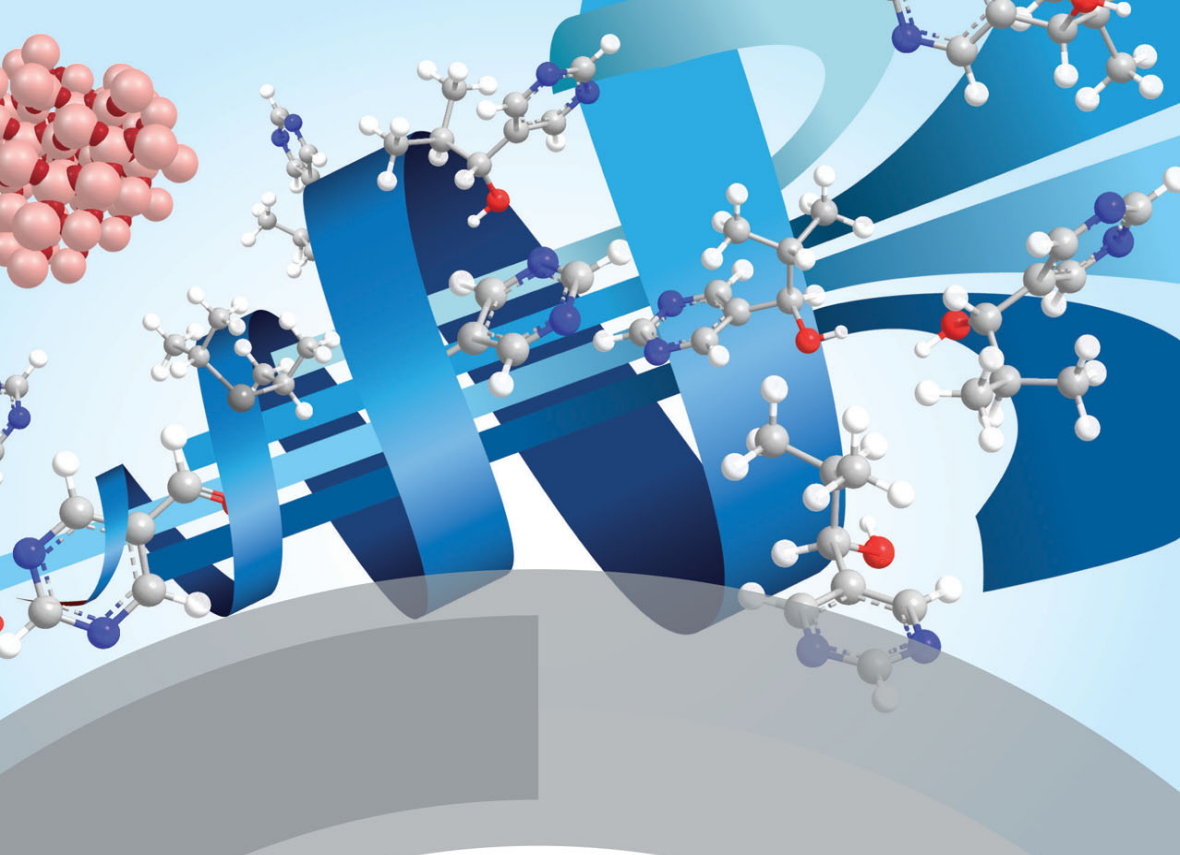

Catalysis Series

Asymmetric Autocatalysis

The Soai Reaction

Edited by Kenso Soai, Tsuneomi Kawasaki
and Arimasa Matsumoto

ROYAL SOCIETY
OF CHEMISTRY

Asymmetric Autocatalysis
The Soai Reaction

Catalysis Series

Editor-in-chief:
Justin S. J. Hargreaves, *University of Glasgow, UK*

Series editors:
Harry Bitter, *Wageningen University, The Netherlands*
Jose Rodriguez, *Brookhaven National Laboratory, USA*

Titles in the series:
1: Carbons and Carbon Supported Catalysts in Hydroprocessing
2: Chiral Sulfur Ligands: Asymmetric Catalysis
3: Recent Developments in Asymmetric Organocatalysis
4: Catalysis in the Refining of Fischer–Tropsch Syncrude
5: Organocatalytic Enantioselective Conjugate Addition Reactions: A Powerful Tool for the Stereocontrolled Synthesis of Complex Molecules
6: N-Heterocyclic Carbenes: From Laboratory Curiosities to Efficient Synthetic Tools
7: *P*-Stereogenic Ligands in Enantioselective Catalysis
8: Chemistry of the Morita–Baylis–Hillman Reaction
9: Proton-Coupled Electron Transfer: A Carrefour of Chemical Reactivity Traditions
10: Asymmetric Domino Reactions
11: C-H and C-X Bond Functionalization: Transition Metal Mediation
12: Metal Organic Frameworks as Heterogeneous Catalysts
13: Environmental Catalysis Over Gold-Based Materials
14: Computational Catalysis
15: Catalysis in Ionic Liquids: From Catalyst Synthesis to Application
16: Economic Synthesis of Heterocycles: Zinc, Iron, Copper, Cobalt, Manganese and Nickel Catalysts
17: Metal Nanoparticles for Catalysis: Advances and Applications
18: Heterogeneous Gold Catalysts and Catalysis
19: Conjugated Linoleic Acids and Conjugated Vegetable Oils
20: Enantioselective Multicatalysed Tandem Reactions
21: New Trends in Cross-Coupling: Theory and Applications
22: Atomically-Precise Methods for Synthesis of Solid Catalysts
23: Nanostructured Carbon Materials for Catalysis
24: Heterocycles from Double-Functionalized Arenes: Transition Metal Catalyzed Coupling Reactions
25: Asymmetric Functionalization of C–H Bonds
26: Enantioselective Nickel-catalysed Transformations
27: N-Heterocyclic Carbenes: From Laboratory Curiosities to Efficient Synthetic Tools, 2nd edition
28: Zeolites in Catalysis: Properties and Applications
29: Biocatalysis: An Industrial Perspective

30: Dienamine Catalysis for Organic Synthesis
31: Metal-free Functionalized Carbons in Catalysis: Synthesis, Characterization and Applications
32: Modern Biocatalysis: Advances Towards Synthetic Biological Systems
33: NO_x Trap Catalysts and Technologies: Fundamentals and Industrial Applications
34: Alternative Catalytic Materials: Carbides, Nitrides, Phosphides and Amorphous Boron Alloys
35: Enantioselective Cobalt-catalysed Transformations
36: Noncovalent Interactions in Catalysis
37: Carbon Nanomaterials in Hydrogenation Catalysis
38: Nanoparticle Design and Characterization for Catalytic Applications in Sustainable Chemistry
39: Catalytic Aerobic Oxidations
40: Catalysis with Earth-abundant Elements
41: Vanadium Catalysis
42: Organocatalytic Dynamic Kinetic Resolution
43: Asymmetric Autocatalysis: The Soai Reaction

How to obtain future titles on publication:
A standing order plan is available for this series. A standing order will bring delivery of each new volume immediately on publication.

For further information please contact:
Book Sales Department, Royal Society of Chemistry, Thomas Graham House, Science Park, Milton Road, Cambridge, CB4 0WF, UK
Telephone: +44 (0)1223 420066, Fax: +44 (0)1223 420247
Email: booksales@rsc.org
Visit our website at www.rsc.org/books

Asymmetric Autocatalysis
The Soai Reaction

Edited by

Kenso Soai
Tokyo University of Science, Japan
Email: soai@rs.tus.ac.jp

Tsuneomi Kawasaki
Tokyo University of Science, Japan
Email: tkawa@rs.tus.ac.jp

and

Arimasa Matsumoto
Nara Women's University, Japan
Email: a-matsumoto@cc.nara-wu.ac.jp

Catalysis Series No. 43

Print ISBN: 978-1-83916-261-9
PDF ISBN: 978-1-83916-627-3
EPUB ISBN: 978-1-83916-628-0
Print: ISSN: 1757-6725
Electronic ISSN: 1757-6733

A catalogue record for this book is available from the British Library

The Royal Society of Chemistry is a charity, registered in England and Wales, Number 207890, and a company incorporated in England by Royal Charter (Registered No. RC000524), registered office: Burlington House, Piccadilly, London W1J 0BA, UK, Telephone: +44 (0) 20 7437 8656.

For further information see our website at www.rsc.org

Printed in the United Kingdom by CPI Group (UK) Ltd, Croydon, CR0 4YY, UK

Preface

Living creatures on Earth have two characteristic features. One is the ability to self-replicate at the molecular, cellular, and individual levels. The second is the overwhelming one-handedness (homochirality) of biomolecules such as L-amino acids and D-sugars. No known life-form can exist without homochiral components. Ever since Pasteur discovered molecular chirality in 1848, the origins and the processes that can lead to enantiopure organic compounds have attracted broad attention. Indeed, Pasteur himself stated in his lecture notes that he tried to induce chirality using a magnet or by inversed movement of sunlight. Thus, research on the origin of chirality of organic compounds has been a historically venerable theme. Although several theories have been proposed to explain the origins of chirality of organic compounds, such as the influence of circularly polarized light or quartz, the enantiomeric excesses (ee) induced by these mechanisms have been very low or below detection levels. Thus, a mechanism by which the very low or even below detection levels of ee induced by the proposed mechanism of the origins of chirality can be amplified to the corresponding highly enantioenriched compounds is crucial.

Asymmetric autocatalysis is a reaction in which a chiral compound acts as a chiral catalyst for its own formation. The process constitutes a catalytic automultiplication of the chiral compound. In 1995, Soai and co-workers discovered asymmetric autocatalysis of 5-pyrimidyl alkanol with amplification of ee in the enantioselective addition of diisopropylzinc to pyrimidine-5-carbaldehyde. Along with automultiplication, asymmetric autocatalysis is capable of amplifying ee from extremely low to near enantiopure levels in the absence of any other chiral factor. Mislow referred to this phenomenon as the Soai reaction, and it has attracted much attention from competent research groups around the world.

This book illustrates recent developments in asymmetric autocatalysis: the Soai reaction. An overview of the Soai reaction is presented with an examination

Catalysis Series No. 43
Asymmetric Autocatalysis: The Soai Reaction
Edited by Kenso Soai, Tsuneomi Kawasaki and Arimasa Matsumoto

Published by the Royal Society of Chemistry, www.rsc.org

of the origins of chirality in conjunction with asymmetric autocatalysis and its application to absolute asymmetric synthesis. The influence of circularly polarized light, chiral inorganic crystals, chiral isotopomers, and chiral organic crystals composed of achiral compounds are also discussed. Reaction models of the Soai reaction that have been developed, such as structures of asymmetric autocatalysts, elucidation of the reaction pathways, application of asymmetric autocatalysis to chiral discrimination, and some unusual aspects of chirality induction detected by using the Soai reaction are also described.

Kenso Soai, Tsuneomi Kawasaki and
Arimasa Matsumoto
Tokyo

Contents

Catalysis Series No. 43
Asymmetric Autocatalysis: The Soai Reaction
Edited by Kenso Soai, Tsuneomi Kawasaki and Arimasa Matsumoto

Published by the Royal Society of Chemistry, www.rsc.org

CHAPTER 1

Asymmetric Autocatalysis: The Soai Reaction, an Overview

KENSO SOAI,*[a,b] TSUNEOMI KAWASAKI[a] AND ARIMASA MATSUMOTO[c]

[a] Department of Applied Chemistry, Tokyo University of Science, Kagurazaka, Shinjuku-ku, Tokyo 162-8601, Japan; [b] Research Organization for Nano & Life Innovation, Waseda University, Wasedatsurumaki-cho, Shinjuku-ku, Tokyo 162-0041, Japan; [c] Department of Chemistry, Nara Women's University, Kita-Uoya Nishi-machi, Nara 630-8506, Japan
*Email: soai@rs.tus.ac.jp

1.1 Introduction

1.1.1 Characteristic Features of Life

1.1.1.1 Self-replication of Organic Molecules

One of the characteristic features of life is self-replication at both cellular and individual levels. Although individuals are mortal, species exist in the long-term because parents produce children. Thus, self-replication provides a mechanism through which a species can exist for longer periods. Self-replication of organic molecules has attracted much attention and has become one of the topics of systems chemistry. Chemical self-replication of nucleotide by forming templates was reported by von Kiedrowski.[1a] Rebek *et al.* reported self-replication of organic compounds.[1b] Gadhiri *et al.* devised self-replicating peptides.[1c] These processes do not produce new stereogenic centers.

Catalysis Series No. 43
Asymmetric Autocatalysis: The Soai Reaction
Edited by Kenso Soai, Tsuneomi Kawasaki and Arimasa Matsumoto

Published by the Royal Society of Chemistry, www.rsc.org

1.1.1.2 *Overwhelming One Handedness,* i.e., *Homochirality, of Biomolecules*

Another characteristic feature of life is the homochirality of biomolecules such as L-amino acids and D-sugars. Why is homochirality essential for life? Let's think about the situation of shaking hands: when both persons use right hands, it is normal shaking hands. When one uses right hand and the other uses left hand, the situation of shaking hands is very different from the normal one. Similarly, dipeptides of L-alanyl-L-alanine and D-alanyl-L-alanine are diastereomers and have different melting points. If D-amino acids are incorporated irregularly in proteins, conformations of proteins change and enzymatic functions do not operate. If L-deoxyribose is incorporated irregularly in DNA, the formation of the helix is disrupted and genetic information cannot be transferred. Eschenmoser *et al.* examined oligomerization of tetranucleotide cyclophosphates of D-pyronosyl-RNA.[2] They found that the incorporation of L-enantiomer instead of D-enantiomer in tetranucleotides results in the efficiency of assembling of tetramers dropping by a magnitude in the order of two. As described, the homochirality of biomolecules is essential for life.

1.1.2 Origin of Homochirality and Amplification of Enantiomeric Excess

Ever since Pasteur discovered the molecular dissymmetry of sodium ammonium tartrate in 1848, the origins of biological homochirality have attracted considerable attention from many scientists.[3a] Indeed, Pasteur himself stated in his lecture notes that he tried to induce chirality using a magnet or by inversed movement of sunlight.[3b] Thus, research on the origin of chirality of organic compounds has been a historically venerable theme. Although theories for the origins of homochirality such as circularly polarized light and quartz have been proposed,[2,4] the enantiomeric excesses induced by these conditions have usually been very low. An amplification process of ee is required to observe the resulting highly enantioenriched organic compounds.[5]

Considering two of the characteristic features of lie, *i.e.*, self-replication and homochirality, it is natural for chemists to conceive the chiral molecule which is capable of self-replicating. In this context, we distinguish the following two concepts: asymmetric autoinduction and asymmetric autocatalysis.

Asymmetric autoinduction is a reaction in which the chiral product has effects on the stereochemical course of the reaction. Alberts and Wynberg reported enantioselective alkylation of benzaldehyde using chiral metal alkoxide of which the chiral ligand and the chiral product have the same structure.[6a] Danda *et al.* reported asymmetric hydrocyanation catalyzed by chiral 2,5-diketopiperadine.[6b] The chiral product increased the enantioselectivity of the catalyst. Soai *et al.* reported asymmetric autoinductive reduction of amino ketone to 1,2-amino alcohol using lithium aluminum hydride modified with the same chiral beta-amino alcohol as the chiral ligand.[6c] In these asymmetric

autoinductions, the chiral catalyst and product have different structures and the amounts of the initial catalysts do not increase.

In this chapter, we describe the trajectory of discovery of asymmetric autocatalysis, state of the art of asymmetric autocatalysis, and research on the origin of homochirality of organic compounds by using asymmetric autocatalysis with amplification of ee.[7]

1.2 Asymmetric Autocatalysis

1.2.1 Principle of Asymmetric Autocatalysis

Asymmetric autocatalysis is a reaction in which a chiral product acts as a chiral catalyst for its own production (see Scheme 1.1). The reaction involves the process of automultiplication, *i.e.*, self-replication, of a chiral compound. Asymmetric autocatalysis has superiority over conventional asymmetric catalysis in four regards. (1) The process involves automultiplication with high efficiency. (2) During the reaction, the amount of catalyst, *i.e.*, the product, increases. In ideal cases, the catalytic activity does not decrease as the amount of catalyst increases during the reaction. On the other hand, in usual asymmetric catalysis, loss of catalyst through imperfect recovery and deterioration of asymmetric catalyst due to the action of heat, acid, base, mechanical damage, *etc.*, is often observed. (3) The process of separation of

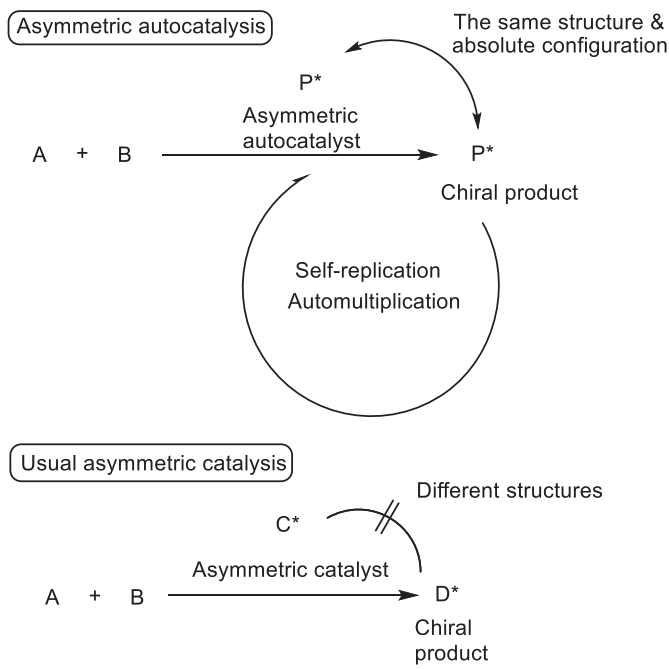

Scheme 1.1 Comparison of the principles of asymmetric autocatalysis and usual asymmetric catalysis.

the product from the catalyst is not necessary because the structure of the catalyst and the product is the same. (4) From the standpoint of green chemistry, three chemical compounds are required in asymmetric autocatalysis: A, B, and P*, whereas four compounds are usually required for asymmetric catalysis: A, B, C*, and D.

1.2.2 Discovery of Asymmetric Autocatalysis of 5-Pyrimidyl, 3-Quinolyl, and 5-Carbamoyl-3-pyridyl Alkanols with Amplification of Enantiomeric Excess: The Soai Reaction

In 1953, Frank proposed a mathematical scheme of asymmetric autocatalysis without referring to any chemical structure.[5c] However, no real asymmetric autocatalysis had been reported until our first report in 1990 on the asymmetric autocatalysis of 3-pyridyl alkanol in the enantioselective addition of dialkylzincs to pyridine-3-carbaldehyde.[8a] In 1995, we found asymmetric autocatalysis of pyrimidyl alkanol **1** with amplification of enantiomeric excess (ee) in the reaction between pyrimidine-5-carbaldehyde **2** and diisopropylzinc (see Scheme 1.2).[9a,b]

Moreover, we found that quinolyl alkanol **4**[10a,b,c] and 5-carbamoylpyridyl alkanol **5**[11a,b] act as asymmetric autocatalysts for amplification of ee in the reactions between quinoline-3-carbaldehyde and 5-carbamoylpyridine-3-carbaldehyde, respectively, with diisopropylzinc (see Scheme 1.3).

Asymmetric autocatalysis with amplification of ee provides an efficient process through which homochirality can be achieved.

1.2.3 Trajectory Leading to the Discovery of Asymmetric Autocatalysis

Enantioselective addition of organometallic reagents to aldehydes using chiral ligands affords enantioenriched *sec*-alcohols. In 1979, Mukaiyama and Soai (one of the present authors) *et al.* reported highly enantioselective addition of alkyllithium and dialkylmagnesium to aldehydes using a chiral β-diaminoalkanol derived from (*S*)-proline as a chiral ligand.[12a] We also observed that diethylzinc adds to benzaldehyde in the presence of diaminoalcohol to afford 1-phenylpropanol in 76% yield.[12a] Given that the reactivity of dialkylzinc to aldehydes is usually low, this result showed amino alcohol accelerates the nucleophilicity of dialkylzinc enough to add to aldehydes. Enantioselective addition of diethylzinc to benzaldehyde using a β-aminoalcohol as a chiral catalyst was reported by Oguni and Omi,[12b] and then by Noyori *et al.*[12c]

Soai *et al.* devised *N*-methyldiphenylprolinol (DPMPM)[12d,e] and *N*,*N*-dibutylnorephedrine (DBNE)[12f,g] as highly enantioselective catalysts for the addition of dialkylzincs to aldehydes.[12h]

(*S*)-*N*-Methyldiphenylprolinol (DPMPM) catalyzes the addition of Et_2Zn to benzaldehyde **6** to afford (*S*)-1-phenylpropanol **7** with 97% ee (see Scheme 1.4). We observed that the catalyst (*S*,*S*)-*threo*-*N*-methylphenylprolinol (PMPM)

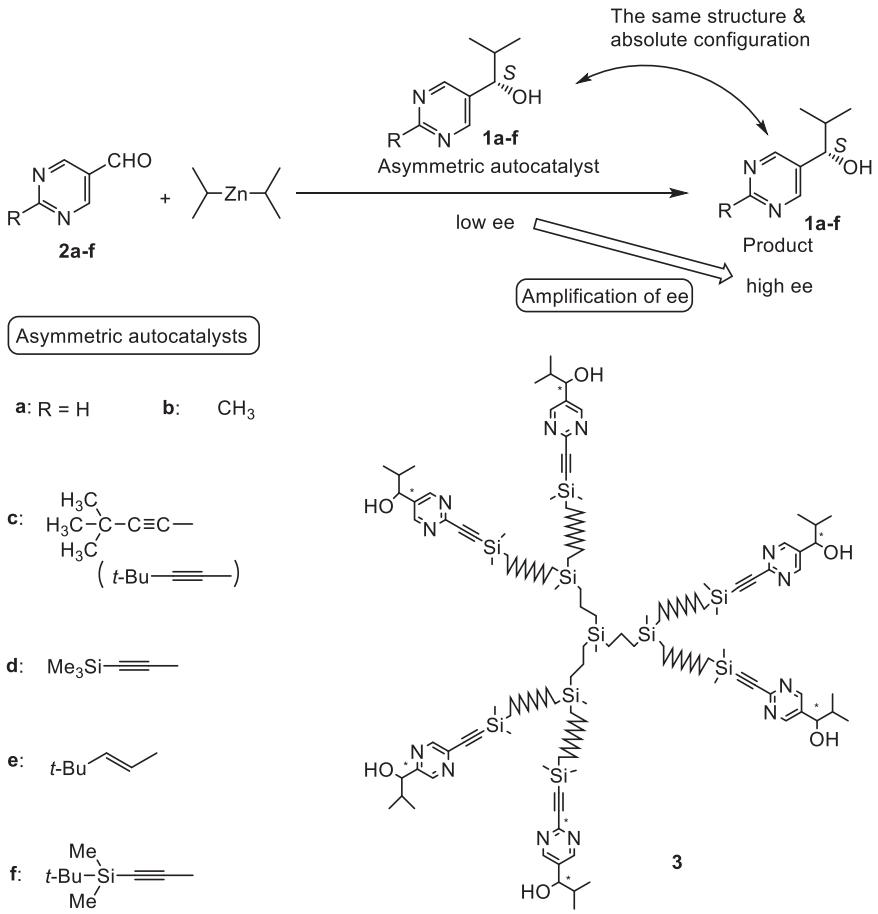

Scheme 1.2 Asymmetric autocatalysis of pyrimidyl alkanol with amplification of enantiomeric excess: The Soai reaction.

affords (*S*)-alkanol **7**, while (*S*,*R*)-*erythro*-PMPM affords (*R*)-alkanol **7**. These results show that the sense of enantioselectivity is controlled by the absolute configuration of the stereogenic center of the alcohol moiety of the catalysts.

We also observed, in 1989, that the reaction of pyridine-3-carbaldehyde **8**, a nitrogen-containing aldehyde, and dialkylzinc catalyzed by (1*S*,2*R*)-DBNE completed within 1 h to afford (*S*)-3-pyridyl alkanol **9**,[10*i*] while the reaction of benzaldehyde **6** needed 16 h to reach completion to afford (*S*)-alkanol **7** (see Scheme 1.5).[10*f*,*g*] We considered that the isopropylzinc alkoxide of pyridyl alkanol, *i.e.*, the product *in situ*, catalyzes the addition of diisopropylzinc to pyridine-3-carbaldehyde **8**.

Based on these observations, we got an idea that a nitrogen-containing chiral alkanol with a suitable structure would act as an asymmetric autocatalyst in the enantioselective addition of dialkylzinc to a nitrogen-containing aldehyde

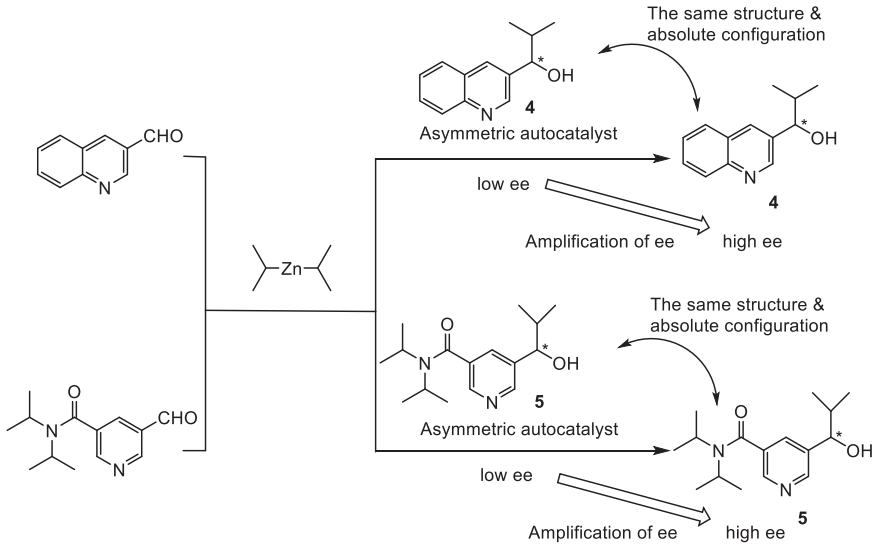

Scheme 1.3 Asymmetric autocatalysis of 3-quinolyl alkanol and 5-carbamoyl-3-pyridyl alkanol with amplification of ee. The Soai reaction.

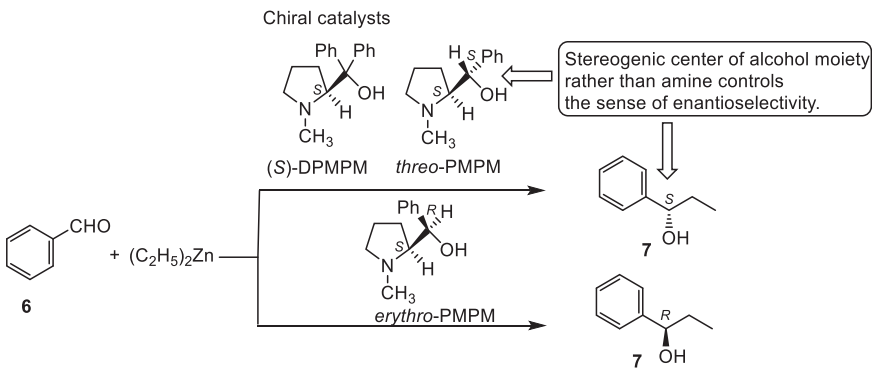

Scheme 1.4 Catalytic enantioselective addition of diethylzinc to benzaldehyde using (*S*)-DPMPM, (*S*,*S*)-*threo*-, and (*S*,*R*)-*erythro*-PMPM.

with a suitable structure. In his stimulating essay, Wynberg challenged "red-blooded" chemists to realize asymmetric autocatalysis.[13]

1.2.4 The First Asymmetric Autocatalysis of 3-Pyridyl Alkanol

In 1990, we found chiral 3-pyridyl alkanols act as asymmetric autocatalysts in the addition of dialkylzincs to pyridine-3-carbaldehyde (see Scheme 1.6).[8a] Although the ee values of products were lower than those of the asymmetric autocatalysts, this stands as the first demonstration of asymmetric autocatalysis.

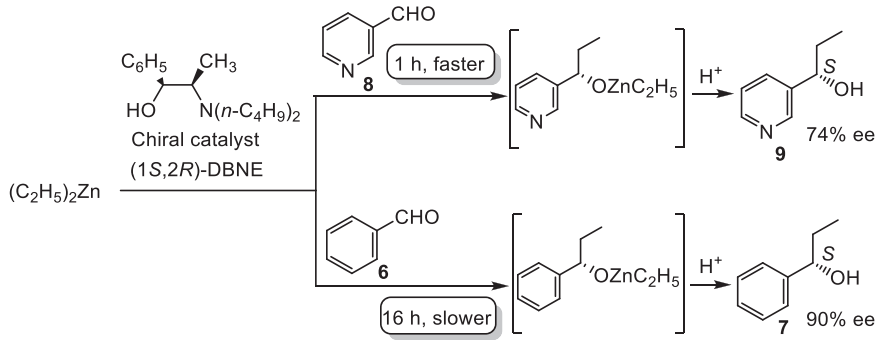

Scheme 1.5 Enantioselective addition of diethylzinc to pyridine-3-carbaldehyde and benzaldehyde catalyzed by (1*S*,2*R*)-DBNE.

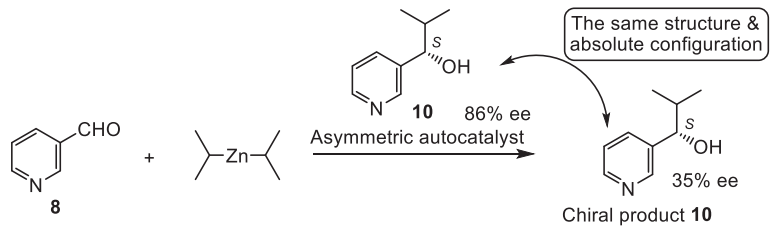

Scheme 1.6 The first asymmetric autocatalysis of 3-pyridyl alkanol in the addition of diisopropylzinc to pyridine-3-carbaldehyde.

1.2.5 Highly Enantioselective Asymmetric Autocatalysis

We continued to search for asymmetric autocatalytic systems with studies on chiral alkanol systems.[8b,c] In 1995, we identified the highly enantioselective asymmetric autocatalysis of pyrimidyl alkanol.[9a,b] Pyrimidyl alkanol acts as a highly enantioselective asymmetric autocatalyst in the enantioselective addition of diisopropylzinc (*i*-Pr_2Zn) to pyrimidine-5-carbaldehyde. (*S*)-Pyrimidyl alkanols[9a,b] with 93–95% ee catalyzed the addition of *i*-Pr_2Zn to pyrimidine-5-carbaldehyde to afford (*S*)-pyrimidyl alkanols[9a,b] with the same structure and absolute configuration with 91–95% ee (see Scheme 1.7).[9b]

After examining the effect of substituents at the 2-position, we found that (*S*)-2-alkynylpyrimidyl alkanol **1c**, with >99.5% ee, was a practically perfect asymmetric autocatalyst to afford itself (*S*)-**1c** with >99.5% ee in >99% yield (see Scheme 1.7).[9c] (*S*)-Pyrimidyl alkanol **1c** obtained in one asymmetric autocatalysis was used as an asymmetric autocatalyst for the next run. Even after 10 rounds of consecutive asymmetric autocatalysis, the yield of (*S*)-**1c** was >99% and the ee was >99.5%. No deterioration of catalytic activity or enantioselectivity was observed. Thus, 2-alkynyl-5-pyrimidyl alkanol **1c** is a practically perfect asymmetric autocatalyst for the addition of *i*-Pr_2Zn to 2-alkynylpyrimidine-5-carbaldehyde **2c**.[9c]

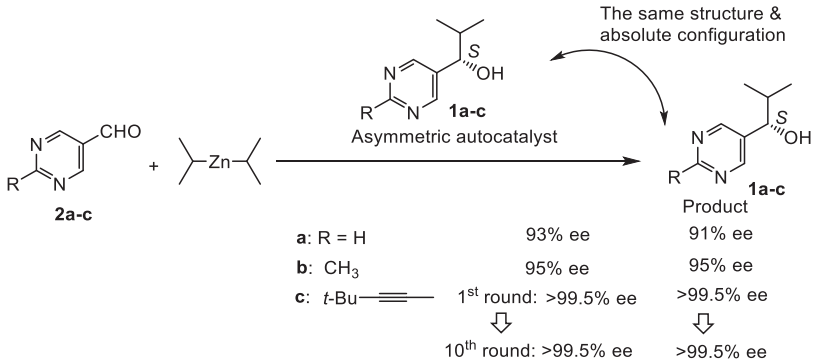

Scheme 1.7 Highly enantioselective asymmetric autocatalysis of 5-pyrimidyl alkanol **1a,b** and practically perfect asymmetric autocatalysis of 2-alkynyl-5-pyrimidyl alkanol **1c**.

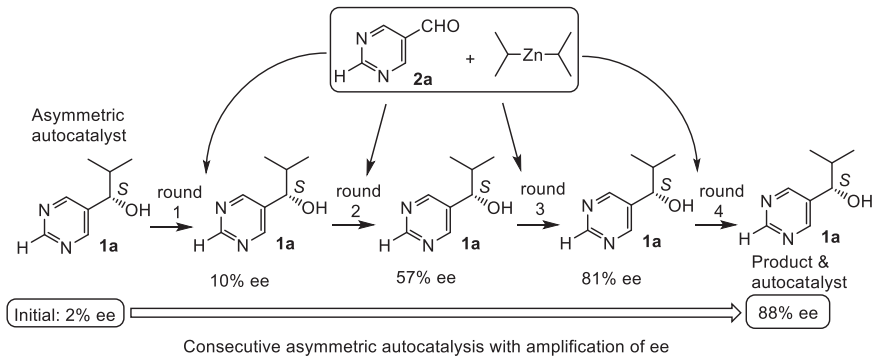

Scheme 1.8 Asymmetric autocatalysis of 5-pyrimidyl alkanol **1a** with amplification of enantiomeric excess from 2 to 88% ee.

1.2.6 Discovery of Asymmetric Autocatalysis with Amplification of Enantiomeric Excess. The Soai Reaction

Moreover in 1995, we found a highly enantioselective asymmetric autocatalysis of pyrimidyl alkanol **1** with amplification of ee in the enantioselective addition of *i*-Pr_2Zn to pyrimidine-5-carbaldehyde **2a** (see Scheme 1.8).[9a] Consecutive asymmetric autocatalysis of pyrimidyl alkanol (*S*)-**1a** with 2% ee in the enantioselective addition of diisopropylzinc (*i*-Pr_2Zn) to pyrimidine-5-carbaldehyde **2a** enabled amplification of ee to 88%.[9a] In the reaction, pyrimidyl alkanol **1a** with 2% ee acts as an asymmetric autocatalyst to afford more of itself with the same absolute configuration and with an amplified 10% ee as a mixture of the newly formed and the initial alkanol. Alkanol **1a** with 10% ee was used as the next round of asymmetric autocatalysis and the ee was amplified to 57%. Subsequent consecutive asymmetric autocatalysis enabled ee amplification from 57% to 81% ee, then to 88% ee.[9a] It should be emphasized

that the origin of amplification of ee was the initial slight enantiomeric imbalance (2% ee) of asymmetric autocatalyst **1a** itself and that, unlike non-autocatalytic systems, no other chiral factor was necessary.

In non-autocatalytic amplification in asymmetric catalysis, the structures of chiral catalysts and products are different.[5a] Therefore, the ee of the product cannot be amplified further.

Soai *et al.* found that the asymmetric autocatalysis of (*S*)-2-alkynylpyrimidyl alkanol[9c,d] exhibits significant amplification of ee (see Scheme 1.9).[9d] Thus, asymmetric autocatalysis of (*S*)-2-alkynylpyrimidyl alkanol **1c** with an extremely low ee of *ca.* 0.00005% (*i.e.*, enantiomeric ratio of *ca.* 50.000025 : 49.999975) afforded (*S*)-alkanol **1c** with significantly amplified 57% ee. Subsequent consecutive asymmetric autocatalysis using (*S*)-alkanol **1c** with 57% ee amplified the ee to 99% ee, and then the third asymmetric autocatalysis increased the ee to >99.5%. During these three consecutive asymmetric autocatalysis runs, the amount of the initial slightly major (*S*)-alkanol **1c** automultiplied by a factor of *ca.* 630 000 times, while the minor (*R*)-alkanol **1c** only *ca.* 950 times.[9d]

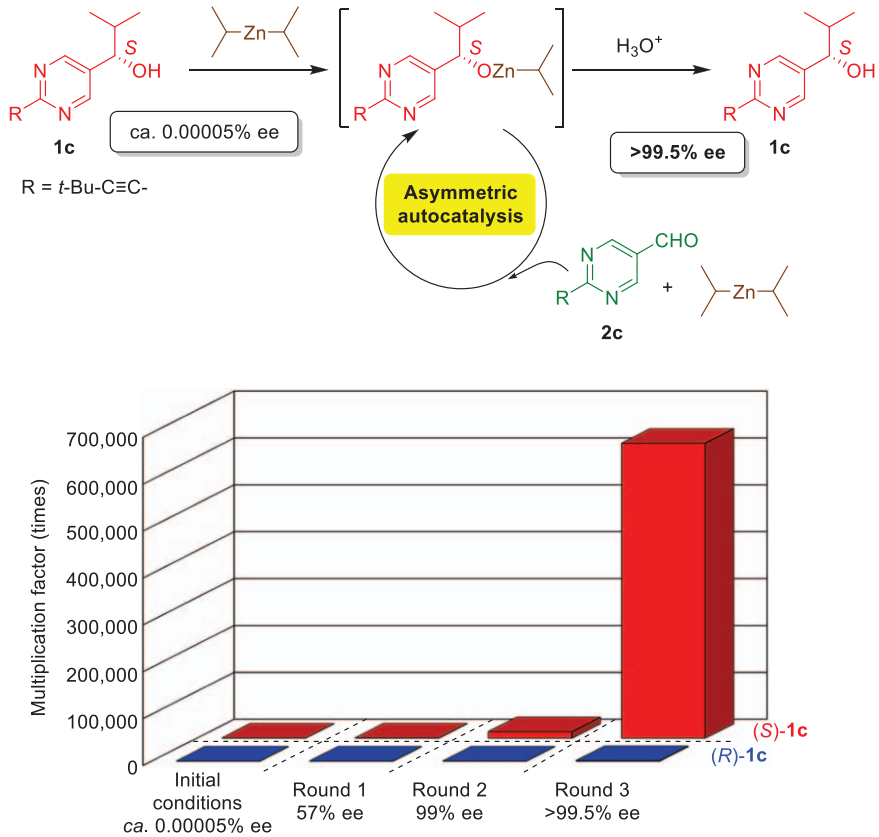

Scheme 1.9 Asymmetric autocatalysis of 2-alkynyl-5-pyrimidyl alkanol **1c** with significant amplification of ee from *ca.* 0.00005% to >99.5% ee.

It was also found that 2-alkenylpyrimidyl alkanol **1e**,[9e] 3-quinolyl alkanol **4**,[10b,c] and 5-carbamoylpyridyl alkanol **5** with one nitrogen atom in the aromatic ring[11b] are highly enantioselective asymmetric autocatalysts with amplification of ee (see Schemes 1.2 and 1.3). Moreover, asymmetric autocatalysis of multiply functionalized pyrimidyl alkanol **3** was achieved.[9f] Ultra-remote intramolecular asymmetric autocatalysis was also observed.[9g]

The most characteristic feature of the present amplification of ee by asymmetric autocatalysis is that the amplification of ee is made possible without the intervention of any chiral factor other than the initial enantiomeric imbalances of the asymmetric autocatalysts themselves. The results proved that there is a real chemical reaction in which very slight enantiomeric excess can be amplified to near enantiopure levels (>99.5% ee) by asymmetric autocatalysis.

1.2.7 Investigation of the Mechanism of Asymmetric Autocatalysis

Asymmetric autocatalysis described in the preceding sections is unique and leads to significant amplification of ee. Thus, mechanistic aspects of asymmetric autocatalysis have attracted great attention. Several groups showed interest in the reaction, and both theoretical and experimental studies of the reaction have been performed using a range of techniques. These are described in other chapters of this book. For non-autocatalytic nonlinear effects in asymmetric catalysis, the dimer mechanism was proposed by Noyori *et al.*[14a] and the ML_n mechanism was put forward by Kagan *et al.*[14b]

We reported the relationship between the reaction time and yield of the product in asymmetric autocatalysis using an enantiopure pyrimidyl alkanol **1c**,[15a] for which a sigmoidal curve of product formation was observed. We also reported kinetic analysis of the relationship between the time and the yield, including ee of the product of asymmetric autocatalysis based on chiral HPLC analysis,[15b] which suggested that dimeric or more highly aggregated catalytic species were involved.

Measurement of heat flow with a microcalorimeter by Blackmond and Brown *et al.* revealed the reaction rate to be a function of the progress of the reaction, which suggested the dimeric catalyst model.[15c] NMR experiments with direct observation of the reaction solution led to the presence of dimeric and tetrameric species being proposed.[15d,e] Structures of catalyst aggregates have also been proposed based on DFT calculations by the groups of Ercolani[15f,g] and Gridnev.[15h,i] Reaction models based on spontaneous mirror-symmetry breaking have also been presented. These approaches led to the proposal of mechanistic frameworks for asymmetric autocatalysis of pyrimidyl alkanol **1c**.[15j–q] Denmark *et al.* employed NMR and react-IR for the study of the reaction using 6-alkynylpyrimidyl alkanol as the substrate.[15r] Trapp *et al.* reported an acetal intermediate based on the *in situ* mass spectrometry study of the reaction.[15s]

Based on X-ray diffraction analysis, we clarified that the crystal structures of asymmetric autocatalysts, *i.e.*, isopropylzinc alkoxide of **1c**, are either tetrameric or oligomeric (see Figure 1.1).[15t,u] The tetrameric crystal structure is formed in the presence of an excess molar amount of *i*-Pr_2Zn (Figure 1.1a,b) whereas higher-order aggregates are formed in the presence of equimolar or a slight excess of *i*-Pr_2Zn. It should be noted that Zn_2O_2 square has a coordinatively unsaturated Zn atom to which the oxygen atom of aldehyde is considered to coordinate (Figure 1.1c). It should also be noted that 6 molecules of activated *i*-Pr_2Zn are involved in the enantiopure crystal structure by coordination with nitrogen atoms of the pyrimidine ring (Figure 1.1a).

Recent reaction modeling also supports the suggestion that the tetramer or higher-order aggregates are significant species in asymmetric autocatalysis.[15v] Circular dichroism (CD) spectroscopy by Matsumoto *et al.* of the catalyst in solution revealed the equilibrium of tetramer and dimer.[15w] Clarification of the overall reaction pathway of asymmetric autocatalysis awaits further investigation.

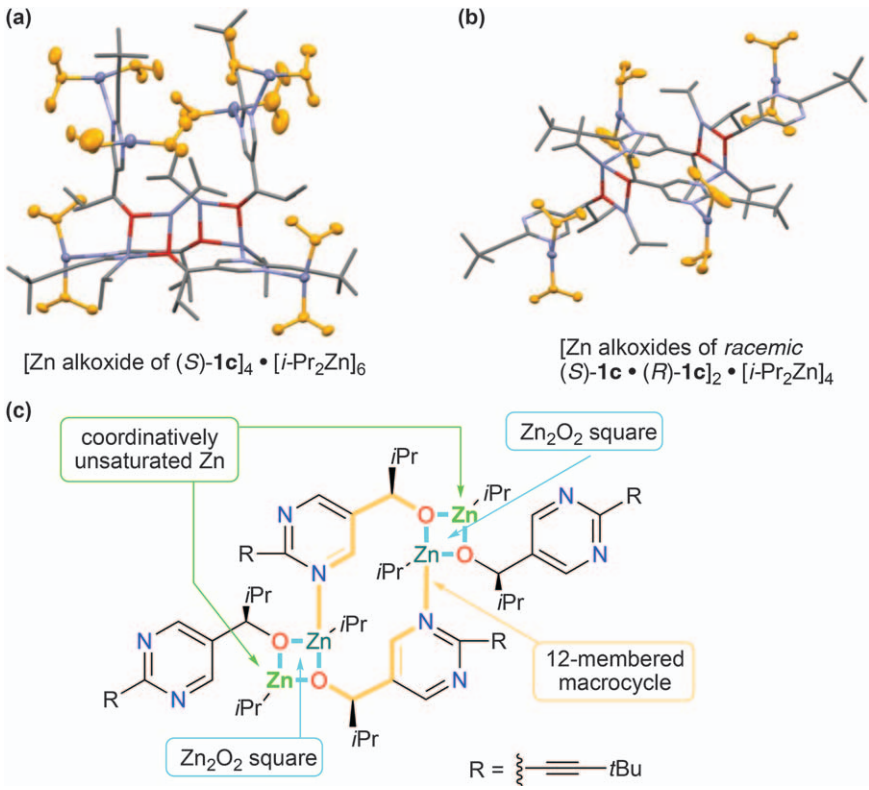

Figure 1.1 X-Ray crystal structures of (a) tetrameric enantiopure isopropylzinc alkoxide of (*S*)-**1c** coordinated with 6 mol *i*-Pr_2Zn and (b) tetrameric racemic isopropylzinc alkoxide with 4 mol *i*-Pr_2Zn. Schematic tetrameric structure (c) with a 12-membered macrocycle and two Zn_2O_2 squares including coordinatively unsaturated Zn atoms.

More detailed description of the theoretical and experimental studies on the mechanisms of asymmetric autocatalysis are described in other chapters of this book.

1.3 Studies on the Origins of Homochirality by Using Asymmetric Autocatalysis

With regard to the origins of homochirality, several theories such as circularly polarized light and chiral inorganic quartz have been proposed. However, the ee values induced by the processes proposed in these theories have usually been very low. We thought that the low ee induced by the origin of homochirality could be enhanced to the highly enantioenriched compound through asymmetric autocatalysis with amplification of ee.

1.3.1 Circularly Polarized Light

Left (*l*) and right (*r*) circularly polarized light (CPL) has been proposed as the origin of chirality of organic compounds.[4c] The generation of relatively strong CPL has been observed in some star-forming regions.[16a] Asymmetric photodecomposition of racemic leucine by CPL leaves leucine with *ca.* 2% ee.[4c] Asymmetric photosynthesis of [6]helicene with low ee by CPL has also been reported.[16b] By using leucine[16c] and [6]helicene with low ee as chiral triggers of asymmetric autocatalysis, enantioenriched pyrimidyl alkanols **1b**,**c** with the corresponding absolute configurations to those of the chiral triggers were obtained. Thus, for the first time, the chirality of CPL has been correlated to the very high ee of the generated organic compound by using asymmetric autocatalysis.[16c]

The direct irradiation with *l*-CPL of racemic (*rac*) asymmetric autocatalyst, *i.e.*, pyrimidyl alkanol **1c**, and subsequent asymmetric autocatalysis with amplification of ee afforded (*S*)-alkanol **1c** with >99.5% ee (see Scheme 1.10).[16d] In sharp contrast, irradiation with *r*-CPL afforded (*R*)-**1c** with >99.5% ee. The correlation between the handedness of *l*- and *r*-CPL and (*S*)-**1c** and (*R*)-**1c** is explained as follows: in their circular dichroism (CD) spectra at 313 nm, (*R*)-**1**

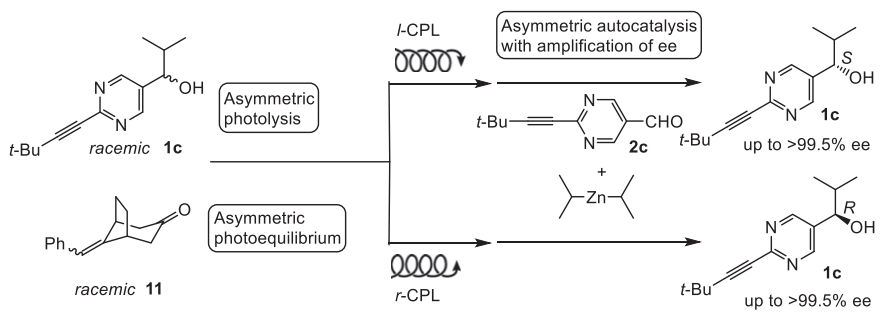

Scheme 1.10 Asymmetric autocatalysis triggered by irradiation with left- or right-circularly polarized light (CPL).

and (*S*)-**1c** exhibited positive and negative Cotton effects, respectively. Therefore, irradiation with l-CPL of *rac*-**1c** would induce the asymmetric photoreaction of (*R*)-**1c** due to its preferential absorbance of *l*-CPL. The less reactive (*S*)-**1c** would then become enriched as the remaining enantiomer over (*R*)-**1c**. Subsequent asymmetric autocatalysis increases the ee of (*S*)-**1c** to >99.5% ee.[16d] The asymmetric photoequilibrium of *rac*-olefin **11** under irradiation with CPL, and the subsequent asymmetric autocatalysis afforded pyrimidyl alkanol **1c** with absolute configuration correlated to CPL.[16e] Thus, the first direct correlation was accomplished between the handedness of CPL and that of an organic compound with very high ee.

Recently, under CPL irradiation, Viedma-type racemization–crystallization of an amino acid derivative was reported.[16f]

1.3.2 Chiral Inorganic Crystals of Quartz, Cinnabar, Sodium Chlorate, Retgersite, and the Enantiotopic Face of Achiral Crystals of Gypsum

Quartz exhibits enantiomorphism and optical activity was found with this mineral. Chiral minerals such as quartz have been proposed as the origin of homochirality.[4g] Several results were reported on attempts to use quartz to induce chirality in organic compounds; however, most of the earlier reports were later disproved.[17a] Only low enantioenrichment was reported for an enantiomer-selective adsorption of racemic amino acid detected by radioactivity.[17b]

We anticipated that *d*- and *l*-quartz could act as a chiral trigger in the reaction between pyrimidine-5-carbaldehyde and diisopropylzinc. The initially formed isopropylzinc alkoxide of pyrimidyl alkanol would be enantioenriched with the absolute configuration corresponding to that of the chiral initiator. Subsequent asymmetric autocatalysis would then amplify significantly the ee of the product pyrimidyl alkanol.[17c] Indeed, asymmetric autocatalysis using pyrimidine-5-carbaldehyde **2c** and *i*-Pr_2Zn in the presence of *d*-quartz gave (*S*)-**1c** with 97% ee in a yield of 95% (see Scheme 1.11).[17c] In contrast, *l*-quartz afforded (*R*)-**1c**

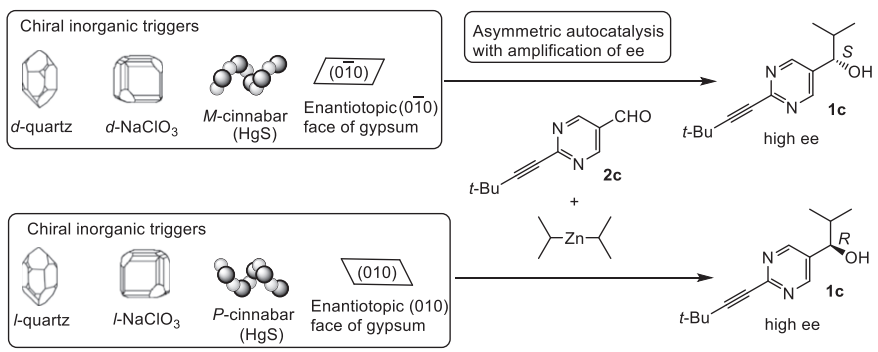

Scheme 1.11 Asymmetric autocatalysis triggered by chiral inorganic crystals such as quartz, cinnabar, and sodium chlorate, and by the enantiotopic face of the achiral crystal of gypsum.

with 97% ee. These results clearly show that *d*- and *l*-quartz act as chiral initiators of asymmetric autocatalysis. Thus, the chirality of *d*- and *l*-quartz was correlated for the first time to the chirality of a near enantiopure organic compound.

Sodium chlorate ($NaClO_3$) and sodium bromate ($NaBrO_3$) are chiral inorganic ionic crystals.[18a,b] It was found that *d*-$NaClO_3$ can also trigger asymmetric autocatalysis to afford (*S*)-**1c** with high ee. In contrast, *l*-$NaClO_3$ triggers the formation of (*R*)-**1c**.[18c] Moreover, *d*-$NaBrO_3$ and *l*-$NaBrO_3$ trigger the formation of (*R*)- and (*S*)-**1c**, respectively.[18d] It should be noted that *d*-$NaClO_3$ and *l*-$NaBrO_3$ of the opposite signs of optical rotation have the same type of enantiomorph.

Enantiomorphic *P*- and *M*-crystals of cinnabar, mercury(II) sulfide (HgS), are constructed with –S–Hg–S–Hg spiral chains. We found that *P*-HgS induces asymmetric autocatalysis to afford (*R*)-**1c** with high ee and that *M*-HgS induces the formation of (*S*)-**1c**.[18e]

Asymmetric autocatalysis triggered by retgersite ($NiSO_4{\cdot}6H_2O$) of [CD(+)390_{Nujol}] afforded (*S*)-**1c** with high ee, whereas retgersite of the opposite [CD(−)390_{Nujol}] afforded (*R*)-**1c** with high ee.[18f] As described, chiral minerals such as quartz, cinnabar, sodium chlorate, and retgersite act as origins of chirality to afford, in conjunction with asymmetric autocatalysis, highly enantioenriched organic compounds.

Gypsum ($CaSO_4{\cdot}2H_2O$; calcium sulfate dihydrate) has been widely used for plaster boards in buildings and for sculptures. Although gypsum has an achiral crystal structure, it exhibits two-dimensional enantiotopic cleavage (010) and ($0\bar{1}0$) faces. Pyrimidine-5-carbaldehyde **2c** was grasped on the enantiotopic (010) face and was exposed to the vapor of *i*-Pr_2Zn. Asymmetric autocatalysis on the enantiotopic (010) face afforded (*R*)-pyrimidyl alkanol **1c**.[19] In contrast, asymmetric autocatalysis on the opposite enantiotopic ($0\bar{1}0$) face afforded (*S*)-alkanol **1c**. Thus, the enantiotopic face of achiral gypsum acts as an origin of chirality.

As described, by using asymmetric autocatalysis, chiral inorganic crystals were shown to act as the origin of chirality to afford highly enantioenriched organic compounds with correlated absolute configurations.

1.3.3 Organic Crystals

1.3.3.1 Chiral Organic Crystals Composed of Achiral Compounds

There are certain classes of achiral organic compounds that form chiral crystals.[20a] Some of the chiral crystals composed of achiral organic compounds have been used as reactants in stereospecific reactions.[4d] However, chiral organic crystals formed from achiral organic compounds have rarely been used as chiral inducers. We found that chiral crystals composed of achiral organic compounds can act as the origin of chirality and trigger asymmetric autocatalysis (see Schemes 1.12 and 1.13).

It is known that glycine is the only achiral amino acid among proteinogenic amino acids and that the crystal structure of γ-glycine polymorph is chiral; nevertheless, it took years to determine the correlation between the

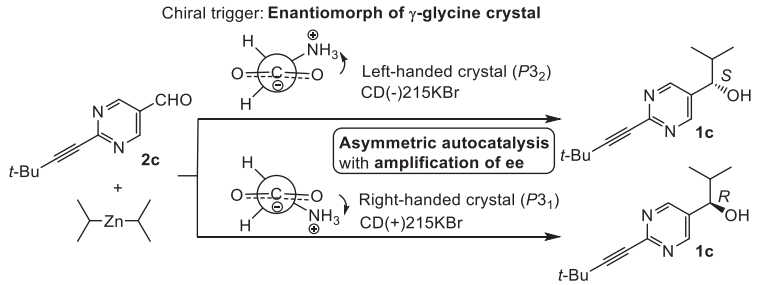

Scheme 1.12 Asymmetric autocatalysis triggered by a chiral γ-polymorph of achiral glycine.

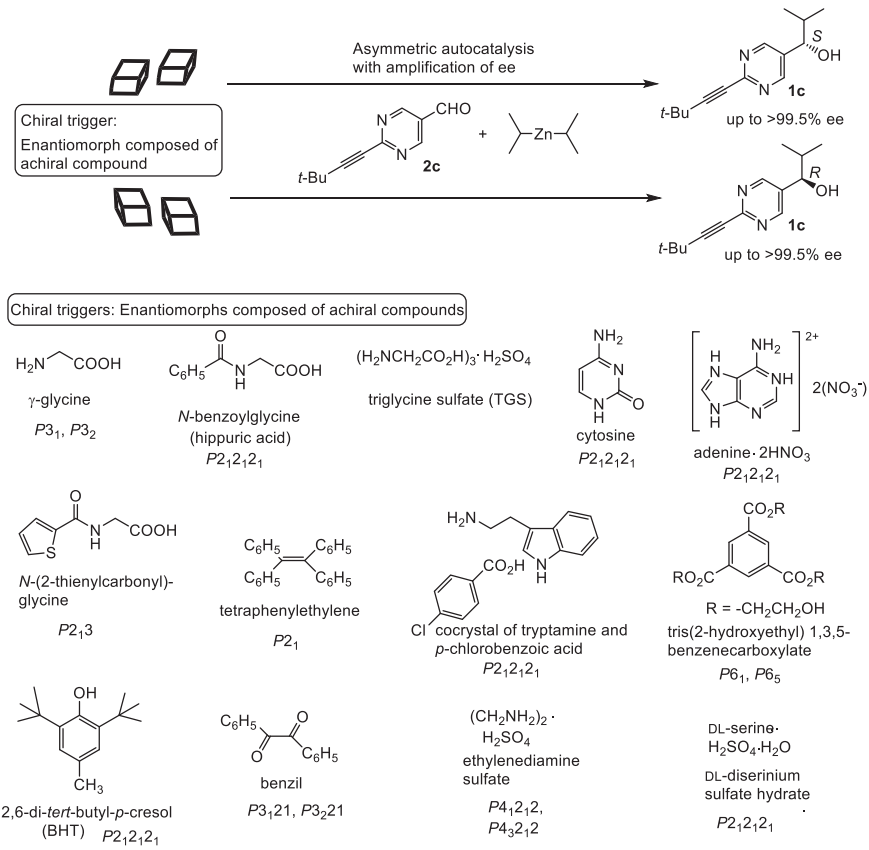

Scheme 1.13 Asymmetric autocatalysis of pyrimidyl alkanol initiated by chiral crystals composed of achiral organic compounds.

optical rotation and the absolute crystal structure of the γ-glycine polymorph. Asahi *et al.*, including the present authors (Kawasaki and Soai), determined the relation between the absolute crystal structure of the

γ-glycine polymorph and the optical rotatory dispersion.[20b] Guillemin reported that γ-glycine exhibits circular dichroism (CD) spectra,[20c] and we then clarified the correlation between the absolute crystal structure of γ-glycine and CD spectra: left-handed crystal ($P3_2$) of γ-glycine exhibits CD(−) at 215 nm observed using a KBr disk, whereas right-handed crystal ($P3_1$) exhibits CD(+).[20d]

We examined asymmetric autocatalysis in the presence of γ-glycine crystal as a chiral trigger. In the presence of a $P3_2$ crystal (left-handed) of γ-glycine, (*S*)-pyrimidyl alkanol **1c** was formed with up to >99.5% ee (see Scheme 1.12).[20d] In contrast, in the presence of a $P3_1$ crystal, (*R*)-alkanol **1c** was obtained with up to >99.5% ee. Thus, achiral glycine acts as the origin of homochirality by forming a chiral γ-polymorph, then triggering the asymmetric autocatalysis with amplification of ee.

Cytosine is an achiral nucleobase. Chiral cytosine crystals formed by crystallization from methanol trigger asymmetric autocatalysis. When a chiral [CD(+)310_{Nujol}]-cytosine crystal was used as a chiral trigger of the reaction between pyrimidine-5-aldehyde **2c** and *i*-Pr_2Zn, asymmetric autocatalysis with amplification of ee afforded (*R*)-pyrimidyl alkanol **1c** (see Scheme 1.13).[20e] In contrast, a [CD(−)310_{Nujol}]-cytosine crystal afforded (*S*)-**1c**. Thus, the chiral cytosine crystal composed of achiral cytosine is capable of acting as the origin of chirality in conjunction with asymmetric autocatalysis.

Crystallization of cytosine from water generates achiral cytosine monohydrate crystals. It was found that a chiral dehydrated cytosine crystal is formed by elimination of crystal water by heating one of the enantiotopic faces of the achiral crystal.[20f] Surprisingly, the chirality of the formed dehydrated cytosine crystal is correlated to the enantiotopic face of the achiral cytosine monohydrate from which heating is applied. It should be noted that dehydration of crystal water of cytosine monohydrate under reduced pressure conditions from one of the enantiotopic faces at room temperature gave the chiral cytosine dehydrated crystal,[20g] but surprisingly again, the formed crystal chirality is opposite to that formed by dehydration upon heating. It should also be noted that the sign of the Cotton effects (CD spectra) of the chiral cytosine crystal are opposite to those observed when using a KBr disk and Nujol mull; that is, CD(+)310_{KBr} (CD plus at 310 nm with KBr disk) and CD(−)310_{Nujol} (CD minus at 310 nm with Nujol mull) arise from the same chirality of cytosine crystal. These results are the first example of the formation of chiral crystals with controlled chirality by dehydration from an achiral crystal monohydrate.

Adenine is another achiral nucleobase that we investigated; a chiral crystal of adenine dinitrate was found to act as a chiral trigger of asymmetric autocatalysis, and highly enantioenriched pyrimidyl alkanols were formed with the absolute configurations corresponding to those of chiral adenine dinitrate (see Scheme 1.13).[20h] These results show that achiral nucleobases, *i.e.*, cytosine and adenine, can act as the origin of chirality in their chiral crystalline form in conjunction with asymmetric autocatalysis with amplification of ee.

Moreover, enantiomorphous crystals composed of achiral *N*-benzoylglycine (hippuric acid),[20i] triglycine sulfate (TGS),[20j] 2-thenoylglycine,[20k] tetraphenylethylene,[20l] certain chiral cocrystals consisting of two achiral compounds,[20m] aromatic trimester,[20n] 2,6-di-*tert*-butyl-*p*-cresol (BHT),[20o] benzil,[20p] and ethylenediammonium sulfate[20q] are all capable of inducing asymmetric autocatalysis as chiral triggers. It is interesting to note that a chiral crystal composed of a racemic serine can also act as a chiral trigger of asymmetric autocatalysis. Thus, *M*-crystals of DL-diserinium sulfate hydrate induce asymmetric autocatalysis to give (*R*)-pyrimidyl alkanol **1c**, while *P*-crystals afford (*S*)-alkanol **1c**.[20r]

1.3.3.2 Enantiotopic Face of the Achiral Organic Crystal of Achiral Organic Compounds

Some achiral organic compounds are known to form achiral crystals with enantiotopic faces. Achiral 2-(*tert*-butyldimethylsilylethynyl)pyrimidine-5-carbaldehyde **2f** forms an achiral crystal ($P\bar{1}$) that has enantiotopic faces. When one of the enantiotopic faces, *i.e.*, *Re*-face of the aldehyde, was exposed to the vapor of *i*-Pr_2Zn in a solvent, (*R*)-pyrimidyl alkanol **1f** was formed (see Scheme 1.14).[21] In contrast, exposure of *i*-Pr_2Zn vapor on the *Si*-face of the aldehyde gave (*S*)-alkanol **1f**. The ee values of the formed pyrimidyl alkanol **1f** were amplified to >99.5% ee by subsequent asymmetric autocatalysis. Thus, it was shown that the enantiotopic faces of an achiral crystal composed of an achiral compound can act as the origin of homochirality in conjunction with asymmetric autocatalysis.

1.4 Absolute Asymmetric Synthesis

The term ''absolute asymmetric synthesis'' has often been used for the asymmetric synthesis ''without using any chiral chemical substance.'' However, Mislow proposed a new definition of absolute asymmetric

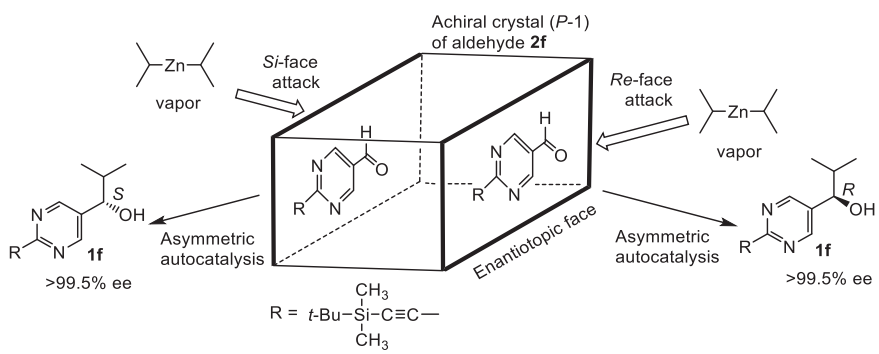

Scheme 1.14 Asymmetric autocatalysis of pyrimidyl alkanol **1f** on the enantiotopic surface of an achiral crystal of 2-(*tert*-butyldimethylsilylethynyl)pyrimidine-5-carbaldehyde **2f**.

synthesis as the formation of an enantioenriched compound "without the intervention of any chiral factor."[4a]

It is known that, when achiral reactants form a chiral product without the intervention of any chiral factor, the chiral product always becomes a racemate. For example, the reaction of benzaldehyde with methylmagnesium bromide always affords racemic 1-phenylethanol. Although the ee is far below the level of detection, the numbers of enantiomers almost always have statistical fluctuations.[4a] By comparison, in the case of flipping a coin 100 times, the probability of flipping 50 heads and 50 tails is only 8%; in the other 92% of cases, some statistical bias exists between the number of heads and tails.

1.4.1 Realization of Absolute Asymmetric Synthesis

As described in the preceding section, asymmetric autocatalysis of pyrimidyl alkanol is capable of amplifying extremely low (*ca.* 0.00005%) ee to near enantiopure (>99.5%) ee.[9d] What will happen if the reaction between pyrimidine-5-carbaldehyde **2** and *i*-Pr_2Zn is run without the intervention of any chiral factor? We envisaged that the reaction of achiral reactants of pyrimidine-5-carbaldehyde **2** and *i*-Pr_2Zn affords enantioenriched product, *i.e.*, zinc alkoxide of pyrimidyl alkanol, as a result of statistical fluctuation, and that the initial ee would be amplified by the subsequent asymmetric autocatalysis (see Scheme 1.15).

Indeed, enantioenriched pyrimidyl alkanol of either *S* or *R* absolute configuration is formed through spontaneous absolute asymmetric synthesis in the reaction between pyrimidine-5-carbaldehyde **2** with *i*-Pr_2Zn without the addition of any chiral substance. We first applied for a patent for this

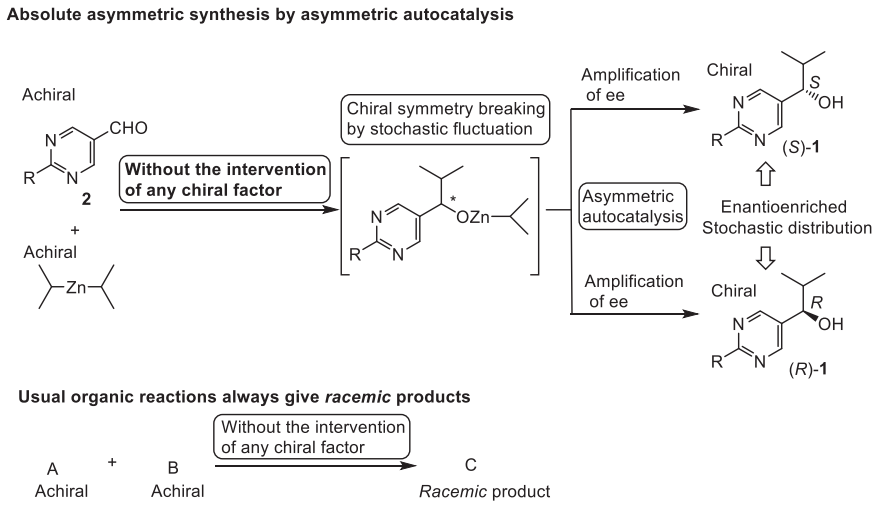

Scheme 1.15 Spontaneous absolute asymmetric synthesis without the intervention of any chiral factor in conjunction with asymmetric autocatalysis.

absolute asymmetric synthesis in 1996.[22a] Enantioenriched (*S*)-pyrimidyl alkanol **1a,b** or (*R*)-pyrimidyl alkanol **1a,b** are formed in the reaction without adding any chiral substance.[22a] When *i*-Pr_2Zn was reacted with aldehyde **2c** in a mixed solvent of ether and toluene without adding any chiral substance, (*S*)-pyrimidyl alkanol **1c** was formed 19 times and (*R*)-**1c** 18 times in a total of 37 reactions (see Figure 1.2(a)).[22b] The formation of *S* and *R* enantiomers of **1c** produced showed a stochastic distribution. The initially formed enantioenriched zinc alkoxide of pyrimidyl alkanol **1c** produced *in situ* is considered to be enantioenriched by statistical fluctuation, and the subsequent amplification of ee by asymmetric autocatalysis gave (*S*)- or (*R*)-**1** with detectable ee values.[22b] Moreover, in the presence of achiral amorphous silica gel, which is used as the stationary phase for column chromatography, the reaction of aldehyde **2c** and *i*-Pr_2Zn afforded (*S*)- or (*R*)-alkanol **1c** with stochastic distribution.[22c] Soai *et al.* reported that achiral diamines promote

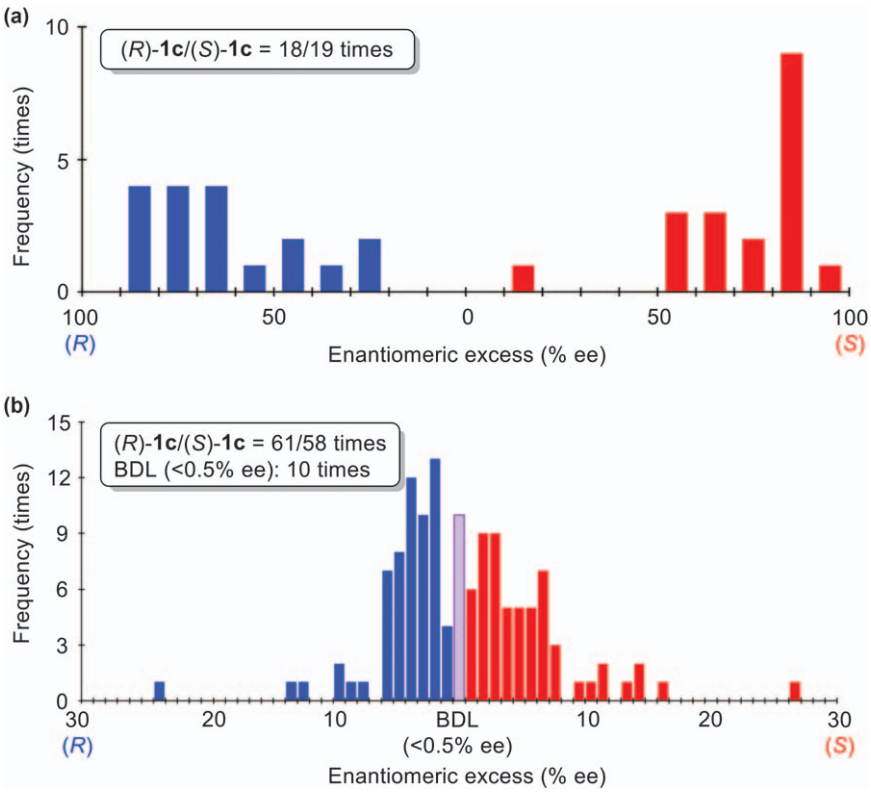

Figure 1.2 Histograms of the frequency, absolute configurations, and ee of pyrimidyl alkanol **1c** formed in spontaneous absolute asymmetric synthesis between pyrimidine-5-carbaldehyde **2c** and *i*-Pr_2Zn without the intervention of any chiral factor. (a) In a mixed solvent of diethylether and toluene. (b) Under the conditions of the powder-like crystal of aldehyde **2c** and vapor of *i*-Pr_2Zn and toluene.

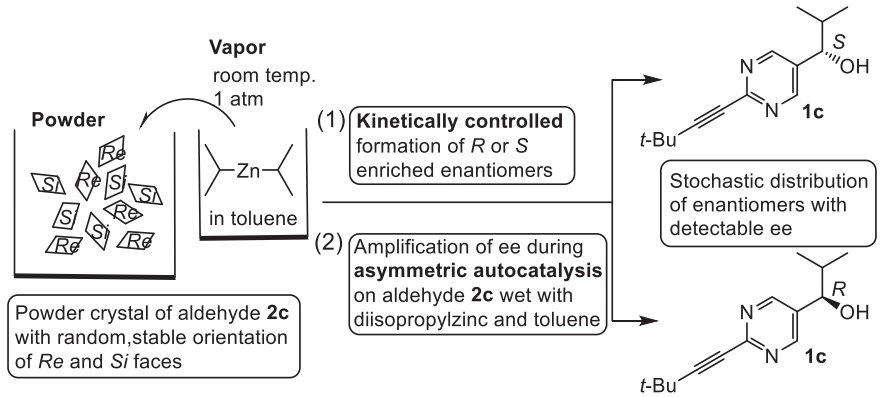

Scheme 1.16 Absolute asymmetric synthesis of pyrimidyl alkanol **1c** under conditions of solid aldehyde **2c** and *i*-Pr_2Zn vapor.

the addition reaction of dialkylzincs to aldehydes.[22d] In the presence of achiral amines, the reaction between aldehyde **2c** and *i*-Pr_2Zn afforded (*S*)- or (*R*)-alkanol **1c** with stochastic distribution.[22e] The stochastic distribution of the product (*S*)- or (*R*)-**1b** has also been reported between pyrimidine-5-carbaldehyde **2b** and *i*-Pr_2Zn.[22f] These results show that the reaction between pyrimidine-5-carbaldehydes and *i*-Pr_2Zn allows spontaneous absolute asymmetric synthesis.[22g–j]

1.4.2 Absolute Asymmetric Synthesis under Solid–Vapor Conditions

In the preceding paragraph, we describe absolute asymmetric synthesis in solution. We here describe absolute asymmetric synthesis under heterogeneous conditions of solid aldehyde–vapor phase *i*-Pr_2Zn (see Scheme 1.16).[22k] In a desiccator, powders of pyrimidine-5-carbaldehyde **2c** in vials were exposed to the vapor of *i*-Pr_2Zn and toluene. (*R*)-Pyrimidyl alkanol **1c** was formed 61 times, and (*S*)-alkanol **1c** 58 times in a total of 129 reactions (**1c** was formed with $<0.5\%$ ee 10 times and was regarded as below the detection level) (see Figure 1.2(b)). These results show that the distribution of (*S*)- and (*R*)-alkanol **1c** is stochastic. The observed various ee values could be amplified to $>99.5\%$ ee by subsequent asymmetric autocatalysis. Thus, spontaneous absolute asymmetric synthesis is achieved under solid–vapor phase conditions.

1.5 Chiral Hydrogen, Carbon, Oxygen, and Nitrogen Isotopomers Act as the Origin of Homochirality in Conjunction with Asymmetric Autocatalysis

Isotopes are defined as atoms of the same atomic number (number of positrons) but with different numbers of neutrons. The number of electrons is the same and the chemical character is very similar. There are a few examples of

the use of chiral isotopomers as chiral auxiliaries for low levels of asymmetric induction by using chiral hydrogen (D/H) isotopomers.[23a,b] Although the difference in atomic weight between H and D is 100%, the difference in atomic weight between ^{12}C and ^{13}C is only 8%; indeed, asymmetric induction by chiral $^{13}C/^{12}C$, $^{15}N/^{14}N$, and $^{18}O/^{16}O$ isotopomers is unprecedented.

Many apparent achiral organic compounds become chiral by substituting carbon (^{12}C), nitrogen (^{14}N), or oxygen (^{16}O) for their isotopes of ^{13}C, ^{15}N, and ^{18}O, respectively. Given that it has two identical methyl groups, 1-methyl-1-phenylethanol **12** is achiral; however, when one of the carbon atoms of the methyl groups is labeled with ^{13}C, the alkanol becomes either chiral (*R*)-1-methyl-1-phenylethanol **12**(^{13}C) or (*S*)-alkanol **12**(^{13}C) (see Scheme 1.17). Because the mass difference of carbon ($^{13}C/^{12}C$) isotopes is so small, asymmetric induction using chiral carbon ($^{13}C/^{12}C$) isotopomers was unprecedented.

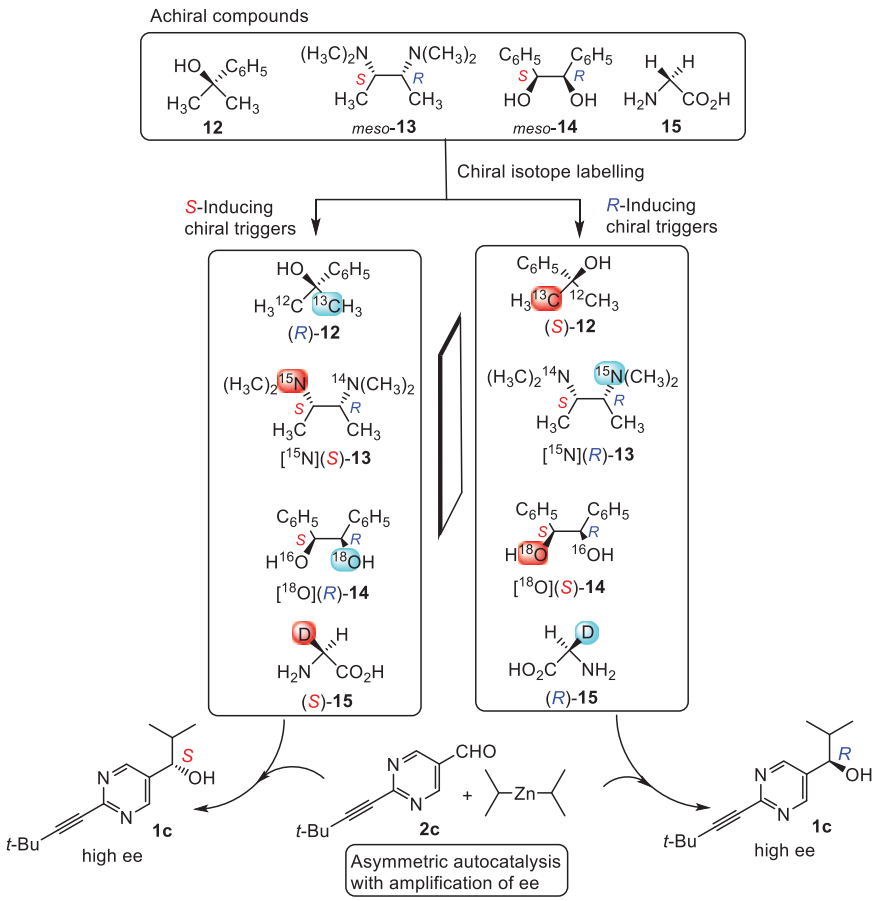

Scheme 1.17 Carbon ($^{13}C/^{12}C$), nitrogen ($^{15}N/^{14}N$), oxygen ($^{18}O/^{16}O$), and hydrogen (D/H) isotopomers act as chiral triggers of asymmetric autocatalysis.

The reaction between pyrimidine-5-carbaldehyde **2c** and *i*-Pr_2Zn was examined in the presence of a chiral carbon ($^{13}C/^{12}C$) isotopomer, namely (*R*)- or (*S*)-1-methyl-1-phenylethanol **12**(^{13}C), as a chiral trigger. Pyrimidyl alkanol **1c** was formed with very high ee with an absolute configuration corresponding to that of the carbon isotopomer (see Scheme 1.17). (*S*)-Pyrimidyl alkanol **1c** with high ee was formed in the presence of (*R*)-carbon isotopomer **12**(^{13}C). In contrast, (*R*)-pyrimidyl alkanol **1c** was formed in the presence of (*S*)-carbon isotopomer **12**(^{13}C).[23c] It was also found that asymmetric autocatalysis is triggered by the chiral nitrogen ($^{15}N/^{14}N$) isotopomer, [^{15}N](*S*), and [^{15}N](*R*)-diamine **13**(^{15}N).[23d] Moreover, pyrimidyl alkanol **1c** with high ee with the corresponding absolute configurations with those of oxygen ($^{18}O/^{16}O$) isotopomers; that is, [^{18}O](*R*) and [^{18}O](*S*)-diol **14**(^{18}O), were formed as the result of asymmetric autocatalysis triggered by oxygen isotopomers **14**.[23e,f] Thus, carbon, nitrogen, and oxygen isotopomers were proved to act as the origin of homochirality in conjunction with asymmetric autocatalysis with amplification of ee.

It was also found that chiral isotopomers labeled with deuterium act as chiral triggers of asymmetric autocatalysis.[23g,h] Achiral glycine **15** becomes chiral by labeling one of the hydrogen atoms of the methylene group with deuterium (D). Chiral (*S*)-glycine-α-D **15**(D) acts as chiral trigger for asymmetric autocatalysis to afford (*S*)-pyrimidyl alkanol **1c** with high ee with the corresponding absolute configurations of the chiral trigger.[23i] Blackmond *et al.* reported mechanistic investigation on asymmetric autocatalysis triggered by a hydrogen (H/D) isotopomer.[23j]

1.6 Various Chiral Materials Including Cryptochiral Compounds as Triggers for Asymmetric Autocatalysis

Asymmetric autocatalysis can also be applied as a chiral sensor of compounds with low ee. Amino acids with low ee are generated from the respective racemate upon CPL irradiation and are often found in meteorites. Asymmetric autocatalysis has been used to correlate the chirality of amino acids with low (*ca.* 0.1%) ee to chiral organic compound with high (see Scheme 1.18).[16c,24a]

Thus, L-alanine (*ca.* 0.1% ee), L-methionine (*ca.* 0.1% ee), and L-valine (*ca.* 0.1% ee) act as chiral triggers for asymmetric autocatalysis in the reaction between 2-(2-*t*-butylethynyl)pyrimidine-5-carbaldehyde **2** and *i*-Pr_2Zn to afford (*S*)-2-(2-*t*-butylethynyl)-5-pyrimidyl alkanol **1c** with enhanced ee (91–92%). However, L-histidine with *ca.* 0.1% ee as a chiral trigger exhibited the opposite sense of enantioselectivity. Thus, (*R*)-pyrimidyl alkanol **1c** was formed with 97% ee. In contrast, D-alanine, D-methionine, and D-valine with low *ca.* 0.1% ee act as chiral triggers to give (*R*)-pyrimidyl alkanol **1c** with an enhanced ee of 72–90%. D-Histidine with *ca.* 0.1% ee as a chiral trigger afforded (*S*)-pyrimidyl alkanol **1c** with 92% ee. Thus, the chirality of amino acids with low ee can be determined by application of asymmetric autocatalysis.[24a]

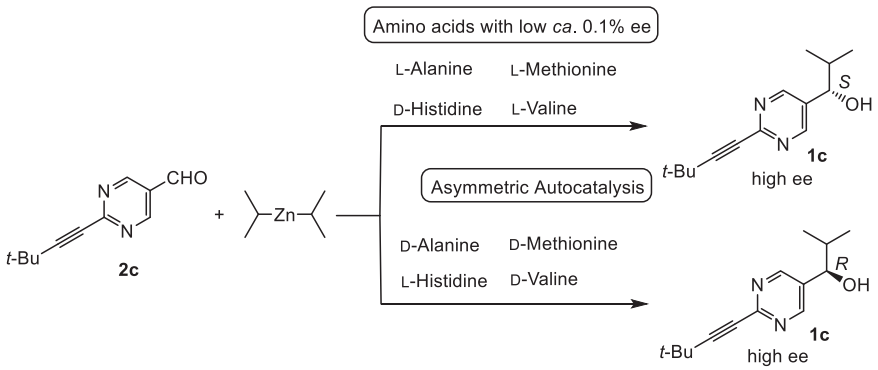

Scheme 1.18 Correlation of the chirality of amino acids with low ee to chiral compounds with high ee by asymmetric autocatalysis with amplification of ee.

[6]Helicene **17**,[24b] tetrathia[7]helicene **18**,[24c] and 2-aza[6]helicene **19**[24d] trigger asymmetric autocatalysis to afford pyrimidyl alkanol **1c** with the corresponding absolute configuration of the chiral triggers (see Scheme 1.19). A cryptochiral saturated quaternary hydrocarbon, (*n*-butyl)ethyl(*n*-hexyl)-(*n*-propyl)methane, *i.e.*, 5-ethyl-5-propylundecane **20**, does not exhibit any detectable value of optical rotation because the differences in the structures of four substituents are so small.[24e]

Asymmetric autocatalysis was found to discriminate the isomers of cryptochiral 5-ethyl-5-propylundecane **20**[24f] and cryptochiral isotactic polystyrene **21**.[24g] The chiralities of artificially designed inorganic helical silica **22**[24h] and mesoporous helical silica **23**[24i] were also discriminated by asymmetric autocatalysis (see Scheme 1.19). In addition, asymmetric autocatalysis discriminates a single-wall carbon nanotube molecule with helical chirality **24**,[24j] and chiral [2.2]paracyclophanes **25**,[24k] chiral metal complexes due to the topology of the coordination of achiral ligands **26**,[24l] ruthenium complex,[24m] **27**[24n] and 1,3-disubstituted hydrocarbon allene **28**.[24o]

1.7 Unusual Phenomena of the Reversal of the Sense of Enantioselectivities Detected by Asymmetric Autocatalysis

Asymmetric autocatalysis revealed unusual inversion of enantioselectivity (see Scheme 1.20). (1*R*,2*S*)-*N*,*N*-Dimethylnorephedrine (DMNE) alone triggers the reaction of aldehyde **2c** and *i*-Pr_2Zn to afford (*R*)-pyrimidyl alkanol **1c**. On the other hand, achiral *N*,*N*-dibutylaminoethanol (DBAE) is considered to promote the formation of racemate. Thus, it is natural to anticipate that the mixture of *R*-affording (1*R*,2*S*)-DMNE and racemate-affording achiral DBNE triggers the reaction to afford (*R*)-alkanol. However, a counterintuitive inversion of the sense of enantioselectivity was observed when the reaction was triggered by a mixture of (1*R*,2*S*)-DMNE and achiral DBAE, that is, the

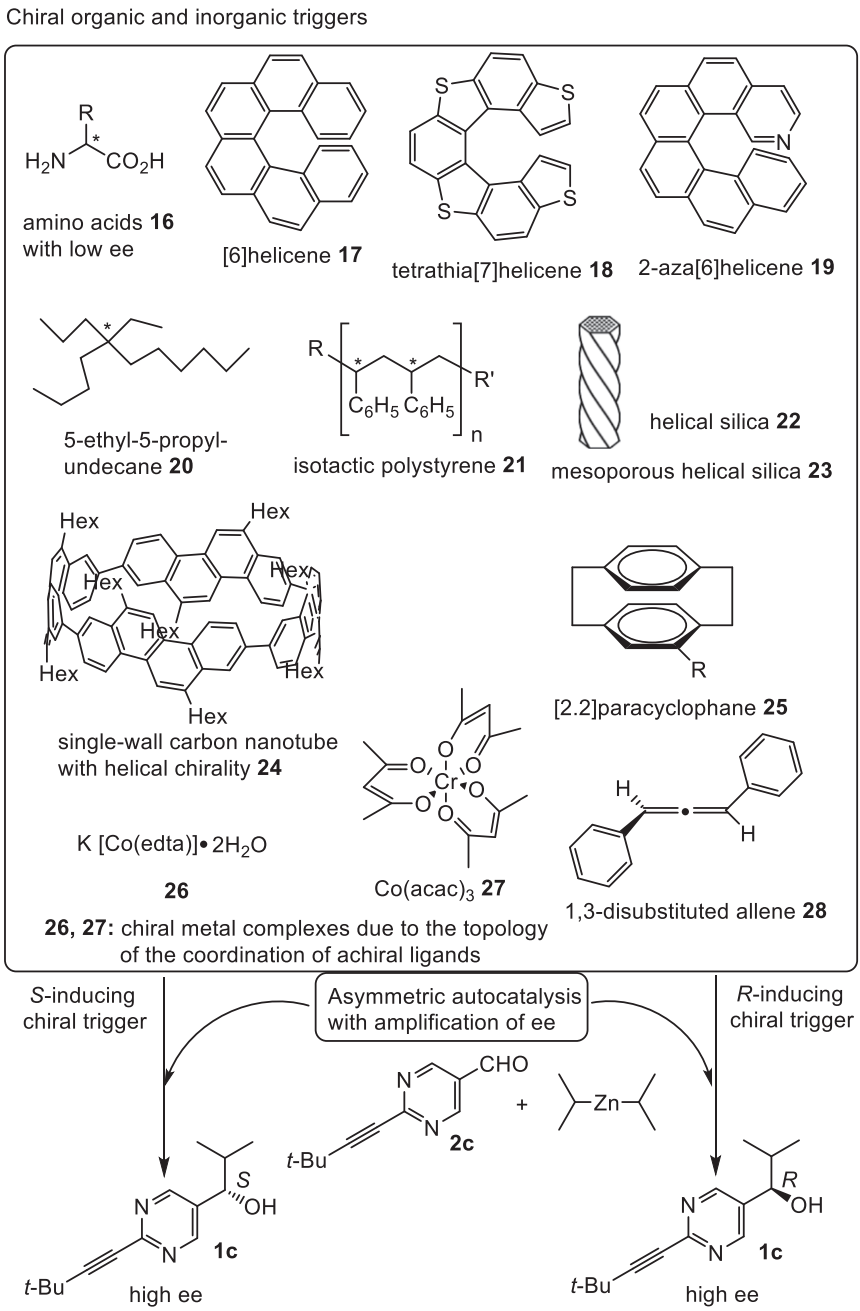

Scheme 1.19 Asymmetric autocatalysis triggered by various chiral compounds, cryptochiral compounds, and chiral inorganic silica.

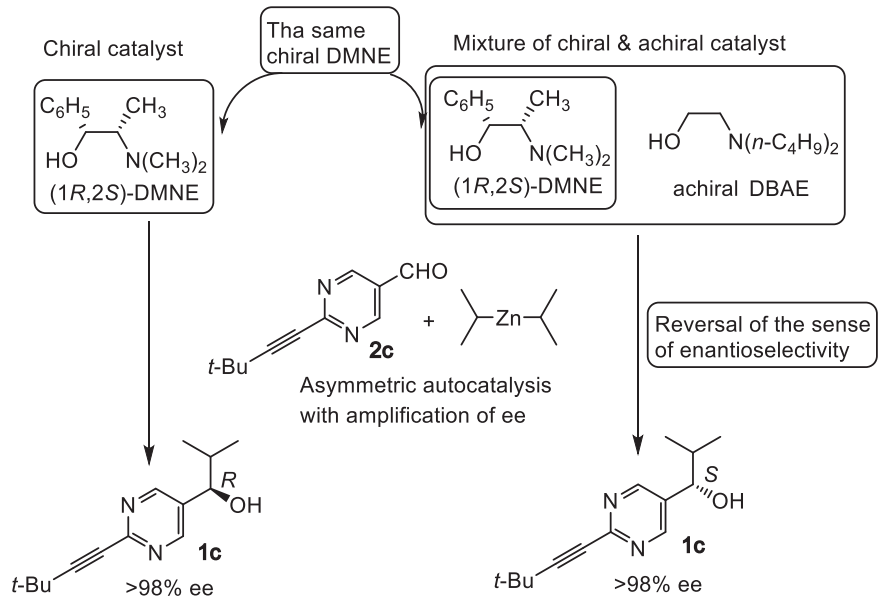

Scheme 1.20 Unusual reversal of the sense of enantioselectivity between chiral catalysts of (1*R*,2*S*)-DMNE and a mixture of [(1*R*,2*S*)-DMNE and achiral DBAE] in asymmetric autocatalysis.

opposite (*S*)-alkanol **1c** instead of anticipated (*R*)-alkanol was formed![25a,b] The formation of aggregation of chiral DMNE and achiral DBAE is the origin of the inversion of the sense of enantioselectivity. Moreover, the mixture of two *R*-affording chiral catalysts, *i.e.*, (1*R*,2*S*)-DMNE and (*R*)-2-[(1-phenylethyl)amino]ethanol, reverses the sense of enantioselectivity to afford the opposite (*S*)-alkanol **1c**.[25c] In asymmetric autocatalysis using chiral aromatic alcohols and amines as chiral triggers, changing the temperature induced the inversion of the sense of enantioselectivity.[25d]

1.8 Application of Asymmetric Autocatalysis for the Synthesis of Various Chiral Compounds

Asymmetric autocatalysis with amplification of ee was successfully applied in asymmetric synthesis of chiral *sec*-alcohols[26a] and asymmetric amplification of alkynyl alkanols.[26b] Carreira *et al.* reported asymmetric synthesis of efavirenz, a chiral drug for the treatment of HIV, by asymmetric autocatalytic alkynylation of ketone.[27]

1.9 Conclusions

Pyrimidyl alkanols, 5-carbamoyl pyridyl alkanol, and 3-quinolyl alkanols act as asymmetric autocatalysts with amplification of ee in the enantioselective addition of *i*-Pr_2Zn to pyrimidine-5-carbaldehydes, 5-carbamoylpyridine, and

quinoline-3-carbaldehydes, respectively. Typically, the ee of (*S*)-2-alkynylpyrimidyl alkanol **1** with very low (*ca.* 0.00005%) ee was enhanced to >99.5% ee during three consecutive asymmetric autocatalysis runs. The amplification of ee by asymmetric autocatalysis is unique in that no chiral factor other than the asymmetric autocatalyst itself, *i.e.*, pyrimidyl alkanol **1**, is necessary. Mislow referred to the asymmetric autocatalysis as the Soai reaction.[4a]

The origins of homochirality were examined by using asymmetric autocatalysis with amplification of ee. Asymmetric autocatalysis with amplification of ee enhanced the initially low ee induced by the origin of chirality. Irradiation with CPL of racemic pyrimidyl alkanol followed by asymmetric autocatalysis correlated for the first time the chirality of CPL and chiral organic compound with very high ee. Chiral inorganic crystals such as quartz and cinnabar also act as chiral triggers of asymmetric autocatalysis. Thus, quartz as the origin of chirality was correlated for the first time to a chiral organic compound with very high ee. Chiral organic crystals composed of achiral compounds such as glycine, cytosine, and adenine also act as chiral initiators of asymmetric autocatalysis to afford highly enantioenriched pyrimidyl alkanol with the corresponding absolute configurations that correlate to those of the chiral initiators. Moreover, absolute asymmetric synthesis, namely, the formation of enantioenriched compound without the intervention of any chiral factor, was achieved for the first time in the reaction between pyrimidine-5-carbaldehdye and *i*-Pr_2Zn followed by asymmetric autocatalysis with amplification of ee. Stochastic distributions of absolute configurations of the products were also observed. Carbon ($^{13}C/^{12}C$), nitrogen ($^{15}N/^{14}N$), oxygen ($^{16}O/^{18}O$), and hydrogen (H/D) isotopomers act as the origin of chirality in asymmetric autocatalysis to afford highly enantioenriched pyrimidyl alkanol with the absolute configurations corresponding to those of the chiral isotopomers.

As described, asymmetric autocatalysis, *i.e.*, the Soai reaction, is the catalytic self-replication of a chiral compound with amplification of ee. Extremely low ee is amplified to very high >99.5% ee by consecutive asymmetric autocatalysis. The reaction is capable of discriminating the chirality of various materials even with low ee. The origin of chirality can thus be examined by using asymmetric autocatalysis. Spontaneous absolute asymmetric synthesis was also achieved by asymmetric autocatalysis. Chiral carbon, nitrogen, and oxygen isotopomers work as the origin of chirality in conjunction with asymmetric autocatalysis. Further aspects of reaction mechanisms will be elucidated through ongoing research by several groups, and it is anticipated that the reaction may be applied to examine the physical origins of chirality in a wide range of systems.

Acknowledgements

Financial support by JSPS KAKENHI (Grant number 15H03781,18H04518, 19K05482 and 19K22190) is gratefully acknowledged. The authors gratefully acknowledge the collaborators whose names appear in the cited literature.

References

1. (a) G. von Kiedrowski, *Angew. Chem., Int. Ed.*, 1986, **25**, 932; (b) T. Tjivikua, P. Ballester and J. Rebek, *J. Am. Chem. Soc.*, 1990, **112**, 1249; (c) K. Severin, D. H. Lee, A. J. Kennan and M. R. Ghadiri, *Nature*, 1997, **389**, 706.
2. M. Bolli, R. Micura and A. Eschenmoser, *Chem. Biol.*, 1997, **4**, 309.
3. (a) L. Pasteur, *Ann. Chim. Phys.*, 1848, **24**, 442; (b) L. Pasteur, *Rev. Sci.*, 1884, **(3)VII**, 2.
4. (a) K. Mislow, *Collect. Czech. Chem. Commun.*, 2003, **68**, 849; (b) B. L. Feringa and R. A. van Delden, *Angew. Chem., Int. Ed.*, 1999, **38**, 3418; (c) Y. Inoue, *Chem. Rev.*, 1992, **92**, 741; (d) I. Weissbuch and M. Lahav, *Chem. Rev.*, 2011, **111**, 3236; (e) K.-H. Ernst, *Phys. Status Solidi*, 2012, **249**, 2057; (f) J. M. Ribó, J. Crusats, F. Sagués, J. Claret and R. Rubires, *Science*, 2001, **292**, 2063; (g) R. M. Hazen and D. S. Sholl, *Nat. Mater.*, 2003, **2**, 367; (h) A. Guijarro and M. Yus, *The Origin of Chirality in the Molecules of Life*, Royal Society of Chemistry, Cambridge, 2009.
5. (a) T. Satyanarayana, S. Abraham and H. B. Kagan, *Angew. Chem., Int. Ed.*, 2009, **48**, 456; (b) M. Kitamura, S. Okada, S. Suga and R. Noyori, *J. Am. Chem. Soc.*, 1989, **111**, 4028; (c) F. C. Frank, *Biochim. Biophys. Acta*, 1953, **11**, 459; (d) D. K. Kondepudi and K. Asakura, *Acc. Chem. Res.*, 2001, **34**, 946; (e) C. Viedma, *Phys. Rev. Lett.*, 2005, **94**, 065504; (f) M. M. Green, J.-W. Park, T. Sato, A. Teramoto, S. Lifson, R. L. B. Selinger and J. V. Selinger, *Angew. Chem., Int. Ed.*, 1999, **38**, 3138; (g) J. Han, O. Kitagawa, A. Wzorek, K. D. Klia and V. A. Soloshonok, *Chem. Sci.*, 2018, **9**, 1718; (h) Y. Hayashi, M. Matsuzawa, J. Yamaguchi, S. Yonehara, Y. Matsumoto, M. Shoji, D. Hashizume and H. Koshino, *Angew. Chem., Int. Ed.*, 2006, **45**, 4593; (i) A. Córdova, M. Engqvist, I. Ibrahem, J. Casas and H. Sundén, *Chem. Commun.*, 2005, 2047; (j) W. L. Noorduin, E. Vlieg, R. M. Kellogg and B. Kaptein, *Angew. Chem., Int. Ed.*, 2009, **48**, 9600; (k) Y. Saito and H. Hyuga, *Rev. Mod. Phys.*, 2013, **85**, 603; (l) C. Moberg, *Acc. Chem. Res.*, 2016, **49**, 2736; (m) T. Buhse, J.-M. Cruz, M. E. Noble-Terán, D. Hochberg, J. M. Ribó, J. Crusats and J.-C. Micheau, *Chem. Rev.*, 2021, **121**, 2147.
6. (a) A. H. Alberts and H. Wynberg, *J. Am. Chem. Soc.*, 1989, **111**, 7265; (b) H. Danda, H. Nishikawa and K. Otaka, *J. Org. Chem.*, 1991, **56**, 6740; (c) T. Shibata, T. Takahashi, T. Konishi and K. Soai, *Angew. Chem., Int. Ed.*, 1997, **36**, 2458.
7. (a) K. Soai, I. Sato and T. Shibata, *Chem. Rec.*, 2001, **1**, 321; (b) K. Soai, T. Shibata and I. Sato, *Acc. Chem. Res.*, 2000, **33**, 382; (c) K. Soai and T. Kawasaki, *Chirality*, 2006, **18**, 469; (d) K. Soai and T. Kawasaki, *Top. Curr. Chem.*, 2008, **284**, 1; (e) T. Kawasaki and K. Soai, *J. Fluor. Chem.*, 2010, **131**, 525; (f) T. Kawasaki and K. Soai, *Bull. Chem. Soc. Jpn.*, 2011, **84**, 879; (g) T. Kawasaki and K. Soai, *Isr. J. Chem.*, 2012, **52**, 582; (h) K. Soai, T. Kawasaki and A. Matsumoto, *Chem. Rec.*, 2014, **14**, 70; (i) K. Soai, T. Kawasaki and A. Matsumoto, *Acc. Chem. Res.*, 2014,

47, 3643; (j) K. Soai, T. Kawasaki and A. Matsumoto, *Tetrahedron*, 2018, **74**, 1973; (k) J. Podlech and T. Gehring, *Angew. Chem., Int. Ed.*, 2005, **44**, 5776; (l) T. Gehring, M. Busch, M. Schlageter and D. Weingand, *Chirality*, 2010, **22**(Suppl 1), E173; (m) K. Soai, *Proc. Jpn. Acad., Ser. B*, 2019, **95**, 89; (n) K. Soai, T. Kawasaki and A. Matsumoto, *Symmerty*, 2019, **11**, 694; (o) K. Soai, A. Matsumoto and T. Kawasaki, *Isr. J. Chem.*, 2021, **61**, 507; (p) D. G. Blackmond, *Chem. Rev.*, 2020, **120**, 4831.

8. (a) K. Soai, S. Niwa and H. Hori, *J. Chem. Soc. Chem. Commun.*, 1990, 982; (b) K. Soai, T. Hayase, C. Shimada and K. Isobe, *Tetrahedron: Asymmetry*, 1994, **5**, 789; (c) K. Soai, T. Hayase and K. Takai, *Tetrahedron: Asymmetry*, 1995, **6**, 637.
9. (a) K. Soai, T. Shibata, H. Morioka and K. Choji, *Nature*, 1995, **378**, 767; (b) T. Shibata, H. Morioka, T. Hayase, K. Choji and K. Soai, *J. Am. Chem. Soc.*, 1996, **118**, 471; (c) T. Shibata, S. Yonekubo and K. Soai, *Angew. Chem., Int. Ed.*, 1999, **38**, 659; (d) I. Sato, H. Urabe, S. Ishiguro, T. Shibata and K. Soai, *Angew. Chem., Int. Ed.*, 2003, **42**, 315; (e) I. Sato, T. Yanagi and K. Soai, *Chirality*, 2002, **14**, 166; (f) T. Kawasaki, M. Nakaoda, Y. Takahashi, Y. Kanto, N. Kuruhara, K. Hosoi, I. Sato, A. Matsumoto and K. Soai, *Angew. Chem., Int. Ed.*, 2014, **53**, 11199; (g) T. Kawasaki, Y. Ishikawa, Y. Minato, T. Otsuka, S. Yonekubo, I. Sato, T. Shibata, A. Matsumoto and K. Soai, *Chem. – Eur. J.*, 2017, **23**, 282–285.
10. (a) T. Shibata, K. Choji, H. Morioka, T. Hayase and K. Soai, *Chem. Commun.*, 1996, 751; (b) T. Shibata, K. Choji, T. Hayase, Y. Aizu and K. Soai, *Chem. Commun.*, 1996, 1235; (c) I. Sato, T. Nakao, R. Sugie, T. Kawasaki and K. Soai, *Synthesis*, 2004, 1419.
11. (a) T. Shibata, H. Morioka, S. Tanji, T. Hayase, Y. Kodaka and K. Soai, *Tetrahedron Lett.*, 1996, **37**, 8783; (b) S. Tanji, Y. Kodaka, A. Ohno, T. Shibata, I. Sato and K. Soai, *Tetrahedron: Asymmetry*, 2000, **11**, 4249.
12. (a) T. Mukaiyama, K. Soai, T. Sato, H. Shimizu and K. Suzuki, *J. Am. Chem. Soc.*, 1979, **101**, 1455; (b) N. Oguni and T. Omi, *Tetradedron Lett.*, 1984, **25**, 2823; (c) M. Kitamura, S. Suga, K. Kawai and R. Noyori, *J. Am. Chem. Soc.*, 1986, **108**, 6071; (d) K. Soai, A. Ookawa, K. Ogawa and T. Kaba, *J. Chem. Soc., Chem. Commun.*, 1987, 467; (e) K. Soai, A. Ookawa, T. Kaba and K. Ogawa, *J. Am. Chem. Soc.*, 1987, **109**, 7111; (f) K. Soai, S. Yokoyama, K. Ebihara and T. Hayasaka, *J. Chem. Soc., Chem. Commun.*, 1987, 1690; (g) K. Soai, S. Yokoyama and T. Hayasaka, *J. Org. Chem.*, 1991, **56**, 4264; (h) K. Soai and S. Niwa, *Chem. Rev.*, 1992, **92**, 833; (i) K. Soai, H. Hori and S. Niwa, *Heterocycles*, 1989, **29**, 2065.
13. H. Wynberg, *Chimia*, 1989, **43**, 150.
14. (a) M. Kitamura, S. Suga, H. Oka and R. Noyori, *J. Am. Chem. Soc.*, 1998, **120**, 9800; (b) D. Guillaneux, S.-H. Zhao, O. Samuel, D. Rainford and H. B. Kagan, *J. Am. Chem. Soc.*, 1994, **116**, 9430.
15. (a) I. Sato, D. Omiya, K. Tsukiyama, Y. Ogi and K. Soai, *Tetrahedron: Asymmetry*, 2001, **12**, 1965; (b) I. Sato, D. Omiya, H. Igarashi, K. Kato, Y. Ogi, K. Tsukiyama and K. Soai, *Tetrahedron: Asymmetry*, 2003, **14**, 975;

(c) D. G. Blackmond, C. R. McMillan, S. Ramdeehul, A. Schorm and J. M. Brown, *J. Am. Chem. Soc.*, 2001, **123**, 10103; (d) M. Quaranta, T. Gehring, B. Odell, J. M. Brown and D. G. Blackmond, *J. Am. Chem. Soc.*, 2010, **132**, 15104; (e) T. Gehring, M. Quaranta, B. Odell, D. G. Blackmond and J. M. Brown, *Angew. Chem., Int. Ed.*, 2012, **51**, 9539; (f) L. Schiaffino and G. Ercolani, *Angew. Chem., Int. Ed.*, 2008, **47**, 6832; (g) G. Ercolani and L. Schiaffino, *J. Org. Chem.*, 2011, **76**, 2619; (h) I. D. Gridnev and A. K. Vorobiev, *ACS Catal.*, 2012, **2**, 2137; (i) I. D. Gridnev and A. K. Vorobiev, *Bull. Chem. Soc. Jpn.*, 2015, **88**, 333; (j) B. Barabás, L. Caglioti, K. Micskei and G. Pályi, *Bull. Chem. Soc. Jpn.*, 2009, **82**, 1372; (k) J. C. Micheau, J. M. Cruz, C. Coudret and T. Buhse, *ChemPhysChem*, 2010, **11**, 3417; (l) J. C. Micheau, C. Coudret, J. M. Cruz and T. Buhse, *Phys. Chem. Chem. Phys.*, 2012, **14**, 13239; (m) K. Micskei, G. Rábai, E. Gál, L. Caglioti and G. Pályi, *J. Phys. Chem. B*, 2008, **112**, 9196; (n) M. Maioli, K. Micskei, L. Caglioti, C. Zucchi and G. Pályi, *J. Math. Chem.*, 2008, **43**, 1505; (o) J. Crusats, D. Hochberg, A. Moyano and J. M. Ribó, *ChemPhysChem.*, 2009, **10**, 2123; (p) É. Dóka and G. Lente, *J. Am. Chem. Soc.*, 2011, **133**, 17878; (q) J.-C. Micheau, C. Coudret, J.-M. Cruz and T. Buhse, *Phys. Chem. Chem. Phys.*, 2012, **214**, 13239; (r) S. V. Athavale, A. Simon, K. N. Houk and S. E. Denmark, *Nat. Chem.*, 2020, **12**, 412; (s) O. Trapp, S. Lamour, F. Maier, A. F. Siegle, K. Zawatzky and B. F. Straub, *Chem. – Eur. J.*, 2020, 15871; (t) A. Matsumoto, T. Abe, A. Hara, T. Tobita, T. Sasagawa, T. Kawasaki and K. Soai, *Angew. Chem., Int. Ed.*, 2015, **54**, 15218; (u) A. Matsumoto, S. Fujiwara, T. Abe, A. Hara, T. Tobita, T. Sasagawa, T. Kawasaki and K. Soai, *Bull. Chem. Soc. Jpn.*, 2016, **89**, 1170; (v) M. E. Noble-Teran, J.-M. Cruz, J.-C. Micheau and T. Buhse, *ChemCatChem*, 2018, **10**, 642; (w) A. Matsumoto, A. Tanaka, Y. Kaimori, N. Hara, Y. Mikata and K. Soai, *Chem. Commun.*, 2021, **57**, 11209.

16. (a) J. Bailey, A. Chrysostomou, J. H. Hough, T. M. Gledhill, A. McCall, S. Clark, F. Ménard and M. Tamura, *Science*, 1998, **281**, 672; (b) H. Kagan, A. Moradpour, J. F. Nicoud, G. Balavoine and G. Tsoucaris, *J. Am. Chem. Soc.*, 1971, **93**, 2353; (c) T. Shibata, J. Yamamoto, N. Matsumoto, S. Yonekubo, S. Osanai and K. Soai, *J. Am. Chem. Soc.*, 1998, **120**, 12157; (d) T. Kawasaki, M. Sato, S. Ishiguro, T. Saito, Y. Morishita, I. Sato, H. Nishino, Y. Inoue and K. Soai, *J. Am. Chem. Soc.*, 2005, **127**, 3274; (e) I. Sato, R. Sugie, Y. Matsueda, Y. Furumura and K. Soai, *Angew. Chem., Int. Ed.*, 2004, **43**, 4490; (f) W. L. Noorduin, A. C. Bode, M. van der Meijden, H. Meekes, A. F. van Etteger, W. J. P. van Enckevort, P. C. M. Christianen, B. Kaptein, R. M. Kellogg, T. Rasing and E. Vlieg, *Nat. Chem.*, 2009, **1**, 729.
17. (a) A. Amariglio, H. Amariglio and X. Duval, *Helv. Chim. Acta*, 1968, **51**, 2110; (b) W. A. Bonner, P. R. Kavasmaneck, F. S. Martin and J. J. Flores, *Science*, 1974, **186**, 143; (c) K. Soai, S. Osanai, K. Kadowaki, S. Yonekubo, T. Shibata and I. Sato, *J. Am. Chem. Soc.*, 1999, **121**, 11235.

18. (a) D. K. Kondepudi, R. J. Kaufman and N. Singh, *Science*, 1990, **250**, 975; (b) J. M. McBride and R. L. Carter, *Angew. Chem., Int. Ed.*, 1991, **30**, 293; (c) I. Sato, K. Kadowaki and K. Soai, *Angew. Chem., Int. Ed.*, 2000, **39**, 1510; (d) I. Sato, K. Kadowaki, Y. Ohgo and K. Soai, *J. Mol. Catal. A: Chem.*, 2004, **216**, 209; (e) H. Shindo, Y. Shirota, K. Niki, T. Kawasaki, K. Suzuki, Y. Araki, A. Matsumoto and K. Soai, *Angew. Chem., Int. Ed.*, 2013, **52**, 9135; (f) A. Matsumoto, H. Ozawa, A. Inumaru and K. Soai, *New J. Chem.*, 2015, **39**, 6742.
19. A. Matsumoto, Y. Kaimori, M. Uchida, H. Omori, T. Kawasaki and K. Soai, *Angew. Chem., Int. Ed.*, 2017, **56**, 545.
20. (a) T. Matsuura and H. Koshima, *J. Photochem. Photobiol., C*, 2005, **6**, 7; (b) K. Ishikawa, M. Tanaka, T. Suzuki, A. Sekine, T. Kawasaki, K. Soai, M. Shiro, M. Lahav and T. Asahi, *Chem. Commun.*, 2012, **48**, 6031; (c) A. V. Tarasevych, A. E. Sorochinsky, V. P. Kukhar, L. Toupet, J. Crassous and J. -C. Guillemin, CrystEngCom*m*, 2015, **17**, 1513; (d) A. Matsumoto, H. Ozaki, S. Tsuchiya, T. Asahi, M. Lahav, T. Kawasaki and K. Soai, *Org. Biomol. Chem.*, 2019, **17**, 4200; (e) T. Kawasaki, K. Suzuki, Y. Hakoda and K. Soai, *Angew. Chem., Int. Ed.*, 2008, **47**, 496; (f) T. Kawasaki, Y. Hakoda, H. Mineki, K. Suzuki and K. Soai, *J. Am. Chem. Soc.*, 2010, **132**, 2874; (g) H. Mineki, Y. Kaimori, T. Kawasaki, A. Matsumoto and K. Soai, *Tetrahedron: Asymmetry*, 2013, **24**, 1365; (h) H. Mineki, T. Hanasaki, A. Matsumoto, T. Kawasaki and K. Soai, *Chem. Commun.*, 2012, **48**, 10538; (i) T. Kawasaki, K. Suzuki, K. Hatase, M. Otsuka, H. Koshima and K. Soai, *Chem. Commun.*, 2006, 1869; (j) T. Kawasaki, Y. Kaimori, S. Shimada, N. Hara, S. Sato, K. Suzuki, T. Asahi, A. Matsumoto and K. Soai, *Chem. Commun.*, 2021, **57**, 5999; (k) D. J. Carter, A. L. Rohl, A. Shtukenberg, S. D. Bian, C. -H. Hu, L. Baylon, B. Kahr, H. Mineki, K. Abe, T. Kawasaki and K. Soai, *Cryst. Growth Des.*, 2012, **12**, 2138; (l) T. Kawasaki, M. Nakaoda, N. Kaito, T. Sasagawa and K. Soai, *Origins Life Evol. Biospheres*, 2010, **40**, 65; (m) T. Kawasaki, K. Jo, H. Igarashi, I. Sato, M. Nagano, H. Koshima and K. Soai, *Angew. Chem., Int. Ed.*, 2005, **44**, 2774; (n) T. Kawasaki, M. Uchida, Y. Kaimori, T. Sasagawa, A. Matsumoto and K. Soai, *Chem. Lett.*, 2013, **42**, 711; (o) A. Matsumoto, S. Takeda, S. Harada and K. Soai, *Tetrahedron: Asymmetry*, 2016, **27**, 943; (p) T. Kawasaki, Y. Harada, K. Suzuki, T. Tobita, N. Florini, G. Palyi and K. Soai, *Org. Lett.*, 2008, **10**, 4085; (q) A. Matsumoto, T. Ide, Y. Kaimori, S. Fujiwara and K. Soai, *Chem. Lett.*, 2015, **44**, 688; (r) T. Kawasaki, T. Sasagawa, K. Shiozawa, M. Uchida, K. Suzuki and K. Soai, *Org. Lett.*, 2011, **13**, 2361.
21. T. Kawasaki, S. Kamimura, A. Amihara, K. Suzuki and K. Soai, *Angew. Chem., Int. Ed.*, 2011, **50**, 6796.
22. (a) K. Soai, T. Shibata and Y. Kowata, *Japan Kokai Tokkyo Koho*, *JP Pat.*, JP1997-268179, 1997. An abstract is readily available as JPH09268179 from the European Patent Office. http://worldwide.espacenet.com; (b) K. Soai, I. Sato, T. Shibata, S. Komiya, M. Hayashi, Y. Matsueda, H. Imamura, T. Hayase, H. Morioka, H. Tabira, J. Yamamoto and

Y. Kowata, *Tetrahedron: Asymmetry*, 2003, **14**, 185; (c) T. Kawasaki, K. Suzuki, M. Shimizu, K. Ishikawa and K. Soai, *Chirality*, 2006, **18**, 479; (d) K. Soai, M. Watanabe and M. Koyano, *Bull. Chem. Soc. Jpn.*, 1989, **62**, 2124; (e) K. Suzuki, K. Hatase, D. Nishiyama, T. Kawasaki and K. Soai, *J. Systems Chem.*, 2010, **1**, 5; (f) D. A. Singleton and L. K. Vo, *Org. Lett.*, 2003, **5**, 4337; (g) G. Lente, *J. Phys. Chem. A*, 2005, **109**, 11058; (h) L. Caglioti, C. Hajdu, O. Holczknecht, L. Zékány, C. Zucchi, K. Micskei and G. Pályi, *Viva Origino*, 2006, **34**, 62; (i) D. Lavabre, J.-C. Micheau, J. Rivera Islas and T. Buhse, *Top. Curr. Chem.*, 2008, **284**, 67; (j) Y. Saito and H. Hyuga, *Top. Curr. Chem.*, 2008, **284**, 97; (k) Y. Kaimori, Y. Hiyoshi, T. Kawasaki, A. Matsumoto and K. Soai, *Chem. Commun*, 2019, **55**, 5223.

23. (a) A. Horeau, A. Nouaille and K. Mislow, *J. Am. Chem. Soc.*, 1965, **87**, 4957; (b) H. Pracejus, *Tetrahedron Lett.*, 1966, **7**, 3809; (c) T. Kawasaki, Y. Matsumura, T. Tsutsumi, K. Suzuki, M. Ito and K. Soai, *Science*, 2009, **324**, 492; (d) A. Matsumoto, H. Ozaki, S. Harada, K. Tada, T. Ayugase, H. Ozawa, T. Kawasaki and K. Soai, *Angew. Chem., Int. Ed.*, 2016, **55**, 15246; (e) T. Kawasaki, Y. Okano, E. Suzuki, S. Takano, S. Oji and K. Soai, *Angew. Chem., Int. Ed.*, 2011, **50**, 8131; (f) A. Matsumoto, S. Oji, S. Takano, K. Tada, T. Kawasaki and K. Soai, *Org. Biomol. Chem.*, 2013, **11**, 2928; (g) I. Sato, D. Omiya, T. Saito and K. Soai, *J. Am. Chem. Soc.*, 2000, **122**, 11739; (h) T. Kawasaki, H. Ozawa, M. Ito and K. Soai, *Chem. Lett.*, 2011, **40**, 320; (i) T. Kawasaki, M. Shimizu, D. Nishiyama, M. Ito, H. Ozawa and K. Soai, *Chem. Commun.*, 2009, 4396; (j) N. A. Hawbaker and D. G. Blackmond, *ACS Cent. Sci.*, 2018, **4**, 776.
24. (a) I. Sato, Y. Ohgo, H. Igarashi, D. Nishiyama, T. Kawasaki and K. Soai, *J. Organomet. Chem.*, 2007, **692**, 1783; (b) I. Sato, R. Yamashima, K. Kadowaki, J. Yamamoto, T. Shibata and K. Soai, *Angew. Chem., Int. Ed.*, 2001, **40**, 1096; (c) T. Kawasaki, K. Suzuki, E. Licandro, A. Bossi, S. Maiorana and K. Soai, *Tetrahedron: Asymmetry*, 2006, **17**, 2050; (d) A. Matsumoto, K. Yonemitsu, H. Ozaki, J. Míšek, I. Starý, I. G. Stará and K. Soai, *Org. Biomol. Chem.*, 2017, **15**, 1321; (e) H. Wynberg, G. L. Hekkert, J. P. M. Houbiers and H. W. Bosch, *J. Am. Chem. Soc.*, 1965, **87**, 2635; (f) T. Kawasaki, H. Tanaka, T. Tsutsumi, T. Kasahara, I. Sato and K. Soai, *J. Am. Chem. Soc.*, 2006, **128**, 6032; (g) T. Kawasaki, C. Hohberger, Y. Araki, K. Hatase, K. Beckerle, J. Okuda and K. Soai, *Chem. Commun.*, 2009, 5621; (h) I. Sato, K. Kadowaki, H. Urabe, J. Hwa Jung, Y. Ono, S. Shinkai and K. Soai, *Tetrahedron Lett.*, 2003, **44**, 721; (i) T. Kawasaki, Y. Araki, K. Hatase, K. Suzuki, A. Matsumoto, T. Yokoi, Y. Kubota, T. Tatsumi and K. Soai, *Chem. Commun.*, 2015, **51**, 8742; (j) S. Hitosugi, A. Matsumoto, Y. Kaimori, R. Iizuka, K. Soai and H. Isobe, *Org. Lett.*, 2014, **16**, 645; (k) S. Tanji, A. Ohno, I. Sato and K. Soai, *Org. Lett.*, 2001, **3**, 287; (l) I. Sato, K. Kadowaki, Y. Ohgo, K. Soai and H. Ogino, *Chem. Commun.*, 2001, 1022; (m) T. Kawasaki, T. Omine, K. Suzuki, H. Sato, A. Yamagishi and K. Soai, *Org. Biomol. Chem.*, 2009, **7**, 1073; (n) T. Kawasaki, T. Omine, M. Sato, Y. Morishita and K. Soai,

Chem. Lett., 2007, **36**, 30; (o) I. Sato, Y. Matsueda, K. Kadowaki, S. Yonekubo, T. Shibata and K. Soai, *Helv. Chim. Acta*, 2002, **85**, 3383.
25. (a) F. Lutz, T. Igarashi, T. Kawasaki and K. Soai, *J. Am. Chem. Soc.*, 2005, **127**, 12206; (b) F. Lutz, T. Igarashi, T. Kinoshita, M. Asahina, K. Tsukiyama, T. Kawasaki and K. Soai, *J. Am. Chem. Soc.*, 2008, **130**, 2956; (c) T. Kawasaki, Y. Wakushima, M. Asahina, K. Shiozawa, T. Kinoshita, F. Lutz and K. Soai, *Chem. Commun.*, 2011, **47**, 5277; (d) A. Matsumoto, S. Fujiwara, Y. Hiyoshi, K. Zawatzky, A. A. Makarov, C. J. Welch and K. Soai, *Org. Biomol. Chem.*, 2017, **15**, 555.
26. (a) I. Sato, H. Urabe, S. Ishii, S. Tanji and K. Soai, *Org. Lett.*, 2001, **3**, 3851; (b) M. Funes-Maldonado, B. Sieng and M. Amedjkouh, *Org. Lett.*, 2016, **18**, 2536.
27. N. Chinkov, A. Warm and E. M. Carreira, *J. Am. Chem. Soc.*, 2011, **50**, 2957.

CHAPTER 2

Asymmetric Autocatalysis Initiated by Enantioenriched Chiral Organic Compounds: The Link Between Circularly Polarized Light and Nearly Enantiopure Organic Compounds

TSUNEOMI KAWASAKI,*[a] ARIMASA MATSUMOTO[b] AND KENSO SOAI[a,c]

[a] Department of Applied Chemistry, Tokyo University of Science, Kagurazaka, Shinjuku-ku, Tokyo 162-8601, Japan; [b] Department of Chemistry, Biology, and Environmental Science, Nara Women's University, Kita-Uoya Nishi-machi, Nara 630-8506, Japan; [c] Research Organization for Nano & Life Innovation, Waseda University, Wasedatsurumaki-cho, Shinjuku-ku, Tokyo 162-0041, Japan
*Email: tkawa@rs.tus.ac.jp

2.1 Introduction

We found that 5-pyrimidyl alkanol **1** with a *tert*-butylethynyl substituent at the 2-position of a pyrimidine ring is a practically perfect asymmetric autocatalyst in the asymmetric addition of diisopropylzinc (*i*-Pr_2Zn) to the corresponding

Catalysis Series No. 43
Asymmetric Autocatalysis: The Soai Reaction
Edited by Kenso Soai, Tsuneomi Kawasaki and Arimasa Matsumoto

Published by the Royal Society of Chemistry, www.rsc.org

pyrimidine-5-carbaldehyde **2**.[1–15] When (*S*)-2-(2-*tert*-butylethynyl)-5-pyrimidyl alkanol **1** with >99.5% enantiomeric excess (ee) was employed as an asymmetric autocatalyst, (*S*)-**1** with the same sense of molecular chirality was found to be synthesized in >99.5% ee and >99% chemical yield by the isopropylation of aldehyde **2**.[16] After 10 rounds of reaction, no decrease of enantioselectivity and chemical yield was observed. Moreover, we found that the asymmetric autocatalysis of 5-pyrimidyl alkanol **1** proceeds with remarkable amplification (see Scheme 2.1). An initial slight enantioimbalance, as low as *ca.* 0.00005% ee, could be significantly amplified to a nearly enantiomerically pure state (>99.5% ee) in only three consecutive cycles of asymmetric autocatalysis.[17] During the reactions, the slightly enriched enantiomer, for example, (*S*)-alkanol **1**, was automultiplied by a factor of *ca.* 630 000, whereas the multiplication factor of the slightly minor (*R*)-enantiomer **1** was <1000. Therefore, the chiral imbalance of 5-pyrimidyl alkanol **1** can be significantly enhanced in the asymmetric autocatalysis without the need for any chiral auxiliary other than the initial tiny ee of the alkanol **1** itself.

Therefore, it could be expected that not only the asymmetric autocatalyst itself but also a chiral compound other than **1** can act as a chiral source to initiate the asymmetric amplification by autocatalysis (see Scheme 2.2).[18] We supposed that a chiral imbalance of asymmetric autocatalyst **1′** (isopropylzinc alkoxide of **1**) induced by the chiral compound might be amplified by the following asymmetric autocatalysis to afford, after the hydrolysis of isopropyl zinc alkoxide, highly enantioenriched alkanol **1**. The absolute configuration of the resulting product **1** would be controlled by the handedness of the source compound. We have demonstrated that various chiral compounds that seemingly do not have significant chiral directing power

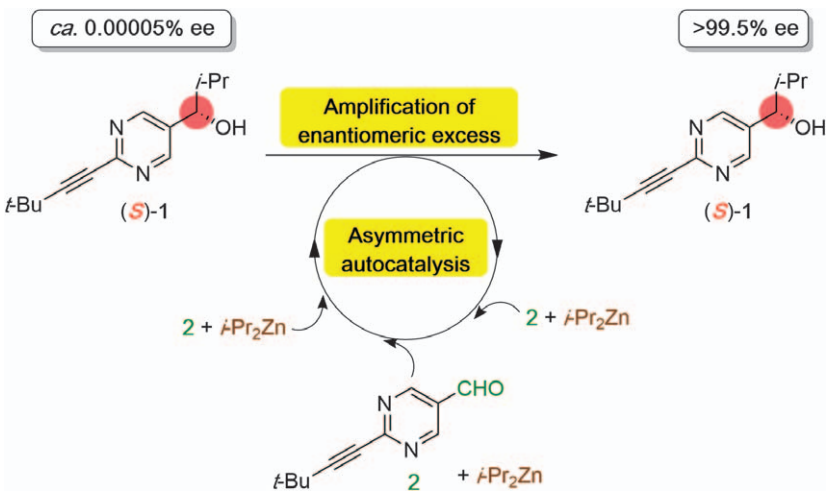

Scheme 2.1 Significant amplification of ee of 5-pyrimidyl alkanol **1** from *ca.* 0.00005% ee to near enantiopure (>99.5% ee) during three consecutive cycles of asymmetric autocatalysis.

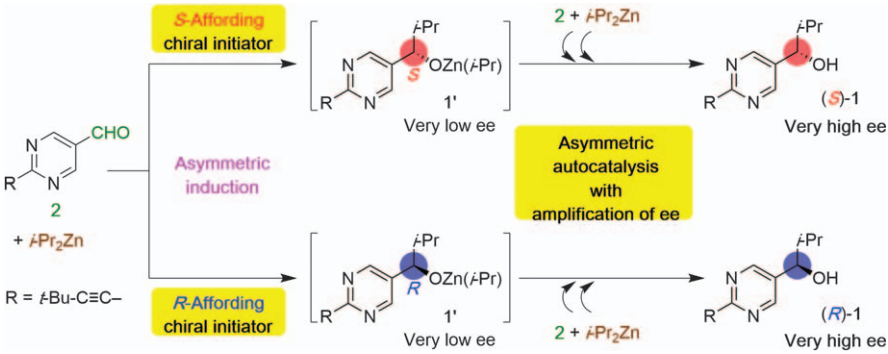

Scheme 2.2 Asymmetric autocatalysis initiated with *S*- and *R*-affording chiral initiators to give (*S*)- and (*R*)-5-pyrimidyl alkanols with amplified high enantioenrichment.

can work as efficient chiral initiators of asymmetric autocatalysis to afford 5-pyrimidyl alkanol **1** with high ee as a result of amplification of ee.

2.2 Asymmetric Autocatalysis Initiated by Various Chiral Compounds

Propylene oxide **3** has been reported as the first interstellar chiral compound detected in the Sagittarius B2 star formation region.[19] The enantioselective addition of *i*-Pr_2Zn to pyrimidine-5-carbaldehyde **2** was examined by using (*S*)- and (*R*)-propylene oxide with low to high ee as a source of chirality for asymmetric autocatalysis (see Scheme 2.3).[20] Upon the addition of *i*-Pr_2Zn to aldehyde **2** in the presence of (*R*)-**3** with 97% ee, (*S*)-5-pyrimidyl alkanol **1** with 96% ee was obtained in 86% yield. On the other hand, (*S*)-**3** with 97% ee induced the formation of the oppositely configured (*R*)-**1** with 94% ee by asymmetric autocatalysis. Even when propylene oxide **3** with low (2–3%) ee was used in the reaction, highly enantioenriched alkanol **1** with a corresponding absolute configuration was obtained. Styrene oxide also acted as a chiral initiator of asymmetric autocatalysis.[20]

Chiral *sec*-alcohols are efficient chiral initiators (see Scheme 2.3).[21] Upon the addition of *i*-Pr_2Zn to aldehyde **2** in the presence of (*S*)-2-butanol **4** with *ca.* 0.1% ee, (*S*)-alkanol **1** with 83% ee was obtained. On the other hand, (*R*)-**4** with *ca.* 0.1% ee induced the formation and amplification of (*R*)-**1** in combination with asymmetric autocatalysis. Chiral organic–inorganic hybrid silsesquioxane **5** has served as a chiral heterogeneous initiator to afford highly enantioenriched alkanol **1** with the absolute configuration corresponding to that of the chiral diaminocyclohexane moiety in the structure (see Scheme 2.3).[22] Chromium(III) complex **6**[23] can act as a chiral homogeneous initiator in the enantioselective addition of *i*-Pr_2Zn to pyrimidine-5-carbaldehyde **2**, affording enantioenriched alkanol **1** with the absolute configurations related to the Δ- and Λ-topology of complex **6** with bidentate

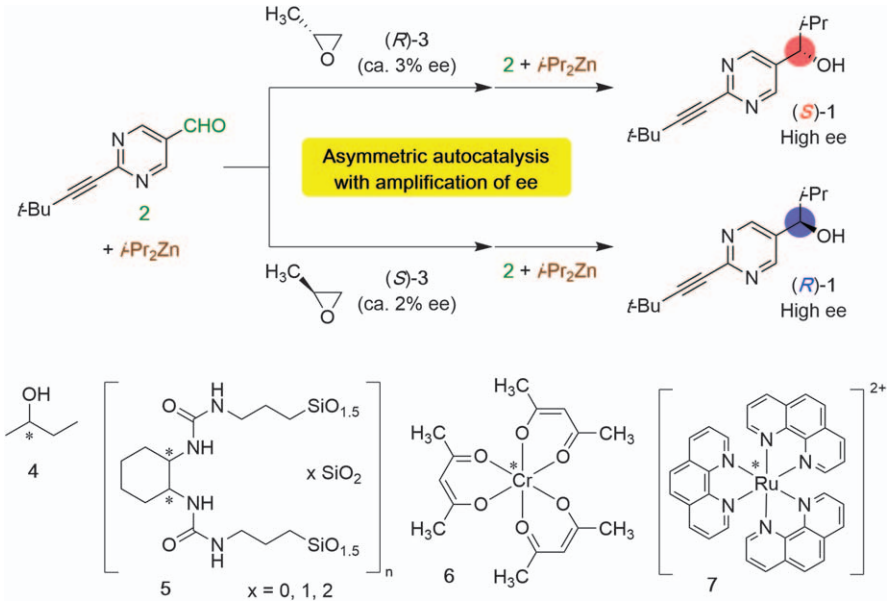

Scheme 2.3 Asymmetric autocatalysis initiated with chiral organic compounds and organic–inorganic hybrid materials affording 5-pyrimidyl alkanol **1** with amplified high enantioenrichment.

acetylacetonate ligands. Furthermore, tris(1,10-phenanthroline) complex of octahedral ruthenium(II) **7** can also act as a highly efficient chiral initiator for asymmetric autocatalysis.[24]

2.3 Chiral Discrimination of Cryptochiral Saturated Quaternary Hydrocarbons

Chiral compounds even without catalytic activity can serve as chiral initiators of asymmetric autocatalysis to induce the enantiomerically imbalanced autocatalyst **1**. Even if only slightly biased ee is induced, asymmetric autocatalysis would greatly enhance the amount and ee of itself to give an easily analyzable outcome, *i.e.,* 5-pyrimidyl alkanol **1**. Thus, it is conceivable that asymmetric autocatalysis can be utilized as a highly sensitive chiral sensor to detect tiny asymmetry in target materials.

Chiral discrimination of saturated quaternary hydrocarbons has been very difficult because of the small difference between the four substituents on the asymmetric carbon atom. (*n*-Butyl)ethyl(*n*-hexyl)(*n*-propyl)methane **8** with the same four methylene (CH_2) groups next to the asymmetric carbon center is a representative example (see Scheme 2.4). Wynberg reported that the enantiomer of **8** exhibits practically no optical rotation between 280 and 580 nm; thus, cryptochirality has occurred.[25] We have demonstrated that cryptochirality is successfully discriminated by asymmetric autocatalysis

with amplification of ee (see Scheme 2.4).[26] Upon the addition of *i*-Pr_2Zn to pyrimidine-5-carbaldehyde **2** in the presence of chiral saturated quaternary hydrocarbon **8** with *R*-configuration, (*S*)-pyrimidyl alkanol **1** with high ee was formed. In contrast, asymmetric autocatalysis in the presence of (*S*)-**8** afforded (*R*)-**1**. Therefore, asymmetric autocatalysis is a highly sensitive reaction that can recognize the cryptochirality of a saturated quaternary hydrocarbon.

Okuda *et al.* reported the synthesis of enantioenriched isotactic polystyrene **9** and demonstrated the dependence of the specific optical rotation on the molecular weight.[27] High-molecular-weight enantioenriched polystyrene **9** ($M_n > 5000$) possesses no detectable value of optical rotation (cryptochirality). Asymmetric autocatalysis can discriminate the cryptochirality of **9** to afford pyrimidyl alkanol **1** with high ee.[28]

We have reported that chiral hydrocarbons such as saturated tertiary alkanes **10**,[26] olefin **11**,[29] binaphthyl **12**,[30] [2,2]paracyclophanes **13**,[31,32] and allene **14**[33] could be successfully utilized as the chiral initiators for asymmetric autocatalysis.

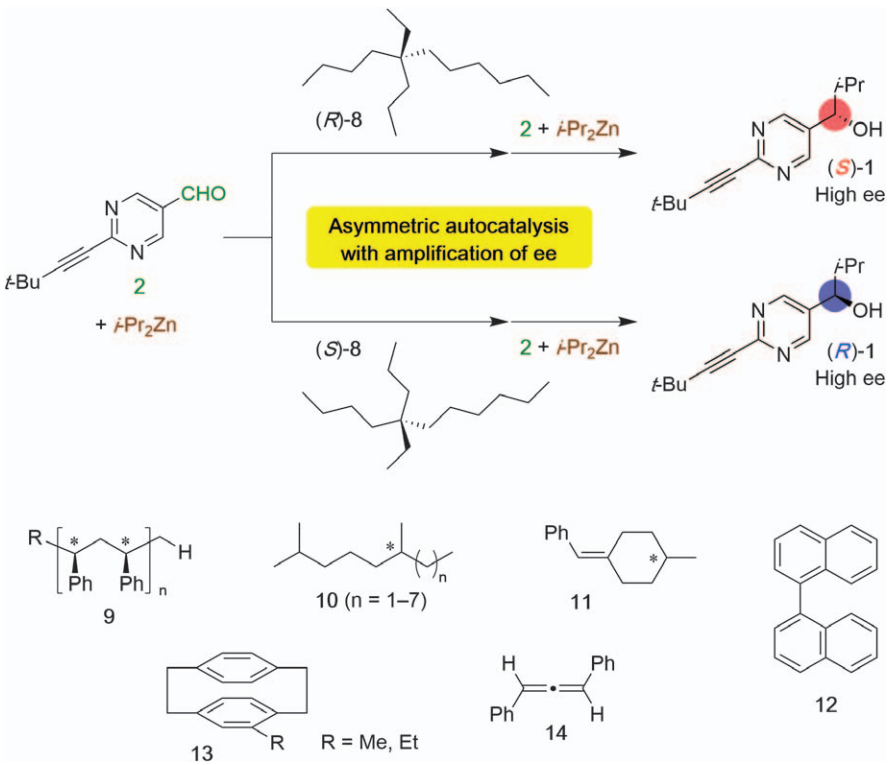

Scheme 2.4 Asymmetric autocatalysis initiated with chiral hydrocarbons, including cryptochiral saturated quaternary hydrocarbon and isotactic polystyrene.

Moreover, chiral compounds arising from isotope substitution can also act as a source of chirality for asymmetric autocatalysis.[34] Therefore, chiral hydrogen,[35–37] carbon,[38] oxygen,[39,40] and nitrogen[41] isotopomers can trigger the asymmetric autocatalysis with amplification of ee to afford highly enantioenriched 5-pyrimidyl alkanol with the corresponding absolute configuration to that of chiral isotopomers.[42]

2.4 Correlation Between Circularly Polarized Light and Highly Enantioenriched Organic Compounds Mediated by Asymmetric Autocatalysis

Circularly polarized light (CPL) has long been suggested as one of the origins of chirality of organic compounds[43–46] and the occurrence of strong CPL has been observed in a star-forming region of the Orion constellation.[47] However, because of the very small anisotropy factors of organic compounds, only low enantioenrichments have been induced by its irradiation. For example, asymmetric photodegradation of racemic leucine by right-handed (*r*) CPL (213 nm) produces L-leucine with only 2% ee (see Figure 2.1).[48] Asymmetric photosynthesis of [6]helicene with low ee was achieved using CPL.[49] Chiral organic compounds with low ee induced by CPL might act as a source of chirality to initiate the asymmetric autocatalysis. Leucine with 2% ee worked as a chiral initiator in the addition of *i*-Pr_2Zn to pyrimidine-5-carbaldehyde with a methyl substituent at the 2-position of the pyrimidine ring to afford the enantiomerically enhanced corresponding alkanol with the absolute configuration correlated to that of leucine.[18] [6]Helicene, although with low enantioenrichment can also induce the asymmetry for autocatalytic formation of 5-pyrimidyl alkanol **1**.[50] Thus, the chirality of CPL has been correlated with that of asymmetric autocatalysts *via* leucine and [6]helicene as the source of chirality.

Asymmetric photoequilibrium of chiral olefins[51] such as benzylidenecyclohexanone **15** has been reported,[52] where CPL can induce only a slight

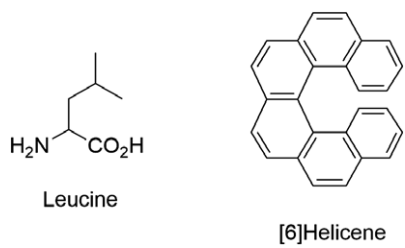

Figure 2.1 Chemical structures of leucine and [6]helicene, whose slight enantioenrichment can be induced by the irradiation of circularly polarized light (CPL).

enantioimbalance (<2% ee). Thus, a racemic olefin was irradiated with *r*- or *l*-CPL and then *i*-Pr_2Zn addition to aldehyde **2** was performed in the presence of the irradiated olefin **15**.[53] Chiral olefin **15** irradiated with *l*-CPL afforded (*S*)-alkanol **1** with high ee. In contrast, **15** irradiated with *r*-CPL induced the formation of (*R*)-**1**. Thus, the correlation between the handedness of CPL and the absolute configuration of 5-pyrimidyl alkanol **1** was reproducibly confirmed (see Scheme 2.5).

The asymmetric autocatalysts, (*R*)- and (*S*)-5-pyrimidyl alkanols **1**, show positive and negative CD spectra at 313 nm, respectively.[54] It could be supposed that the direct irradiation of *l*-CPL to *rac*-**1** would induce the asymmetric photodegradation of (*R*)-alkanol **1** and the residual alkanol **1** should have the slight *S*-enrichment. Although the enantioenrichment of the remaining (*S*)-**1** is extremely low, it would be significantly improved to high ee as a result of subsequent asymmetric autocatalysis. Indeed, direct irradiation of *l*-CPL to *rac*-**1** and the following asymmetric autocatalysis afforded nearly enantiomerically pure (*S*)-alkanol **1** (>99.5% ee) (see Scheme 2.6). On the other hand, irradiation of *r*-CPL induced the amplification and multiplication of (*R*)-alkanol **1** with >99.5% ee.[54] It was found that the photooxidation of **1** proceeded to afford ketone **16** by CPL irradiation in air and, in turn, irradiation under an argon atmosphere, with the photochemical reduction of an alkynyl moiety affording alkenylpyrimidyl alkanol **17** (see Scheme 2.6).[55]

Asymmetric photodecomposition of **1** with CPL and subsequent asymmetric autocatalysis afforded the near enantiopure **1** whose absolute configuration is reproducibly controlled by the handedness of CPL. The process provides a direct correlation of the chirality of CPL, one of the chiral physical factors, with that of organic compounds with high ee.

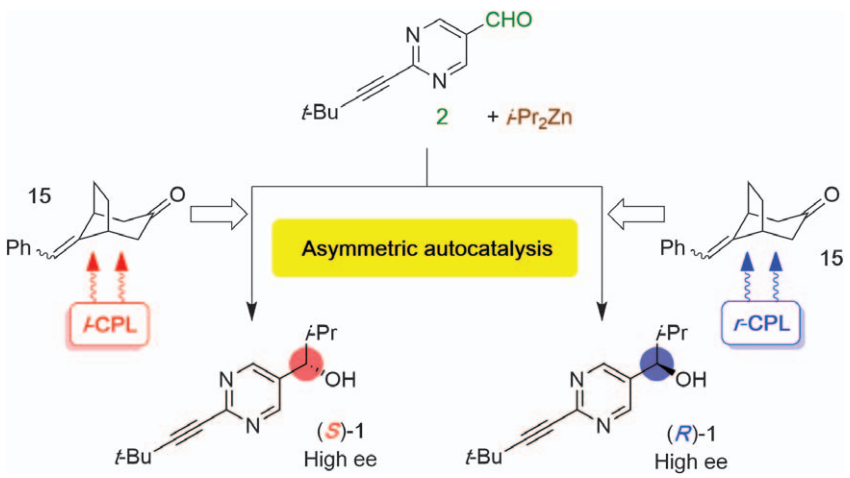

Scheme 2.5 CPL-induced asymmetric amplification of 5-pyrimidyl alkanol **1** mediated by photoequilibrium of chiral olefin in conjunction with asymmetric autocatalysis.

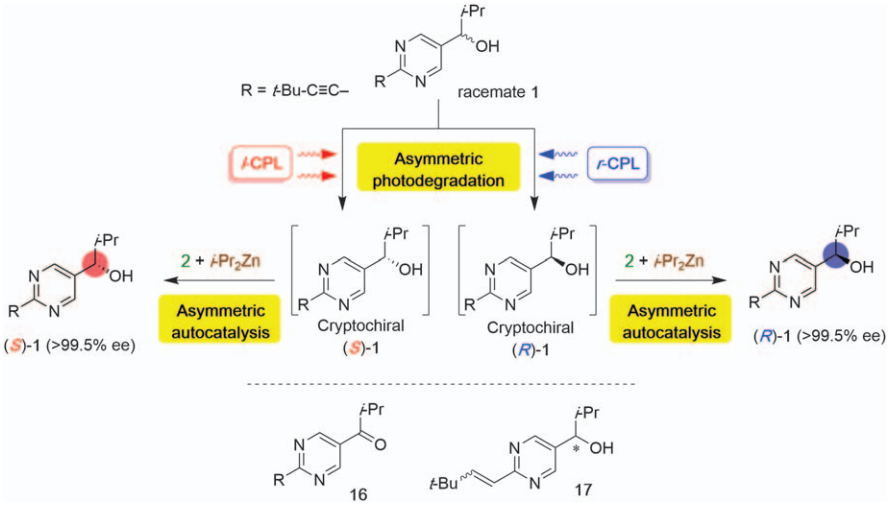

Scheme 2.6 Enantioselective synthesis of near enantiopure organic compounds by CPL irradiation in conjunction with asymmetric autocatalysis.

2.5 Conclusion

We have summarized asymmetric autocatalysis induced by various chiral organic compounds, including organic–inorganic hybrid materials. Although the compounds seem to have a small chiral directing power, asymmetric autocatalysis can recognize the chirality of the initiators to afford highly enantioenriched 5-pyrimidyl alkanol. Thus, asymmetric autocatalysis has sufficient power to discriminate and amplify the cryptochirality, such as that observed in chiral saturated quaternary hydrocarbons and isotactic polystyrene. Moreover, chiral compounds induced by the irradiation of CPL can act as a chiral initiator for the asymmetric autocatalysis of 5-pyrimidyl alkanol. Therefore, one of the chiral physical factors, CPL, is linked with an enantiomerically pure organic compound mediated by the direct irradiation of 5-pyrimidyl alkanol in conjunction with asymmetric autocatalysis with the amplification of ee.

Acknowledgements

This work was financially supported by KAKENHI 19K05482, 19K22190, and 20H04674 from JSPS.

References

1. K. Soai, T. Shibata, H. Morioka and K. Choji, *Nature*, 1995, **378**, 767.
2. K. Soai, T. Kawasaki and A. Matsumoto, *Acc. Chem. Res.*, 2014, **47**, 3643.
3. K. Soai, T. Shibata and I. Sato, *Acc. Chem. Res.*, 2000, **33**, 382.

4. K. Soai, T. Kawasaki and A. Matsumoto, *Tetrahedron*, 2018, **74**, 1973.
5. K. Soai, *Proc. Jpn. Acad., Ser. B*, 2019, **95**, 89.
6. G. Pályi, R. Kurdi and C. Zucchi, *Advances in Asymmetric Autocatalysis and Related Topic*, Elsevier Inc., Cambridge, 1st edn, 2017.
7. G. Pályi, C. Zucchi and L. Caglioti, *The Soai Reaction and Related Topic*, Accad. Nazl. Sci. Lett. Arti, Editioni Artestampa, Modena, 1st edn, 2012.
8. C. Bolm, F. Bienewald and A. Seger, *Angew. Chem., Int. Ed. Engl.*, 1996, **35**, 1657.
9. M. Avalos, R. Babiano, P. Cintas, J. L. Jimonez and J. C. Palacios, *Chem. Commun.*, 2000, 887.
10. D. G. Blackmond, *Proc. Natl. Acad. Sci. U. S. A.*, 2004, **101**, 5732.
11. J. Podlech and T. Gehring, *Angew. Chem., Int. Ed.*, 2005, **44**, 5776.
12. J. M. Brown, I. D. Gridnev and J. Klankermayer, *Top. Curr. Chem.*, 2008, **284**, 35.
13. T. Gehring, M. Busch, M. Schlageter and D. Weingand, *Chirality*, 2010, **22**, E173.
14. O. Fülöp and B. Barabás, *J. Math. Chem.*, 2016, **54**, 10.
15. A. J. Bissette and S. P. Fletcher, *Angew. Chem., Int. Ed.*, 2013, **52**, 12800.
16. T. Shibata, S. Yonekubo and K. Soai, *Angew. Chem. Int. Ed.*, 1999, **38**, 659.
17. I. Sato, H. Urabe, S. Ishiguro, T. Shibata and K. Soai, *Angew. Chem. Int. Ed.*, 2003, **42**, 315.
18. T. Shibata, J. Yamamoto, N. Matsumoto, S. Yonekubo, S. Osanai and K. Soai, *J. Am. Chem. Soc.*, 1998, **120**, 12157.
19. B. A. McGuire, P. B. Carroll, R. A. Loomis, I. A. Finneran, P. R. Jewell, A. J. Remijan and G. A. Blake, *Science*, 2016, **352**, 1449.
20. T. Kawasaki, T. Shimizu, K. Suzuki, I. Sato and K. Soai, *Tetrahedron: Asymmetry*, 2004, **15**, 3699.
21. T. Shibata, K. Iwahashi, T. Kawasaki and K. Soai, *Tetrahedron: Asymmetry*, 2007, **18**, 1759.
22. T. Kawasaki, K. Ishikawa, H. Sekibata, I. Sato and K. Soai, *Tetrahedron Lett.*, 2004, **45**, 7939.
23. T. Kawasaki, T. Omine, M. Sato, Y. Morishita and K. Soai, *Chem. Lett.*, 2007, **36**, 30.
24. T. Kawasaki, T. Omine, K. Suzuki, H. Sato, A. Yamagishi and K. Soai, *Org. Biomol. Chem.*, 2009, **7**, 1073.
25. H. Wynberg, G. L. Hekkert, J. P. M. Houbiers and H. W. Bosch, *J. Am. Chem. Soc.*, 1965, **87**, 2635.
26. T. Kawasaki, H. Tanaka, T. Tsutsumi, T. Kasahara, I. Sato and K. Soai, *J. Am. Chem. Soc.*, 2006, **128**, 6032.
27. K. Beckerle, R. Manivannan, B. Lian, G.-J. M. Meppelder, G. Raabe, T. P. Spaniol, H. Ebeling, F. Pelascini, R. Mülhaupt and J. Okuda, *Angew. Chem., Int. Ed.*, 2007, **46**, 4790.
28. T. Kawasaki, C. Hohberger, Y. Araki, K. Hatase, K. Beckerle, J. Okuda and K. Soai, *Chem. Commun.*, 2009, 5621.
29. I. Sato, R. Sugie, Y. Matsueda, Y. Furumura and K. Soai, *Angew. Chem., Int. Ed.*, 2004, **43**, 4490.

30. I. Sato, S. Osanai, K. Kadowaki, T. Sugiyama, T. Shibata and K. Soai, *Chem. Lett.*, 2002, **31**, 168.
31. S. Tanji, A. Ohno, I. Sato and K. Soai, *Org. Lett.*, 2001, **3**, 287.
32. I. Sato, A. Ahno, Y. Aoyama, T. Kasahara and K. Soai, *Org. Biomol. Chem.*, 2003, **1**, 244.
33. I. Sato, Y. Matsueda, K. Kadowaki, S. Yonekubo, T. Shibata and K. Soai, *Helv. Chim. Acta*, 2002, **85**, 3383.
34. T. Kawasaki and K. Soai, *Bull. Chem. Soc. Jpn.*, 2011, **84**, 879.
35. I. Sato, D. Omiya, T. Saito and K. Soai, *J. Am. Chem. Soc.*, 2000, **122**, 11739.
36. T. Kawasaki, M. Shimizu, D. Nishiyama, M. Ito, H. Ozawa and K. Soai, *Chem. Commun.*, 2009, 4396.
37. T. Kawasaki, H. Ozawa, M. Ito and K. Soai, *Chem. Lett.*, 2011, **40**, 320.
38. T. Kawasaki, Y. Matsumura, T. Tsutsumi, K. Suzuki, M. Ito and K. Soai, *Science*, 2009, **324**, 492.
39. T. Kawasaki, Y. Okano, E. Suzuki, S. Takano, S. Oji and K. Soai, *Angew. Chem., Int. Ed.*, 2011, **50**, 8131.
40. A. Matsumoto, S. Oji, S. Takano, K. Tada, T. Kawasaki and K. Soai, *Org. Biomol. Chem.*, 2013, **11**, 2928.
41. A. Matsumoto, H. Ozaki, S. Harada, K. Tada, T. Ayugase, H. Ozawa, T. Kawasaki and K. Soai, *Angew. Chem., Int. Ed.*, 2016, **55**, 15246.
42. N. A. Hawbaker and D. G. Blackmond, *ACS Cent. Sci.*, 2018, **4**, 776.
43. Y. Inoue, *Chem. Rev.*, 1992, **92**, 741.
44. B. L. Feringa and R. A. van Delden, *Angew. Chem., Int. Ed.*, 1999, **38**, 3418.
45. W. L. Noorduin, A. A. C. Bode, M. van der Meijden, H. Meekes, A. F. van Etteger, W. J. P. van Enckevort, P. C. M. Christianen, B. Kaptein, R. M. Kellogg, T. Rasing and E. Vlieg, *Nat. Chem.*, 2009, **1**, 729.
46. C. Meinert, S. V. Hoffmann, P. C. Chenaï, A. C. Evans, C. Giri, L. Nahon and U. J. Meierhenrich, *Angew. Chem., Int. Ed.*, 2014, 53, 210.
47. J. Bailey, A. Chrysostomou, J. H. Hough, T. M. Gledhill, A. McCall, S. Clark, F. Ménard and M. Tamura, *Science*, 1998, **281**, 672.
48. H. Nishino, A. Kosaka, G. A. Hembury, F. Aoki, K. Miyauchi, H. Shitomi, H. Onuki and Y. Inoue, *J. Am. Chem. Soc.*, 2002, **124**, 11618.
49. A. Moradpour, G. Balavoine, J. F. Nicoud, H. Kagan and G. Tsoucaris, *J. Am. Chem. Soc.*, 1971, **93**, 2353.
50. I. Sato, R. Yamashima, K. Kadowaki, J. Yamamoto, T. Shibata and K. Soai, *Angew. Chem., Int. Ed.*, 2001, **40**, 1096.
51. M. Suarez and G. B. Schuster, *J. Am. Chem. Soc.*, 1995, **117**, 6732.
52. Y. Zhang and G. B. Schuster, *J. Org. Chem.*, 1995, **60**, 7192.
53. I. Sato, R. Sugie, Y. Matsueda, Y. Furumura and K. Soai, *Angew. Chem., Int. Ed.*, 2004, **43**, 4490.
54. T. Kawasaki, M. Sato, S. Ishiguro, T. Saito, Y. Morishita, I. Sato, H. Nishino, Y. Inoue and K. Soai, *J. Am. Chem. Soc.*, 2005, **127**, 3274.
55. I. Sato, T. Yanagi and K. Soai, *Chirality*, 2002, **14**, 166.

CHAPTER 3

Asymmetric Autocatalysis Triggered by the Chirality of Minerals, Organic Crystals, and Surfaces

ARIMASA MATSUMOTO,*[a] TSUNEOMI KAWASAKI[b] AND KENSO SOAI[b,c]

[a] Department of Chemistry, Biology, and Environmental Science, Nara Women's University, Kita-Uoya Nishi-machi, Nara 630-8506, Japan; [b] Department of Applied Chemistry, Tokyo University of Science, Kagurazaka, Shinjuku-ku, Tokyo 162-8601, Japan; [c] Research Organization for Nano & Life Innovation, Waseda University, Wasedatsurumaki-cho, Shinjuku-ku, Tokyo 162-0041, Japan
*Email: a-matsumoto@cc.nara-wu.ac.jp

3.1 Crystal Chirality of Achiral Compounds

Crystal chirality has been an important part of chirality research. The phenomena of optical rotation and circularly polarized light were originally found by studying light transmitted through crystal quartz. Pasteur found molecular chirality by examining the hemihedral crystal shape of salts of tartaric acid. Crystallization can induce spontaneous dememorization[1,2] and, recently, optical resolution by crystallization through Viedma ripening[3–6] attrition-enhanced deracemization of conglomerates has provided a new approach to

Catalysis Series No. 43
Asymmetric Autocatalysis: The Soai Reaction
Edited by Kenso Soai, Tsuneomi Kawasaki and Arimasa Matsumoto

Published by the Royal Society of Chemistry, www.rsc.org

chiral resolution.[7–9] One of the most interesting and important aspects of crystal chirality is the formation of chiral crystals from achiral compounds.

There are 230 space group symmetry identifiers for three-dimensional crystal structures, defining a combination of various symmetry operations such as translation, rotation, inversion, and mirror symmetry. Inversion, mirror, improper rotation, and glide symmetry, classed as second-type symmetry operations, cause an inversion of chirality; in contrast, translation and rotation do not invert the chirality of the molecules. When an enantiopure chiral molecule becomes a crystal, it is always one of the 65 Sohncke space groups, without second-type, chirality inversion symmetry (Table 3.1).[10] However, achiral or racemic molecules do not necessarily crystallize as achiral crystals. The adoption of a helical arrangement of molecules in the crystal or fixing a twist structure can lead to the formation of chiral crystals from achiral or racemic molecules (Figure 3.1).[11,12]

Chiral crystallization of achiral compounds has been considered as a possible origin of biological homochirality. There have been some pioneering reports on the conversion of crystal chirality into molecular chirality by photoreaction in solids[13–16] or by reaction in low-temperature solutions while the conformation in the crystal remains fixed.[17–20] However, it is very difficult to use crystal chirality to control the selectivity of a reaction. The chirality induced by a crystal surface by selective adsorption is typically small and it is difficult to obtain a detectable imbalance of enantiomeric enrichment in the reaction product.

We have been studying asymmetric autocatalytic reactions in which asymmetric amplification occurs. Asymmetric autocatalysis of pyrimidyl alkanol **1**[21–28] is a reaction in which **1** acts as an asymmetric catalyst for asymmetric addition of a *i*-Pr_2Zn to aldehyde **2** to give alkanol **1** with the same structure and absolute configuration as its catalyst **1** (Scheme 3.1). Moreover, this reaction has a positive non-linear effect,[29] in that it gives products with higher enantiomeric excess (ee) even when the ee of the initial catalyst is low. This combination of asymmetric amplification and autocatalysis results in an extreme increase in ee from a small imbalance,

Table 3.1 Sohncke space groups.

System	Point group	Space group
Triclinic	1 (C_1)	$P1$
Monoclinic	2 (C_2)	$P2$, $P2_1$, $C2$
Orthorhombic	222 (D_2)	$P222$, $P222_1$, $P2_12_12$, $P2_12_12_1$, $C222_1$, $C222$, $F222$, $I222$, $I2_12_12_1$
Tetragonal	422 (D_4)	$P422$, $P42_12$, $P4_122$, $P4_12_12$, $P4_222$, $P4_22_12$, $P4_322$, $P4_32_12$, $I422$, $I4_122$
	4 (C_4)	$P4$, $P4_1$, $P4_2$, $P4_3$, $I4$, $I4_1$
Trigonal	32 (D_3)	$P312$, $P321$, $P3_112$, $P3_212$, $P3_121$, $P3_221$, $R32$
	3 (C_3)	$P3$, $P3_1$, $P3_2$, $R3$
Hexagonal	6 (C_6)	$P6$, $P6_1$, $P6_2$, $P6_3$, $P6_4$, $P6_5$
	622 (D_6)	$P622$, $P6_122$, $P6_222$, $P6_322$, $P6_422$, $P6_522$
Cubic	23 (T)	$P23$, $F23$, $I23$, $P2_13$, $I2_13$
	432 (O)	$P432$, $P4_132$, $P4_232$, $P4_332$, $F432$, $F4_132$, $I432$, $I4_132$

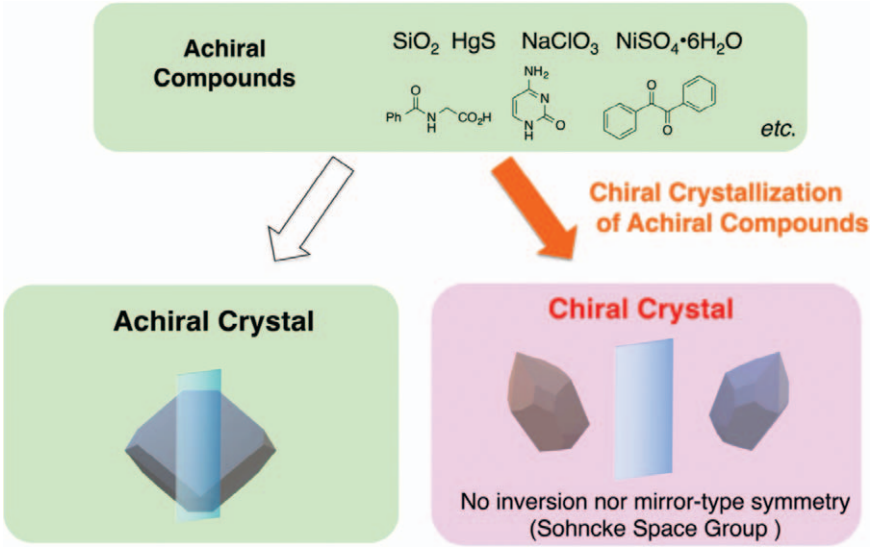

Figure 3.1 Chiral crystallization of achiral compounds.

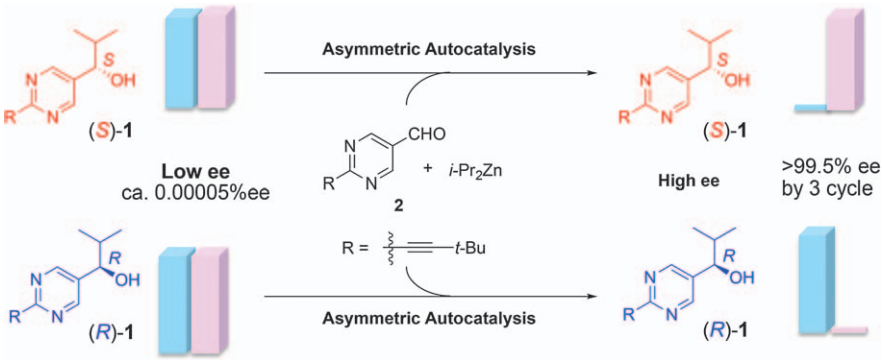

Scheme 3.1 Asymmetric autocatalysis of pyrimidyl alkanol.

attracting the attention of many researchers[30–39] and allowing the recognition of small biases in chirality that would not normally be expected to cause asymmetric reactions such as circular polarized light[40,41] and isotope chirality.[42–48] By taking advantage of this high level of chirality amplification, it is possible to show that the chirality of various crystals does indeed affect the selectivity of the reaction (Scheme 3.2).

3.2 Chirality of Minerals and Inorganic Crystals as a Trigger for Asymmetric Autocatalysis

The question of how the chirality of inorganic minerals such as quartz affects the chirality of organic compounds has long been the focus of attention as a possible origin of molecular chirality. Although there have been

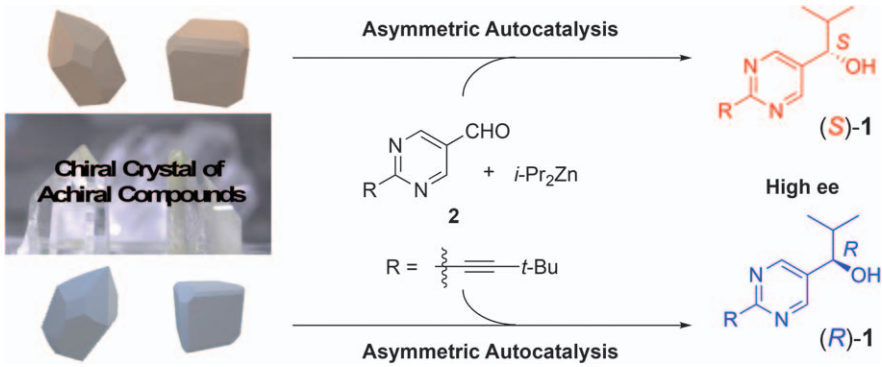

Scheme 3.2 Asymmetric autocatalysis induced by crystal chirality.

pioneering studies on the adsorption of amino acids on the surface of quartz[49] and calcite,[50] it has been difficult to obtain significant selectivity. In this section, we present an example of how the chirality of an inorganic mineral can affect the selectivity of an asymmetric autocatalytic reaction.

3.2.1 SiO_2 Quartz

Quartz (crystals of SiO_2) is one of the most important crystals in the history of chirality. The property of optical rotation was first found by examining quartz crystals and it remains a widely used optical material that is applied for the generation of circularly polarized light. The chirality of the crystal is also manifested in the characteristic crystal shape, which is another reason why quartz was widely recognized as a chiral crystal. However, the terms 'right-handed quartz' and 'left-handed quartz' are often confusing because there is a question of whether the right and left refer to the outer shape of the crystal, the helical axis of the crystal structure, or the direction of light-rotation.[51] Here, crystals with a structure in the space group $P3_221$ that exhibits dextrorotary rotation are described as right-handed, *d*-quartz, and crystal structures in the space group $P3_121$ that exhibit levorotary rotation are described as left-handed, *l*-quartz.

Asymmetric induction or asymmetric adsorption using crystal chirality has often been attempted, but it has been difficult to achieve due to the low asymmetry of crystal surfaces and weak molecular interactions. Using asymmetric amplification with a high degree of asymmetric autocatalysis, the reaction can be carried out in the presence of finely ground quartz crystal. When *d*-quartz is used, an alkanol of the (*S*)-configuration was obtained, and when *l*-quartz is used, an alkanol of the (*R*)-configuration was obtained, reproducibly (Scheme 3.3).[52] This was the first example of how the chirality of quartz, a common mineral on Earth, can affect the selectivity of organic reactions.

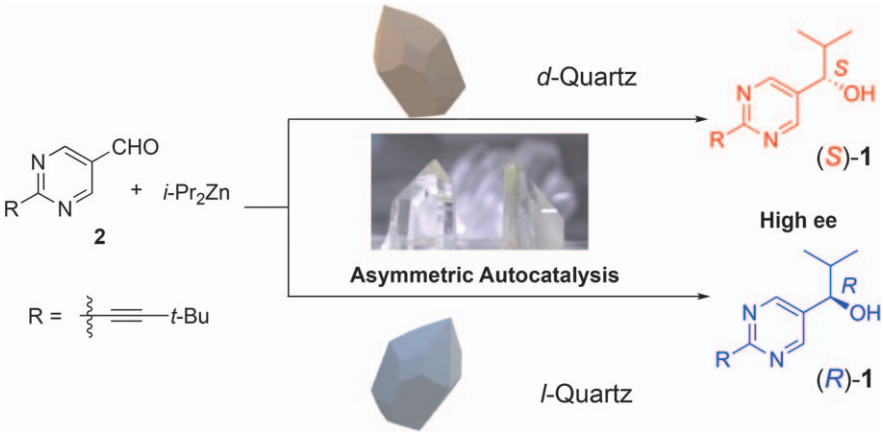

Scheme 3.3 Hemihedral structures of quartz crystals and asymmetric autocatalysis with quartz.

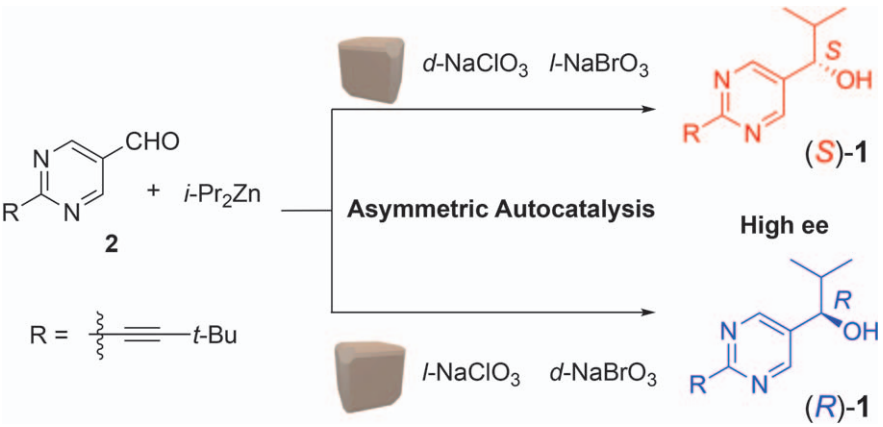

Scheme 3.4 Asymmetric autocatalysis initiated by $NaClO_3$ and $NaBrO_3$.

3.2.2 Sodium Chlorate and Bromate

In the field of chiral crystallization of achiral compounds, sodium chlorate is also a well-known crystal for the study of spontaneous deracemization during recrystallization.[1–3,53] Sodium chlorate ($NaClO_3$) and bromate ($NaBrO_3$) belong to the cubic $P2_13$ space group, giving a cubic structure with high symmetry; the chirality can be easily determined by measuring the direction of rotation with a polarizing microscope. It is important to note that the direction of rotation is reversed for chloride and bromide when the same ion configuration is used.[54,55]

The asymmetric autocatalysis reaction with sodium chlorate or bromate results in the formation of (*S*)-alkanol with *d*-$NaClO_3$ or *l*-$NaBrO_3$ and (*R*)-alkanol formation in the presence of *l*-$NaClO_3$ or *d*-$NaBrO_3$. This result

means that crystals with the same ionic configuration rather than rotatory properties showed the same selectivity (Scheme 3.4).[56,57]

3.2.3 Cinnabar HgS

Cinnabar, a HgS mineral, was used as a vermilion pigment in ancient times, but the fact that it has a chiral structure has not received much attention. It is composed of a series of three helical bonds of mercury and sulfur. Here, the crystal of $P3_121$ with a right-handed triple helical axis is called (*P*)-HgS and the crystal of $P3_221$ with left-handed symmetry is called (*M*)-HgS.

The absolute structure of HgS was determined by single-crystal X-ray diffraction, and asymmetric autocatalysis was performed in the presence of the powder. As a result, (*S*)-alkanol **1** was obtained in the presence of (*P*)-HgS and (*M*)-HgS gave an (*R*)-alkanol (Scheme 3.5).[58]

Furthermore, atomic force microscopy of the surface of cinnabar has been carried out, and differences in the crystal growth of alkanols on its surface were observed depending on the absolute configuration. This suggests that differences in adsorption on the chiral crystals of cinnabar affect the selectivity of asymmetric autocatalysis.

3.2.4 Retgersite

Retgersite (nickel sulfate hexahydrate; $NiSO_4 \cdot 6H_2O$) is a blue-green sulfate mineral that belongs to the $P4_12_12$ or $P4_32_12$ space group. The sulfate ion has tetrahedral symmetry and the Ni ion, with six co-ordinated oxygen atoms, has octahedral symmetry. However, these ions connect through hydrogen bonding and this alignment forms a fourfold screw axis. The crystal chirality can be determined from either the optical rotation or the circular dichroism (CD) spectrum.

The crystal shows several Cotton effects due to the d–d transition of Ni ions, with the signals around 390 and 690 nm being particularly distinctive. The $P4_12_12$ crystal has a negative Cotton effect and the $P4_32_12$ crystal

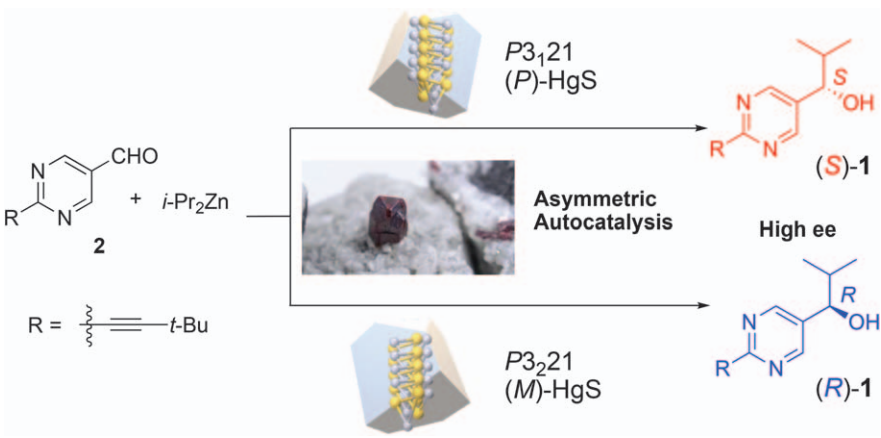

Scheme 3.5 Asymmetric autocatalysis initiated by cinnabar.

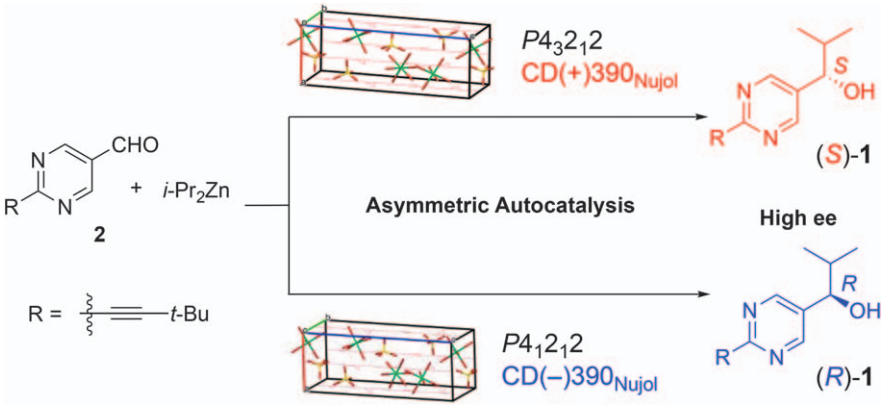

Scheme 3.6 Asymmetric autocatalysis initiated by $NiSO_4 \cdot 6H_2O$.

shows a positive Cotton effect. In the presence of this hydrate crystal, because of the presence of numerous waters of crystallization, the initial reaction is slightly sluggish but the crystal with CD(+)390 gave the (*S*)-alkanol (Scheme 3.6).[59] It was shown that the chirality of crystals can be recognized by asymmetric autocatalysis even if they contain a large amount of crystalline water if the reaction conditions are well chosen.

3.3 Chirality of Organic Compounds

3.3.1 Chiral Crystal of Organic Compounds

Several achiral organic compounds are also known to form chiral crystals. Even if a molecule is considered to be achiral in solution because of its rapid conformational change, it can become an enantiomer in crystals because its conformation becomes fixed. In addition, as in the case of inorganic crystals, the molecules may be arranged in a helical fashion due to intermolecular interactions. This chiral crystallization phenomenon is not a unique case; it has been observed in about 10% of all reported chiral organic crystals.[9,10] This chirality of achiral compounds can be used for absolute asymmetric synthesis and is also of interest for studies on the origin of biological homochirality. In this section, we will show that chiral crystals of various achiral compounds can induce asymmetric autocatalysis.

3.3.2 Chiral Crystal of a Complex

The first asymmetric induction using crystals of an achiral organic compound was achieved using a complex of cobalt. Even in complexes with achiral ligands, chirality is generated depending on the co-ordination mode, such as Λ and Δ types.

Cobalt complexes with EDTA **3** and TRDTA **4** have octahedral geometry and are chiral due to the co-ordination geometry.[60,61] In the solution state,

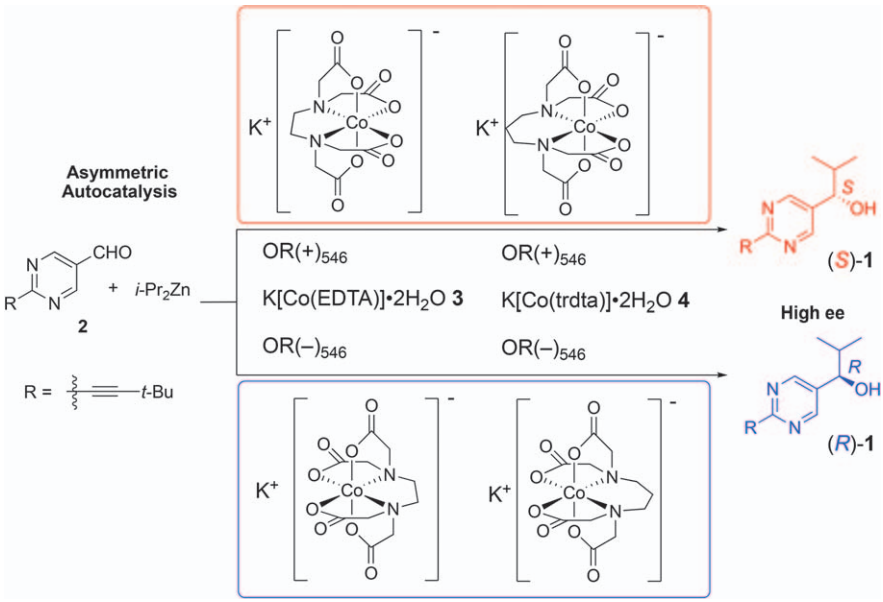

Scheme 3.7 Asymmetric autocatalysis initiated by a chiral cobalt complex.

these enantiomers can racemize; however, this co-ordination chirality is fixed in the crystal and optical rotation (OR) at 546 nm is observed. In the presence of crystals of K[Co(edta)]·2H_2O or K[Co(trdta)]·2H_2O with OR(+), the asymmetric autocatalysis afforded (*S*)-alkanol; in the presence of crystals with OR(−), (*R*)-alkanol was obtained (Scheme 3.7).[62]

3.3.3 Chiral Crystal of Co-crystals

Asymmetric autocatalysis in chiral crystals of non-metallic organic compounds is also possible. Indole amine and indole carboxylate are achiral organic compounds; however, crystallization of indole amine with chlorobenzoic acid and indole carboxylate phenanthridine causes co-crystallization through acid and base interaction and chiral crystals **5** and **6** with space groups $P2_12_12_1$ and $P2_1$, respectively, are formed. Crystals with space groups $P2_12_12_1$ and $P2_1$ are chiral, but their mirror-image space groups are also $P2_12_12_1$ and $P2_1$, so the absolute structure cannot be described by the space groups. For this reason, it is necessary to focus on the arrangement of molecules in the crystal structure to describe the absolute structure: the crystal structure of **5**, which can be regarded as a *P*-helix in the *c*-axis direction, shows a pronounced positive Cotton effect at 225 nm in the CD spectrum in Nujol. For the crystal structure of **6**, which has a *P*-helix molecular arrangement in the *b*-axis direction, a (+) Cotton effect at 250 nm[63–65] was found. In the asymmetric autocatalysis reaction with this chiral

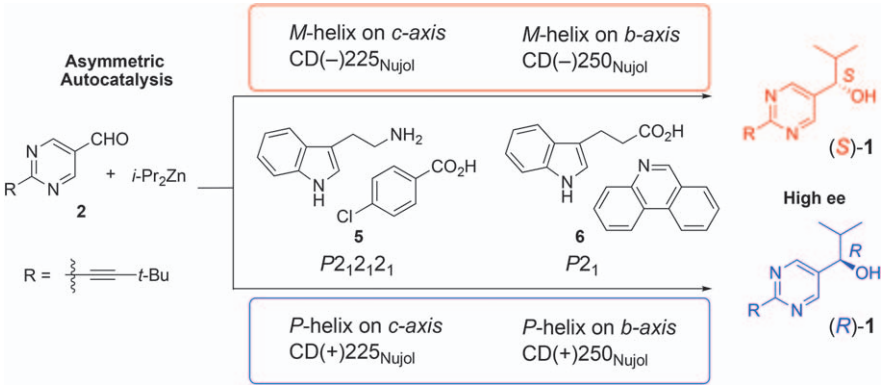

Scheme 3.8 Asymmetric autocatalysis initiated by chiral co-crystals of achiral compounds.

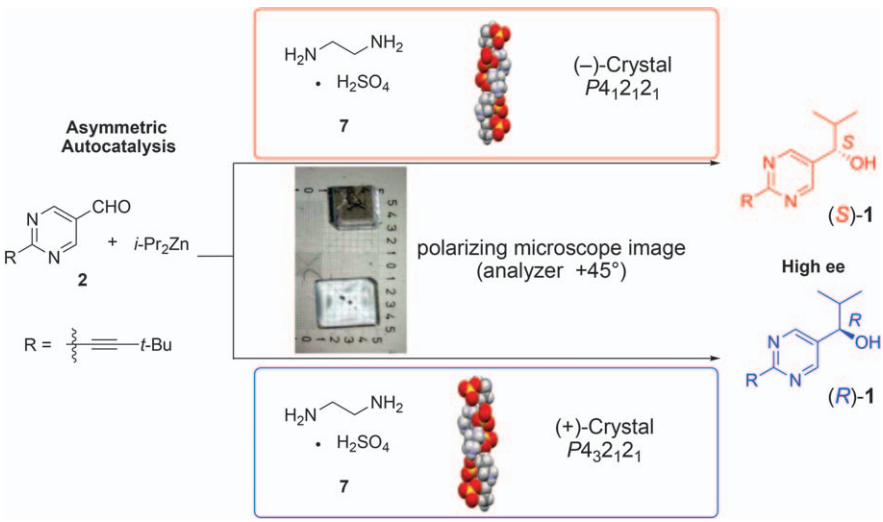

Scheme 3.9 Asymmetric autocatalysis initiated by chiral crystals of ethylenediamine sulfate.

co-crystal, (*S*)-alkanol **1** was obtained with the CD(−) form of crystals of **5** and **6** (Scheme 3.8).[66]

A recent example of asymmetric induction by an acid–base co-crystal is ethylenediamine(ethylenediammonium) sulfate **7**. Ethylenediamine is an achiral diamine but the sulfate crystals have a chiral structure, with $P4_12_12$ or $P4_32_12$ symmetry. Because this tetragonal crystal grows in the form of a large square face orthogonal to the optical axis, the chirality can be easily determined by measuring the direction of rotation with a polarizing microscope.[67] The $P4_12_12$ crystal has (−)-optical rotation and afforded (*S*)-alkanol **1** in the asymmetric autocatalysis (Scheme 3.9).[68]

3.3.4 Chiral Crystal of Simple Organic Compounds

Simple achiral organic compounds also form chiral crystals and can act as chiral initiators in asymmetric autocatalysis. Benzil **8** is a symmetric achiral organic ketone, but it makes chiral crystals. In the crystal structure, the direction of the torsion angle of the two carbonyl groups allows for two conformations that are mirror images of each other; a molecule in one conformation will form a crystal of either $P3_12_12$ or $P3_22_12$. For easier determination of the absolute configuration, dibromobenzil **9**, with bromo groups, gave crystals of $P2_12_12_1$, and the *P*-conformation had a positive Cotton effect at 320 nm in a KBr disk. Using this crystal, it was found that the crystal with a negative Cotton effect CD(−)400_{KBr}-**8** or CD(−)320_{KBr}-**9** induced (*S*)-alkanol **1** in asymmetric autocatalysis (Scheme 3.10).[69]

Simple achiral hydrocarbons can also form chiral crystals. Tetraphenyl ethylene **10** is a well-known aggregation-induced emitting material that forms through intramolecular interaction of the four twisted aromatic rings. This twisted conformation has conformational chirality, and the twisted conformation causes optical resolution due to spontaneous chiral crystallization. Furthermore, this crystal chirality can be recognized by its hemihedral shape in crystal growth. In asymmetric autocatalysis, crystals with CD(+) at 270 nm afforded (*S*)-alkanol. Cl- and Br-substituted derivatives **11** and **12** also form chiral crystals containing *p*-xylene in space group $P2_12_12_1$. The substitution of a heavy element simplifies the determination of the absolute structure by X-ray diffraction. The Cl-substituted crystal **10** has a Cotton effect around 270 nm and the *M*-conformation crystal, which has a negative Cotton effect, afforded (*S*)-alkanol **1** (Scheme 3.11).[70]

A threefold symmetric substituted benzene triester also forms a chiral crystal. In this crystal, molecules stack in a columnar structure with a sixfold rotation helix. A $P6_1$ crystal with sixfold, right-handed helices and a $P6_5$ crystal with a collection of left-handed helices are obtained for which Cotton effects (+ for $P6_1$ and − for $P6_5$) are observed around 224 nm in a KBr disk.[71]

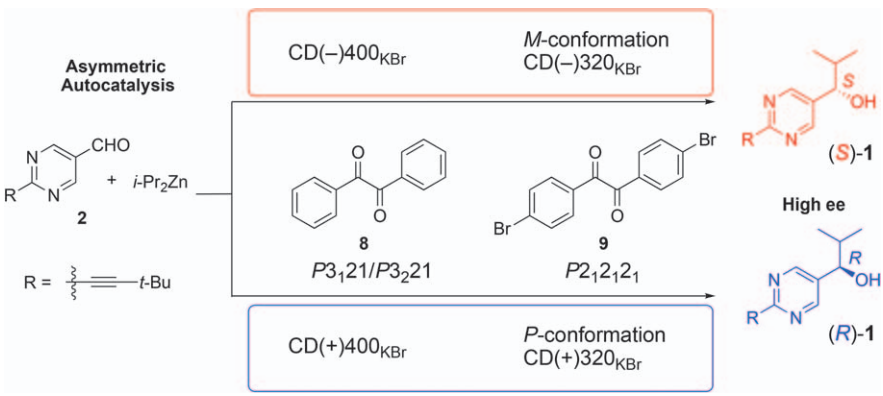

Scheme 3.10 Asymmetric autocatalysis initiated by chiral crystals of benzil derivatives.

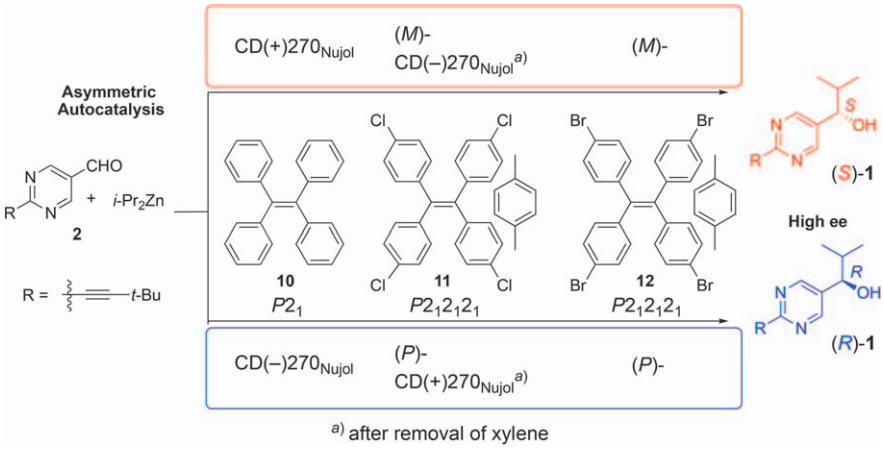

Scheme 3.11 Asymmetric autocatalysis initiated by chiral crystals of a simple hydrocarbon.

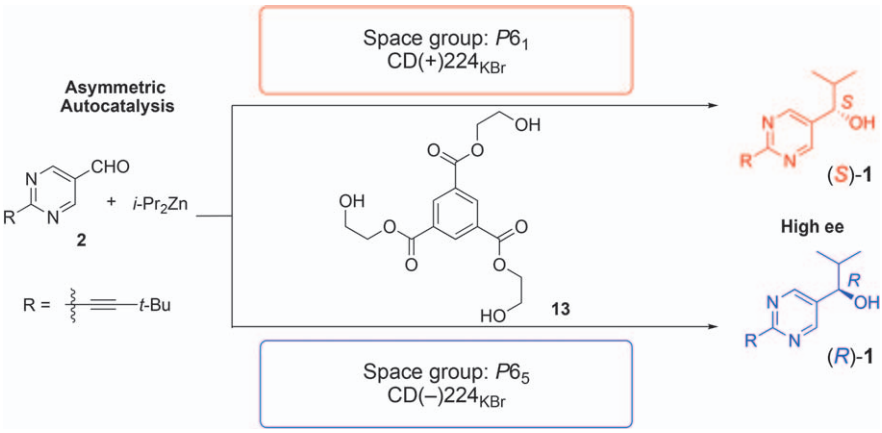

Scheme 3.12 Asymmetric autocatalysis initiated by chiral crystals of benzene triester.

The $P6_1$ crystal gives the (*R*)-product and $P6_5$ gives the (*S*)-product with good reproducibility under asymmetric autocatalysis (Scheme 3.12).[72]

Dibutylhydroxytoluene (BHT) **14** is another example of a chiral crystal of an organic compound.[5,73] This antioxidant is present in many ether solvents as a stabilizer and must be removed in organometallic reactions because it often interferes with the reaction. However, little attention has been paid to the chirality of crystals of this compound. This compound forms a chiral crystal of $P2_12_12_1$. When the direction of the phenol group was considered in the two-helix tilt chirality scheme,[74] the *P* crystal showed a negative Cotton effect at 288 nm and gave the (*R*)-alkanol **1** under asymmetric autocatalysis, whereas the *M* crystal showed the opposite Cotton effect and selectivity (Scheme 3.13).[75]

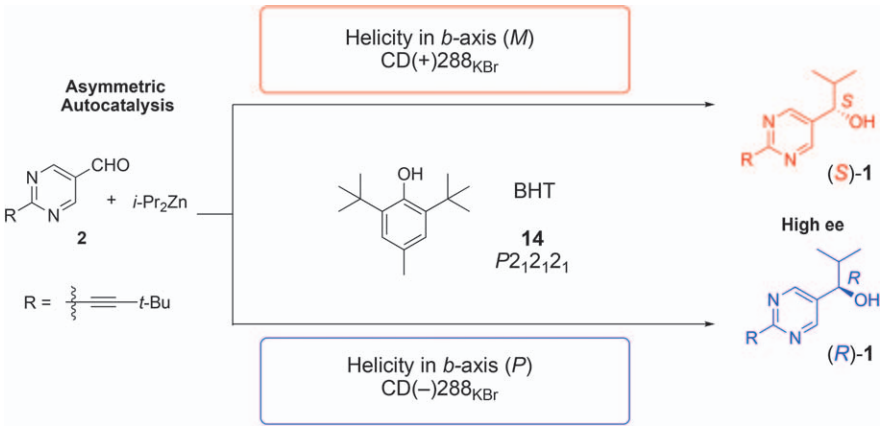

Scheme 3.13 Asymmetric autocatalysis initiated by chiral crystals of BHT.

3.3.5 Chiral Crystal of Amino Acid Related Compounds

Amino acids are the primary bioorganic molecules that make proteins. As is widely known, most of the amino acids in nature are L-amino acids, but the origin of this chirality remains a mystery. However, glycine **15**, the simplest of the amino acids, is an achiral amino acid because it has no side chain and two hydrogens at the α-carbon. Although glycine is the only achiral amino acid, it has chirality in crystals. Glycine has several polymorphs, with the β-form in $P2_1$[76] and the γ-form in $P3_1/P3_2$[77] being chiral.[78] The question of how the chirality of amino acid crystals is related to the chirality of the molecule is also interesting with respect to the homochirality of amino acids.[79]

The fact that γ-glycine crystals tend to form twins and that glycine absorbs only at short wavelengths makes chirality discrimination by X-ray diffraction and CD somewhat difficult.[80] However, it has been shown that $P3_1$ and $P3_2$ γ-glycine have positive and negative Cotton effects, respectively, around 215 nm in KBr. The $P3_1$ crystals give (*R*)-alkanol **1**, whereas the $P3_2$ crystals give (*S*)-alkanol, under autocatalysis (Scheme 3.14).[81]

Hippuric acid **16** and *N*-(2-thienylcarbonyl)glycine **17**, both derivatives of glycine, have also been found to form chiral crystals and to act as chiral inducers of asymmetric autocatalysis.[82,83] In particular, the selectivity of *N*-(2-thienylcarbonyl)glycine has been discussed based on a model of the interaction of pyrimidylalkanols with crystal surfaces.

Another interesting phenomenon noted with glycine is its sulfate salt, triglycine sulfate (TGS) **18**, which is known to be a ferroelectric crystal that forms polar crystals of $P2_1$ and reverses its polarization with an electric field.[84–87] This space group $P2_1$ is also associated with chiral crystals, and this polarity transformation is also a chirality inversion. Using this fact, we have recently succeeded in controlling the selectivity of asymmetric autocatalysis by applying an electric field to TGS crystals (Scheme 3.15).[88]

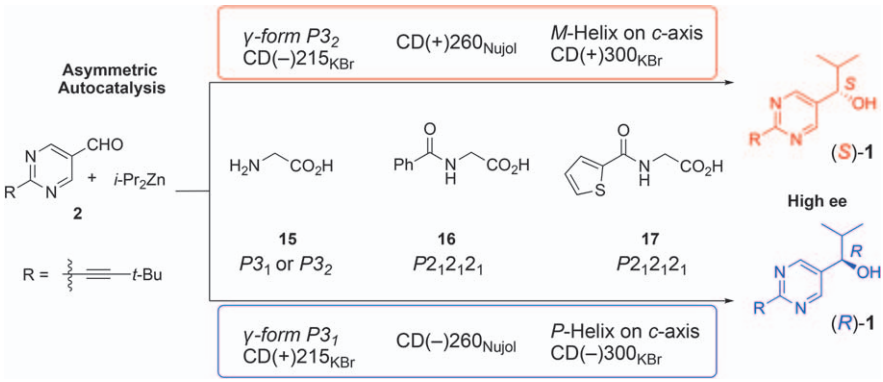

Scheme 3.14 Asymmetric autocatalysis initiated by chiral crystals of achiral glycine and their derivatives.

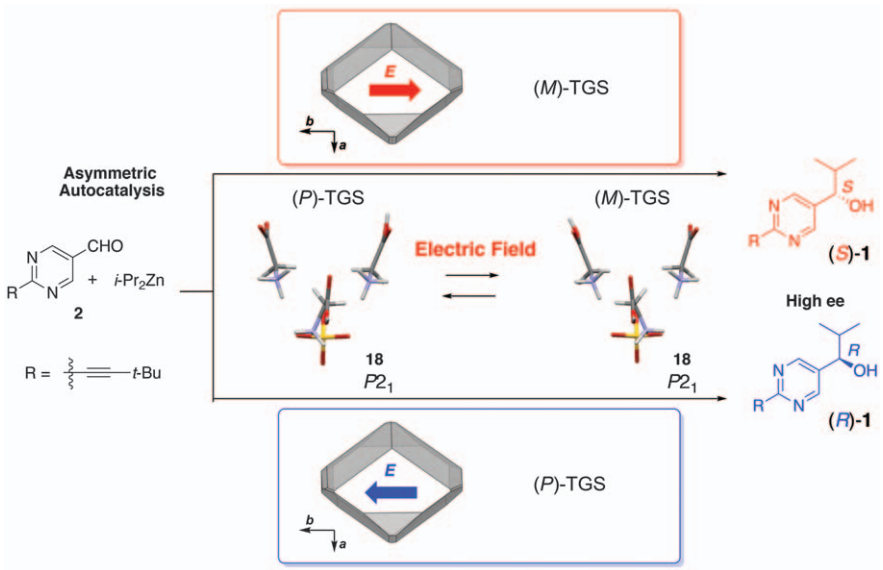

Scheme 3.15 Asymmetric autocatalysis initiated by a ferroelectric crystal of achiral triglycine sulfate. Controlling the selectivity by application of an electric field.

Enantiopure chiral compounds inevitably form chiral crystals, but there are many possibilities for racemic crystals. In some cases, each enantiomer forms a conglomerate as a separate crystal, but, more often, the enantiomers pair to give racemic crystals. However, just as an achiral compound can form a chiral crystal, it is also possible that the crystal structure has chirality even though it is racemic, with enantiomers of each other in the crystal; this is called a kryptoracemate or false conglomerate.[89,90] The sulfate salt of DL-serine **19** is one such rare example, and this racemic DL-serine crystal also acts as a chiral initiator for asymmetric autocatalysis (Scheme 3.16).[91]

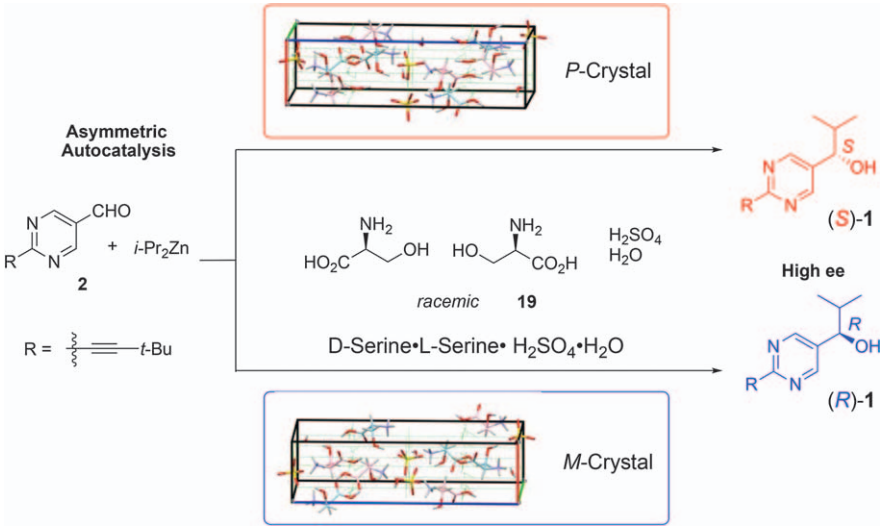

Scheme 3.16 Asymmetric autocatalysis initiated by kryptoracemate, a chiral crystal of racemic DL-serine.

3.3.6 Chiral Crystal of Nucleic Acid Base Compounds

Nucleobases are the primary biomolecules that make up DNA and RNA. Some of these nucleobases also form chiral crystals. Cytosine forms chiral crystals with the $P2_12_12_1$ space group. The chirality of cytosine crystals can be determined from the CD spectrum of the solid state, although it should be noted that the shapes of the CD spectra in KBr and Nujol are so different that the signs are reversed. In Nujol, one of the crystals shows a negative Cotton effect at 250 nm, whereas a crystal with the same chirality shows a positive Cotton effect at 310 nm when measured in KBr. Autocatalysis initiated by chiral crystals of cytosine CD(−)250_{Nujol}-**20** afforded (*S*)-alkanol in high ee (Scheme 3.17).[92] Adenine dinitrate **21** also forms chiral crystals. In this case, crystals with CD(−)310_{Nujol} afforded (*S*)-alkanol and those with CD(−)310_{Nujol} afforded (*R*)-alkanol.[93]

It is also interesting to note that cytosine crystallizes from water as an achiral monohydrate crystal and that the chirality of the dehydrated crystal can be controlled by the method of dehydration and by the exposed face of the crystal. Cytosine monohydrate **20**·H_2O forms monoclinic $P2_1/c$ achiral crystals that grow in a parallelogram shape when viewed from its unique *b*-axis. The direction of the plane was distinguished from the inclination of the parallelogram; from there, the transformation to chiral anhydride crystals by heating and dehydration was repeated many times. As a result, we found that there is a correlation between the plane of dehydration and the chirality of the resulting powder.

Interestingly, the chirality of the crystals obtained by heating the same plane and by depressurization is reversed: CD(−) anhydrate **20** is obtained by heating the b_1-face, whereas CD(+) is obtained by depressurization of the

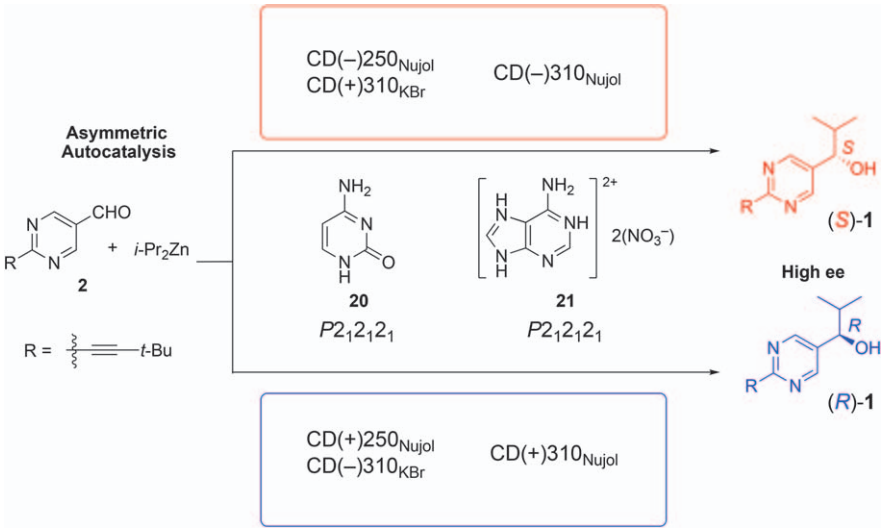

Scheme 3.17 Asymmetric autocatalysis initiated by nucleobases crystals.

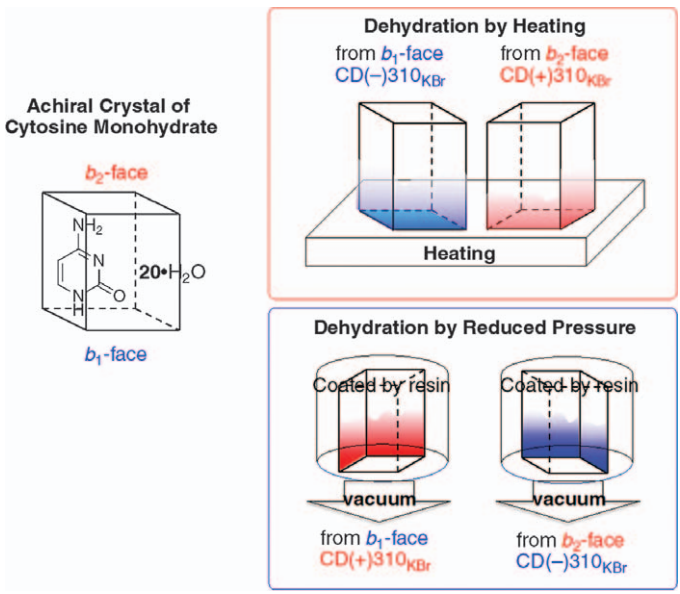

Scheme 3.18 Chiral crystal formation by dehydration of achiral cytosine monohydrate crystals.

same b_1-face (Scheme 3.18).[94,95] This may be due to the difference in the movement of water inside the crystals between dehydration by heating and dehydration by reduced pressure.

3.4 Chirality of Crystal Surfaces

Even if the crystal as a whole is achiral, it is possible that it does not have mirror-image symmetry if we focus on a particular face of the crystal. Just as an achiral planar molecule has enantiotopic *Re*- and *Si*-faces, an achiral crystal also has enantiotropic surfaces. For example, in a crystal whose space group point group is 2/*m*, there is mirror symmetry in the projections along the *a*- and *c*-axes, but only twice rotational symmetry in the projection along the *b*-axis, and the projections along the $+b$- and $-b$-axes are mirror images of each other (Figure 3.2). Even in the most symmetric cubic crystal, a face with all different *hkl* Miller indices, the face pair (*hkl*) and (–h–k–l) becomes an enantiotropic face pair.

The pyrimidyl alkanol derivative **23** also acts as an asymmetric autocatalyst. The corresponding aldehyde **22** forms an achiral crystal of space group $P\bar{1}$. However, when one of the faces is covered with epoxy resin and reacted with a zinc reagent as a vapor from one enantiotropic surface, the product alkanol is formed with high ee, with the selectivity depending on the crystal surface (Scheme 3.19).[96] Note that aldehyde **2** also forms achiral crystals; however, in this case, crystals of **2** typically form merohedral twinning needle crystals, making it difficult to determine the crystal face. The reaction of powdered crystal of aldehyde **1** with diisopropylzinc afforded a stochastic distribution of both enantiomers by a random attack on both enantiotropic faces.[97]

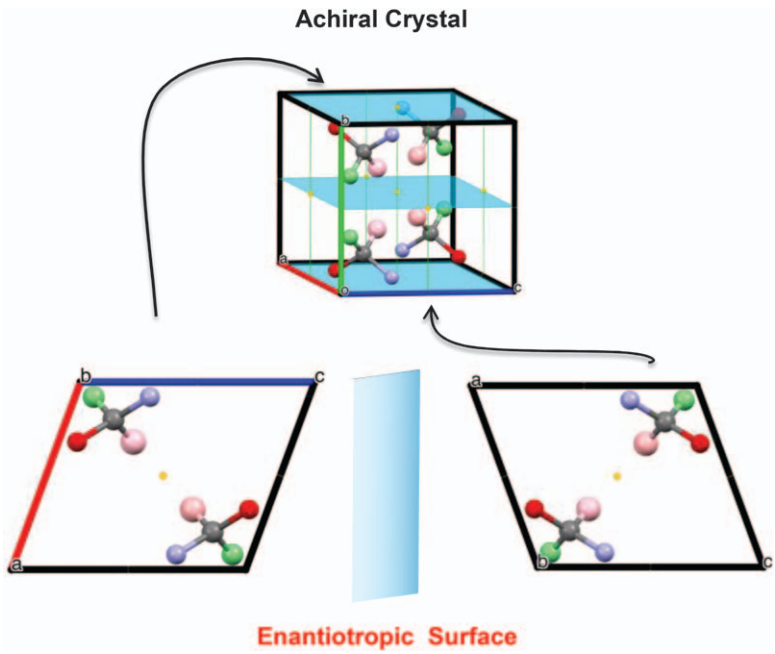

Figure 3.2 Enantiotropic surface of an achiral crystal.

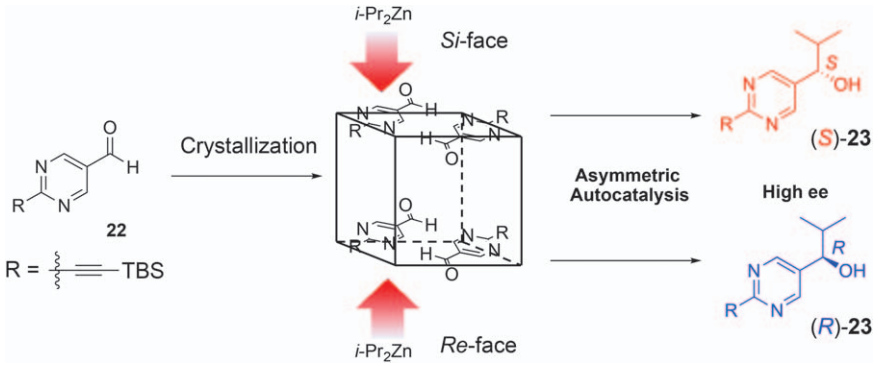

Scheme 3.19 Asymmetric autocatalysis initiated by the crystal surface.

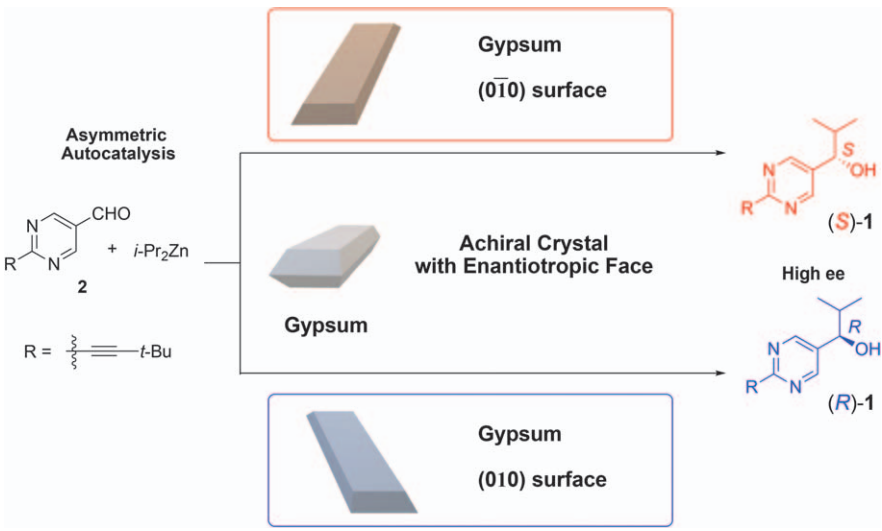

Scheme 3.20 Asymmetric autocatalysis initiated by adsorption on a chiral surface of an achiral mineral gypsum.

Enantiotropic surfaces are also found in inorganic minerals. Gypsum is an achiral crystal that completely cleaves at just the enantiotropic surface, and when the surface of this crystal is coated with aldehyde **2** and reacted with a zinc reagent in the gas phase, a face-correlated alkanol is obtained (Scheme 3.20).

3.5 Summary

In this chapter, we have shown that the crystal chirality and surface chirality of various minerals, achiral or racemic organic compounds, can affect the selectivity of asymmetric autocatalysis. These results indicate that the selectivity of molecular chirality induced by crystal chirality is not a unique case, but rather a widespread phenomenon. The reason why crystal and

surface chirality is not particularly noticed in everyday reactions is that the bias induced directly is small, but it is not zero. The recognition power of asymmetric amplification through asymmetric autocatalysis is very high, allowing the chirality of these crystals to be effectively detected as products with high ee. Asymmetric autocatalysis has the potential to be a method for detecting surface chirality that is not normally recognized. These results also indicate that a scenario in which crystal or surface chirality is the origin of molecular homochirality may be possible.

Acknowledgements

This work was financially supported by JSPS KAKENHI (15H03781, 18H04518, 19K05482, 19K22190, and 20H04674).

References

1. D. K. Kondepudi, R. J. Kaufman and N. Singh, *Science*, 1990, **250**, 975–976.
2. D. K. Kondepudi and K. Asakura, *Acc. Chem. Res.*, 2001, **34**, 946–954.
3. C. Viedma, *J. Cryst. Growth*, 2004, **261**, 118–121.
4. C. Viedma, *Phys. Rev. Lett.*, 2005, **94**, 065504.
5. D. T. McLaughlin, T. P. T. Nguyen, L. Mengnjo, C. Bian, Y. H. Leung, E. Goodfellow, P. Ramrup, S. Woo and L. A. Cuccia, *Cryst. Growth Des.*, 2014, **14**, 1067–1076.
6. C. Xiouras, J. Van Aeken, J. Panis, J. H. Ter Horst, T. Van Gerven and G. D. Stefanidis, *Cryst. Growth Des.*, 2015, **15**, 5476–5484.
7. F. Yagishita, H. Ishikawa, T. Onuki, S. Hachiya, T. Mino and M. Sakamoto, *Angew. Chem., Int. Ed.*, 2012, **51**, 13023–13025.
8. R. R. E. Steendam, J. M. M. Verkade, T. J. B. van Benthem, H. Meekes, W. J. P. van Enckevort, J. Raap, F. P. J. T. Rutjes and E. Vlieg, *Nat. Commun.*, 2014, **5**, 5543.
9. S. Aiba, N. Takamatsu, T. Sasai, Y. Tokunaga and T. Kawasaki, *Chem. Commun.*, 2016, **52**, 10834–10837.
10. H. D. Flack, *Helv. Chim. Acta*, 2003, **86**, 905–921.
11. T. Matsuura and H. Koshima, *J. Photochem. Photobiol. C Photochem. Rev.*, 2005, **6**, 7–24.
12. E. Pidcock, *Chem. Commun.*, 2005, 3457–3459.
13. A. Elgavi, B. S. Green and G. M. J. Schmidt, *J. Am. Chem. Soc.*, 1973, **95**, 2058–2059.
14. B. S. Green, M. Lahav and D. Rabinovich, *Acc. Chem. Res.*, 1979, **12**, 191–197.
15. M. Sakamoto, *Chem. – Eur. J.*, 1997, **3**, 684–689.
16. K. Tanaka, F. Toda, E. Mochizuki, N. Yasui, Y. Kai, I. Miyahara and K. Hirotsu, *Angew. Chem., Int. Ed.*, 1999, **38**, 3523–3525.
17. F. Yagishita, M. Sakamoto, T. Mino and T. Fujita, *Org. Lett.*, 2011, **13**, 6168–6171.

18. M. Sakamoto, T. Iwamoto, N. Nono, M. Ando, W. Arai, T. Mino and T. Fujita, *J. Org. Chem.*, 2003, **68**, 942–946.
19. M. Sakamoto, M. Kato, Y. Aida, K. Fujita, T. Mino and T. Fujita, *J. Am. Chem. Soc.*, 2008, **130**, 1132–1133.
20. F. Yagishita, N. Takagishi, H. Ishikawa, Y. Kasashima, T. Mino and M. Sakamoto, *Eur. J. Org. Chem.*, 2014, **2014**, 6366–6370.
21. K. Soai, T. Shibata, H. Morioka and K. Choji, *Nature*, 1995, **378**, 767–768.
22. T. Shibata, S. Yonekubo and K. Soai, *Angew. Chem., Int. Ed.*, 1999, **38**, 659–661.
23. I. Sato, H. Urabe, S. Ishiguro, T. Shibata and K. Soai, *Angew. Chem., Int. Ed.*, 2003, **42**, 315–317.
24. K. Soai, T. Kawasaki and A. Matsumoto, *Symmetry*, 2019, 11, 694.
25. K. Soai, A. Matsumoto and T. Kawasaki, *Isr. J. Chem.*, 2021, **61**, 507–516.
26. K. Soai, *Proc. Jpn. Acad., Ser. B*, 2019, **95**, 89–110.
27. K. Soai, T. Kawasaki and A. Matsumoto, *Acc. Chem. Res.*, 2014, **47**, 3643–3654.
28. K. Soai, T. Kawasaki and A. Matsumoto, *Chem. Rec.*, 2014, 70–83.
29. T. Satyanarayana, S. Abraham and H. B. Kagan, *Angew. Chem., Int. Ed.*, 2009, **48**, 456–494.
30. D. G. Blackmond, C. R. McMillan, S. Ramdeehul, A. Schorm and J. M. Brown, *J. Am. Chem. Soc.*, 2001, **123**, 10103–10104.
31. D. G. Blackmond, *Chem. Rev.*, 2020, **120**, 4831–4847.
32. T. Gehring, M. Busch, M. Schlageter and D. Weingand, *Chirality*, 2010, **22**(Suppl. 1), E173–E182.
33. I. D. Gridnev, J. M. Serafimov, H. Quiney and J. M. Brown, *Org. Biomol. Chem.*, 2003, **1**, 3811–3819.
34. O. Trapp, S. Lamour, F. Maier, A. F. Siegle, K. Zawatzky and B. F. Straub, *Chem. – Eur. J.*, 2020, 15871–15880.
35. I. D. Gridnev and A. K. Vorobiev, *Bull. Chem. Soc. Jpn.*, 2015, **88**, 333–340.
36. G. Ercolani and L. Schiaffino, *J. Org. Chem.*, 2011, **76**, 2619–2626.
37. É. Dóka and G. Lente, *J. Am. Chem. Soc.*, 2011, **133**, 17878–17881.
38. B. Barabás, C. Zucchi, M. Maioli, K. Micskei and G. Pályi, *J. Mol. Model.*, 2015, **21**, 33.
39. J. Crusats, D. Hochberg, A. Moyano and J. M. Ribó, *ChemPhysChem*, 2009, **10**, 2123–2131.
40. T. Shibata, J. Yamamoto, N. Matsumoto, S. Yonekubo, S. Osanai and K. Soai, *J. Am. Chem. Soc.*, 1998, **120**, 12157–12158.
41. T. Kawasaki, M. Sato, S. Ishiguro, T. Saito, Y. Morishita, I. Sato, H. Nishino, Y. Inoue and K. Soai, *J. Am. Chem. Soc.*, 2005, **127**, 3274–3275.
42. I. Sato, D. Omiya, T. Saito and K. Soai, *J. Am. Chem. Soc.*, 2000, **122**, 11739–11740.
43. T. Kawasaki, M. Shimizu, D. Nishiyama, M. Ito, H. Ozawa and K. Soai, *Chem. Commun.*, 2009, 4396–4398.
44. T. Kawasaki, Y. Matsumura, T. Tsutsumi, K. Suzuki, M. Ito and K. Soai, *Science*, 2009, **324**, 492–495.

45. T. Kawasaki, Y. Okano, E. Suzuki, S. Takano, S. Oji and K. Soai, *Angew. Chem., Int. Ed.*, 2011, **50**, 8131–8133.
46. T. Kawasaki, H. Ozawa, M. Ito and K. Soai, *Chem. Lett.*, 2011, **40**, 320–321.
47. A. Matsumoto, S. Oji, S. Takano, K. Tada, T. Kawasaki and K. Soai, *Org. Biomol. Chem.*, 2013, **11**, 2928–2931.
48. A. Matsumoto, H. Ozaki, S. Harada, K. Tada, T. Ayugase, H. Ozawa, T. Kawasaki and K. Soai, *Angew. Chem., Int. Ed.*, 2016, **55**, 15246–15249.
49. W. A. Bonner, P. R. Kavasmaneck, F. S. Martin and J. J. Flores, *Science*, 1974, **186**, 143–144.
50. R. M. Hazen, T. R. Filley and G. A. Goodfriend, *Proc. Natl. Acad. Sci. U. S. A.*, 2001, **98**, 5487–5490.
51. M. Glazer, *J. Appl. Crystallogr.*, 2018, **51**, 915–918.
52. K. Soai, S. Osanai, K. Kadowaki, S. Yonekubo, T. Shibata and I. Sato, *J. Am. Chem. Soc.*, 1999, **121**, 11235–11236.
53. H. Niinomi, H. Miura, Y. Kimura, M. Uwaha, H. Katsuno, S. Harada, T. Ujihara and K. Tsukamoto, *Cryst. Growth Des.*, 2014, **14**, 3596–3602.
54. H. J. Simon and N. Bloembergen, *Phys. Rev.*, 1968, **171**, 1104–1114.
55. D. Xue and S. Zhang, *Chem. Phys. Lett.*, 1998, **287**, 503–508.
56. I. Sato, K. Kadowaki and K. Soai, *Angew. Chem., Int. Ed.*, 2000, **39**, 1510–1512.
57. I. Sato, K. Kadowaki, Y. Ohgo and K. Soai, *J. Mol. Catal. A: Chem.*, 2004, **216**, 209–214.
58. H. Shindo, Y. Shirota, K. Niki, T. Kawasaki, K. Suzuki, Y. Araki, A. Matsumoto and K. Soai, *Angew. Chem., Int. Ed.*, 2013, **52**, 9135–9138.
59. A. Matsumoto, H. Ozawa, A. Inumaru and K. Soai, *New J. Chem.*, 2015, **39**, 6742–6745.
60. E. C. Gyarfas and D. P. Mellor, *J. Phys. Chem.*, 1955, **59**, 296–297.
61. H. Ogino, M. Takahashi and N. Tanaka, *Bull. Chem. Soc. Jpn.*, 1970, **43**, 424–428.
62. I. Sato, K. Kadowaki, Y. Ohgo, K. Soai and H. Ogino, *Chem. Commun.*, 2001, 1022–1023.
63. H. Koshima, E. Hayashi, T. Matsuura, K. Tanaka, F. Toda, M. Kato and M. Kiguchi, *Tetrahedron Lett.*, 1997, **38**, 5009–5012.
64. H. Koshima, M. Nagano and T. Asahi, *J. Am. Chem. Soc.*, 2005, **127**, 2455–2463.
65. H. Koshima, M. Miyauchi and M. Shiro, *Supramol. Chem.*, 2001, **13**, 137–142.
66. T. Kawasaki, K. Jo, H. Igarashi, I. Sato, M. Nagano, H. Koshima and K. Soai, *Angew. Chem., Int. Ed.*, 2005, **44**, 2774–2777.
67. L. A. Cuccia, L. Koby, J. B. Ningappa and M. Dakessian, *J. Chem. Educ.*, 2005, **82**, 1043.
68. A. Matsumoto, T. Ide, Y. Kaimori, S. Fujiwara and K. Soai, *Chem. Lett.*, 2015, **44**, 688–690.
69. T. Kawasaki, Y. Harada, K. Suzuki, T. Tobita, N. Florini, G. Pályi and K. Soai, *Org. Lett.*, 2008, **10**, 4085–4088.
70. T. Kawasaki, M. Nakaoda, N. Kaito, T. Sasagawa and K. Soai, *Origins Life Evol. Biospheres*, 2010, **40**, 65–78.

71. I. Azumaya, D. Uchida, T. Kato, A. Yokoyama, A. Tanatani, H. Takayanagi and T. Yokozawa, *Angew. Chem., Int. Ed.*, 2004, **43**, 1360–1363.
72. T. Kawasaki, M. Uchida, Y. Kaimori, T. Sasagawa, A. Matsumoto and K. Soai, *Chem. Lett.*, 2013, **42**, 711–713.
73. M. Maze-Baudet, *Acta Crystallogr., Sect. B: Struct. Crystallogr. Cryst. Chem.*, 1973, **29**, 602–614.
74. I. Hisaki, T. Sasaki, N. Tohnai and M. Miyata, *Chem. – Eur. J.*, 2012, **18**, 10066–10073.
75. A. Matsumoto, S. Takeda, S. Harada and K. Soai, *Tetrahedron: Asymmetry*, 2016, **27**, 943–946.
76. Y. Iitaka, *Acta Crystallogr.*, 1960, **13**, 35–45.
77. Y. Iitaka, *Acta Crystallogr.*, 1961, **14**, 1–10.
78. K. Ishikawa, M. Tanaka, T. Suzuki, A. Sekine, T. Kawasaki, K. Soai, M. Shiro, M. Lahav and T. Asahi, *Chem. Commun.*, 2012, **48**, 6031–6033.
79. L. Addadi, Z. Berkovitch-Yellin, N. Domb, E. Gati, M. Lahav and L. Leiserowitz, *Nature*, 1982, **296**, 21–26.
80. K. Ishikawa, M. Tanaka, T. Suzuki, A. Sekine, T. Kawasaki, K. Soai, M. Shiro, M. Lahav and T. Asahi, *Chem. Commun.*, 2012, **48**, 6031–6033.
81. A. Matsumoto, H. Ozaki, S. Tsuchiya, T. Asahi, M. Lahav, T. Kawasaki and K. Soai, *Org. Biomol. Chem.*, 2019, **17**, 4200–4203.
82. T. Kawasaki, K. Suzuki, K. Hatase, M. Otsuka, H. Koshima and K. Soai, *Chem. Commun.*, 2006, **2**, 1869–1871.
83. D. J. Carter, A. L. Rohl, A. Shtukenberg, S. Bian, C. Hu, L. Baylon, B. Kahr, H. Mineki, K. Abe, T. Kawasaki and K. Soai, *Cryst. Growth Des.*, 2012, **12**, 2138–2145.
84. B. T. Matthias, C. E. Miller and J. P. Remeika, *Phys. Rev.*, 1956, **104**, 849–850.
85. A. Lurio and E. Stern, *J. Appl. Phys.*, 1960, **31**, 1125–1126.
86. S. N. Drozhdin and O. M. Golitsyna, *Phys. Solid State*, 2012, **54**, 905–910.
87. J. M. Hudspeth, D. J. Goossens, T. R. Welberry and M. J. Gutmann, *J. Mater. Sci.*, 2013, **48**, 6605–6612.
88. T. Kawasaki, Y. Kaimori, S. Shimada, N. Hara, S. Sato, K. Suzuki, T. Asahi, A. Matsumoto and K. Soai, *Chem. Commun.*, 2021, **57**, 5999–6002.
89. L. Fábián and C. P. Brock, *Acta Crystallogr., Sect. B: Struct. Sci.*, 2010, **66**, 94–103.
90. I. Bernal and S. Watkins, *Acta Crystallogr., Sect. C: Struct. Chem.*, 2015, **71**, 216–221.
91. T. Kawasaki, T. Sasagawa, K. Shiozawa, M. Uchida, K. Suzuki and K. Soai, *Org. Lett.*, 2011, **13**, 2361–2363.
92. T. Kawasaki, K. Suzuki, Y. Hakoda and K. Soai, *Angew. Chem., Int. Ed.*, 2008, **47**, 496–499.
93. H. Mineki, T. Hanasaki, A. Matsumoto, T. Kawasaki and K. Soai, *Chem. Commun.*, 2012, **48**, 10538–10540.
94. T. Kawasaki, Y. Hakoda, H. Mineki, K. Suzuki and K. Soai, *J. Am. Chem. Soc.*, 2010, **132**, 2874–2875.

95. H. Mineki, Y. Kaimori, T. Kawasaki, A. Matsumoto and K. Soai, *Tetrahedron: Asymmetry*, 2013, **24**, 1365–1367.
96. T. Kawasaki, S. Kamimura, A. Amihara, K. Suzuki and K. Soai, *Angew. Chem., Int. Ed.*, 2011, **50**, 6796–6798.
97. Y. Kaimori, Y. Hiyoshi, T. Kawasaki, A. Matsumoto and K. Soai, *Chem. Commun.*, 2019, 5223–5226.

CHAPTER 4

Absolute Asymmetric Synthesis in the Soai Reaction

KENSO SOAI,*[a,b] TSUNEOMI KAWASAKI[a] AND ARIMASA MATSUMOTO[c]

[a] Department of Applied Chemistry, Tokyo University of Science, Kagurazaka, Shinjuku-ku, Tokyo 162-8601, Japan; [b] Research Organization for Nano & Life Innovation, Waseda University, Wasedatsurumaki-cho, Shinjuku-ku, Tokyo 162-0041, Japan; [c] Department of Chemistry, Nara Women's University, Kita-Uoya Nishi-machi, Nara 630-8506, Japan
*Email: soai@rs.tus.ac.jp

4.1 Introduction

The origin of biomolecule homochirality has attracted much attention since Pasteur discovered molecular chirality.[1a] It is well known that organic reactions of achiral reagents always give a racemic mixture of chiral product without the intervention of any chiral factor. To illustrate the formation of racemates, we consider the reduction of acetophenone (methylphenyl ketone) with sodium borohydride ($NaBH_4$) without the intervention of any chiral factor. Attack of the hydride of $NaBH_4$ from the *Re*-face of acetophenone affords (*R*)-1-phenylethanol, while attack from the *Si*-face of acetophenone affords (*S*)-alkanol. The probability of *Re*- and *Si*-face attack is equal (1 : 1), and the number of molecules is huge (laboratory scale of 1 mmol is roughly 10^{20} molecules); thus, the product, 1-phenylethanol, is generated as a practically 1 : 1 mixture of *R*- and *S*-enantiomers. Such a mixture is termed a racemate.

Catalysis Series No. 43
Asymmetric Autocatalysis: The Soai Reaction
Edited by Kenso Soai, Tsuneomi Kawasaki and Arimasa Matsumoto

Published by the Royal Society of Chemistry, www.rsc.org

One of the proposed theories for the origins of homochirality is spontaneous absolute asymmetric synthesis without the intervention of any chiral factor.[2a,b] In the late 19th century, Pearson conceived the formation of enantioenriched chiral molecules by random fluctuations.[2b] Mills presented a mathematical equation describing statistical fluctuations of the number of enantiomers in so-called racemic mixtures that showed that the ee becomes very low as the number of molecules in the system increases.[2c]

In 1953, Frank described a theoretical reaction model[2d] without referring to a chemical structure, in which a chiral molecule catalyzes the production of further molecules of itself with the same absolute structure while suppressing the formation of its antipode. According to this mechanism,[2d] an initial small imbalance of enantiomers becomes overwhelming. Caglioti *et al.* described a mechanism of how the critical first chiral molecule could lead to homochirality in conjunction with a suitable amplification mechanism as exemplified by the Soai reaction.[2e]

Despite the considerations on the spontaneous absolute asymmetric synthesis based on statistical fluctuations as described above, no product ee has been detected; *i.e.*, the ee remains far below the detection level. Thus, it has been a challenging dream of organic chemists to realize the absolute asymmetric synthesis of chiral compounds with significant ee without the intervention of any chiral factor.

4.2 Asymmetric Autocatalysis with Amplification of Enantiomeric Excess: The Soai Reaction

Asymmetric autocatalysis is a reaction in which a chiral product acts as a chiral catalyst for its own formation.[3] The process constitutes an automultiplication of the chiral compound.

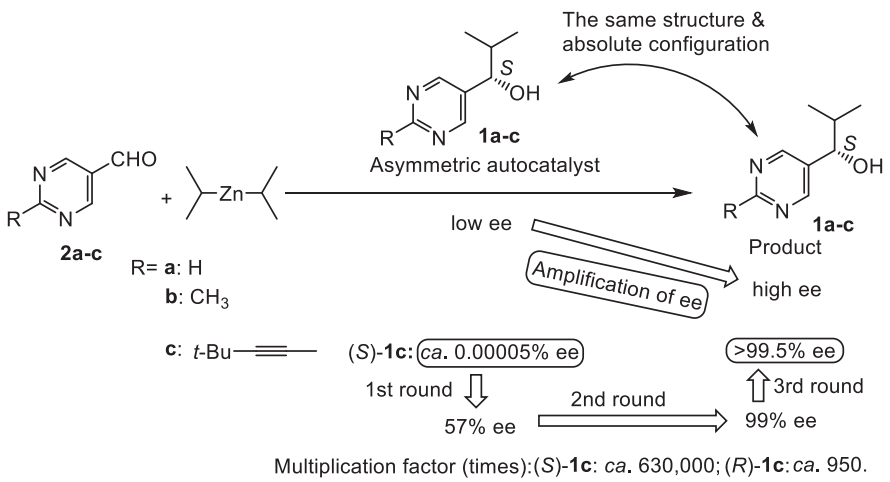

Scheme 4.1 Asymmetric autocatalysis of 5-pyrimidyl alkanols with amplification of enantiomeric excess (ee). The Soai reaction.

In 1995, Soai *et al.* reported a highly efficient asymmetric autocatalysis of 5-pyrimidyl alkanol with amplification of ee (see Scheme 4.1).[4a] Starting with (*S*)-3-alkynyl-5-pyrimidyl alkanol with very low ee (*ca.* 0.00005%) as an asymmetric autocatalyst,[4b] the reaction between 2-alkynyl-5-pyrimidyl alkanol and diisopropylzinc (*i*-Pr_2Zn) afforded (*S*)-pyrimidyl alkanol with the ee amplified to 57%. A second asymmetric autocatalysis using (*S*)-pyrimidyl alkanol with 57% ee gave the same (*S*)-alkanol with 99% ee. With the latter (*S*)-alkanol, a third asymmetric autocatalysis afforded the same alkanol with very high ee (>99.5%).

During these three consecutive asymmetric autocatalysis processes, the initial very slight excess of (*S*)-pyrimidyl alkanol **1c** was automultiplied by a factor of *ca.* 630 000 times, while the initial slightly minor (*R*)-enantiomer **1c** was automultiplied by a factor of *ca.* 950 times.[4b]

These results demonstrated that there is a chemical reaction in which an initial very slight enantiomeric imbalance becomes predominant by the mechanism of asymmetric autocatalysis with amplification of ee. Mislow first referred to the above reaction as the Soai reaction.[2a]

Several theories of the origins of chirality of organic compounds have been proposed.[5] However, the ee values induced by the proposed mechanisms have often been very low and the linkage between the very low ee and high ee observed in nature has been missing. The Soai reaction[3] has also been invoked to describe the origins of homochirality.

We have reported asymmetric autocatalysis in the reaction between pyrimidine-5-carbaldehyde and *i*-Pr_2Zn triggered by amino acids with low ee,[6a,b] chiral inorganic crystals[6c–e] such as quartz,[6c] circularly polarized light (CPL),[6f,g] chiral organic crystals composed of achiral compounds,[7] and chiral isotopomers[8] such as carbon ($^{13}C/^{12}C$),[8c] nitrogen ($^{15}N/^{14}N$),[8d] oxygen ($^{18}O/^{16}O$),[8e] and hydrogen (D/H).[8f,g] Pyrimidyl alkanols with significant ee values were obtained with the absolute configurations determined by the absolute configurations of the chiral triggers. A mechanistic study on the asymmetric autocatalysis initiated by hydrogen (D/H) isotopomer has been reported by Blackmond *et al.*[8h]

4.3 Absolute Asymmetric Synthesis in The Soai Reaction

Based on the results on asymmetric autocatalysis with significant amplification of ee as described above, we examined absolute asymmetric synthesis without the intervention of any chiral factor.[9] That is, the reaction between pyrimidine-5-carbaldehyde and *i*-Pr_2Zn in the absence of added chiral influence. We postulated that the initial uncatalyzed slow reaction would give (*R*)- and (*S*)-isopropylzinc alkoxide of pyrimidyl alkanol with statistical fluctuations of enantiomeric imbalances. This initial formation of the alkoxide with enantiomeric imbalance would, through asymmetric autocatalysis, lead to an amplification of the ee to afford enantioenriched products with detectable ee values (see Scheme 4.2).

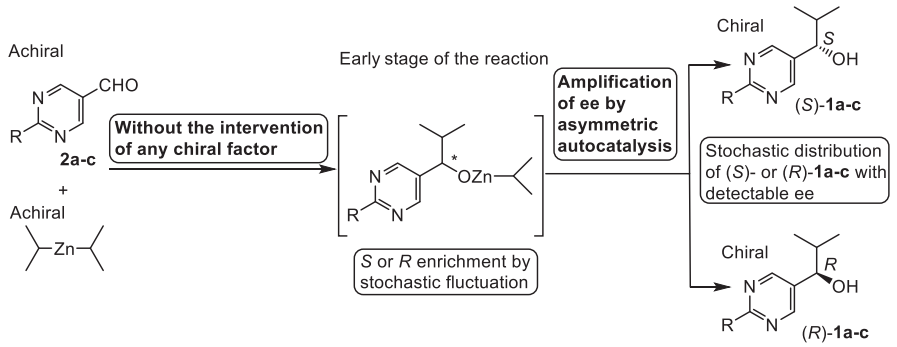

Scheme 4.2 Absolute asymmetric synthesis without the intervention of any chiral factor in conjunction with asymmetric autocatalysis, the Soai reaction.

To illustrate this idea, one can consider a situation in which a coin is tossed 100 times. According to the statistics theory, the probability of exactly 50 heads and 50 tails being recorded is only 8%. That is, there is a 92% probability of the number of either heads or tails being in excess (*e.g.*, 51 to 49 or 52 to 48, *etc.*).

In the initial stage of the reaction, when 99 molecules of the product are formed, the minimum ee ratio is 50 : 49; *i.e.*, $(50-49)/(50+49) = 1/99$, which is greater than 1% ee. When 999 molecules are formed, the minimum is $(500-499)/(500+499) = 1/999$, which is greater than 0.1% ee. Then, the minimum ee ratio of 999 999 molecules, *i.e.*, near one million, should be 1/999 999, which is greater than 0.0001% ee. These ee values are above the threshold (*ca.* 0.00005% ee)[4b] of asymmetric autocatalysis of 2-alkynyl-5-pyrimidyl alkanol described in the previous section.

Although it has not yet been established the exact number of asymmetric autocatalyst centers (*i.e.*, isopropylzinc alkoxide of pyrimidyl alkanol) required for asymmetric autocatalysis with amplification of ee to begin, considering the proposed aggregates of asymmetric autocatalysts, *i.e.*, dimer, tetramer, and oligomer, we postulate that the asymmetric autocatalysis with amplification of ee begins concurrently with the initial uncatalyzed formation of a small number of isopropylzinc alkoxide of pyrimidyl alkanol molecules with stochastic enantiomeric imbalance.

With regard to the initial stochastic distributions of enantiomers in the reaction between achiral reagents to form a chiral product without the intervention of any chiral factor, essentially all reactions are considered to have the same or similar situations. However, unless the initial enantiomeric imbalance is amplified, with the increase in the number of the product according to the law of large numbers,[2c] the ee of the product quickly approaches to below the detection level, *i.e.*, so-called racemate. This is the behavior of usual reactions that always afford racemic products.

The challenging theme is whether the Soai reaction is capable of producing enantioenriched products by amplifying the ee of the initial stochastic fluctuations of the product in the reaction between pyrimidine-5-carbaldehyde and *i*-Pr_2Zn without the intervention of any chiral factor.

4.3.1 Absolute Asymmetric Synthesis Enabled by the Soai Reaction in Solution, in the Presence of Achiral Silica Gel and in the Presence of Achiral Amines

Indeed, we have examined the reaction between pyrimidine-5-carbaldehyde and *i*-Pr_2Zn without the addition of any chiral substance, *i.e.*, chiral trigger. As anticipated, spontaneous absolute asymmetric synthesis led to the formation of enantioenriched pyrimidyl alkanol of either *S*- or *R*-absolute configuration from the reaction between pyrimidine-5-carbaldehyde **2** with *i*-Pr_2Zn without the addition of any chiral substance. As described in a patent application for this absolute asymmetric synthesis lodged in 1996,[9a] enantioenriched (*S*)-pyrimidyl alkanol **1a**,**b** or (*R*)-pyrimidyl alkanol **1a**,**b** are formed in the reaction without adding any chiral substance.[9a]

When *i*-Pr_2Zn was reacted with aldehyde **2c** in a mixed ether/toluene solvent in the absence of added chiral substance, (*S*)- and (*R*)-pyrimidyl alkanol **1c** were formed 19 and 18 times, respectively, in a total of 37 reactions (see Figure 4.1a),[9b] reflecting a stochastic distribution of *S*- and *R*-enantiomers of **1c**. Enantioenriched zinc alkoxide of pyrimidyl alkanol **1c** is likely to be initially produced through statistical fluctuation and this slight ee imbalance is subsequently amplified by asymmetric autocatalysis to give (*S*)- or (*R*)-**1** with detectable ee values.[9b] Moreover, a similar stochastic distribution of (*S*)- or (*R*)-alkanol **1c** was observed for the reaction of aldehyde **2c** and *i*-Pr_2Zn in the presence of achiral amorphous silica gel, which is used as the stationary phase for column chromatography (Figure 4.1b).[9c] Soai *et al.* reported that achiral amines promote the addition of dialkylzincs to aldehydes;[9d] thus, the reaction between aldehyde **2c** and *i*-Pr_2Zn afforded (*S*)- or (*R*)-alkanol **1c** with stochastic distribution in the presence of achiral amines (Figure 4.1c).[9e] A similar stochastic distribution of the product, *i.e.*, (*S*)- or (*R*)-**1b**, has also been reported by Singleton *et al.* for the reaction of pyrimidine-5-carbaldehyde **2b** and *i*-Pr_2Zn.[9f]

These results establish the general principle that the reaction between pyrimidine-5-carbaldehydes and *i*-Pr_2Zn can allow spontaneous absolute asymmetric synthesis.[9g–j]

4.3.2 Absolute Asymmetric Synthesis by the Soai Reaction Under Solid–Vapor Conditions

We previously described systems that enable absolute asymmetric synthesis in solution (see the previous section). We here examine heterogeneous conditions under which absolute asymmetric synthesis can be achieved (see Scheme 4.3).[10]

Consider the system of solid aldehyde–vapor phase *i*-Pr_2Zn. For powder-like crystals of aldehyde, unlike under solution conditions, molecules of pyrimidine-5-carbaldehyde are essentially immobile. With regard to the *Re*- and *Si*-face of the aldehyde, their orientations are considered to be random.

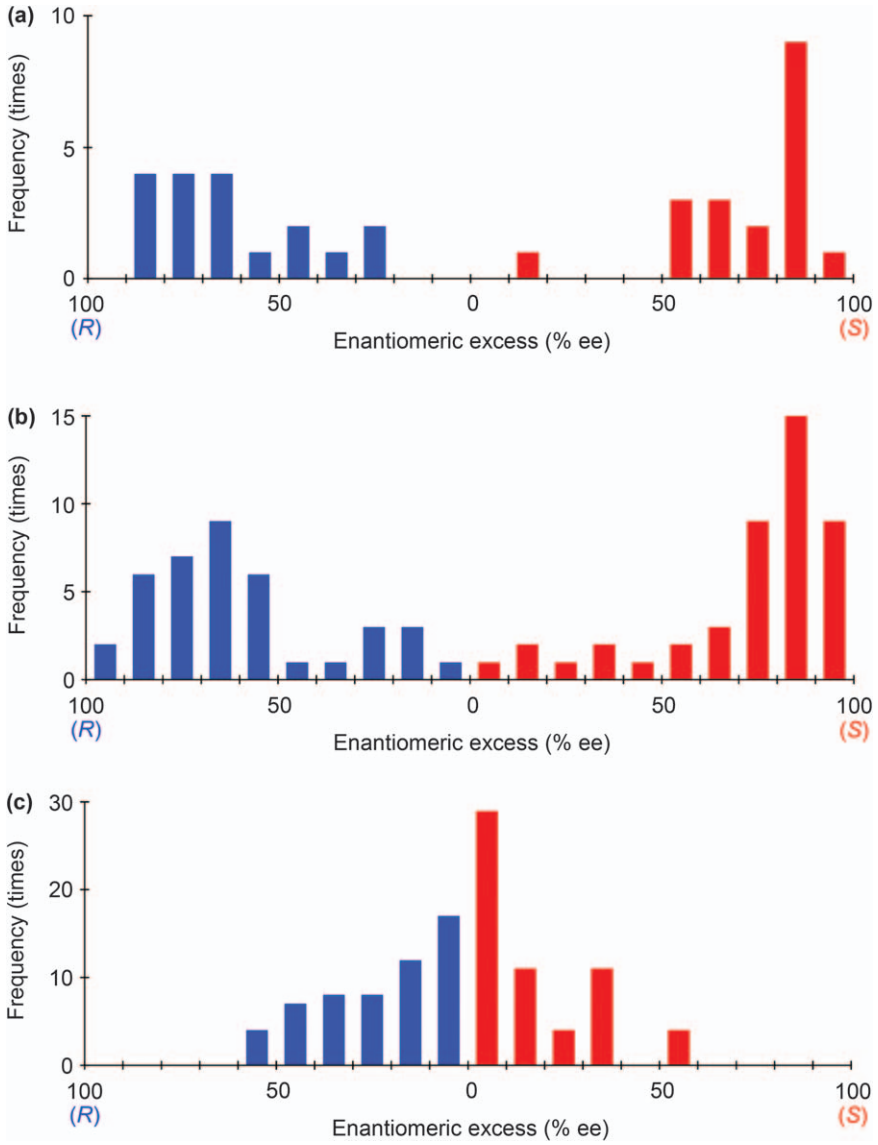

Figure 4.1 Frequency, absolute configurations, and ee histograms reflecting the formation of (*R*)- or (*S*)-pyrimidyl alkanol **1c** through absolute asymmetric synthesis from pyrimidine-5-carbaldehyde **2c** and *i*-Pr_2Zn without the intervention of any chiral factor: (a) in a mixed solvent of diethyl ether and toluene; (b) in toluene in the presence of achiral silica gel; (c) in toluene in the presence of achiral amine.

Moreover, the locations of crystals are different from each other compared to the vapor of *i*-Pr_2Zn and toluene. Thus, when the vapors of *i*-Pr_2Zn and toluene approach the powder-like aldehyde, aldehyde molecules in the most

advantageous position for the initiation of the uncatalyzed reaction afford either *R*- or *S*-enriched enantiomers of isopropylzinc alkoxide of pyrimidyl alkanol. As soon as the isopropylzinc alkoxide is formed, asymmetric autocatalysis with amplification of ee begins between pyrimidine-5-carbaldehyde and *i*-Pr_2Zn in the presence of toluene as a small amount of solvent on the surface of the powder-like crystal. Under heterogeneous conditions, relatively few reaction initiation sites are available and the reactions at these sites do not generally occur simultaneously. Once the reaction occurs, amplification of ee by asymmetric autocatalysis proceeds in a small amount of solvent that comes from the toluene vapor. Isopropylzinc alkoxide in the area of powder-like crystal that is most suitable for the propagation of asymmetric autocatalysis with amplification of ee finally dominates and determines the absolute configuration of the vast majority of pyrimidyl alkanol in a sample.

The above scenario was examined experimentally with a set of vials containing powders of sublimated pyrimidine-5-carbaldehyde **2c** in a desiccator, which were exposed to vapors of *i*-Pr_2Zn and toluene at room temperature.[10] In this system (*R*)- and (*S*)-pyrimidyl alkanol **1c** was formed 61 and 58 times, respectively, in a total of 129 reactions (**1c** was formed in 10 samples with an ee below the detection level of 0.5% ee), reflecting a stochastic distribution of (*S*)- and (*R*)-alkanol **1c** (See Figure 4.2). The ee values could be amplified to >99.5% by subsequent asymmetric autocatalysis.

Thus, solid–vapor phase conditions can also be conducive to spontaneous absolute asymmetric synthesis.

As described, the Soai reaction is capable of achieving absolute asymmetric synthesis without the intervention of any chiral factor.

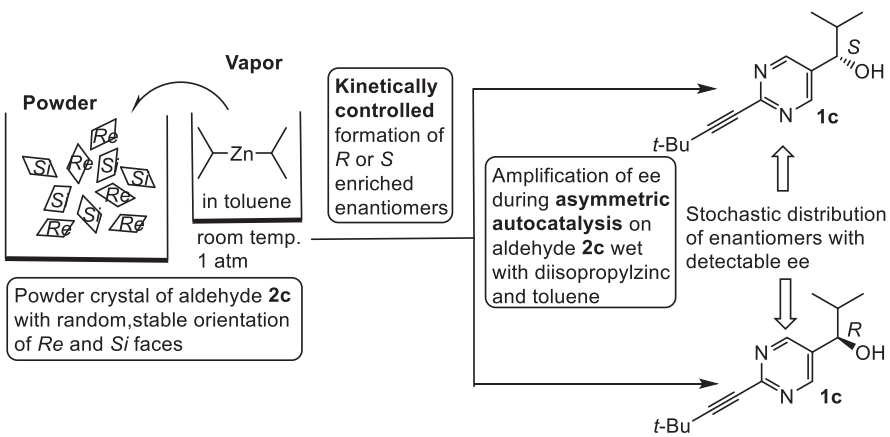

Scheme 4.3 Absolute asymmetric synthesis of pyrimidyl alkanol **1c** from a sublimated powder of pyrimidine-4-carbaldehyde **2c** and vapor of *i*-Pr_2Zn and toluene.

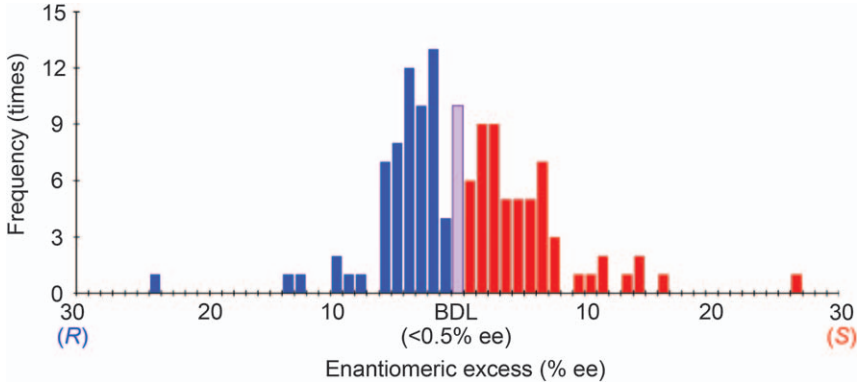

Figure 4.2 Frequency, absolute configurations, and ee histograms reflecting the formation of pyrimidyl alkanol **1c** through absolute asymmetric synthesis from sublimated powder pyrimidine-5-carbaldehyde **2c** and vapor of *i*-Pr_2Zn and toluene.

4.4 Conclusions

In a long history of organic reactions, it has been well accepted that, in the reaction between achiral reagents that form chiral product without the intervention of any chiral factor, the product always become racemate, *i.e.*, a mixture of two enantiomers of equal (1 : 1) ratio. Strictly speaking, the huge numbers of two enantiomers are not the same in most cases, but enantiomeric excesses are practically zero and far below the detection level.

In sharp contrast to the previously known organic reactions, the Soai reaction is capable of producing an enantioenriched product of significant ee with stochastic distribution of enantiomers in the reaction between pyrimidine-5-carbaldehyde and *i*-Pr_2Zn without the intervention of any chiral factor. The initial uncatalyzed formation of enantioenriched molecules of isopropylzinc alkoxide of pyrimidyl alkanol with stochastic fluctuation initiate asymmetric autocatalysis with amplification of ee. Either (*R*)- or (*S*)-pyrimidyl alkanols with significant, *i.e.*, above detection level, ees are formed as the product. Thus, we conclude that the Soai reaction enabled absolute asymmetric synthesis. It should be noted that Lennartson and Håkansson reported absolute asymmetric formation of a chiral five-coordinate copper complex.[11]

Acknowledgements

This work was financially supported by JSPS KAKENHI (15H03781, 18H04518, 19K05482 and 19K22190). Valuable discussion with Professor Kurt Mislow is gratefully acknowledged.

References

1. (a) L. Pasteur, *Ann. Chim. Phys.*, 1848, **24**, 442; (b) L. Pasteur, *Rev. Sci.*, 1884, **7**, 2.

2. (a) K. Mislow, *Collect. Czech. Chem. Commun.*, 2003, **68**, 849; (b) K. Pearson, *Nature*, 1898, **59**, 30; (c) W. H. Mills, *Chem. Ind.*, 1932, **51**, 750; (d) F. C. Frank, *Biochim. Biophys. Acta*, 1953, **11**, 459; (e) L. Caglioti, K. Micskei and G. Palyi, *Chirality*, 2011, **23**, 65.
3. (a) K. Soai and T. Kawasaki, *Top. Curr. Chem.*, 2008, **284**, 1; (b) K. Soai, T. Kawasaki and A. Matsumoto, *Chem. Rec.*, 2014, **14**, 70; (c) K. Soai, T. Kawasaki and A. Matsumoto, *Acc. Chem. Res.*, 2014, **47**, 3643; (d) K. Soai, T. Kawasaki and A. Matsumoto, *Tetrahedron*, 2018, **74**, 1973; (e) K. Soai, *Proc. Jpn. Acad., Ser. B*, 2019, **95**, 89; (f) K. Soai, T. Kawasaki and A. Matsumoto, *Symmetry*, 2019, **11**, 694; (g) K. Soai, A. Matsumoto and T. Kawasaki, *Isr. J. Chem.*, 2021, **61**, 507; (h) D. G. Blackmond, *Chem. Rev.*, 2020, **120**, 4831; (i) T. Buhse, J.-M. Cruz, M. E. Noble-Terán, D. Hochberg, J. M. Ribó, J. Crusats and J.-C. Micheau, *Chem. Rev.*, 2021, **121**, 2147.
4. (a) K. Soai, T. Shibata, H. Morioka and K. Choji, *Nature*, 1995, **378**, 767; (b) I. Sato, H. Urabe, S. Ishiguro, T. Shibata and K. Soai, *Angew. Chem., Int. Ed.*, 2003, **42**, 315; (c) T. Kawasaki, M. Nakaoda, Y. Takahashi, Y. Kanto, N. Kuruhara, K. Hosoi, I. Sato, A. Matsumoto and K. Soai, *Angew. Chem., Int. Ed.*, 2014, **53**, 11199.
5. (a) M. Bolli, R. Micura and A. Eschenmoser, *Chem. Biol.*, 1997, **4**, 309; (b) B. L. Feringa and R. A. van Delden, *Angew. Chem., Int. Ed.*, 1999, **38**, 3418; (c) Y. Inoue, *Chem. Rev.*, 1992, **92**, 741; (d) I. Weissbuch and M. Lahav, *Chem. Rev.*, 2011, **111**, 3236; (e) K.-H. Ernst, *Phys. Status Solidi*, 2012, **249**, 2057; (f) J. M. Ribó, J. Crusats, F. Sagués, J. Claret and R. Rubires, *Science*, 2001, **292**, 2063; (g) R. M. Hazen and D. S. Sholl, *Nat. Mater.*, 2003, **2**, 367; (h) A. Guijarro and M. Yus, *The Origin of Chirality in the Molecules of Life*, Royal Society of Chemistry, Cambridge, 2009.
6. (a) T. Shibata, J. Yamamoto, N. Matsumoto, S. Yonekubo, S. Osanai and K. Soai, *J. Am. Chem. Soc.*, 1998, **120**, 12157; (b) I. Sato, Y. Ohgo, H. Igarashi, D. Nishiyama, T. Kawasaki and K. Soai, *J. Organomet. Chem.*, 2007, **692**, 1783; (c) K. Soai, S. Osanai, K. Kadowaki, S. Yonekubo, T. Shibata and I. Sato, *J. Am. Chem. Soc.*, 1999, **121**, 11235; (d) H. Shindo, Y. Shirota, K. Niki, T. Kawasaki, K. Suzuki, Y. Araki, A. Matsumoto and K. Soai, *Angew. Chem., Int. Ed.*, 2013, **52**, 9135; (e) I. Sato, K. Kadowaki and K. Soai, *Angew. Chem., Int. Ed.*, 2000, **39**, 1510; (f) T. Kawasaki, M. Sato, S. Ishiguro, T. Saito, Y. Morishita, I. Sato, H. Nishino, Y. Inoue and K. Soai, *J. Am. Chem. Soc.*, 2005, **127**, 3274; (g) I. Sato, R. Sugie, Y. Matsueda, Y. Furumura and K. Soai, *Angew. Chem., Int. Ed.*, 2004, **43**, 4490.
7. (a) A. Matsumoto, H. Ozaki, S. Tsuchiya, T. Asahi, M. Lahav, T. Kawasaki and K. Soai, *Org. Biomol. Chem.*, 2019, **17**, 4200; (b) T. Kawasaki, K. Suzuki, Y. Hakoda and K. Soai, *Angew. Chem., Int. Ed.*, 2008, **47**, 496; (c) T. Kawasaki, Y. Hakoda, H. Mineki, K. Suzuki and K. Soai, *J. Am. Chem. Soc.*, 2010, **132**, 2874; (d) H. Mineki, T. Hanasaki, A. Matsumoto, T. Kawasaki and K. Soai, *Chem. Commun.*, 2012, **48**, 10538; (e) T. Kawasaki, K. Suzuki, K. Hatase, M. Otsuka, H. Koshima and

K. Soai, *Chem. Commun.*, 2006, 1869; (f) T. Kawasaki, Y. Kaimori, S. Shimada, N. Hara, S. Sato, K. Suzuki, T. Asahi, A. Matsumoto and K. Soai, *Chem. Commun.*, 2021, **57**, 5999; (g) D. J. Carter, A. L. Rohl, A. Shtukenberg, S. D. Bian, C.-H. Hu, L. Baylon, B. Kahr, H. Mineki, K. Abe, T. Kawasaki and K. Soai, *Cryst. Growth Des.*, 2012, **12**, 2138; (h) T. Kawasaki, K. Jo, H. Igarashi, I. Sato, M. Nagano, H. Koshima and K. Soai, *Angew. Chem., Int. Ed.*, 2005, **44**, 2774; (i) T. Kawasaki, Y. Harada, K. Suzuki, T. Tobita, N. Florini, G. Palyi and K. Soai, *Org. Lett.*, 2008, **10**, 4085; (j) T. Kawasaki, T. Sasagawa, K. Shiozawa, M. Uchida, K. Suzuki and K. Soai, *Org. Lett.*, 2011, **13**, 2361.

8. (a) A. Horeau, A. Nouaille and K. Mislow, *J. Am. Chem. Soc.*, 1965, **87**, 4957; (b) H. Pracejus, *Tetrahedron Lett.*, 1966, **7**, 3809; (c) T. Kawasaki, Y. Matsumura, T. Tsutsumi, K. Suzuki, M. Ito and K. Soai, *Science*, 2009, **324**, 492; (d) A. Matsumoto, H. Ozaki, S. Harada, K. Tada, T. Ayugase, H. Ozawa, T. Kawasaki and K. Soai, *Angew. Chem., Int. Ed.*, 2016, **55**, 15246; (e) T. Kawasaki, Y. Okano, E. Suzuki, S. Takano, S. Oji and K. Soai, *Angew. Chem., Int. Ed.*, 2011, **50**, 8131; (f) I. Sato, D. Omiya, T. Saito and K. Soai, *J. Am. Chem. Soc.*, 2000, **122**, 11739; (g) T. Kawasaki, M. Shimizu, D. Nishiyama, M. Ito, H. Ozawa and K. Soai, *Chem. Commun.*, 2009, 4396; (h) N. A. Hawbaker and D. G. Blackmond, *ACS Cent. Sci.*, 2018, **4**, 776.
9. (a) K. Soai, T. Shibata and Y. Kowata, *Japan Kokai Tokkyo Koho*, *JP Pat.*, JP1997-268179, 1997. An abstract is readily available as JPH09268179 from the European Patent Office. http://worldwide.espacenet.com; (b) K. Soai, I. Sato, T. Shibata, S. Komiya, M. Hayashi, Y. Matsueda, H. Imamura, T. Hayase, H. Morioka, H. Tabira, J. Yamamoto and Y. Kowata, *Tetrahedron: Asymmetry*, 2003, **14**, 185; (c) T. Kawasaki, K. Suzuki, M. Shimizu, K. Ishikawa and K. Soai, *Chirality*, 2006, **18**, 479; (d) K. Soai, M. Watanabe and M. Koyano, *Bull. Chem. Soc. Jpn.*, 1989, **62**, 2124; (e) K. Suzuki, K. Hatase, D. Nishiyama, T. Kawasaki and K. Soai, *J. Systems Chem.*, 2010, **1**, 5; (f) D. A. Singleton and L. K. Vo, *Org. Lett.*, 2003, **5**, 4337; (g) G. Lente, *J. Phys. Chem. A*, 2005, **109**, 11058; (h) L. Caglioti, C. Hajdu, O. Holczknecht, L. Zékány, C. Zucchi, K. Micskei and G. Pályi, *Viva Origino*, 2006, **34**, 62; (i) D. Lavabre, J.-C. Micheau, J. Rivera Islas and T. Buhse, *Top. Curr. Chem.*, 2008, **284**, 67; (j) Y. Saito and H. Hyuga, *Top. Curr. Chem.*, 2008, **284**, 97.
10. Y. Kaimori, Y. Hiyoshi, T. Kawasaki, A. Matsumoto and K. Soai, *Chem. Commun.*, 2019, **55**, 5223.
11. A. Lennartson and M. Håkansson, *New J. Chem.*, 2015, **39**, 5936.

CHAPTER 5

Isotope Chirality and Cosmochemistry†

BÉLA BARABÁS,[a] ROBERT KURDI,[b] MARCO MAIOLI[c] AND GYULA PÁLYI*[d]

[a] Department of Mathematics, University of Technology and Economics, Műegyetem rkp. 3(H-ép.), H-1111 Budapest, Hungary; [b] Institute of Environmental Engineering, University of Pannonia, Egyetem u. 10., H-8200 Veszprém, Hungary; [c] Department of Mathematics, University of Modena and Reggio Emilia, Via Campi 213/B, I-41125 Modena, Italy; [d] Department of Life Sciences, University of Modena and Reggio Emilia, Via Campi 103, I-41125 Modena, Italy
*Email: gyula.palyi@unimore.it

5.1 Introduction

Substitution of achiral molecules by different isotopes of one (or more) of the constituent elements may generate centers of asymmetry in these molecules.[1] If chiral reagents or asymmetric physical fields are not present, these chiral isotopomers form as a ~1 : 1 mixture of their enantiomers, that is – racemates.[2,3] Laws of statistics, however, permit the evolution of more–less enantiomeric excesses in these racemic mixtures.[4–6] Such statistical excesses are enough to operate as inductors of chirality, leading to substantial amplification of the initial enantiomeric excess, in reactions which are sufficiently sensitive to asymmetric induction.[7–12] Presently only one such reaction type

†Electronic supplementary information (ESI) available: See DOI: 10.1039/9781839166273.

Catalysis Series No. 43
Asymmetric Autocatalysis: The Soai Reaction
Edited by Kenso Soai, Tsuneomi Kawasaki and Arimasa Matsumoto

Published by the Royal Society of Chemistry, www.rsc.org

is known, asymmetric autocatalysis (Soai reaction), which is chemically the addition of a dialkyl zinc reagent to N-heterocyclic aldehydes.[13–23] It has been experimentally demonstrated that Soai autocatalysis can amplify the chirality of either very low amounts of chiral auxiliaries[24,25] or even the statistical enantiomeric excesses of the 'racemate' of its own product, the autocatalyst,[26–30] to almost quantitative levels of enantiomeric excess (ee) in the product. This feature turned our attention to the potential effects of isotope chirality in this reaction.[4–6,31] In fact, it has been experimentally demonstrated that isotope-derived chirality of compounds where the only source of chirality is ^{2}H-,[32–34] ^{13}C-,[35,36] ^{15}N-,[37] or $^{17/18}$O-substitution[38,39] causes remarkable chiral induction in the Soai reaction.

These results acquire additional significance in light of recent cosmochemical observations regarding organic material in meteorites (chondrites), comets and cosmic dust.[40–45] An important and attractive direction of this field of cosmochemistry is the stereochemical analysis of chiral compounds in these space-derived objects. Sophisticated analyses unambiguously demonstrated significant enantiomeric excesses (up to 60% ee) of amino acids, hydroxy acids, and (even) carbohydrates which were found in these extraterrestrial bodies.[46–52]

Another interesting line of cosmochemical research concerning the stable isotopic composition of elements in such extraterrestrial samples[53] showed that in the organic compounds from these samples the relative ratio of the heavier isotopes of the light elements (typical for organic compounds, such as H, C, N, O) is much higher than the terrestrial average (see the ESI). The relative abundances of these heavier isotopes can be 3 to 4 orders of magnitude higher than that observed generally in Earth-derived samples.[45] It should be added that these 'anomalies' (with respect to terrestrial abundances, see also values in the ESI) are not general, and several extraterrestrial samples show isotope distributions which are very similar to those observed on Earth.[54]

Some outstanding extraterrestrial enrichment of the heavier isotopes include (for definition of δ see the ESI):

5.1.1 Carbon

Extraterrestrial dust samples showed depletion of ^{13}C ranging to modest accretion. $\delta(^{13}C) = -110 + 10$ to $+(30 + 10)$‰.[55] Cometary carbon isotopic ratios are more stable than those of hydrogen, relatively high heavy isotope enrichment is shown by $^{12}C/^{13}C = 80$ to 85 ($\delta = -48.93$ to 112.40‰).[56] Note that the terrestrial average is 89. Another observation reported $\delta(^{13}C) = -3$ to -17‰ in samples with fairly high deuterium enrichments.[57] In a noteworthy study the carbon isotopic composition of 34 amino acids from the Murchinson meteorite was determined. All compounds showed moderate, but positive values $\delta(^{13}C) = +4.9$ to $+52.8$‰.[50]

5.1.2 Hydrogen

δ(D) ranges from -300‰ to 7500‰ in different meteorites, reaching δ(D) up to 9000‰.[58] In the heterogeneous deuterium distribution from the

Sermakona meteorite domains with $\delta(D)$ up to $\delta(D) \sim 10.000‰$ were found.[59] Data from the comet-forming region showed high deuterium enrichment in the range of $\delta(D) = 500‰$ to 8146‰.[60] Metamorphosis of chondritic organic material can also lead to high deuterium enrichment (up to almost $\delta \sim 12.000‰$) by selective loss of light $^1H_2$ formed in Fe oxidation by water.[61] Extreme deuterium *vs.* ^1H ratios (10 to 30-times terrestrial values) were found in micrometeorites from central Antarctic snow.[62] Interplanetary dust particles collected from the Earth's atmosphere showed deuterium enrichments corresponding to ~50 times of the terrestrial value, $\delta \sim 49\,000‰$.[63] In the organic matter of the well-studied Murchinson meteorite a careful study found maximum $\delta(D) = 2280‰$, while in NWA 801 $\delta(D) = 7500‰$.[64] Another sample of extraterrestrial dust showed $\delta(D) = 5600 + 500‰$.[55]

Cometary deuterium distributions were thoroughly studied.[53] D/H ratios extend over a range from $D/H = (1.61 + 0.24) \times 10^{-4}$ [65] to 2×10^{-4} ($\delta = 33.71$ to 284.11‰).[66] We note that the terrestrial average of D/H ratio is 1.5576×10^{-4}.

5.1.3 Nitrogen

$\delta(^{15}N)$ ranging from 50‰ to 650‰ with eventual domains of $\delta(^{15}N) < 5000‰$ has been observed recently.[67] Organic matter in Murchinson meteorite showed maximum $\delta(^{15}N) = 2590‰$, and in NWA 801 $\delta(^{15}N) = 2200‰$.[64] Extraterrestrial dust samples from meteorites gave ^{15}N enrichment ranging from $\delta(^{15}N) = 360 + 10$ to $1520 + 240‰$.[55] Heavy isotope enrichment in 12 comets was found $^{14}N/^{15}N = 90$ to 190 ($\delta = 431.37$ to 2021.79‰[68]). We note that the terrestrial average of $^{14}N/^{15}N = 272$.

5.1.4 Oxygen

Relatively very high oxygen heavy isotope content, $\delta(^{17}O/^{18}O)$ ranging from 80‰ to 200‰ was found in interplanetary dust particles.[60] Oxygen heavy isotope enrichment in a comet was characterized by the ratio $^{16}O/^{18}O = 300 \pm 150$ ($\delta = -67‰$ to 1794‰[121]).

For the statistical study of these isotopic ''anomalies'' we needed a typical space-born object. The definition of such an object is very difficult, not only because of the large differences in the isotopic concentrations but also because of extremely high variations in other parameters too. Space-derived objects arriving to Earth are of very broad scale of size mass composition and velocity.[41,42,45,69,70] It should be noted, that according to spacecraft observations (*Explorer* 16, *Pioneer* 8 and 9, *Ulysses, Galileo*) approximately 11 to 66 kt material of cosmic (interplanetary) origin falls to Earth in one year.[71] The sum of masses of small particles is much more than that which arrives in the form of larger objects. From the viewpoint of the present study this is very important, since the evolution of statistical chirality effects can more sensitively evolve at smaller objects.[10,31,72] Therefore we shall deal in the following with the relatively small fraction of extraterrestrial objects. Realistically, in the range of 10^{-1} to 10^{-21} kg (hundred gram to attogram),

we have chosen as a representative (relatively light) a mass of 10^{-15} kg (1.0 picogram).[43,71,73–76] The interplanetary (interstellar?) dust particles are of fairly variable composition, contain roughly in average 10% organic material, OM.[45] From this OM 70 to 99% is insoluble, presently still not very well characterized polymer ('insoluble organic matter', IOM),[40,44,58,61,77,78] while the rest is composed of well-known 'soluble' organic compounds (SOC), several of which are basic molecules (or very similar to these) of terrestrial living organisms.[79,80] As a representative value we accepted that IOM is ~80% of OM. Considering these values, we have defined our 1 pg particles, as it contains 10% OM. which is composed of 80% IOM and 20% SOC pro piece of this 'typical stardust'. We calculated isotope chirality effects only in the SOC fraction, which has, consequently, the mass of 20 fg (20 femtogram). We shall consider these data as starting parameters in our calculations.

Here we present stochastic calculations in an effort to explore the magnitude of the effect of the new results of organic and isotopic Cosmochemistry on spontaneous statistical genesis of isotopically chiral structures in simple organic molecules which were (or might have been) involved in the prebiotic or early biotic phase of terrestrial life, at least according to present-day theories. The results will be discussed mainly in the context of the origin(s) of life and of biological chirality.

5.2 Results and Discussion

The selected data shown earlier in this paper and in the rich background literature, indicate that the 'deviations' of the isotopic composition of cosmic/interplanetary matter from the terrestrial standard (average) values are fairly variable and there are also large differences in the enrichment values from element to element. (We deal here only with H, C, N, and O as basic elements for organic chemistry. See ref. 80.) Considering these facts we performed our calculations on model molecules, where one or more of these, but only these, elements are in isotopically prochiral (chirogenic) position(s). The models were selected from simple space-born molecules[44,52,81–86] or are of closely related structures. Some of these are from the most fundamental molecules of terrestrial life[79] and (possibly) are structurally coincident with or at least correlated to organic molecules found in meteorites and/or in extraterrestrial dust particles. These, more–less arbitrarily selected, molecules are listed in Tables 5.1 and 5.2.

The literature on cosmic isotopic distributions gives most frequently the quantitative measure of enrichment or depletion of isotopes in δ [‰] units, calculated with respect to the terrestrial standard values. For our calculations these had to be converted to probability values (px for element X). Some representative values are shown in Table 5.3 together with the formula deduced for $\delta \Rightarrow pX$ conversion.

The stable isotopes of the four atoms, H, C, N, and O, show very asymmetric terrestrial distribution. Therefore we performed our analysis by

Table 5.1 Name, formula, molecular mass (MM [a.u.]), and isotopically prochiral (chirogenic) atoms (X^{CHIR}) in hydrocarbon and simple oxygenate model compounds.

Number	Name	Formulae	MM	X_{CHIR}
1	2-Methyl-*n*-butane	$(H_3C)_2CHCH_2CH_3$ $[C_5H_{12}]$	72.094	H_8C_2
2	Methyl-cyclo-hexane	$CH_2(CH_2CH_2)_2CH(CH_3)$ $[C_7H_{14}]$	98.110	H_8C_4
3	Ethylbenzene	$C_6H_5CH_2CH_3$ $[C_8H_{10}]$	106.078	H_2
4	Ethylene oxide	CH_2OCH_2 $[C_2H_4O]$	44.026	H_4
5	Ethanol	CH_3CH_2OH $[C_2H_6O]$	46.041	H_2
6	Glycolaldehyde	$HOCH_2CHO$ $[C_2H_4O_2]$	60.02113	H_2
7	Propanal	CH_3CH_2CHO $[C_3H_6O]$	58.041	H_2

Table 5.2 Formulae, molecular mass (MM [a.u.]), and isotopically prochiral (chirogenic) atoms (X_{CHIR}) in the biomolecular model compounds.

Number	Name	Formulae	MM	X_{CHIR}
8	Glycine	$H_2N–CH_2–COOH$ $[C_2H_5O_2N]$	75.032	H_2
9	Valine	$(H_3C)_2CH(NH_2)–COOH$ $[C_5H_{11}O_2N]$	117.079	H_6C_2
10	Leucine	$(H_3C)_2CH–CH_2–CH(NH_2)–COOH$ $[C_6H_{13}O_2N]$	131.095	H_8C_2
11	Proline	$HN–(CH_2)_3–CH–COOH$ $[C_5H_9O_2N]$	115.063	H_6
12	Lysine	$H_2N–(CH_2)_4–CH(NH_2)–COOH$ $[C_6H_{14}O_2N_2]$	146.106	H_8
13	Glutamic acid	$HOOC–(CH_2)_2–CH(NH_2)–COOH$ $[C_5H_9O_4N]$	147.053	H_4
14	TMDAB[a]	$H_3C–CH[N(CH_3)_2]–CH[N(CH_3)_2]–CH_3$ $[C_8H_{20}N_2]$	144.163	$H_{20}C_8N_2$
15	DAIB[b]	$H_2N–CH_2–CH(CH_3)–CH_2–NH_2$ $[C_4H_{12}N_2]$	88.100	$H_8C_2N_2$
16	Glycerol	$HO–CH_2–CH(OH)–CH_2–OH$ $[C_3H_8O_3]$	92.048	$H_6C_2O_2$
17	MMA[c]	$HOOC–CH(CH_3)–COOH$ $[C_4H_6O_4]$	118.027	$H_2C_2O_4$
18	DHA[d]	$HO–CH_2–C(O)–CH_2–OH$ $[C_3H_6O_3]$	90.032	H_4

[a]TMDAB = *N,N,N′,N′*-tetramethyl-2,3-diaminobutane.
[b]DAIB = 1,3-diamino-iso-butane.
[c]MMA = methylmalonic acid.
[d]DHA = 1,3-dihydroxyacetone.

supposing mono-isotopic substitution of homoisotopic species of the model compounds. These homoisotopic molecules were constructed from the most abundant stable isotopes (in the present cases the lightest ones) of the four elements. The distribution probabilities of these homoisotopic isotopomers (see Table 5.4) range from 90.49% (compound 14) to 97.50% (compound 4), thus they can be regarded rightfully as suitable representatives.

As the next step of our analysis we calculated for Set A the probabilities (p_{mono}) of monoisotopic substitution of the all-light homoisotopic species considering the numbers of the chirogenic atoms in each model molecule and the terrestrial abundance of the heavier isotopes. These data are shown in Table 5.5.

In a next step of the analysis we calculated the number of chiral molecules in 1 mol sample by the exchange of one chirogenic atom in the all-light

Table 5.3 Isotopic abundance probability factors (pX) corresponding to some typical δ [‰] values.[a]

Carbon (^{13}C)	
Terrestrial abundance, $\delta = 0$‰	$p_C = 0.01123720$
Cosmic abundance,[b] $\delta = 100$‰	$p_C = 0.01220993$
Hydrogen (^{2}H)	
Terrestrial abundance, $\delta = 0$‰	$p_H = 0.000155760$
Cosmic abundance,[b] $\delta = 10\,000$‰	$p_H = 0.001710429$
$\delta = 50\,000$‰	$p_H = 0.007881154$
Nitrogen (^{15}N)	
Terrestrial abundance, $\delta = 0$‰	$p_N = 0.00367600$
Cosmic abundance,[b] $\delta = 5000$‰	$p_N = 0.021580031$
Oxygen (^{17}O + ^{18}O)	
Terrestrial abundance, $\delta = 0$‰	$p_O = 0.00238500$
Cosmic abundance,[b] $\delta = 100$‰	$p_O = 0.002616635$

[a]The following sets of δ values were used in the calculations:
Set A: $\delta(H) = \delta(C) = \delta(N) = \delta(O) = 0$‰; see Tables 5.4–5.9.
Set B: $\delta(H) = 10\,000$‰. $\delta(C) = \delta(N) = \delta(O) = 0$‰; see Tables 5.10, 5.12 and 5.14.
Set C: $\delta(H) = 50\,000$‰. $\delta(C) = 100$‰. $\delta(N) = 5000$‰. $\delta(O) = 100$‰; see Tables 5.11, 5.13 and 5.15.
[b]'Cosmic abundance' means arbitrarily chosen δ values near to experimentally observed abundances of the heavier isotopes in extraterrestrial samples (for details see the text).

Table 5.4 Natural terrestrial abundances of light and heavy stable isotopes and their ratio (in the case of oxygen heavy means ^{17}O and ^{18}O together). Probabilities of all-light homoisotopic molecules (phomo).[a]

Set A	C	H	N	O
Atomic mass, light [a.u.]	12	1.007825	14.003074	15.994914
Light	0.988887867	0.999844264	0.996336471	0.997620575
Heavy	0.011112133	0.000155736	0.003663529	0.002379425
Ratio	0.011237	0.00015576	0.003677	0.0023851

No.	Number of atoms in a molecule, compounds **1–18**				Probability of all-light homoisotopic molecules (p_{homo})
1	5	12	0	0	0.94389472
2	7	14	0	0	0.92274643
3	8	10	0	0	0.9130614
4	2	4	0	1	0.97496479
5	2	6	0	1	0.97466114
6	2	4	0	2	0.97264494
7	3	6	0	1	0.96383058
8	2	5	1	2	0.9689307
9	5	11	1	2	0.93611245
10	6	13	1	2	0.92542193
11	5	9	1	2	0.93640409
12	6	14	2	2	0.92188803
13	5	9	1	4	0.93195318
14	8	20	2	0	0.90497303
15	4	12	2	0	0.94752039
16	3	8	0	3	0.95895055
17	4	6	0	4	0.94633291
18	3	6	0	3	0.95924931

[a]Remark: calculation of probabilities has been explained in the ESI 5.4.

Table 5.5 Number of isotopically prochiral (chirogenic) atoms, probability of one light isotope ⇒ heavy isotope exchange, probability of at least one chirogenic isotope exchanged (multiple exchanges were neglected).[a]

Set A	Number of isotopically prochiral (chirogenic) atoms (X_{CHIR})				Probability of one $^{12}C \Rightarrow {}^{13}C$ exchange	Probability of one $^{1}H \Rightarrow {}^{2}H$ exchange	Probability of one $^{14}N \Rightarrow {}^{15}N$ exchange	Probability of one $^{16}O \Rightarrow {}^{17+18}O$ exchange	Probability of at least one chirogenic isotope exchanged (p_{mono})
	C	H	N	O					
1	2	8	0	0	0.02121309	0.001176168	0	0	0.02238926
2	4	8	0	0	0.041475606	0.001149816	0	0	0.04262542
3	0	2	0	0	0	0.000284437	0	0	0.00028444
4	0	4	0	0	0	0.000607442	0	0	0.00060744
5	0	2	0	0	0	0.000303626	0	0	0.00030363
6	0	2	0	0	0	0.000302998	0	0	0.00030299
7	0	2	0	0	0	0.000300253	0	0	0.00030025
8	0	2	0	0	0	0.000301841	0	0	0.00030184
9	2	6	0	0	0.021038191	0.000874853	0	0	0.02191304
10	2	8	0	0	0.020797933	0.00115315	0	0	0.02195108
11	0	6	0	0	0	0.000875126	0	0	0.00087513
12	0	8	0	0	0	0.001148746	0	0	0.00114875
13	0	4	0	0	0	0.000580644	0	0	0.00058064
14	8	20	2	0	0.081353455	0.002819172	0.006655172	0	0.0908278
15	2	8	2	0	0.021294573	0.001180686	0.006968065	0	0.02944332
16	2	6	0	2	0.021551455	0.000896197	0	0.00457439	0.02702204
17	2	2	0	4	0.021267886	0.000294802	0	0.00902839	0.03059108
18	0	4	0	0	0	0.000597651	0	0	0.00059765

[a]Remark: calculation of probabilities has been explained in the ESI 5.5.

homoisotopic molecules. The results in units as pieces of molecules and as molar quantities are shown in the ESI-Table 5.1. Analogously one can obtain the number of potentially chiral isotopomers also at smaller quantities, which are in the range of the size of the ''typical cosmic sample, 1 pg'', defined earlier (see the ESI-Table 5.2).

These numbers provide the *expectable enantiomeric excess* (ee) with a certain confidence interval by the Pars–Mills equation (Mills, 1932, Barabás *et al.*, 2008). The formula for 50% confidence is as follows:

$$ee_{50\%} = \text{const.}\ (n)^{-1/2},$$

where the const. is 67.5 for $ee_{50\%}$ in % units and 0.675 for $ee_{50\%}$ in units of probability.

Here in this formula n is the number of molecules (or: chiral centers) in the sample (for details see the ESI-5.6).

It is an important consequence of the mathematical structure of this equation that the expectable enantiomeric excess is dependent of the sample size. We present here results of calculations of $ee_{50\%}$ values for 1 attomol and 1 femtomol sample sizes of Set A in Tables 5.6 and 5.7, respectively. For chemical purposes it is more significant to see these quantities in terms of the number of molecules corresponding to the statistically expectable enantiomeric excess in the samples of different sizes. These molecule numbers and the corresponding quantities in molar units (zeptomol, 10^{-21} mol) are presented for 1 attomol and 1 femtomol sample sizes, for Set A in Table 5.8.

Table 5.6 Percentage of enantiomer excesses in 1 attomol samples according to the Pars–Mills equation with 50% confidence ($ee_{50\%}$).[a]

Set A	If only one C isotope exchange	If only one H isotope exchange	If only one N isotope exchange	If only one O isotope exchange	Due to isotopic chirality
1	0.597209	2.536259	—	—	0.581311
2	0.427102	2.565158	—	—	0.421302
3	—	5.157454	—	—	5.157454
4	—	3.529197	—	—	3.529197
5	—	4.991816	—	—	4.991816
6	—	4.996987	—	—	4.996987
7	—	5.019784	—	—	5.019784
8	—	5.006555	—	—	5.006555
9	0.599686	2.940768	—	—	0.587594
10	0.60314	2.561448	—	—	0.587084
11	—	2.94031	—	—	2.94031
12	—	2.566352	—	—	2.566352
13	—	3.609719	—	—	3.609719
14	0.304958	1.638202	1.066225	—	0.288615
15	0.596065	2.531402	1.042011	—	0.506915
16	0.592502	2.905539	—	1.286062	0.529138
17	0.596439	5.065979	—	0.915426	0.497314
18	—	3.557989	—	—	3.557989

[a]Remark: calculation of the enantiomer excess has been explained in the ESI 5.6.

Table 5.7 Percentage of enantiomer excesses in 1 femtomol samples according to the Pars–Mills equation with 50% confidence ($ee_{50\%}$).[a]

Set A	If only one C isotope exchange	If only one H isotope exchange	If only one N isotope exchange	If only one O isotope exchange	Due to isotopic chirality
1	0.018885	0.080204	—	—	0.018383
2	0.013506	0.081117	—	—	0.013323
3	—	0.163093	—	—	0.163093
4	—	0.111603	—	—	0.111603
5	—	0.157855	—	—	0.157855
6	—	0.158019	—	—	0.158019
7	—	0.15874	—	—	0.15874
8	—	0.158321	—	—	0.158321
9	0.018964	0.092995	—	—	0.018581
10	0.019073	0.081	—	—	0.018565
11	—	0.092981	—	—	0.092981
12	—	0.081155	—	—	0.081155
13	—	0.114149	—	—	0.114149
14	0.009644	0.051805	0.033717	—	0.009127
15	0.018849	0.08005	0.032951	—	0.01603
16	0.018737	0.091881	—	0.040669	0.016733
17	0.018861	0.1602	—	0.028948	0.015726
18	—	0.112514	—	—	0.112514

[a]Remark: calculation of the enantiomer excess has been explained in ESI 5.6.

Table 5.8 Enantiomer excesses in terms of number of molecules with 50% confidence.[a]

Set A	In 1 attomol	$ee_{50\%}$ *R* or *S* excess	In 1 femtomol	$ee_{50\%}$ *R* or *S* excess
1	6742	78	6 741 562	2479
2	12 835	108	12 834 813	3420
3	86	9	85 646	279
4	183	13	182 905	408
5	91	9	91 424	289
6	91	9	91 235	288
7	90	9	90 408	287
8	91	9	90 887	288
9	6598	78	6 598 171	2452
10	6610	78	6 609 625	2454
11	264	15	263 507	490
12	346	18	345 896	561
13	175	13	174 836	399
14	27 349	158	27 348 886	4992
15	8 866	90	8 865 591	2842
16	8137	86	8 136 525	2723
17	9211	92	9 211 189	2897
18	180	13	179 957	405

[a]Remark: calculation of the enantiomer excess in terms of number of molecules has been explained in the ESI 5.7.

Table 5.9 Molecular mass, number of chiral molecules, and enantiomer excesses ($ee_{50\%}$) in 20 femtogram samples.

Set A	Molecular mass [a.u.]	Number of chiral molecules in 1 mol (times 10^{23}) see the ESI-Table 1	Number of chiral molecules in 20 femtogram	ee (50%)%	Half the number of chiral molecules in 20 femtogram	*R* or *S* excess with 50% confidence
1	72.0939	0.134831	22 525 419	0.01422222	11 262 709	3204
2	98.10955	0.256696	31 512 953	0.01202428	15 756 477	3789
3	106.07825	0.001713	194 487	0.15305874	97 244	298
4	44.026214	0.003658	1 000 749	0.06747473	500 375	675
5	46.041864	0.001828	478 320	0.09759882	239 160	467
6	60.021128	0.001825	366 157	0.11155008	183 079	408
7	58.041864	0.001808	375 212	0.11019586	187 606	413
8	75.032027	0.001818	291 785	0.12496027	145 893	365
9	117.078977	0.131963	13 575 489	0.01832002	6 787 745	2487
10	131.094627	0.132192	12 145 146	0.01936879	6 072 573	2352
11	115.063327	0.00527	551 652	0.09088059	275 826	501
12	146.105526	0.006918	570 281	0.08938388	285 141	510
13	147.053155	0.003497	286 396	0.12613049	143 198	361
14	144.162648	0.546978	45 698 056	0.00998516	22 849 028	4563
15	88.100048	0.177312	24 240 546	0.01370985	12 120 273	3323
16	92.047342	0.16273	21 293 082	0.01462799	10 646 541	3115
17	118.026606	0.184224	18 799 513	0.01556792	9 399 757	2927
18	90.031692	0.003599	481 486	0.09727739	240 743	468

By calculations using the same algorithm one can obtain the number of chiral molecules and the expectable enantiomeric excess ($ee_{50\%}$) in 20 fg samples (as defined above), for Set A these are shown in Table 5.9.

In the previous part of the present study we calculated the expectable enantiomeric excesses for the model molecules **1** to **18** ($ee_{50\%}$) in percentage (Tables 5.6 and 5.7) and in terms of number of molecules (Tables 5.8 and 5.9). These data serve as a comparison basis for the exploration of the effect of isotopic changes (enrichment of the heavier isotopes) on the basis of astrophysical observations cited above. In the following part of this paper we present the results of the same calculations conducted with (supposed) ''cosmic'' isotopic abundances, as defined for Set B and Set C in Table 5.3. The data for the initial steps of the calculations are presented in the ESI-5.7, and the final results in $ee_{50\%}$ and molar units are shown in Tables 5.10–5.15, respectively.

In the course of the present study we have chosen more–less arbitrarily the size of the sample. Due to the mathematical structure of the Pars–Mills equation,[4,72] increasing or decreasing the sample mass by a factor f, the resulting $ee_{50\%}$ parameter will change by a factor $f^{-1/2}$, that is if the sample mass increases, for example, by 2 orders of magnitude, this causes 1 order of magnitude diminution of the $ee_{50\%}$ value, while if the sample mass decreases by 2 orders of magnitude, the $ee_{50\%}$ value increases 10-fold.

Table 5.10 Percentage of enantiomer excesses in 1 attomol sample of Set B according to the Pars–Mills equation with 50% confidence.

Set B	If only one C isotope exchanged	If only one H isotope exchanged	If only one N isotope exchanged	If only one O isotope exchanged	Due to isotopic chirality
1	0.602811	0.771884	—	—	0.475097
2	0.43178	0.781895	—	—	0.377977
3	—	1.567177	—	—	1.567177
4	—	1.06741	—	—	1.06741
5	—	1.512132	—	—	1.512132
6	—	1.511345	—	—	1.511345
7	—	1.520604	—	—	1.520604
8	—	1.515417	—	—	1.515417
9	0.604841	0.894296	—	—	0.501012
10	0.609272	0.780157	—	—	0.480189
11	—	0.892767	—	—	0.892767
12	—	0.782259	—	—	0.782259
13	—	1.096019	—	—	1.096019
14	0.309741	0.501683	1.082946	—	0.256081
15	0.601657	0.770406	1.051786	—	0.432285
16	0.596202	0.881523	—	1.294092	0.461399
17	0.59923	1.534598	—	0.919709	0.477178
18	—	1.077794	—	—	1.077794

Table 5.11 Percentage of enantiomer excesses in 1 attomol sample of Set C according to the Pars–Mills equation with 50% confidence.

Set C	If only one C isotope exchanged	If only one H isotope exchanged	If only one N isotope exchanged	If only one O isotope exchanged	Due to isotopic chirality
1	0.598202	0.373101	—	—	0.316573
2	0.431623	0.380713	—	—	0.285516
3	—	0.75409	—	—	0.75409
4	—	0.50253	—	—	0.50253
5	—	0.71633	—	—	0.71633
6	—	0.711617	—	—	0.711617
7	—	0.720744	—	—	0.720744
8	—	0.722275	—	—	0.722275
9	0.603957	0.434965	—	—	0.352957
10	0.612506	0.382022	—	—	0.324143
11	—	0.431537	—	—	0.431537
12	—	0.387744	—	—	0.387744
13	—	0.529909	—	—	0.529909
14	0.321398	0.253561	0.481141	—	0.183945
15	0.607655	0.378997	0.454838	—	0.262577
16	0.583911	0.420528	—	1.267415	0.329507
17	0.583643	0.728041	—	0.895785	0.405937
18	—	0.51098	—	—	0.51098

The changes in the mass-related parameters, N_{ee} and M_{ee} are of the opposite direction. Obviously, in the case of more than one chirogenic element in the molecule the changes are more complicated, but the tendency is the same.

Table 5.12 Enantiomer excesses in terms of number of molecules in Set B samples with 50% confidence.

	In 1 attomol	$ee_{50\%}$	In 1 femtomol	$ee_{50\%}$
Set B	Half the number of chiral molecules	*R* or *S* excess with 50% confidence	Half the number of chiral molecules	*R* or *S* excess with 50% confidence
1	10 093	96	10 092 846	3033
2	15 946	121	15 945 782	3812
3	928	29	927 558	919
4	1999	43	1 999 471	1350
5	996	30	996 318	953
6	997	30	997 357	953
7	985	30	985 247	948
8	992	30	992 003	951
9	9076	91	9 075 724	2876
10	9880	95	9 879 934	3001
11	2858	51	2 858 259	1614
12	3723	58	3 722 855	1842
13	1896	42	1 896 449	1315
14	34 739	178	34 739 417	5626
15	12 191	105	12 190 931	3333
16	10 701	99	10 700 985	3123
17	10 005	95	10 005 004	3019
18	1961	42	1 961 128	1337

Table 5.13 Enantiomer excesses in terms of the number of molecules in Set C samples with 50% confidence.

	In 1 attomol	$ee_{50\%}$	In 1 femtomol	$ee_{50\%}$
Set C	Half the number of chiral molecules	*R* or *S* excess with 50% confidence	Half the number of chiral molecules	*R* or *S* excess with 50% confidence
1	22 732	144	22 731 561	4551
2	27 946	160	27 945 815	5046
3	4006	60	4 006 192	1911
4	9021	91	9 020 971	2867
5	4440	64	4 439 670	2011
6	4499	64	4 498 683	2025
7	4385	63	4 385 462	1999
8	4367	63	4 366 886	1995
9	18 287	129	18 286 660	4082
10	21 682	141	21 682 262	4445
11	12 233	106	12 233 255	3339
12	15 153	118	15 152 586	3716
13	8113	86	8 112 877	2719
14	67 329	248	67 328 569	7833
15	33 042	174	33 041 732	5487
16	20 982	138	20 982 007	4373
17	13 825	112	13 824 826	3549
18	8 725	89	8 725 082	2820

Table 5.14 Molecular mass, number of chiral molecules, and enantiomer excess in 20 femtogram samples of Set B.

Set B	Molecular mass [a.u.]	Number of chiral molecules in 1 mol (times 1023)	Number of chiral molecules in 20 femtogram	ee (50%)	Half the number of chiral molecules in 20 femtogram	*R* or *S* excess with 50% confidence
1	72.0939	0.2018569	33 722 980	0.01162360	16 861 490	3920
2	98.10955	0.3189156	39 151 227	0.01078776	19 575 613	4224
3	106.07825	0.0185512	2 106 326	0.04650942	1 053 163	980
4	44.026214	0.0399894	10 939 931	0.02040781	5 469 966	2233
5	46.041864	0.0199264	5 212 621	0.02956485	2 606 310	541
6	60.021128	0.0199471	4 002 738	0.03373845	2 001 369	1350
7	58.041864	0.0197049	4 088 977	0.03338078	2 044 489	1365
8	75.032027	0.0198401	3 184 764	0.03782380	1 592 382	1205
9	117.078977	0.1815145	18 672 960	0.01562058	9 336 480	2917
10	131.094627	0.1975987	18 154 320	0.01584214	9 077 160	2876
11	115.063327	0.0571652	5 983 778	0.02759409	2 991 889	1651
12	146.105526	0.0744571	6 137 907	0.02724543	3 068 953	1672
13	147.053155	0.037929	3 106 545	0.03829702	1 553 272	1190
14	144.162648	0.6947883	58 047 112	0.00885959	29 023 556	5143
15	88.100048	0.2438186	33 332 781	0.01169144	16 666 391	3897
16	92.047342	0.2140197	28 004 211	0.01275534	14 002 106	3572
17	118.026606	0.2001001	20 419 645	0.01493756	10 209 823	3050
18	90.031692	0.0392226	5 247 125	0.02946748	2 623 563	1546

Table 5.15 Molecular mass, number of chiral molecules, and enantiomer excess in 20 femtogram samples of Set C.

Set C	Molecular mass [a.u.]	Number of chiral molecules in 1 mol (times 1023)	Number of chiral molecules in 20 femtogram	ee (50%)	Half the number of chiral molecules in 20 femtogram	*R* or *S* excess with 50% confidence
1	72.0939	0.4546312	75 952 415	0.00774521	37 976 207	5883
2	98.10955	0.5589163	68 614 568	0.00814884	34 307 284	5591
3	106.07825	0.0801238	9 097 378	0.02237926	4 548 689	2036
4	44.026214	0.1804194	49 357 457	0.00960788	24 678 728	4742
5	46.041864	0.0887934	23 227 829	0.01400553	11 613 914	3253
6	60.021128	0.0899737	18 054 773	0.01588575	9 027 387	2868
7	58.041864	0.0877092	18 200 566	0.01582200	9 100 283	2880
8	75.032027	0.0873377	14 019 611	0.01802751	7 009 806	2527
9	117.078977	0.3657332	37 624 117	0.01100451	18 812 059	4140
10	131.094627	0.4336452	39 841 028	0.01069396	19 920 514	4261
11	115.063327	0.2446651	25 610 375	0.01333816	12 805 188	3416
12	146.105526	0.3030517	24 982 215	0.01350480	12 491 107	3374
13	147.053155	0.1622575	13 289 585	0.01851604	6 644 792	2461
14	144.162648	1.3465714	112 501 282	0.00636392	56 250 641	7159
15	88.100048	0.6608346	90 343 623	0.00710158	45 171 812	6416
16	92.047342	0.4196401	54 909 389	0.00910920	27 454 694	5002
17	118.026606	0.2764965	28 215 685	0.01270745	14 107 843	3585
18	90.031692	0.1745016	23 344 521	0.01397048	11 672 261	3261

The structure of the molecule under investigation is also a critical factor to the extent of chirality evolved by isotope substitution. We demonstrate this effect through the isomers of leucine (compound **6** in the tables). Iso-leucine (**15**) or *allo*-iso-leucine have the same elemental composition as leucine, but only two prochiral (chirogenic) hydrogen atoms, much less than the H_8C_2 structure of leucine itself.

As shown in Table 5.16, this slight structural alteration (formal 1,2-methyl-shift of a methyl group) radically changes the parameters describing the isotopically induced chirality. While the normal ⇒ iso rearrangements increase the expectable enantiomeric excesses ($ee_{50\%}$), the absolute quantities (expressed in terms of number of molecules or in molar quantity in the sample) are decreasing. The ratios (R) of the absolute quantities with 'cosmic' isotope distributions to the 'terrestrial' value are near the same parameters found for other molecules with deuterium substitution as the only source of isotope chirality (see Table 5.17). Hypothetic only-deuterium substitution of leucine (6) with the highest deuterium enrichment considered ($\delta(H) = 50\,000‰$) provides lower expectable enantiomeric excess ($ee_{50\%}$) but higher absolute quantity of excess chiral molecules than in the case of 'terrestrial' isotopic distribution (see Table 5.16).

Table 5.16 Effect of molecular structure on the statistically generated enantiomeric excess ($ee_{50\%}$ [%]), its quantity in the number of excess chiral molecules (N_{ee}), in molar units (M_{ee}, [zeptomol]) and on the 'cosmic'/'terrestrial' ratio (R): comparison of iso-leucine (**15**) with leucine (**6**).

	Set A		Set B		Set C	
Iso-leucine						
$\sum ee_{50\%}$	0.39900		0.12040		0.05609	
$\sum N_{ee}$	114.20	**∼114**	378.40	**∼378**	812.27	**∼812**
M_{ee}	0.1896	**∼0.19**	0.6284	**∼0.63**	1.3488	**∼1.3**
R	(1)		3.3158	**∼3.3**	7.1228	**∼7.1**
Leucine						
$\sum ee_{50\%}$	0.24647		0.10717		0.07311	
$\sum N_{ee}$	1198.24	**∼1198**	1726.66	**∼1727**	2635.60	**∼2636**
M_{ee}	1.9897	**∼2.0**	2.8562	**∼2.9**	4.3765	**∼4.4**
R	(1)		1.4416	**∼1.4**	2.2003	**∼2.2**
R (leucine/iso-leucine; [mol mol^{-1}])						
	10.5088	**∼10.5**	4.5688	**∼4.6**	3.2463	**∼3.2**

Table 5.17 Statistical enantiomeric excess ($ee_{50\%}$, [%]), number of excess chiral molecules (N_{ee}), and molar quantity of excess chiral molecules (M_{ee}, [zeptomol]) in leucine (6) resulting from only-deuterium substitution at $\delta(2H) = 50\,000‰$ enrichment.

$ee_{50\%} = 0.02845$
$N_{ee} = 1624.54$ **∼1624**
$M_{ee} = 2.6976$ **∼2.7**
R ('cosmic'/'terrestrial', [mole mole^{-1}]) $= 1.3564$ **∼1.4**

5.3 Conclusions

The above-outlined results lead to the following points:

(a) Substitution of homoisotopic molecules by a different isotope of one of its constituents could generate centers of chirality by the asymmetric distribution of isotopes. These ''new'' stereogenic centers could transform an achiral molecule to a chiral one (*e.g.* in the case of glycine, **8**, the only achiral proteinogenic amino acid) as well as could transform an already chiral molecule to a pair of diastereomers (*e.g.* as in the case of lysine, **12**). Both transformations can be of primary significance in the stereochemical behavior (reactions, structural features, *etc.*) of these molecules.

(b) Increasing the proportion of the less abundant isotopes (*e.g.* ^{2}H) causes diminution in the percentage of the statistically expectable enantiomeric excess in samples of the same mass, of cosmic origin. This tendency, however, is overcompensated by the absolute quantities of excess chiral molecules which were formed statistically by isotopic substitution.

(c) The quantity of statistically formed excess chiral molecules is sufficient for the generation of much higher quantity of these chiral molecules if the system is part, or, is in contact with a sufficiently sensitive asymmetric autocatalytic reaction. Today the best documented example of this kind of reaction is Soai autocatalysis,[15–22,30] which was found by preparative experiments to be suitable for amplification of levels of excess chirality comparable to those shown in Tables 5.8, 5.9, and 5.12–5.15 to very high, sometimes even near-quantitative (ee $>$ 90%) levels,[10,11,16,24,29,34,87,88] for model compounds composed of H, C, N, and O.

(d) The fact that isotope chirality due to isotopic substitution in molecules containing the same chemical elements as the model compounds studied in the present work could successfully be used as chiral inductors in asymmetric autocatalysis[13,32,35–39] compared with the presently most accepted theories on the origin of biological chirality around the dawn of terrestrial life[4,12,20–22,26,89–95] leads to the hypothesis that changes of isotope ratios deriving from extraterrestrial sources could play a certain role in the initial phase of evolution of biological chirality as observed presently in terrestrial life. Obviously, changes in the extent of isotope ratios of biogenic elements could critically influence the spontaneous formation of stereogenic centers by isotope substitution.

(e) Isotope selectivity observed in present-day living organisms,[96–102] however, might indicate that the isotope-generated chirality in the course of the molecular evolution from the beginning of life to the present, did not necessarily have a kind of 'promoting' effect in the history of chemical evolution. Even more, just due to its statistical character it

could counteract to the tendency of establishing more and more order in the function of living organisms.[103–107] In this sense, 'imported' excess extraterrestrial statistical chirality could have acted also as (one of the) inducer(s) of selectivity in presently observed isotopic composition of living matter.

(f) Enantiomeric excesses from extraterrestrial sources were observed prominently in meteorites. These experimentally observed values reach up to 60% ee.[47,48,51] If these high ee values were somehow connected to statistical isotopic chirality, there should have been a noteworthy chirality amplification step in between, either with similar efficiency as that of the Soai reaction[16,19–22] or by a step-by-step 'spontaneous' mechanism.[12]

(g) Chirality is a kind of binary code. Therefore the high level of enantioselectivity in living organisms (biological (''homo'')chirality)[122] is an important carrier of biological information.[108,109] The spontaneous statistically formed excesses of chirality and their changes under the influence of changes in the isotopic abundance of biogenic elements represent an unjustly neglected challenge in biochemical/bioinformatical research.

(h) In the present paper the consequences of isotopic monosubstitution in homoisotopic molecules are analyzed. These homoisotopic molecules, especially in the case of relatively small molecules and because of the very asymmetric isotopic distribution of the elements studied here (H, C, N, O) are mathematically much easier to be handled than 'real' molecules with (terrestrial) natural abundance of stable isotopes. It is, however, to be mentioned, that in a subsequent phase of the present research these natural abundance-based species as well as isotopically disubstituted (and polysubstituted) species will also be analyzed. The latter appears to be negligible because of its low probability, but recent experimental work[110,111] concluded that such species could be carriers of important information on the molecular history of certain fossil organic compounds.

(i) The quantity of extraterrestrial material arriving to Earth was estimated between 5 to 270 t per day, which is 1825 to 98 550 t per year.[43] Considering that our calculations indicated ~0.25 to ~10 zeptomol of 'pure' excess chiral material as a product of spontaneous statistical enantiomeric excess from 20 femtomol SOM, one can calculate (very approximately!), supposing 100 a.u. 'average' molecular mass, that the excess chiral material ranges between 0.012 μg and 1.93 mg per km^2 per year. Obviously this can accumulate substantially over a few thousand years, which still enables conservation of the configuration. If, however, these small amounts encounter such asymmetric autocatalytic mechanisms, which were experimentally demonstrated by K. Soai and co-workers,[15,16,20–24,112] which enable amplification factors reaching 600 000 to 2 800 000 values, this 'imported' chirality can reach ~34 mg per km^{-2} per year to ~5.4 kg per km^{-2} per year.

Considering, that according to recent theories[7–9,108,113,118–121] the chemical evolution of terrestrial life could have started from very small quantities (few or even one molecule), these amounts of 'excess chirality' appear to be serious candidates of initial enantioselective molecular events in the prebiotic or early biotic phase of life.

(j) It should be pointed out, however, that statistical spontaneous formation of enantiomeric excesses, as found in the present work, are much lower than the enantiomeric excesses (up to ~60% ee) found in meteorites by Pizzarello and co-workers.[47–52,114,120] Thus, the primary causes of these excesses of chirality should be attributed to mechanisms (*e.g.* circularly polarized radiation;[115] quantum tunneling in interstellar grains;[84,116] noise-induction[87,117]) which are different from statistical ones. It should be mentioned that these exceptionally high ee values were not yet (?) found in cosmic dust particles only in larger extraterrestrial objects (to the best of our knowledge).

It was the main goal of the present study, to call the attention of the scientific community to a possible connection of 'irregular' isotopic compositions found in the rapidly increasing number of observations of extraterrestrial objects and terrestrial excess of biological chirality, particularly in small molecules related both to recent cosmochemical observations and to terrestrial life and (possibly) its origin. It appears from the results that such a link may exist and, as happens frequently, many additional experimental and theoretical studies appear to be desirable in the future for the more exact definition and estimation of the size of this effect.

References

1. D. Arigoni and E. L. Eliel, *Top. Stereochem.*, 1969, **4**, 127.
2. K. Mislow, *Collect. Czech. Chem. Commun.*, 2003, **68**, 849.
3. G. Pályi, K. Micskei, L. Zékány, C. Zucchi and L. Caglioti, *Magy. Kem. Lapja*, 2005, **60**, 17.
4. B. Barabás, L. Caglioti, K. Micskei, C. Zucchi and G. Pályi, *Origins Life Evol. Biospheres*, 2008, **38**, 317.
5. B. Barabás, R. Kurdi and G. Pályi, *Symmetry*, 2016, **8**, 2.
6. B. Barabás, R. Kurdi and G. Pályi, Isotope chirality in the reagents and intermediates of the Soai reaction, in *Advances in Asymmetric Autocatalysis and Related Topics*, ed. G. Pályi, R. Kurdi and C. Zucchi, Elsevier, Cambridge (MA, USA), 2017, pp. 259–276.
7. L. Caglioti, C. Zucchi and G. Pályi, *Chem. Today*, 2005, **23**(5), 38.
8. L. Caglioti, K. Micskei and G. Pályi, *Viva Origino*, 2007, **35**, 82.
9. L. Caglioti, K. Micskei and G. Pályi, *Chirality*, 2011, **23**, 65.
10. M. Maioli, G. Varadi, R. Kurdi, L. Caglioti and G. Pályi, *J. Phys. Chem. B*, 2016, **120**, 7438.
11. K. Micskei, M. Maioli, C. Zucchi, L. Caglioti and G. Pályi, *Tetraherdon: Asymmetry*, 2006, **17**, 2960.

12. J. M. Ribó, D. Hochberg, J. Crustas, Z. El-Hachemi and A. Moyano, *J. R. Soc., Interface*, 2017, **14**, 20170699.
13. T. Kawasaki and K. Soai, *Isr. J. Chem.*, 2012, **52**, 582–590.
14. T. Shibata, H. Morioka, T. Hayase, K. Choji and K. Soai, *J. Am. Chem. Soc.*, 1996, **118**, 471.
15. K. Soai, Asymmetric autocatalysis and the origin of chiral homogeneity of biologically relevant molecules, in *Fundamentals of Life*, ed. G. Pályi, C. Zucchi and L. Caglioti, Elsevier, Paris, 2002, pp. 427–436.
16. K. Soai, Asymmetric autocatalysis, absolute asymmetric synthesis and the origin of homochirality of biomolecules, in *Progress in Biological Chirality*, ed. G. Pályi, C. Zucchi and L. Caglioti, Elsevier, Oxford (GB), 2004, pp. 355–364.
17. K. Soai and T. Kawasaki, *Top. Curr. Chem.*, 2008, **284**, 1.
18. K. Soai, T. Shibata, H. Morioka and K. Choji, *Nature*, 1995, **378**, 767.
19. K. Soai, T. Shibata and I. Sato, *Acc. Chem. Res.*, 2000, **33**, 382.
20. K. Soai, T. Kawasaki and A. Matsumoto, *Acc. Chem. Res.*, 2014, **47**, 3643.
21. K. Soai, T. Kawasaki and A. Matsumoto, *Chem. Record*, 2014, **14**, 70.
22. K. Soai, T. Kawasaki and A. Matsumoto, *Tetrahedron*, 2018, **74**, 1973.
23. K. Soai, A. Matsumoto and T. Kawasaki, Asymmetric autocatalysis and the origins of homochirality of organic compounds. An overview, in *Advances in Asymmetric Autocatalysis and Related Topics*, ed. G. Pályi, R. Kurdi and C. Zucchi, Elsevier–Academic Press, Cambridge, MA, USA, 2017, pp. 1–30.
24. I. Sato, H. Urabe, S. Ishiguro, T. Shibata and K. Soai, *Angew. Chem., Int. Ed.*, 2003, **42**, 315.
25. T. Shibata, S. Yonekubo and K. Soai, *Angew. Chem., Int. Ed.*, 1999, **38**, 659.
26. B. Barabás, L. Caglioti, C. Zucchi, M. Maioli, E. Gál, K. Micskei and G. Pályi, *J. Phys. Chem. B*, 2008, **111**, 11506.
27. B. Barabás, L. Caglioti, K. Micskei and G. Pályi, *Bull. Chem. Soc. Jpn.*, 2009, **82**, 1372.
28. T. Kawasaki, K. Suzuki, M. Shimizu, K. Ishikawa and K. Soai, *Chirality*, 2006, **18**, 479.
29. K. Soai, I. Sato, T. Shibata, S. Komiya, M. Hayashi, Y. Matsueda, H. Imamura, T. Hayase, H. Morioka, H. Tabira, J. Yamamoto and Y. Kowata, *Tetrahedron: Asymmetry*, 2003, **14**, 185.
30. K. Soai, T. Shibata and Y. Kowata, *Jpn. Kokai Tokkyo Koho*, 1997, **9**, 179.
31. B. Barabás, R. Kurdi, C. Zucchi and G. Pályi, *Chirality*, 2018, **30**, 913.
32. N. A. Hawbaker and D. G. Blackmond, *ACS Cent. Sci.*, 2018, **4**, 776.
33. I. Sato, D. Omiya, T. Saito and K. Soai, *J. Am. Chem. Soc.*, 2000, **122**, 11739.
34. T. Kawasaki, M. Shimizu, D. Nishiyama, M. Ito, H. Ozawa and K. Soai, *Chem. Commun.*, 2009, 4396.
35. T. Kawasaki, Y. Matsumura, T. Tsutsumi, K. Suzuki, M. Ito and K. Soai, *Science*, 2009, **324**, 492.
36. T. Kawasaki and K. Soai, *Bull. Chem. Soc. Jpn.*, 2011, **84**, 879.

37. A. Matsumoto, H. Ozaki, S. Harada, K. Tada, T. Ayugase, H. Ozawa, T. Kawasaki and K. Soai, *Angew. Chem., Int. Ed.*, 2016, **55**, 15246.
38. T. Kawasaki, Y. Okano, E. Suzuki, S. Takano, S. Oji and K. Soai, *Angew. Chem., Int. Ed.*, 2011, **50**, 8131.
39. A. Matsumoto, S. Oji, S. Takano, K. Tada, T. Kawasaki and K. Soai, *Org. Biomol. Chem.*, 2013, **11**, 2928.
40. E. Dartois, C. Engrand and R. Brunetto, *Geochem. J.*, 2014, **48**, 511.
41. S. Kwok, *Origins Life Evol. Biospheres*, 2015, **45**, 113.
42. S. Kwok, *Astrophys. Rev.*, 2016, **24**, 8.
43. J. M. C. Plane, *Chem. Soc. Rev.*, 2012, **41**, 6507.
44. S. A. Sandford, C. Engrand and A. Rotundi, *Elements*, 2016, **12**, 185.
45. D. H. Wooden, H. A. Ishi and M. E. Zolensky, *Philos. Trans. R. Soc., A*, 2017, **375**, 20160260.
46. T. Kawasaki, K. Hatase, Y. Fujii, Y. K. Jo, K. Soai and S. Pizzarello, *Geochim. Cosmochim. Acta*, 2006, **70**, 5395.
47. S. Pizzarello, *Life*, 2016, 6, 18.
48. S. Pizzerello, *Métode*, 2016, **6**, 161.
49. S. Pizzarello, Y. Huang and M. R. Alexandre, *Proc. Natl. Acad. Sci. U. S. A.*, 2008, **105**, 3700.
50. S. Pizzarello, Y. Huang and M. Fuller, *Geochim. Cosmochim. Acta*, 2004, **68**, 4963.
51. S. Pizzarello and T. L. Groy, *Geochim. Cosmochim. Acta*, 2011, **75**, 645.
52. S. Pizzarello and E. Shock, *Cold Spring Harbor Perspect. Biol.*, 2010, **2**, a002105.
53. D. Bocklée-Morvan, U. Calmonte and S. Charnley, *Space Sci. Rev.*, 2015, **197**, 47.
54. H. Yabuta, T. Noguchi and S. Itoh, *Geochim. Cosmochim. Acta*, 2017, **214**, 172.
55. C. Vollmer, D. Kepaptsoglou, J. Leitner, H. Busemann, N. Spring, Q. M. Ramasse, P. Hoppe and L. R. Nittler, *Proc. Natl. Acad. Sci. U. S. A.*, 2014, **111**, 15338.
56. P. Rousselot, E. Jehin, J. Manfroid and D. Hutsemékers, *Astron. Astrophys.*, 2012, **545**, A24.
57. N. A. Starkey and I. A. Franchi, *Geochim. Cosmochim. Acta*, 2013, **105**, 73.
58. L. Remusat, F. Robert and S. Derenne, *C. R. Geosci.*, 2007, **339**, 895.
59. L. Piani, F. Robert and L. Remusat, *Earth Planet. Sci. Lett.*, 2015, **415**, 154.
60. N. A. Starkey, I. A. Franchi and M. R. Lee, *Geochim. Geophys. Acta*, 2014, **142**, 115.
61. C. M. O. D. Alexander, G. D. Cody, B. T. De Gregorio, L. R. Nittler and R. M. Stroud, *Geochemistry*, 2017, **77**, 227.
62. J. Duprat, E. Dobriča, C. Engrand, J. Aléon, Y. Marocchi and F. Robert, *Science*, 2010, **328**, 742.
63. S. Messenger, *Planet. Space Sci.*, 2002, **50**, 1221.
64. M. Hashiguchi, S. Kobayashi and H. Yurimoto, *Geochem. J.*, 2015, **49**, 377.

65. P. Hartogh, D. C. Lis and D. Bocklée-Morvan, *Nature*, 2011, **478**, 218.
66. J. Crovisier, D. Bockléer-Morvan, P. Colom, N. Biver, D. Despois and D. C. Lis, *Astron. Astrophys.*, 2004, **418**, 1141.
67. E. M. M. E. van Kooten, K. Nagashima and T. Kasama, *Geochim. Cosmochim. Acta*, 2017, **205**, 119.
68. P. Rousselot, O. Pirali, E. Jehin, M. Vervolet, D. Hutsemékers, J. Manfroid, D. Cordier, A.-M. Martin-Drumel, S. Gruet and C. Arpigny, *Astrophys. J.*, 2014, **780**, L17.
69. J. D. Carillo-Sánchez, D. Nesvorny, P. Pokorny, D. Janches and J. M. C. Plane, *Geophys. Res. Lett.*, 2016, **43**, 11979.
70. J. D. Carrillo-Sánchez, J. M. C. Plane, W. Feng, D. Nesvorny and D. Janches, *Geophys. Res. Lett.*, 2015, **42**, 6518.
71. H. A. Zook, Spaccraft measurements of the cosmic dust flux, in *Accretion of Extraterrestrial Matter Throughout Earth's History*, ed. B. Peucker-Ehrenbrink and B. Schmitz, Springer Science + Business Media, New York, 2001, pp. 75–92.
72. W. H. Mills, *Chem. Ind.*, 1932, 750.
73. E. Grün, H. A. Zook, H. Fechtig and R. H. Giese, *Icarus*, 1985, **62**, 244.
74. J. D. Carrillo-Sánchez, J. M. C. Plane, W. Feng, D. Nesvorny and D. Janches, *Geophys. Res. Lett.*, 2015, **42**, 6518.
75. R. Noguchi, N. Ohashi, S. Tsujimoto, T. Mitsunari, J. P. Bradley, T. Nakamura, S. Toh, T. Stephan, N. Iwata and N. Imae, *Earth Planet. Sci. Lett.*, 2015, **410**, 1.
76. G. Dorlshagen, D. Koschny, S. Dorlshagen, J. Kretschmer and B. Poppe, *Planet. Space Sci.*, 2017, **143**, 21–27.
77. G. J. Flynn, L. R. Nittler and C. Engrand, *Elements*, 2016, **12**, 177.
78. M. A. Sephton, I. P. Wright, I. Gilmour, J. W. de Leeuw, M. M. Grady and C. T. Pillinger, *Planet. Space Sci.*, 2002, **50**, 711.
79. R. H. Garrett and C. M. Grisham, *Biochimica*, Zanichelli, Bologna, 5th edn, 2002.
80. M. Kajtár, *Variations on Four Elements (Organic Chemistry)*, Gondolat, Budapest, 1984, vol. 1–2, [in Hungarian].
81. H. M. Cuppen, C. Walsh, T. Lamberts, D. Semenov, R. T. Garrod, E. Penteado and S. Ippolo, *Space Sci. Rev.*, 2017, **212**, 1.
82. P. de Marcellus, C. Meinert, J. Myrgorodska, L. Nahon, T. Buhse, L. L. S. d'Hendecourt and U. J. Meierhenrich, *Proc. Natl. Acad. Sci. U. S. A.*, 2015, **112**, 965.
83. Z. Martins, P. Modica, B. Zanda and L. L. S. d'Hendecourt, *Meteorit. Planet. Sci.*, 2015, **50**, 926.
84. Y. Oba, N. Watanabe, Y. Osamura and A. Kouchi, *Chem. Phys. Lett.*, 2015, **634**, 53.
85. M. A. Sephton, *Philos. Trans. R. Soc., A*, 2005, **363**, 2729.
86. L. Markó, *Organic Chemistry*, Pannon University Press, Veszprém, 2000, vol. I, pp. 42–65.
87. M. Maioli, K. Micskei, C. Zucchi, L. Caglioti and G. Pályi, *J. Math. Chem.*, 2008, **43**, 1505.

88. K. Micskei, G. Rábai, E. Gál, L. Caglioti and G. Pályi, *J. Phys. Chem. B*, 2008, **112**, 9196.
89. B. Barabás, J. Tóth and G. Pályi, *J. Math. Chem.*, 2010, **48**, 457.
90. D. G. Blackmond, *Phil. Trans. R. Soc. B*, 2011, **366**, 2878.
91. R. Breslow, *J. Am. Chem. Soc.*, 2012, **134**, 6887.
92. V. A. Pavlov and E. I. Klabunovskii, *Chem. Revs*, 2015, **84**, 121.
93. V. A. Pavlov and T. N. Pavlova, *Curr. Org. Chem.*, 2017, **21**, 872.
94. L. Silva-Dias and A. Lopez-Castillo, *Phys. Chem. Chem. Phys.*, 2017, **19**, 29424.
95. V. Sojo, *Origins Life Evol. Biospheres*, 2015, **45**, 219.
96. A. A. Berezin and V. V. Gridin, *Nonlinear Dyn. Psychol. Life Sci.*, 2017, **21**, 485.
97. J. W. Boeckeln, C. T. Yarnes, B. A. Cook and A. C. James, *Ann. Rev. Ecol. Evol. Syst.*, 2011, **42**, 411.
98. B. F. Murphey and A. D. Nier, *Phys. Rev.*, 1941, **59**, 771.
99. A. D. Nier and E. A. Gulbarnsen, *J. Am. Chem. Soc.*, 1939, **61**, 697.
100. N. Ohkouchi, N. O. Ogawa, Y. Chikaraishi, H. Tanaka and E. Wada, *Progr. Earth Panet. Sci.*, 2015, **2**, 1.
101. M. Schidlowski, Sedimentary carbon isotope archives as recorders of early life: implications for extraterrestrial scenarios, in *Fundamentals of Life*, ed. G. Pályi, C. Zucchi and L. Caglioti, Elsevier, Paris, 2002, pp. 307–329.
102. H. Urey, *Science*, 1948, **108**, 489.
103. M. Liu, L. Zhang and T. Wang, *Chem. Rev.*, 2015, **115**, 7304.
104. M. E. Price, *Coplexity*, 2017, 4745379.
105. L. Smolin, *The Life of the Cosmos*, Oxford University Press, New York, NY, USA, 1997.
106. J. T. Trevors, *J. Microbiol. Meth.*, 2010, **83**, 341.
107. J. T. Trevors and M. H. Sainer, *C. R. Biol.*, 2011, **334**, 1.
108. L. Caglioti, C. Zucchi, N. Florini and G. Pályi, Open questions about chirality, in *Organometallic Chirality*, ed. G. Pályi, C. Zucchi and L. Caglioti, Mucchi Editore, Modena, 2008, pp. 7–27.
109. G. Pályi, C. Zucchi, L. Bencze and L. Caglioti, Biological chirality: A tool of information in vivo and in vitro, in *New Avenues in Bioinformatics*, ed. J. Seckbach and E. Rubin, Springer, Berlin, 2004, pp. 81–98.
110. M. Clog, M. Lawson, B. Peterson, A. A. Ferreira, E. V. Santos Neto and J. M. Eiler, *Geochim. Cosmochim. Acta*, 2018, **223**, 229.
111. J. M. Eiler, *Ann. Rev. Earth Planet. Sci.*, 2013, **41**, 411.
112. T. Kawasaki, A. Matsumoto, I. Sato and K. Soai, Synthesis of pyrimidine—terminated chiral large molecular architectures with functions of self-replication and self-improvement by asymmetric autocatalysis, in *Advances in Asymmetric Autocatalysis and Related Topics*, ed. G. Pályi, R. Kurdi and C. Zucchi, Elsevier, Academic Press, Cambridge, MA, USA, 2017, pp. 149–165.
113. G. F. Arnaud, B. Barabás and L. Caglioti, *et al.*, Towards absolute enantioselective synthesis, in *The Soai Reaction and Related*, ed. G. Pályi,

C. Zucchi and L. Caglioti, Artestampa – Accad. Nazl. Sci. Lett. Arti, Modena, 2012, pp. 241–273.
114. S. Pizzarello, *Rend. Fis. Acc. Lincei*, 2011, **22**, 153.
115. J. Bailey, *Origins Life Evol. Biospheres*, 2001, **31**, 167.
116. Y. Oba, Y. Takano, H. Naraoka, A. Kouchi and N. Watanabe, *Astrophys. J.*, 2017, **849**, 122.
117. F. Jafarpour, T. Biancalani and N. Goldenfeld, *Phys. Rev. E*, 2017, **95**, 032407.
118. J. D. Carroll, *Chirality*, 2009, **21**, 354–358.
119. W. Fuss, *Colloids Surf., B*, 2009, **74**, 498.
120. S. Pizzarello, G. W. Cooper and G. J. Flynn, The nature and distribution of the organic material in carbonaceous chondrites and interplanetary dust particles, in *Meteorites and the Early Solar System, II*, ed. D. S. Lauretta and H. Y. McSween Jr., University of Arizona Press, Tucson, AZ, USA, 2006, pp. 625–651.
121. C. Decock and J. Six, *Eur. J. Soil Sci.*, 2013, **64**, 610.
122. G. Pályi, *Biological Chirality*, Elesevier, Academic, Oxford, UK, 2020.

CHAPTER 6

Reaction Mechanism in the Study of Amplifying Asymmetric Autocatalysis

JOHN M. BROWN

CRL, Department of Chemistry, University of Oxford, Oxford OX1 3TA, UK
Email: John.brown@chem.ox.ac.uk

6.1 Introduction

6.1.1 Scope of and Limitations to the Study of Reaction Mechanisms

Absolute solutions to mechanistic problems are not attainable, since it is impossible to prove hypotheses with any certainty. That statement on the nature of provability, originating from Popper and Miller, is provocative and has led to vigorous discussion concerning its application to the sciences.[1] Platt's paper on ''Strong Influence'' provides some endorsement, advising experimentalists to: ''*set down explicitly at each step just what the question is*, *what all the alternatives are*, *and then to set up crucial experiments to try to disprove some*.''[2] Hence progress in mechanistic understanding may be made, either by providing additional supportive evidence for an existing hypothesis or by disproof of alternative explanations. In the absence of any clear refutation this approach offers an acceptable *status quo*, but one that is subject to modification, if and when additional evidence becomes available in the future. This leads to the conclusion that complementary approaches

Catalysis Series No. 43
Asymmetric Autocatalysis: The Soai Reaction
Edited by Kenso Soai, Tsuneomi Kawasaki and Arimasa Matsumoto

Published by the Royal Society of Chemistry, www.rsc.org

to a specific problem are beneficial for promoting general acceptance of a reaction mechanism by the scientific community. This acceptance of a mechanism is subject to change at a future date, as new experimental evidence arises. The overall status is summarized by Feynman's view that progression of understanding in the Sciences is always from good to better but never goes as far as perfection.[3]

Given the fact that the Soai reaction of di-iso-propylzinc with N-heterocyclic aldehydes provides the only robust examples of AAA to date, a range of methods to test the mechanism have already been applied and significant progress has been made toward understanding this complex and challenging system. More general interest has been further heightened by the first demonstrations of absolute asymmetric synthesis by Soai and by Singleton, that have been analyzed in detail in an informative review.[4] Even before the experimental demonstrations of AAA, it has been discussed and reviewed as a potential contender for the origins of chirality in Nature.[5]

6.1.2 General Features of Autocatalytic Mechanisms

In the elucidation of any reaction mechanism, a primary aim is to define the structure and energy of reactive intermediates up to the point of the first irreversible step. Catalyzed reactions introduce some further considerations through possibilities that catalytic efficiency may alter over time, through aggregation or degradation. Where the catalytic cycle involves bi- or multimolecular steps, possible ambiguity arises in defining that first irreversible step of the catalytic cycle, as the relative energies of individual steps will depend on the initial concentration of the reactant and catalyst and on temperature. AAA introduces further complexity, since the catalyst of each cycle associates with the product and is incorporated into the next cycle; the catalyst concentration increases with each catalytic cycle and a rate maximum is observed. This is demonstrated schematically in Figure 6.1 for the rate of a first order in both reactant and catalyst, compared to a reaction that is first order in reactant and autocatalyst.

For these reasons, any mechanistic analysis of catalysis and particularly autocatalysis needs to specify the reaction conditions fully. This consideration is particularly important when catalytic turnover involves an irreversible step that possesses a low energy barrier, since the relative energies may change with changing autocatalyst concentration.

The time-dependence of product formation in autocatalysis commonly has characteristic features; a hysteresis-shaped curve is observed on plotting product concentration (or substrate decay) *versus* time (Figure 6.2). Questions need to be answered about each phase of the cycle. Initiation step, in which the catalyst is generated; what reactions and what association phenomena are involved? Burst phase, what is the aggregation state of the catalyst and is it structurally identical to the product in its resting state? What is the timescale of dynamic equilibria relative to turnover? Is the initially formed product identical in structure to the equilibrium state?

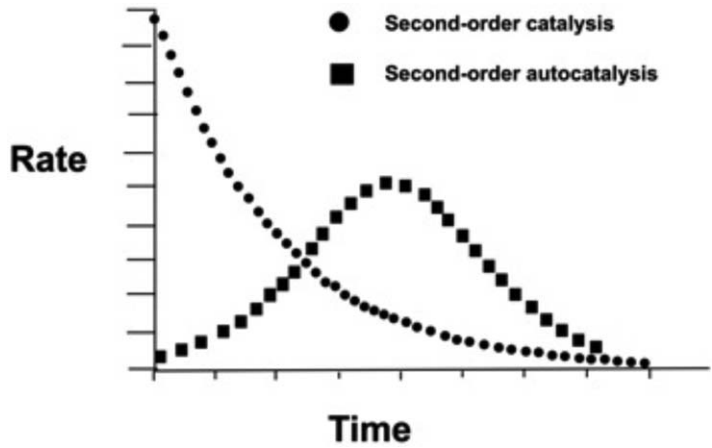

Figure 6.1 A comparison of the decay curves for a simple catalytic reaction catalysis compared to the corresponding autocatalytic reaction.

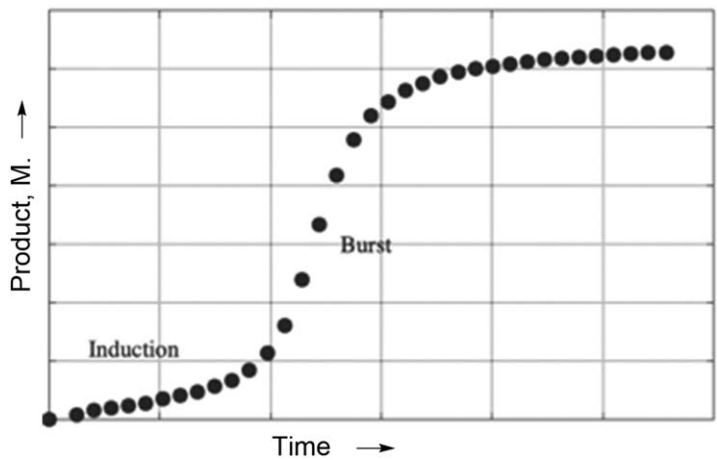

Figure 6.2 Typical hysteresis curve for the output from an autocatalytic reaction.

To summarize, this requires both kinetic analysis and also insights into molecular structure by physicochemical techniques, including X-ray structure determination. Computation, generally through accessible DFT methodologies, plays an important role by assessing the viability of structures proposed from experiment and information on the structure and energy of intermediates that are experimentally inaccessible. The constraints in defining an autocatalytic mechanism apply equally to computational approaches. Electronic energies as computed are derived through the Hartree–Fock equation and may be converted into enthalpies through standard methods.[6] A specific advantage of DFT methods lies in the additional ability to calculate transition state energies and structures. For multi-stage catalytic reaction this provides access to models for the full reaction pathway.

6.2 The Key Steps Towards Amplifying Asymmetric Autocatalysis (AAA)

6.2.1 Catalytic Asymmetric Synthesis

Recognition of the intrinsic chirality in the natural world dates back to early observations made by crystallography or polarimetry, together with Pasteur's defining contributions, as summarized.[7] In a similar manner, the origin of single-handedness of chiral molecules in the natural world had long been debated.[8] Experimental organic chemistry developed rapidly in the 19th century, and it was originally considered that Nature's chirality was beyond replication in the laboratory. Natural products exhibited consistent optical purity on polarimetric assay; organic synthesis could not independently create an asymmetric center and imitate Nature. Emil Fischer was the first to challenge this principle,[9] but successful demonstration of an asymmetric synthesis awaited Mackenzie's work; he had observed diastereoselectivity in Grignard reactions of a menthyl keto-ester in 1904. After hydrolysis of the initial product to the α-hydroxy acid by removing the chiral auxiliary enantiomerically enriched product was obtained.[10] A more general approach to asymmetric synthesis without the need for a chiral auxiliary was provided by Bredig. He showed that the addition of HCN to benzaldehyde **1** (Scheme 6.1A and B), and likewise to other aldehydes in their later paper, in the presence of catalytic amounts of quinine or quinidine gave optically active cyanohydrin **2**. The product was predominantly dextrorotatory with quinine and levorotatory with quinidine.[11,12]

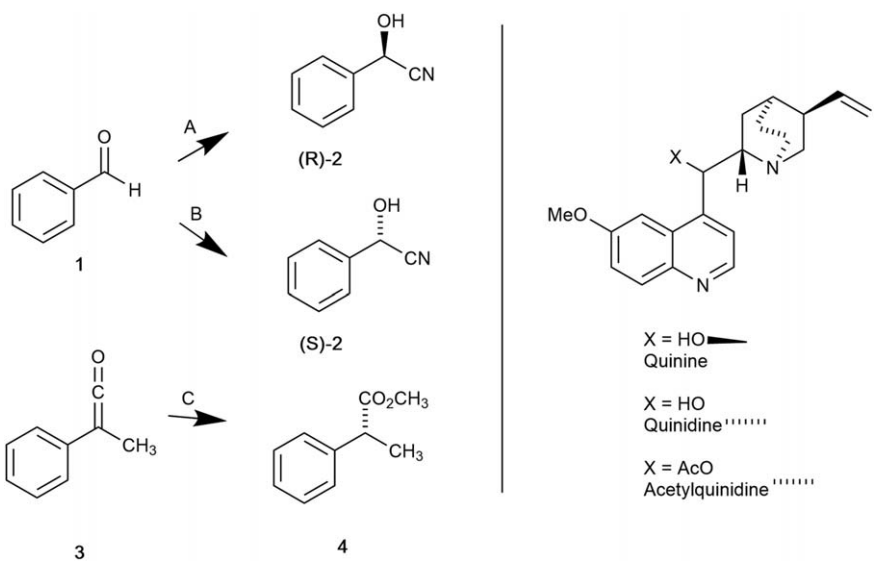

Scheme 6.1 Early contributions to asymmetric synthesis from Bredig (A and B) and from Pracejus (C).

The field progressed, but only slowly over more than sixty years, with occasional significant papers, exemplified by Prelog's work.[13] Successes like the early example of organocatalysis by Pracejus were rare. He studied asymmetric addition of methanol to phenyl methyl ketene **3** catalyzed by the alkaloid base acetylquinidine, and reported that e.e.'s of up to 74% in product **4** were observed when the reaction was carried out at −110 °C.[14]

Two separate demonstrations of efficient catalytic asymmetric synthesis led to rapid change thereafter. These key initial contributions involved the asymmetric aldol reaction catalyzed by proline (1971),[15,16] and asymmetric hydrogenation with enantiomerically pure rhodium phosphine complex catalysts (1968–1971).[17,18] After Kagan's use of DIOP **5** (Scheme 6.2), easily synthesized from tartaric acid, chelating diphosphines became the standard ligands for asymmetric hydrogenation. Their paper provides the first example of enamide hydrogenation as a route to enantiomerically enriched amino-acids.[19] The path to Knowles's chelating ligand was taken through discovery of far more efficient monophosphines where the key factor was incorporation of a 2-methoxyphenyl group in the ligand.[20] The chelating biphosphine ligand DIPAMP **6** ensued and was utilized in the first commercial application of asymmetric hydrogenation for production of the aromatic amino-acid L-DOPA soon afterwards.[21] Integration of ruthenium catalysts using Noyori's BINAP ligand **7** and close relatives that demonstrated high ee's in asymmetric hydrogenation,[22] and likewise the transfer hydrogenation of ketones,[23] further extended the range of applications.

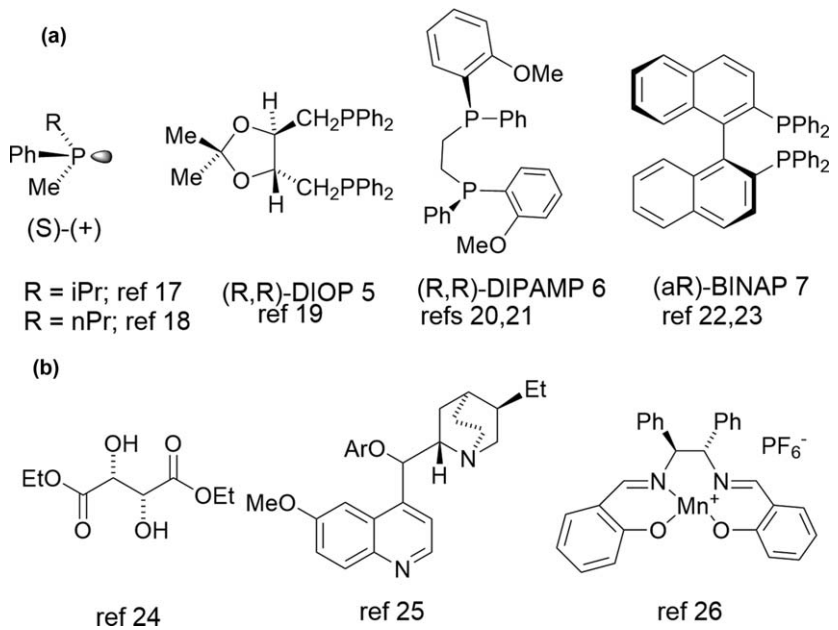

Scheme 6.2 Effective ligands for catalytic asymmetric synthesis. (a) Hydrogenation and (b) C–O bond formation.

Discoveries of the asymmetric epoxidation of allylic alcohols by Sharpless and Katsuki,[24] asymmetric dihydroxylation of alkenes by Sharpless and Jacobsen,[25] and asymmetric epoxidation of simple alkenes by Jacobsen,[26] widened the synthesis of asymmetric catalysis to C–O bond formation, in industry and academia. These rapid developments had been summarized, just over twenty years after the key discoveries.[27]

6.2.2 Non-linear Effects (NLE)

Non-linear effects (NLE)[†] in the context of organic reactivity refers to a non-linear relationship between the enantiomeric purity of a catalyst or reagent and the enantiomeric purity of the reaction product. In 1937 Langenbeck suggested circumstances in which this might be likely to occur.[28] His research activity had been directed toward simple molecular systems that provided models for the action of common enzymes, including esterases and dehydratases. This led him to consider the specificity of chirality in Nature and make comparisons between enzymatic and organic reactions. The conclusion he came to, as translated in Heller's review of the early examples of NLE,[29] indicates his view that: ''*It must be possible using a highly stereochemically specific catalyst*, *and where an equilibrium is formed with the substrate*, *to realize an increase in the optical purity when one allows an optically impure catalyst to catalyze a reaction*, *starting with an optically impure substrate*''. Langenbeck's ideas were not developed further at the time, partly because of the relatively slow pace of progress in asymmetric synthesis. The importance of this pioneering paper was recognized and propagated by Heller soon after Kagan's initial papers had provided robust experimental evidence for NLE in asymmetric synthesis and catalysis.[30]

There were other significant advances in the intervening period, however, that hinted at the broader picture that would emerge. Occasional observations and interpretation of anomalous stereochemical effects both in spectroscopy and in synthesis had been made. Horeau had observed non-linearity in polarimetry when he plotted the rotation of α-methyl-α-ethyl-succinic acid, resolved to varying degrees, against the known optical purity of the samples at constant concentrations in $CHCl_3$.[31] He subsequently reviewed the relevant literature up to 1974 on related stereochemical disparities.[32] He concluded that effects observed by polarimetry, NMR, and calorimetry may be explained by diastereomeric interactions of enantiomers in solution. On this basis, he challenged the existence of a spurious effect involving ''racemates in solution'' (preferred (*R*,*S*) association) that had previously been postulated.

Wynberg and Feringa examined the difference between the oxidative phenolic coupling of enantiomerically pure (*S*) or racemic substrates, where the sterically-hindered product may possess (*R*,*R*), (*S*,*S*), or (*R*,*S*)-configuration

[†]NLE = non-linear effect – in a stereochemical context.

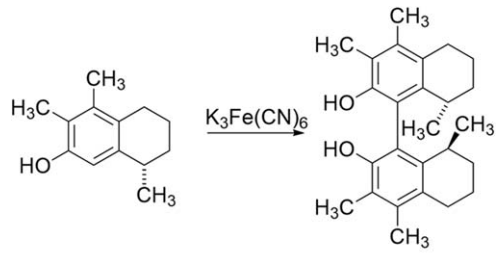

8 9

Scheme 6.3 Oxidative coupling that forms a new stereogenic axis, through hindered biaryl rotation.

and also possesses a stereogenic axis as a consequence of hindered biaryl rotation. They found that oxidation of the pure (*S*,*S*)-enantiomer of **8** gave pure (*S*,*S*,*aR*)-enantiomer **9** as expected (Scheme 6.3). By contrast, the main product from racemic **8** had an (*S*S**,*aR**) configuration but was formed together with a minor quantity of racemic (*S**,*S**,*aS**)-**9**. Similar behavior was found in the analysis of the products from reductive dimerization of enantiopure and racemic camphor. Their results challenged the prevailing idea of ''enantiomeric self-recognition'' (preference to form racemates) and they concluded that for a reaction involving a chiral starting material, both the rate and the optical yield will be dependent upon the ee of the reactant.[33]

In addition to recording the first authentic examples of both positive and negative NLE's in asymmetric synthesis, Kagan has been responsible for definitive and comprehensive reviews on this topic, covering the literature prior to the publication date of his later article in 2009.[34,35] His rigorous enumeration of the consequences of NLE for enantioselectivity and reactivity, in reactions conducted with a scalemic catalyst or auxiliary, has provided a template for many subsequent quantitative analyses.[36] His publications led to a step growth in the appreciation and application of NLE's, particularly in their application to catalytic reactions.

6.2.3 Autocatalysis

Autocatalytic reactions[37] involve a product or precursor of a product as a catalyst, affecting both the reaction rate and product distribution. Early demonstrations of *in vitro* autocatalytic behavior were largely based on the self-replication of small or medium-sized nucleotides, with key papers from von Kiedrowski and Nicolaou.[38,39] Rebek's publications, where autocatalytic turnover was achieved in designed chemical systems based on H-bonding recognition between catalyst and reactants, gave generality to the emerging field.[40,41] In a further development, Sutherland demonstrated H-bonding catalysis for a Diels–Alder reaction where the diene and dienophile may both form multiple H-bonds with their reacting partner, and the product further facilitates the reaction by H-bonding to both components of the reactant

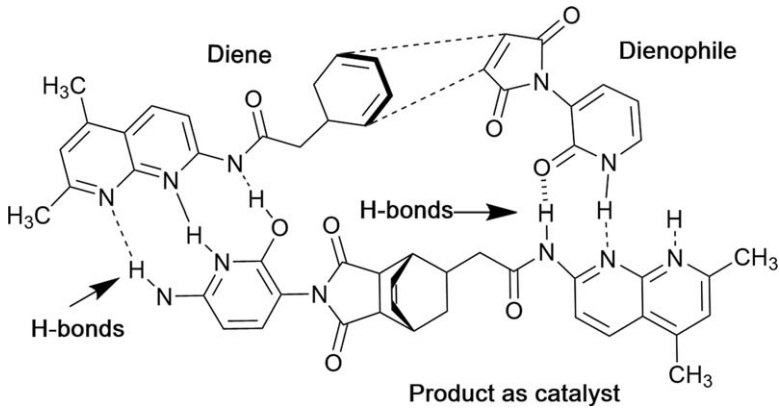

Figure 6.3 Autocatalysis through multiple H-bonding of the product to the reactants. Adapted from ref. 42 with permission from the Royal Society of Chemistry.

pair. In the absence of added product, evolution of the reaction follows a hysteresis curve and is in accordance with the model shown in Figure 6.3.[42]

Cycloadditions involving a chiral reactant may produce an additional stereogenic center in the product and high levels of diastereoselectivity have been demonstrated in some cases.[43,44] Autocatalysis based on the recognition of catalyst and reactant through H-bonding arrays has developed strongly within the general framework of systems chemistry.[45]

6.2.4 Chiral Amplification Through Phase Change

For scalemic compounds, many processes that involve a change of phase have the potential to alter ee's. This is a diverse area that has been thoroughly reviewed;[46] only a brief overview will be attempted here. It is interesting that iso-propyl substituents play a significant role in several examples.

Chromatography of scalemic samples on achiral supports can lead to changes in enantiomeric purity between elution fractions. In this way Kagan noted that the leading fractions from chromatography of sulfoxide **10** (Scheme 6.4) of 86% ee on an achiral silica gel column were of 99% ee, and late fractions were of lower ee than the original sample.[47]

There are many recorded cases where the sublimation of a scalemic sample leads to fractionation with either the sublimed material or the residue becoming enriched in one enantiomer. In an early example, Kwart demonstrated that very slow sublimation of scalemic sulfide **11** led to enantiomerically pure sublimate and racemic residue.[48] Sublimation of scalemic amino-acids can lead to amplification of ee, which is accompanied by rapid interconversion of racemic and conglomerate crystals in the solid phase.[49] Examples of enantiomer separation through fractional distillation are more rare, and require association of monomers in the gas phase and differentiated stabilities of (*R*R**) and (*R*S**) dimers or aggregates.

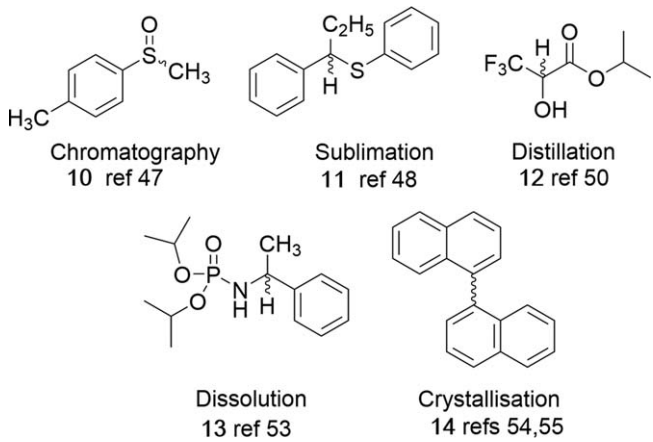

Scheme 6.4 Asymmetric amplifications involving a phase change.

The classic case is iso-propyl trifluorolactate **12** that has the potential for strong intermolecular H-bonding, favoring the homochiral form.[50]

The simple process of dissolution of scalemic amino-acids in water may lead to amplification.[51] Conversely, through consideration of the phase diagram for proline, the likelihood of amplification on dissolution of racemic amino-acids was noted. This was observed in several cases, with racemic phenylalanine possessing 83% ee at the eutectic point.[52] Feringa has reported a more recent example of ee enhancement through dissolution of phosphoramidite **13** in water and standing at 0 °C. Under these conditions, a scalemic starting material gives rise to enantiomer enriched product in up to 95% ee. It was suggested that amplification arose from the better steric matching of monomers in the homochiral dimer than in its heterochiral counterpart, a suggestion supported by the X-ray structure of the homochiral dimer. H-bonding from water to the substrate may also play a role. Their approach was successfully extended to related ring-substituted derivatives and esters of common amino-acids.[53]

Starting from crystals of racemic 1,1′-binaphthyl **14**, spontaneous deracemization from the stirred molten phase had initially been investigated by Pincock.[54,55] The compound crystallizes in either racemic $P4_12_12$ or chiral c_2/c space groups, and the relative stability of the two solid forms is temperature dependent. Above 75 °C the racemic compound is gradually converted into the enantiomerically pure forms. In a set of 200 crystallizations from molten binaphthyl at 150 °C, seeded externally by local dry ice contact, all experiments led to optical activity in the product, close to equi-distribution between (*R*,*R*)- and (*S*,*S*)-forms and with variable ee averaging around 20%.[56] Asakura and Kondepudi later showed that the ee of the product is critically dependent on the stirring speed, and uniformly high with a stochastic distribution in multiple runs between (*R*)- and (*S*)-binaphthyl crystals, obtained upon fast stirring of the melt at 180 °C.[57]

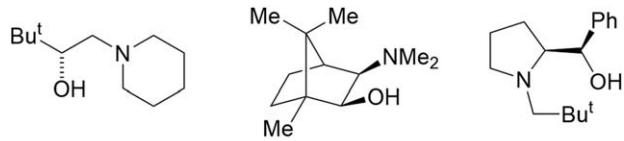

15 ref. 59 16 ref. 60 17 ref. 61

Scheme 6.5 Key compounds in the early application of NLE to catalysis.

6.2.5 Asymmetric Catalysis Creating Amplification Through NLE

Further progress toward an effective procedure for AAA required a reaction that also showed a strong non-linear effect; one that also generated suitable functionality for further catalytic activity, and progress came from catalytic organozinc chemistry. This was initiated by Oguni's 1984 paper.[58] The key finding there was that enantiomerically pure β-aminoalcohols catalyzed the addition of diethylzinc to aldehydes, in moderate enantiomer excess. With further improvement of catalytic enantioselectivity, he demonstrated a positive non-linear effect, of clear interest in a catalytic asymmetric reaction leading to the formation of a new C–C bond. Typically, ee amplification of 6.5% to 74% occurred in a single step with **15** (Scheme 6.5) as the source of catalysis.[59] The ability to make C–C bonds in a catalytic asymmetric reaction attracted many groups to design alternative catalysts for the same reaction. Two sets of results stood out for the high levels of enantioselectivity that were achieved. Noyori's application of the monoterpene derived β-aminoalcohol DAIB[‡] **16**, contributed both synthetic developments and mechanistic insights.[60] Soai's simply prepared norephedrine-based pre-catalyst was effective for both aliphatic and aromatic aldehydes, and his proline-related catalysts **17** performed well, giving access to both enantiomers of the alkylation product.

6.2.6 Absolute Asymmetric Synthesis (AAS)

This topic has been well-covered in Mislow's review (ref. 4) and is discussed elsewhere in the present book but covered only briefly here. AAS has been widely discussed as a potential origin of biological homochirality, with two feasible pathways. For the first, Kuhn showed that circularly polarized light (CPL) was capable of inducing asymmetry in racemic mixtures by photodestruction.[61] Kagan demonstrated an asymmetric synthesis from achiral precursors through the agency of CPL for the first time, in 1971. He was able to achieve this by obtaining hexahelicene with *ca.* 0.2% optical purity through a CPL-induced photocyclization.[62]

Mills had shown in principle that AAS could be created by a reaction using a racemic catalyst that reacted with substrate to form a product with a new

[‡]DAIB = acronym for dimethylamino-iso-borneol.

stereogenic center.[63] Provided that the total number of molecules of the catalyst was sufficiently small, a random but measurable enantiomer excess would be the most likely outcome. The average enantioselectivity X is given by the expression:

$$X = 0.7643/n^{0.5}$$

where n is the number of molecules of catalyst. Solving this for a pool of 500 000 molecules of racemic catalyst gives an average ee of 0.1%. The significance of this deduction for natural chirality is recognized in Ritchie's prescient article.[64]

Frank's 1953 paper provided a framework for linking these ideas to the prebiotic world. He considered that absolute or spontaneous asymmetric synthesis was fundamental to the origin of life. He offered a mechanism through which the low enantiomer excess in a small pool of self-reproducing enantiomers could be amplified through a systematic series of steps and described a full algebraic analysis for this process. Amplification to complete optical purity only occurred, however, only after he had incorporated an additional step of "mutual antagonism" between the enantiomers.[65] This publication has been highly influential, both in understanding spontaneous asymmetric synthesis, and in the development of models for the origin of Nature's homochirality.

6.3 The Pathway That Led to the First Examples of AAA

Wynberg discussed the feasibility of AAA in reviewing its potential and how it might be realized.[66] He indicated that the dialkylzinc alkylation of aldehydes might provide a possible candidate, although his own system proved ineffective for that purpose. Soai's research from that point onwards demonstrates his perception of the problem and systematic progress towards a solution. In his first demonstration of asymmetric autocatalysis, he showed that the enantiomerically-enriched product from the addition of $Zn^{i}Pr_2$ to 3-formylpyridine **18** acted as a catalyst for further reaction of the same substrates, albeit with a reduction of ee between the catalyst and product. As indicated by the dashed lines for reactant **18** in Scheme 6.6,

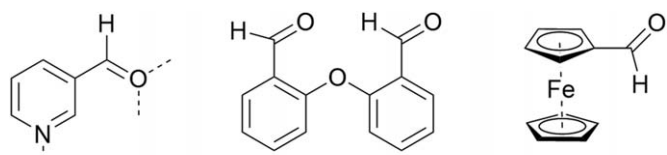

18 ref. 67 19 ref. 68 20 ref. 69

Scheme 6.6 Progress in autocatalysis toward AAA.

the lone-pair vectors in the substrate preclude formation of a monomeric chelate between the aldehyde and pyridine nitrogen; they cannot cooperate to form a monocyclic zinc complex.[67] This result encouraged further examples of autocatalysis, using zinc alkyl reagents together with compounds **19** or **20**, that did not induce amplification of ee when tested. They did underscore the crucial information that using $Zn^{i}Pr_2$ as a reagent gave superior results to the use of $ZnEt_2$, however.[68,69]

These papers provided guidelines for reactant design that soon led to the desired breakthrough, since three distinct examples of AAA were observed through further variation in the structure of the reactant. All of these involved heterocyclic aldehydes as the substrate, namely pyrimidine **21**,[70] quinoline **22**,[71,72] or substituted pyridine **23** (Scheme 6.7).[73,74] The pyrimidine aldehyde **21** was conspicuously the most effective case. An ee of 90% was observed, by a three-step sequence starting from an alkanol catalyst precursor of 5% ee and then using the product from one step as the catalyst for the next step. In a separate publication, autoinduction was demonstrated for the same reactants; high levels of enantiomeric purity in the pyrimidine reactant were maintained through several additional catalytic cycles.[75] Further positive results were obtained for both the quinoline **22** and the 3-substituted pyridine **23**. For the quinoline **22**, three cycles of sequential optimization increased the ee of the final product from 8.9% to 81.3%. For the substituted pyridine, six cycles of optimization increased the final ee from 4% to 86%.

The efficiency of pyrimidine-based AAA was improved through the introduction of a 2-methyl substituent in **24**, (Scheme 6.8)[76] but was dramatically enhanced by incorporation of a 2-alkynyl group.[77] The preferred alkyne substituents were *t*-butyl in **25** or trimethylsilyl in **26**, raising the ee in just a single cycle from 5.5% to 69.6% for the former and 8.4% to 74.2% for the latter. Under optimized conditions using cumene/toluene as the solvent, a product of >99% ee could be amplified to five-fold the original mass in a single cycle, retaining the same level of stereospecificity. For many years afterwards, Soai's heterocyclic autocatalysts remained the only successful examples of AAA, and further developments (*e.g.* **27**) would be largely based on 2-alkynylpyrimidine substrates,[78] (Scheme 6.8) with the more recent exception of pyridine analogs of **25** and **26**.

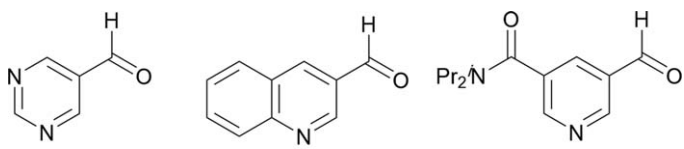

Scheme 6.7 Substrates that demonstrated successful AAA upon reaction with $Zn^{i}Pr_2$.

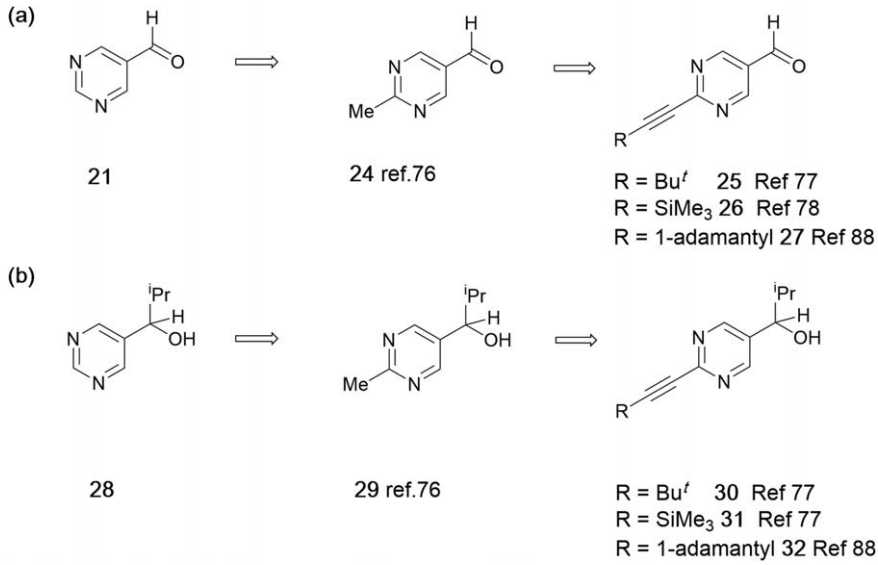

Scheme 6.8 (a) Reactants and (b) products in progressively more efficient AAA reactions.

6.4 The Progression of Mechanistic Understanding of the Soai Reaction

6.4.1 Background: The Catalyzed Reaction of Dialkyl Zinc with Aldehydes

The Soai reaction provides a case of asymmetric synthesis benefitting from NLE, and uniquely catalyzed by the reaction product. More generally, such reactions are catalyzed by β-aminoalkoxyzinc reagents that are capable of forming five-membered chelates, but they do not demonstrate AAA. The most thoroughly studied system in this class is Noyori's bicyclic DAIB reagent. When enantiomerically pure, it catalyzed the conversion of benzaldehyde to 1-phenylpropan-1-ol occurring in 98% ee.[79] The efficiency led to a detailed mechanistic study,[80] a further quantification of NLE effects,[81,82] and both *ab initio* and DFT analyses.[83] There is a strong non-linear effect demonstrated by reaction with Et_2Zn reagent and 8 mol% (*S*)-catalyst (ee = 15%) leading to (*S*)-product, ee = 90%. Arising from the mechanistic studies, the origin of amplification through NLE lies in the higher stability of the racemic (*R*,*S*)-catalyst dimer compared to the homochiral (*R*,*R*) and (*S*,*S*)-dimers. The racemic dimer is the major component in a rapidly equilibrating pool, whereas the reactive form of the catalyst is the monomer (EtZn(DAIB)) based on information from X-ray, cryoscopic, and kinetic measurements. X-ray structures were obtained for analogous homochiral and heterochiral dimers from $ZnMe_2$, with the zinc atoms present in a (Zn–O–Zn–O–) square motif

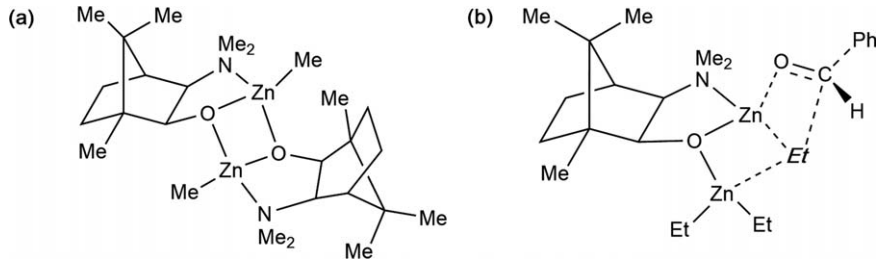

Figure 6.4 (a) The racemic $[Zn–O]_2$ dimer (R = Me) from X-ray. (b) The transition-state model for the preferred pathway from monomeric catalyst, minimizing Et/Ph contact.

(Figure 6.4). In toluene solution at concentrations relevant to catalysis, a heterochiral dimer dominates; significantly, enantiomerically-pure monomers are far less prone to association. The product-determining step in Figure 6.4b is alkyl transfer occurring in accordance with steric constraints, predominantly to the (*S*)-product.

6.4.2 Kinetic Approaches to the Mechanism of AAA

Soai's first contribution to elucidating the kinetics of AAA involved reactions at 0 °C or −45 °C and the following progress by analyzing aliquots from the reaction mixture by HPLC. On the basis of the results obtained that showed characteristic autocatalytic plots of [product] *vs.* time, and a pathway that is second order in the autocatalyst was preferred.[84] In a later contribution using the same methodology,[85] the development of ee during AAA with scalemic catalysts was followed. For three separate runs, the final ee was slightly higher in practice than his model indicated. Hence the possibility of product inhibition, where the catalytically active complex of the reactive enantiomer is inhibited by the unreactive enantiomer, was suggested as an interpretation compatible with Frank's ''mutual antagonism''.

6.4.2.1 Microcalorimetry

This technique measures the heat generated or lost in a chemical process. The strongly exothermic Soai reaction, involving the exothermic conversion of a Zn–C bond in the reagent to a Zn–O bond in the product, is an ideal candidate. Blackmond and Brown showed that the rate of reaction was consistent with the involvement of a dimeric intermediate; the reaction rate for aldehyde and Zn^iPr_2 with enantiomerically pure catalyst **29** *vs.* time could be superimposed on the same curve as an identical run with racemic catalyst, with the former reacting at twice the rate of the latter. This clearly makes the mechanistic pathway incompatible with a monomeric catalyst (*cf.* ref. 80). With a scalemic catalyst, the curve could not be superimposed on

those from either racemic or enantiomerically-pure runs. Taken together, this led to their proposal that the active catalyst was dimeric, and the source of AAA was the kinetic inertness of the racemic dimer with comparable energies for the racemic and enantiomerically-pure zincates in an unbiased and assumed rapid equilibrium. This process played the role of Frank's "mutual antagonist" that was necessary for amplification of ee as the reaction progressed.[86] Further constraints on the mechanism were placed by the rate equation that was derived in Blackmond's later paper that showed dependency on $[A]^2[C]^1[ZniPr_2]^0$, where [A] is aldehyde and [C] is pyrimidinol. Two aldehydes together with a dimeric catalyst indicated a tetrameric transition state.[87]

In later work using Gehring's adamantyl–ethynyl reactant and *in situ* prepared catalyst, some further observations were made. Using RPKA to analyze the data,[88] the reaction order was confirmed, albeit with a fractional best fit of $[A]^{1.6}$. The fractional order in [A] was attributed to an intermediate stage in the catalytic cycle where the second aldehyde adds to an intermediate that already includes the first one. Absence of Zn reagent from the rate equation suggests its active participation only occurs after the first irreversible step. These postulates were supported by further analysis of the experimental data and discussion of the broader context.[89]

6.4.2.2 IR

Denmark and Houk were encouraged by the fact that pyridine-derived enantiomerically-pure Zn alkoxides and those derived from alkanols exhibited tetrameric structures by DOSY (*vide infra*, Section 6.5.1). They introduced IR monitoring techniques for following the decay of the aldehyde C=O stretching vibration at *ca.* 1700 cm^{-1}. For aldehyde **33** (Scheme 6.9) as the reactant, a slow decay curve exhibiting the hysteresis shape characteristic of autocatalysis was observed. In the absence of added catalyst, a racemic product was formed. With **34** of 42% ee as the catalyst, amplification gave **34** (R = Pr^i) of 82% ee after five turnovers, verifying AAA activity (Section 6.4.2.1). A study of the scope and limitations of AAA for related pyridine structures was conducted,

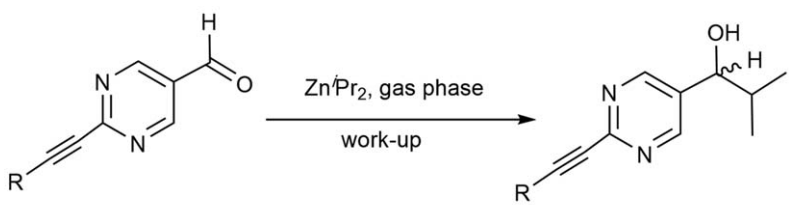

35; R = Bu^tCMe_2; chiral space group
25; R = Bu^t; achiral space group, enantiotopic faces

36; R = Bu^tCMe_2
30; R = Bu^t

Scheme 6.9 A reactive substrate for pyrimidine AAA.

demonstrating that substrates with F- or Me-substituents at the unoccupied *meta*-position of **33** were also viable. A direct comparison showed that **33** reacted more slowly than pyrimidine **31.** A closely related aldehyde to **34** (R = Et) does not exhibit AAA under these conditions. Analysis of the reaction kinetics was made cautiously but indicated that the reaction might exhibit a distinct rate profile to that observed with pyrimidines, first-order in aldehyde. The authors are cautious about over-interpreting their data but recognize the mechanistic importance of inhibition by excess Zn^iPr_2 reagent.[90]

6.4.2.3 MS

Modern mass spectrometry provides a useful resource for research into the reaction mechanism, particularly in organometallic chemistry.[91] General ES-MS techniques permit the accurate determination of the masses of positive ions and allow insight into reactive intermediates in catalysis.[92] MS methodologies had not previously applied to AAA, but Trapp and co-workers have thoroughly demonstrated their potential.[93] Positive-ion ES-MS analysis is enabled by gas-phase protonation of a pyrimidine nitrogen atom. Zinc-containing ions are readily identified because each zinc atom contributes five isotopes, four having a natural abundance of ≥4%. The MS setup was calibrated up to 800 amu, permitting the analysis of species up to trimeric for the zincate from **29** and dimeric for the zincate from **30.** By continuous sampling of the reaction (FTMS/APCI), a number of ions were detected derived from mono-, di-, and trizincate species. From a mechanistic point of view the two most significant were the di- and trizinc hemiacetal species, identified by HRMS from parent and daughter ions. As part of the same paper they obtained kinetic data, monitoring the decay of aldehyde and the growth of product in the presence of 1% alcohol of 99.9% enantiomeric purity by chiral HPLC. No loss of enantiomeric purity in the product was observed over time and their derived rate equation was in accord with Blackmond's results derived by microcalorimetry; $[A]^{1.9}[C]^1[Zn^iPr_2]^0$, [C] being the added pyrimidinol. The paper emphasizes the importance of hemiacetal intermediates in the AAA catalytic cycle and provides a mechanism where the trimeric intermediate fulfills a catalytic role.

6.4.3 Computational Approaches to the Mechanism of AAA

The $(Zn–O)_2$ square arising from Noyori's X-ray analysis of homo-and heterochiral dimers from the reaction between DAIB and Me_2Zn was the preferred initial building block for computations. The early DFT work of Gridnev and Brown was designed to establish the relative energies of oligomers based on the pyrimidine Zn–alkoxide monomer, with $ZnMe_2$ as the reagent to simplify computation.[94] This work established two reasonable geometries for dimers: square and macrocyclic with N–Zn–O coordination, the square dimer is the more stable by 6.8 kcal mol^{-1}. At the tetramer level, at least five viable

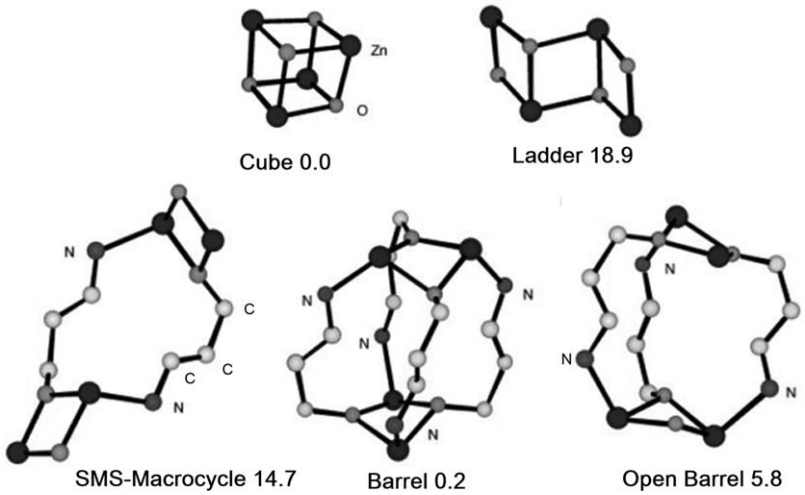

Figure 6.5 DFT calculations (gas-phase, B3LYP) showing the atom connectivity of different ring frameworks in minimized structures, using $ZnMe_2$; (energies quoted in kcal mol^{-1}). Reproduced from ref. 94 with permission from the National Academy of Sciences.

structures were found (Figure 6.5). The cubic geometry suggested by Noyori,[38] being the one that is prevalent for simple Zn alkoxides in the CCDC database, was calculated to be the structure of lowest energy. Barrel structures, where three or four extended links are made between two Zn squares, were found to be of comparably low energy; the Open Barrel structure with three links is coordinatively unsaturated. The Ladder variant where two Zn–O squares are *trans*-disposed is disfavored. The Square-Macrocycle-Square (SMS)[§] is likewise energetically disfavored, but otherwise an attractive proposition because of the flexible macrocyclic ring with the potential for substrate binding.

Related DFT calculations by Klankermayer *et al.* changed the perspective, however. $Zn^{i}Pr_2$ was used in these later calculations since it is the only effective reagent for AAA. This work demonstrated that the SMS tetramer suffers far less steric strain than the Cube and other closer-packed tetramers that all experience unavoidable steric clashes between iso-propyl groups. This made the SMS-tetramer an attractive candidate for the structure of the resting state in solution.[95]

Gridnev and Vorobiev carried out further computational studies, supported by low temperature NMR. These results form part of an ambitious attempt to correlate all the available information on the Soai autocatalytic pathway prior to 2012.[96] This paper also systematically calculated the energies of potential intermediates in AAA, using the B3LYP functional, since

[§]SMS = abbreviation of square-macrocycle-square.

this was in better accord with experimental observations on the relative strength of Zn–O and Zn–N bonds than the M05-2x functional. The authors analyzed the conformational flexibility of both homochiral and heterochiral species by calculating the ground-state energies of accessible minima. They conclude that distinct ground-state geometries can exist that distinguish the homochiral and heterochiral forms. The authors discuss the possibility of barrel tetramers being involved in catalysis and consider it to be less likely, based on their own low temperature NMR analyses. They conclude on the basis of their experiments that the reaction pool of AAA exists mainly as interconverting square dimers, with access to SMS tetramers.

6.4.4 Spectroscopic Approaches to the Mechanism of AAA

6.4.4.1 NMR

DOSY is informative on RMM but alone provides no details of the underlying structural framework. That information can be provided by other NMR analyses. Under conditions that are comparable to AAA reaction conditions, the ^{1}H spectra are complicated by dynamic broadening and do not provide details that define the preferred connectivity. Assuming that the catalyst needs to be coordinatively saturated limits the structures that need to be considered and additional information can be revealed by NMR. For the aldehyde alone, reagent binding is detectable by chemical shifts in ^{1}H and ^{15}N NMR spectra that indicates the pyrimidine nitrogen is the binding site, weak at 273 K and best measured at 213 K (Figure 6.6). Stronger binding of the zinc reagent to Zn alkoxide was observed in separate experiments, where a comparable binding constant of 5.5 mol^{-1} was derived at 273 K. This indicates that under the typical low concentrations employed for the Soai reaction, the zinc reagent is largely dissociated from available pyrimidine sites.[97,98]

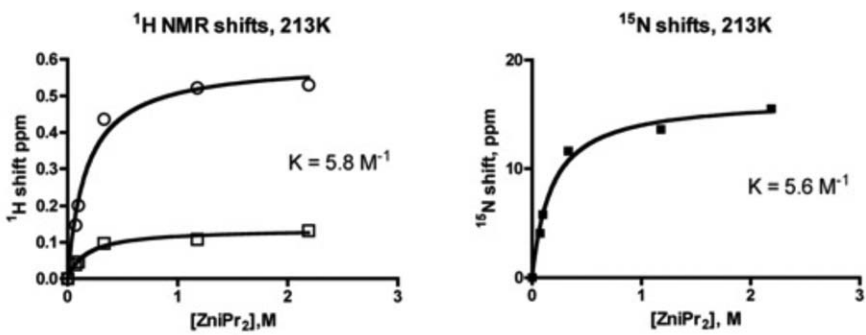

Figure 6.6 Weak association of aldehyde with Zn^{i}Pr$_2$, by NMR titration at low temperature. Reproduced from ref. 98*b* with permission from Springer Nature, Copyright 2008.

The reagent binding experiments do not provide information on the solution state of the catalyst, although that may be deduced from dynamic NMR experiments on a racemic mixture, shown in Figure 6.7. At 323 K and below, two signals are observed in the aromatic region that correspond to two species, homochiral and heterochiral, at comparable concentrations. These are in rapid equilibrium at higher temperatures through a dissociation–recombination mechanism. Although the dynamic behavior is compatible with a dimeric structure, the DOSY results require a tetramer. The (*R*,*R*,*R*,*R*)-tetramer has a pair of pyrimidines that form part of the macrocyclic ring and a pair that are pendants. On the NMR timescale at temperatures where autocatalytic turnover is efficient there are just two magnetic environments for the pyrimidine, implying that any conformational equilibria in the macrocycle are rapid.

In further experiments, the comparative dynamic behavior of the homochiral and heterochiral Zn alkoxides was analyzed in both THF and toluene by ^{1}H NMR. In THF, where AAA does not function, sharp signals were observed for the heterochiral species, but the homochiral species was broader. At low temperatures in toluene, concentration-dependent line-broadening reveals further associative reactions involving the homochiral tetramer; above RT a dissociation/recombination process governs site exchange between homo- and hetero-chiral forms, as shown in Figure 6.7.

Using the 1-adamantyl aldehyde **33**, where there is a high degree of solubility over a wide temperature range, the progress of AAA was followed by NMR in toluene-d_8.[99] Significant line broadening was noted that limited the scope, but as the reaction progressed there were marked chemical shift changes associated with the ZnCH signal; plotted over time a hysteresis curve that tracked the progress of reaction was followed. An anomalous

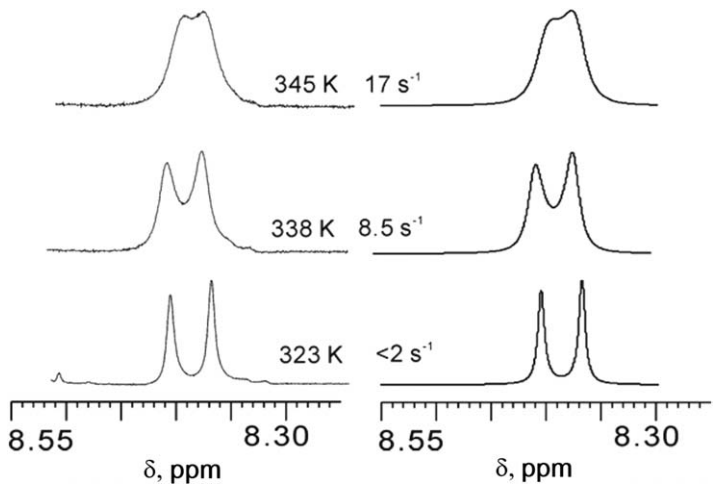

Figure 6.7 Samples from the ^{1}H DNMR analysis of racemic catalyst from 24 in toluene-d_8, showing site exchange between the homochiral and heterochiral components.

signal consistently appeared at the onset of the burst phase and disappeared before the reaction was complete. The most evident signals were in the 6 ppm region of the ^{1}H spectrum and identified as a trimeric acetal moiety from spectral correlations. At 253 K this transient persisted ($t_{1/2}$ *ca.* 1 h) and at 233 K it persisted throughout the reaction and involved ≥10% of the product; warming to RT after completion of AAA led to disappearance of all associated signals and regeneration of two equivalents of starting aldehyde, indicating that the zinc hemiacetal species is thermally labile. This reactive species was analyzed further by Gridnev,[100] with the reasonable conclusion that a reaction between transiently-formed square dimer species and aldehyde reactant is responsible for the appearance of the observed acetal signals. Any requirement for the independent existence of a square dimer is significant and is in accordance with DNMR observations, since it implies that the overall AAA reaction is more complex than a simple templating of four reactants by a tetrameric product.

6.4.5 X-ray Crystallography for Mechanistic Insights into AAA

6.4.5.1 X-ray

Crystallization and X-ray analysis indicate the feasibility of a postulated species in catalysis rather than defining its precise role in the catalytic cycle. This has the potential to provide the most important advances in understanding of a catalytic mechanism. For this reason, the structures of tetrameric Zn alkoxides reported by Matsumoto and Soai give confidence to the proposals that have arisen in the course of NMR and DFT studies.[101,102] Together with one $ZnEt_2$ analog, six related structures were completed, all requiring either crystallization in the presence of excess reagent or THF in addition to the hydrocarbon solvent. These structures were derived from both enantiomerically-pure alkoxide and racemic alkoxide. All the tetramers possess the SMS-framework as a core; a combination of (*S*,*S*) and (*R*,*R*) dimeric units are observed in the racemic cases. Additional Zn^iPr_2 in the structures is mainly coordinated to the free pyrimidine lone pairs. Different structures reveal distinct conformations of the macrocyclic component unit, that alter the way the two $(Zn–O)_2$ squares are disposed to one another. In the homochiral tetramer, they are *syn*-related, but they are *anti*-related in the heterochiral tetramer. The *syn*-form possesses a cavity that can accommodate the substrate, and exocyclic pyrimidines able to bind the reagent. This combination permits a low energy reaction pathway for product formation, but only for the homochiral tetramer, and this structure is in accord with the model proposed by Denmark and Houk on the basis of their DFT calculations. The variations in the core structure between different crystals suggest a high level of conformational mobility for the tetrameric species in solution (Figure 6.8). It is notable that only the simple homochiral tetramer has *syn*-related square dimers that would enable it to function as a catalytic pocket for AAA turnover.

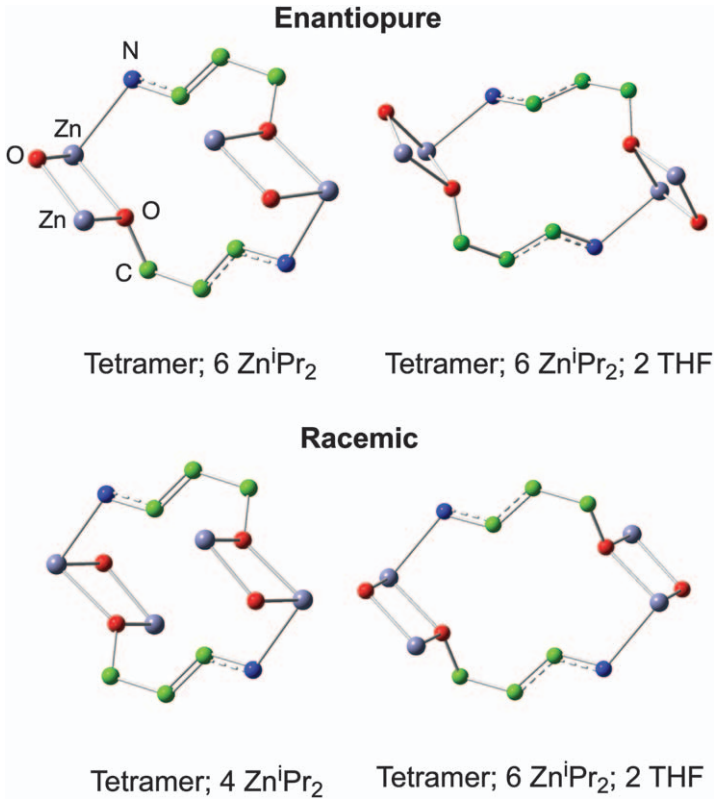

Figure 6.8 The central core atoms of the two Zn^iPr_2 complexed tetramer structures and the two THF-complexed Zn^iPr_2 complexed tetramer structures. Models were based on the CCDC X-ray coordinates for structures 1420664, 1420666, 1420667, and 1477025.[101,102]

6.5 Current Understanding of the AAA Catalytic Cycle

6.5.1 Molecular Weights from Diffusion-ordered Spectroscopy

Among the methods available for measuring RMM[¶] values in solution, diffusion-ordered NMR spectroscopy (DOSY) is convenient and rapid. In a solvent of known viscosity, the procedure estimates the hydrodynamic radius of a large molecule at a given temperature that can be converted into molecular weight according to the Stoke–Einstein equation. The standard procedure assumes that the analyte is a sphere and results are normally standardized by including compounds of known RMM;[103] more detailed and precise methods are currently accessible.[104] Estimates made in this way for

[¶]RMM = reduced molecular mass.

the RMM of the resting state in AAA are in accord with a tetrameric structure, independent of the temperature.

The tetrameric zincate from **31** that is proposed to be the resting state of AAA has an RMM of 1423 and the zincate from **32** has an RMM of 1672. When DOSY measurements were made in toluene at 233 K and compared to mono and dimeric porphyrins of known molecular weight the results, based on the assumption of tetrameric zincates, fit very well when diffusion coefficients from DOSY measurements in toluene at 233 K (Figure 6.9). This is in accord with results obtained at 298 K (see ref. 98, Figure 8). Early DOSY results that were obtained for the Zn alkoxide derived from alkanol **29** by comparison with cubic $(^{i}PrZn–O)_4$ suggest that it is also more aggregated than dimeric.[105]

Denmark and Houk recognized the need for systematic analysis of the structural constraints required for AAA, and synthesized a series of analogs of Soai's pyrimidinols, varying the aromatic ring and considering both ethylzinc and iso-propylzinc-derived species. After reaction with ZnR_2 (R = Et, ^{i}Pr), DOSY analysis (*vide infra*) was used to establish RMM values for the zinc alkoxides. With additional NMR experiments, they established that the trimethylsilylalkynyl analog of **34** was an SMS-tetramer.[106]

Whilst there is a reasonable consensus on a tetrameric structure for the pyrimidine Zn alkoxide at equilibrium in both solution and the solid state, there is less so for the catalytic species involved in the first irreversible step of AAA. If the reaction is first order in a catalyst that is tetrameric, it places constraints on the entities that may be involved. Any rapid equilibration, for example dissociation to dimers that are the catalytically-active entity, must occur without perturbing the concentration of tetramers significantly in

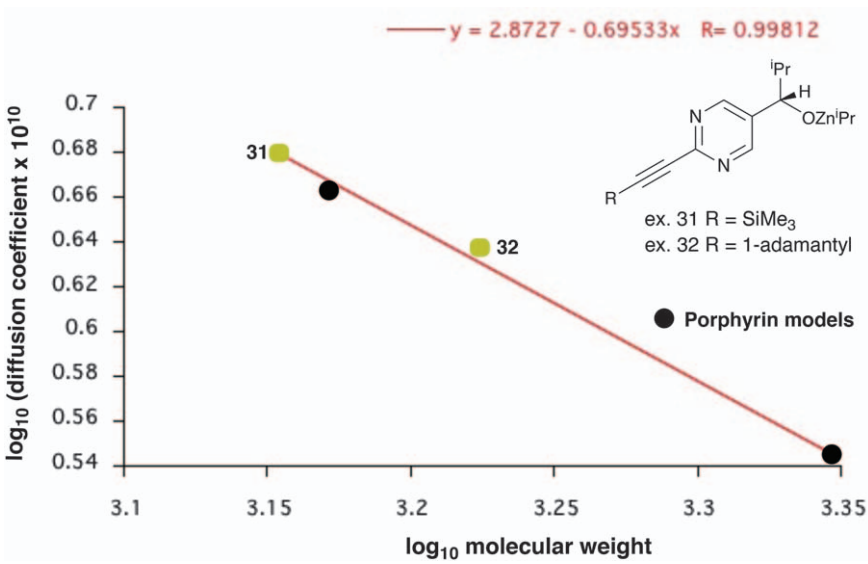

Figure 6.9 Results from the DOSY analysis of the iso-propylzincates from **31** and **32**.

order to retain the defined kinetic order in the catalyst. NMR observations indicate that the equilibrated resting state is dynamic in toluene solution over most of the temperature range that AAA is effective. This means that further insight is only readily obtained through kinetic analysis or computation, or by selective irreversible trapping of transient intermediates. Once the first monomeric Zn alkoxide is formed from the aldehyde substrate in a new cycle of catalysis, it must accumulate three further aldehyde molecules to create a new tetramer. This can occur either through further dimerization of an intermediate dimer or by sequential aggregation steps. The model arising from Blackmond's microcalorimetry limits the range of possible pathways, since it requires the involvement of two aldehyde moieties and one Zn alkoxide in the first irreversible step without participation of $Zn^{i}Pr_2$.[107] This puts constraints on the structure of the resting state but also on the species involved in the first irreversible step of the AAA cycle, since a concentration-dependent dissociative process would deviate from first-order kinetics unless the equilibrium strongly favored the tetramer. The DNMR results demonstrate rapid intermolecular exchange between equal partners that are assembled from two homochiral dimer units and the heterochiral tetramer must be assembled by pairing (*R*,*R*)- and (*S*,*S*)-dimers. Additionally, 3 : 1 aggregation of stereoisomers is disfavored. The overall outcome is compatible with a predominant tetrameric model for both homo- and hetero-chiral forms retained through the catalytic cycle. Even at the time when it was considered that dimers were the resting state in solution, a tetrameric catalyst with SMS structure was suggested. At the time of writing, SMS is the best candidate for the AAA catalyst structure in solution, but access to other conformations (and alternative pathways for AAA catalysis) cannot be ruled out. These considerations apply equally to the more complex chemistry discussed in Sections 6.6 and 6.7.

From an alternative earlier viewpoint, Ercolani and Schiffino proposed that a dimeric autocatalyst model underestimates the observed ee increase as AAA proceeds, when starting with an autocatalyst that was initially of low ee. This led them to consider a trimeric species as a precursor to a product of Barrel structure. When their DFT studies failed to provide a viable pathway for that route, they explained the progression of ee during AAA in a manner analogous to Noyori's reservoir model that they named the ''extended dimer''. In this, the favorable production of racemic over enantiopure tetramers is hypothesized as the existence of an inactive tetrameric reservoir, with a suggested contribution from both SMS and Barrel tetramers (*cf.* Figure 6.5).[108]

6.6 Phase Variation in AAA

Autocatalysis with $Zn^{i}Pr_2$ condensed directly from the vapor phase provides interesting results. Kawasaki and Soai grew large crystals of aldehyde **35** that crystallized in the $P\bar{1}$ space group with enantiotopic faces. When subjected to $Zn^{i}Pr_2$ vapor an AAA reaction took place through the exposed single crystal

surface and it was established that an excess of (*R*)- or (*S*)-product **36** was formed predictably from each crystal, depending on whether the (001) or (00$\bar{1}$) face was the one exposed to reagent vapor. ee values for the single stage process without any bias beyond the exposed surface were in the 15–67% range.[109] In more recent work, similar experiments were conducted by exposing large crystals of aldehyde **25** to the vapor of a solution of Zn^iPr_2 in toluene (Scheme 6.10). This compound crystallizes in an achiral space group but with identifiable mirror image plane faces. When only one face is exposed to the reagent, AAA occurs to give an excess of one hand; the other face gives an excess of the opposite hand. When random crystal faces are exposed, the result is consistently stochastic, with low ee.[110]

Amedjkouh conducted reactions directly between Zn^iPr_2 vapor and pyridinal **33** (Scheme 6.11) in toluene at 0 °C and observed enantiomerically-enriched products without any additional source of chirality involved. Along with the normal AAA product formed in moderate ee a complex mixture of side-products was formed through an intermediate hemiacetal formed from the aldehyde and zinc alkoxide, followed by further aldehyde capture. The main final products are an ester, as a result of MPV-like hydride transfer

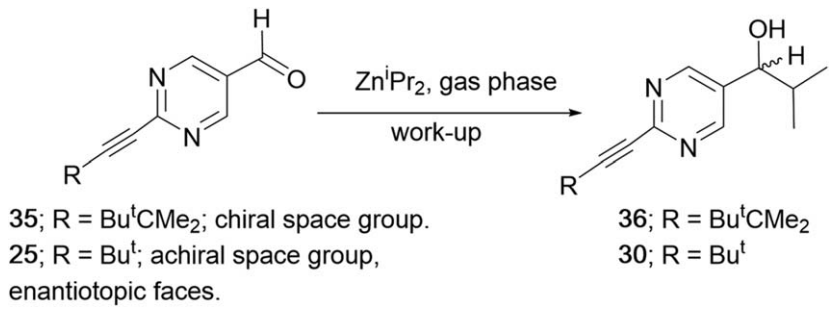

Scheme 6.10 Solid–gas reactions with controlled access to defined crystal faces.

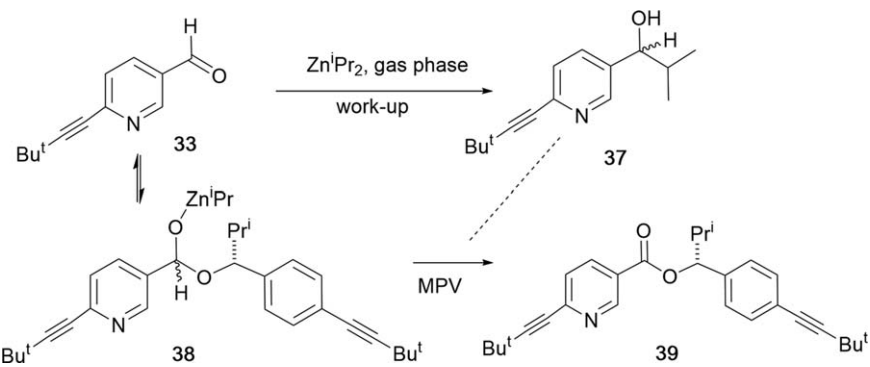

Scheme 6.11 Side-reactions arising from the formation of a hemiacetal **38** and subsequent redox chemistry.

from the hemiacetal to the substrate together with the ketone formed by oxidation of **37** in the hydride transfer step; both possess a maximum ee of 74%.[111]

6.7 The Sensitivity of AAA to Internal and External Factors

Within the first few years of the initial discovery, the extreme sensitivity of Soai's AAA to initiation by triggers of low ee became clear. Starting with the product (R = Me) of 0.018% ee, three *in situ* cycles of catalysis with the corresponding aldehyde substrate led to further product of 87%% ee.[112] Later on, a similar experiment using the analog (R = Bu^{t}C≡C–) with 0.00005% ee (one molecule excess in 100 000) three *in situ* cycles led to product of 99.5% ee invariably defined by the configuration of the enantiomer that was initially in slight excess.[113] The high level of response of AAA had already led to reports of spontaneous asymmetric synthesis (*vide supra*). The sensitivity is not restricted to the added autocatalyst, since the presence of a wide range of chiral solutes at low concentration and low ee leads to effective AAA that reproducibly gives a single enantiomer of product. The sense of asymmetric induction was consistently dictated by the initial configuration of the additives, present in 0.15% ee, that included mandelic acid, methyl mandelate, butan-2-ol, or *N*,α-dimethylbenzylamine. The autocatalytic products were produced in 38–85% ee.[114] Partially resolved [5]- or [6]-helicenes are also effective triggers for pyrimidine AAA even at ee's below 1%, with the (*aS*)-enantiomer leading to (*R*)-alkanol, and the (*aR*)-enantiomer to (*S*)-alkanol; thiahelicenes gave similar results.[115,116] The selective photodegradation of racemic leucine by CPL is an effective trigger for AAA.[117] Insoluble solids,[118,119] where the chirality at an exposed crystal face can act as a trigger for AAA are also effective, exemplified by powdered quartz or sodium chlorate.

The relationship between the configurations of trigger compound and autocatalytic product depended on the trigger in a way that was not well understood. Allowing two very similar triggers of opposite configuration, at identical concentration in toluene, to compete in initiating AAA produced interesting results that could not be fully rationalized. Further work to elucidate the origins and better understand the role of triggers followed.[120] Chiral and achiral β-aminoalcohols, that might be expected to compete with pyrimidinols for sites in the AAA catalyst, were employed.[121] The effectiveness of switching an (*S*)-directing autocatalyst to the (*R*)-pathway was judged by the ratio of achiral trigger **40** to chiral trigger **41** at the inflexion point, with lower values indicating a more powerful response, with R = *n*-Bu the most effective (Scheme 6.12). The structures of triggers that are effective in reversing the stereochemical course of autocatalysis suggests the possibility that the trigger competes with a pyrimidinol monomer for sites in the catalytic aggregate. The resulting mixed species produces the opposite enantiomer of product to unperturbed autocatalyst. The switching efficiency of

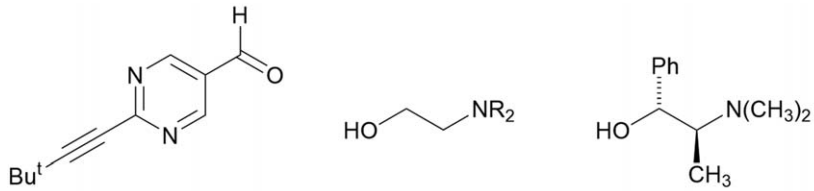

Reactant, **30** Achiral trigger **40** Chiral trigger **41**

Inflexion points: R = CH_3, 60%; R = C_2H_5, 40%; R = n-Octyl, 30%; R = n-Butyl, 25%

Scheme 6.12 Triggering autocatalysis whilst varying the composition of a mixture of enantiomerically-pure and achiral β-aminoalcohols.

the achiral component is indicated by the inflexion point where the product configuration switches from ≥95%(*R*) to ≥95%(*S*); the lower the more efficient. Similar observations were made through variation of the relative proportions of two chiral triggers, one (*R*), the other (*S*)-directing.[122]

Amedjkouh examined the possibility of AAA occurring with the pyridine analog **33** of pyrimidine **25**, but this was not observed under their conditions. With added enantiomerically pure pyrimidinol **30** as the catalyst, using an inverse addition protocol such that the concentration of free Zn^iPr_2 remained low, **33** reacts in competition with **25**. Pyridine **33** reacts the faster, and to a higher final ee than pyrimidine **25**. Under their conditions, the pyridine did not demonstrate AAA independently, but this was induced by co-reaction with the pyrimidine. Using enantiomerically-pure pyrimidine as a trigger, a range of substituted pyridines react to give amplified product in high ee.[123,124]

The response of Soai's autocatalytic reaction to extremely low concentrations of added Zn reagent was tested both by Singleton,[125] and by Gridnev and Brown.[126,127] Results from the latter work that include both experiments with controlled reverse addition of Zn^iPr_2 reagent to (*S*)-alkanols and in the presence or absence of trace alcohol are shown in Figure 6.10. Above 1 μM, the results show a lowering of product ee with decreasing concentration, but with reasonable run to run reproducibility. The lowest concentration of homochiral catalyst was 0.5 μM, and at this level the response is more random, although (*S*)-catalyst always gives (*S*)-product. Without a catalyst, the results show stochastic behavior.

Sensitivity is tested to the limit by isotopically chiral triggers. Examples of the effectiveness of ^2H (partially CH_3-deuterated *N*-benzoyl-2-methylalanine),[128] ^{13}C (Mono $^{13}CH_3$-2-phenylpropan-2-ol),[129] and ^{18}O isotopic chirality in defining the product configuration of AAA have been recorded. The results with single enantiomers of 1-^{18}O-diphenyl-1,2-ethanediol are striking. Dropwise addition of aldehyde and Zn^iPr_2 to a 1% solution of the trigger in toluene at 0 °C gave a product of 75–98% ee, over eighteen examples; after three cycles of amplification with all-(*S*) product from (*R*)-configured trigger

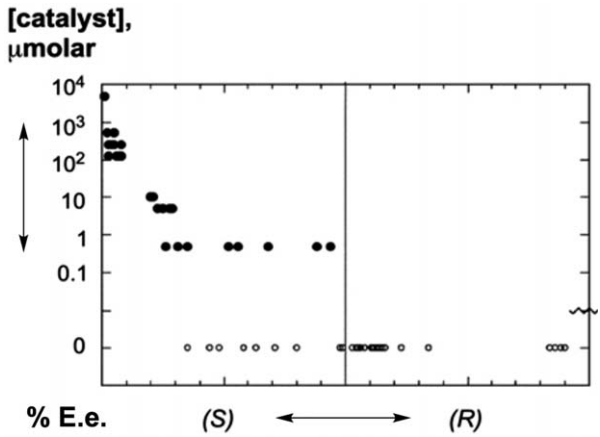

Figure 6.10 Studies of AAA at very low concentrations of added (*S*)-alkanol catalyst (●) and without added catalyst, (○). Adapted from ref. 126 with permission from the Royal Society of Chemistry.

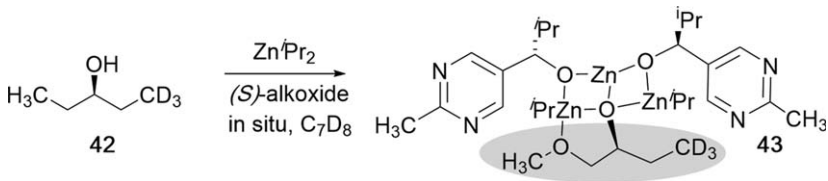

Scheme 6.13 Sensitivity of the Soai reaction to isotopic chirality. The shaded part indicates the preferred isotopomer in the proposed inhibitory intermediate.

and all-(*R*) product from (*S*)-configured trigger.[130] Since AAA is sensitive to isotopic chirality, the process must reveal a KIE whose origin should further explain the phenomenon.

Blackmond studied an ^{18}O-enriched enantiomerically-pure alcohol that acts as initiator of AAA and concluded that the stereochemical control of AAA in its presence was governed by stereoselective complexation of initiator **42** with the autocatalyst. The hypothesis was supported by NMR observations on the reaction mixture containing the resulting 2 : 1 complex **43** and by DFT calculations.[131] Since the energy involved in discrimination must be exceedingly small, the limit was tested by gradual reduction of the enantiomeric purity of added (*R*)-directing initiator until the response was stochastic rather than weighted to (*R*)-product (Scheme 6.13). On this basis the energy required for chiral discrimination by the initiator was estimated at being within the range 1.5×10^{-7} to 1.5×10^{-8} kJ mol^{-1}. Although tiny, this is some orders of magnitude greater than the influence of parity conservation, and currently provides an impressive model for the extreme sensitivity of the Soai reaction.[132]

Acknowledgements

The author thanks Christopher McMillan, Dr Andrea Schorm, Prof. Ilya Gridnev, Dr Jörg Serafimov, Prof. Jürgen Klankermayer, and Dr Timo Gehring for their essential contributions to the Oxford autocatalysis project, Prof. Stephen Fletcher for critical appraisal of a draft, and the Leverhulme Foundation for their support.

References

1. K. Popper and D. Miller, *Nature*, 1983, **302**, 687–688.
2. J. R. Platt, *Science*, 1964, **146**, 347–357.
3. R. P. Feynman, *The Character of Physical Law*, Penguin Books, London, 1992.
4. K. Mislow, *Collect. Czech. Chem. Commun.*, 2003, **68**, 849–864.
5. W. A. Bonner, *Origins Life Evol. Biospheres*, 1991, **21**, 59–111.
6. T. Helgaker, T. A. Ruden, P. Jorgensen, J. Olsen and W. Klopper, *J. Phys. Org. Chem.*, 2004, **17**, 913–933.
7. G. M. Richardson, *The Foundations of Stereo Chemistry; Memoirs by Pasteur, Van t'Hoff, LeBel and Wislicenus, 1901*, Reprinted by Franklin Classics Trade Press, 2018, p. 152, (ISBN-10:0353055204; ISBN-13:978-0353055209).
8. V. I. Goldanskii and V. V. Kuz'min, *Z. Phys. Chem.*, 1988, **269**, 216–274.
9. E. Fischer and M. Slimmer, *Ber. Dtsch. Chem. Ges.*, 1903, **36**, 2575–2587.
10. A. MacKenzie, *J. Chem. Soc., Trans.*, 1904, 1248–1262.
11. G. Bredig and P. S. Fiske, *Biochem. Z.*, 1913, **46**, 7–23.
12. G. Bredig and M. Minaeff, *Biochem. Z.*, 1932, **249**, 241–244.
13. V. Prelog and M. Wilhelm, *Helv. Chim. Acta*, 1954, **37**, 1634–1660.
14. H. Pracejus, *Ann. Chem.*, 1960, **634**, 9–22.
15. U. Eder, G. Sauer and R. Wiechert, *Angew. Chem., Int. Ed.*, 1971, **10**, 496–497.
16. Z. G. Hajos and D. R. Parrish, *J. Org. Chem.*, 1974, **39**, 1615–1621.
17. W. S. Knowles and M. J. Sabacky, *Chem. Commun.*, 1968, 1445–1446.
18. L. Horner, H. Siegel and H. Buethe, *Angew. Chem., Int. Ed. Engl.*, 1968, **7**, 942.
19. H. B. Kagan and T. P. Dang, *J. Chem. Soc., Chem. Commun.*, 1971, 481.
20. W. S. Knowles, M. J. Sabacky and B. D. Vineyard, *Chem. Commun.*, 1972, 10–11.
21. W. S. Knowles, M. J. Sabacky, B. D. Vineyard and D. J. Weinkauff, *J. Am. Chem. Soc.*, 1975, **97**, 2567–2568.
22. H. Takaya, T. Ohta, N. Sayo, H. Kumobayashi, S. Akutagawa, S. Inoue, I. Kasahara and R. Noyori, *J. Am. Chem. Soc.*, 1987, **109**, 1596–1597.
23. M. Kitamura, T. Ohkuma, S. Inoue, N. Sayo, H. Kumobayashi, S. Akutagawa, T. Ohta, H. Takaya and R. Noyori, *J. Am. Chem. Soc.*, 1988, **110**, 629–631.
24. T. Katsuki and K. B. Sharpless, *J. Am. Chem. Soc.*, 1980, **102**, 5974–5976.

25. E. N. Jacobsen, I. Marko, W. S. Mungall, G. Schroeder and K. B. Sharpless, *J. Am. Chem. Soc.*, 1988, **110**, 1968–1970.
26. W. Zhang, J. L. Loebach, S. R. Wilson and E. N. Jacobsen, *J. Am. Chem. Soc.*, 1990, **112**, 2801–2803.
27. *Catalytic Asymmetric Synthesis*, ed. I. Ojima, Wiley-VCH, New York, 1993, ISBN 3527895329.
28. W. Langenbeck and G. Triem, *Z. Phys. Chem.*, 1936, **177**, 401–408.
29. D. Heller, H.-J. Drexler, C. Fischer, H. Buschmann, W. Baumann and B. Heller, *Angew. Chem., Int. Ed.*, 2000, **39**, 495–499.
30. C. Puchot, O. Samuel, E. Dunach, S. Zhao, C. Agami and H. B. Kagan, *J. Am. Chem. Soc.*, 1986, **108**, 2353–2357.
31. A. Horeau, *Tetrahedron Lett.*, 1969, 3121–3124.
32. A. Horeau and J. P. Guette, *Tetrahedron*, 1974, **30**, 1923–1931, and refs. therein.
33. H. Wynberg and B. Feringa, *Tetrahedron*, 1976, **32**, 2831–2834.
34. C. Girard and H. B. Kagan, *Angew. Chem., Int. Ed.*, 1998, **37**, 2923–2959.
35. T. Satyanarayana, S. Abraham and H. B. Kagan, *Angew. Chem., Int. Ed.*, 2009, **48**, 456–494.
36. C. Puchot, O. Samuel, E. Dunach, S. Zhao, C. Agami and H. B. Kagan, *J. Am. Chem. Soc.*, 1986, **108**, 2353–2357.
37. A. J. Bissette and S. P. Fletcher, *Angew. Chem., Int. Ed.*, 2013, **52**, 12800–12826.
38. T. Li and K. C. Nicolaou, *Nature*, 1994, **369**, 218–221.
39. D. Sievers and G. von Kiedrowski, *Nature*, 1994, **369**, 221–224.
40. T. Tjivikua, P. Ballester and J. Rebek, *J. Am. Chem. Soc.*, 1990, **112**, 1249–1250.
41. J. Rebek, Jr., *Acc. Chem. Res.*, 1990, **23**, 399–404.
42. B. Wang and I. O. Sutherland, *Chem. Commun.*, 1997, 1495–1496.
43. A. Dieckmann, S. Beniken, C. D. Lorenz, N. L. Doltsinis and G. von Kiedrowski, *Chem. – Eur. J.*, 2011, **17**, 468–480.
44. C. C. Robertson, H. W. MacKenzie, T. Kosikova and D. Philp, *J. Am. Chem. Soc.*, 2018, **140**, 6832–6841.
45. A. I. Hanopolskyi, V. A. Smaliak, A. I. Novichkov and S. N. Semenov, *ChemSystemsChem*, 2021, **3**, e2000026.
46. J. Han, O. Kitagawa, A. Wzorek, K. D. Klika and V. A. Soloshonok, *Chem. Sci.*, 2018, **9**, 1718–1739.
47. P. Diter, S. Taudien, O. Samuel and H. B. Kagan, *J. Org. Chem.*, 1994, **59**, 370–373.
48. H. Kwart and D. P. Hoster, *J. Org. Chem.*, 1967, **32**, 1867–1871.
49. C. Viedma, J. E. Ortiz, T. de Torres and P. Cintas, *Chem. Commun.*, 2012, **48**, 3623–3625.
50. T. Katagiri, C. Yoda, K. Furuhashi, K. Ueki and T. Kubota, *Chem. Lett.*, 1996, **25**, 115.
51. R. Breslow and M. S. Levine, *Proc. Natl. Acad. Sci. U. S. A.*, 2006, **103**, 12979–12980.

52. M. Klussmann, H. Iwamura, S. P. Mathew, D. H. Wells, Jr., U. Pandya, A. Armstrong and D. G. Blackmond, *Nature*, 2006, **441**, 621–623.
53. V. Daskova, J. Buter, A. K. Schoonen, M. Lutz, F. de Vries and B. L. Feringa, *Angew. Chem., Int. Ed.*, 2021, **60**, 11120–11126.
54. R. E. Pincock and K. R. Wilson, *J. Am. Chem. Soc.*, 1971, **93**, 1291–1292.
55. R. E. Pincock, R. R. Perkins, A. S. Ma and K. R. Wilson, *Science*, 1971, **174**, 1018–1020.
56. D. K. Kondepudi, K. L. Bullock, J. A. Digits and P. D. Yarborough, *J. Am. Chem. Soc.*, 1995, **117**, 401–404.
57. D. K. Kondepudi, J. Laudadio and K. Asakura, *J. Am. Chem. Soc.*, 1999, **121**, 1448–1451.
58. N. Oguni and T. Omi, *Tetrahedron Lett.*, 1984, **25**, 2823–2824.
59. N. Oguni, Y. Matsuda and T. Kaneko, *J. Am. Chem. Soc.*, 1988, **110**, 7877–7878.
60. M. Kitamura, S. Suga, K. Kawai and R. Noyori, *J. Am. Chem. Soc.*, 1986, **108**, 6071–6072.
61. W. Kuhn and E. Knopf, *Z. Phys. Chem., Abt. B*, 1930, **7**, 292–310.
62. H. Kagan, A. Moradpour, J. F. Nicoud, G. Balavoine and G. Tsoucaris, *J. Am. Chem. Soc.*, 1971, **93**, 2353–2354.
63. W. H. Mills, *Chem. Ind.*, 1932, **51**, 750–759.
64. P. D. Ritchie, *Adv. Enzymol. Relat. Subj. Biochem.*, 1947, 65–110.
65. F. C. Frank, *Biochim. Biophys. Acta*, 1953, **11**, 459–463.
66. H. Wynberg, *J. Macromol. Sci., Chem.*, 1989, **A26**, 1033–1041.
67. K. Soai, S. Niwa and H. Hori, *Chem. Commun.*, 1990, 982–983.
68. K. Soai, T. Hayase, C. Shimada and K. Isobe, *Tetrahedron: Asymmetry*, 1994, **5**, 789–792.
69. K. Soai, T. Hayase and K. Takai, *Tetrahedron: Asymmetry*, 1995, **6**, 637–638.
70. K. Soai, T. Shibata, H. Morioka and K. Choji, *Nature*, 1995, **378**, 767–768.
71. T. Shibata, K. Choji, H. Morioka, T. Hayase and K. Soai, *Chem. Commun.*, 1996, 751–752.
72. T. Shibata, K. Choji, T. Hayase, Y. Aizu and K. Soai, *Chem. Commun.*, 1996, 1235–1236.
73. T. Shibata, H. Morioka, T. Hayase, Y. Kodaka and K. Soai, *Tetrahedron Lett.*, 1996, **37**, 8783–8786.
74. S. Tanji, Y. Kodaka, A. Ohno, T. Shibata, I. Sato and K. Soai, *Tetrahedron: Asymmetry*, 2000, **11**, 4249–4253.
75. T. Shibata, H. Morioka, T. Hayase, K. Choji and K. Soai, *J. Am. Chem. Soc.*, 1996, **118**, 471–472.
76. T. Shibata, J. Yamamoto, N. Matsumoto, S. Yonekubo, S. Osanai and K. Soai, *J. Am. Chem. Soc.*, 1998, **120**, 12157–12158.
77. T. Shibata, S. Yonekubo and K. Soai, *Angew. Chem., Int. Ed.*, 1999, **38**, 659–661.
78. K. Soai, T. Kawasaki and A. Matsumoto, *Acc. Chem. Res.*, 2014, **47**, 3643–3654.
79. M. Kitamura, S. Suga, K. Kawai and R. Noyori, *J. Am. Chem. Soc.*, 1986, **108**, 6071–6072.

80. M. Kitamura, S. Okada, S. Suga and R. Noyori, *J. Am. Chem. Soc.*, 1989, **111**, 4028–4036.
81. M. Kitamura, S. Suga, M. Niwa and R. Noyori, *J. Am. Chem. Soc.*, 1995, **117**, 4832–4842.
82. M. Kitamura, S. Suga, H. Oka and R. Noyori, *J. Am. Chem. Soc.*, 1998, **120**, 9800–9809.
83. M. Yamakawa and R. Noyori, *Organometallics*, 1999, **18**, 128–133.
84. I. Sato, D. Omiya, K. Tsukiyama, Y. Ogi and K. Soai, *Tetrahedron: Asymmetry*, 2001, **12**, 1965–1969.
85. I. Sato, D. Omiya, H. Igarashi, K. Kato, Y. Ogi, K. Tsukiyama and K. Soai, *Tetrahedron: Asymmetry*, 2003, **14**, 975–979.
86. D. G. Blackmond, C. R. McMillan, S. Ramdeehul, A. Schorm and J. M. Brown, *J. Am. Chem. Soc.*, 2001, **123**, 10103–10104.
87. F. G. Buono and D. G. Blackmond, *J. Am. Chem. Soc.*, 2003, **125**, 8978–8979.
88. M. Quaranta, T. Gehring, B. Odell, J. M. Brown and D. G. Blackmond, *J. Am. Chem. Soc.*, 2010, **132**, 15104–15107.
89. D. G. Blackmond, *Proc. Natl. Acad. Sci. U. S. A.*, 2004, **101**, 5932–5936.
90. S. V. Athavale, A. Simon, K. N. Houk and S. E. Denmark, *Nat. Chem.*, 2020, **12**, 412–423.
91. C. Iacobucci, S. Reale and F. De Angelis, *Angew. Chem., Int. Ed.*, 2016, **55**, 2980–2993.
92. K. L. Vikse, Z. Ahmadi and J. S. McIndoe, *Coord. Chem. Rev.*, 2014, **279**, 96–114.
93. O. Trapp, S. Lamour, F. Maier, A. F. Siegle, K. Zawatzky, O. Trapp, S. Lamour and B. F. Straub, *Chemistry*, 2020, **26**, 15871–15880.
94. I. D. Gridnev and J. M. Brown, *Proc. Natl. Acad. Sci. U. S. A.*, 2004, **101**, 5727–5731.
95. J. Klankermayer, I. D. Gridnev and J. M. Brown, *Chem. Commun.*, 2007, 3151–3153.
96. I. D. Gridnev and A. K. Vorobiev, *ACS Catal.*, 2012, **2**, 2137–2149.
97. I. D. Gridnev, J. M. Serafimov and J. M. Brown, *Angew. Chem., Int. Ed.*, 2004, **43**, 4884–4887.
98. (a) I. D. Gridnev and J. M. Brown, invited lecture delivered by IDG, *209th ACS Symposium*, Anaheim, CA, 2005; (b) J. M. Brown, I. Gridnev and J. Klankermayer, *Top. Curr. Chem.*, 2008, **284**, 35–65.
99. T. Gehring, M. Quaranta, B. Odell, D. G. Blackmond and J. M. Brown, *Angew. Chem., Int. Ed.*, 2012, **51**, 9539–9542.
100. I. D. Gridnev and A. K. Vorobiev, *Bull. Chem. Soc. Jpn.*, 2015, **88**, 333–340.
101. A. Matsumoto, T. Abe, A. Hara, T. Tobita, T. Sasagawa and K. Soai, *Angew. Chem. Int. Ed.*, 2015, **54**, 15218–15221.
102. A. Matsumoto, S. Fujiwara, T. Abe, A. Hara, T. Tobita, T. Sasagawa, T. Kawasaki and K. Soai, *Bull. Chem. Soc. Jpn.*, 2016, **89**, 1170–1177.
103. T. C. Chan, H. T. Li and K. Y. Li, *J. Phys. Chem. B*, 2015, **119**, 15718–15728.
104. R. Evans, *Prog. Nucl. Magn. Reson. Spectrosc.*, 2020, **117**, 33–69.
105. A. Schorm, Research Report, German Research Foundation (DFG), Dyson Perrins Laboratory, Oxford, 2001, p. 14.

106. S. V. Athavale, A. Simon, K. N. Houk and S. E. Denmark, *J. Am. Chem. Soc.*, 2020, **142**, 18387–18406.
107. D. G. Blackmond, *Tetrahedron: Asymmetry*, 2006, **17**, 584–589.
108. L. Schiaffino and G. Ercolani, *ChemPhysChem*, 2009, **10**, 2508–2515.
109. T. Kawasaki, S. Kamimura, A. Amihara, K. Suzuki and K. Soai, *Angew. Chem., Int. Ed.*, 2011, **50**, 6796–6798.
110. Y. Kaimori, Y. Hiyoshi, T. Kawasaki, A. Matsumoto and K. Soai, *Chem. Commun.*, 2019, **55**, 5223–5226.
111. G. Rotunno, D. Petersen and M. Amedjkouh, *ChemSystemsChem*, 2020, **2**, e1900060.
112. T. Shibata, T. Hayase, J. Yamamoto and K. Soai, *Tetrahedron: Asymmetry*, 1997, **8**, 1717–1719.
113. I. Sato, H. Urabe, S. Ishiguro, T. Shibata and K. Soai, *Angew. Chem., Int. Ed.*, 2003, **42**, 315–317.
114. T. Shibata, J. Yamamoto, N. Matsumoto, S. Yonekubo, S. Osanai and K. Soai, *J. Am. Chem. Soc.*, 1998, **120**, 12157–12158.
115. I. Sato, R. Yamashima, K. Kadowaki, J. Yamamoto, T. Shibata and K. Soai, *Angew. Chem., Int. Ed.*, 2001, **40**, 1096–1098.
116. T. Kawasaki, K. Suzuki, E. Licandro, A. Bossi, S. Maiorana and K. Soai, *Tetrahedron: Asymmetry*, 2006, **17**, 2050–2053.
117. I. Sato, R. Sugie, Y. Matsueda, Y. Furumura and K. Soai, *Angew. Chem., Int. Ed.*, 2004, **43**, 4490–4492.
118. A. J. Gellman and K.-H. Ernst, *Catal. Lett.*, 2018, **148**, 1610–1621.
119. I. Weissbuch and M. Lahav, *Chem. Rev.*, 2011, **111**, 3236–3267.
120. F. Lutz, T. Igarashi, T. Kawasaki and K. Soai, *J. Am. Chem. Soc.*, 2005, **127**, 12206–12207.
121. F. Lutz, T. Igarashi, T. Kinoshita, M. Asahina, K. Tsukiyama, T. Kawasaki and K. Soai, *J. Am. Chem. Soc.*, 2008, **130**, 2956–2958.
122. T. Kawasaki, Y. Wakushima, M. Asahina, K. Shiozawa, T. Kinoshita, F. Lutz and K. Soai, *Chem. Commun.*, 2011, **47**, 5277–5279.
123. C. Romagnoli, B. Sieng and M. Amedjkouh, *Eur. J. Org. Chem.*, 2015, 4087–4092.
124. C. Romagnoli, B. Sieng and M. Amedjkouh, *Chirality*, 2020, **32**, 1143–1151.
125. D. A. Singleton and L. K. Vo, *Org. Lett.*, 2003, **5**, 4337–4339.
126. I. D. Gridnev, J. M. Serafimov, H. Quiney and J. M. Brown, *Org. Biomol. Chem.*, 2003, **1**, 3811–3819.
127. J. M. Serafimov, MSc thesis, Oxford, 2002.
128. T. Kawasaki, H. Ozawa, M. Ito and K. Soai, *Chem. Lett.*, 2011, **40**, 320–321.
129. T. Kawasaki and K. Soai, *Bull. Chem. Soc. Jpn.*, 2011, **84**, 879–892.
130. T. Kawasaki, Y. Okano, E. Suzuki, S. Takano, S. Oji and K. Soai, *Angew. Chem., Int. Ed.*, 2011, **50**, 8131–8133.
131. N. A. Hawbaker and D. G. Blackmond, *ACS Cent. Sci.*, 2018, **4**, 776–780.
132. N. A. Hawbaker and D. G. Blackmond, *Nat. Chem.*, 2019, **11**, 957–962.

CHAPTER 7

Spontaneous Emergence of Chirality in Autocatalytic Cycle Models of the Soai Reaction

THOMAS BUHSE,*[a] MARÍA E. NOBLE-TERÁN,[a] DAVID HOCHBERG,[b] JOSEP M. RIBÓ[c] AND JEAN-CLAUDE MICHEAU[d]

[a] Centro de Investigaciones Químicas-IICBA, Universidad Autónoma del Estado de Morelos, 62209 Cuernavaca, Morelos, Mexico; [b] Department of Molecular Evolution, Centro de Astrobiología (CSIC-INTA), 28850 Torrejón de Ardoz, Madrid, Spain; [c] Department of Organic and Inorganic Chemistry, Institute of Cosmos Science (IEEC-UB), University of Barcelona, 08028 Barcelona, Catalonia, Spain; [d] Laboratoire des IMRCP, UMR au CNRS No. 5623, Université Paul Sabatier, F-31062 Toulouse, France
*Email: buhse@uaem.mx

7.1 Introduction

The long-standing objective of organic chemists has been to achieve total asymmetric synthesis in a homogeneous reaction system,[1–3] and in the absence of an external chiral induction. This dream came true after Soai's discovery.[4] The Soai reaction, the addition of diisopropylzinc to prochiral pyrimidine carbaldehydes (see Scheme 7.1), yields unprecedented biases from the racemate (see ref. 5–9 and references therein). The chiral induction is exerted by the same final chiral product acting as an enantioselective catalyst, and this means that the Soai reaction is an autocatalytic enantioselective reaction.

Catalysis Series No. 43
Asymmetric Autocatalysis: The Soai Reaction
Edited by Kenso Soai, Tsuneomi Kawasaki and Arimasa Matsumoto

Published by the Royal Society of Chemistry, www.rsc.org

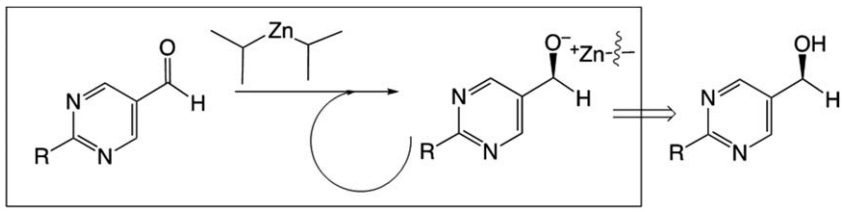

Scheme 7.1 Principle of the enantioselective autocatalysis of the Soai reaction. Initial carbaldehyde and final alkoxide form a diversity of oligomeric complexes with diisopropylzinc. These complexes may be chiral and nowadays it is widely accepted that some of them act as enantioselective catalysts and that additional heterochiral coupling reactions between oligomers, containing the final chiral alkoxides, form a Frank-like reaction network (ref. 10) yielding spontaneous mirror-symmetry breaking (SMSB).

The first efforts to study the Soai reaction were aimed at inferring the mechanisms showing autocatalysis (see Box 7.1). It was realized that this is not a simple direct autocatalysis,[11] but rather one implying a complex reaction network of intermediates (see Section 7.3). The high exergonicity of the alkyl Zn(II) addition to the carbaldehyde points to kinetic control of the reaction before the reverse reaction has had time to racemize the alkoxides. Therefore, the reaction outputs should correspond to transient stationary states.

Several characteristics of the Soai reaction point to a quite different thermodynamic scenario than that of the common asymmetric inductions of organic synthesis. This is an energy dissipative chemical system (see Box 7.2), where the final non-equilibrium stationary state (NESS) does not have the racemic composition: the expected racemate is an unstable NESS, and there is an energetically degenerate enantiomeric pair of scalemic NESS's, which have high enantiomeric excess (ee) values (see Section 7.2). This is an unfamiliar feature compared to the common enantioselective kinetic control of classical asymmetric synthesis. The experimental example of the Soai reaction agrees with a scenario of irreversible non-equilibrium thermodynamics, where a reaction network showing higher order nonlinear enantioselective autocatalysis (Box 7.1) operates at far from equilibrium conditions (Box 7.2). Then, beyond a critical value, an increase in the entropy production converts the racemic NESS into an unstable stationary (saddle) point, from which, by the effect of a chiral fluctuation (Box 7.3), the system evolves towards the corresponding stable scalemic NESS.

In summary, nowadays all rationalizations of the Soai reaction consider a reaction network similar to that of the Frank mechanism[10] (first-order autocatalysis coupled to a heterochiral reaction coupling, called the mutual inhibition step) in which enantioselective autocatalysis and mutual inhibition are provided by the involvement of oligomeric intermediates

Box 7.1 Reaction mechanisms which potentially may yield SMSB

Reaction with linear kinetic dependences on the enantiomers. A common transformation from achiral to chiral products, reversible or irreversible, as for example:

$$A + B \leftrightarrows D(L) \quad \text{or} \quad A + B \rightarrow D(L),$$

can only lead to the racemate in the deterministic limit and in the absence of any chiral polarization.

Reaction showing enantioselective autocatalysis (enantioselective non-linear dependences). When the transformation from achiral to chiral is autocatalytic, the growth dynamics follows[12] either reversibly (left) or irreversibly (right):

$$A + B + nD \leftrightarrows (n+1)D(L) \quad \text{or} \quad A + B + nD \rightarrow (n+1)D(L).$$

The outcome of this reaction depends on the nature of the system and on the autocatalytic order.

If the autocatalytic order is sufficiently high ($n > 1$),

In closed systems in equilibrium with their surroundings, the reversible reaction (left) yields the racemate, while the irreversible one (right) may show racemic biases even if the initial conditions start from extremely low enantiomeric excesses:[13,14] unavoidable initial stochastic fluctuations from the racemate are more efficiently transferred in the deterministic limit of the transformation. For the case of a reversible reaction, but sufficiently exergonic, some transient chiral excursions may be detected.

In open far from equilibrium systems, even the reversible transformation may lead to scalemic non-equilibrium stationary states (NESS's) (see Box 7.2).[12]

If the autocatalytic order is too low ($n \leq 1$) scalemic NESS's cannot be obtained. This is the case, for instance, of first-order autocatalysis ($n = 1$) which requires coupling with other enantioselective reactions[11] in order to yield SMSB and to achieve the enantiomer growth dynamics up to observable levels.

(Section 7.3). Furthermore, the thermodynamic scenario for SMSB is that far from equilibrium thermodynamics. Figure 7.1 attempts to describe the confluence of these two topics in the discussion of the Soai reaction. This, in open systems, should lead to final stable NESS, but in closed systems to transient stationary scalemic states of similar composition. On the basis of all these considerations and on the basis of previously reported reductionist models (Section 7.2), the design of realistic models (Section 7.4) should be possible.

Box 7.2 Soai reaction as a bifurcation in a dissipative system

Open system. The characteristic methodology of the Soai reaction of successive additions of reagents to the exhausted reaction outcome, in order to achieve the amplification to higher ee values, is an approximation to an open flow reactor, such as previously reported.[15,16] Therefore, the understanding of the reaction is more suited to the framework of systems open to matter exchange.

Dependence on the boundary conditions. The reaction exhibits high sensitivity to the reaction parameters, the total chemical mass being an important one, and to the boundary conditions. This means for the same reaction mechanisms, that the final reaction outcome may be a racemic or a scalemic mixture depending on whether the system parameters achieve or not the value of the critical entropy production for the bifurcation.[12]

Stochastic distribution of chiral sign between experiments. In the absence of any external chiral polarization, the spontaneous mirror-symmetry breaking (SMSB) in the Soai reaction must lead to a stochastic distribution of chiral signs between experiments, due to the stochastic distribution of chiral signs of the fluctuations (see Box 7.3). On the contrary, under chiral polarization, acting at the bifurcation point,[17] the SMSB leads to a deterministic chiral sign.

Box 7.3 Effect of fluctuations in the bifurcation scenario

Chiral compositional fluctuations take the system away from its saddle point and the unstable racemic NESS. By their nature they are stochastic, and therefore must lead to a stochastic distribution of chiral signs between experiments. Early reports on the Soai reaction showed biases from the expected 50%/50% bimodal distribution of opposite chiral signs between experiments. However, later reports had shown how the stochastic distribution of chiral signs between experiments may be obtained by optimizing and controlling the experimental conditions.[18]

Sensitivity of cryptochiral inductions. The Soai reaction shows unprecedented sensitivities to very weak chiral inductions. For example, those of asymmetric centres arising from isotopic substitution ($^{1}H/^{2}H$, but also $^{12}C/^{13}C$, $^{16}O/^{18}O$, and $^{14}N/^{15}N$).[19–22] This is the confirmation of previous theoretical reports indicating that a very small chiral polarization may convert a perfect bifurcation into an imperfect one,[17] *i.e.*, different experiments would lead always to the NESS of the same chiral sign. From a factual point of view, such evolution appears as a chiral amplification, but it is a consequence of the instability of the racemic NESS of the

evolution towards a stable NESS. Note that such an effect of a cryptochiral polarization is a selection of the chiral sign but not an asymmetric induction, because with or without the chiral polarization the final NESS is always chiral and practically of the same absolute ee value. It is only the *distribution* of the final chiral signs that differs.

The effect of cryptochirality in the Soai reaction would be also manifested, not only by a cryptochiral substance, but also by the presence of chiral compounds at very low concentrations. In our opinion, the first Soai reaction reports show a divergence from the stochastic bimodal distribution of chiral signs that is probably due to traces of chiral contaminants.[6]

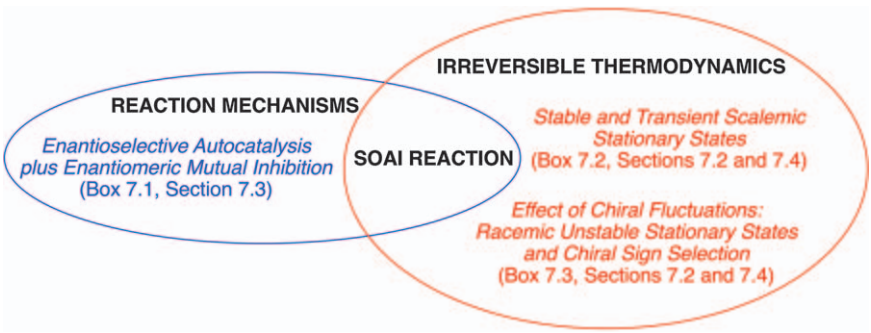

Figure 7.1 Main elements to be considered for the understanding of the Soai reaction.

7.2 Reductionist Frank Models of the Soai Reaction

The main features of the Soai reaction can be summarized in three points: (i) the Soai reaction leads to random outcomes of the chiral sign[18,23–25] starting from the tiny statistical chiral fluctuations about the ideal racemic composition,[26,27] (ii) extremely small chiral polarizations, such as those furnished by isotopic enantiomers[20,28–31] are sufficient to determine the chiral sign of the final reaction outcome, and (iii) the experimental procedure, based on sequential reactions where the reaction product is used in the next reaction stage, leads to amplification of chirality from initial experimentally undetectable ee's to final ee values close to homochirality.[18,24] These features (see Boxes 7.2 and 7.3) have inspired kinetic modeling efforts, based on the Frank reaction network[10] with enantioselective autocatalysis (see Box 7.1) and mutual inhibition, and which have successfully reproduced the variety of the striking phenomena observed in the Soai reaction.[32,33] We discuss briefly selected results from two reductionist approaches.

7.2.1 Models of Rivera Islas *et al.*

The kinetic models defined by Rivera Islas *et al.*[32] are summarized in Table 7.1. Model 1 represents the minimal set of processes that can reproduce qualitatively the main features of the Soai reaction. Reactions **3–5** coincide with Frank's original model, whereas **1** and **2** allow for the direct production of the enantiomers. Model 2 aims at more chemical realism by including the organozinc reactant Z in steps **1′–4′** as well as the reversible formation of the heterochiral (**6**) and homochiral dimers, **7–8**. Lastly, Model 3 allows for the possibility of replacing the monomer-catalyzed steps **3′** and **4′** by dimer catalysis in **9** and **10**. Model 3 includes the steps **1′**, **2′**, and **5–11**.

The minimal Model 1 leads to a large racemic bias in a bifurcation scenario (see Figure 7.2) under batch conditions in which any kinetic parameter or achiral substrate concentration can drive the system into either a racemic or scalemic state from achiral initial conditions. The amplification strength depends on the ratio of heterodimerization to enantioselective autocatalysis: (k_2/k_1). The enantiomeric excess is defined as $ee = ([R]_{tot} - [S]_{tot})/([R]_{tot} + [S]_{tot})$, where $[S]_{tot} = [S] + [RS] + 2[SS]$, and similarly for $[R]_{tot}$. As shown in Figure 7.2 the bifurcation threshold depends on the mutual inhibition rate constant (k_2) and the value of the initial ee_0. For curve A no chiral catalyst was added, for curve B, $ee_0 = 1\%$, curve C, $ee_0 = 10\%$ and curve D, $ee_0 = -1\%$. Note, for strictly racemic initial conditions, the expected final outcome must also be racemic, so that the results in curve A are a consequence of the numerical round-off error. Hence, beyond the bifurcation threshold the final outcome of a positive or negative ee is random (curve A). Simulations for which this numerical noise is suppressed are presented in Section 7.2.2.

Model 2 behaves almost identically to Model 1 in so far as reproducing the mirror-symmetry breaking and the amplification of ee are concerned. By contrast, regarding parameter fits, the monomeric model requires a homodimer *vs.* heterodimer energy difference of 6.3 kcal mol^{-1} while for the dimeric model the requisite is only 2.7 kcal mol^{-1}, with the heterodimer being more stable. Figure 7.3 shows a fit to the aldehyde concentration during a one-step Soai reaction.[23]

Table 7.1 The kinetic models proposed by Rivera-Islas *et al.*[32] based on Frank's scheme.[10] Forward and reverse reaction rate constants are indicated by the ordered pairs: (k_{for}, k_{rev}).

Model 1	Model 2	Model 3
$A \rightarrow R$ (k_0) [**1**]	$A + Z \rightarrow R$ (k_0') [**1′**]	$A + Z + RR \rightarrow R + RR$ (k_6) [**9**]
$A \rightarrow S$ (k_0) [**2**]	$A + Z \rightarrow S$ (k_0') [**2′**]	$A + Z + SS \rightarrow S + SS$ (k_6) [**10**]
$A + R \rightarrow 2R$ (k_1) [**3**]	$A + Z + R \rightarrow 2R$ (k_1') [**3′**]	$A + Z + RS \rightarrow 0.5\ S + 0.5\ R + RS$ (k_7) [**11**]
$A + S \rightarrow 2S$ (k_1) [**4**]	$A + Z + S \rightarrow 2S$ (k_1') [**4′**]	
$R + S \rightarrow RS$ (k_2) [**5**]	$RS \rightarrow R + S$ (k_3) [**6**]	Model 3 includes steps **1′**, **2′** and **5–11**.
	$R + R \leftrightarrow RR$ (k_4, k_5) [**7**]	
	$S + S \leftrightarrow SS$ (k_4, k_5) [**8**]	

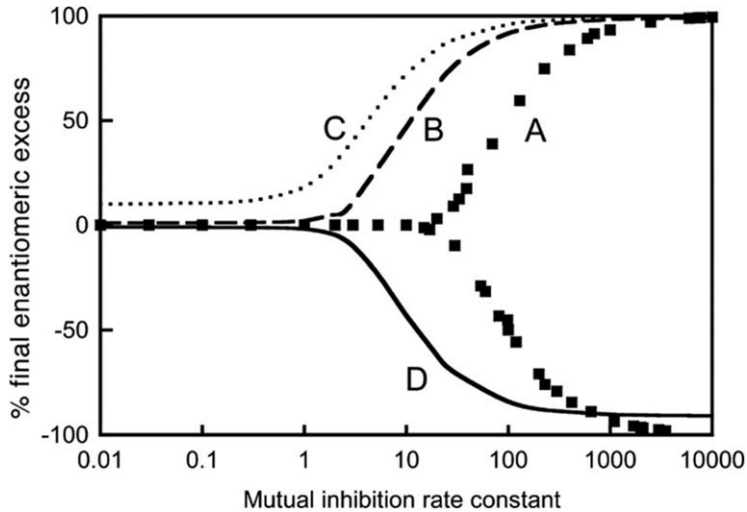

Figure 7.2 Mirror-symmetry breaking and amplification of ee in Model 1. $[A]_0 = 1$ M, $k_0 = 10^{-6}$ $M^{-1}s^{-1}$, $k_1 = 1$ $M^{-1}s^{-1}$. Curve A, racemic initial conditions: $[R]_0 = [S]_0 = 0$; curve B, $[R]_0 = 5.05\times10^{-3}$ M, & $[S]_0 = 4.95\times10^{-3}$ M (1% catalyst, ee = 10%); curve C, $[R]_0 = 5.50\times10^{-3}$ M & $[S]_0 = 4.50\times10^{-3}$ M (1% catalyst, ee = −10%); curve D, $[R]_0 = 4.95\times10^{-2}$ M & $[S]_0 = 5.05\times10^{-2}$ M (10% catalyst, ee = −1%). Reproduced from ref. 32 with permission from the National Academy of Sciences.

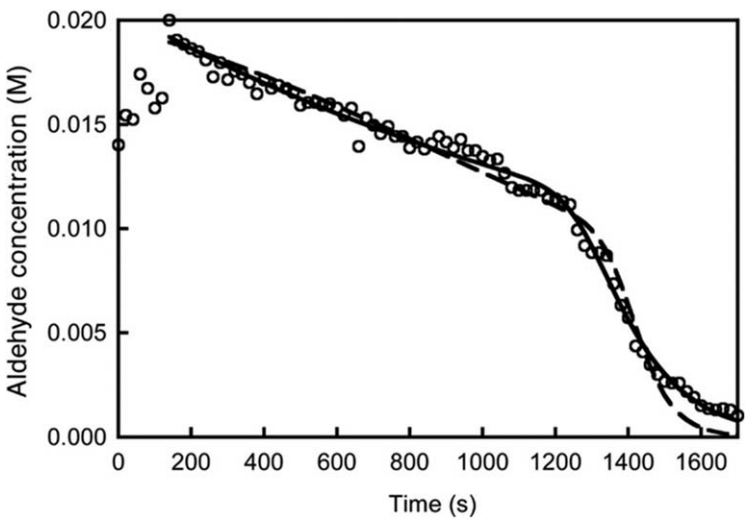

Figure 7.3 Evolution of the aldehyde concentration during a typical Soai reaction (open circles). Fit by Model 2 (continuous line) and by Model 3 (broken line). Initial concentrations (M): $[A] = 1.92\times10^{-2}$ & $[Z] = 0.04$; rate parameters Model 2 (Model 3): $k_0 = 5.2\times10^{-3}$ (3.7×10^{-3}) $M^{-1}s^{-1}$; $k_1 = 69$ $M^{-2}s^{-1}$ ($k_6 = 154$ $M^{-2}s^{-1}$), $k_7 = 2.1\times10^{-4}$ $M^{-2}s^{-1}$, $k_2 = 4.5\times10^{5}$ (9.2×10^{5}) $M^{-1}s^{-1}$; $k_3 = 5.2\times10^{-2}$ (6.4×10^{-4}) s^{-1}; $k_4 = 4.8\times10^{3}$ (1.1×10^{4}) $M^{-1}s^{-1}$; $k_5 = 21$ (6.4×10^{-4}) s^{-1}. Reproduced from ref. 32 with permission from the National Academy of Sciences.

We remark that more detailed dynamical perspectives show that the simplified reductionist direct autocatalysis, such as, *e.g.* $A + B \rightarrow 2B$, actually derives from a more involved autocatalytic cycle in which dimers, trimers, and tetramers are implicated (see Section 7.4). In this approach, the hetero-oligomers provide the self-inhibition.[34] Comprehensive kinetic analyses of autocatalytic cycle models based on the various oligomeric orders of the assumed catalytic species have been carried out in ref. 35.

7.2.2 Models of Crusats *et al.*

Fully reversible reaction networks in closed systems, based on the Frank model,[10] and in the absence of any chiral polarization, have been considered in detail, see Table 7.2 for the reaction scheme and the corresponding thermodynamic constraint.[33] First, we point out that the network (I) + (II) by itself cannot explain SMSB of the Soai reaction, because it is unable to amplify chirality from an initial enantiomeric excess[33] (see also Box 7.1). The case of limited enantioselectivity (I) + (II) + (III) does no better. In either open or closed systems, this network can only lead to stable final racemic states, and as a consequence of the thermodynamic constraint. By contrast, the network (I) + (II) + (V) (Frank model) may lead to a kinetically controlled SMSB. The amplification by (II) of the initially low non-linear effect of (V) is greater when the initial total concentration of catalysts is low. This implies that the sequential reaction procedure of the Soai reaction works well when it is carried out not only for constant initial concentrations of A and B, but also when the dilution of the previous outcome is performed.[18,24] Soai's repetitive sequential reaction procedure uses the outcome from one reaction as a catalyst for the next reaction. Indeed, in order to increase the ee value of the reaction to significant values, the Soai reaction uses a sequential reaction procedure: the exhausted final reaction mixture is used for a new reaction batch at the same initial conditions. However, this works well only under dilution of the previous batch of the reaction: either by using a larger reaction volume (generally 1 : 10) or by using only a small aliquote of the previous reaction product.[24,36] The point is not intuitive, but it is a simple

Table 7.2 A and B are two achiral reactants. The reversible reactions are (I): direct production of enantiomers L or D, (II) enantioselective autocatalysis, (III) non-enantioselective catalysis, (IV) homodimerization, and (V) heterodimerization. Inset: Thermodynamic constraints that relate (I), (II), and (III) through their corresponding (forward, reverse) reaction rate constants (k_f,k_r).

Reactions	Thermodynamic constraint
$A + B \leftrightarrow L$, $A + B \leftrightarrow D$ (k_1,k_{-1}) (**I**) $A + B + L \leftrightarrow 2L$, $A + B + D \leftrightarrow 2D$ (k_2,k_{-2}) (**II**) $A + B + L \leftrightarrow L + D$, $A + B + D \leftrightarrow D + L$ (k_3,k_{-3}) (**III**) $L + L \leftrightarrow LL$, $D + D \leftrightarrow DD$ (k_4,k_{-4}) (**IV**) $L + D \leftrightarrow LD$ (k_5,k_{-5}) (**V**)	$\frac{k_1}{k_{-1}} = \frac{k_2}{k_{-2}} = \frac{k_3}{k_{-3}}$

consequence of the non-linearity of the autocatalysis. Such as that noted by other authors,[15] this behavior is a consequence of the fact the typical sequential methodology of the Soai reaction is an approximation to an open flow reactor system.[16]

Figure 7.4 indicates how a significant ee_t would be obtained following the dilution procedure after 6 sequential reactions, but not for a repetitive procedure involving only the addition of new reagents A and B. In the latter case, the value of ee_t remains below the limits of experimental detection. This behavior is in agreement with the experimental reports that have led to the optimization of the work-up of the Soai reaction.[18,24,28]

The role of the limited enantioselectivity and homodimerization reactions, (III) and (IV), respectively, when included in the Frank model, (I) + (II) + (V), can be appreciated in Figure 7.5. The formation of the homodimers LL and DD, (IV), does not change the maximum value of ee_t value are lower than for the basic network: compare the curves (b) and (d). The purpose of the formation of the heterodimer LD, (V), is to increase the ee by racemate elimination.

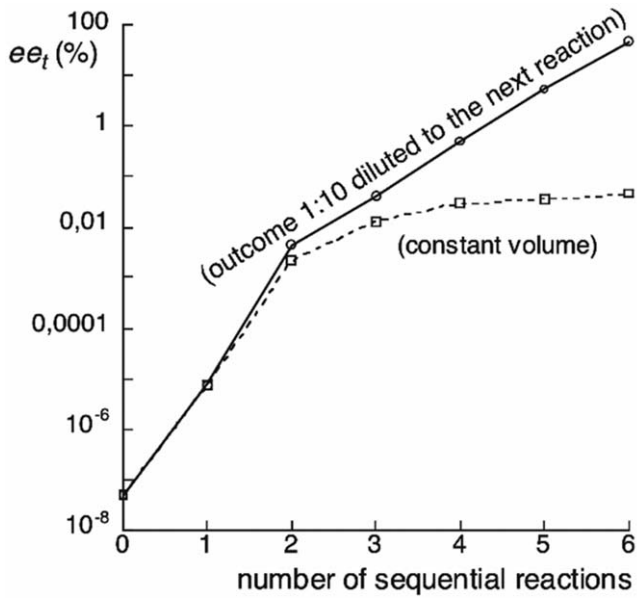

Figure 7.4 Evolution of ee_t by a sequential repetitive asymmetric amplification in a system (I) + (II) + (V) (see Table 7.2) with a low exergonic formation of LD ($K_V = 10$); $[A]_0 = 1$ M, $[B]_0 = 1$ M, $k_1 = 1\times10^{-5}$, $k_{-1} = 1\times10^{-10}$, $k_2 = 1$, $k_{-2} = 1\times10^{-5}$, $k_5 = 1\times10^{6}$, $k_{-5} = 1\times10^{5}$. The first reaction starts with an initial ee_t below that corresponding to the inherent statistical deviation of the racemic composition (log scale). The dashed line corresponds to a procedure without dilution of the previous reaction outcome and the solid line to a procedure where the reaction volume is increased by a factor of ten in each new reaction (see the text for an explanation). Reproduced from ref. 33 with permission from John Wiley & Sons,

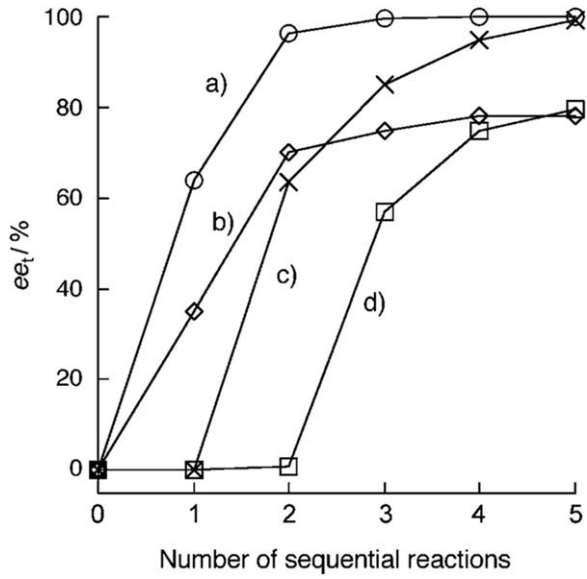

Figure 7.5 The change in ee_t (defined in Table 7.1) *versus* the sequential reaction work-up (1 : 10 volume increase in each stage); $[A]_0 = [B]_0 = 1$ M and in the first reaction $[L]_0 = (1\times10^{-7} + 1\times10^{-16})$ M, $[D]_0 = 1\times10^{-7}$ M. Other parameters are: $k_1 = 1\times10^{-5}$, $k_2 = 1$, $k_3 = 0.1$, and $\frac{k_i}{k_{-i}} = 1 \times 10^5$; $k_4 = 10^6$, $k_{-4} = 3.33\times10^4$, $k_5 = 1\times10^6$, $k_{-5} = 3.33\times10^3$. (a) (I) + (II) + (V), (b) (I) + (II) + (III) + (V), (c) (I) + (II) + (IV) + (V), (d) (I) + (II) + (III) + (IV) + (V); see Table 7.2 and the text for explanation of the curves in (a), (b), (c), and (d). Reproduced from ref. 33 with permission from John Wiley & Sons, Copyright © 2009 Wiley-VCH Verlag GmbH & Co. KGaA, Weinheim.

The formation of the homodimers LL and DD, (IV), competes with this process, thus limiting its effect. Limited enantioselectivity, (III), tends to racemize the system and so lowers the final enantiomeric excess.

7.3 Mechanistic Investigations of the Soai Reaction

7.3.1 Hemiacetal and Aldehyde Involvement Within the Autocatalytic Scaffold

From the experimental/structural point of view, the biggest actual question refers to the nature of the autocatalyst.[37–40] To address this problem, the Trapp group[39,40] has carried-out detailed kinetic analyses including the record of more than 20 kinetic evolutions of both the starting aldehyde and the produced carbinols. By the clever use of an unprecedented combination of flow-injection enantioselective HPLC and *in situ* high-resolution mass spectrometric measurements, a transient formation of hemiacetal complexes has been unveiled and it has been assumed that they can establish an

autocatalytic cycle. This result is a confirmation of the previous NMR analysis of a hemiacetal formation by Gehring *et al.*[41] However, if the transient has been scaled by NMR at less than 2% of the initial aldehyde (at 0 °C with an adamantly substituted pyrimidinic aldehyde), mass spectrometry does not allow such quantitation although the bell-shaped kinetic was very similar. Fortunately, thanks to a kinetic modeling approach giving rise to the forward and reverse rate constants of acetalization, it is possible to estimate the maximum amount of hemiacetal in a typical Trapp experiment (run at 20 °C with a *tert*-butylacetylenyl substituted aldehyde). Figure 7.6 displays the numerical simulation of the establishment of the hemiacetalization equilibrium between aldehyde and added carbinol before the addition of the alkylzinc. Note that the equilibrium is shifted towards the reactant side and that the amount of hemiacetal is about 0.3% of the minor reactant (the added carbinol).

This value is compatible with the transient hemiacetal bell-shaped kinetic curve, but the involvement of a so-small amount in the catalytic cycle has been already questioned by Gridnev *et al.*[42] Trapp *et al.* recognize themselves that the process is apparently inefficient, but thanks to a well-performed experiment they confirm the autocatalytic properties of the Soai reaction mixture. The experiment consisted of matching a reference Soai reaction with a doped one, *i.e.* the same reaction, but which has received at its starting point, a small injection of a currently running Soai reaction mixture. The results are gathered in Table 7.3.

While these results confirm the catalytic role of the Soai reaction mixture, they don't give any information about the catalyst structure. The claimed sentence: "*It has to be pointed out, that adding 60 μL of a completed Soai reaction does not influence the induction period*", might suggest that both aldehyde and carbinol are needed to build the catalyst. However, as it is well known that the carbinol alone is catalytic,[5] such an assumption requires complementary experiments. Their proposed mechanism has been then translated into a reaction network which was subsequently analyzed by using 26 differential equations allowing the authors to calculate the concentration profiles and the ee in various conditions. Unfortunately, no direct comparison between the experiments and the model were provided. The question about the involvement of the aldehyde within the catalytic cycle is still open.

The key question about the possible involvement of the aldehyde within the catalytic scaffold in the Soai reaction is related to the apparent second kinetic order of the aldehyde. First discovered by Blackmond *et al.*,[43,44] then confirmed by Trapp,[39] this result must be considered carefully. If the kinetic order appears as useful in simple linear kinetic systems, it can be misleading in the case of nonlinear systems such as the Soai autocatalytic reaction. For instance, this second-order story guided Ercolani *et al.* to compute several catalytic scaffolds involving one or two aldehyde moieties, but without acetalization.[45,46] Examples of such calculations are displayed in Scheme 7.2.

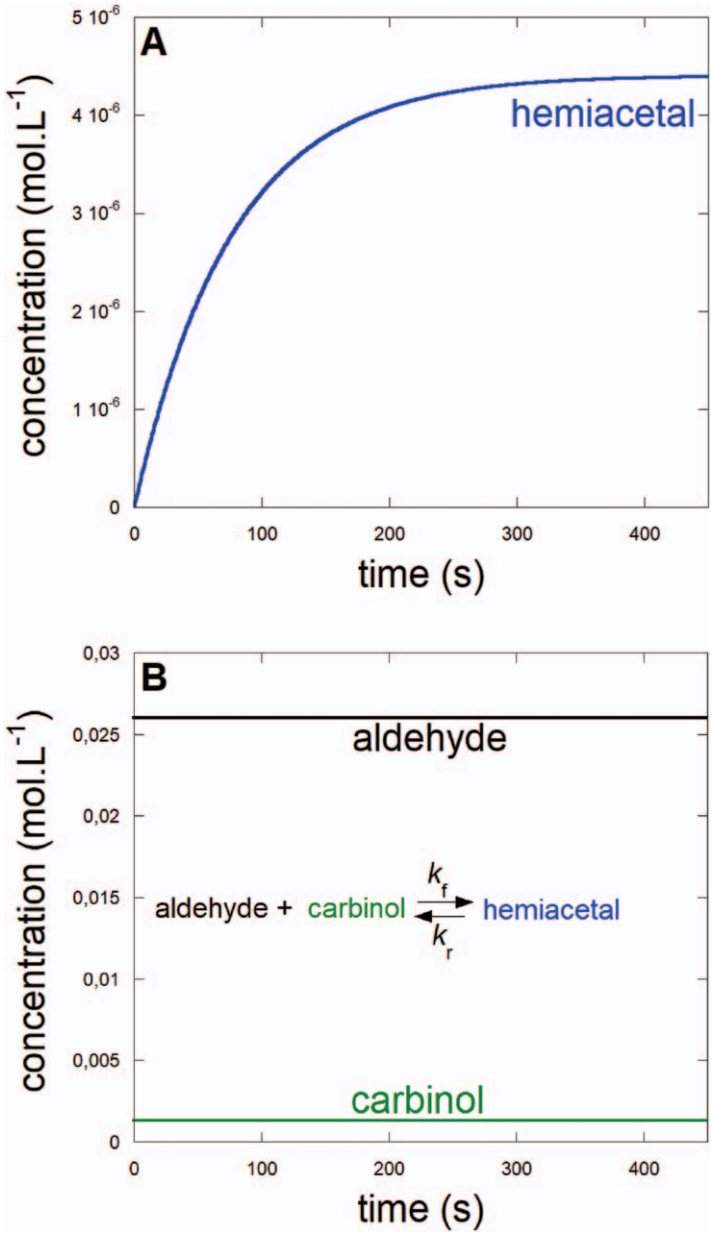

Figure 7.6 (A) Numerical simulation of the establishment of the hemiacetalization equilibrium using the Trapp's published[39] forward and reverse rate constants and initial concentrations: $k_f = 1.7 \times 10^{-3}\ M^{-1}\ s^{-1}$; $k_r = 1.3 \times 10^{-2}\ s^{-1}$; (B) initial concentrations of the aldehyde (26 mM) and the alcohol (1.3 mM) are not significantly affected by the establishment of this equilibrium.

Table 7.3 Analysis of the reference and doped experiments.

	Reference	Doped	Comment
Initial rate (mol s^{-1})	4.2×10^{-3}	1.4×10^{-2}	From S.I.[39]
Inflexion time (s)	254.9	199.5	From S.I.[39]

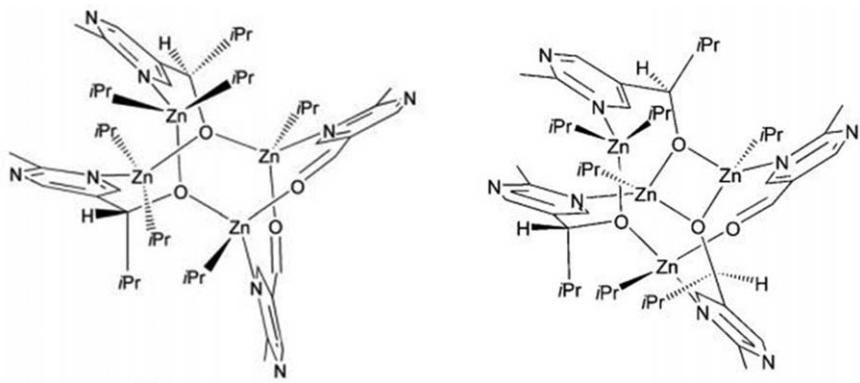

Scheme 7.2 Self-assembled tetramolecular complexes including two or one aldehyde as they were computed by Schiaffino and Ercolani Reproduced from ref. 45 with permission from John Wiley & Sons, Copyright © 2008 Wiley-VCH Verlag GmbH & Co. KGaA, Weinheim.

To conclude this kinetic second-order diversion, we invite the reader to look at the supplementary information part of the ref. 34 (see Table S5 and Figures S6 and S7) where an aldehyde second-order has been demonstrated in a model in which there is only one involvement of the aldehyde with the autocatalytic cycle.

7.3.2 Background Uncatalyzed Racemic Alkylation

Among all the kinetic runs, those with a smaller amount of added carbinol are of particular interest because the added carbinol could mask any autocatalytic effect. In fact, it has been known since 2003, that the Soai reaction can be run without the addition of any chiral catalyst.[18] This property is due to a slow uncatalyzed racemic alkylation. This process has been unveiled by Rivera Islas *et al.*[32] at around $4.5 \pm 1\times10^{-3}$ M^{-1} s^{-1} for the trimethysilylethynyl pyrimidinic aldehyde[23] in C_7D_8 at 273 K and subsequently confirmed by Noble-Terán *et al.*[47] at 1.3×10^{-3} for the *tert*-butyl-ethynyl pyrimidinic aldehyde[48] at 248 K and 3.8×10^{-4} M^{-1} s^{-1} for the adamantly-ethynyl pyrimidinic aldehyde[49] at 298 K. The presence of such racemic background alkylation has also been recognized recently by Hawbaker and Blackmond.[50]

7.3.3 Varying Zinc Alkoxides and Aldehydes Structures

Denmark and co-workers conducted extensive structural and mechanistic study by combining various zinc alkoxides and aldehyde substrates.[37] *In situ*

IR monitoring at 1710 cm^{-1} of the residual aldehyde allowed them to sample the reaction mixture for the simultaneous determination of the ee. The reactions were started according to the Soai procedure, *i.e.* the aldehyde was added as the final component, such that it was never contacted to the free carbinol as in Trapp's experiment. Figure 7.7 shows that a very nice sigmoidal aldehyde evolution has been recorded by mixing a bulky pyrimidinic aldehyde with di-isopropyl zinc in the absence of any added catalyst. The final ee (≈2%) is a sign that spontaneous mirror-symmetry breaking is on the doorstep. On the other hand, the addition of 20% of carbinol gives rise to fast consumption of the initial aldehyde. This catalyst produces a rate about 4 times faster than the rate at inflexion in the sigmoidal run. Such comparison could provide an estimation of the amount of autocatalyst, which has been produced spontaneously in the absence of added carbinol. Interestingly, these results also provide a talented confirmation of the previous Klankermayer *et al.* results that the amplifying asymmetric autocatalysis is dependent on the unique steric properties of the isopropyl group.[51]

Another series of experiments has been carried out in order to compare the classical alkylating agent (di-isopropyl zinc) with the simpler one, diethyl zinc using a trimethylsilyl-ethynyl pyrimidinic di-isopropyl carbinol additive. The observed enantiomeric ratio amplifications are gathered in Table 7.4. However, in the absence of any recorded kinetic evolution showing a characteristic sigmoidal shape, any enantiomeric amplification does not allow us to conclude that chiral autocatalysis is operating. It can be just a simple catalyst association, the so-called ''nonlinear effect in asymmetric synthesis''.[52]

Nevertheless, the Denmark *et al.* approach is very complete and original, and a lot of interesting DFT calculations have been carried out. Two competing tetrameric SMS Klankermayer-like[51] transition states have been computed, the favored one delivers the isopropyl group from the side which produces the homomorphic alkoxide, while the higher energy other gives rise to the heteromorphic product *via* the delivery of the isopropyl group from the enantiomeric side. Depending on the structure of the carbaldehyde (pyridinic or trimethylsilyl-ethynyl pyridinic), an energy difference lying between 2.2 to 4.4 kcal mol^{-1} is compatible with the observed final high enantiomeric ratio at 99 : 1 (see Section 7.4).

A simplified reaction model for autocatalysis has been developed and used to fit semi-quantitatively several kinetic runs. Unfortunately, neither the chirality, the reversibility of the aggregation steps, nor the contribution of an uncatalyzed background alkylation has yet been taken into account in this model.

The question of the number of nitrogen atoms within the aromatic cycle of the aldehyde has been debated by Denmark,[37,38] and also by Amedjkouh.[55] Azaaryl aldehydes (pyridine-like) represent only a limited-version of the Soai aldehyde; in homogeneous solution, their amplification power is weak. It is likely that they are not able to build an autocatalytic scaffold as is expected with the pyrimidinic Soai aldehyde.

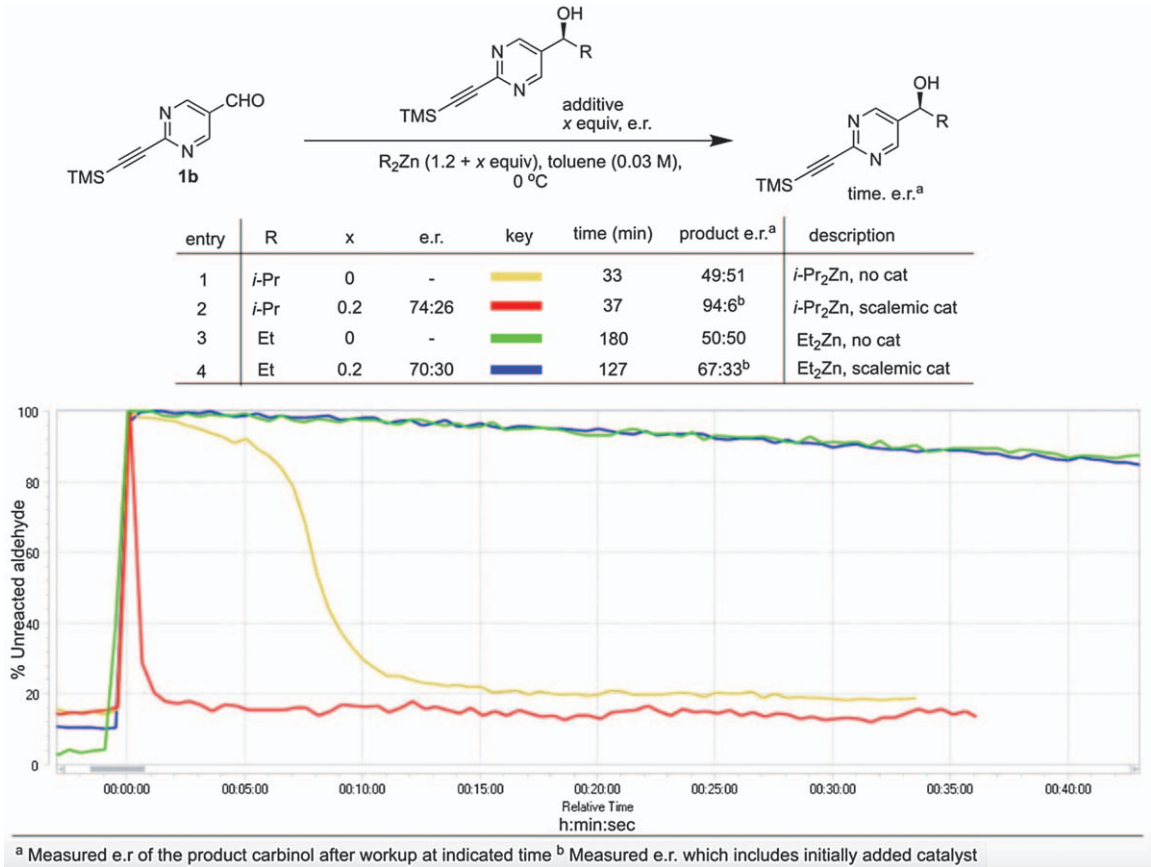

entry	R	x	e.r.	key	time (min)	product e.r.[a]	description
1	*i*-Pr	0	-		33	49:51	*i*-Pr_2Zn, no cat
2	*i*-Pr	0.2	74:26		37	94:6[b]	*i*-Pr_2Zn, scalemic cat
3	Et	0	-		180	50:50	Et_2Zn, no cat
4	Et	0.2	70:30		127	67:33[b]	Et_2Zn, scalemic cat

[a] Measured e.r of the product carbinol after workup at indicated time [b] Measured e.r. which includes initially added catalyst

Figure 7.7 Non-catalytic and catalytic alkylation of the trimethylsilyl-ethynyl pyrimidinic carbaldehyde with di-isopropyl zinc (**1**, **2**) and di-ethyl zinc (**3**, **4**). Reproduced from ref. 38 with permission from American Chemical Society, Copyright 2020.

Table 7.4 Enantiomeric ratio (e.r.) amplification during the alkylation of several carbaldehydes by di-isopropyl and di-ethyl zinc in the presence of 20% trimethylsilyl–ethynyl pyrimidinic di-isopropyl carbinol additive. Note the nonlinear character of the amplification gain ($e.r._{pdt}/e.r._{cat}$). Higher gain is witnessed for higher catalyst enantiomeric ratios.

Carbaldehydes	Trimethylsilyl-ethynyl-pyridinic	Pyridinic	Triisopropylsilyl-ethynyl-pyrimidinic	*t*-Butyl-ethynyl-pyrimidinic
Di-isopropyl zinc	1.18 to 6.75[53] 3 to 49[23]	3 to 10.1[38]	1.188 to 1.193[53] 2.57 to 11.5[38]	1.12 to 5.58[53] 1.0000005 to 3.65[54]
Di-ethyl zinc	3 to 5.66[38]	3 to 1.22[38]	2.85 to 3.17[38]	

However, the Amedjkouh group has described two specific situations where the Soai-like character of such limited-version aldehydes can be revealed. The first one is a chemical system combining asymmetric amplification of Soai's autocatalyst (pyrimidinic) alongside a catalytic addition of $Zn(iPr)_2$ to azaaryl (pyridinic) aldehydes.[56,57] The idea was to use the Soai's autocatalyst as a catalyst in an ensuing enantioselective alkylation (or alkynylation[55,57]) of azaaryl aldehydes with moderate to good levels of asymmetric induction. This work demonstrates that the Soai autocatalytic scaffold can play the role of a 'classical' chiral catalyst beyond the traditional chiral pool and indicates a potentially novel approach to access enantiomerically pure molecules. Moreover, the ee increase of the azaarylcarbinol over time suggests some autocatalytic effect, *i.e.* the slow building of a powerful reactive species, the structure of which has yet to be established. The second one is to work in heterogeneous conditions, *i.e.* when aldehyde crystals are contacted by $Zn(iPr)_2$ vapor, a mirror-symmetry breaking has been witnessed.[58] This effect is the signature of chiral autocatalysis. The mechanism is complex since several side products were identified. Moreover, the autocatalytic character is confirmed by monitoring the progress of ee over time. It is likely that the confined reactive layer was favorable to the building-up of some autocatalytic scaffold which does not occur in fluid solution.

7.3.4 Influence of the Isotopic Chirality

The sensitive response of the Soai reaction to the minute isotope chirality, as recorded for $^{12}C/^{13}C$,[20] H/D,[19] $^{16}O/^{18}O$,[21] and recently for $^{14}N/^{15}N$ moieties,[22] is definitely the most remarkable feature among all other additive effects.[59,60] In this regard, Hawbaker and Blackmond studied the effect of H/D chirality using (*R*)- or (*S*)-1-methoxy-(^{2}H)-3-methoxy propanol as the additive (Scheme 7.3).[61]

The authors found that the additive, as a function of its concentration, increasingly slows down the overall velocity of the reaction (Figure 7.8).

To rationalize this inhibitory effect, they conducted kinetic, NMR, and DFT studies that indicated a selective interaction between the assumed

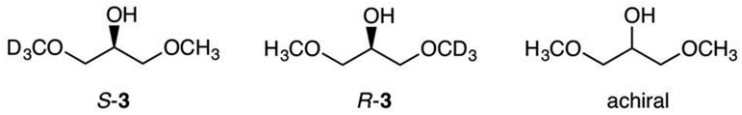

Scheme 7.3 Structures of the ^{2}H-labeled chiral dimethoxy propanol and achiral parent.

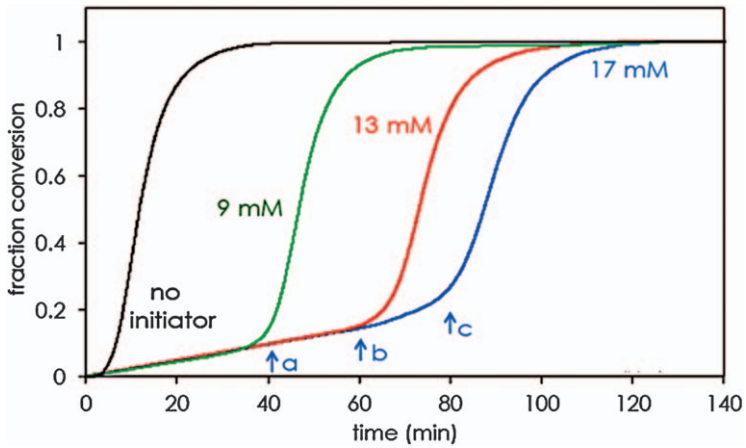

Figure 7.8 Inhibitory effect on the overall velocity of the Soai reaction by the presence of different concentrations of 1-methoxy-(^{2}H)-3-methoxy propanol as an isotopically chiral additive. Reproduced from ref. 61 with permission from American Chemical Society, Copyright 2018.

homochiral dimeric zinc alkoxide autocatalyst (R_2 and S_2) and the chiral additive (X) that inhibits the autocatalytic pathway. It is argued that the additive–catalyst interaction can trap the autocatalyst through the stereoselective formation of inactive diastereomeric species R_2X and S_2X thus promoting one enantiomer over the other during the autocatalytic stage. Such chiral additive–catalyst inhibition was already anticipated in 2007 in the framework of kinetic understanding of the enantioselectivity reversal by achiral additives in the Soai reaction.[62,63]

Taking into account the similitude of the isotopically-labeled enantiomers, it is likely that the energy difference between the two diastereoisomers is tiny. This is the reason why a subsequent study by the same authors was carried-out in order to identify the magnitude of the energy imbalance that gives rise to directed symmetry breaking and asymmetric amplification in the Soai reaction.[50] The idea was to perform a long series of Soai reactions in the presence of the same amount of the ^{2}H-labeled chiral dimethoxy propanol by decreasing gradually its ee. These experiments demonstrated that when the ee of the initiator was $\geq$1.0%, it directed the chiral outcome of the reaction. On the other hand, when the ee of the initiator was less than 1.0%,

fluctuations overtook its influence and gave a stochastic outcome. In order to interpret this result, a Kondepudi–Nelson-like stochastic model[50,64] was programmed to simulate the experiments run at initiator ee = 1.0% and 0.1%. Repeated simulations were useful to estimate whether the outcome would be stochastic or directed. The value of the tiny energy difference between the two diastereoisomers was tuned until all of the ee = 1.0% simulations showed a directed outcome and the 0.1% ones, a stochastic result. The authors estimated this value to be in the range of 10^{-8}–10^{-7} kJ mol^{-1}.

7.4 Critical Analysis of Two Specific Realistic Models: Noble-Terán *vs.* Trapp Cycles

7.4.1 The Noble-Terán Cycle

The Noble-Terán cycle is a kinetic and thermodynamic model of the Soai reaction which integrates the results of the most recently published XRD structural data and DFT calculations and selected experimental kinetic data. The cycle includes the aldehyde: A, the alkyl Zn: Z: ($(iPr)_2Zn$), and the carbinol: R.[23,41,65] The carbinol appears under the form of alcoholates: RZ,[66] square-dimer: R2,[67] alcoholate dimer: R2Z2,[68] alcoholate tetramer: R4Z4[46,65] and the activated tetramer: R4Z5 (catalytic scaffold).[68] A doubly-activated tetramer (R4Z6) has been crystallized and isolated under its enantiomeric form: S4Z6. Among the heterochiral pool, there are the hetero-square dimer RS and the hetero tetramer R2S2Z4 which has been crystallized and isolated. Figure 7.9 displays the structures of all the recognized intermediates that are involved in the cycle.

For the sake of chemical realism, homo- and heterochiral configurations of all oligomeric species were taken into account. All reversible processes were defined by their equilibrium constants and by their relaxation time constants that describe the rate by which the equilibrium is established. The unique irreversible process is the highly exergonic alkylation (Figure 7.10).

The Noble-Terán scaffold (R4Z5) is made of carbinol only. Such structures are reminiscent to previous transition states proposed by Gridnev and Vorobiev[68] as well as by Denmark and co-workers[38] (see Figure 7.11).

The 3D homochiral tetramer cavity displays a suitable shape complementarity for the aldehyde to be positioned. The electrophilicity of the aldehyde group is increased upon Zn coordination, whereas its orientation is insured by the bulky ethynyl substituent. Under these conditions, the two prochiral planes of the aldehyde are discriminated in order to form the carbinol with the same configuration as the tetrameric catalyst. After the alkyl transfer, the catalyst can split reversibly into dimeric[69] and monomeric alcoholates.

Finally, the Noble-Terán cycle model reproduces the simultaneous evolution of the ee and conversion of two independent experiments. The model is also able to mimic strong amplification from extremely low initial ee and

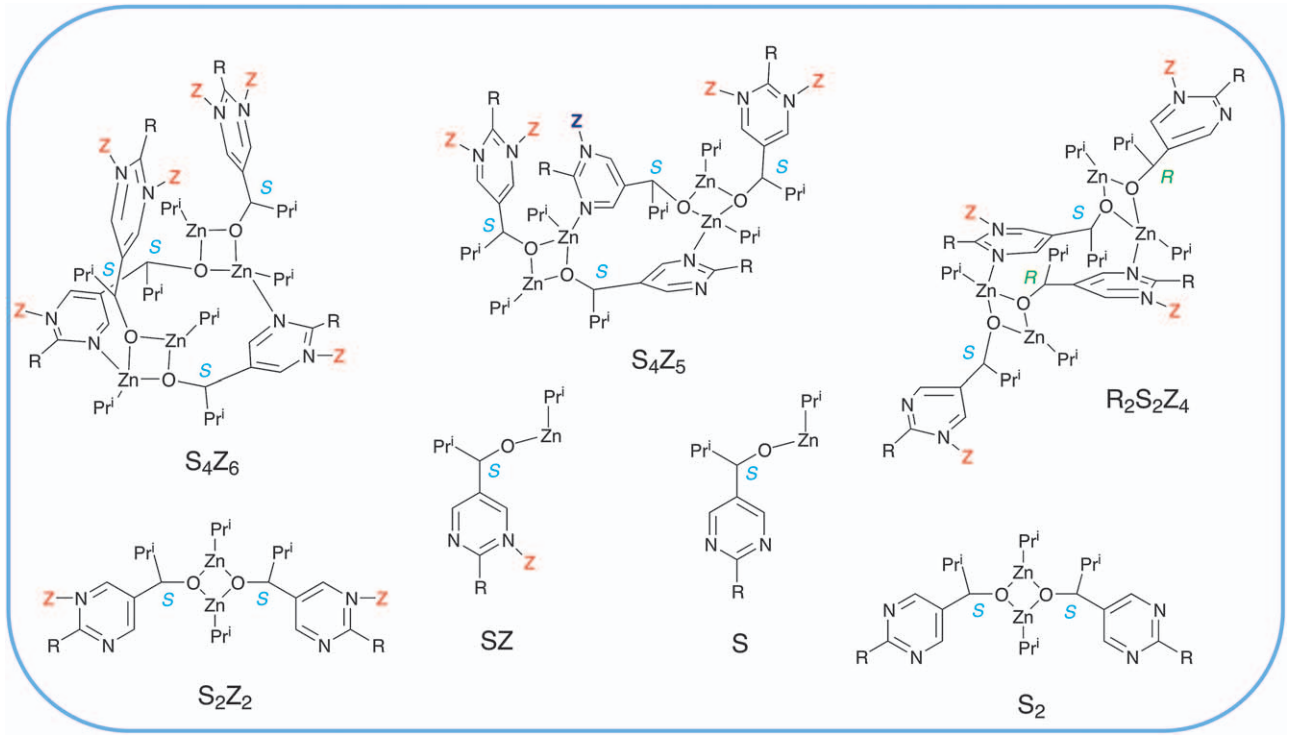

Figure 7.9 The structures of the various intermediates were either determined by using XRD or NMR spectroscopy or were computed by DFT. Reproduced from ref. 47 with permission from John Wiley & Sons, Copyright © 2018 Wiley-VCH Verlag GmbH & Co. KGaA, Weinheim.

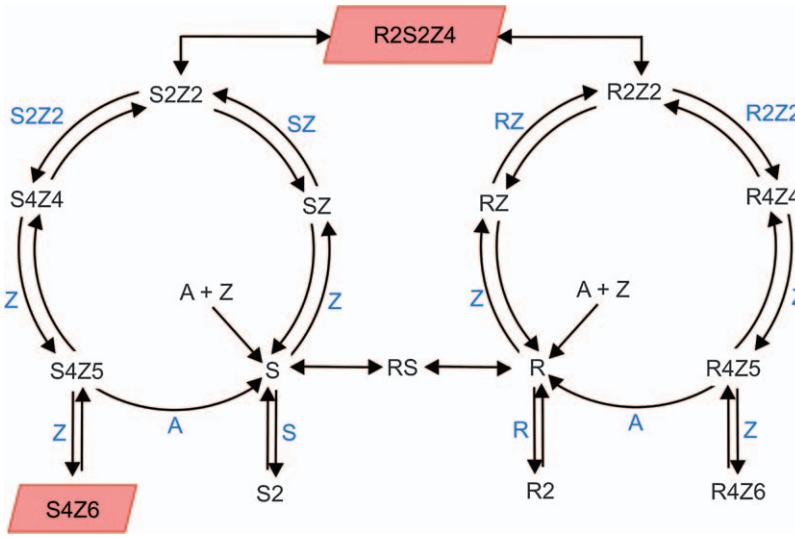

Figure 7.10 Noble-Terán mechanism:[47] A: aldehyde; Z: $(i\text{-Pr})_2$Zn; R carbinol; RZ alcoholates; R2: square-dimer; R2Z2: alcoholate dimer; R4Z4: alcoholate tetramer; R4Z5: activated tetramer (ready for alkylation); R4Z6: doubly-activated tetramer, has been crystallized and isolated under its enantiomeric form: S4Z6 (rhombohedra). Among the heterochiral pool, there are the hetero-square dimer RS and the hetero tetramer R2S2Z4 which has been crystallized and isolated (rhombohedra). Reproduced from ref. 47 with permission from John Wiley & Sons, Copyright © 2018 Wiley-VCH Verlag GmbH & Co. KGaA, Weinheim.

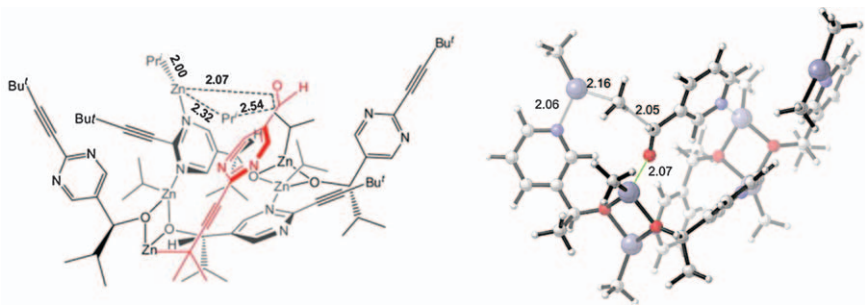

Figure 7.11 Gridnev's (left) and Denmark's (right) schedules of supposed tetrameric transition states. The main difference lies in the number of aromatic nitrogens involved in the oligomerization process. In the case of Denmark, the aromatic cycles are pyridinic. Reproduced from ref. 68 (left) and ref. 38 (right) with permission from American Chemical Society, Copyright 2012 and 2020.

spontaneous mirror-symmetry breaking under ''initial zero-catalyst'' conditions. It also reproduces the crystallization conditions by exhibiting the preferential accumulation of the corresponding oligomeric species in solution.

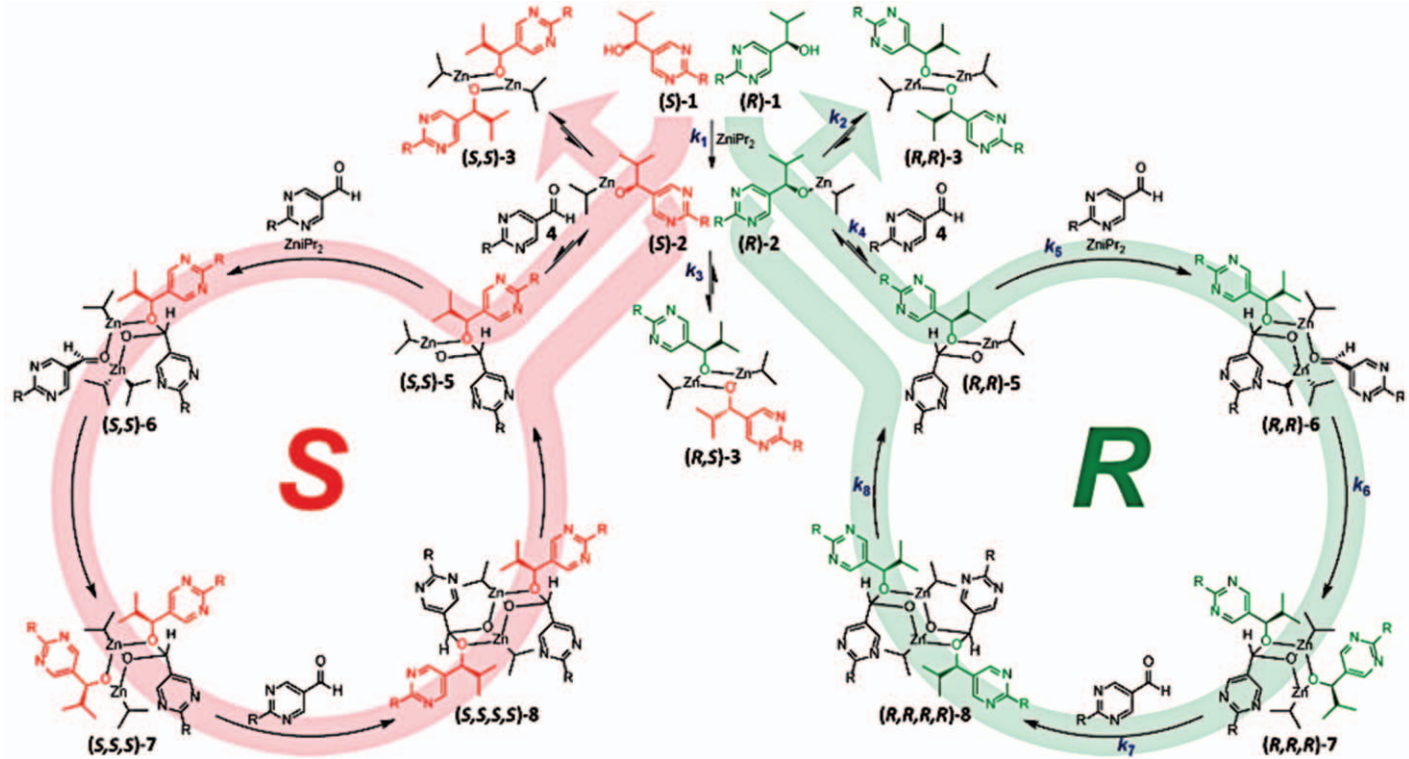

Figure 7.12 Trapp mechanism: involvement of a transient chiral acetal catalyst as a key step intermediate. All the structures proposed have been identified by the *in situ* high-resolution mass spectrometric experiments. Reproduced from ref. 39 with permission from John Wiley & Sons, Copyright © 2020 The Authors. Published by Wiley-VCH GmbH.

7.4.2 The Trapp Cycle

The Trapp cycle mechanism[39,40] has been established from *in situ* high-resolution mass spectrometric measurements, detailed kinetic analyses, and doping with reacting reaction mixtures (see Figure 7.12). It shows some similarities with the Noble-Terán cycle: the aldehyde, carbinols, Zn-alcoholates, and homo- and hetero-square dimers appear as common elements of both mechanisms. Another point of similarity is the building of a catalytic scaffold including the carbinols or the Zn-alcoholates which is in both cases at the origin of the autocatalysis. But the similarity ends here, since it includes the transient formation of hemiacetal complexes which can establish the autocatalytic cycle.

Let us examine the four main intermediates of the Trapp's cycle.

A: SS-5 is the so-called hemiacetal (Scheme 7.4):

In SS-5, the 2 ''S'' do not have the same meaning: one is from carbinol (in red), the other is from acetal (in black). The formation of the acetal results from the reaction of the CO of the aldehyde on the Zn–O bond of the alcoholate: C bonds with the O and O bonds Zn. Only the acetal can be readily racemized by returning back to the aldehyde.

B: SS-6 (Scheme 7.5):

SS-6 includes the SS-5 structure. An aldehyde is now complexed, and it is ready to be alkylated by a di-isopropylzinc also complexed in an appropriate position.

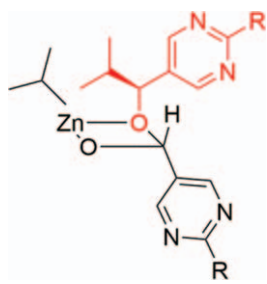

Scheme 7.4

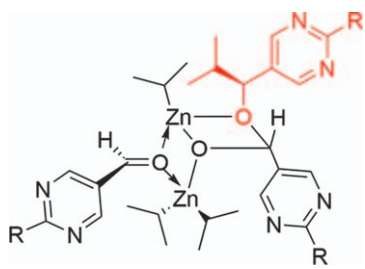

Scheme 7.5

C: SSS-7 (Scheme 7.6):

SSS-7 is the key structure, the aldehyde has been alkylated, and a new stable chiral carbon has been formed; this alkylation step is highly exergonic, the reverse which is expected to be very slow is a racemizing one.

D: SSSS-8 (Scheme 7.7):

This intermediate is the result of a second hemiacetalization according to Scheme 7.8.

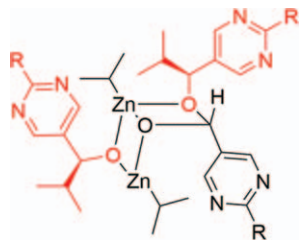

Scheme 7.6

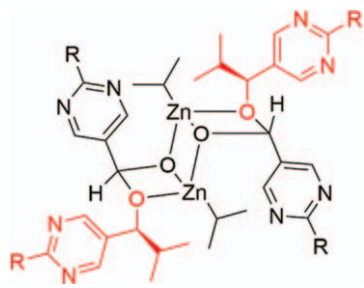

Scheme 7.7

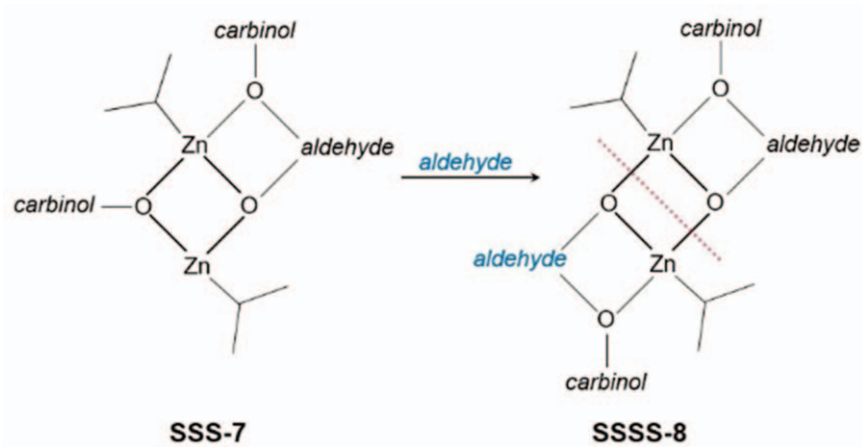

Scheme 7.8 Attack of a second aldehyde on SSS-7 after breaking the newly formed carbinol Zn bond. A subsequent split of SSSS-8 along the dashed red line gives rise to SS-5 hemiacetal, thus closing the Trapp cycle.

While many transient intermediates have been identified from mass spectrometry, none of these mechanistic assumptions have been really validated. First principles DFT calculations help to define some structures and confirm spectroscopic investigations, but it should be remembered that the structure of the catalytic step can be rather difficult to discern. The Trapp cycle mechanism has been modeled to calculate the concentration profiles and the ee in various conditions. Unfortunately, no direct comparison between the experiments and the model were provided.

7.5 Conclusion

The Soai reaction represents a unique example of total asymmetric synthesis in a homogeneous reaction system. Nowadays it is widely accepted that it forms a Frank-like reaction network where enantioselective autocatalysis and mutual inhibition are provided by the involvement of oligomeric intermediates. The typical sequential methodology of the Soai reaction is an approximation to an open flow reactor system. The high exergonicity of the alkyl Zn(II) addition to the carbaldehyde points to a kinetic control of the reaction. This is an energy dissipative chemical system, where the final non-equilibrium stationary state (NESS) does not have the racemic composition: the expected racemate is an unstable NESS, and there is an energetically degenerate enantiomeric pair of scalemic NESS's, which have high ee values. This is an unfamiliar feature compared to the common enantioselective kinetic control of classical asymmetric synthesis.

In the absence of any external chiral polarization, spontaneous mirror-symmetry breaking (SMSB) must lead to a stochastic distribution of chiral signs between experiments, due to the stochastic distribution of chiral signs of the fluctuations. On the contrary, under a chiral polarization, acting at the bifurcation point, the SMSB leads to a deterministic chiral sign. For example, those of asymmetric centers arising from isotopic substitution are sufficient to direct the chiral sign of the Soai reaction.

Several more or less realistic models inspired by a Frank-like reaction network have been provided. They differ by the structure of the catalyst and by the involvement of reversible steps. More often, these models include a slow uncatalyzed racemic alkylation. It is likely that the true autocatalyst is in equilibrium with a lot of inactive oligomers and that these equilibria are displaced towards the autocatalyst one, once the exergonic alkylation is occurring. These models reproduce the main features of the Soai reaction including the ee amplification through the repetitive sequential reaction procedure which uses the outcome from one reaction as the catalyst for the next reaction. A realistic model based on isolated XRD structures and DFT calculations results has been established including an all-alcoholate tetrameric catalytic scaffold. This scaffold has been confirmed from recent DFT calculation and *in situ* IR monitoring. However, the possible involvement of the aldehyde within the catalytic scaffold is still questioned.

It appears now that several independent teams are involved in Soai's reaction experimental investigations. All of them confirm the necessary specific structures of the reactants involved, namely di-isopropyl Zn and pyrimidinic bulky aldehydes. This feature makes the Soai's reaction very unique. However, this uniqueness should not be a barrier for the development of new experimental situations and multidimensional monitoring techniques. Much more than varying the structures, this is the concept of a catalytic oligomeric supramolecular scaffold which deserves to be exploited.

Acknowledgements

J. M. R. and D. H. acknowledge financial support from the coordinated project PID2020-116846GB-C21 and PID2020-116846GB-C22, respectively, from the Ministerio de Ciencia e Innovación (Spain). T. B. acknowledges financial support by project CF19-2272 from the Consejo Nacional de Ciencia y Tecnología (Mexico).

References

1. B. L. Feringa and R. A. van Delden, *Angew. Chem., Int. Ed.*, 1999, **38**, 3418.
2. J. M. Ribó, C. Blanco, J. Crusats, Z. El-Hachemi, D. Hochberg and A. Moyano, *Chem. - Eur. J.*, 2014, **20**, 17250.
3. J. Crusats and A. Moyano, *Synlett*, 2021, **32**, A.
4. T. Shibata, H. Morioka, T. Hayase, K. Choji and K. Soai, *J. Am. Chem. Soc.*, 1996, **118**, 471.
5. K. Soai, A. Matsumoto and T. Kawasaki, in *Advances in Asymmetric Autocatalysis and Related Topics*, ed. G. Pályi, R. Kurdi and C. Zucchi, Academic Press, London, 2017, ch. 1, pp. 1–30.
6. T. Buhse, J.-M. Cruz, M. E. Noble-Teran, D. Hochberg, J. M. Ribó, J. Crusats and J. C. Micheau, *Chem. Rev.*, 2021, **121**, 2147.
7. K. Soai, *Proc. Japan Acad. Ser. B Phys. Biol. Sci.*, 2019, **95**, 89.
8. K. Soai, T. Kawasaki and A. Matsumoto, *Tetrahedron*, 2018, **74**, 1973.
9. K. Soai, T. Kawasaki and A. Matsumoto, *Symmetry*, 2019, 694.
10. F. C. Frank, *Biochim. Biophys. Acta*, 1953, **11**, 459.
11. R. Plasson, A. Brandenburg, L. Jullien and H. Bersini, *J. Phys. Chem. A*, 2011, **115**, 8073.
12. J. M. Ribó and D. Hochberg, *Phys. Chem. Chem. Phys.*, 2020, **22**, 14013.
13. G. Lente, *J. Phys. Chem. A*, 2004, **108**, 9475.
14. G. Lente, *J. Phys. Chem. A*, 2005, **109**, 11058.
15. R. Plasson, D. K. Kondepudi, H. Bersini, A. Commeyras and K. Asakura, *Chirality*, 2007, **19**, 589.
16. A. Blokhuis, D. Lacoste and P. Gaspard, *J. Chem. Phys.*, 2018, **148**, 144902.
17. D. K. Kondepudi and G. W. Nelson, *Phys. Rev. Lett.*, 1983, **50**, 1023.

18. K. Soai, I. Sato, T. Shibata, S. Komiya, M. Hayashi, Y. Matsueda, H. Imamura, T. Hayase, H. Morioka, H. Tabira, J. Yamamoto and Y. Kowata, *Tetrahedron: Asymmetry*, 2003, **14**, 185.
19. T. Kawasaki, M. Shimizu, D. Nishiyama, M. Ito, H. Ozawa and K. Soai, *Chem. Commun.*, 2009, 4396.
20. T. Kawasaki, Y. Matsumura, T. Tsutumi, K. Suzuki, M. Ito and K. Soai, *Science*, 2009, **324**, 492.
21. T. Kawasaki, Y. Okano, E. Suzuki, S. Takano, S. Oji and K. Soai, *Angew. Chem., Int. Ed.*, 2011, **50**, 8131.
22. A. Matsumoto, H. Ozaki, S. Harada, K. Tada, T. Ayugase, H. Ozawa, T. Kawasaki and K. Soai, *Angew. Chem., Int. Ed.*, 2016, **55**, 15246.
23. I. D. Gridnev, J. M. Serafimov, H. Quiney and J. M. Brown, *Org. Biomol. Chem.*, 2003, **1**, 3811.
24. D. A. Singleton and L. K. Vo, *Org. Lett.*, 2003, **5**, 4337.
25. Y. Kaimori, Y. Hiyoshi, T. Kawasaki, A. Matsumoto and K. Soai, *Chem. Commun.*, 2019, **55**, 5223.
26. W. H. Mills, *J. Soc. Chem. Ind.*, 1932, **51**, 750.
27. K. Mislow, *Collect. Czech. Chem. Commun.*, 2003, **68**, 849.
28. K. Soai, T. Shibata and I. Sato, *Acc. Chem. Res.*, 2000, **33**, 382.
29. I. Sato, D. Omiya, T. Saito and K. Soai, *J. Am. Chem. Soc.*, 2000, **122**, 11739.
30. I. Sato, K. Kadowaki, H. Urabe, J. H. Jung, Y. Ono, S. Shinkai and K. Soai, *Tetrahedron Lett.*, 2003, **44**, 721.
31. T. Kawasaki, H. Tanaka, T. Tsutsumi, T. Kasahara, I. Sato and K. Soai, *J. Am. Chem. Soc.*, 2006, **128**, 6032.
32. J. Rivera Islas, D. Lavabre, J.-M. Grevy, R. H. Lamoneda, H. R. Cabrera, J.-C. Micheau and T. Buhse, *Proc. Natl. Acad. Sci. U. S. A.*, 2005, **102**, 13743.
33. J. Crusats, D. Hochberg, A. Moyano and J. M. Ribó, *Chem. Phys. Chem.*, 2009, **10**, 2123.
34. J. C. Micheau, J. M. Cruz, C. Coudret and T. Buhse, *Chem. Phys. Chem.*, 2010, **11**, 3417.
35. J. C. Micheau, C. Coudret, J. M. Cruz and T. Buhse, *Phys. Chem. Chem. Phys.*, 2012, **14**, 13239.
36. D. A. Singleton and L. K. Vo, *J. Am. Chem. Soc.*, 2002, **124**, 10010.
37. S. V. Athavale, A. Simon, K. N. Houk and S. E. Denmark, *Nat. Chem.*, 2020, **12**, 412.
38. S. V. Athavale, A. Simon, K. N. Houk and S. E. Denmark, *J. Am. Chem. Soc.*, 2020, **142**, 18387.
39. O. Trapp, S. Lamour, F. Maier, A. F. Siegle, K. Zawatzky and B. F. Straub, *Chem. – Eur. J.*, 2020, **26**, 15871.
40. O. Trapp, *Front. Chem.*, 2020, **8**, 615800.
41. T. Gehring, M. Quaranta, B. Odell, D. G. Blackmond and J. M. Brown, *Angew. Chem., Int. Ed.*, 2012, **51**, 9539.
42. I. D. Gridnev and A. K. Vorobiev, *Bull. Chem. Soc. Jpn.*, 2015, **88**, 333.
43. F. G. Buono and D. G. Blackmond, *J. Am. Chem. Soc.*, 2003, **125**, 8978.
44. D. G. Blackmond, *Tetrahedron: Asymmetry*, 2006, **17**, 584.

45. L. Schiaffino and G. Ercolani, *Angew. Chem., Int. Ed.*, 2008, **47**, 6832.
46. L. Schiaffino and G. Ercolani, *Chem. – Eur. J.*, 2010, **16**, 3147.
47. M. E. Noble-Terán, J. M. Cruz, J. C. Micheau and T. Buhse, *ChemCatChem*, 2018, **10**, 642.
48. I. Sato, D. Omiya, H. Igarashi, K. Kato, Y. Ogi, K. Tsukiyama and K. Soai, *Tetrahedron: Asymmetry*, 2003, **14**, 975.
49. M. Quaranta, T. Gehring, B. Odell, J. M. Brown and D. G. Blackmond, *J. Am. Chem. Soc.*, 2010, **132**, 15104.
50. N. A. Hawbaker and D. G. Blackmond, *Nat. Chem.*, 2019, **11**, 957.
51. J. Klankermayer, I. D. Gridnev and J. M. Brown, *Chem. Commun.*, 2007, 3151.
52. M. E. Noble-Terán, T. Buhse, J. M. Cruz, C. Coudret and J. C. Micheau, *ChemCatChem*, 2016, **8**, 1836.
53. T. Shibata, S. Yonekubo and K. Soai, *Angew. Chem., Int. Ed.*, 1999, **38**, 659.
54. I. Sato, H. Urabe, S. Ishiguro, T. Shibata and K. Soai, *Angew. Chem., Int. Ed.*, 2003, **42**, 315.
55. C. Romagnoli, B. Sieng and M. Amedjkouh, *Chirality*, 2020, **32**, 1143.
56. C. Romagnoli, B. Sieng and M. Amedjkouh, *Eur. J. Org. Chem.*, 2015, 4087.
57. M. Funes-Maldonado, B. Sieng and M. Amedjkouh, *Eur. J. Org. Chem.*, 2015, 4081.
58. G. Rotunno, D. Petersen and M. Amedjkouh, *ChemSystemsChem*, 2020, **2**, e1900060.
59. T. Kawasaki, Y. Kaimori, S. Shimada, N. Hara, S. Sato, K. Suzuki, T. Asahi, A. Matsumoto and K. Soai, *Chem. Commun.*, 2021, **57**, 5999.
60. G. Rotunno, G. Kaur, A. Lazzarini, C. Buono and M. Amedjkouh, *Chem. - Asian J.*, 2021, **16**, 2361.
61. N. A. Hawbaker and D. G. Blackmond, *ACS Cent. Sci.*, 2018, **4**, 776.
62. D. Lavabre, J. C. Micheau, J. Rivera Islas and T. Buhse, *J. Phys. Chem. A*, 2007, **111**, 281.
63. D. Lavabre, J.-C. Micheau, J. Rivera Islas and T. Buhse, *Top. Curr. Chem.*, 2008, **284**, 67.
64. D. K. Kondepudi and G. W. Nelson, *Nature*, 1985, **314**, 438.
65. A. Matsumoto, T. Abe, A. Hara, T. Tobita, T. Sasagawa, T. Kawasaki and K. Soai, *Angew. Chem., Int. Ed.*, 2015, **54**, 15218.
66. J. M. Brown, I. Gridnev and J. Klankermayer, *Top. Curr. Chem.*, 2008, **284**, 35.
67. I. D. Gridnev, J. M. Serafimov and J. M. Brown, *Angew. Chem., Int. Ed.*, 2004, **43**, 4884.
68. I. D. Gridnev and A. K. Vorobiev, *ACS Catal.*, 2012, **2**, 2137.
69. A. Matsumoto, A. Tanaka, Y. Kaimori, N. Hara, Y. Mikata and K. Soai, *Chem. Commun.*, 2021, **57**, 11209.

CHAPTER 8

Mechanism of the Soai Reaction – DFT and Kinetic Computations of the Catalytic Cycle

ILYA D. GRIDNEV,*[a,b] ANDREY KH. VOROBIEV[b] AND ALEXEY V. BOGDANOV[b]

[a] N. D. Zelinsky Institute of Organic Chemistry, Leninsky Prospekt 47, Moscow 119991, Russian Federation; [b] Department of Chemistry, M. V. Lomonosov Moscow State University, Leninskie Gory, Moscow 119991, Russian Federation
*Email: ilyaiochem@gmail.com

8.1 Introduction

The problems of chirality amplification and spontaneous chiral symmetry breaking are quite a broad area nowadays.[1,2] Nevertheless, the Soai reaction (Scheme 8.1) remains the single clear-cut example of a reaction in solution that demonstrates remarkable levels of chirality amplification[3] and statistically reproducible phenomenon of spontaneous generation of chirality from achiral substrates.[4] This puts it in the center of intensive research with the ultimate goal of conscious design of other systems that could behave similarly *via* deep understanding of the chemical mechanism of the reaction.

Catalysis Series No. 43
Asymmetric Autocatalysis: The Soai Reaction
Edited by Kenso Soai, Tsuneomi Kawasaki and Arimasa Matsumoto

Published by the Royal Society of Chemistry, www.rsc.org

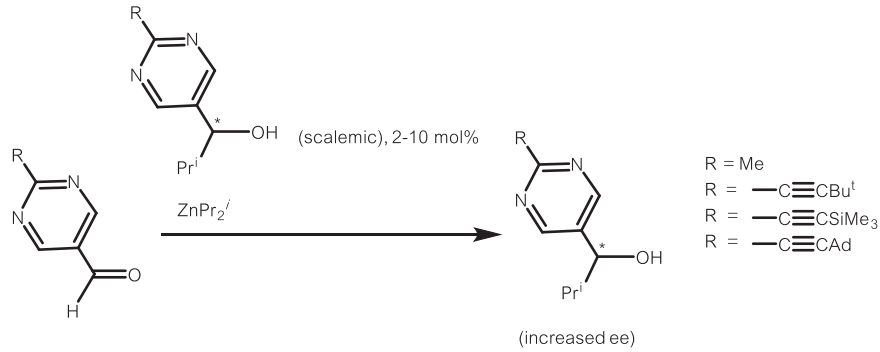

Scheme 8.1 Autoamplifying Soai reaction (SR).

Broad interest for this field results in frequent reviewing,[1,2] so the interested reader is well-informed on the recent achievements. Hence, in this chapter we tried to make a compact glossary of DFT and kinetics simulation results in illuminating the problems that still exist in the accumulation of data and their interpretation to promote further fruitful research.

8.2 Structure of the Product in Solution as a Source for Calibration of Computation Results

After experiments and computations described in ref. 5–10 there is a consensus in the literature on the solution structure of the product (Scheme 8.2). The main component of the reaction mixture at ambient temperature is the homochiral square dimer **SD** (only homochiral species will be discussed here if no special note will state otherwise). Excessive diisopropylzinc can coordinate either to oxygen or nitrogen atom of a square dimer molecule, the latter binding mode is more prominent.

These observations have been quantified that provide a lead for appropriate choice of a functional for further computations. Apparently, while B3LYP gives nice qualitative agreement in all studied cases, the M05x functional strongly overestimates the strength of donor–acceptor interactions.

We are not trying to advertise exclusively the B3LYP for the computational studies of SR. Rather, we would like to the draw attention of researchers to the fact that the dependence of the results on the applied functional can be very strong. Hence, when a new computational level is applied, it is necessary to compute the whole catalytic cycle on the same level. Otherwise, it is impossible to evaluate the energetics of the catalytic cycle and decide whether the energy of the rate limiting transition state is reasonable compared to that of the starting compounds and not only to the immediate precursors as is seen in some recent publications.

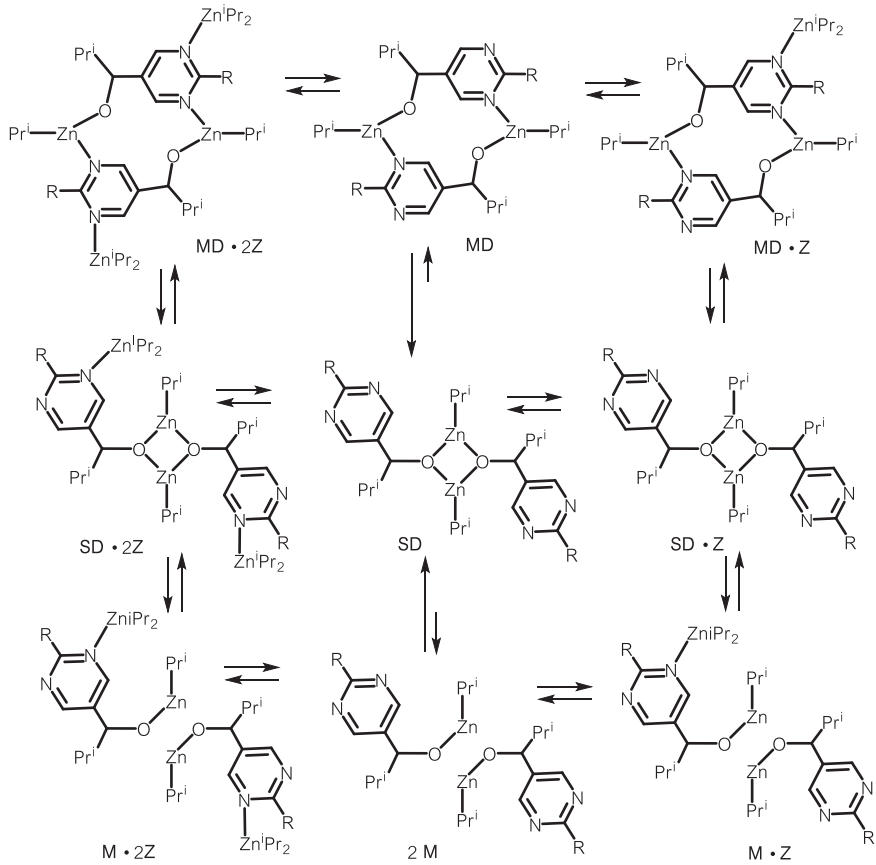

Computed parameters R=^{t}Bu, 6-31G*(pcm, toluene), kcal/mol

Process	ΔE(ZPVE)	ΔG(298.15)	ΔG(273.15)	ΔG(193.15)	ΔG(298.15) exp.
2 M —> SD					
B3LYP	-30.6	-16.0	-17.2	-21.1	-19.1
M05-2X	-54.0	-29.2	-30.9	-38.1	
SD —> SD • Z					
B3LYP	-4.8	3.7	2.8	-0.1	no separate signals for SD•Z in NMR
M05-2X/6-31G	-19.1	-10.4	-10.8	-12.7	
SD —> SD • 2Z					
B3LYP	-14.9	11.2	9.1	2.3	
M05-2X)	-36.1	-12.3	-14.3	-20.3	
SD —>MD[a]					
B3LYP	8.7-9.1			11.1-15.6	
M05-2X	6.4-11.8			5.4-11.0	
SD • Z —> MD • Z[a]					
B3LYP	10.0-14.7			13.5-20.0	
M05-2X	7.4-13.7			10.0-17.5	

[a] Depending on conformation

Scheme 8.2 Equilibria between monomeric and dimeric alcoholates and their $ZnPr^i_2$ complexes.

Processes taking place in the reaction pool of the SR at decreased temperatures have been further studied with NMR spectroscopy.[11,12] In the ^{1}H NMR of the most stable conformation of the tetramer the in-cavity protons (shown red in Scheme 8.3) exhibit abnormally low-field shifted signals that enabled estimation of the thermodynamic parameters of tetramerization and formation of an adduct between tetramer and Zn^iPr_2. From inspecting the data shown in Scheme 8.3 one can conclude that the B3LYP functional again performs significantly better.

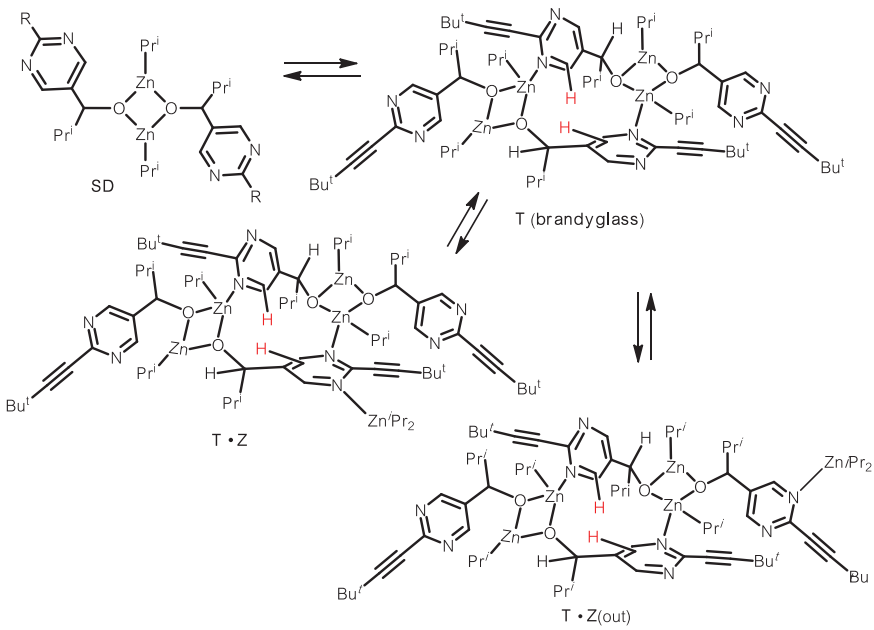

Computed parameters R=^{t}Bu, 6-31G*(pcm, toluene), kcal/mol

Process	ΔE(ZPVE)	ΔG(298.15)	ΔG(273.15)	ΔG(193.15)
2 SD —> T				
B3LYP	-30.6	5.8	4.1	-1.5
M05-2X	-42.2	-24.0	-25.4	-29.3
Experimental		2.9	1.0	-5.2
T + Z —> T•Z				
B3LYP	-8.3	6.7	5.5	1.5
M052-X	-21.0	-11.4	-12.0	-14.2
Experimental		1.2	1.0	-3.0
T + Z —> T•Z(out)				
B3LYP	-11.8	3.7	5.5	1.5
M052-X	-21.1	-10.7	-12.0	-14.2

Scheme 8.3 Equilibria between dimeric and tetrameric alcoholates and their Zn^iPr_2 complexes.

8.3 Comparison of the Computed Catalytic Cycles

8.3.1 DFT Mechanisms – A General Consideration

The main problem of all existing DFT computations of the SR mechanism is the analysis of a single mechanistic possibility silently suggesting that all other possibilities do not exist. For example, a nice mechanism for the reaction is found for a homochiral oligomer being the catalyst. It is automatically assumed that the only reaction capable of competing with this pathway is catalyzed by a heterochiral dimer of approximately the same structure (or non-enantioselective reaction of the homochiral oligomer). However, this is not an entirely accurate approach. The competing reaction can also be catalyzed by an oligomer of a different structure, or a different order of aggregation.

Another problem is calculation of only one transition state with its immediate precursor without computing the whole catalytic cycle.[13,14] This together with the difference in functionals outlined above makes an accurate comparison of different cycles difficult. For example, Figure 8.1 shows the data for the uncatalyzed alkylation (B3LYP/6-31G(d)/SMD(toluene) level of theory.

As can be seen from Figure 8.1, the data from one computational job may vary by 75% depending on the chosen reference and precise kind of value reported. Especially striking is the high value of $\Delta G^{\ddagger}$ when referred to the mixture of reagents. This is caused by the well-known issue in computation of entropies in bimolecular reactions.[15–17] In a multi-stage catalytic cycle such systematic errors are accumulated, hence it is reasonable to report computed enthalpies or ZVPC energies. Nevertheless, to obtain these data frequency analysis is also necessary that requires a lot of resources. As a result, in the historically first mechanism suggested for the SR only electronic energies are reported that is, at least to some extent, misleading.

The difference between the numbers obtained for the mixture of starting compounds and their adducts is not so dramatic (Figure 8.1), but one must keep in mind their accumulation, especially during the formation of oligomers. Hence, it is impossible to evaluate properly any mechanism if the energy of the whole catalytic cycle is not estimated. For this reason we will not discuss in detail the recent mechanistic suggestions with only one stage computed.[13,14]

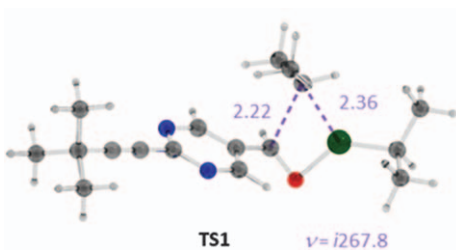

Activation energy, kcal/mol

Relative to	A · Z	A + Z
E	20.6	24.3
E_{zpve}	22.0	25.0
H	22.0	24.0
G	27.9	35.6

Figure 8.1 Computed activation parameters for the uncatalyzed reaction.[12]

8.3.2 Dimer Catalyst Mechanism – *Barrels* Empty and Full

The first conclusion of an explorer encountering the chemistry of the SR is the multitude of possibilities opened for the construction of various structures looking potentially competent for the role of amplifying catalyst. Sooner or later this multitude of possibilities leads to the necessity of some bias that would justify consideration of only a limited number of structures to ably describe the corresponding mechanism. It is no doubt that the mechanism described in the ref. 18–21 was inspired by the beauty and apparent symmetry (see, however, further) of the *barrel* structure (Figure 8.2). It would be interesting to know what exact reason was decisive for the choice between a catalyst and a product in the catalytic cycle. We can see at least two perfectly sound reasons why the latter choice was taken. Indeed, the *barrel* structure itself is so cumbersome that one can hardly afford the addition of any further guests for the dinner since this would make the visualization

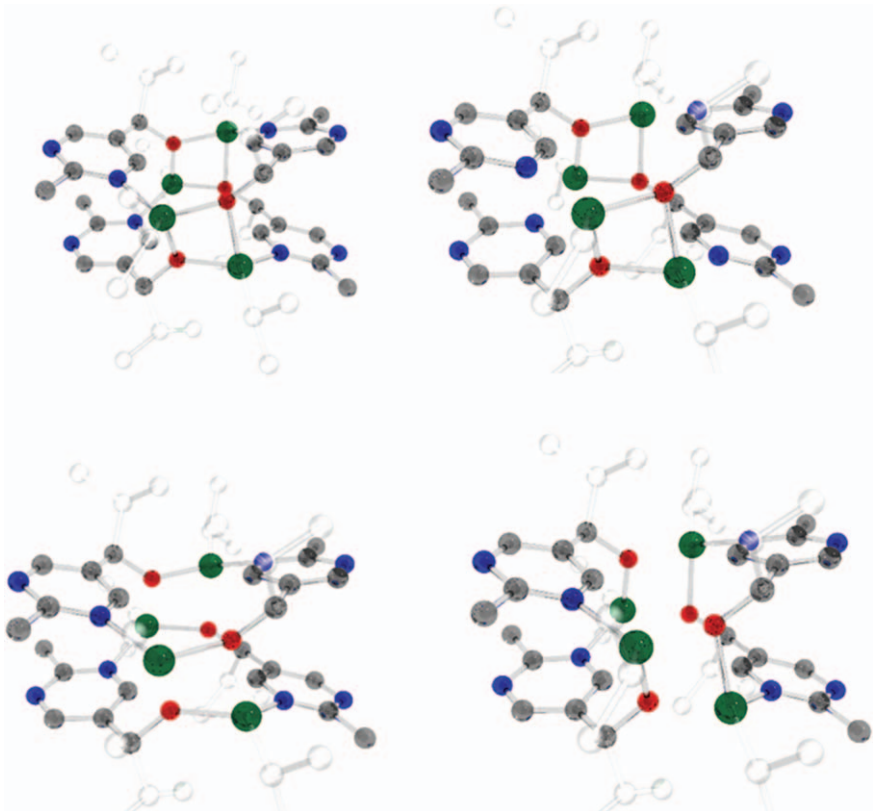

Figure 8.2 One of the possible barrel structures (left up) and different possible ways for its dissociation to dimers: two square dimers (right up), two macrocyclic dimers in the layer conformation (left, below), and two macrocyclic dimers in waterglass conformation (right, below).

practically impossible. Besides, at that time the idea of a dimeric catalyst has been under thorough investigation (apparently, also due to its relative simplicity).[21]

The catalytic cycle begins from a molecule of **SD** which makes an adduct with two molecules of diisopropylzinc **SD** · **2Z** (Figure 8.2). The latter rearranges to **MD** · **2Z** which accommodates two molecules of the substrate to make **MD** · **2Z** · **2A.** Two consequent alkylation stages give a tetramer **B** which gives upon dissociation two molecules of **SD** instead of one borrowed in the beginning.

The five-molecular adduct **MD** · **2Z** · **2A** has a specific structure: a molecule of macrocyclic dimer in a flat *pancake* conformation is decorated first with two diisopropylzinc moieties, which are later used for the two-points docking of two substrates each using its oxygen and one of its nitrogen atoms to

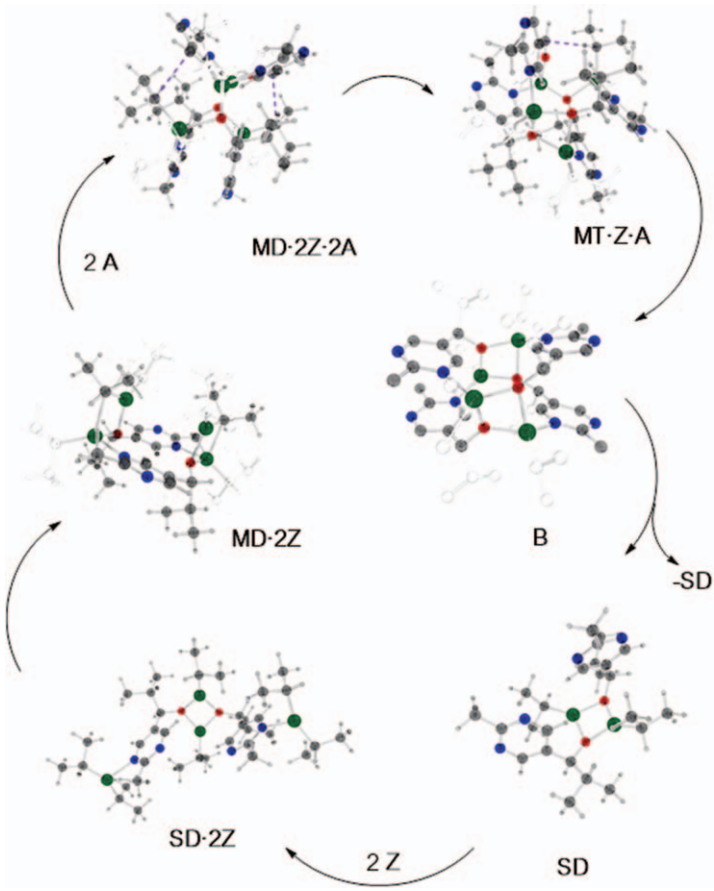

Figure 8.3 Catalytic cycle of the SR with a macrocyclic dimer in layer conformation as a catalyst and barrel tetramer as a product.

form the Zn–O and Zn–N bonds, respectively, and acquire the appropriate conformation for accepting an isopropyl group from Z (Figure 8.3).

To keep all this ensemble together the authors must apply the M05x functional in their computations. They report a striking weakening of the associates when the B3LYP is attempted. Using the M05X, however, is not a universal cure, since the *barrel* itself becomes quite a stable structure, and computed with M05X gives rather uncertain perspectives for the regeneration of the catalyst (computed $\Delta E^{\ddagger}$ is around 55 kcal mol^{-1}; unfortunately a frequency analysis, essential for taking into account entropy, has not been performed).[20]

Rationalization of enantioselectivity of the SR is a tough part of this mechanism. It is difficult to illuminate some idea without telling the whole story which is quite long and cumbersome. Nevertheless, a very useful set of data is given by 10 different computed transition states for the isopropyl group transfer ranging in the corresponding activation barriers from 6 to 18 kcal mol^{-1}.[21] Although these data are just electronic energies and cannot be compared to anything else, the diligent structural analysis demonstrates that there are many circumstances to account if you challenge the mechanism of the SR.

Moreover, the kinetic treatment of the computed results is accurate and convincing (*vide infra*).

8.3.3 Tetrameric Mechanism – *Brandy* Party[11,12]

Since the **SD** structure fails to catalyze the SR, it was important to get a closer look at the 12-membered macrocyclic oligomers, which are conformationally flexible. Scanning the energy changes upon varying the angle between the pyrimidinyl rings and the dihedral angle between two Zn–O bonds, numerous minima for the homo- as well as for the hetero-chiral dimer were located. Although any of these conformations could be used as a building ground for the reactive assemblies, no notable distinctions between homo- and hetero-chiral species at the dimer level of oligomerization have been seen. Nevertheless, it was realized that macrocyclic tetramers that could reversibly form *via* dimerization of the square dimers (Scheme 8.3) may have more distinct conformations due to the presence of Zn–O–Zn–O squares in their structure.

These efforts resulted in an important finding – although a multitude of possible conformations could be located for the tetrameric macrocycles, there was a notable difference between homo- and hetero-chiral species. For the homochiral species a C_2-symmetrical conformation with two almost orthogonal pyrimidinyl rings became dominant in the equilibrium mixture (Figure 8.4). Although a similar conformation is possible for the heterochiral tetramer, in this case it is notably less stable, and the angle between the pyridinyl rings is further from 90°. On the other hand, heterochiral tetramers were much more inclined to form structurally opposite conformations – with almost coplanar pyrimidyl rings (Figure 8.4).

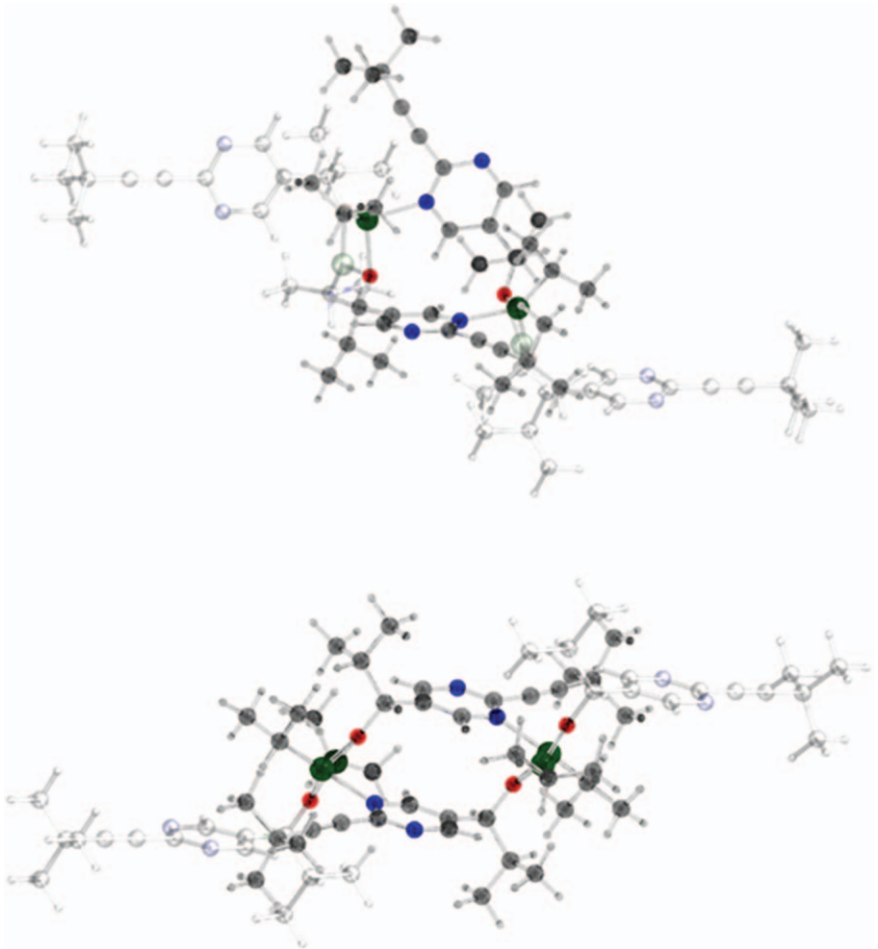

Figure 8.4 The most stable conformations of the heterochiral tetramer: up – homochiral brandyglass (the angle between pyrimidinyl rings is close to 90°) bottom – heterochiral layer (the angle between pyrimidinyl rings is close to 0°).

This example of structural diversification between homo- and hetero-chiral structures together with the beautiful cavity capable of accommodating a molecule of aldehyde resulted in the suggestion that the homochiral *brandyglass* tetramer is an active catalyst of the SR.

Moreover, computational study of the diisopropylzinc coordination to homo- and hetero-chiral *brandyglass* tetramers revealed a still more distinct structural diversification (Figure 8.5): whereas in the homochiral case the angle between the pyridinyl rings was kept around 90°, in both possible isomers of the $Zn^{i}Pr_2$ complex of the heterochiral *brandyglass* this angle was significantly decreased (Figure 8.5), thus closing the cavity appropriate for accommodating a substrate.

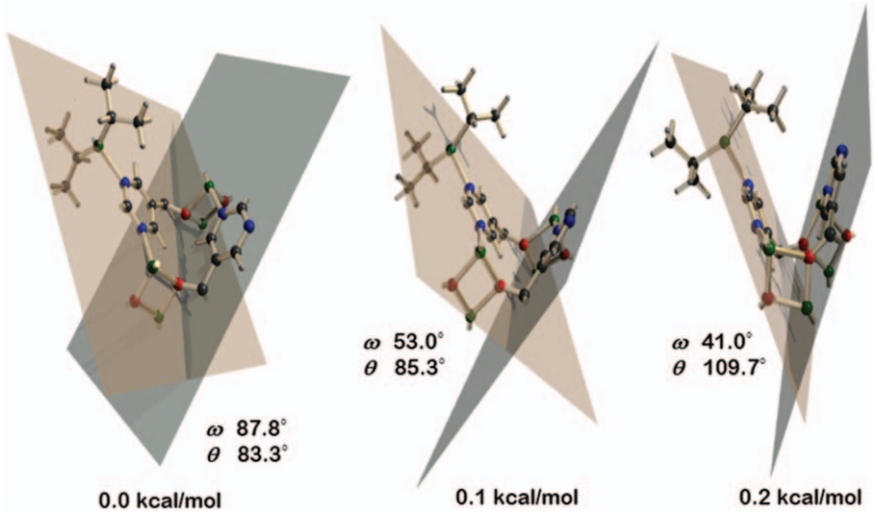

Figure 8.5 Structural diversification between homo- and hetero-chiral brandyglass tetramers upon coordination of the diisopropylzinc molecule. Left – homochiral brandyglass (cavity is open). Right – two isomers of hetero-chiral brandyglass (cavity is closed).

This could be a perfect opportunity for the realization of Frank's scheme *via* removing the concurrence from the heterocyclic catalyst, and the corresponding transition state applying the homochiral *brandyglass* tetramer as a catalyst was located.[12]

The located transition state (Figure 8.6) has several important features for the SR. First, the reaction catalyzed by the homochiral *brandyglass* tetramer provides the same handedness of the product as was seen in the catalyst. Moreover, this reaction is perfectly enantioselective, since the aldehyde is unable to approach the coordinated $Zn^{i}Pr_2$ with another prochiral plane. Another important trait is the clear role of the *t*-Bu–C≡C– substituent, which helps to keep the substrate appropriately coordinated for the facile transfer of the isopropyl group (Figure 8.6).

The catalytic cycle using the homochiral *brandyglass* tetramer as the catalyst was computed and explicit kinetic equations were derived for kinetics simulations. This approach allowed us to simulate adequately important characteristics of the SR such as: chirality amplification, sigmoidal shape of the kinetic curves, and reverse Arrhenius dependence of the reaction rate.

Interestingly, the primary product of the outlined catalytic cycle is a monomer. DFT calculations coupled with kinetic simulations showed that the formation of the experimentally intercepted metastable acetal species is best explained by the reaction of the monomer alcoholate formed in the reaction with a highly concentrated square dimer taking place before alcoholate could find another partner for dimerization.[22]

In the next section a kinetic approach for the elucidation of the mechanism of SR will be discussed.

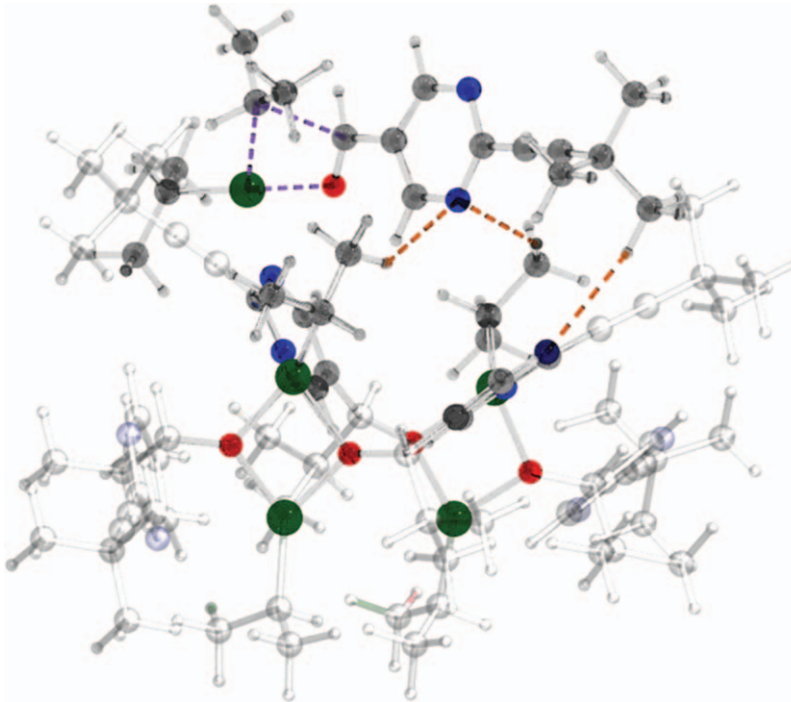

Figure 8.6 Transition state for the alkyl transfer catalyzed by homochiral brandyglass tetramer. Dashed lines illustrate the docking mode of the substrate molecule: the aldehyde group is coordinated to Zn, whereas three C–H–···π (hetero) interactions (around 3 Å each) fix the molecule of the substrate in the appropriate orientation.

8.4 Kinetic Approach for Exploring the Mechanism of the Soai Reaction

Although quite a few experimental and theoretical studies of the Soai reaction have been reported, its mechanism is still vigorously discussed. Kinetics of sophisticated reactions can often serve as a key for elucidation of their mechanisms,[23–28] hence it is not surprising that many researches challenged the kinetic analysis of the Soai reaction. As a result of these efforts, it is universally accepted that the chirality amplification and spontaneous break of chirality, as well as the specific kinetic features of this reaction are stipulated by its autocatalytic character and follow the Frank's catalytic scheme.[29] There is also consensus on the catalytic stage being the rate-determining one. On the other hand, some extremely important questions remain unanswered:

– Chemical nature of the catalytically active species, *i.e.* the molecule in which alkylation occurs;

- What stages in the catalytic cycle are fast enough to be described by the steady-state approximation;
- Which stages can be considered as quasi-equilibrium ones.

Elucidation of mechanisms using chemical kinetics applies the following steps:

- Interception of all products (if possible, also intermediates) *via* chemical and spectral methods; making a list of possible stages based on the experimental data;
- Determination of the kinetic and thermodynamic characteristics of every stage (reaction order, molecularity, equilibrium constant, activation energy, *etc.*);
- Checking the experimentally found parameters against the results of quantum-chemical computations;
- Design of the stage-by-stage reaction scheme and kinetic simulation of the entire intricate process.

This kind of approach to the kinetic investigation gives the most reliable results and has a high predictive power. Neglecting any of the stages listed above makes the conclusions unreliable and quite often erroneous. Unfortunately, such examples can be found in the literature describing kinetic studies of the SR. For example, the hypothesis of participation of an acetal intermediate in the catalytic alkylation stage[14] is not consistent with the estimation of its life span and with the DFT computations of the energetics of such reaction.[22]

In the next section we will analyze the kinetic results described in the literature.

8.4.1 Browsing the Known Kinetic Data

All known experimental characterizations of the individual processes in the Soai reaction are collected in Table 8.1.

There are significant contradictions in the data shown in Table 8.1. Thus, the reaction orders for different reagents vary from 0 to 2 in aldehyde, 0 or 1 in diisopropylzinc, and 1 or 2 in the catalyst. Such inconsistent data are not appropriate for discrimination between various hypotheses on the mechanism of a multi-stage reaction. We have found the following reasons for the origin of these inconsistencies:

1. Use of the concept of ''reaction progress kinetic analysis'' as a kinetic method adapted for synthetic chemists, leads to erroneous results. The merits and demerits of this procedure in general deserves special treatment. In the case of the Soai reaction the weak points of this approach are:
   - The fractional orders strongly deviating from integers just prove the multi-stage character and variability of the empirical order during

Table 8.1 Compilation of the known kinetic data for the Soai reaction.

No.	Substrate, temperature	What is measured	Ref.
1	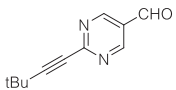 228–273 K	Overall reaction orders (assumed): 1st in aldehyde, 1st in Zn^iPr_2, 2nd in product	30, 2001
		Product of kinetic constant of autocatalytic step, k, and equilibrium dimerization constant, K (from simulation of the overall reaction kinetic curve): $kK = 1.5\times10^3\ M^{-3}\,s^{-1}$ (228 K) $kK = 3.0\times10^3\ M^{-3}\,s^{-1}$ (248 K) $kK = 1.2\times10^4\ M^{-3}\,s^{-1}$ (273 K)	31, 2003
2	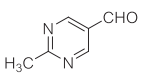 298 K	Overall reaction orders (from analysis of dependence of reaction rate on fraction conversion): 2nd in aldehyde, 0th in Zn^iPr_2, 1st in homochiral dimeric autocatalyst	32, 2003
3	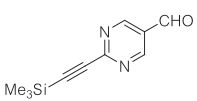 213–308 K	Kinetic constant of zinc-alkoxide dimer dissociation (extrapolated from temperature dependence of NMR line shapes at 323–353 K) $k_{diss} = 0.025\ s^{-1}$ (273 K)	5, 2003
		Equilibrium association constant of zinc-alkoxide dimer with Zn^iPr_2 (from dependence of NMR line shifts on Zn^iPr_2 concentrations): $k_a = 4.6\ M^{-1}$ (308 K, toluene)	6, 2004
		Equilibrium association constant of aldehyde with Zn^iPr_2 (from dependence of NMR line shifts on Zn^iPr_2 concentrations): $k_a = 5.6\ M^{-1}$ (213 K, toluene)	10, 2008
4	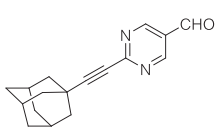 263–298 K	Temperature dependence of overall reaction kinetic curve Overall reaction orders (from analysis of dependence of reaction rate on fraction conversion): 1.6 in aldehyde, 0th in Zn^iPr_2, 1st in zinc-alkoxide	33, 2010

5	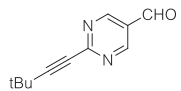	Equilibrium association constant of 2 dimer–tetramer (from temperature dependence of NMR signals) $\Delta H = -20.3$ kcal mol^{-1}; $\Delta S = -78$ cal mol^{-1} K^{-1}; $\Delta G(298) = 2.9 \pm 4.2$ kcal mol^{-1}; $\Delta G(193) = -5.2 \pm 3.3$ kcal mol^{-1}; Equilibrium association constant Zn^iPr_2 of zinc-alkoxide with oligomers of zinc-alkoxide (from the temperature dependence of NMR signals) $\Delta H = -10.7$ kcal mol^{-1}; $\Delta S = -40$ cal mol^{-1} K^{-1}; $\Delta G(298) = 1.2$ kcal mol^{-1}; $\Delta G(193) = -5.2 \pm 3.3$ kcal mol^{-1};	12, 2012
6	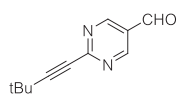 293 K	Overall reaction orders (from measurement of initial reaction rates at different reagent concentrations): 1.9 in aldehyde, 0th in Zn^iPr_2, 1st in alcohol. In accordance with kinetic curves presented in the ESI, the initial rates of reaction are near zero and cannot be estimated with appropriate accuracy. The physical meaning of the values of k_0 plotted in the figures and dimension of this value are not disclosed in the paper.	14, 2020
7	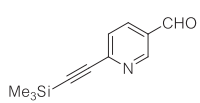 263–293 K	For reaction of unsubstituted 3-pyridylaldehyde with Zn^iPr_2 (from measurement of initial reaction rates at different reagent concentrations): 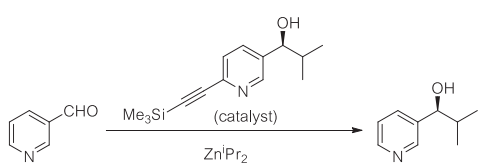 Kinetic orders: 0th in aldehyde, 0th in Zn^iPr_2, 1st in catalyst Rate constant: $$k = \frac{k_B T}{h} \exp\left(-\frac{\Delta H^{\ddagger}}{RT} + \frac{\Delta S^{\ddagger}}{R}\right)$$ $\Delta H^{\ddagger} = 8.50$ kcal mol^{-1}; $\Delta S^{\ddagger} = -35.6$ cal mol^{-1} K^{-1}; $\Delta G^{\ddagger}(273) = 17.68$ kcal mol^{-1}	13, 2020

the reaction. Hence the fractional orders are non-specific and do not provide any information on the mechanism;
- Replacement of the appropriate mathematical treatment of the kinetic equations with graphical representation, including the neglect of the starting parts of the kinetic curves and induction period, which is an important and specific feature of the Soai reaction.
- Attempts to replace kinetic experiments at various reagent concentrations with complex formal analysis of a single kinetic curve of the brutto reaction.

2. Unjustified use of the mass action law *via* application of equations like $v = kA^aZ^zP^p$. Elementary reactions of only first or second order are common in Nature. Since triple molecular encounters are a rare phenomenon, only few elementary reactions are approximately described by third order. Getting an empirical order of 3 and more just means that the reaction under study is multi-stage and involves a quasi-equilibrium stage or stages.

Let us consider a simple example of a reaction possible only for a dimer if the dimer–monomer equilibrium is fast:

$$2\mathrm{M} \overset{K}{\rightleftarrows} \mathrm{D} \overset{k}{\rightarrow} \mathrm{P}$$

Chemical analysis of the reaction mixture at any time would provide the concentration of the reagent:

$$M_t = M + 2D;\ \ K = \frac{D}{(M_t - 2D)^2};$$

The current dimer concentration in that case can be found as a solution of the square equation:

$$D = \frac{1 + 4K \cdot M_t - \sqrt{1 + 8K \cdot M_t}}{8K},$$

Showing that:

if $K \cdot M_t \gg 1$, the dimer concentration approximately is $D \approx M_t/2$

if $K \cdot M_t \ll 1$, $\sqrt{1 + 8K \cdot M_t} \approx 1 + 4K \cdot M_t - 8K^2 \cdot M_t^2 + \ldots;\quad D \approx KM_t^2$

then at intermediate concentrations the rate is described by the expression

$$v = kD = k\frac{1 + 4K \cdot M_t - \sqrt{1 + 8K \cdot M_t}}{8K}$$

with the reaction order changing during the process. Similarly, it is easy to get expressions for the complexation of diisopropylzinc with the alcoholate and other possible quasi-equilibrium stages of the Soai

reaction, as well as for the equilibrium formation of the triple complex aldehyde/diisopropylzinc/catalyst. It is clear that simple appearance of the expression for the rate constant containing multiplication of concentrations in integer orders can be observed only in artificially designed specific conditions.

3. Negligence of the restrictions stipulated by the conditions of the material balance. Thus, considering the material balance of the Soai reaction, the kinetic equation $v = kA^a Z^z P^p$ is transformed to $v = kA^a(Z_0 - A_0 + A)^z(P_0 + A_0 - A)^p$ meaning that the experimental reaction order becomes non-integer and variable throughout the reaction. In the case where a real kinetic equation becomes indeterminate and cannot serve anymore as a sensible kinetic feature helpful for the mechanism elucidation.
4. Carrying out all kinetic experiments within a narrow range of the reagent concentrations mimicking the synthetic conditions. It is evident that reactions exhibiting zero order by reagent in the whole concentrations range do not exist. Finding conditions when the reaction rate begins to depend on the reagent concentration, could provide information on the strength of binding of this reagent in the reactive complex.
5. The known results of the kinetic measurements for the Soai reaction are based on the idea of one single- or multi-stage sophisticated reaction. In fact, there are two simultaneously running reactions leading to different products, that are enantiomers. These two reactions compete for the starting compounds and inhibit each other. Namely, these features are the basis of the Frank's scheme. From a kinetic point of view, the co-existence of two competing chemical processes requires at least two kinetic equations for an adequate description of the system. These considerations were not sufficiently addressed in the known experimental studies. As a rule, two competing catalysts are introduced to the system simultaneously, whereas the kinetic equation describes the total concentration of the products of two competing reactions.

Despite numerous flaws pointed out above let us try to extract the most relevant kinetic features of the Soai reaction.

Zeroth order in diisopropylzinc was reported in several studies.[14,21,32,33] This finding can be considered as more or less reliable. Note however, that two other studies[30,31] reported the first order under approximately the same conditions.

The characteristic time of the dimer dissociation was reported as ~30 s (273 K) from the temperature dependence of NMR line-shapes.[5,6,10] The constant of the dimer–monomer equilibrium was estimated as 4×10^6 M^{-1} based on a guess for the dimerization kinetic constant. Unfortunately, the method of elucidation of the latter value is unclear. Nevertheless, the NMR data qualitatively prove the high value of the equilibrium constant of the monomer–dimer equilibrium. In other words, it is possible to accept with some confidence that the product (catalyst) mostly exists as a dimer in the temperature and concentration intervals normally used for the Soai reaction.

The binding constants for the adducts of diisopropylzinc with aldehyde and dimer were estimated as 5.6 M^{-1} at 213 K and 4.6 M^{-1} at 308 K, respectively.[6] Unfortunately, the absence of the temperature dependence for these constants makes it difficult to adjust them for the experimental conditions. Nevertheless, it should be noted that the latter data allow estimation of the level of binding of the dimer with diisopropylzinc as 14–50% of the total concentration of the dimer contradicting the reported zero order of the reaction for Zn.

The Gibbs energy for dimerization of zinc alcoholate was estimated from NMR line-shape analysis as 19 kcal mol^{-1}.[12] We have also estimated by NMR data the equilibrium constant for the formation of tetramer from the dimer. These data testify that the formation of tetramer is possible already at ambient temperature ($\Delta G(298) = 2.9 \pm 4.2$ kcal mol^{-1}) and becomes thermodynamically favorable upon decreasing the temperature ($\Delta G(193) = -5.2 \pm 3.3$ kcal mol^{-1}). Although the ΔH and ΔS values obtained for this process are in accord with the results of DFT calculations, they are still not accurate enough for the quantitative estimations of the tetramer concentrations.

Estimated thermodynamic parameters of the association of diisopropylzinc with oligomers ($\Delta G(298) = 1.2$ kcal mol^{-1}; $\Delta G(193) = -5.2 \pm 3.3$ kcal mol^{-1})[12] show rather weak binding of diisopropylzinc and correlate with the estimations made previously. Nevertheless, they contradict to the observed zero order of the reaction by Zn.

The most reliable kinetic data were obtained for the model substrate 3-pyridylaldehyde.[13] Authors of this work avoided most of the methodological flaws mentioned above. The experimental orders of the reaction (0th in aldehyde, 0th in $Zn^{i}Pr_2$, 1st in catalyst) testify that the measurements were carried out under conditions of saturation of the reactive complex with both substrates. The Gibbs activation energy for the rate limiting stage was measured to be 17.68 kcal mol^{-1}. This value agrees well with the DFT computations for the measured substrate as well as with our DFT results obtained for the *t*-Bu–C≡C– substituted substrate (activation enthalpy 17 or 18 kcal mol^{-1} depending on the method).[12]

In general, the research results outlined above demonstrate that experimental kinetic data available now are insufficient to be used for the discrimination between suggested mechanisms or the verification of the developed models.

8.4.2 Simulations of the Kinetics in the Soai Reaction

A significant number of attempts to simulate the kinetics of the Soai reaction have been described.[2,14,19,34–36] Some of the suggested schemes contain more than 10 kinetic stages and 6–8 fitting parameters. There is a saying well-known among professionals: ''if you use 4 adjustment parameters for describing your kinetic curve, you can describe a horse. If you add the 5th parameter, your horse would friendly wag its tail''. As in any other joke, there is some truth in this saying. Having this in mind, it is not surprising that it

was possible to adjust the simulation results to the experimental kinetic curves for any chosen model: monomer catalyst, dimer catalyst, tetramer catalyst, acetal catalyst, *etc.* upon sufficient variation of the adjustment parameters. Hence, these examples of quantitative simulations of the kinetic curves are not appropriate for the discrimination or verification of the suggested mechanisms. On the other hand, the merit of these efforts is that they demonstrate a principal possibility to describe the kinetics of the Soai reaction *via* modified Frank's schemes.

Since the experimental data are insufficient, one can consider the following tactics for the discrimination between different models:

- Limit the reaction scheme to the minimal number of stages taking into consideration only the experimentally characterized processes. One must take into account the well-established strong predominance of the square dimers in the reaction pool. Since the estimated high activation energy of the alkylation stage allows considering it as the rate-limiting one, it is reasonable to consider other stages of the process in quasi-equilibrium approximation.
- Use in the models the principal processes – autocatalysis and mutual inhibition. Since two enantiomeric products are formed in the reaction, the system of kinetic equations must contain no less than two equations describing the evolution of both products. This can be a system of equations for the concentrations of both enantiomers or a system of related equations for the total concentrations of the products and enantiomeric excess.
- Abandon the quantitative description of the kinetic curves due to inevitable simplification of the kinetic model. Instead, target the semi-quantitative and qualitative description of specific reaction features, *e.g.* enantiomeric excess, anormal temperature dependence, *etc.*
- Use instead of lacking experimental parameters the results of quantum-chemical computations which are sufficiently accurate for the qualitative description of the Soai reaction.

This approach was more or less successfully attempted by Schiaffino and Ercolani.[19,20] They have used a minimal kinetic scheme and compact kinetic equations connecting the concentration of the substrate (or the total concentration of the reaction products and enantiomeric excess that is the same) for the model of a dimeric catalyst, all forms of which are rapidly equilibrating. The authors compare the solutions of the suggested equations with the enantiomeric excess, achieved experimentally under different reaction conditions. A good agreement was obtained for the ambient temperature. However, to reproduce in the calculations the experimentally observed temperature dependence of the enantiomeric excess, it was necessary to introduce additional assumptions and use supplementary parameters describing the properties of the different oligomers.

We have applied a similar approach for the description of the accumulation of the enantiomeric excess in the case of a tetrameric catalyst.[12] The corresponding system of equations simultaneously describing the kinetics of the product accumulation and the kinetics of the enantiomeric excess changes is shown below.

$$\frac{dC}{dt} = (C_0 + A_0 - C) \times \mathrm{Zn} \times \left[4k_r D^2((1+ee)^4 - (1-ee)^4) + 2k_0\right]$$

$$\frac{dee}{dt} = \frac{(C_0 + A_0 - C)\cdot \mathrm{Zn} \cdot D}{1 + K_{D\mathrm{Zn}}\mathrm{Zn}} \left[2k_r \cdot \left((1+ee)^4(1-ee) - (1+ee)\right) - \frac{k_0 \cdot ee}{K_D^2}\right]$$

where C_0 and A_0 are the starting concentrations of alcoholate and aldehyde, and the concentrations of non-bound dimers D and non-bound diisopropylzinc Zn are determined by the following equations:

$$\mathrm{Zn}_\Sigma = \mathrm{Zn}_0 - C + C_0$$

$$D = \left(\sqrt{(1/K_{D\mathrm{Zn}} + \mathrm{Zn}_\Sigma - C/2)^2 + 2C/K_{D\mathrm{Zn}}} - 1/K_{D\mathrm{Zn}} - \mathrm{Zn}_\Sigma + C/2\right)/2$$

$$\mathrm{Zn} = \mathrm{Zn}_\Sigma/(1 + K_{D\mathrm{Zn}}D)$$

and the observed rate constant $k_r = \frac{k_1 K_A K_{T\mathrm{Zn}} K_T}{2^6}$ contains the equilibrium constants: K_T is the equilibrium constant between dimer and tetramer species, $K_{T\mathrm{Zn}}$. $K_{D\mathrm{Zn}}$ are equilibrium constants for diisopropylzinc attachment to tetramer and dimer species, respectively, K_A is the equilibrium constant for substrate attachment to the tetramer–diisopropylzinc complex.

Solving this system of equation showed that by using the thermodynamic parameters close in values to those obtained by DFT computations one can qualitatively reproduce the anormal temperature dependence of the SR.

Additionally, we have shown that in the case of co-existence of two types of associates of the levels n and l, suggesting existence of a quasi-equilibrium, the kinetic equations acquire the following form:

$$\frac{dA}{dt} = -k_r A(C_0 + A_0 - A)^{n/l}[(1+ee)^n + (1-ee)^n] - 2k_0 A,$$

$$\frac{dee}{dt} = k_r \frac{A}{C_0 + A_0 - A}\left[(C_0 + A_0 - A)^{n/l}[(1+ee)^n(1-ee) + (1-ee)^n(1+ee)]\right] - \frac{2k_0 A ee}{C_0 + A_0 - A}$$

Using these equations, we have found that the experimentally measured changes of the enantiomeric excesses during the reaction can be easily described by a tetramer catalyst model suggesting a statistical content of the

dimeric and tetrameric associates. This is a good argument in favor of the tetrameric catalyst model. On the other hand, it was also shown that changing the equilibrium constants of the equilibria between the associates of different orders, (*i.e.* suggesting a non-statistical formation of the associates and variation of the additional equilibrium constant) one can achieve a good description of the enantiomeric excess changes for a monomeric or dimeric catalyst as well. This observation is an additional illustration of the fact that increasing the number of the variable parameters leads to results not applicable for the discrimination between various models.

8.4.3 Deterministic *vs.* Stochastic Kinetic Modeling

Both deterministic and stochastic modeling are used for description of the Soai reaction.[37–39] At first glance, the statistical approach has obvious advantages, especially, for description of the handedness of enantiomeric symmetry breaking. The excellent example of stochastic modeling for elucidation of the symmetry breaking process is presented in ref. 39. On the other hand, the stochastic modeling is related with some troubles. Indeed, the thermodynamic fluctuations occur in small fragments of the large solution space. As the result of fluctuations, the predominance of the enantiomer in one point of reactive space is inevitably accompanied by predominance of another enantiomer in another point of reactive space. The autocatalytic enhancement in these points should proceed simultaneously and then begin to compete in the course of diffusion mixing. The comprehensive consideration of the overall kinetics of the reaction in this condition should solve the known theoretical ''reaction–diffusion'' problem.[40–42] In the case of nonlinear reactions this problem remains unsolved until now. It is known, nevertheless, that the reaction–diffusion systems can demonstrate spatial symmetry breaking, producing the oscillations, Turing patterns, concentration waves, and other complicated kinetic phenomena.[43–45] Thus, consistent stochastic modeling is complicated and is feasible for consideration of the specific kinetic features only. Thus, the simple deterministic kinetic modeling seems to be preferable for description of kinetics for the purpose of elucidation of the chemical reaction mechanism in conditions where statistical fluctuation can be neglected.

8.5 Conclusions and the Objectives of a Kinetic Description

The analysis of the kinetics of the Soai reaction shown above cannot substitute experimental data that give significantly more detailed and reliable knowledge of the reaction mechanism. On the other hand, it can suggest some useful recommendations for the conditions of a productive kinetic experiment:

1. Reliable values of the reaction orders and rate constants in a complex reaction are possible only in specially organized limiting conditions.

For example, the simplest method is carrying out the reactions in a large excess/deficiency of the chosen reagents.
2. Two enantiomers can be formed in the Soai reaction. The simplest method for reducing the number of kinetic equations and more reliable measurement of the rate constants is to perform all reactions with an enantiomerically pure catalyst. Another possibility is the large excess of a strictly racemic catalyst.
3. Dependence of the reaction rate on the concentration of the inhibitor (opposite enantiomer) should be measured for the determination of the kinetic characteristics of the inhibition process.
4. An impulse introduction of a portion of the chosen component into the reaction mixture under continuous spectral monitoring of the reaction rate can be used for the determination of the dependence of the reaction rate on the regents and other components (inhibitor, catalyst, solvent, *etc.*).

The experimental studies of the Soai reaction are quite difficult. Therefore, thorough kinetic experiments must be justified by achievements of important goals. In our opinion, the kinetic studies must give the answers for the following questions:

- Why does the Soai reaction demonstrate such a strong dependence on the substrate structure?
- Why until now has the Soai reaction remained the only transformation repeatedly demonstrating the chiral symmetry breaking?
- What requirements must obey other chemical transformations for realization of enantiomeric amplification?

In our opinion, careful kinetic studies (combined with DFT modeling) could help to get the answers for these questions.

References

1. T. Buhse, J. M. Cruz, M. E. Noble-Teran, D. Hochberg, J. M. Ribo, J. Crusats and J. C. Micheau, *Chem. Rev.*, 2021, **121**, 2147.
2. D. G. Blackmond, *Chem. Rev.*, 2020, **120**, 4831.
3. K. Soai, T. Shibata, H. Morioka and K. Choji, *Nature*, 1995, **378**, 767.
4. K. Soai, T. Shibata and Y. Kowata, *Jpn. Kokai Tokkyo Koho, JP Pat.*, 9-268179, 1997.
5. I. D. Gridnev, J. M. Serafimov, H. Quiney and J. M. Brown, *Org. Biomol. Chem.*, 2003, **1**, 3811.
6. I. D. Gridnev, J. M. Serafimov and J. M. Brown, *Angew. Chem., Int. Ed.*, 2004, **43**, 4884.
7. I. D. Gridnev and J. M. Brown, *Proc. Natl. Acad. Sci. U. S. A.*, 2004, **101**, 5727.

8. I. D. Gridnev, *Chem. Lett.*, 2006, 148.
9. J. Klankermayer, I. D. Gridnev and J. M. Brown, *Chem. Commun.*, 2007, 3151.
10. J. M. Brown, I. D. Gridnev and J. Klankermayer, *Top. Curr. Chem.*, 2008, **284**, 35.
11. I. D. Gridnev, A. K. Vorob'ev and E. A. Raskatov, Role of Oligomerization in Soai Reaction: Structures, Energies, Possible Reactivity, in *The Soai Reaction and Related Topic*, ed. G. Pályi, C. Zucchi and L. Caglioti, Artestampa, Modena, 2012, pp. 79–122.
12. I. D. Gridnev and A. Kh. Vorobiev, *ACS Catal.*, 2012, **2**, 2137.
13. S. V. Athavale, A. Simon, K. N. Houk and S. E. Denmark, *Nat. Chem.*, 2020, **2**, 412.
14. O. Trapp, S. Lamour, F. Maier, A. F. Siegle, K. Zawatzky and B. F. Straub, *Chem. – Eur. J.*, 2020, **26**, 15871.
15. C. Červinka, M. Fulem and K. Růžička, *J. Chem. Eng. Data*, 2013, **58**, 1382.
16. C. E. Chang, W. Chen and M. K. Gilson, *J. Chem. Theory Comput.*, 2005, **1**, 1017.
17. J. Carlsson and J. Aqvist, *J. Phys. Chem. B*, 2005, **109**, 6448.
18. L. Schiaffino and G. Ercolani, *Angew. Chem., Int. Ed.*, 2008, **47**, 6832.
19. L. Schiaffino and G. Ercolani, *Chem. Phys. Chem.*, 2009, **10**, 2508.
20. L. Schiaffino and G. Ercolani, *Chem. Eur. J.*, 2010, **16**, 3147.
21. G. Ercolani and L. Schiaffino, *J. Org. Chem.*, 2011, **76**, 2619.
22. I. D. Gridnev and A. Kh. Vorobiev, *Bull. Chem. Soc. Jpn.*, 2015, **88**, 333.
23. J. R. E. Smith and C. N. Hinshelwood, *Proc. R. Soc. A*, 1942, **180**, 237.
24. N. N. Semenoff, *Chemical Kinetics and Chain Reactions*, Oxford University Press, London, 1935, pp. xii + 480.
25. R. M. Noyes, R. Field and E. Koros, *J. Am. Chem. Soc.*, 1972, **94**, 8649.
26. T. Engel and G. Ertl, *Adv. Catal.*, 1979, **28**, 1.
27. E. P. Dougherty and H. Rabitz, *J. Chem. Phys.*, 1980, **72**, 6571.
28. K. Smallbone, *et al.*, *FEBS Lett.*, 2013, **587**, 2832.
29. F. C. Frank, *Biochim. Biophys. Acta*, 1953, **11**, 459.
30. I. Sato, D. Omiya, K. Tsukiyama and K. Soai, *Tetrahedron: Asymmetry*, 2001, **12**, 1965.
31. I. Sato, D. Omiya, H. Igarashi, K. Kato, Y. Ogi, K. Tsukiyama and K. Soai, *Tetrahedron: Asymmetry*, 2003, **14**, 975.
32. F. G. Buono and D. G. Blackmond, *J. Am. Chem. Soc.*, 2003, **125**, 8978.
33. M. Quaranta, T. Ghering, B. Odell, J. M. Brown and D. G. Blackmond, *J. Am. Chem. Soc.*, 2010, **132**, 15104.
34. T. Buhse, *Tetrahedron: Asymmetry*, 2003, **14**, 1055.
35. D. Lavabre, J.-C. Micheau, J. R. Islas and T. Buhse, *J. Phys. Chem. A*, 2007, **111**, 281.
36. M. E. Noble-Terán, J.-M. Cruz, J.-C. Micheau and T. Buhse, *ChemCatChem*, 2018, **10**, 642.
37. D. K. Kondepudi and K. Asakura, *Acc. Chem. Res.*, 2001, **34**, 946.
38. G. Lente and T. Ditroi, *J. Phys. Chem. B*, 2009, **113**, 7237.

39. N. A. Hawbaker and D. G. Blackmond, *Nature Chem.*, 2019, **11**, 957.
40. G. Nicolis and I. Prigogine, *Self-organization in Non Equilibrium Systems*, Wiley, New York, 1977.
41. I. R. Epstein and J. Pojman, *An Introduction to Nonlinear Chemical Dynamics*, Oxford University Press, Oxford, 1998.
42. A. De Wit, *Adv. Chem. Phys.*, 1999, **109**, 435.
43. *Oscillations and Traveling Waves in Chemical Systems*, ed. R. L. Field and M. Burger, Wiley, New York, 1985.
44. V. Castets, E. Dulos, J. Boissonade and P. De Kepper, *Phys. Rev. Lett.*, 1990, **64**, 2953.
45. V. K. Vanag and I. R. Epstein, *Chaos*, 2007, **17**, 037110.

CHAPTER 9

Stochastic Modeling of Asymmetric Autocatalysis in the Soai Reaction

GÁBOR LENTE

Department of Physical Chemistry and Materials Science, University of Pécs, Hungary
Email: lenteg@gamma.ttk.pte.hu

9.1 Introduction

The Soai reaction, whose essence is carbon–carbon bond formation by the addition of an organozinc reagent onto a pyrimidinyl carbaldehyde, results in the formation of a new asymmetry center and is therefore a reaction that produces chiral molecules under completely non-chiral external conditions. Since it was first reported in 1995,[1] it has been thoroughly investigated from a synthetic experimental point of view.[2–11] In the initial report,[1] which has also been analyzed scientometrically to prove its major influence on the chemical literature,[12] the main emphasis was on the combination of two long-known phenomena, autocatalysis and enantioselective catalysis. A process is usually termed autocatalytic if at least one of the products formed in it has a verifiable accelerating effect on its own formation (catalyst and product at the same time). This effect can typically be made obvious by adding the suspected autocatalytic product deliberately before initiating the actual reaction, which should cause a very substantial shortening in the reaction time. Enantioselective catalysis, on the other hand, means that in a

Catalysis Series No. 43
Asymmetric Autocatalysis: The Soai Reaction
Edited by Kenso Soai, Tsuneomi Kawasaki and Arimasa Matsumoto

Published by the Royal Society of Chemistry, www.rsc.org

reaction yielding a chiral product from non-chiral initial conditions, the influence of one of the enantiomers of a chiral catalyst (typically different from the product) results in a notable imbalance of the enantiomers of the product formed. Their combination, enantioselective autocatalysis, therefore means the rare phenomenon where the chiral product of the reaction is also an enantioselective catalyst.

After the initial discovery, several more delicate phenomena have been reported in the Soai reaction. For example, it was demonstrated that the reaction's sensitivity also extends to unusual and normally neglected sources of chirality such as the one caused by the difference between the carbon isotopes ^{12}C and ^{13}C, and also hydrogen isotope chirality.[5,6] For the present article, the most important single feature, which was uncovered in later reports, is the possibility to generate highly noticeable stochastic effects in chemical processes.[2–4] This means that under certain conditions, the organozinc reagent addition can be carried out in such a way that the resulting chiral, tertiary alcohol product will be far away from the expected racemic mixture. In these experiments, the enantiomeric composition of the product mixture changes from experiment to experiment even if major efforts are made to ensure identical external conditions. This phenomenon seems to be known both as 'symmetry breaking' or 'absolute asymmetric synthesis' and its observation is still inspiring theoretical research up to the present day.[13–60]

Although the concept of reproducibility is very much emphasized in the training of most chemists, the fact that certain conditions will lead to stochastic results in chemical processes has been known for a long time. As early as 1940, Delbrück pointed out that an autocatalytic process might deviate from the usual deterministic models of chemical kinetics.[61] The stochastic approach to chemical kinetics was developed in fine detail in later years.[62,63] It seems likely that the lack of spectacular and obvious experimental examples was the dominating reason why this approach, which is mathematically slightly less demanding than the usual deterministic one, never gained the attention it deserved.

In 1953, Frank published a model[64] that gave some theoretical framework for later attempts at understanding absolute asymmetric synthesis. The analysis of the scheme used the deterministic kinetic approach and showed the phenomenon of chiral amplification: although no enantiomeric excess was formed in it starting from completely non-chiral conditions, the slightest fluctuation from these symmetric conditions gave rise to gradually higher and higher enrichment of one of the enantiomers. Chiral autocatalysis was one of the important features of this model in addition to mutual antagonism, which meant that the two enantiomers of the same chiral product molecule have the ability to 'neutralize' each other in a chemical way. It is probably the effect of this early paper combined with the scarce knowledge of the development of stochastic kinetics that led to a prevailing view of the already mentioned theoretical attempts in the last two decades,[13–60] which is based on the deterministic approach and shows amplification properties. So the interpretation of absolute asymmetric

synthesis is dependent on the initial fluctuations, but these are not described in any reasonable mathematical way in most of these works. Altogether, this attitude may lead to a reasonable qualitative interpretation but never to a fully quantitative one. Also, this paper might be responsible for the baseless assumption that mutual antagonism is a necessary element in chiral amplification models. In fact, Frank himself[64] did not make such a claim at all in his classic paper.

This chapter aims to present an outline of the fully quantitative modeling efforts of the Soai reaction that are based on stochastic kinetics.[62,63] As the most striking, the experimentally confirmed stochastic feature in the process is the sizable fluctuation in the enantiomeric distribution of the product tertiary alcohol, and most emphasis will be put on a comparison of measured and theoretically predicted distributions. First, a brief summary of stochastic kinetics will be given, then the particle-based, discrete approach to racemates will be introduced and compared to actual observations in the Soai reaction. After this, the development of a minimal kinetic model of absolute enantioselective synthesis will be summarized, followed by a more detailed version based on an actual chemical scheme. Finally, some remarks will be offered on the possibility of interpreting asymmetric distributions, also based on the observation made in the Soai reaction. All these modeling efforts rely on detailed and thoroughly proven mathematical theorems. The proofs will not be reproduced here, they are available in the original sources.[14,18,23,28,37,38,40,46] The main focus will be given to the underlying concepts and the comparison with experimental results.

9.2 Fundamentals of Stochastic Kinetics

Chemical kinetics is normally part of the training of chemists in higher education. Unfortunately, it is seldom emphasized that the classical kinetics taught is one of several possible approaches: the one that is called deterministic in this chapter. The alternatives are several different stochastic approaches, but none of them are typically mentioned in undergraduate or even graduate courses and remain unknown to the majority of researchers as well.

The main underlying idea of usual deterministic kinetics is that the concentration of a substance is sufficiently approximated mathematically by a continuous function (the independent variable is time). If this is so, this function may have derivatives, which provide the basis for defining rates of chemical reactions, and these rates are determined by the concentrations in addition to other possible external conditions (most notably, temperature), but the rates themselves are never dependent on time in an explicit manner: their changes can be described using only the changes in concentrations and other notable external conditions. The connection between the rate and the concentration is called the rate equation. As the starting concentration in a process is typically controlled by the experimenter and the rates are functions of the concentrations (*i.e.* any particular set of concentrations

determines the rate without ambiguity), the concentrations can be given as a function of time by solving the set of differential equations generated by the rate equation. This set of differential equations is typically non-linear as it is common that two concentrations are multiplied or one concentration is raised to a power different from 0 or 1 in the rate equation. Also, a symbolic solution of this rate equation can only be found in the simplest cases: mostly for one-step reactions.

In contrast, probabilities have central roles in stochastic kinetics. The approach described here is called continuous time discrete state (CDS) and its mathematics is already developed in fine detail, which is available from monographs.[63,65,66] As the term 'discrete state' implies, the concentration is not thought to be a continuous function here: it can only assume discrete values because of the particulate nature of matter. So in this sense, CDS kinetics is closer to reality than the deterministic approach. Because of the non-continuous nature, it is much more convenient to use particle numbers (always integers) rather than concentrations derived from these integers by division with the Avogadro constant and volume. Furthermore, a non-continuous function does not have derivatives. Therefore, a quantity called infinitesimal transition probability replaces the deterministic concept of rates in CDS. Even if the initial particle numbers are known with certainty in the process, the molecular events can be described only in terms of probabilities in the system, so the particle numbers do not have certain values, either, after the initial time. Rather, they are quantified with probabilities. It should also be noted that individual particle numbers are never independent of others, so CDS results in a time-dependent set of the joint probabilities of the various particle numbers. One particular set of possible particle numbers in a system is called a state. In the most common mathematical handling of CDS kinetics, a set of linear, first-order differential equations, called the master equation of the process, is written for the state probabilities.

In comparison with deterministic kinetics, CDS kinetics is technically simpler as the differential equations are always linear, which is a consequence of the fact that only one state can occur at any given time (the term 'Markov chain' is also used for this property in mathematics). However, the number of states is way higher than the number of concentrations in a system, which often necessitates creative mathematical handling in order to obtain useful theoretical predictions that are directly comparable to experimental data. This is probably the most difficult aspect of CDS kinetics and this is also why deterministic kinetics is preferred whenever the error introduced by using continuous functions in it is tolerable. However, when the observations themselves are stochastic, then using CDS kinetics becomes a necessity.

9.3 A Particle-based View on Racemates

A racemic mixture of a chiral compound is typically defined as one in which the concentrations of the two mirror-image enantiomers are equal. This is a

viable definition for most of the practical cases but is not entirely acceptable in a strictly particle-based approach. For example, no racemic mixture could exist when the total number of molecules is 1 or any other odd integer. This conceptual problem has been recognized,[22,67,68] and it was pointed out that the number of different enantiomer molecules are characterized by a symmetric binomial distribution in equilibrium. The base assumption here is that every chiral molecule has exactly 50% chance of being one of the two enantiomers, and their stereochemistry is independent of the presence of other molecules. In a mathematical formula, the symmetric binomial distribution is stated simply. Out of N chiral molecules, where the enantiomers are designated R and S, the probability of finding exactly r molecules of R is:

$$P(r) = \binom{N}{r} 2^{-N} \tag{9.1}$$

The symbol within the parentheses is a binomial coefficient in this equation. Of course, by conservation of matter, the number of S molecules is $s = N - r$. The probability distribution shown in eqn (9.1) is shown in Figure 9.1 for the cases where $N = 20$, 50, and 100.

Some important remarks should be made based on the curves shown in Figure 9.1. The first is that the number of chiral molecules (N) was selected to be extremely low (20, 50, and 100) in order to illustrate the scientific points in an optimal way. The second is that each distribution is symmetric with a maximum at $r/N = 0.5$ in agreement with the fact that the energies of the two enantiomers are strictly equal ('exact racemate'). The third notable effect is that the maximum probability decreases as N increases. Although the most probable outcome is the one where the number of molecules for the two enantiomers is equal, the absolute probability of this specific state is

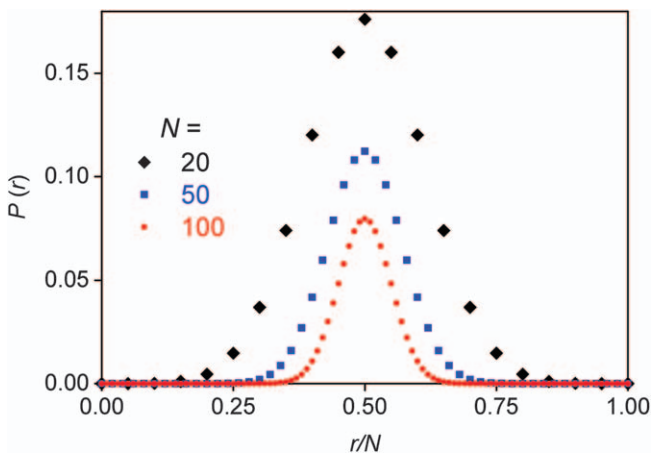

Figure 9.1 Binomial distribution of enantiomers for $N = 20$, 50, and 100 chiral molecules.

decreasing as the overall number of molecules (N) increases. In fact, the probability of the occurrence of any state decreases as N increases simply because the number of states increases, and the sum of the probabilities of all states must be 1 in every case. It can be estimated that with a chemically meaningful amount of substance such as $N = 10^{20}$, the probability of obtaining an 'exact racemate', where the number of the molecules for the two enantiomers is strictly equal, is vanishingly low $\left(\cong 1/\sqrt{N\pi} = 5.6 \times 10^{-11}\right)$. Fourth, the distribution shown in Figure 9.1 becomes narrower as N increases. This means that the expected relative deviations from the 'exact racemate' gradually decrease in magnitude despite the fact that the probability of the occurrence of the 'exact racemate' also decreases. This is in agreement with the well-known property of the binomial distribution that its relative standard deviation scales with the inverse of the square root of N.

Figure 9.1 also illustrates a very important point: using probabilities directly in comparing experimental data and theoretical predictions is not advantageous because of the very low probabilities of individual states. Instead, it is much more favorable to use the cumulative probability distributions. In the distributions of enantiomers, this cumulative distribution function (F) is very simply calculated by adding the probabilities of all states in which the value of r is lower than a pre-set limit:

$$F(r) = \sum_{i=1}^{r} P(i) \tag{9.2}$$

With this definition, $F(r)$ still has a clear meaning: it shows the probability of obtaining not more than r molecules of R in a mixture. The scale of these cumulative probabilities is always between 0 and 1 as illustrated by Figure 9.2, where the $F(r)$ functions are shown for the cases for which simply the probabilities were graphed in Figure 9.1. It is also straightforward to extend the cumulative distribution function to continuous random variables, where the probabilities shown in Figure 9.1 would have to be replaced by probability densities and would be a reason for further concern.

It is important to conclude at this point that although the experimental data on absolute asymmetric synthesis are typically displayed as histograms first,[3,4] which are analogous to probabilities, a direct comparison of histograms to theoretical predictions is heavily distorted by the low number of individual events in a histogram category. Therefore, it is very much advisable to use cumulative distribution functions instead of histograms in such analysis.

Theoretical considerations, thus far unconfirmed by experiments, suggest that the energies of two enantiomeric molecules might be very slightly different because of the well understood asymmetry in weak nuclear forces. This difference is called parity-violating energy difference and is projected to be about 10^{-13} J mol^{-1} for small molecules (*i.e.* 1 attoelectronvolt),[69] a calculation which was also carried out specifically for the product of the Soai

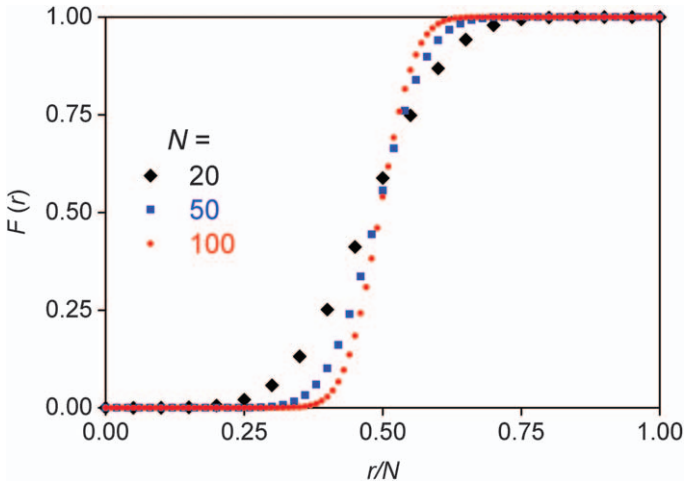

Figure 9.2 Cumulative distribution function of the binomial distribution of enantiomers for $N = 20$, 50, and 100 chiral molecules.

reaction as well.[27] This tiny energy difference may cause a slight asymmetry in the distribution of enantiomers. The consequences of this possible effect were analyzed in two papers.[23,28] The resulting distribution is still a binomial one, but this time it is asymmetric. This can be described by introducing a parameter ε, which can be simply calculated from the parity-violating energy difference,[28] and is equivalent to half of the difference of the probabilities at which the two different enantiomers form under completely non-chiral conditions. Here, R will be selected to be the more stable enantiomer for demonstration purposes. The distribution is given with the following formula:

$$P(r) = \binom{N}{r}(0.5+\varepsilon)^r(0.5-\varepsilon)^{N-r} \tag{9.3}$$

It should be emphasized again that ε is a really small number, it is about 10^{-17} if the 10^{-13} J mol^{-1} estimate for the parity-violating energy difference holds.[28] This slight possible asymmetry was proposed as a potential reason for the accumulation of a preferred isomer in schemes showing chiral amplification and eventually as a possible reason for biological homochirality. In detailed analysis,[23,28] however, this scenario was shown to be very unlikely. A descriptor $R(N)$ was defined for the binomial distribution that shows the excess probability of obtaining a higher number of molecules for the more stable enantiomer. The mathematical definition is as follows:

$$R(N) = \sum_{i=0}^{[N/2]} (P(N-i) - P(i)) \tag{9.4}$$

The notation [...] means the integer part of a number here (the highest integer not higher than the number itself). For the asymmetric binomial distribution, the following formula was derived to approximate the values of $R(N)$ as a function of N and parameter ε:

$$R(N) \cong 4\varepsilon\sqrt{\frac{N}{2\pi}} \tag{9.5}$$

This formula and the analysis of its role in possible amplification scenarios show that for the parity-violating energy difference to have a substantial role in a process, the amount of substance involved would have to exceed the mass of planet Earth.[28]

As already mentioned, the phenomenon of absolute asymmetric synthesis was experimentally observed in the Soai reaction.[2–4] In two cases,[3,4] sufficiently detailed enantiomeric distributions were published and they were analyzed in detail in later works.[18,21–23,28–30,33,36–38,40,43,44,46] It should be added that other, perhaps somewhat less spectacular experimental examples were also published in different reactions,[13,70–73] but the analysis in this chapter will focus on the results obtained by the Soai group in the mentioned two examples.[3,4] The two distributions are shown in Figure 9.3.

The two distributions in Figure 9.3 are labeled as '37 points'[3] and '84 points',[4] which indicates the number of repetitions of identical experiments that were carried out to define them. It must be emphasized that extreme care was taken to ensure that the reactions in a single series were run under the same conditions.[3,4] A surprising feature of the comparison of the two distributions is that they look very similar despite the fact that the

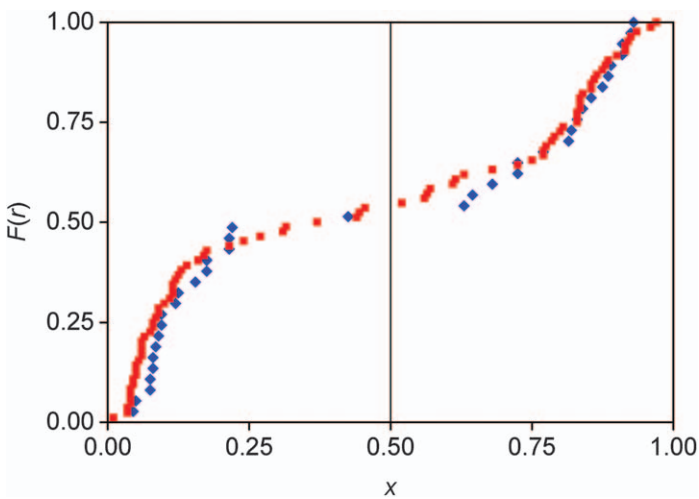

Figure 9.3 Experimentally measured and distributions in the Soai reaction and a comparison with a binomial distribution. Experimental data were published in the papers of Soai *et al.*[3,4]

experimental conditions were quite different in the two series.[3,4] Indeed, statistical analysis showed that the differences between the two distributions are not significant at all.[36,37] Figure 9.3 also displays the binomial distribution relevant for the number of product molecules formed under the experimental conditions. The measured data obviously do not fit to this binomial distribution. First, this fact clearly proves that the direct racemization of the product tertiary alcohol cannot take place in the time frame of the experiments, as this alone would result in a binomial distribution of enantiomers independently of other chemical reactions in the system. Second, it is also clear that the enantioselective autocatalysis confirmed in the system[1] has a major role in governing the final outcome. In the beginning of this chapter, it was emphasized that one of the conditions of observing the binomial distribution is the independence of product formation events from one another. In a statistical sense, enantioselective autocatalysis introduces strong correlation between reaction events, which are not independent any more. In an oversimplified explanation of absolute asymmetric synthesis, one can consider the formation of the very first chiral molecule in a slow direct (*i.e.* not autocatalytic) reaction as the product is not present yet. This first molecule must be one of the two possible enantiomers, and there is no middle ground between the two cases on a molecular level. Whichever enantiomer forms as the first molecule, its strong enantiomeric catalysis provides a powerful, positive feedback for its own further formation and results in an overwhelming excess of that enantiomer in the final mixture. So in an extreme case, the process may continue to produce a single enantiomer only. Of course, this explanation is somewhat exaggerated: in reality, the final result is a high enantiomeric excess. It can be safely concluded that the reasons for observing absolute asymmetric synthesis and the stochastic fluctuations in the enantiomeric distribution of the product lie in chemical kinetics, so with the common wording of organic chemistry, the synthesis process is under kinetic control.

9.4 Minimal Models of the Soai Reaction

The first step of building a successful model of a previously unknown phenomenon is usually to look for the minimum requirements under which the essence of the finding is already shown by theoretical considerations. In this particular case, this strategy means that finding a mechanism that already shows the large stochastic fluctuations in the enantiomeric excess of the product is a step forward even if the mechanism certainly cannot be valid for the Soai reaction itself. Also, the model should be minimal to be useful for this purpose, which means that it should not contain more reaction steps than necessary. This is reflected in the first efforts that were published based on CDS kinetics[15,18] to interpret the enantiomeric distribution observed in the Soai reaction.[3]

If an autocatalytic process is started without the product being present, then there is always a need for a reaction that produces the autocatalytic

product without autocatalysis (direct or uncatalyzed reaction).[74] The autocatalytic reaction must be a separate one. So this simple consideration shows that at least two distinct reactions are needed in a minimal model. As the reaction produces enantiomers of a chiral material, symmetry requirements double the number of reactions, but not the number of rate constants. The simplest kinetic assumption is that a reaction is first order with respect to each of its reagents. The considerations already presented define the chemical scheme shown in Table 9.1, where A denotes the non-chiral starting material, whereas *R* and *S*, as previously stated, stand for the enantiomers of the product. It should be noted that the order of reaction ξ is included in the autocatalytic rate equation for some generality: $\xi = 1$ holds in the simplest model.

Table 9.1 shows the four reactions (two pairs of symmetry-related processes) and the deterministic rate equations, which are more familiar for chemical experts than the stochastic formalism. A general property of the CDS model is that the master equation can be unambiguously stated if the deterministic rate equations are known.[65] The first stochastic publication on the Soai reaction[15] devised a method that was able to give the final enantiomeric distribution predicted by the model without approximations and also without the need for giving the time dependence of state probabilities as it only depends on the ratio of the two rate constants k_u and k_c. The discrete distribution is given as follows:

$$P(r) = \binom{N}{r} \frac{\prod_{j=0}^{r-1} (0.5 + \alpha j) \prod_{j=0}^{N-r-1} (0.5 + \alpha j)}{\prod_{j=0}^{N-1} (1 + \alpha j)} \tag{9.6}$$

Here the new parameter α is defined as the dimensionless ratio of the uncatalytic and catalytic rate constants k_u and k_c (N_A is the Avogadro constant, *V* is the volume of the reactor):

$$\alpha = \frac{k_c}{k_u N_A V} \tag{9.7}$$

Interestingly, a very close continuous approximation has also been found for the distribution shown in eqn (9.6). If the value of *N* exceeds 100 (in most

Table 9.1 The minimal chemical mechanisms for interpreting absolute asymmetric synthesis.

Reaction step	Deterministic rate equation
$A \rightarrow R$	$k_u[A]$
$A \rightarrow S$	$k_u[A]$
$A + \xi R \rightarrow (\xi + 1)R$	$k_c[A][R]^{\xi}$
$A + \xi S \rightarrow (\xi + 1)S$	$k_c[A][S]^{\xi}$

chemical systems, 100 molecules are not even detectable), the following formula can be used instead of eqn (9.6) without any practical loss of accuracy:

$$P(r/N) = \frac{\Gamma(1/\alpha)}{\Gamma(0.5/\alpha)\Gamma(0.5/\alpha)} \left(\frac{r}{N}\right)^{\frac{0.5}{\alpha}-1} \left(1-\frac{r}{N}\right)^{\frac{0.5}{\alpha}-1} \tag{9.8}$$

The notation Γ here refers to the gamma function, which is basically the factorial function (*e.g.* $N!$), originally defined only on integers, extended to the kingdom of real numbers. It should be pointed out that the ratio r/N appears in this formula. This quantity is termed the molar fraction of enantiomer *R* and was already used in Figures 9.1–9.3 as the independent variable on the *x*-axis. It is very interesting to note that N does not appear in any other place in the formula of eqn (9.8). This fact implies that the predicted distribution, if considered in terms of the molar fraction rather than the absolute molecule number r, is independent of the amount of product molecules formed so eventually it is independent of the amount of substance of the reactant. In effect, it is the value of the dimensionless parameter α that solely determines the shape of the distribution. In addition, the distribution shown in eqn (9.8) is not unknown in other fields of mathematics, it is referred to as the symmetric beta distribution.[75] Its cumulative distribution function is also known in the form of a function called the regularized incomplete beta function.[75] For the simple model with $\xi = 1$, a full symbolic solution was also derived using the technique of Laplace transformation and published later.[76] This work also addressed the case when some of the chiral molecules are present in the initial mixture as well.[76]

Occasionally, cases are encountered in the literature of autocatalytic reactions when the order of the reaction with respect to the autocatalyst is higher than 1, a phenomenon sometimes termed supercatalysis.[77] There are many examples when supercatalysis results in effects qualitatively different from those observed under linear autocatalysis. The same was confirmed[18] for the models shown in Table 9.1: whenever $\xi > 1$ (it does not need to be an integer), the independence of the distribution of N is no longer true.[18] In this case, given a sufficiently high value of N, the final state is always one where one of the two enantiomers totally dominates in the final mixture ($r/N = 0$ or $r/N = 1$). In addition to proving this in a mathematical sense, further analysis of the model was also carried out for $\xi = 2$ (second-order autocatalysis). Unlike in the case of first-order autocatalysis, the actual experimental value of N (3×10^{20}) had to be considered in these calculations, for which a new algorithm was developed.[18]

The cases of $\xi = 1$ and $\xi = 2$ were also used to generate predicted distributions that fit the experimental observations of the Soai reaction[3,4] best. In both cases, only the value of a single parameter, the ratio of the uncatalytic and catalytic rate constants k_u and k_c was optimized. The best fits are shown in Figure 9.4.

Looking at Figure 9.4 reveals that the two theoretical predictions are indeed quite close to the experimentally measured results. The best fit to the second-

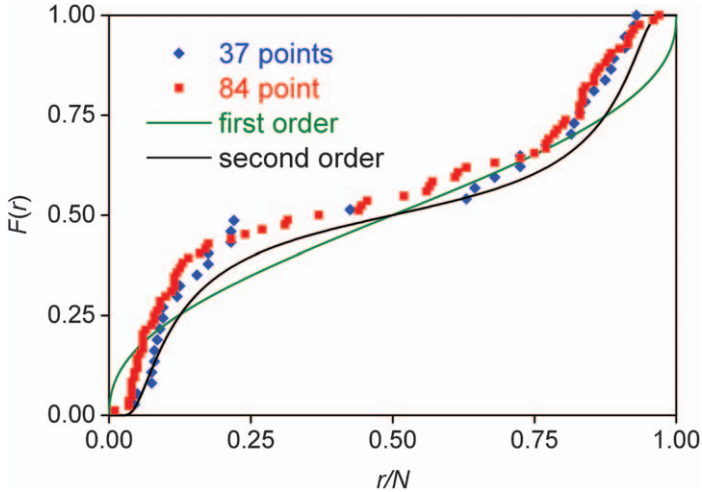

Figure 9.4 Experimentally measured distributions in the Soai reaction and a comparison with the predictions of the minimal models in Table 9.1. Experimental data were published in the papers of Soai *et al.*[3,4] Theoretical distributions were derived by Lente.[15,18]

order autocatalytic curve seems slightly better by the naked eye, this is also confirmed by statistical testing,[18] which proved that this is a significantly better fit than the first-order case. It should be emphasized again that whilst the first-order case can be simply described by a closed formula (eqn (9.8)), calculating the distribution predicted by second-order autocatalysis requires extensive numerical calculations of a highly non-routine nature.

9.5 Mechanism-based Modeling

Once a suitable minimal model of an observed phenomenon is found in chemical kinetics, it can be improved further by refining it, considering the chemical details of the process.[74,78–80] This was reported by the CDS approach in two separate publications.[38,40] Fortunately, T. Buhse already published a reasonable, fully chemical mechanism of the Soai reaction in 2003,[14] which accommodated many of the non-kinetic chemical observations made in the system. In later works, this model was also used in a study about oscillatory symmetry breaking in the Soai reaction.[31] This mechanism is shown in Table 9.2.

Although Table 9.2 shows 18 individual reactions, these only mean four different processes, two of which are reversible. The seemingly high number of individual steps comes from the symmetry requirements of stereochemistry. The chemical essence of the model is summarized as follows: after the initial formation of the chiral zinc alcoholate (*R* and *S*) from the reactants pyrimidinyl carbaldehyde (A) and alkyl zinc (Z), some intervention of dimeric (B) and trimeric (C) species occurs. The trimeric species

Table 9.2 The chemical mechanisms proposed for the Soai reaction by T. Buhse.[13]

Reaction step	Deterministic rate equation
$A + Z \rightarrow R$	$k_1[A][Z]$
$A + Z \rightarrow S$	$k_1[A][Z]$
$2R \rightarrow B_{RR}$	$k_2[R]^2$
$B_{RR} \rightarrow 2R$	$k_{-2}[B_{RR}]$
$2S \rightarrow B_{SS}$	$k_2[S]^2$
$B_{SS} \rightarrow 2S$	$k_{-2}[B_{SS}]$
$R + S \rightarrow B_{RS}$	$k'_2[S][R]$
$B_{RS} \rightarrow R + S$	$k_{-2}[B_{SR}]$
$B_{RR} + A \rightarrow C_{RR}$	$k_3[A][B_{RR}]$
$C_{RR} \rightarrow B_{RR} + A$	$k_{-3}[C_{RR}]$
$B_{SS} + A \rightarrow C_{SS}$	$k_3[A][B_{SS}]$
$C_{SS} \rightarrow B_{SS} + A$	$k_{-3}[C_{SS}]$
$B_{RS} + A \rightarrow C_{RS}$	$k_3[A][B_{RS}]$
$C_{RS} \rightarrow B_{RS} + A$	$k_{-3}[C_{RS}]$
$C_{RR} + Z \rightarrow B_{RR} + R$	$k_4[C_{RR}][Z]$
$C_{SS} + Z \rightarrow B_{SS} + S$	$k_4[C_{SS}][Z]$
$C_{RS} + Z \rightarrow B_{RR} + R$	$k_4[C_{RS}][Z]$
$C_{RS} + Z \rightarrow B_{RR} + S$	$k_4[C_{RS}][Z]$

subsequently opens an enantioselective, catalytic pathway for the original reaction of A and Z.

From the CDS kinetics point of view, the mechanism shown in Table 9.2 already constitutes a highly complicated system. For example, the number of different individual states is about 10^{160} in it, which is an extremely large number (*e.g.* the estimated number of elementary particles in the entire known universe is about 10^{80}). Modeling efforts to obtain a predicted distribution had to rely on the extensive use of creative mathematics. First, the technique of deterministic continuation was developed. This means that stochastic calculations based on the master equation were only carried out until the number of product molecules formed reached a pre-set limit (10 000). After this limit, the numerical handling of the deterministic approach was used.[74] This is possible because at tens of thousands of molecules present, the continuous approximation of concentrations is already acceptable in a sense that its use does not cause higher errors than typically inherent in experimental observations. A second trick was the use of Monte Carlo simulations in the form of the Gillespie algorithm for the CDS calculations.[65,81–83] With this method, individual simulation runs are carried out instead of directly solving the master equation of the process, and the distributions are estimated by comparing the results of repetitive runs. Third and probably most important, an equivalent of the rapid pre-equilibrium approach was developed in CDS kinetics, and the two reversible processes were handled stochastically as rapid pre-equilibria.[38]

Finally, the technique of symmetrization was also employed: as the chirally symmetric chemical reactions in the model require a symmetric distribution (a fact also proved by mathematical precision[38]), this property was forced onto the simulation results by interpreting the result of each simulation as one side of a symmetric pair.

The combination of these special mathematical techniques facilitated the computation of a theoretical prediction for the final distribution of the enantiomers in the process. Some parameters were partially optimized compared to the original model[14] to find reasonable agreement between the predicted and observed distributions.[38] This comparison is shown in Figure 9.5.

When analyzing Figure 9.5, it should be kept in mind that it does not show the best fit as the relatively high number of parameters made it unfeasible to find a global minimum for the sum squares in the analysis. The curve merely illustrates that very good agreement with the experiments can be reached using this model and a reasonable parameter set. In addition, Figure 9.5 also shows the best fit for the simple, second-order autocatalytic model. A striking characteristic is that this best fit is very close to the mechanism-based prediction for the distribution, which serves as clear evidence that the essence of the phenomenon is already quite nicely captured in the simpler model as well. Extensive analysis was reported in a later work[46] to show that a series of quasi-stationary (steady sate) assumptions for various minor species in the system can be employed to reduce the model into one whose non-elementary rate equation in fact shows second-order autocatalysis very similarly to the one assumed in the simple model with $\xi = 2$. In effect, some

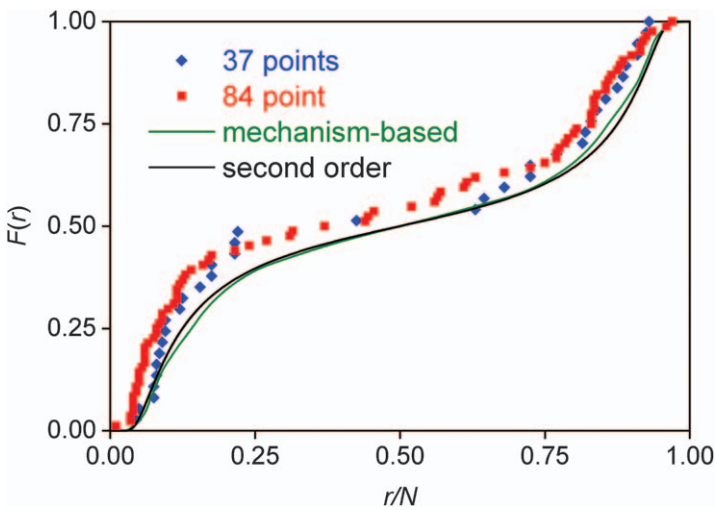

Figure 9.5 Experimentally measured and distributions in the Soai reaction and a comparison with the predictions of one minimal model and the mechanism-based model. Experimental data were published in the papers of Soai *et al.*[3,4] Theoretical distributions were derived by Lente[18,40] and Dóka and Lente.[38]

form of kinetic equivalence was established between the detailed and the minimal model that was valid for the final distribution for enantiomers. This phenomenon of a kinetic equivalence, which typically means that multiple different mechanisms lead to identical rate equations, was well understood in a number of earlier cases,[74,78] but it was most probably this model of the Soai reaction where it was first deduced for enantioselective autocatalysis.[46]

9.6 Distribution Asymmetry

Some additional analysis of the two reported distributions[3,4] was also carried out without using any kinetic models.[18,25] These tests established the fact that there is no significant asymmetry in the 37-point distribution,[3] in agreement with what has already been stated when the technique of symmetrization was introduced. Of course, this symmetry is clearly expected based on the fact that the models are symmetric with respect to the chemical species. However, the same statistical tests showed that there is a slight, but already significant asymmetry in the 84-point distribution.[25,37] This was extremely strange at first, because similar statistical tests also showed that the 37-point and 84-point distributions were not significantly different: how can one then be symmetric and the other asymmetric? The key to resolving this virtual contradiction is the different number of points in the two distributions. If the same relative deviation from symmetry is seen in the two data sets, it remains not significant because of the lower number of experimental points in the first case. It was already mentioned in the present chapter that the parity-violating energy difference[27] was ruled out as a possible source of such asymmetry.[23,28] Therefore, a suitable explanation was sought in a modeling study[37] that was primarily based on the mathematical techniques developed for the earlier attempts.

The basic idea in this modeling effort was that the slight asymmetry is caused by some sort of uncontrolled external chiral influence on the reaction system. Since there are a high number of possibilities in reality, the influence of such external effects was semi-quantized as a few molecules of the product added before the onset of the reaction. Because of the high sensitivity of the system through enantioselective autocatalysis, this results in a distortion of the symmetry of the distribution. It was also assumed that the introduction of these product molecules into the initial system is stochastic in nature, and several different distributions were tested in the calculations. The probability that the initial number of R enantiomers was exactly r is given by a function $T(r)$. The first tested possibility was the geometric distribution:

$$T(r) = p(1-p)^r \tag{9.9}$$

The second distribution that was investigated was the Poisson distribution:

$$T(r) = \frac{p^r}{r!}\mathrm{e}^{-p} \tag{9.10}$$

Parameter p here is the characteristic single parameter of the two distributions. The same symbol is used for simplicity in the two cases, but their meaning is actually different.

As the mechanism-based model of the Soai reaction was shown to be kinetically equivalent to the case of second-order autocatalysis, only the minimal models were used as rate equations in the analysis. Similarly to the previous work, both $\xi = 1$ and $\xi = 2$ were considered.[37] So altogether, four different models were set up and their parameters optimized. These are the first-order geometric, first-order Poisson, second-order geometric, and second-order Poisson models. The best fits are shown in Figure 9.6. To obtain these fits, two parameters were optimized: the value of distribution parameter p, and the dimensionless ratio of the uncatalytic and catalytic rate constants k_u and k_c.

A close look at Figure 9.6 reveals that the best fit is again given by second-order autocatalysis, but it does not matter much whether the initial amount of the product follows geometric or Poisson distribution. The best fitting value of p was 21 ± 1 for the Poisson, and 0.044 ± 0.003 for the geometric distribution.[37] From these parameters, the expectation for the initial number of product molecules can be calculated. For the Poisson distribution, this is exactly the value of $p = 21$, whereas $p^{-1} - 1 = 22$ for the geometric distribution.[37] So the calculations show that a very small amount, roughly two dozen molecules of the product present initially on average can give rise to the slight but significant asymmetry of the distribution. In the original

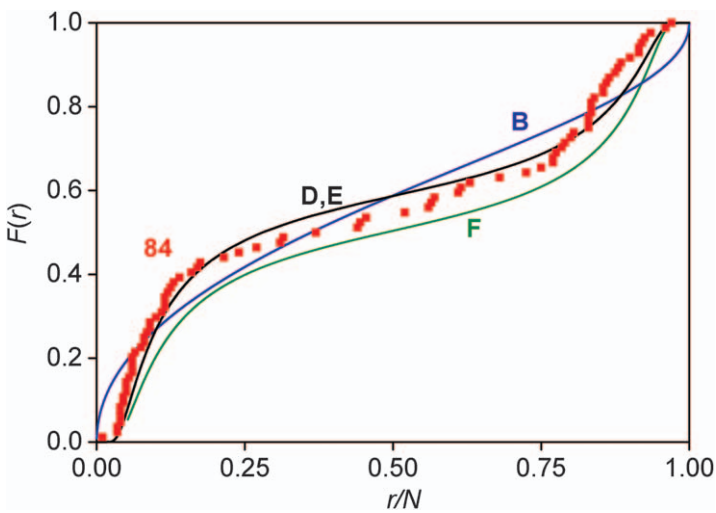

Figure 9.6 Experimentally measured asymmetric distribution in the Soai reaction and a comparison with predictions of minimal models. Experimental data were published in the papers of Soai *et al.*[4] Theoretical distributions were derived by Lente.[37] Notations used: B: first order geometric model, D, E: second order Poisson and geometric models, F: second order symmetric model.

publication,[37] a histogram-based comparison was also presented, but it also showed that this method is greatly inferior to the one based on comparing cumulative distribution functions.

9.7 Conclusion

The most important message of this chapter is that kinetic tools already exist for interpreting stochastic experimental observations in chemistry. As the training of chemists emphasizes the concept of reproducibility very much, this is less obvious in this field of science than in physics or biology. In contrast with deterministic kinetics, which is based on continuous concentration–time functions, the continuous time discrete state (CDS) stochastic approach considers the particulate nature of matter. The mathematical background of CDS has already been developed in sufficient detail to solve complex problems. The successful quantitative interpretation of the experimentally measured enantiomeric distributions in the Soai reaction provides an example that the resourceful use of mathematical tools can give spectacular results even if the system seems highly complex at first. Evidence shows that the theoretically predicted parity-violation energy difference between the two enantiomers of the same chiral molecule cannot have significant consequences in processes occurring on the surface of the Earth. A final and highly important point is that whenever stochastic phenomena measured experimentally are compared to theoretical predictions, the use of the cumulative distribution functions must be preferred to histograms and probability density functions despite the fact the latter techniques are easier to visualize and imagine.

Acknowledgements

This work was supported by the Higher Education Institutional Excellence Programme of the Ministry of Human Capacities in Hungary, within the framework of the 1st thematic programme of the University of Pécs. The National Research, Development, and Innovation Office of Hungary also supported this work under grant No. SNN 125739.

References

1. K. Soai, T. Shibata, H. Morioka and K. Choji, *Nature*, 1995, **378**, 767.
2. K. Soai, T. Shibata and Y. Kowata, *Japan Kokai Tokkyo Koho, JP Pat.*, 9-268179, 1997. Application date: February 1 and April 18, 1996 (in Japanese).
3. K. Soai, I. Sato, T. Shibata, S. Komiya, M. Hayashi, Y. Matsueda, H. Imamura, T. Hayase, H. Morioka, H. Tabira, J. Yamamoto and Y. Kowata, *Tetrahedron: Asymmetry*, 2003, **14**, 185.
4. T. Kawasaki, K. Suzuki, M. Shimizu, K. Ishikawa and K. Soai, *Chirality*, 2006, **18**, 479.

5. T. Kawasaki, M. Shimizu, D. Nashiyama, M. Ito, H. Ozawa and K. Soai, *Chem. Commun.*, 2009, 4396.
6. T. Kawasaki, Y. Matsamura, T. Tsutsumi, K. Suzuki, M. Ito and K. Soai, *Science*, 2009, **324**, 492.
7. K. Soai and T. Kawasaki, *Chim. Oggi*, 2009, **27**, 3.
8. K. Soai, T. Kawasaki and A. Matsumoto, *Tetrahedron: Asymmetry*, 2018, **74**, 1973.
9. Y. Kaimori, Y. Hiyoshi, T. Kawasaki, A. Matsumoto and K. Soai, *Chem. Commun.*, 2019, **55**, 5223.
10. K. Soai, *Proc. Jpn. Acad., Ser. B*, 2019, **95**, 89.
11. K. Soai, T. Kawasaki and A. Matsumoto, *Symmetry*, 2019, **11**, 694.
12. O. Fülöp and B. Barabás, *J. Math. Chem.*, 2016, **54**, 10.
13. I. D. Gridnev, J. M. Serafimov, H. Quiney and J. M. Brown, *Org. Biomol. Chem.*, 2003, **1**, 3811.
14. T. Buhse, *Tetrahedron: Asymmetry*, 2003, **14**, 1055.
15. G. Lente, *J. Phys. Chem. A*, 2004, **108**, 9475.
16. J. Rivera Islas, D. Lavabre, J. M. Grevy, R. Hernández Lamoneda, H. Rojas Cabrera, J. C. Micheau and T. Buhse, *Proc. Natl. Acad. Sci. U. S. A.*, 2005, **102**, 13743.
17. L. Caglioti, C. Zucchi and G. Pályi, *Chim. Oggi*, 2005, **23**, 38.
18. G. Lente, *J. Phys. Chem. A*, 2005, **109**, 11058.
19. I. D. Gridnev, *Chem. Lett.*, 2006, **35**, 148.
20. D. Hochberg and M. P. Zorzano, *Chem. Phys. Lett.*, 2006, **431**, 185.
21. K. Micskei, G. Póta, L. Caglioti and G. Pályi, *J. Phys. Chem. A*, 2006, **110**, 5982.
22. L. Caglioti, C. Hajdu, O. Holczknecht, L. Zékány, C. Zucchi, K. Micskei and G. Pályi, *Viva Origino*, 2006, **34**, 62.
23. G. Lente, *J. Phys. Chem. A*, 2006, **110**, 12711.
24. Y. Saito, T. Sugimori and H. Hyuga, *J. Phys. Soc. Jpn.*, 2007, **76**, 044802.
25. B. Barabás, L. Caglioti, C. Zucchi, M. Maioli, E. Gál, K. Micskei and G. Pályi, *J. Phys. Chem. B*, 2007, **111**, 11506.
26. D. Lavabre, J. C. Micheau, J. Rivera Islas and T. Buhse, *J. Phys. Chem. A*, 2007, **111**, 281.
27. F. Faglioni, P. Lazzeretti and G. Pályi, *Chem. Phys. Lett.*, 2007, **435**, 346.
28. G. Lente, *Phys. Chem. Chem. Phys.*, 2007, **9**, 6134.
29. B. Barabás, L. Caglioti, K. Micskei, C. Zucchi and G. Pályi, *Orig. Life Evol. Biospheres*, 2008, **38**, 317.
30. B. Barabás, L. Caglioti, F. Faglioni, N. Florini, P. Lazzaretti, M. Maioli, K. Micskei, G. Rábai, F. Taddei, C. Zucchi and G. Pályi, *AIP Conf. Proc.*, 2008, **963B**, 1150.
31. K. Micskei, G. Rábai, E. Gál, L. Caglioti and G. Pályi, *J. Phys. Chem. B*, 2008, **112**, 9196.
32. T. Sugimori, H. Hyuga and Y. Saito, *J. Phys. Soc. Jpn.*, 2008, **77**, 064606.
33. L. Caglioti, B. Barabás, F. Faglioni, N. Florini, P. Lazzeretti, M. Maioli, K. Micskei, G. Rábai, F. Taddei, C. Zucchi and G. Pályi, *Chim. Oggi*, 2008, **26**, 30.

34. J. M. Cruz, P. Parmananda and T. Buhse, *J. Phys. Chem. A*, 2008, **112**, 1673.
35. D. Hochberg, *Phys. Rev. Lett.*, 2009, **102**, 248101.
36. B. Barabás, L. Caglioti, K. Micskei and G. Pályi, *Bull. Chem. Soc. Jpn.*, 2009, **82**, 1372.
37. G. Lente, *Tetrahedron: Asymmetry*, 2011, **22**, 1595.
38. É. Dóka and G. Lente, *J. Am. Chem. Soc.*, 2011, **133**, 17878.
39. J. C. Micheau, C. Coudret, J. M. Cruz and T. Buhse, *Chem. Chem. Phys.*, 2012, **14**, 13239.
40. G. Lente, in *The Soai reaction and related topic*, ed. G. Pályi, C. Zucchi and L. Caglioti, Artestampa - Accademia Nazionale di Scienze, Lettere ed Arti, Modena, 2012, pp. 123–147.
41. Y. Saito and H. Hyuga, *Rev. Mod. Phys.*, 2013, **85**, 603.
42. J. M. Ribó, C. Blanco, J. Crusats, Z. El-Hachemi, D. Hochberg and A. Moyano, *Chem. – Eur. J.*, 2014, **20**, 17250.
43. B. Barabás, C. Zucchi, M. Maioli, K. Micskei and G. Pályi, *J. Mol. Model.*, 2015, **21**, 33.
44. B. Barabás, R. Kurdi and G. Pályi, *Symmetry*, 2016, **8**, 2.
45. L. Silva-Dias and A. López-Castillo, *Phys. Chem. Chem. Phys.*, 2017, **19**, 29424.
46. G. Lente, in *Advances in Asymmetric Autocatalysis and Related Topics*, ed. G. Pályi, R. Kurdi and C. Zucchi, Academic Press, London, 2017, pp. 167–181.
47. N. A. Hawbaker and D. G. Blackmond, *ACS Cent. Sci.*, 2018, **4**, 6776.
48. V. A. Pavlov and S. G. Zlotin, *Curr. Org. Chem.*, 2018, **22**, 2029.
49. A. J. Gellman and K. H. Ernst, *Catal. Lett.*, 2018, **148**, 1610.
50. K. P. Bryliakov, *ACS Catal.*, 2019, **9**, 5418.
51. T. Sawato, N. Saito and M. Yamaguchi, *Phys. Chem. Chem. Phys.*, 2019, **21**, 25406.
52. T. Sawato, N. Saito and M. Yamaguchi, *ACS Omega*, 2019, **4**, 5879.
53. S. V. Athavale, A. Simon, K. N. Houk and S. E. Denmark, *J. Am. Chem. Soc.*, 2020, **142**, 18387.
54. J. M. Ribó, *Symmetry*, 2020, **12**, 1982.
55. K. P. Bryliakov, *Research*, 2020, 5689246.
56. C. Tschierske and C. Dressel, *Symmetry*, 2020, **12**, 1098.
57. D. Kondepudi and Z. Mundy, *Symmetry*, 2020, **12**, 769.
58. J. M. Ribó and D. Hochberg, *Phys. Chem. Chem. Phys.*, 2020, **22**, 14013.
59. T. Buhse, J. M. Cruz, M. E. Noble-Terán, D. Hochberg, J. M. Ribó, J. Crusats and J. C. Micheau, *Chem. Rev.*, 2021, **121**, 2147.
60. J. Crusats and A. Moyano, *Synlett*, 2021, **32**, 2013.
61. M. Delbrück, *J. Chem. Phys.*, 1940, **8**, 120.
62. P. Érdi and J. Tóth, *React. Kinet. Catal. Lett.*, 1976, **4**, 81.
63. P. Érdi and J. Tóth, *Mathematical Models of Chemical Reactions*, Manchester University Press, Manchester, 1989.
64. F. C Frank, *Biochim. Biophys. Acta*, 1953, **11**, 459.

65. P. Érdi and G. Lente, *Stochastic Chemical Kinetics - Theory and (Mostly) Systems Biological Applications*, Springer, Cham, 2014.
66. J. Tóth, A. L. Nagy and D. Papp, *Reaction Kinetics: Exercises*, *Programs and Theorems. Mathematica for Deterministic and Stochastic Kinetics*, Springer, New York, 2018.
67. W. Mills, *Chem. Ind.*, 1932, **51**, 7509.
68. K. Mislow, *Collect. Czech. Chem. Commun.*, 2003, **68**, 849.
69. M. Quack, *Angew. Chem., Int. Ed.*, 2002, **41**, 4619.
70. D. A. Singleton and L. K. Vo, *J. Am. Chem. Soc.*, 2002, **124**, 10010.
71. D. A. Singleton and L. K. Vo, *Org. Lett.*, 2003, **5**, 4337.
72. M. Mauksch, S. B. Tsogoeva, S. Wei and I. M. Martynova, *Chirality*, 2007, **19**, 816.
73. K. Asakura, A. Ikumo, K. Kurihara, S. Osanai and D. K. Kondepudi, *J. Phys. Chem. A*, 2000, **104**, 2689.
74. G. Lente, *Deterministic Kinetics in Chemistry and Systems Biology, The Dynamics of Complex Reaction Networks*, Springer, Cham, 2015.
75. N. L. Johnson, S. Kotz and N. Balakrishnan, *Continuous Univariate Distributions*, Wiley, New York, 2nd edn, 1995, vol. 2.
76. J. Shao and L. Liu, *J. Phys. Chem. A*, 2007, **111**, 9570.
77. A. K. Horváth, *Chem. Phys. Chem.*, 2020, **21**, 1703.
78. J. H. Espenson, *Chemical Kinetics and Reaction Mechanisms*, McGraw-Hill, New York, 2nd edn, 1995.
79. G. Lente and I. Fábián, *Inorg. Chem.*, 1998, **37**, 4204.
80. G. Lente and J. H. Espenson, *Inorg. Chem.*, 2000, **39**, 4809.
81. T. Sipos, J. Tóth and P. Érdi, *React. Kinet. Catal. Lett.*, 1974, **1**, 113.
82. T. Sipos, J. Tóth and P. Érdi, *React. Kinet. Catal. Lett.*, 1974, **1**, 209.
83. D. T. Gillespie, *J. Comput. Phys.*, 1976, **22**, 403.

CHAPTER 10

Demystifying the Soai Reaction[†]

SOUMITRA V. ATHAVALE AND SCOTT E. DENMARK*

Roger Adams Laboratory, Department of Chemistry, University of Illinois, Urbana, Illinois 61801, USA
*Email: sdenmark@illinois.edu

> The reaction can be likened to a pearl and the mechanism to an oyster. The pearl is prized for its luster and simplicity; the oyster is a complex living beast whose innards give rise to this mysteriously beautiful gem.[1]

10.1 Introduction

10.1.1 Biological Homochirality, Absolute Asymmetric Synthesis, and Asymmetric Autocatalysis

In a quaint 1953 publication, F. C. Frank presented a kinetic model that rationalized spontaneous symmetry breaking and the generation of enantioenriched products in a chemical reaction without any chiral intervention (absolute asymmetric synthesis).[2] Although the idea was motivated by the need to articulate a mechanistic proposal that could account for the origin of biological homochirality, it is generally applicable for the evolution of homochirality in any closed chemical system. This scheme necessitates three conditions: (1) autocatalysis, (2) enantioselective catalysis, and (3) mutual inhibition. The fate of a hypothetical Grignard reaction of benzaldehyde (**1a**), if it were to follow the Frank model, is illustrated in Figure 10.1. In this imaginary autocatalytic version, the product is a catalyst

[†]A full account of the original research described in this chapter can be found in ref. 13, 71 and 72.

Catalysis Series No. 43
Asymmetric Autocatalysis: The Soai Reaction
Edited by Kenso Soai, Tsuneomi Kawasaki and Arimasa Matsumoto

Published by the Royal Society of Chemistry, www.rsc.org

for its own formation. This activity is enantioselective: catalysis by the (*R*)-**2a** product results in exclusive formation of new (*R*)-**2a** whereas catalysis by the (*S*)-**2a** product results exclusively in the formation of new (*S*)-**2a**. Most critically, the final requirement implies that in some manner, the autocatalysts are also mutual inhibitors: the (*R*)-**2a** product inhibits the formation of new (*S*)-**2a** and *vice versa.* Frank demonstrated mathematically that a reaction meeting these boundary conditions is predisposed to yield enantiomerically enriched products over time. After the reaction initiates, a slight, statistical excess of one product enantiomer will be generated. Owing to autocatalysis, this enantiomer population will grow at a faster rate than its counterpart. Furthermore, the production of the minor enantiomer will be inhibited more efficiently than its competitor. The result will be an exponential amplification of the initial excess enantiomer at the expense of the minor enantiomer. The precise extent of enantioenrichment will depend on the relative rates of autocatalysis, mutual inhibition, and autocatalyst selectivity, but in the ideal case, the system will inevitably converge to the generation of a highly enantioenriched product.

In 1989, Hans Wynberg coined the term asymmetric autocatalysis to describe a system that satisfies the first two Frank conditions.[3] Incorporation of mutual inhibition effects would result in asymmetric amplification – formally, *amplifying* asymmetric autocatalysis. Wynberg also proposed exploration of specific reactions that may demonstrate this striking phenomenon, unfortunately with no success. Clearly, the identification or design of a chemical system that proficiently satisfies all three conditions is a formidable challenge. For an authoritative treatment of the historical development of concepts related to absolute asymmetric synthesis, statistical symmetry breaking and asymmetric autocatalysis, especially in relation to the Soai reaction, the reader is directed to Mislow's masterful commentary on the subject.[4]

Seeds for practical realization of this obscure theoretical concept were sown through the development of amino-alcohol catalyzed enantioselective alkylation of aldehydes with dialkylzinc reagents in the 1980s.[5–7] Apart from synthetic utility, these reactions have since assumed special pedagogical importance for their remarkable mechanistic peculiarity. Typically, a strong positive non-linear effect (NLE) is observed, with product enantioenrichment significantly higher than that of the employed catalyst. Figure 10.2 describes such a NLE in the case of dimethylaminoisoborneol (DAIB).[8,9] With diethylzinc, even when the catalyst enantiopurity is 60 : 40 e.r. (enantiomeric ratio), product selectivity in excess of 90 : 10 e.r. is obtained. A detailed discussion of the myriad models proposed to explain NLEs in asymmetric catalysis is beyond the scope of this section and the reader is encouraged to refer to a number of excellent reviews on the subject.[10,11] At this point, it is sufficient to note that the origin of non-linear behavior in an asymmetric catalytic reaction can be traced to differential activity of the various homochiral and heterochiral species resulting from catalyst aggregation. In relation to Frank's proposal, a positive non-linear effect is a general term for

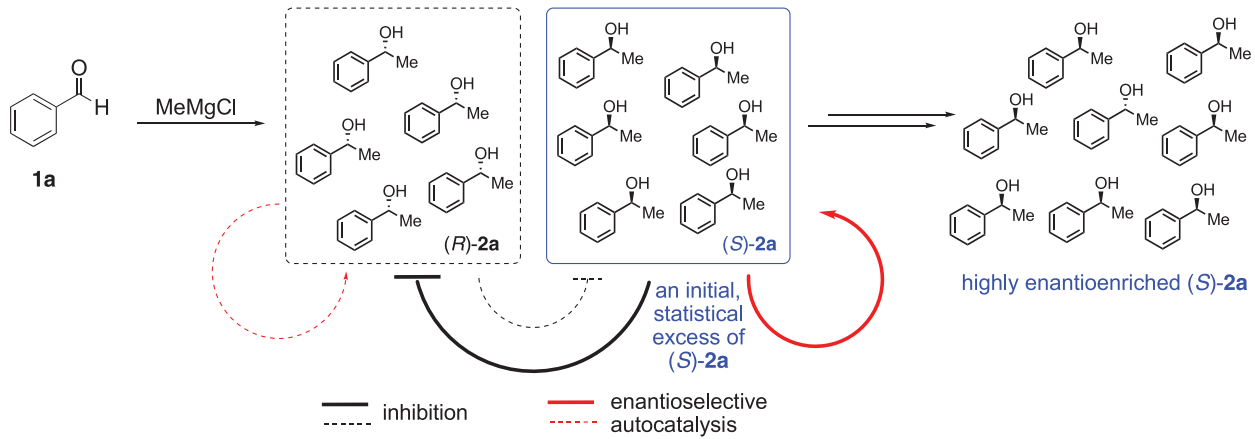

Figure 10.1 A hypothetical version of Grignard alkylation operating under the Frank model will yield enantioenriched products starting from achiral materials.

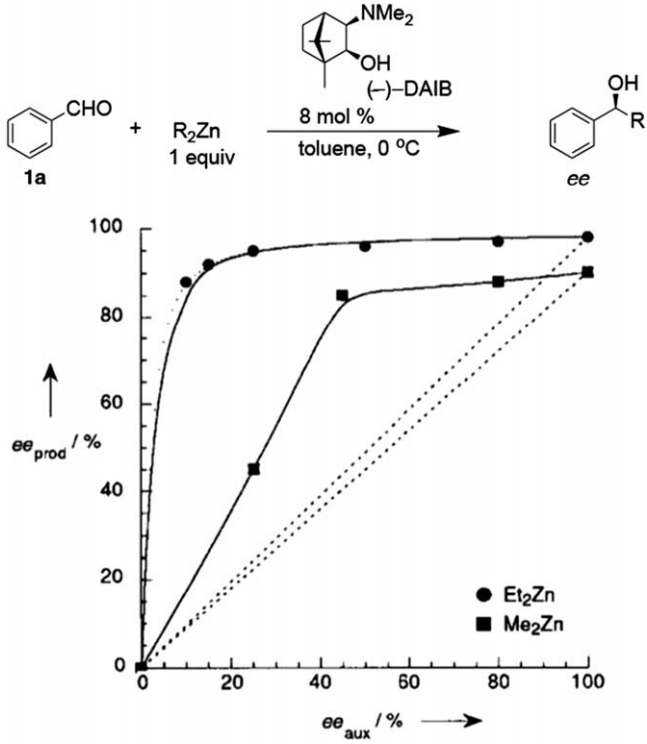

Figure 10.2 Positive NLE in the (−)-DAIB catalyzed dialkylzinc addition to benzaldehyde. Adapted from ref. 10 with permission from John Wiley & Sons, Copyright © 1998 Wiley-VCH Verlag GmbH, Weinheim, Fed. Rep. of Germany.

the phenomenological outcome of asymmetric amplification resulting from some form of mutual inhibition. Dialkylzinc chemistry was thus inherently predisposed to satisfy one critical chemical constraint necessary to achieve amplifying asymmetric autocatalysis.

The provocative idea of F. C. Frank, Wynberg's promotion of the asymmetric autocatalysis formalism, the active developments of non-linear effects in dialkylzinc chemistry, and the overarching romanticism of the origin of biological homochirality and absolute asymmetric synthesis found their combined expression in Soai's groundbreaking discoveries.

10.1.2 The Soai Reaction

In 1995, Soai *et al.* realized the objective of amplifying asymmetric autocatalysis in their seminal report describing the diisopropylzinc alkylation of pyrimidine-5-carbaldehyde (**3a**) (Figure 10.3b). Inclusion of the scalemic product carbinol **4a** at the beginning of the reaction resulted in the newly-formed product being more enantioenriched than the initial additive.[12] Near

racemic autocatalyst with only 51 : 49 e.r. provided a higher enantioenriched product with 55 : 45 e.r. The product from one reaction could be used as a catalyst for a subsequent reaction and it was shown that in successive reaction cycles, the enantioenrichment of **4a** could be increased to up to 94.5 : 5.5 e.r. Note that the actual 'catalyst' and product is the isopropylzinc alkoxide. The carbinol is obtained only after workup and does not exist under the reaction conditions. When the carbinol is included as an additive, it is immediately quenched by diisopropylzinc to give the alkoxide, which is the species of interest. Here and elsewhere, the carbinol is interchangeably referred to as the catalyst only for simplicity. Asymmetric amplification is

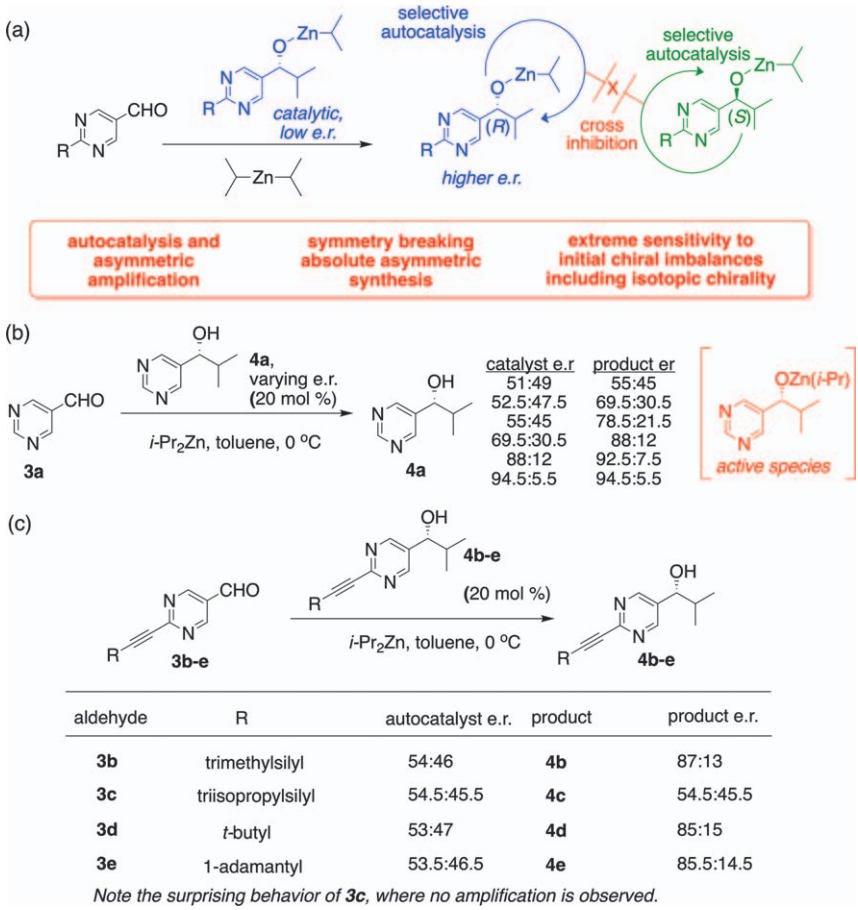

aldehyde	R	autocatalyst e.r.	product	product e.r.
3b	trimethylsilyl	54:46	**4b**	87:13
3c	triisopropylsilyl	54.5:45.5	**4c**	54.5:45.5
3d	*t*-butyl	53:47	**4d**	85:15
3e	1-adamantyl	53.5:46.5	**4e**	85.5:14.5

*Note the surprising behavior of **3c**, where no amplification is observed.*

Figure 10.3 (a) The Soai reaction, with the general scheme of amplifying autocatalysis and salient features. (b) Seminal report with substrate **3a**. (c) Improved performance with alkynyl substituted substrates, except in the case of **3c**. Adapted from ref. 13 with permission from American Chemical Society, Copyright 2020.

seen because the product alkoxide, in some manner, acts as a highly enantioselective catalyst for its own production while concomitantly inhibiting catalysis by its enantiomeric counterpart. Thus, the dominant enantiomer reinforces itself with time, resulting in continuous enantioenrichment with reaction progression, satisfying the Frank scheme (Figure 10.3a). Following this discovery, it was demonstrated that in general, the reaction of diisopropylzinc with 2-substituted pyrimidinyl carbaldehydes displayed autocatalytic, asymmetric amplification.[14–19] In particular, a bulky alkynyl substituent (examples in Figure 10.3c) drastically increased the performance of these reactions in terms of the degree of asymmetric amplification, final enantioenrichment achieved, reaction times, and isolated yields (note however, the surprising contrary behavior of the TIPS substrate **3c**).

In the case of the *tert*-butyl alkynyl substituted aldehyde **3d**, which has become the workhorse substrate for the Soai group, with a nearly racemic autocatalyst (*ca.* 5×10^{-5}% e.e.), enantiopure product in high yield is obtained in three reaction cycles (the product from a previous reaction is used as a catalyst for the subsequent one) (Figure 10.4).[20] This outcome indicates that all three factors in the Frank model – (1) autocatalytic efficiency, (2) catalyst selectivity, and (3) positive non-linear effect, are satisfied with high proficiency in this system. With such a profound capacity for chiral amplification, the system is a supreme candidate for absolute asymmetric synthesis. Soai and Singleton have tested this proposal in landmark experiments.[21–25] It was demonstrated that in the absence of any added catalyst, multiple runs of the reaction inevitably lead to enantioenriched product, that is, the reaction demonstrates spontaneous symmetry breaking. This phenomenon is believed to occur by an autocatalytic amplification of the stochastically generated, statistical excess of one enantiomer produced by uncatalyzed diisopropylzinc alkylation in the initial phases of the reaction. These experiments in principle prove that the Soai reaction is predisposed to evolve toward homochirality and can affect absolute asymmetric synthesis arising from runaway autocatalytic amplification of

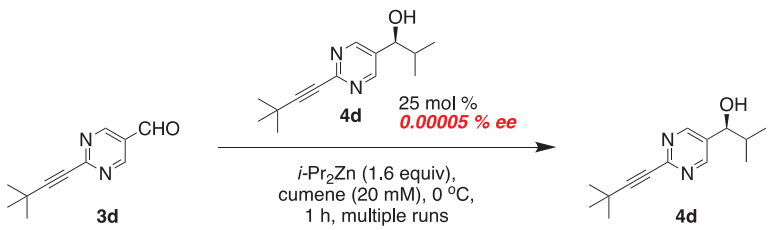

run	product er	product yield (%)
1	78.5:21.5	96
2	99.5:0.5	96
3	>99.9:0.1	90

Spontaneous, stochastic symmetry breaking is seen in the absence of any initially added (auto)catalyst.

Figure 10.4 Highly efficient asymmetric autocatalytic amplification with substrate **3d**.

statistical symmetry breaking – a spectacular experimental demonstration of the Frank model!

A large variety of chiral additives ranging from amino acids,[26] enantiomorphic crystals,[27] helical hydrocarbons,[28] and even cryptochiral molecules[29] can influence the outcome of the reaction by biasing an initial imbalance of one of the enantiomers.[30] Remarkably, even circularly polarized light[31] and isotopic chirality[32–34] have been demonstrated to result in a nonracemic product. One may state that in multiple cycles of the Soai reaction, symmetry breaking and enantioenrichment is inevitable. The Soai reaction hence qualifies as a chemical transformation with a predisposition to evolve toward homochirality. Soai's seminal discoveries have received widespread attention in diverse chemical fields and have revived discussions regarding absolute asymmetric synthesis, symmetry breaking, and the origin of biological homochirality.[35–39] Multiple reviews provide further details, accounts, and descriptions of the remarkable properties of the Soai reaction.[30,40,41]

10.1.3 Mechanistic Challenges and Prior Art

Since its discovery, elucidation of the mechanism of the Soai reaction stood as a monumental challenge. Conceptually, the reaction represents a fortuitous confluence of three themes in catalysis: autocatalysis, enantiospecific catalysis, and non-linear effects. In this respect, it has no parallel among known chemical transformations. Four central issues regarding the reaction mechanism remained enigmatic: (1) an elucidation of the precise identity and modus operandi of the autocatalyst, (2) a transition state structure rationalizing the basis of asymmetric autocatalysis, (3) an explanation for the origin of positive, non-linear (auto)catalysis, and (4) a justification of the puzzling, restrictive, and idiosyncratic substrate requirements that allow successful amplifying autocatalysis.

The remarkable properties of the Soai system have motivated numerous studies to elucidate the mechanism of this iconic transformation.[42–62] In light of Franks's proposal and lessons learnt from non-linear effects in dialkylzinc chemistry, the recognition that product alkoxide aggregation (which in this case amounts to catalyst aggregation) must be a critical factor in the origin of (auto)catalysis as well as non-linearity has driven efforts in identifying the exact nature of this aggregation, which should then lead to insights in catalysis.

Structural proposals resulting from these studies (prior to 2020) are highlighted in Figure 10.5. For the 3-formyl-6-methylpyrimidine-carbaldehyde system, a kinetic comparison of enantiopure and racemic autocatalyst reactions indicate a dimeric alkoxide aggregate as the catalytic species, whereas subsequent investigations with an enantiopure catalyst suggest two aldehyde substrates in a tetrameric complex.[44,47,58] The first structural studies in 2004, employing ^{1}H NMR spectroscopy with the **4b**-derived isopropylzinc alkoxide were consistent with a dimeric model but could not

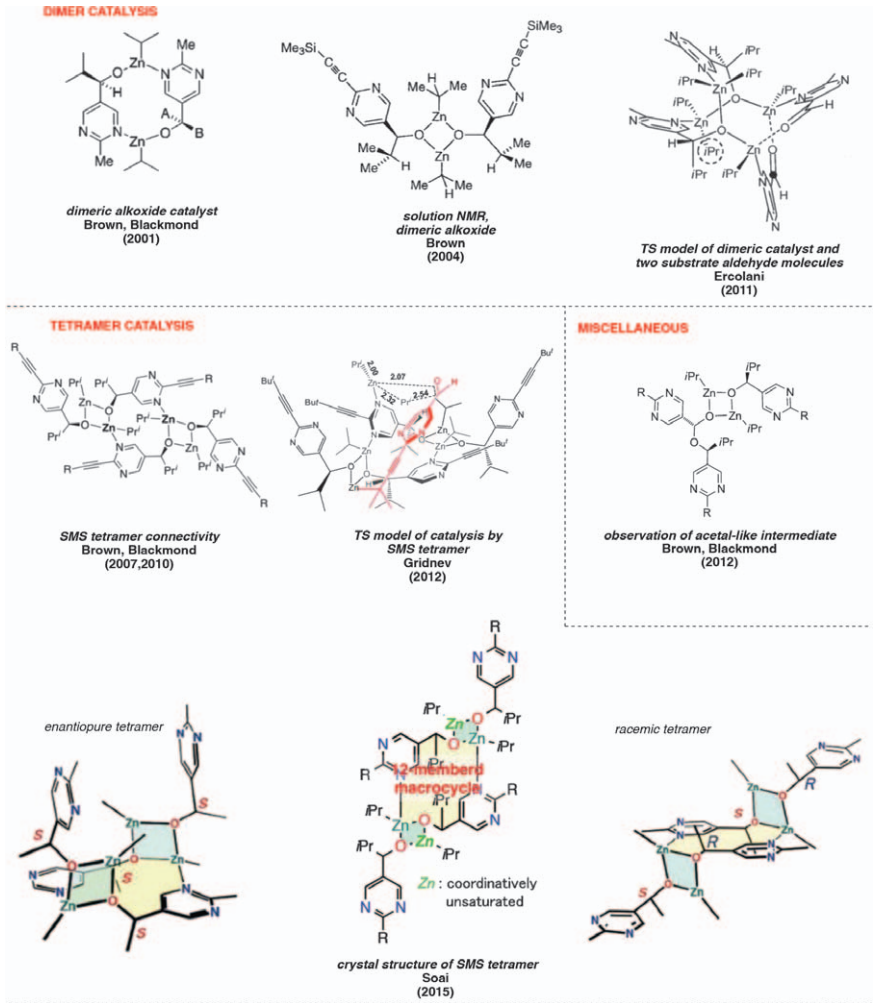

Figure 10.5 Notable structural proposals prior to 2020. Reproduced from ref. 44 and 57–59 with permission from American Chemical Society, Copyright 2001, 2010, 2011, 2012. Reproduced from ref. 48, 60 and 65 with permission form John Wiley & Sons, Copyright © 2004 Wiley-VCH Verlag GmbH & Co. KGaA, Weinheim, 2015, Copyright © 2012 Wiley-VCH Verlag GmbH & Co. KGaA, Weinheim, Copyright © 2015 The Authors. Published by Wiley-VCH Verlag GmbH & Co. KGaA.

conclusively distinguish between dimers and higher order aggregates.[48,49] For the alkynyl substituted systems, modeling studies indicate that the extraordinarily high experimentally observed amplification efficiency is not possible with dimeric catalysis, implicating the involvement of higher order aggregates in the catalytic cycle.[46,55,63] Theoretical suggestions for possible higher order aggregate structures, most notably, the square-macrocycle-square (SMS) tetramer were made for the first time by Brown and

Gridnev.[52,64] Subsequent investigations provided further momentum for a tetrameric catalyst model. Reaction progress kinetic analysis (RPKA) experiments[57] with substrate **3e** indicate the reaction rate to be 0th order in diisopropylzinc, 1st order in the catalyst (product alkoxide), and 1.6 order in aldehyde. An intriguing inverse temperature dependence on the reaction rate is also observed. On the basis of kinetic and spectroscopic clues, the suggestion that the SMS tetrameric alkoxide might be the active catalyst was raised for the first time. A DFT study to model these tetramers was reported by Gridnev in 2012.[59] The same year, Brown and Blackmond reported the observation of an acetal-like intermediate in the Soai reaction with substrate **3e**.[65] However, its actual relevance to the catalytic process remains unproven.

In 2015, Soai *et al.* reported the first crystal structures of the isopropylzinc alkoxide of **4d**. A tetrameric or oligomeric aggregate was obtained, depending on the crystallization conditions.[60,66] The homochiral and heterochiral tetramers possess a 12-member macrocycle with a connectivity resembling the SMS tetrameric structure proposed earlier. The assembly is a concatamer of two Zn–O square dimers, ligated through pyrimidine–Zn coordination. In the homochiral aggregate, the unbound pyrimidine units (referred to as the tetramer 'arms') are oriented on the same face of the macrocycle. The racemic, heterochiral tetramer possesses a similar overall connectivity but the arms are placed on opposite sides of the macrocycle. In both the homochiral (enantiopure) and heterochiral (racemic) tetramers, a pair of three-coordinate, unsaturated (alkoxy)zinc atoms are present as part of the pyrimidinyl arms.

The remaining six pyrimidinyl nitrogen atoms are bound by diisopropylzinc molecules (these are not shown in the structure in Figure 10.5). These landmark results provide a definitive structural understanding of the solid-state SMS tetramer and reveal the differences in the homochiral and heterochiral tetrameric assemblies.

Although these pioneering enquiries have converged on the consensus of the SMS tetramer as the likely autocatalyst, they have fallen short in providing any answers as to how this species, if it indeed is the autocatalyst, operates and executes the Frank scheme. Neither a structural basis for enantioselective (auto)catalysis, nor an explanation for the origin of non-linearity has been proposed.

Limitations in mechanistic understanding are also apparent from the lack of a compelling model that can rationalize the remarkable substrate constraints of the Soai reaction. For example, in the footnote of two reports, the reaction with diethylzinc is mentioned to display chiral erosion.[14,66] It is presumed that with other dialkylzinc reagents, analogous reactions are either not autocatalytic, not amplifying, or both. Brown *et al.*[43] claim that dicyclopropylzinc, di-*tert*-butylzinc, and dicyclopentylzinc[52] fail to provide autocatalytic asymmetric amplification with **3a** although no data was provided. Thus, although systematic studies are lacking, it is assumed that amplifying autocatalysis is unique to diisopropylzinc. Soai *et al.* also described isolated reports wherein amplifying autocatalysis with diisopropylzinc was

demonstrated with some specific substituted quinoline-3-carbaldehydes[67,68] and 5-formyl-nicotinamides,[68] however, these reactions are not as efficient as the substituted pyrimidine analogs and have not been a subject of further studies. Pyridine analogs are believed to be incompetent; pyridine-3-carbaldehyde (**5a**), for example does not demonstrate amplifying autocatalysis.[69] Although 2-alkynyl-pyrimidine-5-carbaldehydes are superlative substrates, it was noted that surprisingly, the inclusion of a triisopropylsilyl (TIPS) group (**3c**, Figure 10.3) was detrimental to chiral amplification.[15] Amplifying asymmetric autocatalysis is seen only when severe, non-obvious structural constraints are met.

10.2 Demystifying the Evolution of the Structure and Function of the SMS Tetramer

10.2.1 Competency of a Pyridine System – One of the Nitrogen Atoms in the Pyrimidine Core is Dispensable in the Soai Reaction

The reaction of 5-(trimethylsilylethynyl)pyridine-3-carbaldehyde (**5b**) with diisopropylzinc represents the simple change from a pyrimidine-to-pyridine core in the Soai system. On the basis of the known structural constraints of the Soai reaction, this transformation is not expected to display amplifying asymmetric autocatalysis. Indeed, in a 2015 publication by Amedjkouh and co-workers, the analogous reaction of the closely related substrate 5-(*tert*-butyl)pyridine-3-carbaldehyde (**5d**) was reported to display chiral erosion.[70]

In light of this literature precedent, our discovery of efficient amplifying asymmetric autocatalysis in the diisopropylzinc alkylation of **5b** was unexpected and surprising (Figure 10.6a).[71] Product carbinol **6b**, when included in this reaction as a scalemic catalyst, afforded a newly generated product with higher enantioenrichment. The reaction was homogenous even at high concentrations and was conveniently monitored by tracking aldehyde consumption using *in situ* IR spectroscopy. The transformation displayed all the characteristics of an amplifying, autocatalytic process (Figure 10.6b). Without the added catalyst, sigmoidal aldehyde consumption, with an initial induction period, followed by a rapid reaction is observed, characteristic of autocatalysis (entry 1, blue dashed curve). Inclusion of the scalemic product carbinol eliminated the induction period, leading to the rapid production of product with higher enantioenrichment than the initially added autocatalyst (entry 2, red dashed curve). At lower concentrations, the background reaction without added product was sluggish and inefficient (entry 3, solid blue curve). However, inclusion of either enantioenriched (entry 4, solid red curve) or racemic (entry 5, solid green curve) carbinol resulted in accelerated reactions and efficient product generation. In the case of the enantioenriched autocatalyst (entry 4), a highly enantioenriched product was obtained whereas the racemic autocatalyst

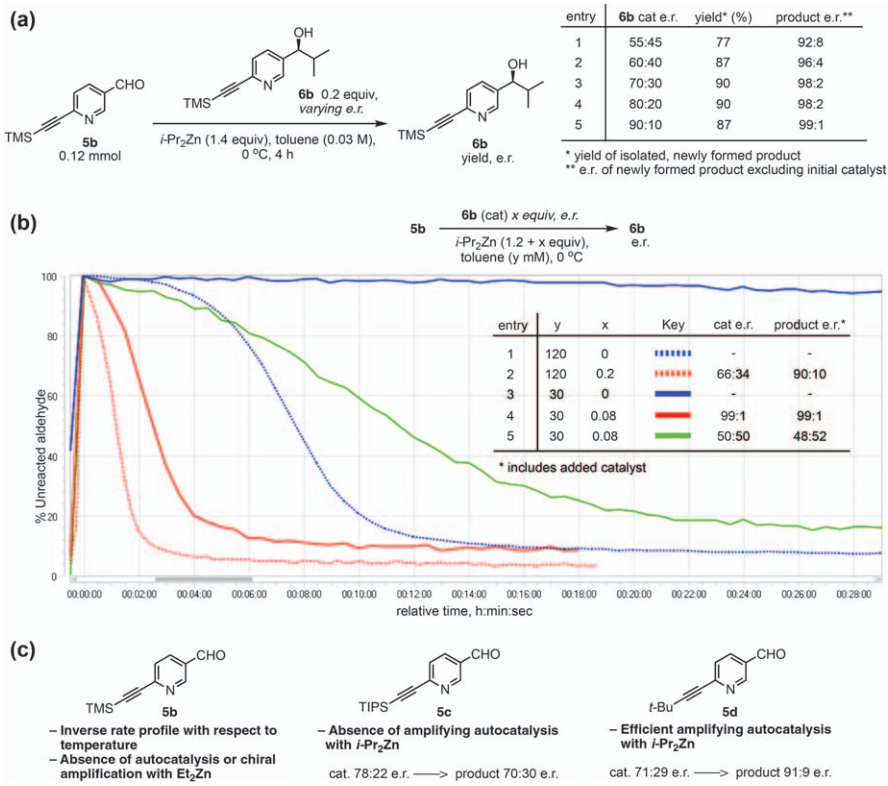

Figure 10.6 (a) Asymmetric autocatalysis with chiral amplification in alkylation of **5b** with diisopropylzinc. (b) Observation of sigmoidal aldehyde consumption profiles and non-linear autocatalysis upon monitoring aldehyde consumption by *in situ* IR spectroscopy ($t = 0$ denotes time of aldehyde addition). (c) Pertinent observations further highlighting the striking similarity of the pyridine system to the original pyrimidine system. Adapted from ref. 71 with permission from Springer Nature, Copyright 2020.

(entry 5) yielded a racemic product. Crucially, the latter reaction was much slower than the former indicating the lower catalytic activity of the racemic autocatalyst species, further highlighting the non-linear effect. These observations establish that, just as in the case in the iconic Soai pyrimidine-system, non-linear amplifying autocatalysis is also operative in the reaction of **5b** and diisopropylzinc.

Furthermore, the new system also shared the other non-obvious, idiosyncratic characteristics typical to the iconic pyrimidine substrate (Figure 10.6c, for details, refer to the Supplementary Information in ref. 71). An inverse rate profile with respect to temperature was noted, with a rate maximum at ~0 °C. Note that a similarly intriguing temperature effect was also reported previously in the Soai reaction of the pyrimidine substrate **3e**.[57] The analogous reaction with diethylzinc did not result in asymmetric

amplification or rate enhancement. Remarkably, the reaction of diisopropylzinc with 5-(triisopropylsilylethynyl)pyridine-3-carbaldehyde (**5c**) was sluggish and demonstrated neither asymmetric amplification nor autocatalytic rate enhancement. Consistent with this trend of observations, we find efficient amplifying autocatalysis also with substrate **5d**, thus contradicting Amedjkouh's report.[13]

Such striking similarities with the behavior of the original pyrimidine substrates clearly demonstrate that one of the nitrogen atoms in the pyrimidine ring is dispensable in the Soai reaction system. We believe that this is a significant development in terms of structural considerations of a mechanistic hypothesis because it constrains the possible coordination/interaction sites in any proposed catalytic assembly.

10.2.2 Structure–Activity Relationships of the Pyridinyl Autocatalyst

In the Soai reaction of **5b**, amplifying autocatalysis is affected by the unique activity of the isopropylzinc alkoxide of **6b** (henceforth termed **PyII**). Understanding the basis for this activity is essential for gaining meaningful mechanistic insights.

To evaluate contributions of the alkyl group on the carbinol center in the (auto)catalyst and the O–Zn-alkyl group, a qualitative comparison of catalysis by four different zinc alkoxides (**PyII**, **PyEE**, **PyIE**, and **PyEI**) was made by *in situ* IR monitoring of dialkylzinc additions to **5b** in catalyzed and uncatalyzed reactions (Figure 10.7) (nomenclature: Py/Ph = pyridine/phenyl indicating the aromatic core, I/E = isopropyl/ethyl indicating the carbinol alkyl group, and I/E = isopropyl/ethyl indicating the alkylzinc group). Note that owing to alkyl exchange, the choice of dialkylzinc reagent employed is dictated by the identity of the alkylzinc alkoxide (for example, **PyII** and **PyEI** cannot be used in a reaction with diethylzinc; likewise, **PyEE** and **PyIE** cannot be used in a reaction with diisopropylzinc).

Under these conditions, the uncatalyzed reactions (entries 1 and 4) were sluggish, showed low conversion, and ultimately stalled. Inclusion of either **PyEE** (entry 5) or **PyIE** (entry 6) showed no appreciable rate enhancement. In the case of **PyEE**, the product carbinol had a lower enantiomeric composition than the added catalyst whereas a minor positive non-linear effect was seen in the case of **PyIE**. Entry 2 representing the autocatalytic reaction with diisopropylzinc, reiterates the high catalytic efficiency and strong nonlinear behavior of catalyst **PyII**. Finally, with alkoxide **PyEI** (entry 3), a sigmoidal aldehyde decay with high final product e.r. was achieved, but with an absence of initial rate enhancement. This behavior is interpreted to arise from a low catalytic activity of **PyEI** giving rise to an initial production of **PyII** followed by strong asymmetric autocatalysis from a buildup of **PyII**.

Taken together, these observations prove that in this alkoxide series, only **PyII** possesses the requisite structural requirements for efficient, amplifying

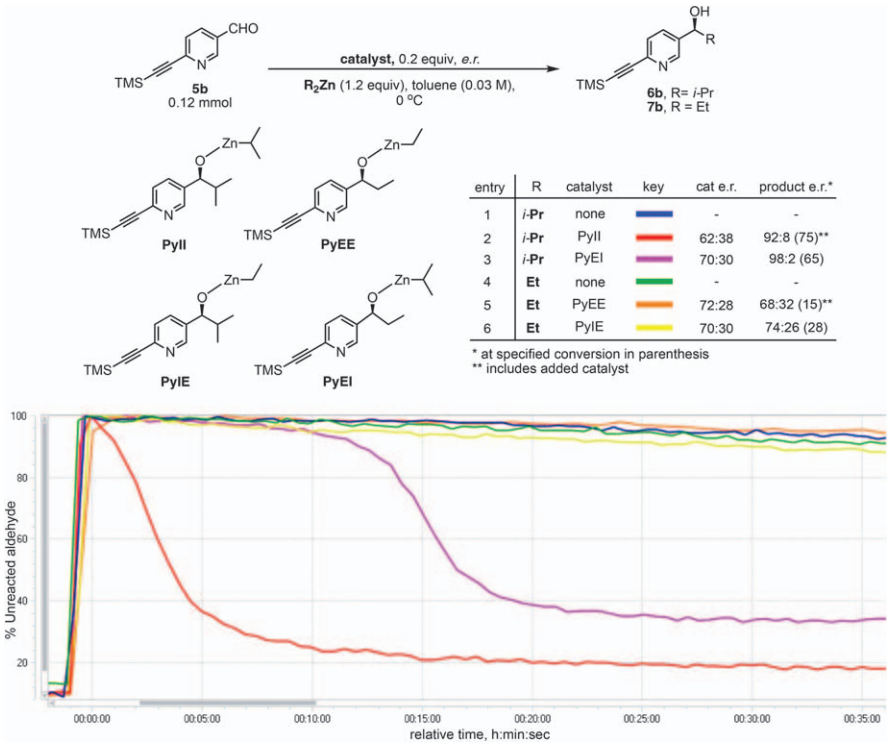

Figure 10.7 Qualitative comparison of catalytic activities and non-linear effect of alkoxides **Py*XX*** in dialkylzinc addition to **5b** by *in situ* IR monitoring of aldehyde consumption. Adapted from ref. 71 with permission from Springer Nature, Copyright 2020.

catalysis and replacement of either or both isopropyl groups results in alkoxides (**PyEE**, **PyIE** and **PyEI**) that possess markedly inferior catalytic efficiencies.

10.2.3 Spectroscopy of Zinc Alkoxides and the 'Cube-Escape' Model for the Assembly of the SMS Tetramer

To gain insights into the structural requirements for efficient catalysis, a spectroscopic study to characterize the solution state structures of phenyl (**PhEE**, **PhEI**, **PhIE**, and **PhII**) and pyridyl (**PyEE**, **PyEI**, **PyIE**, and **PyII**) zinc alkoxides in toluene was undertaken (Figure 10.8). These eight alkoxides represent a close chemical space around the **PyII** structure and may allow a delineation of the structural contributions that lead to catalysis only with **PyII**. The absence of a coordinating nitrogen atom in phenyl alkoxides, make them a simpler starting point for interpreting structural effects. Both enantioenriched and racemic samples of all eight alkoxides in deuterated toluene were studied. Multidimensional and variable temperature NMR

experiments as well as Diffusion Ordered Spectroscopy (DOSY; for molecular weight estimation of aggregates) was employed. For brevity, only the main conclusions from this study are presented in Figure 10.8 (for detailed discussion and data analysis, refer to ref. 71).

In all cases, spectra obtained from racemic samples showed greater multiplicity of signals and additional peaks compared to spectra obtained from enantioenriched samples, proving the multimeric nature of these alkoxides. Based on a comparison of chemical shifts of diagnostic protons, racemate analysis, and DOSY studies, clear patterns emerge. Several alkoxides form similar aggregate species in solution – these are highlighted with the same color. **PhEE**, **PhEI**, **PhIE**, and **PyEE** exist exclusively as a cubic tetrameric aggregate (species 'a') and are highlighted with yellow. Among the observations that support this conclusion, the comparison of enantioenriched and racemic samples is particularly decisive. In the case of **PhEI**, a remarkable quadruplet splitting pattern in the racemic aggregate was observed in comparison to the enantiopure aggregate (Figure 10.8 lower panel). Such a pattern, also seen in all cases where species a is detected, is a smoking gun for a symmetric, cubic tetramer structure, which finds ample precedent.[73,74]

In contrast, the spectrum of the autocatalytically competent **PyII** displayed significant differences with the spectral characteristics of species a and appears to form a distinct, exclusive aggregate structure (species b; colored blue). Species b is still tetrameric but is not a cubic tetramer. **PyEI** appears to form a mixture of species a and b. **PyIE**, in addition to species a and b, also forms another tetrameric aggregate – species c. Finally, **PhII** forms a mixture of two trimeric aggregates – species d and e.

Rationalizing the effect of structure on alkoxide aggregation begins with the assumption that a cubic tetramer is the preferred state of these alkoxides. It was hypothesized that replacement of ethyl groups around the cube core by bulkier isopropyl groups results in destabilization of the cube structure by steric repulsion to the point at which the cube is no longer viable as in cases of **PhII** and **PyII**. A weakened cube can be further disrupted by a pyridine nitrogen through coordination to the zinc alkyls to assist in the formation of alternative tetrameric aggregates. This hypothesis was tested by the addition of excess pyridine to solutions of the zinc alkoxides. In the case of **PhEI**, **PhIE**, and **PhII**, this modification resulted in disruption of the aggregate structure to a pyridine coordinated saturated dimer (Figure 10.9 and 10.10a), whereas **PhEE** remained unaffected. The results demonstrate that a cubic tetramer weakened by unfavorable steric interactions (**PhEI**, **PhIE**, and **PhII** but not **PhEE**) is poised to be disrupted by pyridine coordination to the zinc atoms.

This analysis can be extended to the pyridyl alkoxides (Figure 10.10b) with the recognition that these molecules already possess a pyridine nitrogen for intra-aggregate coordination. With a pyridine nitrogen available for coordination to zinc, alkoxides **PyEE**, **PyEI**, **PyIE**, and **PyII** are poised to escape the cube only if the core is sufficiently weakened. Whereas **PyEE** maintained a cubic tetramer constitution (species a) because its core is sufficiently stable to resist intramolecular pyridine disruption, **PyEI** and **PyIE** exhibited

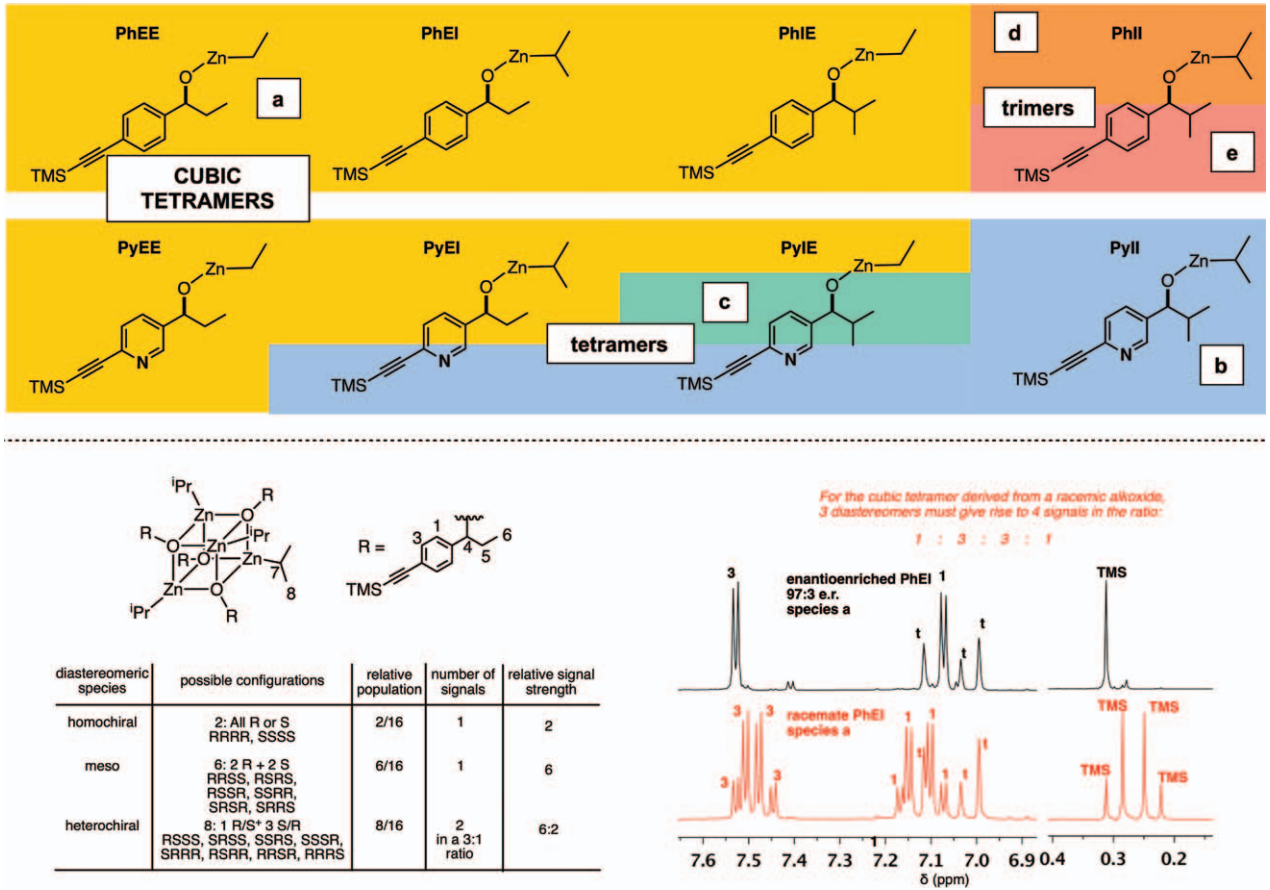

diastereomeric species	possible configurations	relative population	number of signals	relative signal strength
homochiral	2: All R or S RRRR, SSSS	2/16	1	2
meso	6: 2 R + 2 S RRSS, RSRS, RSSR, SSRR, SRSR, SRRS	6/16	1	6
heterochiral	8: 1 R/S+ 3 S/R RSSS, SRSS, SSRS, SSSR, SRRR, RSRR, RRSR, RRRS	8/16	2 in a 3:1 ratio	6:2

Figure 10.8 Top panel – summary of solution state alkoxide aggregates (top panel). Bottom panel – diastereomeric species possible in a racemic cubic tetramer with their relative peak distributions. ^{1}H NMR of the aryl and TMS region for racemic **PhEI** displays this predicted quadruplet pattern (t = residual toluene). Adapted from ref. 71 with permission from Springer Nature, Copyright 2020.

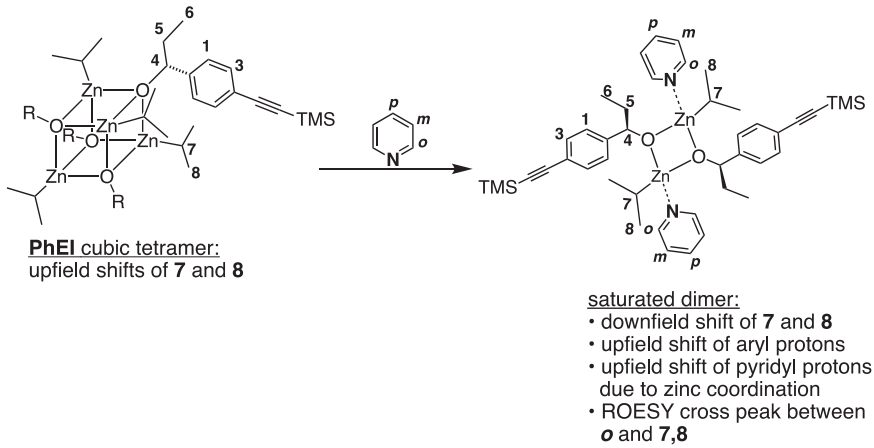

Figure 10.9 Disruption of the cubic tetrameric aggregate by pyridine coordination. Diagnostic changes in the ^{1}H NMR spectrum are noted.

formation of other tetrameric species (species b and c) owing to partial cube escape facilitated by nitrogen coordination. Finally, **PyII**, through complete cube escape, accesses an exclusive, alternative aggregate structure. Reconciling the observation that **PyII** exists as a non-cubic tetrameric aggregate, the simplest way in which such a cube-escape can occur is an intramolecular coordination of the pyridyl nitrogen to expand the cube to a square-macrocycle-square (SMS) connectivity (Figure 10.10b).

This proposed connectivity of **PyII** is identical to the pyrimidine SMS tetramer (Figure 10.5) whose crystal structure was described by Soai. For the first time, these studies provide a systematic logic for its solution-state assembly and establish how only a single nitrogen atom is required in the aromatic core to build this tetramer. The next tantalizing question is – can this aggregate lead to a compelling model for non-linear enantioselective catalysis in the Soai system?

10.2.4 Substrate Binding by the SMS Tetramer

To act as a catalyst, the SMS tetramer must in some way engage diisopropylzinc and the substrate. Crucially, if benzaldehyde (**1a**) or the trimethylsilyl–alkynyl substituted benzaldehyde (**1b**) is employed as a substrate, only trace alkylation was observed (Figure 10.11). However, pyridine-3-carbaldehyde (**5a**) is a competent substrate and the SMS tetramer catalyzes a rapid diisopropylzinc alkyl transfer with a positive non-linear effect. The nitrogen atom in the substrate seems indispensable for strategic coordination to some location on the SMS tetramer. Identical substrate limitation is also seen in reactions catalyzed by the isopropylzinc alkoxide of **4b** (the analogous pyrimidine SMS tetramer).

Note that the **PyII** catalyzed addition of diisopropylzinc to **5a** is a non-autocatalytic reaction because the corresponding product is catalytically inactive. This observation indicates the general attributes that make **PyII** an

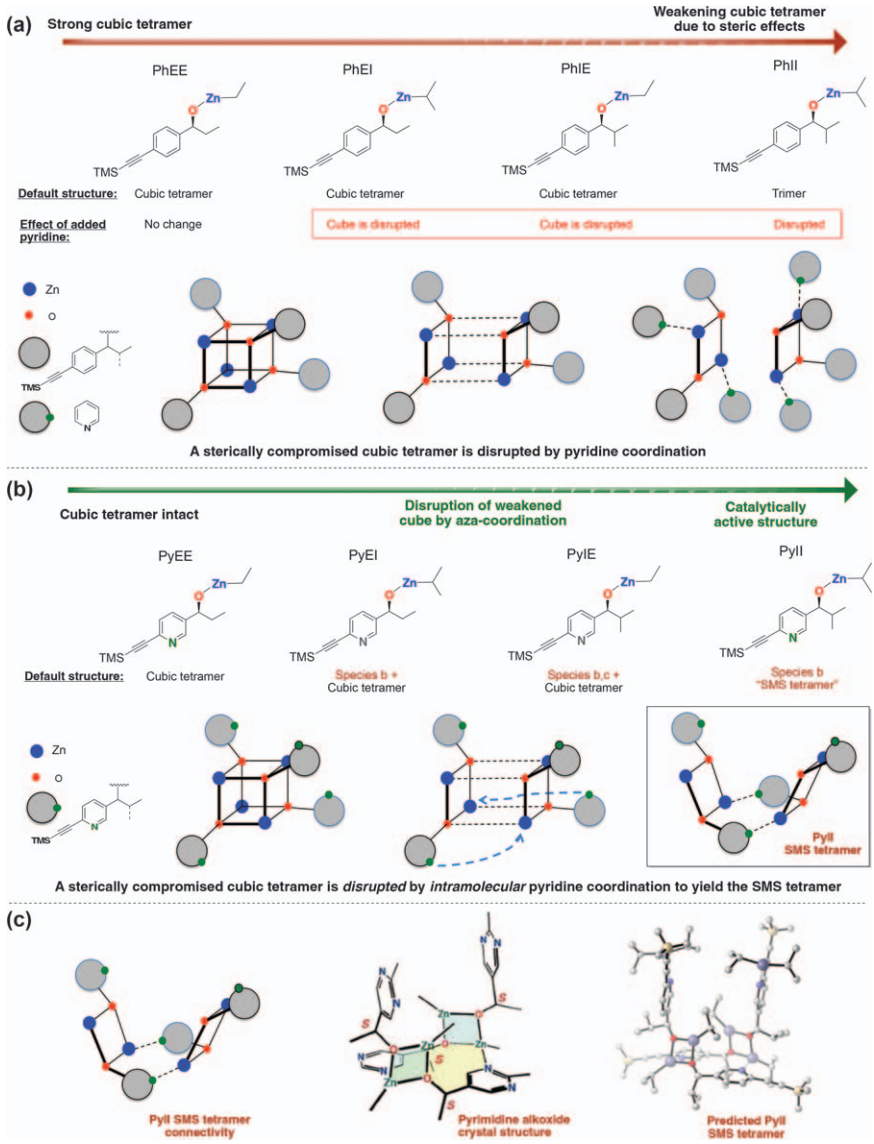

Figure 10.10 (a) Sterically weakened **PhXX** cubic tetramers are disrupted by pyridine. (b) A conceptually similar 'cube escape' occurs in the **PyXX** alkoxides with intramolecular pyridine coordination yielding the SMS tetramer. (c) The predicted identity of the cube-escaped **PyII** SMS tetramer by analogy with the Soai pyrimidine alkoxide crystal structure. Adapted from ref. 71 with permission from Springer Nature, Copyright 2020.

enantioselective catalyst. The autocatalytic behavior is simply a special case wherein the substrate is matched to give the same product as the catalyst. With this perspective, it becomes clear that the fundamental catalytic

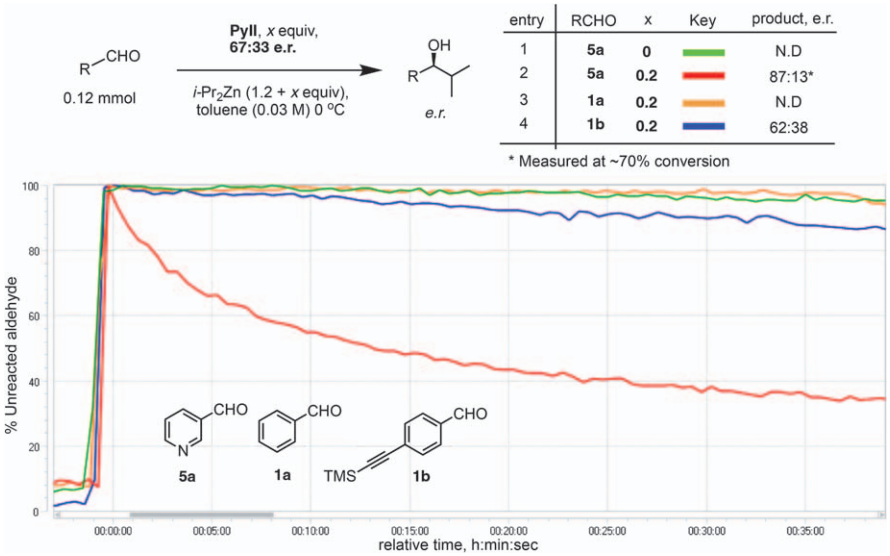

Figure 10.11 Aldehyde consumption is monitored by *in situ* IR spectroscopy in catalyzed reactions to assess substrate compatibility for alkyl transfer by **PyII**. Poor reactivity is seen with benzaldehydes but pyridine-3-carbaldehyde is a competent substrate, resulting in isopropyl transfer with a strong positive NLE. Adapted from ref. 71 with permission from Springer Nature, Copyright 2020.

properties of the **PyII** tetramer can be studied with any competent substrate – in fact, use of pyridine-3-carbaldehyde simplifies the complicated autocatalytic behavior to that of a conventional catalyst–substrate system. Initial rate kinetic studies with this surrogate substrate revealed that the reaction rate was 0th order in both the substrates and first order in the **PyII** tetramer. At least with **5a,** this indicates saturation binding of both reactants to the SMS tetramer followed by a rate limiting alkyl transfer.

Insights into the nature of the binding of substrate (**5a** or **5b**) and diisopropylzinc to the **PyII** tetramer were obtained by further NMR spectroscopy investigations. Interactions between the two reactants – diiisopropylzinc and **5a** (as well as **5b**) unambiguously proved (data not shown, refer to the Supplementary Information of ref. 71 and 72) that the carbonyl oxygen has no affinity to diisopropylzinc and both **5a** and **5b** bind to diisopropylzinc exclusively through the nitrogen center. This binding is characterized by an upfield shift of the aromatic protons (including the carbonyl proton) and a concomitant downfield shift of the alkylzinc protons (with the shift magnitude increasing at lower temperatures). This change in NMR signals arising from a pyridine–dialkylzinc coordination finds literature precedent.[75,76] Quantitative NMR measurements established the binding constant of diisopropylzinc and **5b** to be about 109 M^{-1} at −18 °C. Likewise, the

addition of diisopropylzinc to **PyII** shows reagent coordination to the 'pyridine arms' of the SMS tetramer.

Experiments directly probing the binding of **5a** to **PyII** were also attempted in the absence of diisopropylzinc (Figure 10.12b). Orienting experiments were performed with **PhEE** and **PhII** (Figure 10.12a). The region of the ^{1}H-NMR spectrum denoting the substrate protons is shown. In Figure 10.12a, a *downfield* shift (~0.1 ppm) of the aldehyde proton (H_a) was observed only in the presence of **PhII** (blue). In the cubic tetrameric **PhEE**, all four zinc atoms are coordinatively saturated by alkoxide binding and are unavailable for carbonyl coordination. In contrast, **PhII**, existing as a mixture of trimers, presumably contains at least one unsaturated zinc center, which binds the carbonyl oxygen and causes the downfield chemical shift. Note that this *downfield* shift of H_a, as well as the absence of shifts of $H_{b/c}$ rule out binding *via* the nitrogen of **5a**. A similar observation – a downfield chemical shift (~0.5 ppm) for H_a – was noted in the experiment with **PyII** (Figure 10.12b, blue). Taken together, these investigations indicate that the

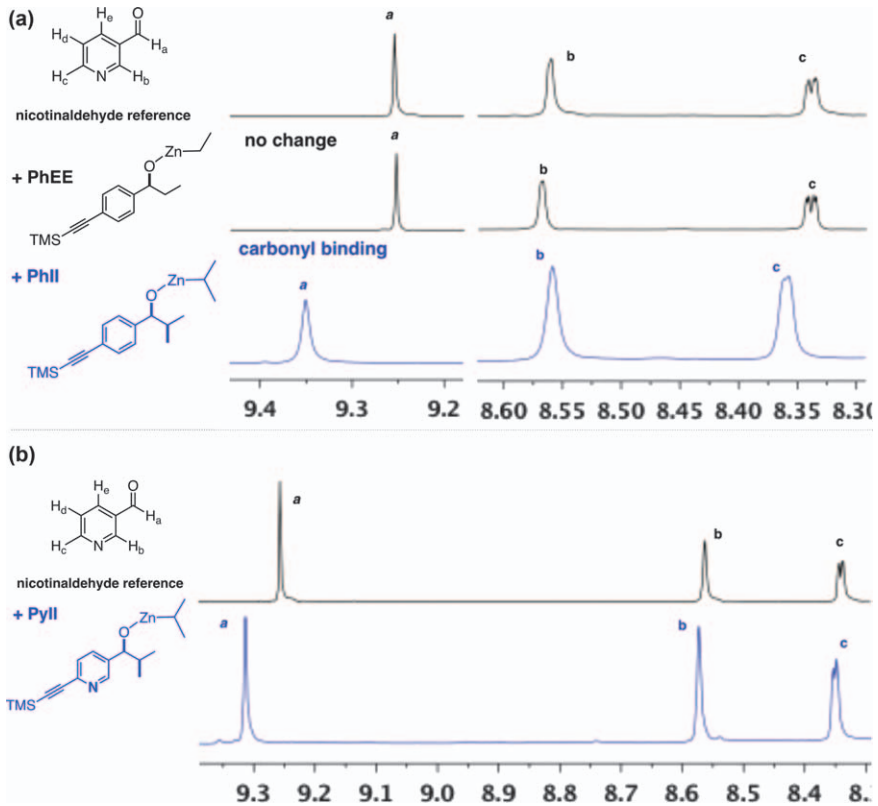

Figure 10.12 Downfield region of the ^{1}H-NMR spectrum of **5a** and, (a) **PhEE** and **PhII** and (b) **PyII**. All spectra recorded at 0 °C in deuterated toluene.

carbonyl oxygen of **5a** can bind to the unsaturated zinc center of the **PyII** SMS tetramer.

10.2.5 Enantioselective Alkyl Transfer by the SMS Tetramer

Considering these observations, two binding models of the reactants to the **PyII** SMS tetramer are proposed (Figure 10.13): (1) floor-to-floor and (2) floor-to-arm. In both cases, two diisopropylzinc molecules, each bound to a pyridine-arm saturate the tetramer. In both cases, the carbonyl oxygen of the substrate **5a** is bound to an unsaturated zinc center located in the Zn–O square of the tetramer. The site of substrate nitrogen coordination distinguishes the two models. In the former, this site is the second unsaturated zinc center on the opposite Zn–O square whereas in the latter, binding occurs to a diisopropylzinc molecule ligated to a catalyst arm. Hence, in the floor-to-floor model, the substrate, through a two-point binding, bridges the two distal unsaturated zinc alkoxide centers in the Zn–O squares whereas in the floor-to-arm model, the substrate through a two-point binding, bridges an unsaturated zinc alkoxide atom in the Zn–O square and a dialkylzinc atom on the opposite arm. Note that in both models, the reactants are electronically activated toward alkyl transfer – the aldehyde (rendered more electrophilic) by coordination to the Lewis acidic zinc center and diisopropylzinc (rendered more nucleophilic) by coordination to the Lewis basic nitrogen. Density functional theory (DFT) calculations were employed to identify the most favorable alkyl transfer pathway arising from these ground state binding modes. The floor-to-floor binding is preferred by 4.5 kcal mol^{-1}. In this mode,

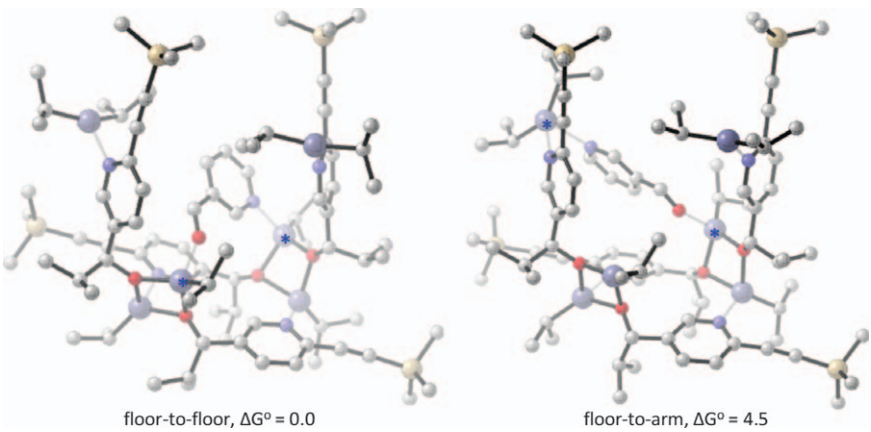

Figure 10.13 Proposed models for two-point binding of substrate **5a** to the **PyII** SMS tetramer. Blue asterisks signify bound zinc atoms. Structures represent optimized minima calculated at the M06-2X/def2-TZVPP-SMD (toluene)//B3LYP/6-31G(d) level of theory. Relative energies (ΔG°) reported in kcal mol^{-1}. Purple, zinc; yellow, silicon; red, oxygen; blue, nitrogen; gray, carbon. Hydrogens are hidden for clarity. Adapted from ref. 71 with permission from Springer Nature, Copyright 2020.

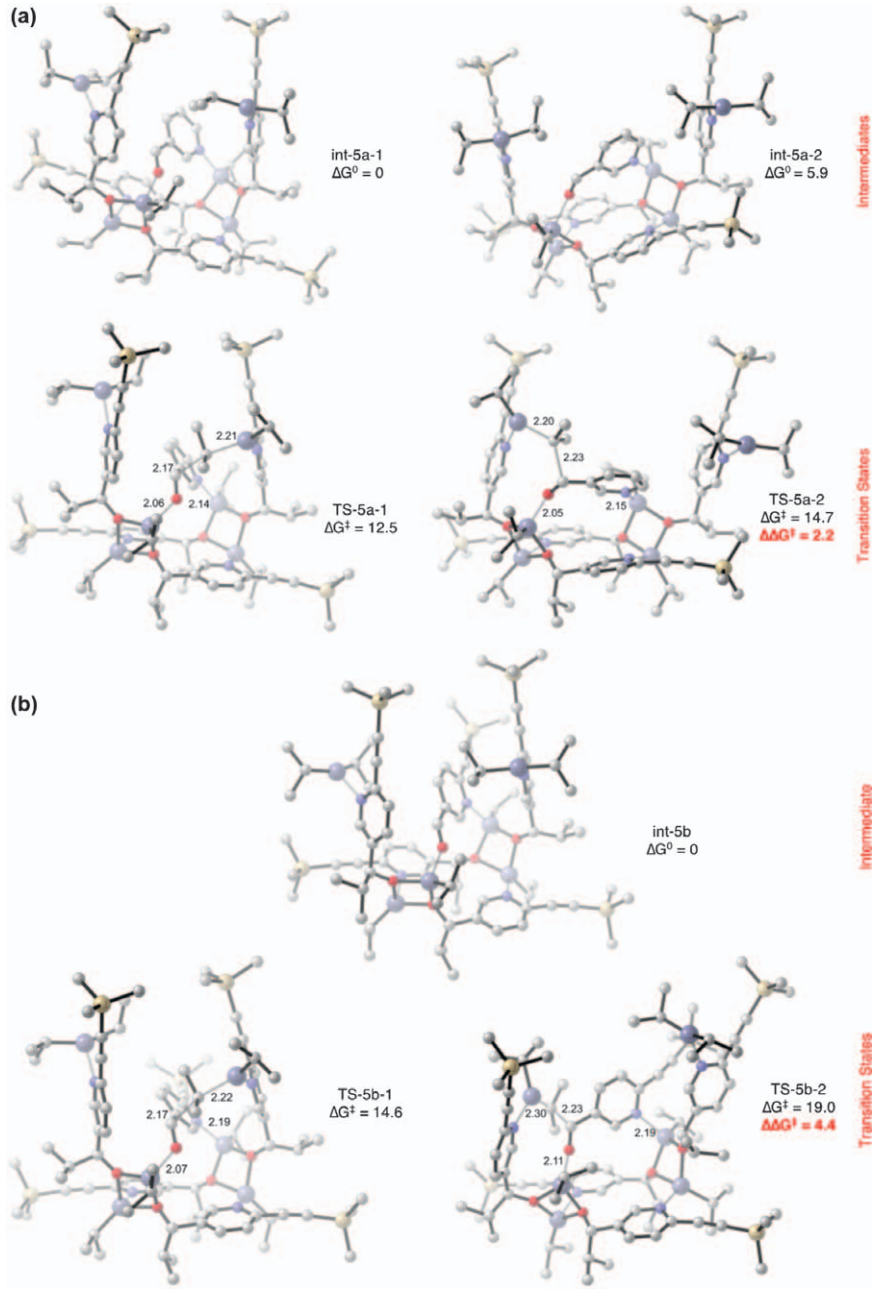

Figure 10.14 Catalysis by the **PyII** SMS tetramer – DFT studies for floor-to-floor substrate docking and alkyl transfer. (a) Catalysis with **5a** as substrate. (b) (Auto)catalysis with **5b** as substrate. Transition structures and optimized minima are calculated at the M06-2X/def2-TZVPP-SMD (toluene)// B3LYP/6-31G(d) level of theory. Energies reported in kcal mol^{-1}. Purple, zinc; yellow, silicon; red, oxygen; blue, nitrogen; gray, carbon. Hydrogens are hidden for clarity. ΔG°, free energy of activation. $\Delta\Delta G^{\ddagger}$, relative free energy activation barrier. Adapted from ref. 71 with permission from Springer Nature, Copyright 2020.

the diisopropylzinc molecules bound to the tetramer arms appear to be stereoelectronically predisposed for carbonyl addition. Indeed, floor-to-floor binding leads to the most favorable alkyl transfer pathway, with predicted selectivity consistent with the observed experimental stereoselectivity. In contrast, the floor-to-arm binding, in addition to being energetically unfavorable, leads to alkyl transfer pathways that are prohibitively high in energy.[71]

In the floor-to-floor model, alkyl group transfer by diisopropylzinc is primed for delivery to the *Si* face of the aldehyde in **int-5a-1** (most stable ground state intermediate), which would lead to the observed *S* stereoisomer (Figure 10.14a). Conversely, the *Re* face is accessible only through a rotation of both the substrate and one arm of the tetramer as shown in **int-5a-2**, which is unfavorable by 5.9 kcal mol^{-1}. The stereocontrolling transition structures **TS-5a-1** and **TS-5a-2** arising respectively from **int-5a-1** and **int-5a-2**, have activation free energy barriers of 12.5 kcal mol^{-1} and 14.7 kcal mol^{-1} respectively. This energy difference ($\Delta\Delta G^{\ddagger} = 2.2$ kcal mol^{-1}, red) agrees with the observed stereoselectivity of **PyII** with pyridine-3-carbaldehyde **5a** (95 : 5 e.r., $\Delta\Delta G^{\ddagger} = 1.7$). Thus, the enantioselective alkylation of **5a** by **PyII** can be computationally justified to result from the favored pathway of two-point, floor-to-floor substrate binding followed by preferred alkyl delivery from an arm-bound diisopropylzinc molecule.

The transition structures and minima for the autocatalytic reaction of aldehyde **5b** and tetramer **PyII** were also investigated computationally (Figure 10.14b). Only a single binding intermediate (**int-5b**, geometry similar to **int-5a-1**) is found (the structure analogous to **int-5a-2** is not a stable intermediate). The lowest-energy transition structure **TS-5b-1** leads to the alcohol (*S*)-**6b**, and the next higher energy transition structure **TS-5b-2** ($\Delta\Delta G^{\ddagger} = 4.4$ kcal mol^{-1}, red) leads to the (*R*)-**6b** product. This large difference in energy comports with an enantioselective autocatalytic mechanism. **TS-5b-1** is analogous to **TS-5a-1**, in which facile alkyl transfer takes place from diisopropylzinc in the ground state geometry **int-5b-1**. Contrariwise, **TS-5b-2** represents a higher-energy pathway because the left arm of the tetramer does not rotate for alkyl transfer to the *Re*-face of the aldehyde as in **int-5a-1**. This conformation is inaccessible for aldehyde **5b** because to arrange this substrate to receive the isopropyl group would require that the trimethylsilylethynyl substituent be in the same space as the opposite arm (*N.B.*, the C(5) position of aldehyde **5a** in both **int-5a-2** and **TS-5a-2**, which corresponds to the trimethylsilylethynyl-substituted position of **5b**).

To summarize, the **PyII** SMS tetramer structure provides two unsaturated, Lewis acidic zinc atoms in the Zn–O squares adjoining the macrocyclic floor, which anchor the substrate (in a floor-to-floor arrangement) and activate it toward nucleophilic attack. The diisopropylzinc nucleophile, bound to each catalyst arm is in turn activated by the Lewis basic, pyridyl nitrogen coordination. Alkyl delivery from one arm is highly favored over the other, leading to the generation of the homochiral product (in this case, the *S* configuration). Transition state models of the surrogate substrate **5a** are

reflective of and can be extended to the reaction with substrate **5b**, which switches enantioselective catalysis by **PyII** into an asymmetric autocatalytic transformation and imparts improved selectivity by virtue of the conformationally restrictive trimethylsilylalkynyl substitution. With this model, the reason for the incompetence of benzaldehydes as substrates (Figure 10.11) is obvious since they cannot engage with the **PyII** tetramer in a floor-to-floor binding.

10.2.6 The Origin of Non-linearity

The floor-to-floor transition state model provides an elegant solution to the origin of non-linearity in catalysis, which is the basis for asymmetric amplification.[71] The catalytic competence of the heterochiral (racemic) **PyII** tetramer was computationally investigated (Figure 10.15). The heterochiral aggregate was modeled according to the Soai crystal structure for the isopropylzinc alkoxide tetramer derived from racemic **3d.** The heterochiral tetramer is energetically preferred to the homochiral **PyII** tetramer by 2.1 kcal mol^{-1} (G_{rel}, blue). From inspection of this structure, it is clear that substrate binding in a two-point, floor-to-floor arrangement is impossible because the requisite, unsaturated zinc atoms (purple circles) are positioned on opposite sides of the macrocycle. Indeed, any alkyl transfer pathway from a single-point binding was calculated to be energetically prohibitive.

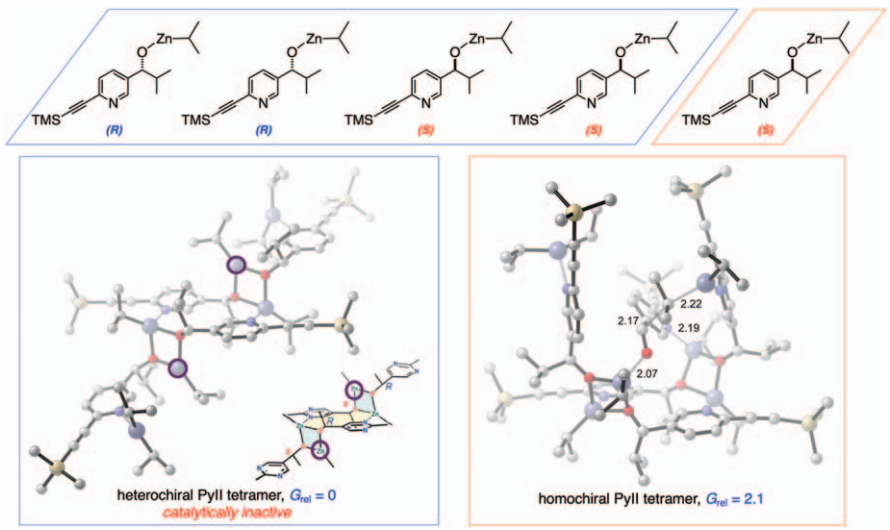

Figure 10.15 Origin of non-linearity in the alkyl transfer by the SMS tetramer. In a scalemic (60 : 40 e.r.) mixture of the zinc alkoxide, the heterochiral aggregate is preferentially formed but is catalytically inactive since a two-point floor to floor binding is impossible. Adapted from ref. 71 with permission from Springer Nature, Copyright 2020.

The phenomenological outcome is akin to a reservoir effect model in non-linear enantioselective catalysis.[11] Consider a scalemic (60 : 40, *S*/*R* e.r.) mixture of the **PyII** alkoxide. The racemic constituent of this mixture (blue box) will preferentially form the heterochiral SMS tetramer, which is catalytically inactive. The excess, enantiopure component (in this case the *S* stereoisomer, red box) will assemble into the catalytically active homochiral **PyII** aggregate. Owing to the highly selective catalysis by the homochiral autocatalyst, this bifurcation of the scalemic alkoxide will give rise to a strong positive non-linear effect – in this case, formally manifesting as autocatalytic, asymmetric amplification.

10.3 Structural Contributions to Amplifying Autocatalysis in the Soai Reaction

10.3.1 'Mixed Catalyst–Substrate' Experiments

The reaction between **PyII** and **5a** (Figure 10.11) is referred to as a 'mixed catalyst substrate' experiment because the alkylation of the substrate produces a species distinct from the initial catalyst. Because the product contributes minimally to catalysis, we hypothesized that such combination experiments can provide an empirical understanding about independent contributions from the catalyst and reactant structures like any classical, non-autocatalytic system. Results from reactions catalyzed by pyrimidinyl alkoxides **PmII** and **PmIE** (nomenclature: Pm = pyrimidine indicating the aromatic core, I/E = isopropyl/ethyl indicating the carbinol alkyl group, and I/E = isopropyl/ethyl indicating the alkylzinc group) with various substrates are presented in Figure 10.16. Consistent with the floor-to-floor model, benzaldehydes are incompetent substrates (entries 5 and 6). The extremely rapid reaction with **5b** (entry 1) is expected because the diisopropylzinc alkylation of **5b** itself is autocatalytic. Substrates **5a**, **3c**, and **5c** (entries 2–5), neither of which demonstrate amplifying autocatalysis with diisopropylzinc are competent substrates for alkylation with **PmII** and yield products with a positive NLE. Clearly, the TIPS substituted substrates **3c** and **5c** are viable if presented with a competent catalyst (in this case, **PmII**). Thus, the failure of such substrates in the Soai reaction (diisopropylzinc alkylation) must arise from the catalytic incompetence of the TIPS-derived alkoxides, rather than the substrates themselves. Furthermore, the relative rates of reactions suggest that the alkynyl substituent retards the rate of alkylation (compare entries 2 and 4) by the SMS tetramer and that pyrimidinyl substrates (**3c**) show a faster rate than pyridine substrates (**5c**), perhaps because of the higher electrophilicity of the former (compare entries 3 and 4). Note that analogous trends were also seen in the case of experiments with **PyII** (data not shown here, refer to ref. 13 and 72).

Catalysis experiments with **PmIE** (Figure 10.16b) indicate that the SMS tetramer can also catalyze the transfer of diethylzinc. A rapid alkylation

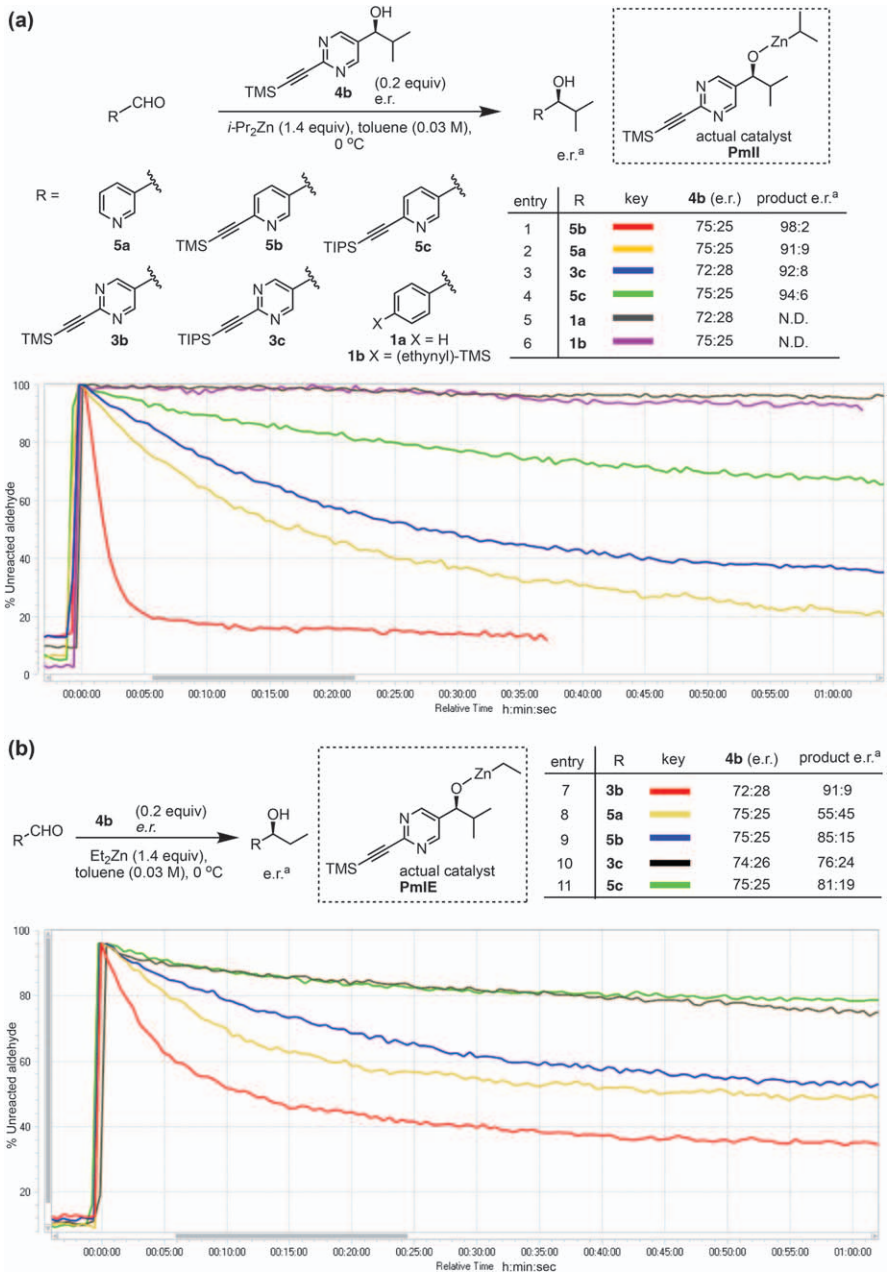

Figure 10.16 'Mixed-catalyst substrate' reactions monitored by *in situ* IR spectroscopy. (a) Diisopropylzinc alkylations catalyzed by **PmII**. (b) Diethylzinc alkylations catalyzed by **PmIE**. [a] Measured e.r. of product carbinol after workup; N.D. not determined (no product was detected). Adapted from ref. 13 with permission from American Chemical Society, Copyright 2020.

with a positive NLE is seen when **3b** is provided as a substrate (entry 7). Presumably, the cube escaped **PmIE** SMS tetramer is present in sufficient concentrations to affect such alkylations. Rate and selectivity vary considerably with aldehyde structure (entries 8–11) and a positive nonlinear effect is observed with all substrates except **5a** (entry 8). Only marginal catalysis was observed with the challenging TIPS-substituted substrates, **3c** and **5c** (entries 10 and 11). Phenyl substrates **1a** and **1b** were unreactive (data not shown). Although **5b** reacts slower than **5a**, the substituted pyrimidine **3b** is more reactive than either of these, suggesting that a balance of two opposing factors determine aldehyde reactivity: (1) activation by the pyrimidine ring and (2) deactivation from 2-alkynyl substitution, consistent with the trend seen in the **PmII** catalyzed (Figure 10.16a) reactions. Likewise, comparison of entries 8, 9, and 10 suggests that the 2-alkynyl substituent improves substrate-controlled selectivity and among them, an optimum balance of reactivity and selectivity is achieved for aldehyde **5b**.

Such 'mixed catalyst substrate' experiments enable a qualitative understanding of the structural contributions in the Soai reaction. For the sake of brevity, only selected experiments are described here in the hope of conveying the rationale and utility of such an approach; further details can be found in ref. 13, 72. General conclusions from these studies and knowledge gained during the formulation of the cube-escape, floor to floor model – summarized in Figure 10.17 are as follows: (1) the bulky isopropyl groups enable cube escape from the catalytically inactive cubic tetramer, (2) only a single nitrogen atom is necessary in the aromatic core to assemble the autocatalytically active SMS tetramer, (3) the SMS tetramer can process substrates belonging to the pyridine-3-carbaldehyde scaffold (including pyrimidine carbaldehydes); the aromatic nitrogen is indispensable for two-point binding, (4) the substrate alkynyl substituent increases alkyl transfer enantioselectivity by disfavoring the minor transition state through an unfavorable steric interaction, (5) the substrate alkynyl substituent decreases reactivity (while increasing selectivity) – the pyrimidine substrates are more reactive, presumably because of their increased electrophilicity in comparison to the pyridine substrates (DFT calculated LUMO energies, computed at wb97x-d/aug-cc-pVDZ in gas phase – benzaldehyde, 1.906 eV; pyridine-3-carbaldehyde, 1.017 eV; pyrimidine-5-carbaldehyde, 0.700 eV; likewise for a comparison of Hammett parameters, see ref. 77), (6) diethylzinc, in principle, can be accepted as a reagent by the SMS tetramer to affect carbonyl alkylation, albeit with lower enantioselectivity, as compared to diisopropylzinc, and (7) from the perspective of the autocatalyst, the alkynyl substituent contributes to efficient, enantioselective activity by: (a) improving solubility characteristics, (b) directing the alkoxide away from unproductive aggregates by providing a steric shield on one side of the molecule, and (c) favoring a specific conformation of the SMS tetramer that increases enantioselectivity to meaningful levels.

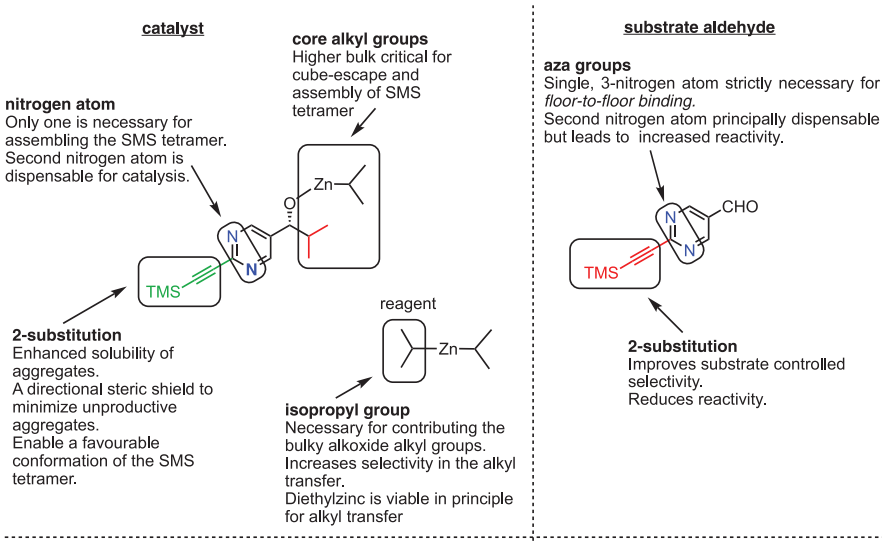

Figure 10.17 A summary of the roles played by various structural constituents in effecting catalysis and selectivity in the Soai system. Reproduced from ref. 13 with permission from American Chemical Society, Copyright 2020.

10.3.2 Insights from the Soai Reaction of a Fluoro-substituted Pyridine System

While surveying the competency of other substituted pyridines in the Soai reaction, the diisopropylzinc alkylation of 5-fluoro-6-((trimethylsilyl)ethynyl)nicotinaldehyde (**5e**) was found to demonstrate efficient amplifying autocatalysis (Figure 10.18a). The autocatalytic isopropylzinc alkoxide of **6e** is designated as **FPyII** (FPy = fluoropyridine, I = isopropyl) in further discussions.

The autocatalytic systems arising from substrates **3b**, **5b**, and **5e** (corresponding to **PmII**, **PyII**, and **FPyII** respectively) differ only in the heteroaromatic core. The pyrimidine nitrogen, with lower Lewis basicity than the pyridine,[78,79] is expected to display weaker binding to the Lewis acidic diisopropylzinc reagent as well as to the O–Zn moiety. Likewise, the **FPyII** nitrogen should be less Lewis basic than the **PyII** nitrogen (pK_a: pyridine = 5.23, 3-fluoropyridine = 3.0, pyrimidine = 1.30).[78,80] The comparison of these three provided an interesting opportunity to study the effects of such electronic changes on autocatalytic behavior.

To compare the inherent activities of the three alkoxide catalysts (**PmII**, **PyII**, and **FPyII**), a comparison of initial rates with the common substrate pyridine-3-carbaldehyde (**5a**) was undertaken (Figure 10.18b). These three catalysts provide product carbinol **6e** in comparable enantioenrichment. However, initial rates of **FPyII** and **PmII** while comparable to each other, are at least twofold lower than the rate with **PyII**. This observation may be rationalized by considering the floor-to-floor TS model for the alkyl transfer

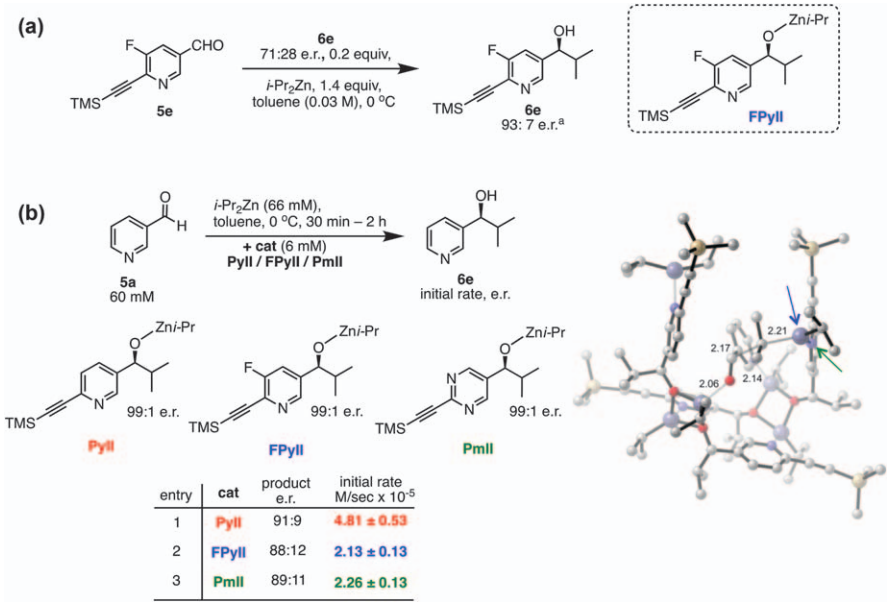

Figure 10.18 (a) Amplifying autocatalysis in the Soai reaction of **5e** ([a]e.r. includes initially added **6e**). (b) Comparison of alkyl transfer rates of **PyII**, **FPyII**, and **PmII**. TS model for the alkyl transfer with **PyII** highlighting the transferring diisopropylzinc moiety (blue arrow) bound to the activating arm nitrogen (green arrow). Reproduced from ref. 13 with permission from American Chemical Society, Copyright 2020.

step. Because of the weaker Lewis basicity of the coordinating nitrogen, the transferring diisopropylzinc in the **PmII** and **FPyII** tetramer is deactivated (as compared to **PyII**), resulting in a slower elementary alkyl transfer step. Thus, for an identical substrate, the activities of the three catalysts are in the order **PyII** > **PmII** ~ **FPyII**.

10.3.3 Inhibition of Autocatalysis by Excess Diisopropylzinc in the Pyridine Systems

Consistent with earlier reports,[57] autocatalytic progression of the **PmII** system was found to be insensitive to diisopropylzinc concentration but, similar experiments with the **PyII** system resulted in inhibition of reaction progression with increasing reagent concentration. This phenomenon was also noted for the **FPyII** system. Increasing diisopropylzinc concentration also adversely affected the selectivity of the reaction, presumably by accelerating the uncatalyzed background addition while concomitantly compromising the catalytic pathway. Although the **PyII** system otherwise resembles the behavior of the autocatalytic **PmII** system,[71] this inhibition by excess diisopropylzinc is an important point of divergence.

Figure 10.19 presents the results of comparative experiments among the three autocatalytic systems (all runs are reproducible and represent one among duplicate experiments). The reactions were carried out under identical conditions, with varying concentration of diisopropylzinc. The yellow curves represent reactions with the **PmII** system, which are extremely rapid, invariant in rate with respect to diisopropylzinc concentration, and provide the product with >99 : 1 e.r. in all cases. Reaction profiles with the **PyII** and **FPyII** system are represented by solid and dashed curves respectively. Although the autocatalytic reaction of **PyII** was faster than that of **FPyII** at lower concentrations of zinc reagent (compare entries 1 and 5), with increasing diisopropylzinc concentration, reactions of the former were inhibited more significantly than the latter (entries 1 to 8). Thus, at diisopropylzinc concentrations upward of 2.4 equivalents, the **FPyII** reactions were faster than those of **PyII** (compare entries 2 and 6, 3 and 7, 4 and 8). These results demonstrate that the extent of inhibition by excess diisopropylzinc is greater for **PyII** than for **FPyII** and is entirely absent for **PmII** (*i.e.* **PyII** > **FPyII** ≫ **PmII**).

This intriguing trend is in principle consistent with the floor-to-floor model. On the basis of the mechanistic knowledge gained so far, a minimal set of elementary steps can be compiled for the definition of the autocatalytic reaction pathway (the simplified floor-to-floor – 'SF' model,

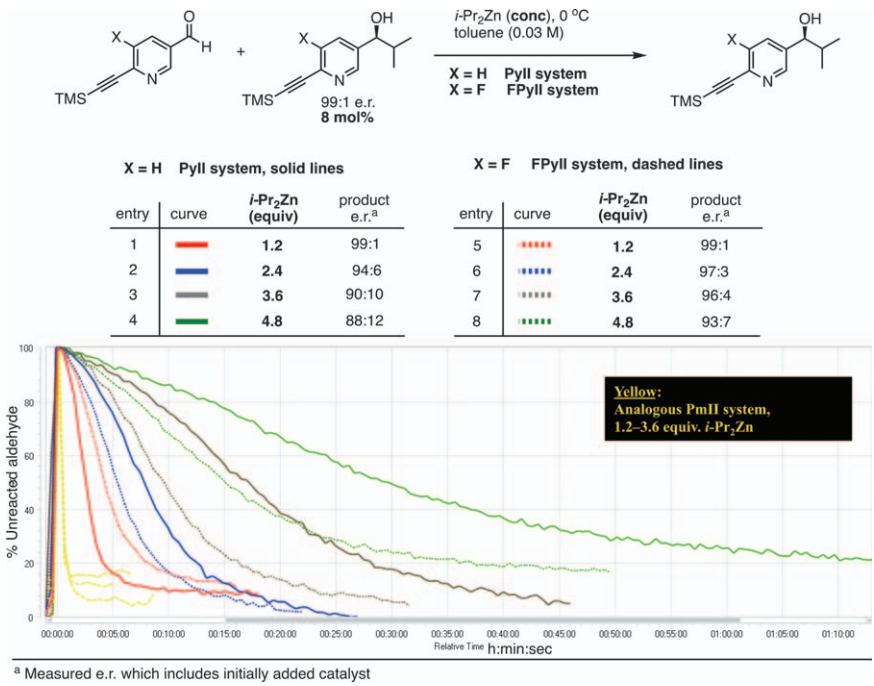

Figure 10.19 Inhibition of autocatalytic progression in **PyII** and **FPyII** systems with increasing diisopropylzinc. Reproduced from ref. 13 with permission from American Chemical Society, Copyright 2020.

Figure 10.20). These steps are: (1) equilibrium binding of substrate aldehyde (A) and diisopropylzinc (Z) to yield the N–Zn bound adduct (AZ), (2) equilibrium binding of the catalyst (C) to diisopropylzinc (Z) at the pyridyl arm (binding by only one arm is considered for simplicity) to yield the active species (CZ), (3) equilibrium binding of substrate aldehyde (A) to the catalyst-diisopropylzinc adduct (AZ) to yield the activated complex (ACZ), (4) alkyl transfer from the SMS tetramer active complex (ACZ) to yield the catalyst-bound product alkoxide adduct (PC), (5) equilibrium

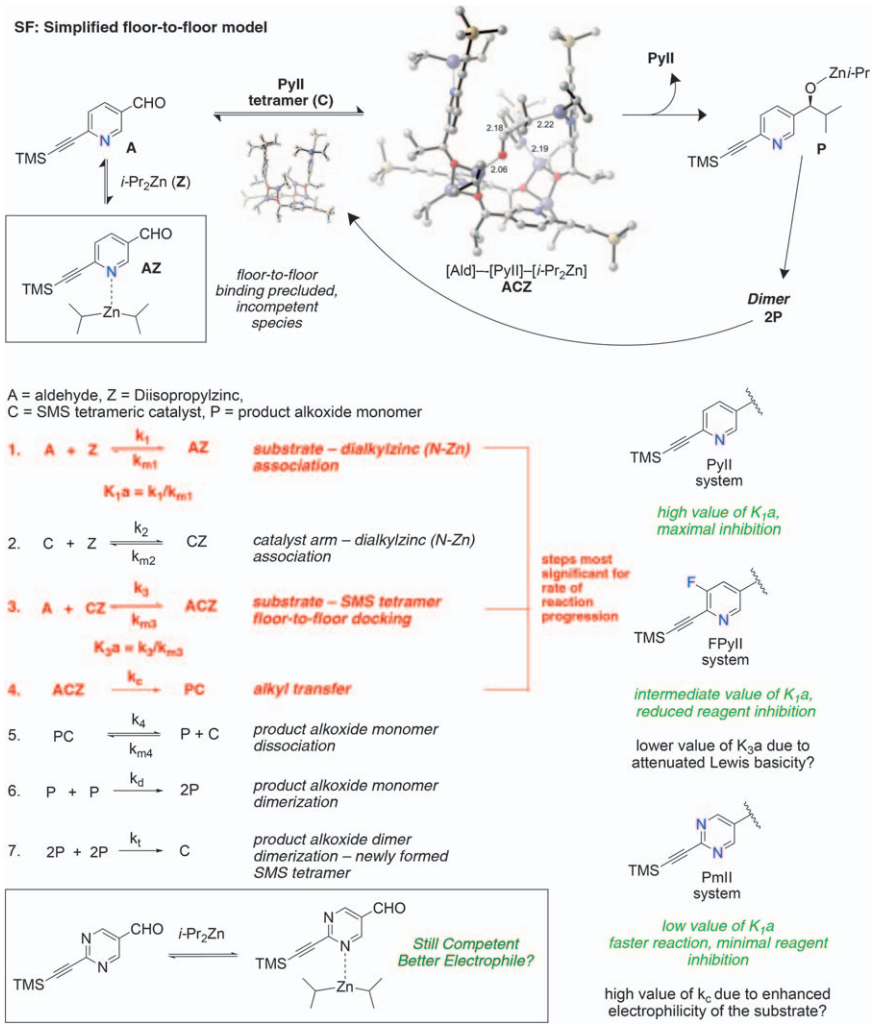

Figure 10.20 The SF model of autocatalysis. Steps affecting the rate of reaction progression are highlighted in red. The consequence of these steps in the **PyII**, **FPyII,** and **PmII** systems are indicated. Adapted from ref. 13 with permission from American Chemical Society, Copyright 2020.

dissociation of the product monomer alkoxide (P) to regenerate the SMS tetramer (C), (6) dimerization of the monomeric alkoxide (P) product to a dimeric unit (2P), and (7) dimerization of the dimeric unit (2P) to yield the newly constituted SMS tetramer (C). Rate constants for each step are designated. This is a simplified picture of the actual catalytic process and additional steps can be envisaged. For example, the binding of two molecules of diisopropylzinc to the catalyst are ignored; the order of binding of the reagent and aldehyde to the SMS tetramer may be different than the one suggested here; reagent binding to the product alkoxide may exist; the precise mechanism of tetramer reformation is unclear; the contribution of an uncatalyzed background alkylation is ignored. However, the scheme incorporates all fundamental binding events necessary and sufficient to achieve compatibility with the 'SMS tetramer – floor to floor' (SF) autocatalysis model.

This model could qualitatively reproduce the autocatalytic reaction profiles for the **PyII** system, including the inhibitory effect of diisopropylzinc.[13,72] Model simulations reveal that among the seven proposed elementary steps, the rate of reaction progression is sensitive only to the kinetic parameters of steps 1, 3, and 4 (Figure 10.20, red) in the following manner: (1) decreasing the association constant K_{1a} results in faster reactions and decreasing extent of diisopropylzinc inhibition, mimicking the transitions from the **PyII** (to **FPyII**) to **PmII** systems, (2) an increase in the value of K_{3a} results in faster reactions, and (3) an increase in the value of k_c results in faster reactions.

To a first approximation, the relative rates of the **PyII**, **FPyII**, and **PmII** systems, and the differences in severity of diisopropylzinc inhibition originate from divergent contributions from the three autocatalytic-progression determining steps in the SF model (Figure 10.20). Considering the Lewis basicity of the aromatic nitrogen atoms, the K_{1a} values for the three systems are expected to be in the order: **PmII** $\ll$ **FPyII** $<$ **PyII**.[78–80] Moreover, the adduct for the pyrimidine system is in principle, a competent species because floor-to-floor binding is still feasible with the second pyrimidine nitrogen atom. The binding constant for reagent coordination to this second nitrogen (necessary to render the adduct incompetent) is expected to be very low. Taken together, these factors must contribute to a very low effective value of K_{1a} in the pyrimidine system, thus accounting for its extraordinary rate and absence of inhibitory behavior (this is reproduced in the model simulations). The qualitative prediction of K_{3a} and k_c is not straightforward. In the three systems, the Lewis basicity of the substrate nitrogen atoms and the Lewis acidities of the unsaturated tetramer zinc atoms follow opposite trends, thus complicating a comparative estimate of the association constant for step 3. Similarly, the nucleophilicity of the catalyst-arm bound diisopropylzinc molecule and the electrophilicity of the bound substrate follow opposite trends in the three systems, which complicate a comparative estimate of the alkyl transfer rate constant. An interplay of contributions from these steps must dictate the overall trend of reaction progression. Kinetic simulations

are consistent with this hypothesis; modifying the values of K_{1a}, K_{3a}, and k_c to mimic the three systems can indeed reproduce their relative rate profiles. Furthermore, we speculate that the origin of the inverse rate dependence in the autocatalytic reactions is also a manifestation of the change in relative contributions of these steps with varying temperature.

Taken together, these preliminary modeling studies reveal how the substrate–reagent binding equilibrium, catalyst–substrate binding equilibrium, and the alkyl transfer rate contribute to the rate of autocatalytic progression, the origin of the extraordinarily rapid reactions in the **PmII** system, and the origin of inhibition in the **PyII** and **FPyII** systems.

10.4 Outlook: Competing Mechanistic Models

In the past two decades, numerous mechanistic models have been proposed for the Soai reaction. Common to these is the formulation that alkoxide aggregates (monomers, dimers, trimers, tetramers, and higher oligomers) are the active catalysts. These hypotheses have been developed predominantly on the basis of kinetic analysis of the reaction and aim to reproduce the rate behavior and observed enantiomeric amplification (for a summary, see ref. 42). It must be noted that the complexity of the reaction and likely presence of multiple equilibria, resulting from the dynamic nature of aggregate species may be the reason why different models (given enough parameters) may simultaneously succeed in being consistent with the observed kinetic behavior. Is it conceivable that multiple reaction pathways are operational? We believe that a far more comprehensive experimental data set, which will provide reaction profiles exploring extensive boundary conditions with a common system (preferably the 2-alkynylpyrimidine aldehyde **3b**, **3d**, or **3e** or the newly described pyridine system of **5b**) may be required to distinguish these models. Nonetheless, the consensus of the SMS tetramer model has been considerably strengthened by Soai's crystal structure studies.

10.4.1 The Significance of Structure–Activity Relationships

The structure–activity observations presented here are assumed to be different manifestations of a common mechanistic manifold and can stand as a test for any proposed model. The same catalyst should be operational in all five cases in Figure 10.21; cases 3–5 represent scenarios wherein the nonlinear, enantioselective, catalytic action of the active species is conveniently separated from the autocatalytic aspect of the Soai reaction. In other words, the only difference in cases 1 and 2, and case 3 for instance, is that the latter represents a conventional (non-autocatalytic) reaction system, in which the catalyst acts on a substrate that does not produce an active product. Similarly, case 5 demonstrates that this active species can also promote a diethylzinc transfer, although with lower selectivity (thus, only the alkynyl substituted substrates produce a positive NLE). This behavior is not surprising – just as any enantioselective catalyst can have a range of substrate

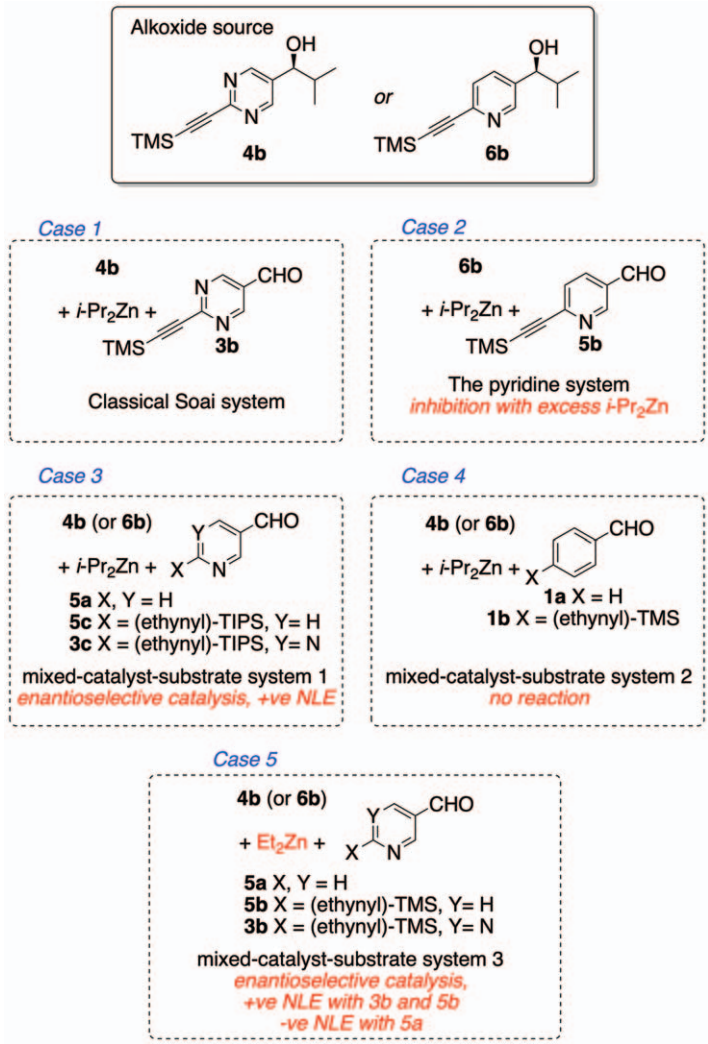

Figure 10.21 Various manifestations of a common mechanistic manifold.

scope, the active species in the Soai reaction also has one – although this is limited narrowly to the pyridine-3-carbaldehyde scaffold. Autocatalysis (cases 1 and 2) is simply a special case wherein the substrate is matched to the catalyst structure. This perspective dictates that a transition state model proposed for cases 3 or 5 should also be applicable to cases 1 and 2. Indeed it is predicted that the relative simplicity of the former systems (cases 3 and 5) may make investigations more tractable. Investigations of the catalytic action of **PyII** with surrogate substrate **5b** (an example of case 3, see Figures 10.11–10.14) were motivated by this thinking. An explanation for the

behavior of all five cases, including the inhibitory effect seen in the pyridine system (case 2) arises naturally through the SF model (simplified floor-to-floor, Figure 10.20).

10.4.2 The 'Hemiacetal Model'

Recently, a radically different mechanistic proposal has been presented by Trapp and co-workers.[81] On the basis of mass spectrometry and kinetic studies of the Soai reaction of substrate **3d**, a model invoking hemiacetal-like intermediates as active species was proposed (Figure 10.22). Previously in 2012, brown and co-workers provided evidence for the detection of a putative acetal-like species in the Soai reaction (see Figure 10.9), although an argument against its involvement in the catalytic cycle was forwarded in 2015 by Gridnev.[65,82] In their studies, Trapp and co-workers could detect hemiacetal-like intermediates by mass spectrometry. It is important to note that this hemiacetal (**A1** in Figure 10.22) constituted by an alkoxide monomer and substrate aldehyde, is different from Brown's acetal intermediate, which in contrast is composed of an alkoxide dimer and the aldehyde substrate. Trapp and co-workers found the autocatalytic reaction rate to have an order of 1.9 with respect to aldehyde concentration, suggesting the involvement of two aldehyde molecules in the (auto)catalytic cycle – one of them contributed by the hemiacetal fragment. The model could accurately reproduce rate behavior and enantiomeric amplification in the diisopropylzinc alkylation of **3d**. The crucial structures suggested are **A1–A4** (Figure 10.22). The **A1** hemiacetal is proposed to be the active species in equilibrium with the aldehyde (**3d**) and monomeric alkoxide (**M**). **A1** can bind both reactants in a Zn–O square interaction, leading to the trimeric intermediate **A2** preceding the irreversible alkyl transfer (k_6).

10.4.3 Comparison and Critiques of the Hemiacetal Model and the Floor-to-Floor Model

The Trapp proposal is an important development which warrants further investigation and refinement. In its current form, it does not provide a compelling explanation for some aspects of the structure–activity relationships observed previously (see Figure 10.21). For instance, the reason for the incompetency of benzaldehydes as substrates in mixed catalyst–substrate reactions is not apparent. The model structures do not indicate why the TIPS substituted systems (Soai reactions of **3c** and **5c**) fail to display amplifying autocatalysis. Initial rate studies of the **PyII** catalyzed diisopropylzinc transfer to the surrogate substrate pyridine-3-carbaldehyde (see Section 10.2.4 and ref. 71) indicate zeroth order dependence on aldehyde concentration – whether this observation is consistent with the hemiacetal mechanism remains to be seen. Crucially, since diisopropylzinc (found to have 0th order dependence on reaction rate – implying saturation binding) is

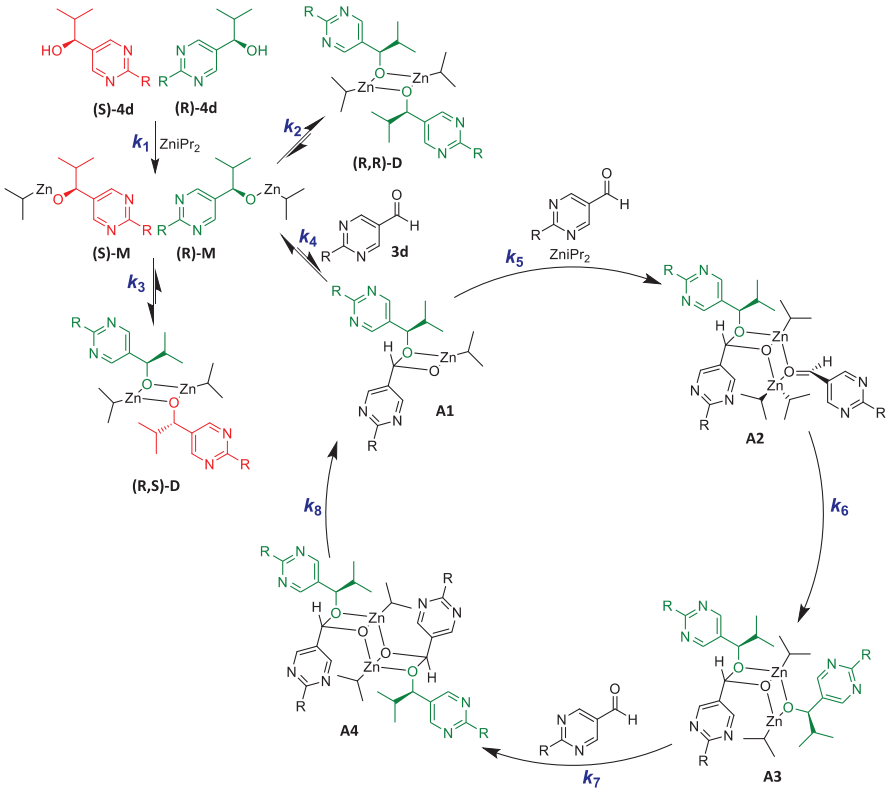

Figure 10.22 A mechanistic model by Trapp and co-workers that suggests hemiacetal-like intermediates (**A1–A4**) as active species. For simplicity, only the pathway for the *R* enantiomer is depicted. Adapted from ref. 81 with permission from John Wiley & Sons, Copyright © 2020 The Authors.

involved in only one associative step (k_5), its inhibitory effect observed in the pyridine system cannot be reconciled. A shortcoming of the structures of the Trapp proposal is the absence of any productive, associative interactions mediated through the aromatic nitrogen. Our studies strongly suggest that binding of both the Lewis basic centers (aromatic nitrogen and carbonyl oxygen) of the substrate to the active species is important for catalysis. A revision of the Trapp model that incorporates these considerations in the proposed hemiacetal-like intermediates is suggested as a way forward.

The floor-to-floor model is strongly supported by structural data and is consistent with a wide variety of empirical characteristics of the Soai system. Preliminary kinetic simulations of the SF model can provide an explanation for several intriguing rate phenomena. However, there is still a need for subjecting it to further, rigorous kinetic analysis. For example, the model does not provide an intuitive confirmation of the 2nd order rate dependence on aldehyde concentration in the autocatalytic reactions. It must be noted

that an apparent 2nd order does not necessarily imply a two-aldehyde bimolecularity and the observed order dependence can arise because of the complexity of the kinetic network. A trimeric model by Buhse and coworkers, in which binding of two aldehydes was never considered, was nonetheless shown to reproduce the 2nd order dependence.[42] Thus, especially in the complex autocatalytic pyrimidine and pyridine systems, care must be exercised in interpreting reaction orders. A kinetic analysis for the autocatalytic pyridine system has not been performed. The results described herein clearly indicate that the reaction rate of the autocatalytic pyridine system shows a negative order in diisopropylzinc concentration; obtaining reaction orders for the remaining constituents will allow further comparisons with the pyrimidine system. Furthermore, the nature of steps after the aldehyde alkylation, which include product dissociation and catalyst reformation is not well enunciated in the SF model.

10.5 Summary

The unprecedented observation of asymmetry amplifying autocatalysis in the alkylation of 5-(trimethylsilylethynyl)pyridine-3-carbaldehyde (**5b**) using diisopropylzinc was pivotal in deconstructing the Soai system. Comprehensive spectroscopic analysis of phenyl and pyridyl zinc alkoxides reveals the structural rationale for the assembly of the active, square-macrocycle-square (SMS) tetrameric autocatalyst that is formed by a pyridine-assisted cube-escape. Kinetic analysis with a surrogate substrate allows the interrogation of the crucial alkyl transfer step in the catalytic pathway. Augmented by computational studies, this approach led to the identification of the floor-to-floor catalysis model, wherein a two-point docking of the substrate to the autocatalyst is followed by alkylation from a preferred arm-bound diisopropylzinc molecule, leading to the homochiral product. The binding mode is inaccessible to the more stable, heterochiral SMS tetramer, thus providing a simple resolution for the origin of non-linearity.

The strategy of mixed catalyst–substrate experiments allowed extensive study of structure activity relationships in the pyrimidine and pyridine system. Ensuing results enable a formulation of the roles played by structural constituents in effecting catalysis and selectivity in the Soai reaction which are consistent with the predictions of the mechanistic model. The **FPyII** system (the Soai reaction of 5-fluoro-6-((trimethylsilyl)ethynyl)nicotinaldehyde (**5e**)) represents Lewis basicity (of the aromatic nitrogen atom) properties intermediate between the **PyII** and **FPyII** systems. A comparison of the three autocatalytic systems (**PyII**, **FPyII**, and **PmII**) uncovers an unexpected inhibitory effect of diisopropylzinc in the pyridine systems. A simple autocatalytic mechanism scheme derived from the floor-to-floor model (the SF model) qualitatively reproduces this effect with appropriate chemical parameters. Moreover, reaction simulations enable the identification of three mechanistic steps, which dictate autocatalytic rate progression. The low Lewis basicity of the pyrimidine as well as the presence of

two nitrogen atoms overcome the inhibitory effect and contributes to the extraordinary efficiency of the pyrimidine system. Likewise, an intricate balance of the equilibrium/rate constants of these steps result in the relative rates of the pyridine systems.

These results provide a compelling model of the autocatalyst identity, assembly, and its *modus operandi* as well as the origin of the non-linear effect. New structure–activity relationships are presented, and their rationalization is provided. The new findings should also stand as a test for any alternative mechanistic proposal.

Acknowledgements

We are grateful for generous financial support from the University of Illinois. S. V. A. is grateful to the University of Illinois for Graduate Fellowships. We thank the support services of the NMR, mass spectrometry, and microanalytical laboratories of the University of Illinois at Urbana – Champaign. Computational studies were performed in collaboration with Dr Adam Simon and Prof. Kendall N. Houk at the University of California, Los Angeles, USA. We thank Dr. Sharath Chandra Mallojjala for computing LUMO energies. We are grateful for stimulating discussions with Prof. Kenso Soai and Prof. Oliver Trapp.

References

1. Inspired from a similar quote on mathematical theorems and proofs that appears in D. R. Hofstadter, *Gödel, Escher, Bach: An Eternal Golden Braid*, Basic Books, New York, 20th anniversary edn, 1999.
2. F. C. Frank, *Biochim. Biophys. Acta*, 1953, **11**, 459–463.
3. H. Wynberg, *J. Macromol. Sci., Part A: Pure Appl. Chem.*, 1989, **26**, 1033–1041.
4. K. Mislow, *Collect. Czech. Chem. Commun.*, 2003, **68**, 849–864.
5. N. Oguni and T. Omi, *Tetrahedron Lett.*, 1984, **25**, 2823–2824.
6. M. Kitamura, S. Suga, K. Kawai and R. Noyori, *J. Am. Chem. Soc.*, 1986, **108**, 6071–6072.
7. K. Soai, S. Yokoyama, K. Ebihara and T. Hayasaka, *J. Chem. Soc., Chem. Commun.*, 1987, 1690.
8. M. Kitamura, S. Suga, H. Oka and R. Noyori, *J. Am. Chem. Soc.*, 1998, **120**, 9800–9809.
9. M. Kitamura, S. Okada, S. Suga and R. Noyori, *J. Am. Chem. Soc.*, 1989, **111**, 4028–4036.
10. D. Ferwick and H. B. Kagan, in *Topics in Stereochemistry*, ed. S. E. Denmark, John Wiley and Sons, 1999, ch. 5, vol. 22.
11. T. Satyanarayana, S. Abraham and H. B. Kagan, *Angew. Chem., Int. Ed.*, 2009, **48**, 456–494.
12. K. Soai, T. Shibata, H. Morioka and K. Choji, *Nature*, 1995, **378**, 767–768.
13. S. V. Athavale, A. Simon, K. N. Houk and S. E. Denmark, *J. Am. Chem. Soc.*, 2020, **142**, 18387–18406.

14. T. Shibata, H. Morioka, T. Hayase, K. Choji and K. Soai, *J. Am. Chem. Soc.*, 1996, **118**, 471–472.
15. T. Shibata, S. Yonekubo and K. Soai, *Angew. Chem., Int. Ed.*, 1999, **38**, 659–661.
16. I. Sato, T. Yanagi and K. Soai, *Chirality*, 2002, **14**, 166–168.
17. F. Lutz, T. Kawasaki and K. Soai, *Tetrahedron: Asymmetry*, 2006, **17**, 486–490.
18. M. Busch, M. Schlageter, D. Weingand and T. Gehring, *Chem. Eur. J.*, 2009, **15**, 8251–8258.
19. T. Kawasaki, S. Kamimura, A. Amihara, K. Suzuki and K. Soai, *Angew. Chem., Int. Ed.*, 2011, **50**, 6796–6798.
20. I. Sato, H. Urabe, S. Ishiguro, T. Shibata and K. Soai, *Angew. Chem., Int. Ed.*, 2003, **42**, 315–317.
21. K. Soai, T. Shibata and Y. Kowata, *Japan Kokai Tokkyo Koho, JP Pat.*, 9-268179, 1997. Application date: February 1 and April 18, 1996.
22. D. A. Singleton and L. K. Vo, *J. Am. Chem. Soc.*, 2002, **124**, 10010–10011.
23. K. Soai, I. Sato, T. Shibata, S. Komiya, M. Hayashi, Y. Matsueda, H. Imamura, T. Hayase, H. Morioka, H. Tabira, J. Yamamoto and Y. Kowata, *Tetrahedron: Asymmetry*, 2003, **14**, 185–188.
24. D. A. Singleton and L. K. Vo, *Org. Lett.*, 2003, **5**, 4337–4339.
25. Y. Kaimori, Y. Hiyoshi, T. Kawasaki, A. Matsumoto and K. Soai, *Chem. Commun.*, 2019, **55**, 5223–5226.
26. I. Sato, Y. Ohgo, H. Igarashi, D. Nishiyama, T. Kawasaki and K. Soai, *J. Organomet. Chem.*, 2007, **692**, 1783–1787.
27. T. Kawasaki, K. Jo, H. Igarashi, I. Sato, M. Nagano, H. Koshima and K. Soai, *Angew. Chem., Int. Ed.*, 2005, **44**, 2774–2777.
28. I. Sato, R. Yamashima, K. Kadowaki, J. Yamamoto, T. Shibata and K. Soai, *Angew. Chem., Int. Ed.*, 2001, **40**, 1096–1098.
29. T. Kawasaki, H. Tanaka, T. Tsutsumi, T. Kasahara, I. Sato and K. Soai, *J. Am. Chem. Soc.*, 2006, **128**, 6032–6033.
30. K. Soai, T. Kawasaki and A. Matsumoto, *Acc. Chem. Res.*, 2014, **47**, 3643–3654.
31. T. Kawasaki, M. Sato, S. Ishiguro, T. Saito, Y. Morishita, I. Sato, H. Nishino, Y. Inoue and K. Soai, *J. Am. Chem. Soc.*, 2005, **127**, 3274–3275.
32. T. Kawasaki, Y. Matsumura, T. Tsutsumi, K. Suzuki, M. Ito and K. Soai, *Science*, 2009, **324**, 492–495.
33. T. Kawasaki, Y. Okano, E. Suzuki, S. Takano, S. Oji and K. Soai, *Angew. Chem., Int. Ed.*, 2011, **50**, 8131–8133.
34. A. Matsumoto, H. Ozaki, S. Harada, K. Tada, T. Ayugase, H. Ozawa, T. Kawasaki and K. Soai, *Angew. Chem., Int. Ed.*, 2016, **55**, 15246–15249.
35. D. G. Blackmond, *Cold Spring Harbor Perspect. Biol.*, 2010, **2**, a002147.
36. R. M. Flügel, *Chirality and Life: A Short Introduction to the Early Phases of Chemical Evolution*, Springer-Verlag Berlin, Heidelberg, 1st edn, 2011.
37. I. Weissbuch and M. Lahav, *Chem. Rev.*, 2011, **111**, 3236–3267.
38. P. Cintas*Biochirality: Origins, Evolution and Molecular Recognition*, Springer-Verlag Berlin, Heidelberg, 1st edn, 2013.

39. B. Barabás and O. Fülöp, in *Advances in Asymmetric Autocatalysis and Related Topics*, ed. G. Palyi, R. Kurdi and C. Zucchi, Academic Press, 2017, ch. 3.
40. T. Gehring, M. Busch, M. Schlageter and D. Weingand, *Chirality*, 2010, **22**, E173–E182.
41. K. Soai, A. Matsumoto and T. Kawasaki, in *Advances in Asymmetric Autocatalysis and Related Topics*, ed. G. Palyi, R. Kurdi and C. Zucchi, Academic Press, 2017, ch. 1.
42. T. Buhse, M. E. Noble-Terán, J.-M. Cruz, J.-C. Micheau and C. Coudret, in *Advances in Asymmetric Autocatalysis and Related Topics*, ed. G. Palyi, R. Kurdi and C. Zucchi, Academic Press, 2017, ch. 4.
43. I. D. Gridnev, J. M. Serafimov, H. Quiney and J. M. Brown, *Org. Biomol. Chem.*, 2003, **1**, 3811–3819.
44. D. G. Blackmond, C. R. McMillan, S. Ramdeehul, A. Schorm and J. M. Brown, *J. Am. Chem. Soc.*, 2001, **123**, 10103–10104.
45. T. Buhse, *Tetrahedron: Asymmetry*, 2003, **14**, 1055–1061.
46. I. Sato, D. Omiya, H. Igarashi, K. Kato, Y. Ogi, K. Tsukiyama and K. Soai, *Tetrahedron: Asymmetry*, 2003, **14**, 975–979.
47. F. G. Buono and D. G. Blackmond, *J. Am. Chem. Soc.*, 2003, **125**, 8978–8979.
48. I. D. Gridnev, J. M. Serafimov and J. M. Brown, *Angew. Chem., Int. Ed.*, 2004, **43**, 4884–4887.
49. J. M. Brown, I. Gridnev and J. Klankermayer, in *Amplification of Chirality*, ed. K. Soai, Springer Berlin Heidelberg, Berlin, Heidelberg, 2008, pp. 35–65.
50. J. R. Islas, D. Lavabre, J.-M. Grevy, R. H. Lamoneda, H. R. Cabrera, J.-C. Micheau and T. Buhse, *Proc. Natl. Acad. Sci. U. S. A.*, 2005, **102**, 13743–13748.
51. K. Micskei, G. Póta, L. Caglioti and G. Pályi, *J. Phys. Chem. A.*, 2006, **110**, 5982–5984.
52. J. Klankermayer, I. D. Gridnev and J. M. Brown, *Chem. Comm.*, 2007, 3151–3153.
53. L. Schiaffino and G. Ercolani, *Angew. Chem., Int. Ed.*, 2008, **47**, 6832–6835.
54. K. Micskei, G. Rábai, E. Gál, L. Caglioti and G. Pályi, *J. Phys. Chem. B*, 2008, **112**, 9196–9200.
55. L. Schiaffino and G. Ercolani, *ChemPhysChem*, 2009, **10**, 2508–2515.
56. J.-C. Micheau, J.-M. Cruz, C. Coudret and T. Buhse, *ChemPhysChem*, 2010, **11**, 3417–3419.
57. M. Quaranta, T. Gehring, B. Odell, J. M. Brown and D. G. Blackmond, *J. Am. Chem. Soc.*, 2010, **132**, 15104–15107.
58. G. Ercolani and L. Schiaffino, *J. Org. Chem.*, 2011, **76**, 2619–2626.
59. I. D. Gridnev and A. K. Vorobiev, *ACS Catal.*, 2012, **2**, 2137–2149.
60. A. Matsumoto, T. Abe, A. Hara, T. Tobita, T. Sasagawa, T. Kawasaki and K. Soai, *Angew. Chem., Int. Ed.*, 2015, **54**, 15218–15221.
61. A. Matsumoto, T. Kawasaki and K. Soai, in *Advances in Asymmetric Autocatalysis and Related Topics*, ed. G. Palyi, R. Kurdi and C. Zucchi, Academic Press, 2017, ch. 10.

62. N. A. Hawbaker and D. G. Blackmond, *ACS Cent. Sci.*, 2018, **4**, 776–780.
63. D. G. Blackmond, *Chem. Rev.*, 2019, **120**, 4831–4837.
64. I. D. Gridnev and J. M. Brown, *Proc. Natl. Acad. Sci. U. S. A.*, 2004, **101**, 5727–5731.
65. T. Gehring, M. Quaranta, B. Odell, D. G. Blackmond and J. M. Brown, *Angew. Chem., Int. Ed.*, 2012, **51**, 9539–9542.
66. A. Matsumoto, S. Fujiwara, T. Abe, A. Hara, T. Tobita, T. Sasagawa, T. Kawasaki and K. Soai, *Bull. Chem. Soc. Jpn.*, 2016, **89**, 1170–1177.
67. T. Shibata, K. Choji, H. Morioka, T. Hayase and K. Soai, *Chem. Comm.*, 1996, 751–752.
68. T. N. Itaru Sato, *Synthesis*, 2004, **9**, 1419–1428.
69. K. Soai, S. Niwa and H. Hori, *J. Chem. Soc., Chem. Commun.*, 1990, 982–983.
70. C. Romagnoli, B. Sieng and M. Amedjkouh, *Eur. J. Org. Chem.*, 2015, **2015**, 4087–4092.
71. S. V. Athavale, A. Simon, K. N. Houk and S. E. Denmark, *Nat. Chem.*, 2020, **12**, 412–423.
72. S. V. Athavale, PhD thesis, University of Illinois, Urbana Champaign, 2019.
73. J. G. Noltes and J. Boersma, *J. Organomet. Chem.*, 1968, **12**, 425–431.
74. S. Jana, R. J. H. Berger, R. Frohlich, T. Pape and N. W. Mitzel, *Inorg. Chem.*, 2007, **46**, 4293–4297.
75. S. Schulz, R. Schäper, D. Krech, D. Schuchmann, D. Bläser and R. Boese, *Z. Anorg. Allg. Chem.*, 2011, **637**, 83–86.
76. W. Brüser, L. Hilfert, V. Lorenz, C. G. Hrib, K. Bode, A. Adam, J. Vogt and F. T. Edelmann, *J. Organomet. Chem.*, 2016, **806**, 77–82.
77. C. Hansch, A. Leo and R. W. Taft, *Chem. Rev.*, 1991, **91**, 165–195.
78. A. Albert, R. Goldacre and J. Phillips, *J. Chem. Soc.*, 1948, 2240–2249.
79. C. Laurence and J.-F. Gal, *Lewis Basicity and Affinity Scales: Data and Measurement*, John Wiley & Sons Ltd., 2010.
80. K. Clarke and K. Rothwell, *J. Chem. Soc.*, 1960, 1885.
81. O. Trapp, S. Lamour, F. Maier, A. F. Siegle, K. Zawatzky and B. F. Straub, *Chem. Eur. J*, 2020, **26**, 15871–15880.
82. I. D. Gridnev and A. K. Vorobiev, *Bull. Chem. Soc. Jpn.*, 2015, **88**, 333–340.

CHAPTER 11

Elucidation of Soai's Asymmetric Autocatalysis

OLIVER TRAPP

Department of Chemistry, Ludwig-Maximilians-University Munich, Butenandtstr. 5-13, 81377 Munich, Germany
Email: oliver.trapp@cup.uni-muenchen.de

11.1 Introduction

The ubiquitous mostly single-handedness of molecular building blocks (amino acids, carbohydrates, *etc.*) in nature, which are an integral feature of biologically relevant polymeric structures and metabolisms is considered a signature of life.[1–9] Interestingly, homochirality gives the impression of a complication, however it leads to an out-of-equilibrium chemical system per definition and is even a simplification, because it would create another dimension of complexity to specifically control every single stereocentre in building blocks, oligomers, and polymers. Several mostly theoretical approaches,[10–14] how biological homochirality developed from a predominantly achiral environment, have been investigated over recent decades and many findings show how enantiomer enrichment may have occurred by physical processes or chemical reactions. In Scheme 11.1 some proposals for asymmetric amplification of initial small imbalances by autocatalytic reactions are summarized[15–18] and have been reviewed in detail previously.[19,20]

Autocatalysis and in particular self-amplifying chemical processes are of great interest as they provide an explanation for the efficient replication of molecules with intrinsic error correction.[21,22] Asymmetric autocatalysis, enantioselective self-amplifying chemical processes[23–39] (see Figure 11.1),

Catalysis Series No. 43
Asymmetric Autocatalysis: The Soai Reaction
Edited by Kenso Soai, Tsuneomi Kawasaki and Arimasa Matsumoto

Published by the Royal Society of Chemistry, www.rsc.org

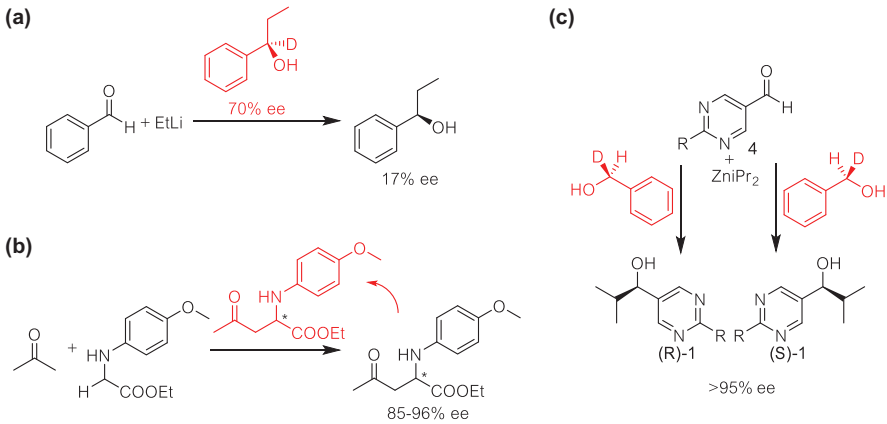

Scheme 11.1 Examples for asymmetric amplification of initial small imbalances by autocatalytic reactions introduced by (a) Alberts and Wynberg, (b) Tsogoeva, and (c) Soai and Kawasaki. R = –C≡C–C(CH$_3$)$_3$.

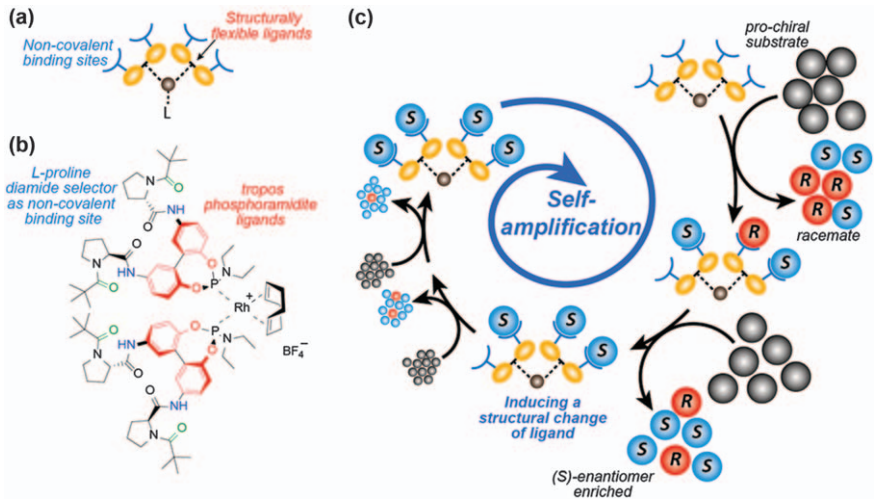

Figure 11.1 Example for enantioselective self-amplifying catalysis. (a) The stereodynamic self-amplifying catalyst is designed with non-covalent binding sites to interact with the targeted product enantiomers formed in the catalyzed reaction. (b) Structure of a rhodium(I) complex with tropos phosphoramidite ligands which are self-aligned upon preferential interaction of the non-covalent binding sites with one of the formed product enantiomers. (c) Turnover steps leading to enantioselective self-amplifying catalysis. After activation of the pre-catalyst the product is formed in no or low enantioselectivity at the catalytically active metal center. The catalyst interacts at the product interaction sites with the initially formed racemic reaction product. This product–catalyst interaction induces a change in the catalyst structure, which leads to enhanced enantioselectivity of the catalyst.

and recycling processes[40] are fundamental symmetry breaking mechanisms[41] and might be related to the emergence of life.[42–47]

In asymmetric transformations – catalytic and non-catalytic – it is expected that the enantiomeric excess (ee) of the reagent or catalyst used will be transferred linearly to the product formation. Positive nonlinear effects (+NLE),[48–51] where an enantiomerically enriched reagent or catalyst leads to a significant increase in the product ee, are rarely observed. Mechanistic explanations for such reactions with a +NLE were discussed by Kagan[32,33,35,52] and Noyori[53,54] considering reversible monomer–dimer associations. Kitamura and Noyori discovered a reaction showing a strong +NLE, which involves the enantioselective addition of diethylzinc to benzaldehyde,[55] promoted by catalytic amounts of the β-aminoalcohol (−)-3-*exo*-(dimethylamino)isoborneol (DAIB) yielding (*S*)-1-phenylpropanol in high enantiomeric purity (see Scheme 11.2). The reaction mechanism and origin of high +NLE have been elucidated by kinetic measurement, alkyl scrambling experiments, single-crystal X-ray analysis, $^{1}H/^{13}C$ NMR studies, and cryoscopic molecular weight determination in benzene. Reaction of (−)-DAIB and dimethylzinc in a 1 : 1 molar ratio produces a single binuclear zinc chelate complex, which does not alkylate benzaldehyde but acts as a catalyst precursor. The alkylation proceeds *via* a binuclear zinc complex containing the (−)-DAIB auxiliary, an aldehyde ligand, and three alkyl groups, where it is the bridging alkyl group, rather than the terminal alkyls, that migrates from zinc to the aldehyde carbon. The reaction is first order in (−)-DAIB auxiliary, zeroth order in dialkylzinc. With aldehyde concentrations lower than 0.3 M, the reaction is first order in the aldehyde.

Frank[56] postulated a theoretical model leading to a spontaneous asymmetric synthesis. If dimers can be formed from their monomeric building blocks, *e.g.* by intermolecular interactions, they are of the same configuration (homochiral) or of opposite configuration (heterochiral). Since these homochiral and heterochiral dimers are diastereomeric to each other, they have different intrinsic properties, which are reflected in their solubility, rate of formation, and other physical properties. The formation of heterochiral dimers from an enantiomerically enriched mixture can increase the enantiomeric excess of the free monomeric major enantiomer.

In 1995, Soai[57–63] reported an extremely remarkable reaction. When pyrimidine-5-carbaldehyde **4** reacts with diisopropylzinc (*i*-Pr_2Zn) in the presence of a catalytic amount of pyrimidyl alcohol **1** with a low ee, asymmetric autocatalytic amplification of the enantiomeric excess gives the pyrimidine alcohol **1** with high ee as the final product (see Scheme 11.3).

Autocatalysis and amplification are also observed in pyridyl-3-carbaldehydes,[65–68] which was published in 1990, however the 2-alkynyl substituted pyrimidine analogs are superior in amplification of the ee. Even the presence of traces of chiral compounds[69,70] such as an extremely low ee of the initial catalyst of only $\sim 5 \times 10^{-5\%}$[71] or other chiral triggers like $^{1}H/^{2}H$, $^{12}C/^{13}C$, $^{14}N/^{15}N$, and $^{16}O/^{18}O$ isotopically labeled cryptochiral compounds,[72–79] cryptochiral compounds,[80] circularly polarized light,[81,82] enantiomorph crystals,[83–93] and

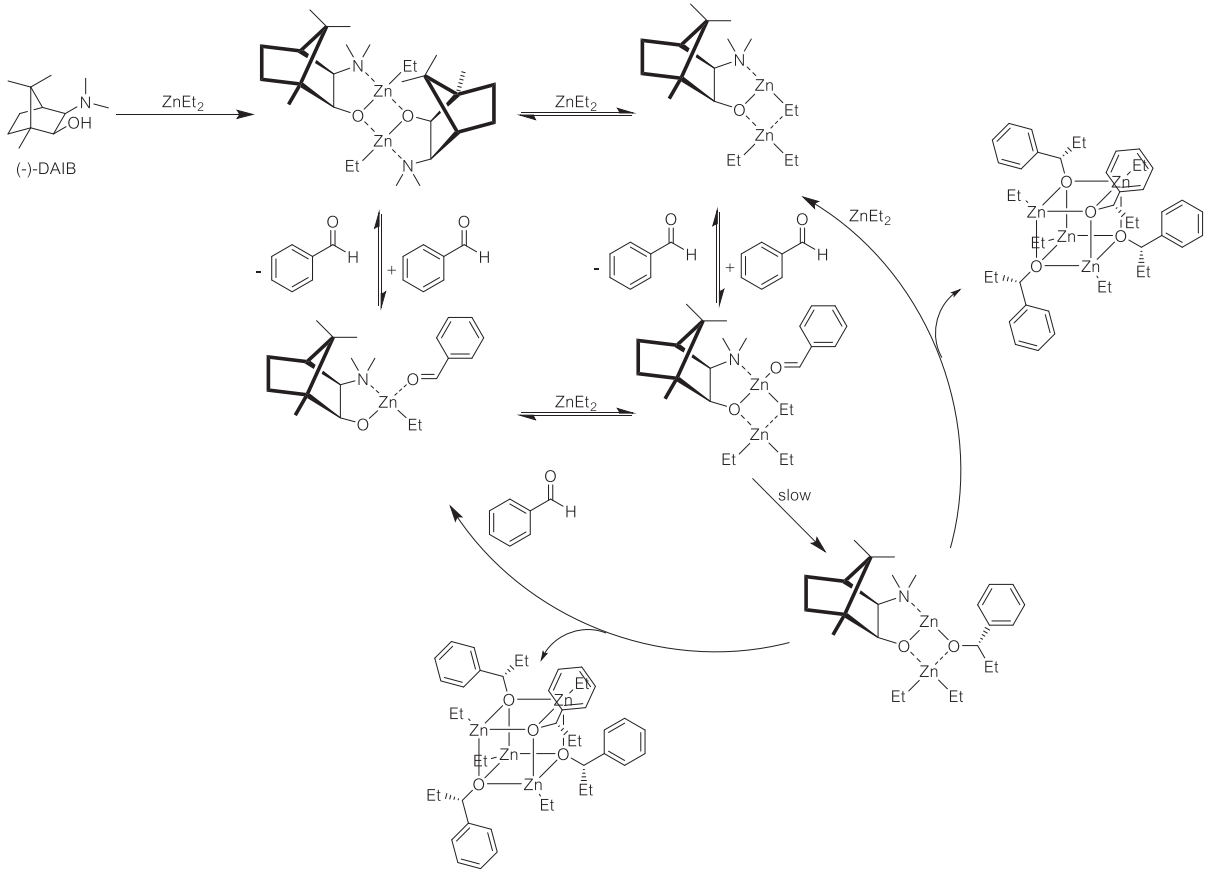

Scheme 11.2 Proposed mechanism of the enantioselective addition of diethylzinc to benzaldehyde, promoted by catalytic amounts of the β-aminoalcohol (−)-3-*exo*-(dimethylamino)isoborneol (DAIB) yielding (*S*)-1-phenylpropanol in high enantiomeric amounts as elucidated by Noyori and co-workers.

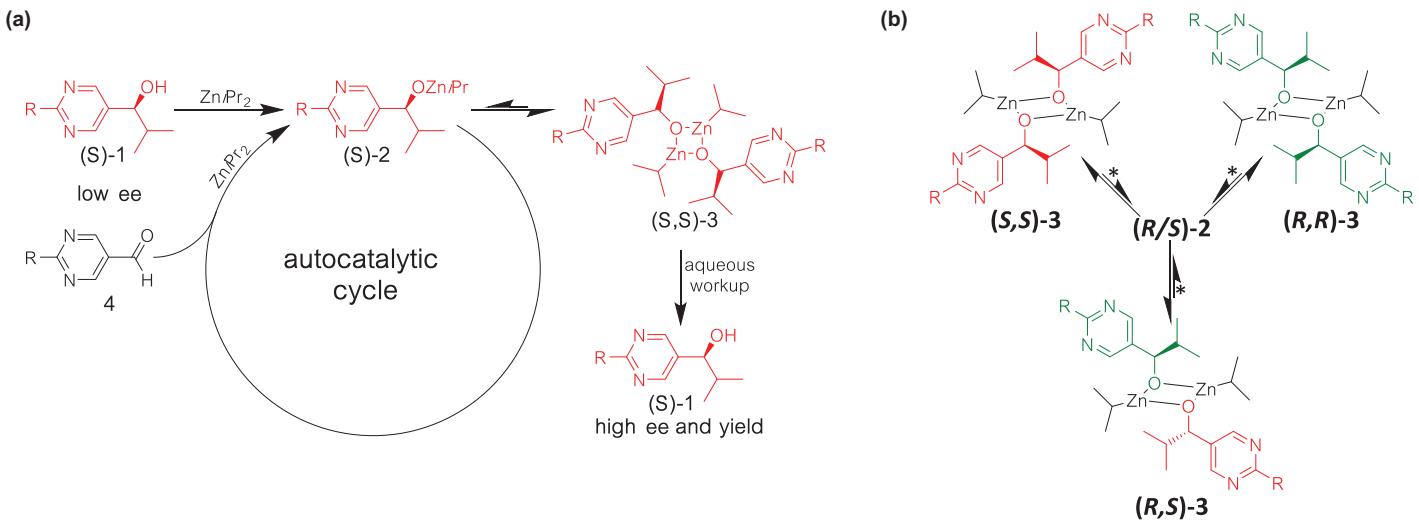

Scheme 11.3 Soai's asymmetric autocatalytic reaction. (a) Conversion of pyrimidine-5-carbaldehyde **4** with diisopropylzinc (i-Pr_2Zn) in the presence of a catalytic amount of pyrimidyl alcohol **1**. (b) Formation of homochiral (***R,R***)-**3**/(***S,S***)-**3** and heterochiral (***R,S***)-**3** dimers of the isopropylzinc pyrimidyl alkoxides **2**. The dimers can exchange their monomeric moieties without the formation of the monomers **2**. R = $(H_3C)_3C–C{\equiv}C–$. Adapted from ref. 64 with permission from John Wiley & Sons,

other compounds[94–99] are able to induce enantioselectivities, leading to an amplification greater than 99.5% ee in a few reaction cycles. The latest addition to this list of intriguing examples is the chiral induction triggered by a ferroelectric crystal of triglycine sulfate, whose polarization is altered by an electric field.[100]

A highly interesting feature of the reaction is that spontaneous symmetry breaking with stochastic distribution of the final (***R***)-**1** or (***S***)-**1** product is possible, even when no chiral additive is employed.[101]

The elucidation of the mechanism of Soai's asymmetric autocatalysis is highly challenging due to complex reaction equilibria and elusive intermediates.[102–111] It is well established that isopropylzinc pyrimidyl alkoxides **2** can form dimers, tetramers,[112,113] and oligomeric compounds. The dimers can be either homochiral ((***R***,***R***)-**3** or (***S***,***S***)-**3**) or heterochiral ((***R***,***S***)-**3**) (Scheme 11.3b).[114] It is important to note that the interconversion of dimer **3** can proceed by direct exchange of the monomeric moieties without formation of the monomers.[114] This could potentially proceed *via* tetrameric cube type structures which allow an exchange of Zn–alkoxide moieties without formation of the monomers in the equilibrium of the homo- and heterochiral dimers.

The implication of this equilibrium between the homochiral and heterochiral dimers is that the equilibrium constant for the heterochiral dimer formation K_{hetero} is twice the equilibrium constant for the homochiral dimer formation $K_{\text{hetero}}/K_{\text{homo}} = 2$.[115] Thus, a nonlinear effect can be well explained because an imbalance of the enantiomers leads to amplification as soon as more stable heterochiral dimers (***R***,***S***)-**3** have formed. Blackmond and Brown developed a model considering dimer **3** as catalytically active species based on reaction progress analysis by calorimetric measurements and NMR spectroscopy. These Zn–alkoxide dimers, tetramers,[112,113] and oligomers[116] were characterized by NMR spectroscopy and the group of Soai was able to isolate crystals, so that single-crystal X-ray diffraction analysis could be performed,[117] which showed ladder type structures, where the Zn–alkoxides are coordinated by the nitrogen atoms of the pyrimidyl moieties. These findings are supported by quantum chemical computations.[118] Kinetic studies corroborate these results with pronounced effects of the additive concentration[119] and ee leading to an induction period and a sigmoidal kinetic profile typical for autocatalytic processes. Schiaffino performed quantum chemical calculations of the kinetic constants at the M05-2X/6-31G(d) level of theory and investigated the effect of the aza group in the pyrimidine moiety to activate the zinc reagent in the tetrameric complex.[120–123]

In 2012 Brown, Blackmond and co-workers[124] reported the identification of a transient hemiacetal intermediate in the Soai reaction of 2-(adamantylacetylene-1-yl)pyrimidine-5-carbaldehyde and 2-(adamantylacetylene-1-yl)pyrimidyl alcohol by ^{1}H NMR spectroscopic kinetic studies. Gridnev and Vorobiev investigated by quantum chemical DFT calculations and kinetic analysis potential acetal intermediates. They concluded that the acetals are off-loop species because they are not precursors of the reaction product.[109] However it has to be pointed out that the structures shown in the publication of Gridnev *et al.* involve pyrimidin-5-ol derivatives (Scheme 11.4, structure P_2A in

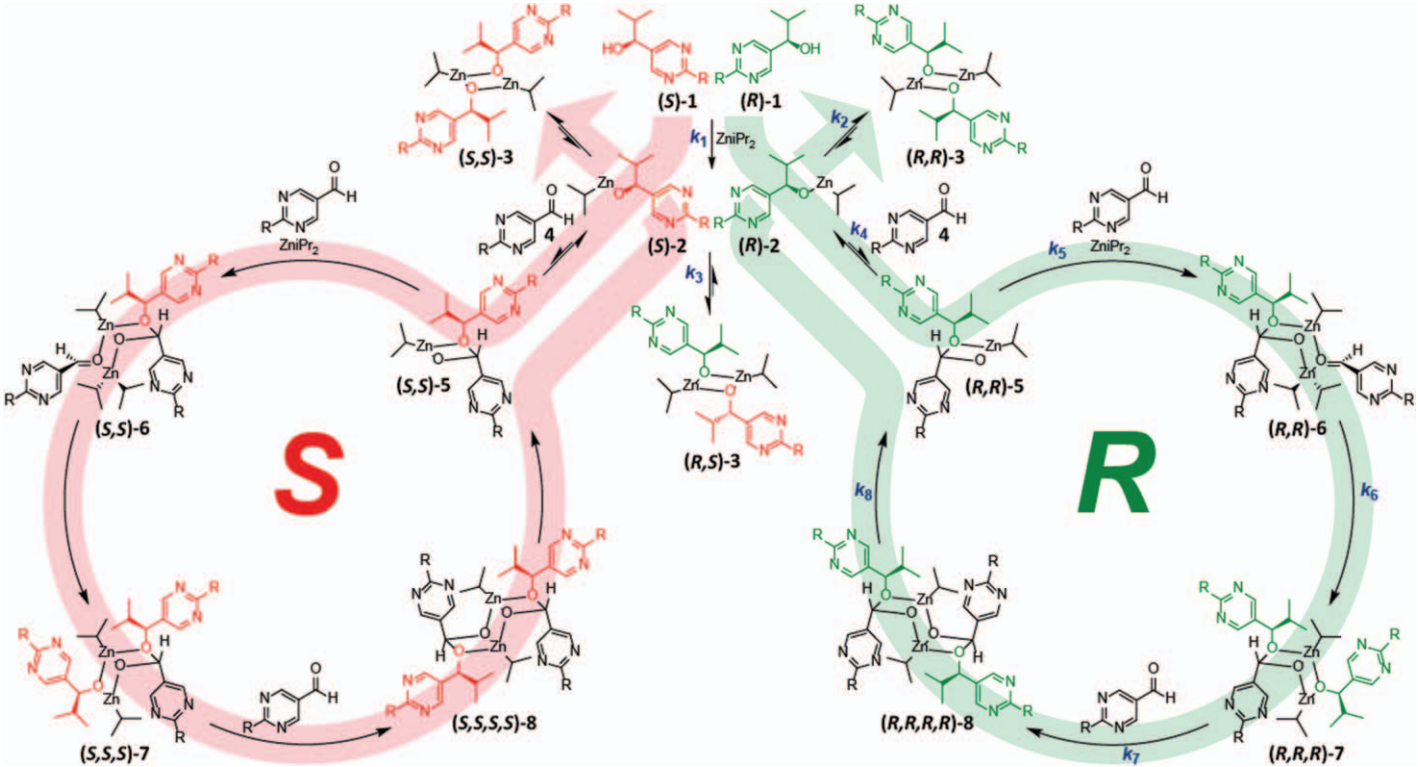

Scheme 11.4 Proposed mechanism of the Soai-reaction with the formation of the transient Zn–hemiacetalate catalyst **5** as the key step intermediate. All structures identified by the *in situ* high-resolution mass spectrometric experiments were considered in the mechanism. The green and red reaction arrows show the pathways to the reaction products, dimers **3**, *via* Zn–hemiacetalate catalysis. R = –C≡C–C(CH$_3$)$_3$. Reproduced from ref. 64 with permission from John Wiley & Sons, Copyright © 2020 The Authors.

ref. 109) and the assumed kinetic data and activation parameters (Table 3 in ref. 109) are not in agreement with experimentally measured data of the formation of hemiacetals.

In this context, another highly remarkable discovery was reported by Hawbaker and Blackmond, where hydroxy ethers interfere with the Soai reaction and even inhibit the reaction.[79]

Denmark and co-workers[125,126] investigated the Soai reaction using pyridyl-3-carbaldehyde as the surrogate ('Trojan-Horse' substrate) with focus on the role of the nitrogen atoms in the pyrimidine/pyridyl moiety, the structure of the Zn–alkoxides in solution by NMR spectroscopic studies, and *in situ* IR reaction monitoring. A mechanism is proposed, considering a 'cube escape' model, similar to the structures proposed in the enantioselective addition of dialkylzincs to aldehydes promoted by chiral β-amino alcohols, *i.e.* (−)-3-*exo*-(dimethyl-amino)isoborneol (DAIB) (*vide supra*, Scheme 11.2). Such Zn–alkoxides cubes have been discussed by Brown and co-workers[102] in the context of the Soai reaction as a potential tetrameric structure of the Zn–alkoxides.

It is interesting to note that tetrameric cube-type structures would allow the exchange of the monomeric Zn–alkoxide moieties without formation of the monomers in the equilibrium of the homo- and hetero-chiral dimers.

11.2 Looking Back to the Beginning of Our Mechanistic Investigations on Soai's Asymmetric Autocatalysis: An Analysis

We began our mechanistic investigations of Soai's asymmetric autocatalysis in 2009 with the goal of elucidating the underlying mechanism in order to apply these findings to the design of other autocatalytic processes and to explore possibilities for broadening the current reaction spectrum. First, we made a detailed analysis of the characteristics of the Soai reaction and compiled open questions:

(Q1) The Soai reaction is characterized by a significant amplification efficiency, which is hard to explain by equilibria resulting from homo- and hetero-chiral dimers, tetramers, or higher oligomers. What boosts this reaction to yield these exceptionally high ee's? What is the origin of the enantioselectivity?

(Q2) Why are pyrimidyl-5-carbaldehydes and also pyridyl-5-carbaldehydes privileged structures in this reaction? Is this due to the possible coordination of the nitrogen containing pyridyl or pyrimidyl rings and the associated activation of the alkyl zinc compounds as well as the formation of supramolecular structures?

(Q3) The Soai reaction is characterized by a prolonged induction period. What is the cause for this period and how can we precisely characterize this period? Which factors influence the induction period?

(Q4) There is an unusual inverse temperature dependence on the reaction kinetics, and the reaction rate increases significantly with decreasing reaction temperature.[127] Is there a process involved, which is favored at lower temperature? Higher aggregates of Zn–alkoxides are favored at lower temperature, but they are also formed by aging or crystallization. Why is no difference in the kinetics and induction period observed, when a reaction is doped with such additives?

(Q5) How can we continuously monitor the individual formation of the product enantiomers without quenching the reaction? Time-resolved quantification of the product alcohol enantiomers is mandatory for kinetic analysis, because it is the convolution of the complete reaction. So far only NMR spectroscopy, IR spectroscopy, and calorimetry were used for kinetic studies. These techniques give no information about the change of the enantiomeric excess during the reaction.

(Q6) Is it possible to identify and elucidate structures of intermediates or is the reaction really limited to the formation of dimeric, tetrameric, and oligomeric Zn–alkoxides.

(Q7) How can we perform a detailed kinetic analysis, not based on curve fitting algorithms but on experimentally determined steps?

We started with the preparation of a broad variety of unsubstituted and 2-substituted pyrimidine-5-carbaldehydes, and their corresponding pyrimidyl alcohols as racemate and enantiomerically pure compounds as reference substances and additives. Preparing racemic pyrimidyl alcohols by the Soai reaction is indeed challenging, which requires cleaned glassware and operations avoiding any chiral contamination.

11.3 Kinetic Analysis

For the continuous reaction monitoring of the individual product alcohol enantiomers and the aldehyde substrate we employed multiplexing chromatography,[128–131] which we developed for GC and HPLC separations to achieve a high-throughput even for complex mixtures. This HPLC setup in the flow-injection mode[132] turned out to be ideal to perform reaction progress analysis, because the analytical time intervals can be exactly controlled, and the reaction can be performed under inert and defined reaction conditions. Furthermore, it allows us to separate the product enantiomers by using the chiral stationary phase Chiralpak IB[133] (25 cm, i.d. 4.6 mm, particle size 5 μm) with *n*-hexane/THF 55 : 45 as the eluent (1.2 mL min^{-1}) (see Figure 11.2a), which solved question 5 of the task list (Q5, *vide supra*). The first injection takes place 1 min after adding the organozinc solution, the next injections followed with a time interval of 2.1 min (see Figure 11.2b). It is important to note that the injected sample is hydrolyzed by residual water in the eluent on the column, so that the total amount of the aldehyde and the (*R*)- and (*S*)-alcohol can be quantified.

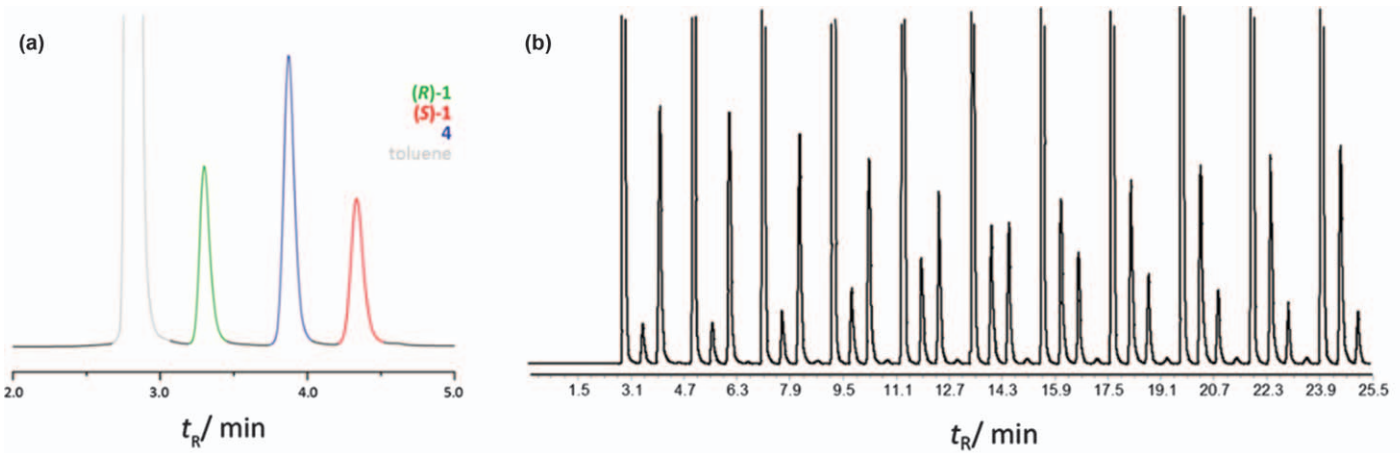

Figure 11.2 (a) Enantioselective HPLC chromatogram to separate the product enantiomers **1** of the Soai reaction and the 2-(*tert*-butylacetylene-1-yl)pyrimidyl-5-carbaldehyde **4** on a Chiralpak IB column (25 cm, i.D. 4.6 mm, particle size 5 μm) with *n*-hexane/THF 55 : 45 as the eluent (1.2 mL min^{-1}). The elution order is depicted by the colored peaks **(*R*)-1** in green, **(*S*)-1** in red, and **4** in blue. Toluene is used as the reaction solvent and is colored in gray. (b) Typical chromatogram for reaction progress analysis obtained by flow-injection analysis using enantioselective HPLC to separate the product enantiomers. (26.0 mmol L^{-1} 2-(*tert*-butylacetylene-1-yl)pyrimidyl-5-carbaldehyde **4**, 1.3 mmol L^{-1} (*R*)-2-(*tert*-butylacetylene-1-yl)pyrimidyl-5-(iso-butan-1-ol) (ee > 99.9%), and 40 mmol L^{-1} $Zn(iPr)_2$; 20 °C).

Furthermore, the Soai reaction is performed in toluene, so that under these conditions no change of the solvent is necessary and the reaction can be performed under the original reaction conditions.

Overall, we performed over 800 kinetic measurements with various pyrimidyl-5-carbaldehydes. Here I show an example data set, where we systematically varied the concentrations of the reactants and additives of the Soai reaction (2-(*tert*-butylacetylene-1-yl)pyrimidyl-5-carbaldehyde **4**: 10.6–41 mM (see Figure 11.3), ((*R*)-2-(*tert*-butylacetylene-1-yl)pyrimidyl-5-(iso-butan-1-ol) **(*R*)-1** (ee > 99.9%): 0.266–4 mM (see Figure 11.4); *i*-Pr_2Zn: 30–130 mM (see Figure 11.5).

Kinetic analysis of these data (see Figure 11.6) gives a reaction order of 1.9 in the aldehyde (2-(*tert*-butylacetylene-1-yl)pyrimidyl-5-carbaldehyde **4**), first order in the alcohol (2-(*tert*-butylacetylene-1-yl)pyrimidyl-5-(iso-butan-1-ol) **1**), and zeroth order in iPr_2Zn, confirming previous studies:[127]

$$\frac{d[ROH]}{dt} = k^0[RCHO]^{1.9}[ROH]^1[iPr_2Zn]^0 \qquad (11.1)$$

It is important to note, that the reaction orders in Soai's asymmetric autocatalysis are the same as determined by the initial rate method or by the graphical method,[134] which reflects the maximum rate, here the inflection point of the s-shaped autocatalytic reaction profile, which means that there is no change in the course of the reaction.

At the very beginning of our mechanistic studies we made a surprising observation, which attracted our attention. When we performed the HPLC separation of the reaction mixture using isopropanol, which is typically the standard additive solvent for the Okamoto type chiral stationary phases instead of THF, we observed the enantiomers of another compound connected by plateau formation with **4**. We identified these peaks as the isopropyl hemiacetals **(*R*)-5$_{iPr}$** or **(*S*)-5$_{iPr}$** (see Figure 11.7a), *i.e.* in the case of chiral alcohols diastereomeric hemiacetals are expected (*vide infra*).

Remarkably, these hemiacetals **5$_{iPr}$** are subject to a dynamic interconversion, which we investigated by temperature-dependent enantioselective dynamic HPLC (DHPLC)[135–143] (see Figure 11.7b). It is interesting to note that the enantiomers of the hemiacetals can be separated by enantioselective HPLC, which demonstrates also experimentally an important feature: The dynamic formation of a new stereocenter, in the case of a chiral alcohol the formation of diastereomers, which gives additional selectivity in the case of an enantiomerically pure alcohol, *i.e.* the alcohol formed in the Soai reaction.

The thermodynamic parameters of the formation of the hemiacetal **5$_{iPr}$** were determined by linear regression of the thermodynamic Gibbs free energies $\Delta G(T)$, obtained from the equilibrium constants K, *vs.* the temperatures T (correlation coefficient $r = 0.9949$) to be $\Delta G^0 = 3$ kJ mol^{-1}, $\Delta H^0 = -15.6$ kJ mol^{-1}, and $\Delta S^0 = -62.5$ J (K mol)$^{-1}$ (see Figure 11.8).

The activation enthalpies $\Delta H^{\ddagger}$ for the hemiacetal **5$_{iPr}$** formation and decomposition were obtained *via* the slope and the activation entropies $\Delta S^{\ddagger}$

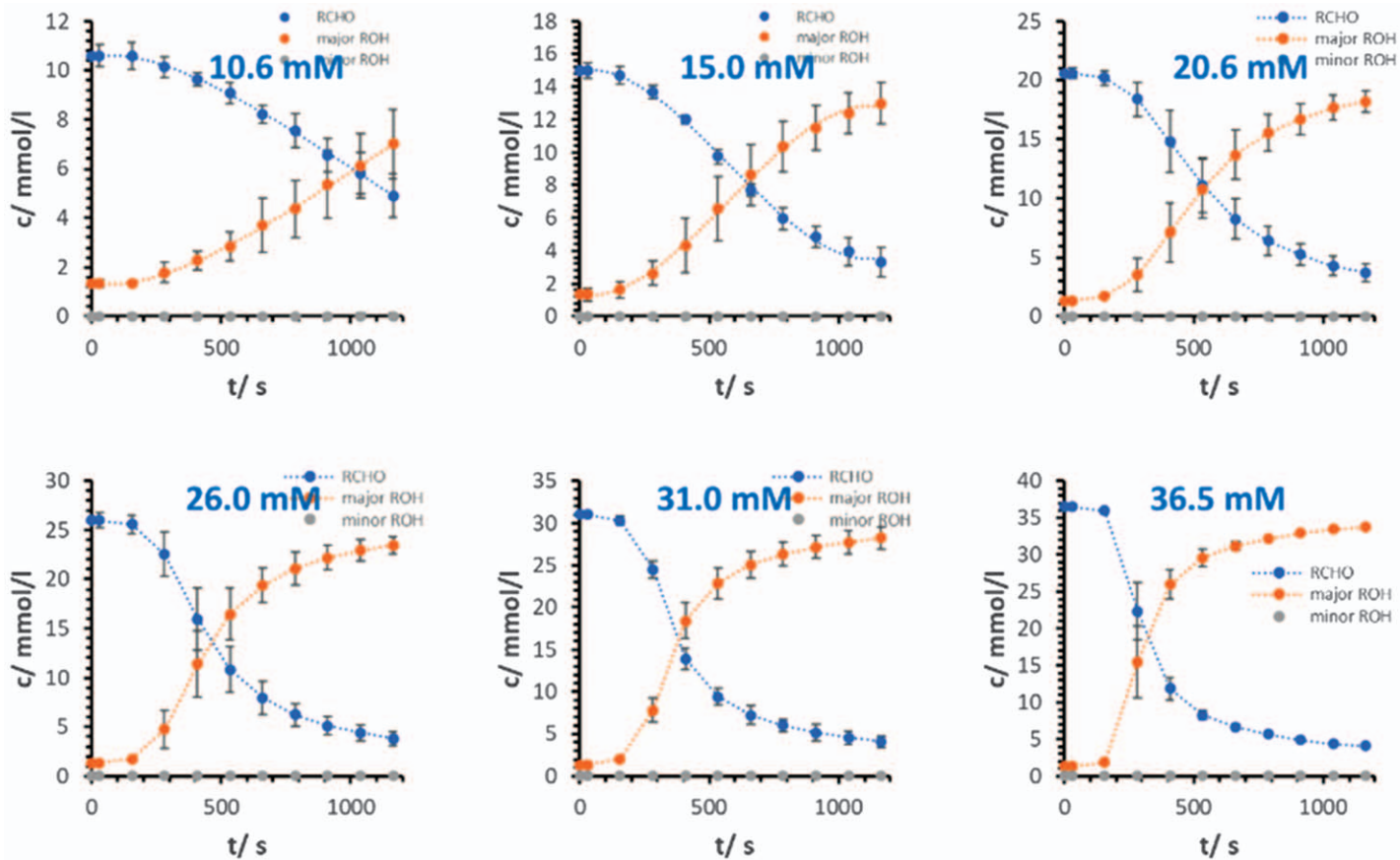

Figure 11.3 Reaction progress analysis by variation of the 2-(*tert*-butylacetylene-1-yl)pyrimidyl-5-carbaldehyde 4 concentration from 10.6 mmol L^{-1} to 36.5 mmol L^{-1} (1.3 mmol L^{-1} (*R*)-2-(*tert*-butylacetylene-1-yl)pyrimidyl-5-(iso-butan-1-ol) (ee > 99.9%), 40 mmol L^{-1} $Zn(iPr)_2$). All measurements were repeated three times.

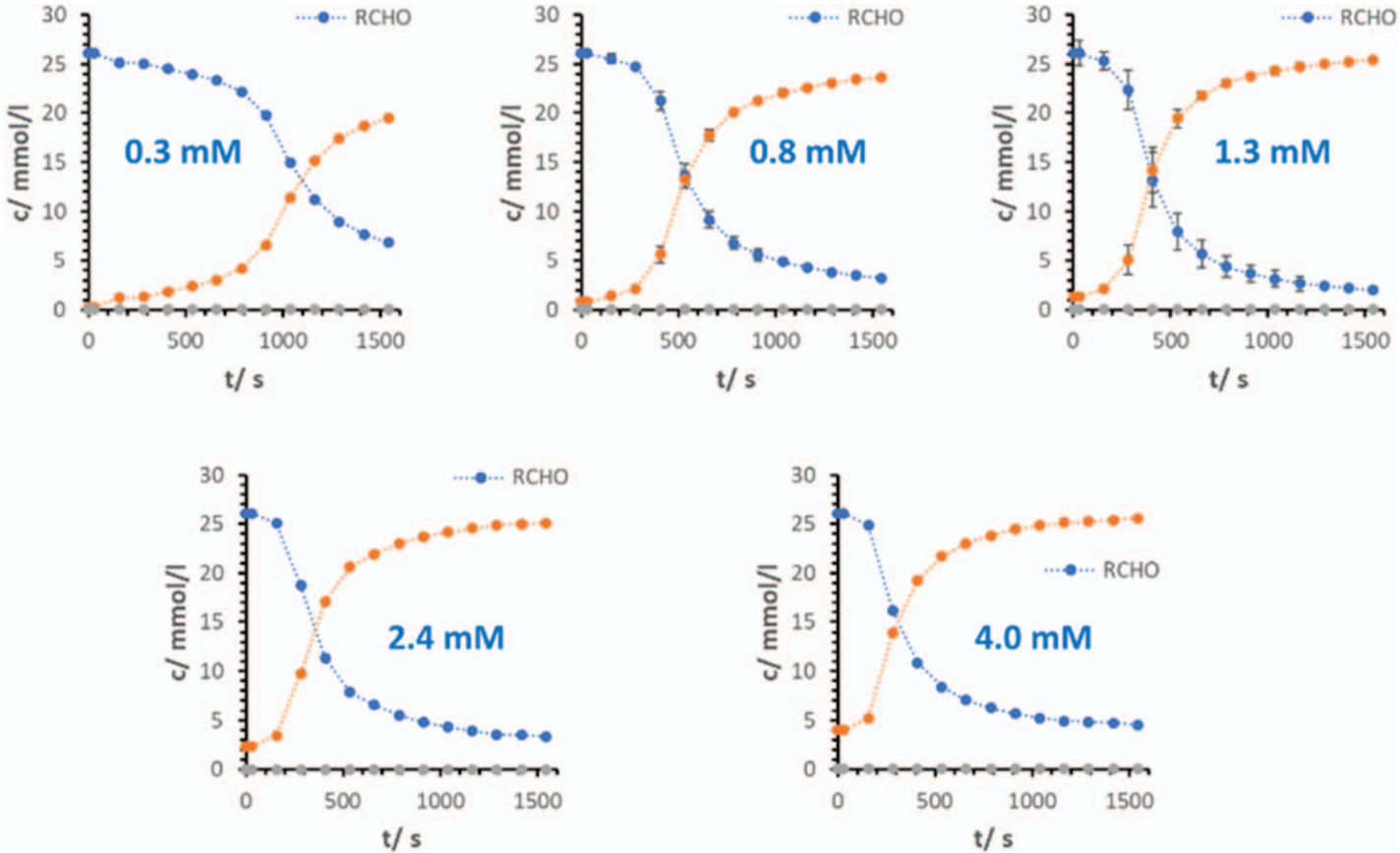

Figure 11.4 Reaction progress analysis by variation of the (*R*)-2-(*tert*-butylacetylene-1-yl)pyrimidyl-5-(iso-butan-1-ol) (ee > 99.9%) concentration from 0.266 mmol L^{-1} to 4 mmol L^{-1} (26.1 mmol L^{-1} 2-(*tert*-butylacetylene-1-yl)pyrimidyl-5-carbaldehyde, 40 mmol L^{-1} $Zn(iPr)_2$.

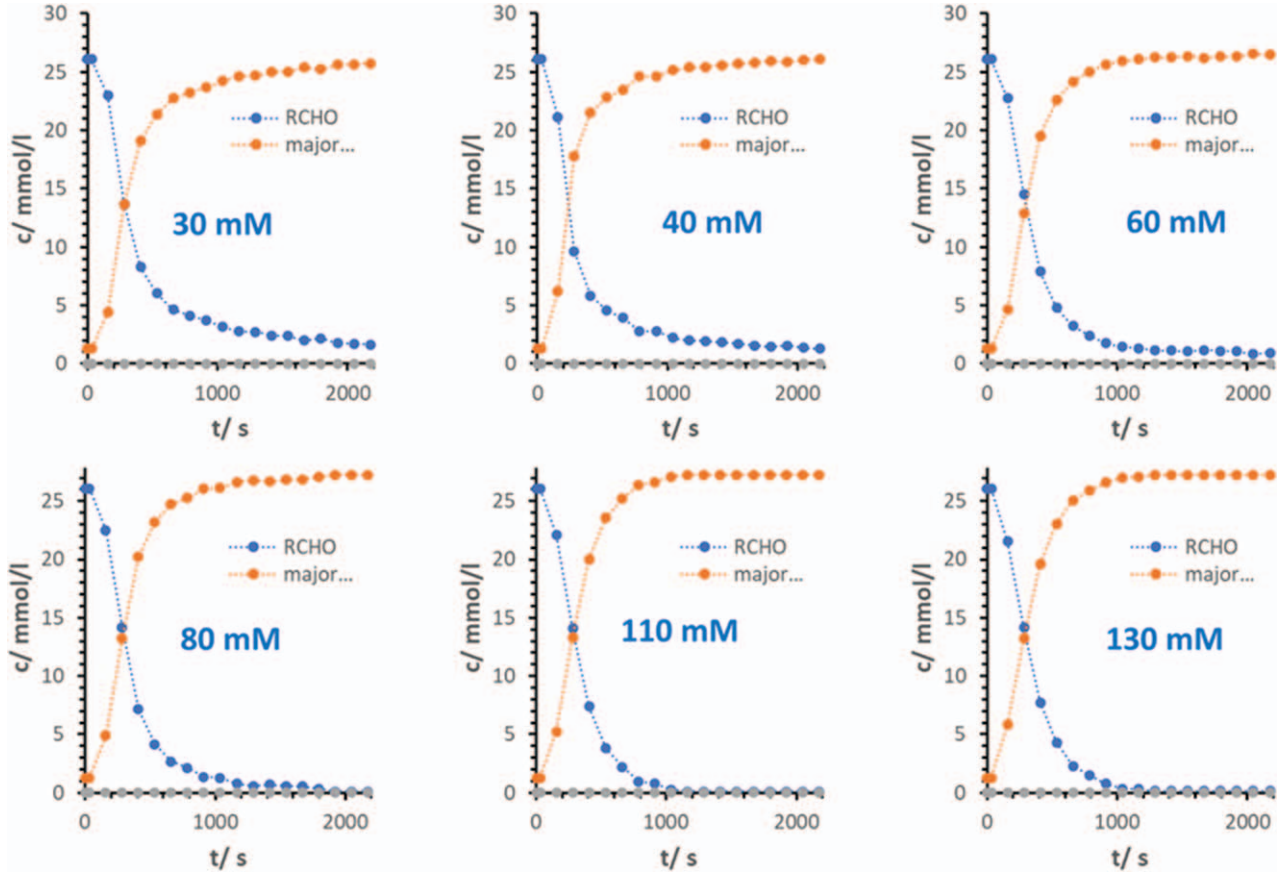

Figure 11.5 Reaction progress analysis by variation of the $Zn(iPr)_2$ concentration from 30 mmol L^{-1} to 130 mmol L^{-1} (26.1 mmol L^{-1} 2-(*tert*-butylacetylene-1-yl)pyrimidyl-5-carbaldehyde, 1.3 mmol L^{-1} (*R*)-2-(*tert*-butylacetylene-1-yl)pyrimidyl-5-(iso-butan-1-ol) (ee > 99.9%)).

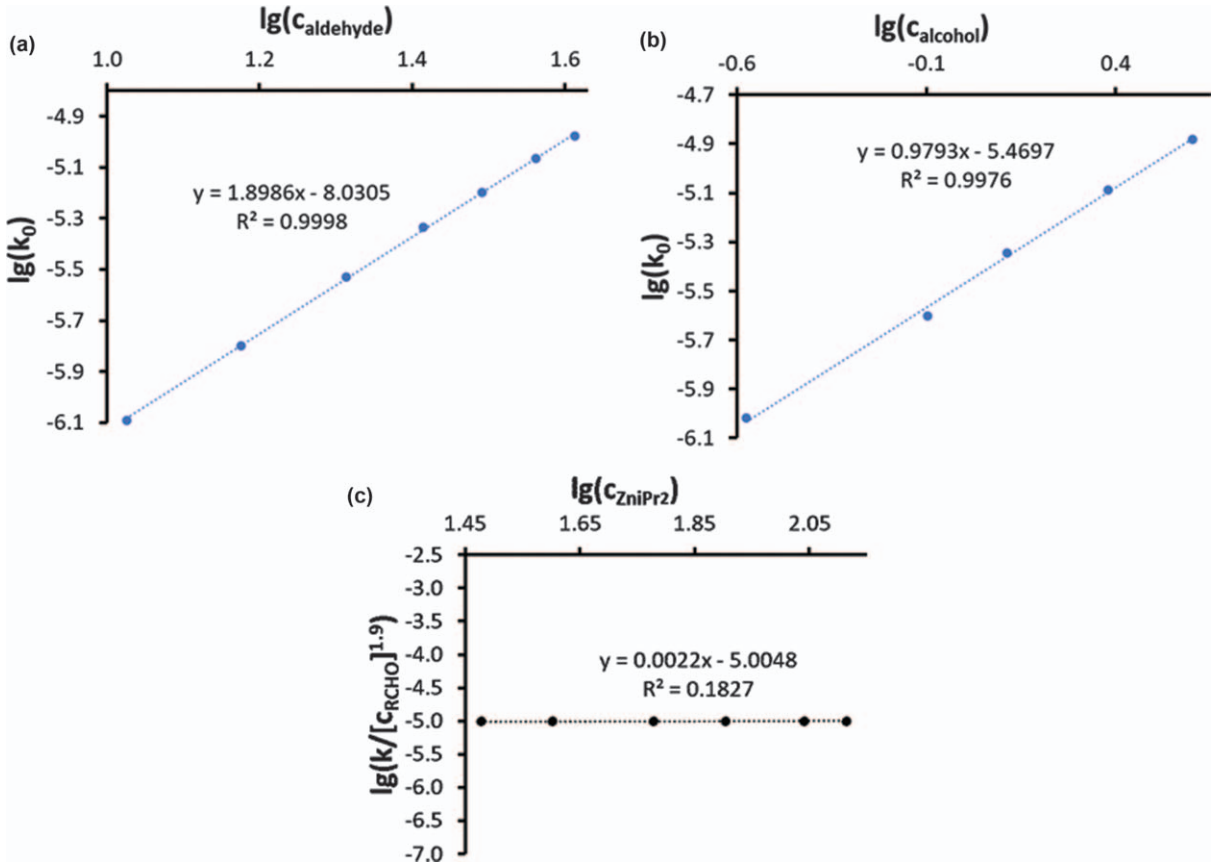

Figure 11.6 Determination of the reaction order for (a) aldehyde 4 by linear regression analysis of $\lg(k_0)$ *vs.* $\lg(c_{\text{aldehyde}})$, (b) for alcohol **1** by linear regression analysis of $\lg(k_0)$ *vs.* $\lg(c_{\text{alcohol}})$, and (c) for diisopropyl zinc by linear regression analysis of $\lg(k_0/[c_{\text{RCHO}})^{1.9}$) *vs.* $\lg(c_{\text{diisopropyl zinc}})$. The slope of the regression lines gives the reaction order.

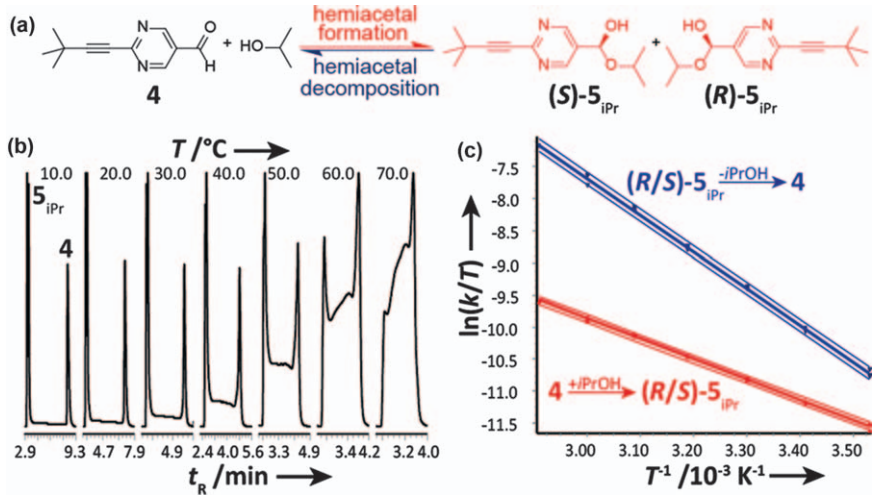

Figure 11.7 (a) Hemiacetal formation of 4 in the presence of i-propanol. (b) Temperature-dependent enantioselective DHPLC measurements of the formation of the hemiacetal $\mathbf{5_{iPr}}$ with isopropanol (Chiralpak IC-3 (15 cm, I.D. 4.6 mm, particle size 3 μm), *n*-hexane/isopropanol 60 : 40 (v/v), 1.0 mL min^{-1}. (c) Eyring plot for the determination of the activation parameters $\Delta H^{\ddagger}$ and $\Delta S^{\ddagger}$ of the hemiacetal formation (red data points) and the hemiacetal decomposition (blue data points) obtained from the DHPLC experiment. The upper and lower curves represent the error bands (21 data points each) of the linear regression with a level of confidence of 95%. Reproduced from ref. 64 with permission from John Wiley & Sons, Copyright © 2020 The Authors.

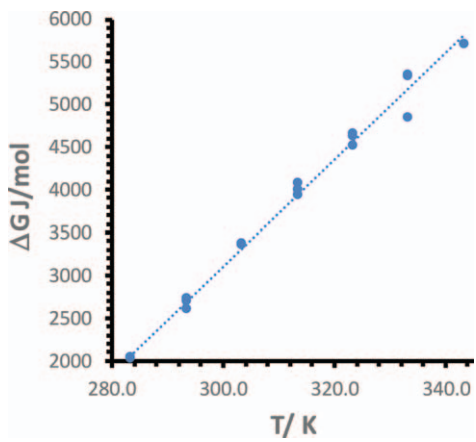

Figure 11.8 Determination of the thermodynamic parameters ΔH and ΔS by plotting the Gibbs free energy ΔG as a function of T.

via the intercept of the Eyring plots ($\ln(k/T)$ *vs.* $1/T$) (see Figure 11.7c). Deviations of the activation parameters $\Delta H^{\ddagger}$ and $\Delta S^{\ddagger}$ have been calculated by error band analysis of the linear regression with a level of confidence of 95%. The activation parameters of the hemiacetal **5$_{iPr}$** formation are $\Delta H^{\ddagger} = 26.3 \pm 0.2$ kJ mol^{-1} and $\Delta S^{\ddagger} = -195 \pm 34$ J (K mol)$^{-1}$ ($r = 0.9990$, residual deviation $s_y = 0.0306$) and the hemiacetal **5$_{iPr}$** decompositions are $\Delta H^{\ddagger} = 47.7 \pm 0.2$ kJ mol^{-1} and $\Delta S^{\ddagger} = -112 \pm 1$ J (K mol)$^{-1}$ ($r = 0.9994$, $s_y = 0.0630$) (see Figure 11.7c). The formation of hemiacetal **5$_{iPr}$** from **4** is endergonic, however this is a highly dynamic process and interestingly, the kinetic parameters $k_1(293\ \text{K}) = 4.1 \times 10^{-3}$ (mol s)$^{-1}$ and $k_{-1}(293\ \text{K}) = 1.3 \times 10^{-2}$ s^{-1} agree very well with the observed induction period, which is in the range of minutes depending on the substrate and additive concentrations.

These experimental observations attracted our attention. So, we started to examine this hypothesis, that the catalyst might be dynamically formed, which could explain the prolonged induction period we analyzed in question 3 of the task list (Q3, *vide supra*).

Furthermore, the thermodynamic data indicate that the formation of the hemiacetal is favored at lower temperature and if it is involved in the autocatalytic cycle, it correlates with the observation that the Soai reaction is accelerated at lower temperature which was question 4 of the task list (Q4, *vide supra*).

^{1}H NMR spectroscopic studies in CD_3OD reveal that the electron-deficient pyrimidine moiety of **4** and the unsubstituted pyrimidyl-5-carbaldehyde **4$_H$** promote the formation of deuterated methyl hemiacetals (characteristic hemiacetal proton at $\delta = 5.7$ ppm in 95% yield at room temperature, while for comparison benzaldehyde yields only 9% (see Table 11.1). Temperature-dependent measurements confirm the trend that the hemiacetal formation is favored at lower temperature. This formation of hemiacetals is also observed in toluene, the solvent used in the Soai reaction: Reaction of **4** and **4$_H$** with *rac*-2-methyl-1-phenylpropan-1-ol in [D_8]toluene gives diastereomeric hemiacetals in 11% and 9% yield, respectively. More important, the diastereomeric ratio of 1 : 2.6 for the unsubstituted pyrimidine hemiacetal improves to 1 : 5.2 for the 2-(*tert*-butylacetylene-1-yl substituted pyrimidine hemiacetal. These results are also in line with high-resolution mass spectrometric experiments we performed with the Soai alcohol and aldehyde, which allowed the identification and quantification of the formed hemiacetals.

More importantly, this reveals the unique properties of pyrimidine-5-carbaldehydes, which are excellent in forming hemiacetals (Q2, *vide supra*).

It is important to note that of course these properties can be tuned by the substituent in position 2 of the pyrimidine ring. However, this not only influences the formation of the hemiacetal, but changes also other properties, *e.g.* the solubility, which in turn influences the properties of the homo- and hetero-chiral dimers and the residence time of the catalyst in solution.

In this context, it is important to note that the formation of stereolabile hemiacetals offers the conceptual mechanism of minor enantiomer

Table 11.1 Determination of equilibrium constants of the formation of hemiacetals from benzaldehyde and pyrimidyl-5-carbaldehydes by reaction with alcohols. Quantification was performed by ^{1}H NMR spectroscopy. Reproduced from ref. 9 with permission from Frontiers, Copyright 2020.

Aldehyde	Alcohol	Hemiacetal	Yield/%	K/M^{-1}	K_{minor}/ M^{-1}	K_{major}/ M^{-1}
	CD_3OH	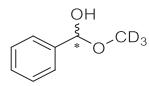	9	0.0040	—	—
 4_H	CD_3OH	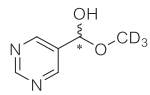	95	0.7733	—	—
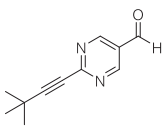 4	CD_3OH	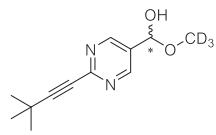	95	0.7722	—	—
 4_H	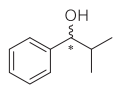	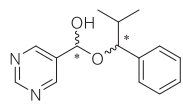	9	0.0544	0.0151	0.0393
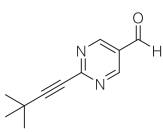 4	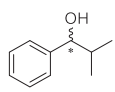	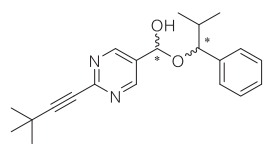	11	0.1195	0.0193	0.1002

recycling[40,144–147] leading to the amplification of the major enantiomer/diastereoisomer.

Hemiacetals, formed from the pyrimidine-5-carbaldehyde and its corresponding alcohol can function as a transient chiral ligand to activate the dialkylzinc reagent, very similar to the β-dialkylamino alcohols in Noyori's DAIB catalysis[53] or Blackmond's hydroxy ethers.[79]

The *in situ* formation of a transient catalyst by reaction or interaction of molecules participating in the reaction is a fundamental mechanism leading immediately to autocatalysis and amplification. Similar mechanisms are well known in substrate activated enzyme catalysis to regulate biochemical reaction networks and in artificial systems.[148,149]

11.4 Identification and Reaction Progress Analysis of Intermediates of Soai's Asymmetric Autocatalysis by *In Situ* Reaction High-resolution Orbitrap Mass Spectrometry

We were aware that although we had a good starting point and a strong hypothesis for the mechanism of the Soai reaction, it would take another 3 years of research to provide the capability for an *in situ* reaction study and to unambiguously identify possible intermediates during the reaction. The difficulty here is that, on the one hand, such intermediates of organometallic compounds are extremely sensitive and, on the other hand, the time window for such an investigation, as can be seen from the kinetic progress analysis, has to be very fast and with high sensitivity. In addition, we were also aware that such an investigation would require the highest precision and reproducibility, as this would represent a significant paradigm shift. Here we were focused on the clarification of question 1 (Q1), which is closely related to questions 2–4 (Q2–Q4) as well as the experimental implementation of questions 5 and 6 (Q5 and Q6, *vide supra*).

The technique of choice for this purpose was high-resolution mass spectrometry (Q6, *vide supra*). The relocation to the Ludwig-Maximilians-University Munich provided the opportunity to acquire an Orbitrap mass spectrometer, which opened up completely new opportunities for the identification and characterization of reactions.

We investigated the Soai reaction by *in situ* high-resolution mass spectrometric experiments, where the reaction is performed in a syringe. In these experiments there is no separation column involved to avoid quenching of the reaction intermediates. We monitored the course of the Soai reaction under inert conditions (anhydrous toluene, argon atmosphere) by feeding the reacting reaction mixture continuously (10 $\mu L\,min^{-1}$) but pulsed (time interval of 30 s) *via* a 5 μL sample loop of a 6-port valve (anhydrous toluene as eluent, flow rate 200 $\mu L\,min^{-1}$) into a high-resolution Orbitrap mass spectrometer using atmospheric pressure chemical ionization (APCI) under mild ionization conditions ($T = 150\ ^{\circ}C$, N_2).

To identify all intermediates and transient intermediates during the Soai reaction, all pulsed injections were summed up over the complete reaction progress and the mass range between *m*/*z* 180 and 800 in a first step (see Figure 11.9). This high-resolution mass spectrum shows the complexity of intermediates formed in the Soai reaction. We identified the alcohol **1a** and its fragment **1b**, the monomeric Zn–alkoxides **2a** and **2b**, the dimeric Zn–alkoxides **3a** and **3b** (different charge states), pyrimidine-5-carbaldehyde **4**, the Zn-complex of the hemiacetalate **5a**, the hemiacetal fragments **5b** and **5c**, a hydroxylated structure **5d**, which is probably formed by the ionization process, hemiacetal **5e** with iPr_2Zn coordinated to it (this can be bridged or

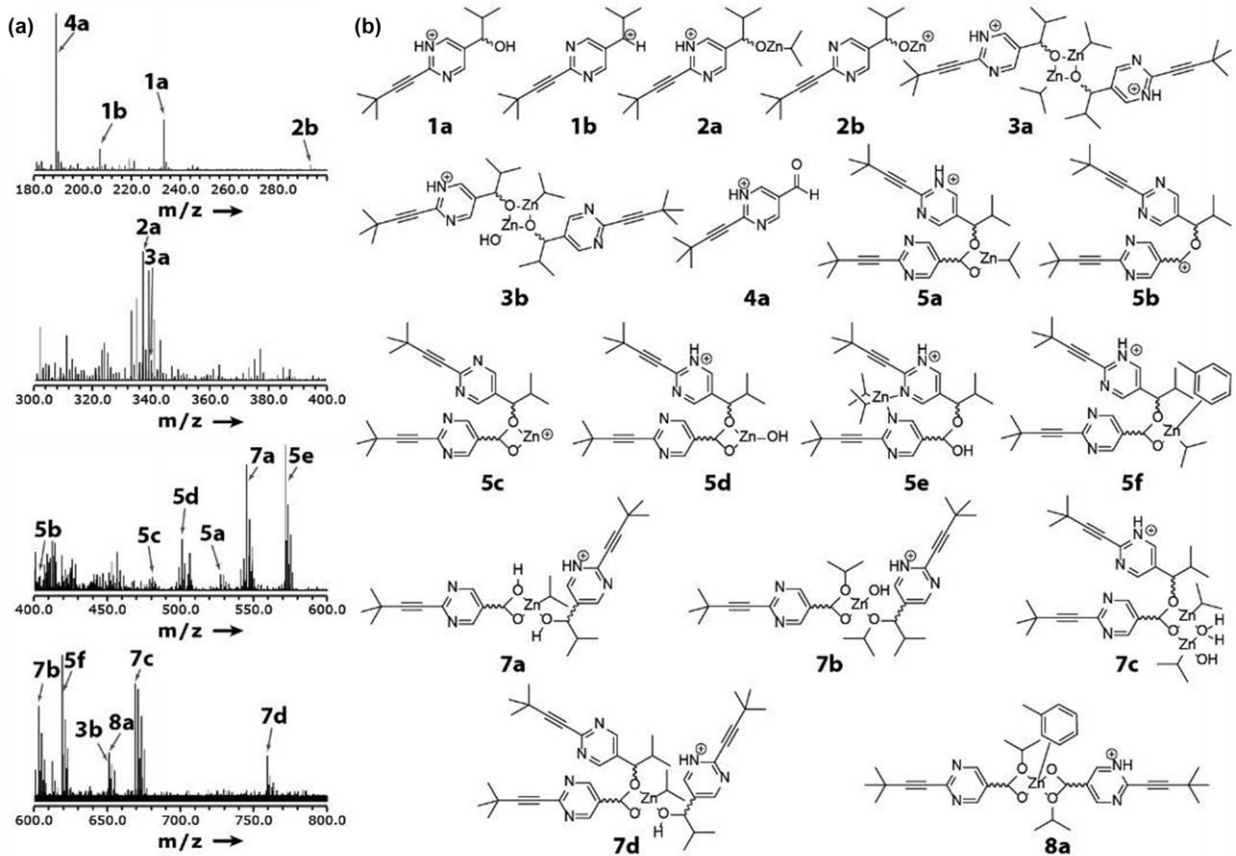

Figure 11.9 Identification of intermediates and transient intermediates of the Soai reaction by *in situ* high-resolution mass spectrometry. (a) Summarized mass spectra and assigned peaks covering *m*/*z* 180–800. (b) Structures identified by high-resolution MS. Reproduced from ref. 64 with permission from John Wiley & Sons, Copyright © 2020 The Authors.

open), and the hemiacetalate with coordinated toluene **5f**. Structures **7a–7d** are Zn–hemiacetalate complexes with another molecule or fragment of alcohol **1** coordinated, and structure **8** represents a dimeric Zn–hemiacetal complex.

The identification of the Zn complexes is facilitated by the characteristic isotope pattern of Zn (see Figure 11.10a, right mass spectrum). For

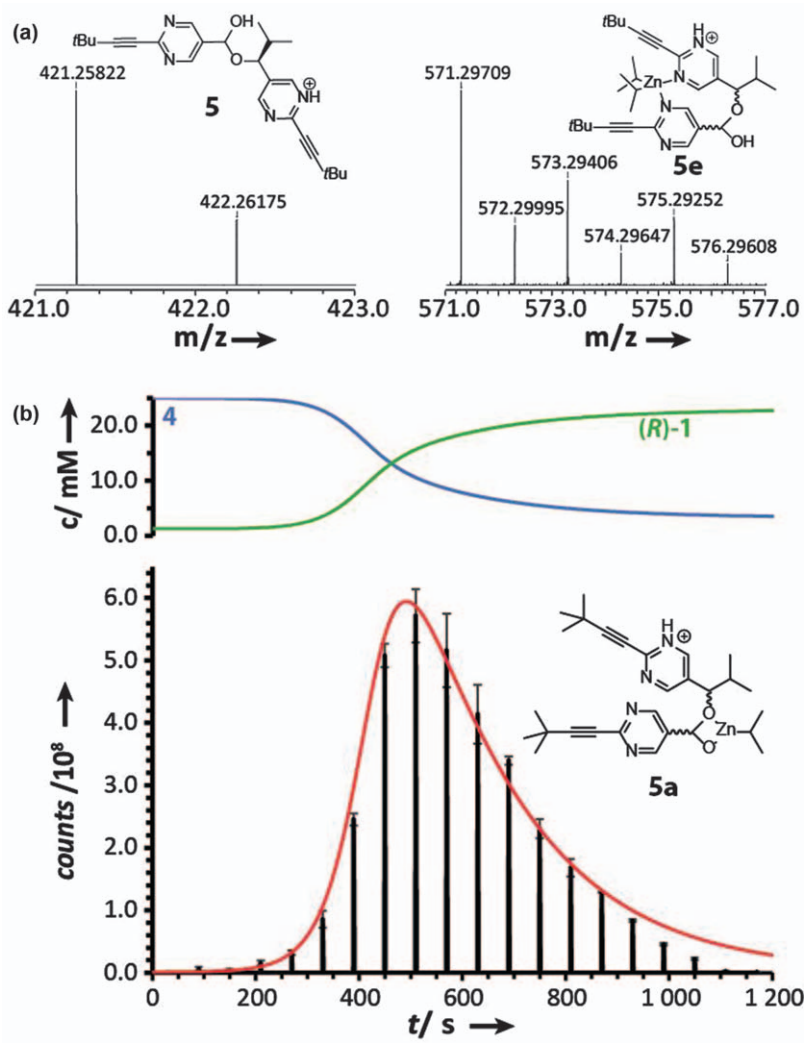

Figure 11.10 Investigation of the Soai reaction by *in situ* high-resolution mass spectrometry. (a) High-resolution mass spectrum of the hemiacetal **5** (left) and transient hemiacetal structure **5c** (right) obtained by *in situ* MS reaction monitoring of the Soai reaction. (b) Monitoring of the ion counts (bottom) of **5a** (*m/z* 527.234115) and **5e** (*m/z* 571.297085) *vs.* time during the Soai reaction (top). Reaction conditions: 25.0 mM **4**, 1.25 mM **(*R*)-1** (ee > 99.9%), and 50 mM *i*-Pr_2Zn in toluene at 20 °C. Reproduced from ref. 64 with permission from John Wiley & Sons, Copyright © 2020 The Authors.

comparison, the high-resolution MS spectrum on the left side in Figure 11.10a shows the formation of hemiacetal **5** (*m*/*z* 421.25822) by mixing **1** and **4** in toluene, which is the proof, that the hemiacetal is formed from the reactants of the Soai reaction in toluene. These structures were also confirmed by MS/MS measurements.

By the temporal resolution of the injection pulses in the experimental setup, the relative concentration of the transient hemiacetal intermediate **5** can be monitored in the course of the Soai reaction (see Figure 11.10b). Interestingly, the apex of this profile coincides with the inflection point of the sigmoidal kinetic profile of the Soai reaction (see Figure 11.10b, top), which suggests that the transient Zn–hemiacetalate **5** is slowly built up during the induction period, and is then amplified in the autocatalytic cycle and finally depleted.

The coordination of *i*-Pr_2Zn to the *N* atoms of the pyrimidine rings not only activates the zinc reagent, but also favors the formation of hemiacetals by spatial arrangement (tweezer effect) and electronic effects. Interestingly, no bridged pyrimidyl alcohols **1**, pyrimidyl alkoxides **2**, or pyrimidine-5-carbaldehydes **4** are observed, which can be attributed to the noncovalent nature of such complexes, which are not stable under the conditions of the APCI.

To investigate the role of the dialkylzinc reagent and the alcohol additive in the Soai reaction we performed mixing experiments. We systematically varied *i*-Pr_2Zn and diethylzinc (Et_2Zn) as a reagent in the reaction itself and to pre-form Zn–alkoxides **2**.

11.5 The Doping Experiment: Formation of a Transient Catalyst During the Autocatalysis

A doping experiment corroborates that the Soai reaction is catalyzed by a transient catalyst formed in the course of the reaction. For this purpose, we transferred the reaction solution of a running Soai reaction to a just started Soai reaction. Four Soai reactions (25 mM 2-(*tert*-butylacetylene-1-yl)-pyrimidyl-5-carbaldehyde **4**, 1.25 mM 2-(*tert*-butylacetylene-1-yl)pyrimidyl-5-(iso-butan-1-ol) (***R***)-**1** (ee > 99.9%), 20 °C, all concentrations are final concentrations after the addition of the iPr_2Zn solution) were prepared from the same stock solutions and distributed in 4 vials under inert reaction conditions. 2 vials were used as reference vials, one started simultaneously (1st vial) with a 2nd vial, in which the transient catalyst is formed during the reaction (see Figure 11.11).

The Soai reactions are triggered by the addition of iPr_2Zn (125 mM final concentration). After 210 s the 3rd Soai reaction is started by the addition of *i*-Pr_2Zn (125 mM final concentration). 218 s after the start of the reference reaction and the Soai reaction in the 2nd vial 60 μL of the reaction solution are transferred from the 2nd vial into the 3rd vial. The 2nd ref. (4th vial) was started after the completion of reactions 1 and 2. All reactions were

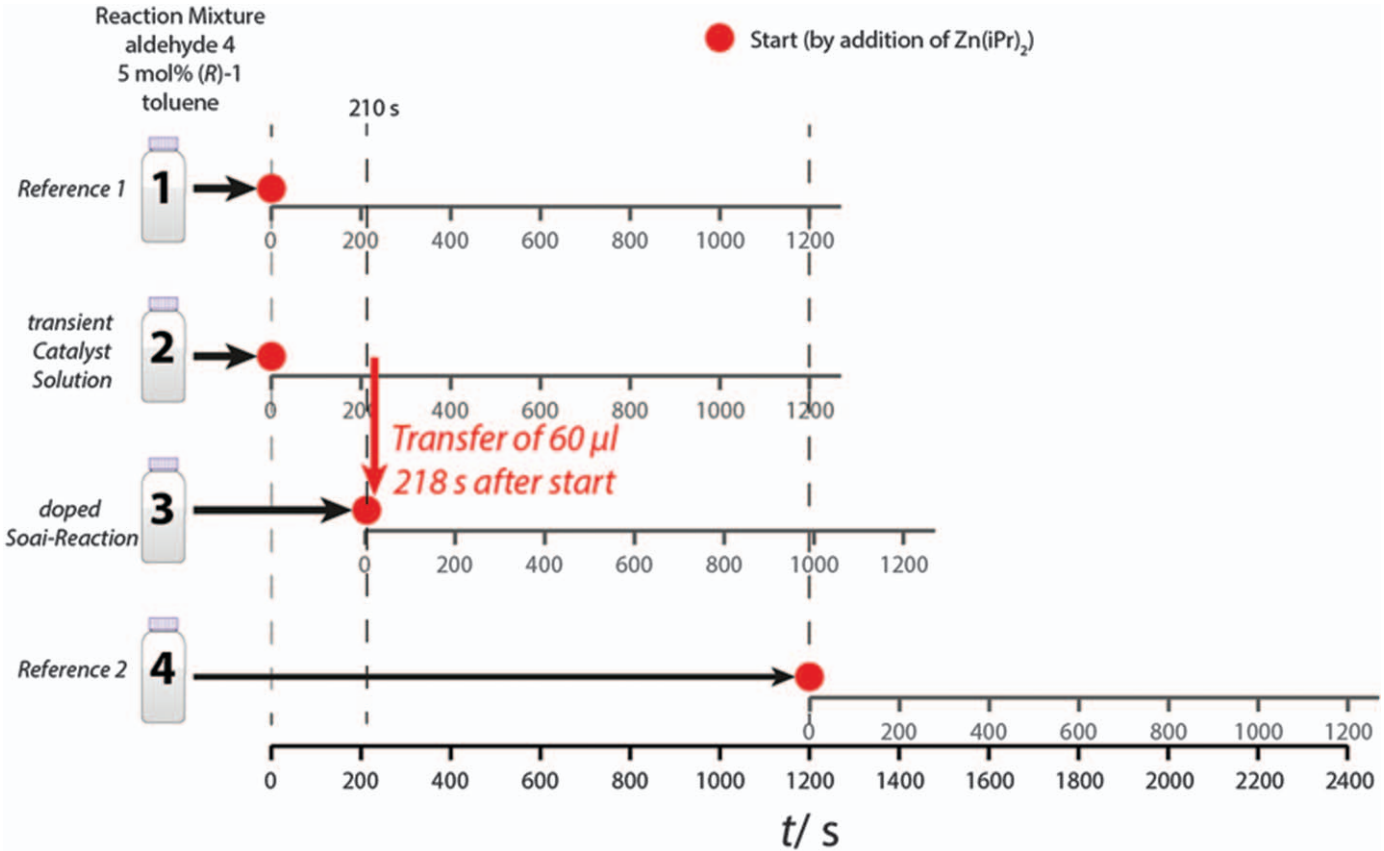

Figure 11.11 Timing scheme of the doping experiment. Reproduced from ref. 64 with permission from John Wiley & Sons, Copyright © 2020 The Authors.

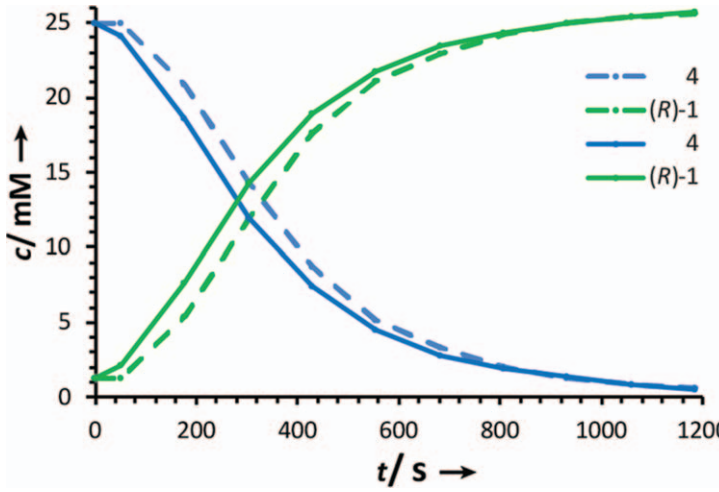

Figure 11.12 Reaction progress of concentrations **(*R*)-1** and **4** *vs.* time *t* of the doping experiment. The solid lines represent the Soai reaction doped with the transient catalyst solution (60 μL) formed from an immediately preceding ($t = 218$ s) Soai reaction. The dashed lines represent the reaction progress of the reference Soai reaction. Reaction conditions: 25.0 mM **4**, 1.25 mM **(*R*)-1** (ee > 99.9%), and 125 mM *i*-Pr_2Zn in toluene at 20 °C. Reproduced from ref. 64 with permission from John Wiley & Sons, Copyright © 2020 The Authors.

monitored by multiplexing HPLC in the flow-injection mode. Analysis of the kinetic data (see Figure 11.12) shows that the induction period is reduced in the doped experiment. Quantitative kinetic analysis confirms that the inflection point (maximum reaction rate) of the 'normal' Soai reaction (25.0 mM **4**, 1.25 mM **(*R*)-1** (ee > 99.9%) and 125 mM *i*-Pr_2Zn in toluene at 20 °C) is at 255 s with an initial reaction rate of 4.2×10^{-3} mol s^{-1}, while in the doped experiment the inflection point is at 200 s and the initial reaction rate is 1.4×10^{-2} mol s^{-1}.1 This means that the induction period is shifted by 55 s in the doped experiment!

It is important to highlight that adding 60 μL of a completed Soai reaction does not influence the induction period!

11.6 Proposed Mechanism of Soai's Asymmetric Autocatalysis *via* the Formation of a Transient Hemiacetalate-catalyst

Taking all the kinetic and thermodynamic data of the hemiacetal formation, the structural puzzle pieces determined by the *in situ* high-resolution mass spectrometric reaction monitoring, the transient formation of the Zn–hemiacetalate **5** during the Soai reaction, and the doping experiment into consideration, a novel reaction mechanism that can explain the high

amplification of the experimentally observed enantioselectivity (see Scheme 11.4) was proposed.

This mechanism (see Scheme 11.4) starts with the formation of the isopropylzinc pyrimidyl alkoxides **2** from (***R***)-**1** and/or (***S***)-**1**. The isopropylzinc pyrimidyl alkoxides **2** are in equilibrium with the homochiral (***R,R***)-**3**/(***S,S***)-**3** and heterochiral (***R,S***)-**3** dimers. Depending on this first selection process the dominating enantiomer directs whether the autocatalytic cycle proceeds to the right autocatalytic *R*-cycle (green) or the left autocatalytic *S*-cycle (red).

The key step is the formation of the transient hemiacetal catalyst **5**, which is in dynamic equilibrium between the Zn–alkoxide **2** and aldehyde **4** forming diastereomeric complexes (***R,R***)-**5** or (***R,S***)-**5**, if (***R***)-**1** dominates, or forming diastereomeric complexes (***S,S***)-**5** or (***S,R***)-**5**, if (***S***)-**1** dominates. DFT calculation at the PBE0-D3/LACVP** level of theory of the optimized structures of (***R,R***)-**5** and (***R,S***)-**5** indicate that the diastereomer (***R,R***)-**5** is favored by 6 kJ mol^{-1}.

In the following only the autocatalytic *R*-cycle on the right side will be discussed, which is mirror-symmetrical to the autocatalytic *S*-cycle.

In the consecutive step of this cycle pyrimidine-5-carbaldehyde **4** and *i*-Pr$_2$Zn are coordinated to the hemiacetal (***R,R***)-**5** forming adduct (***R,R***)-**6**. This spatial alignment of the carbaldehyde results in a transfer of the adjacent isopropyl group from the *re* side giving (***R,R,R***)-**7**. DFT calculations provide an energy barrier of 54 kJ mol^{-1}.

Insertion of another molecule of the pyrimidine-5-carbaldehyde **4** leads to the dimeric hemiacetal (***R,R,R,R***)-**8**, which splits into two monomeric hemiacetals (***R,R***)-**5**, which explains the rapid sigmoidal increase in the formation of catalytically highly active (***R,R***)-**5** and is typical for an autocatalytic process. The dimeric hemiacetal (***R,R,R,R***)-**8** represents a diastereomeric complex and in combination with the dissociation into the monomeric hemiacetals (***R,R***)-**5**, which can dynamically control the stereocenter of the hemiacetal group, giving a natural mechanism of autocorrection.

It has to be noted that (***R,R,R***)-**7** can be also converted into (***R,R***)-**5** and (***R***)-**2** (and its corresponding dimer (***R,R***)-**3**).

11.7 Evaluation of the Kinetic Data

The evaluation of the kinetic data was an enormous task. We started to evaluate data from the reaction progress analysis by means of the graphical method[134] already in 2010 and in parallel we began to develop a method that systematically evaluates the experimental data to determine the reaction rates.

The idea, in contrast to a fitting of the kinetic reaction data, is the following: a reaction model can be used to set up the corresponding differential equations of the system and to calculate reaction profiles with the given initial experimental concentrations. Here, a large matrix is generated with up to 2.25 million combinations of reaction rate constants that are

systematically varied. The profiles calculated in this way are then compared with the experimental profiles and sorted by matching. This matching must be satisfied with all experimental reaction profiles under different starting conditions (concentrations). In the example shown above, these are 18 reaction profiles determined several times and thus the number of profiles is significantly larger than the number of reaction rate constants to be determined. In addition, rate constants already determined by direct measurement can be taken into account. By multiple refinements of the reaction parameter space, the rate constants can be further narrowed down. However, this systematic approach requires a very efficient calculation. In total, we have developed seven programs over time, which also considered models of the proposed mechanism described in the literature. The algorithm for the mechanism described above (see Scheme 11.4) takes into account 26 differential equations and was created and implemented in the Soai 7 software package, written in object-oriented Pascal (Delphi XE/RAD Studio). This program allows us to calculate kinetic reaction profiles using an adaptive Runge–Kutta routine to solve the system of differential equations with the initial experimental parameters, *i.e.* concentrations of the additives (***R***)-**1** and (***S***)-**1** (ee), the pyrimidin-5-carbaldehyde **4** and iPr_2Zn, the reaction time, reaction rate constants k_n, and equilibrium constants K_n. This program allows to define large data sets (2.25 million kinetic profiles each) with variable ranges for the reaction rate constants k_n and equilibrium constants K_n. The calculated kinetic profiles are compared with the experimentally determined kinetic profiles of (***R***)-**1**, (***S***)-**1**, and **4** to refine the kinetic parameters. This method was applied iteratively to all kinetic data sets (in total 81 million kinetic profiles) and thus the rate constants for the respective partial steps were determined. The results of the kinetic and thermodynamic parameters are summarized in Table 11.2.

Table 11.2 Kinetic data of the Soai-reaction of aldehyde **4** with *i*-Pr_2Zn forming alcohol **1** obtained by comprehensive simulation of the proposed reaction mechanism. Reproduced from ref. 64 with permission from John Wiley & Sons, Copyright © 2020 The Authors.

n^a	$k_n{}^b$	$K_n{}^c$	$k_{-n}{}^d$
1	$1.5\times10^2 \pm 7\ M^{-1}\,s^{-1}$	—	—
2	$7.0\times10^2 \pm 32\ M^{-1}\,s^{-1}$	$81 \pm 4\ M^{-1}$	$8.6 \pm 0.8\ s^{-1}$
3	$7.0\times10^2 \pm 32\ M^{-1}\,s^{-1}$	$162 \pm 8\ M^{-1}$	$4.3 \pm 0.4\ s^{-1}$
4	$1.7\times10^{-3} \pm 1.2\times10^{-4}\ M^{-1}\,s^{-1}$	$0.136 \pm 0.001\ M^{-1}$	$1.3\times10^{-2} \pm 1.0\times10^{-3}\ s^{-1}$
5	$63 \pm 5\ M^{-2}\,s^{-1}$	—	—
6	$0.11 \pm 0.01\ s^{-1}$	—	—
7	$13.2 \pm 0.2\ M^{-1}\,s^{-1}$	—	—
8	$0.23 \pm 0.02\ s^{-1}$	—	—

[a]Reaction step as denoted in Scheme 11.3.
[b]Forward reaction rate constants.
[c]Equilibrium constants.
[d]Backward reaction rate constants.

The formation of the isopropylzinc pyrimidyl alkoxides **2** is a rapid process and agrees very well with kinetic data of the reaction of alkylzinc compounds with alcohols described in the literature.[150] The equilibrium between monomeric **2** and homochiral (***R,R***)-**3**/(***S,S***)-**3** and heterochiral (***R,S***)-**3** is dynamic and not extremely shifted to the side of the dimers, as is also observed in the mass spectra. More interesting is the equilibrium and the kinetic parameters of the hemiacetal **5** formation, which are in excellent agreement with the kinetic parameters determined by enantioselective DHPLC for the formation of $\mathbf{5_{iPr}}$ ($k_1(293\ \mathrm{K}) = 4.1\times10^{-3}\ (\mathrm{mol\,s})^{-1}$ and $k_{-1}(293\ \mathrm{K}) = 1.3\times10^{-2}\ \mathrm{s}^{-1}$) and equilibria of the derivatives by ^{1}H NMR spectroscopy. In the autocatalytic cycle the rate determining step is the transfer of the isopropyl group, while the other steps are energetically balanced.

The proposed mechanism and the kinetic model allow us not only to predict kinetic reaction profiles of the conversion of the pyrimidine-5-carbaldehyde **4** into the reaction product **1** of the Soai reaction, but even more important the precise prediction of the nonlinear amplification of the ee and the induction period in dependence on the ee. When starting with an ee of 1% in **1** (2 mmol L^{-1}), 9.25% ee in the 1st step, 59.4% ee in the 2nd step, 94.6% ee in the 3rd step, 99.4% ee in the 4th step, and 99.9% ee in the 5th step are obtained (see Figure 11.13).

A systematic variation of the initial ee_0 of **1** and the corresponding final product ee is plotted in Figure 11.14a. Interestingly, if the reaction is performed under conditions where the formed product with amplifying ee propagates through a reaction mixture, *i.e.* by diffusion or starting with seeding on a chiral or enantiomorph surface, extraordinary ee amplifications

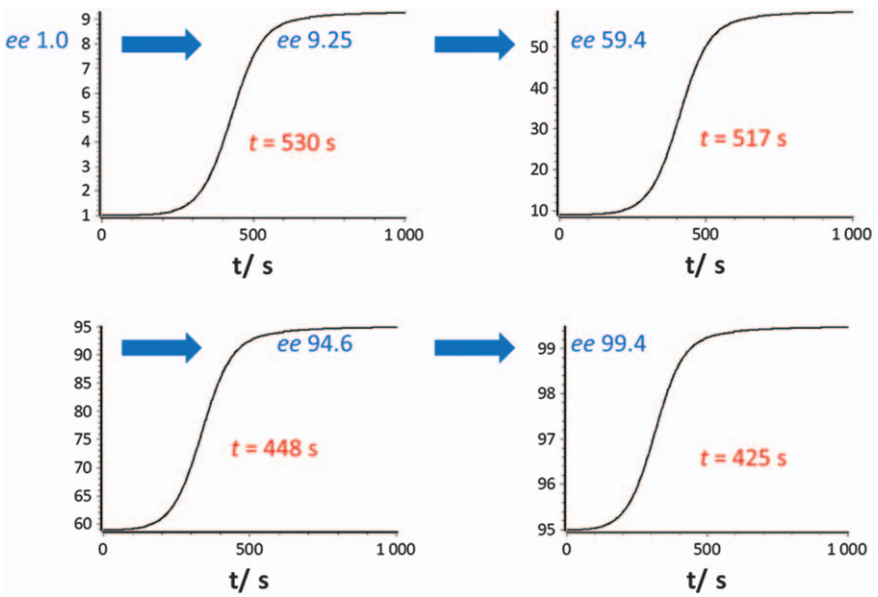

Figure 11.13 Amplification of the enantiomeric excess in the Soai reaction.

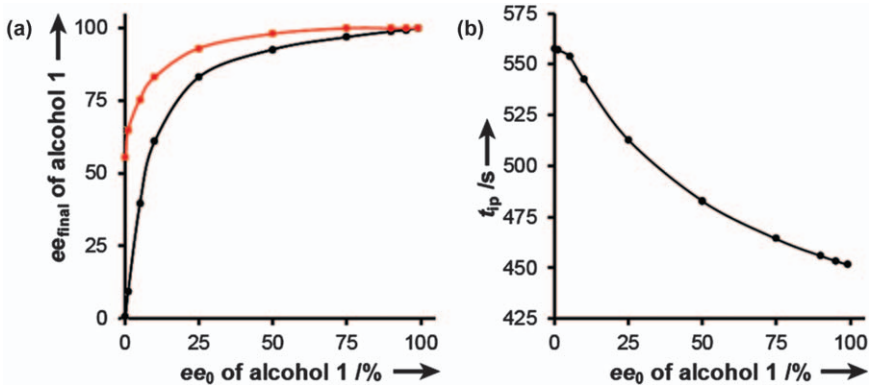

Figure 11.14 Enantiomeric excess and time of the inflection point in dependence on the initial ee of the added pyrimidine alcohol **1** predicted by the mechanistic model and reaction rate constants obtained by comprehensive analysis of the kinetic data. Simulations were obtained by calculations with Soai 7. (a) Amplification of the ee (final ee *vs.* initial ee of the alcohol **1**). The black line represents a homogeneous and stirred reaction mixture, the red line represents a Soai reaction slowly propagating through a reaction mixture. (b) Shift of the inflection point t_{ip} in dependence on the initial ee of 1. Starting concentrations used for the simulation: 25.0 mM **4**, 2 mM **1** (ratio of **(*R*)-1** and **(*S*)-1** depending on the corresponding ee) and 50 mM *i*-Pr_2Zn. Reproduced from ref. 64 with permission from John Wiley & Sons, Copyright © 2020 The Authors.

can be predicted, jumping immediately from 1×10^{-5}% to 55% and finally >99.9% (see Figure 11.14, red line). Experimental investigations of reactions with variation of the starting ee of the alcohol additive and concentrations were compared with the prediction of ee values by simulation with the program Soai 7, giving excellent correlation between the experiment and simulation.

Furthermore, the simulations correctly predict the prolonged induction period, which is caused by the slow hemiacetal formation, and the time of the inflection point t_{ip} dependent on the initial ee of the pyrimidine alcohol **1** (see Figure 11.14b).

11.8 Summary and Outlook

The results of the high-resolution mass spectrometric measurements and the comprehensive kinetic analyses suggest the formation of a transient Zn–hemiacetalate complex, which is catalytically active in the Soai reaction. This intermediate can establish an autocatalytic cycle and the extraordinary amplification of the enantiomeric excess. This is supported by mass spectrometric profiling of the transient hemiacetal intermediate and by doping experiments, which demonstrate that the Soai reaction can be accelerated by adding the *in situ* formed catalyst. Kinetic and thermodynamic data of the

highly dynamic formation and decomposition of the hemiacetal explain the unusual inverse temperature dependence on the reaction kinetics, the induction period, and time shift of the inflection point. Furthermore, the results suggest that the formation of the transient diastereomeric Zn–hemiacetalates amplify any initial imbalance of the formed product enantiomers, which is interestingly always given for an odd number of formed molecules. These results give new guidance to structures envisioning potential processes leading to symmetry breaking.

Acknowledgements

I acknowledge financial support from the European Research Council ERC under Grant Agreements No. StG 258740. I thank all my former PhD students who were involved in the Soai's asymmetric autocatalysis project for the fruitful and inspiring research. It was sometimes like a sailing expedition to discover new continents, the daily struggle with equipment, with the uncertainty of "where the journey is going", and flaring euphoria that carried the enthusiasm for science. Many thanks to Dr Frank Maier (2013), Dr Skrollan Stockinger (2014), Dr Kerstin Zawatzky (2015), Dr Alexander Siegle (2016), and Dr Saskia Lamour (2019). Furthermore, I would like to thank Prof. Dr Kenso Soai and Dr. John Brown for the discussions.

References

1. R. A. Hegstrom, *Origins Life*, 1984, **14**, 405–411.
2. D. G. Blackmond, *Proc. Natl. Acad. Sci. U. S. A.*, 2004, **101**, 5732–5736.
3. T. Kawasaki, K. Suzuki, Y. Hakoda and K. Soai, *Angew. Chem., Int. Ed.*, 2008, **47**, 496–499.
4. D. G. Blackmond, *Phil. Trans. R. Soc. B*, 2011, **366**, 2878–2884.
5. N. A. Hawbaker and D. G. Blackmond, *Nat. Chem.*, 2019, **11**, 957–962.
6. J. S. Teichert, F. M. Kruse and O. Trapp, *Angew. Chem., Int. Ed.*, 2019, **58**, 9944–9947.
7. F. M. Kruse, J. S. Teichert and O. Trapp, *Chem. – Eur. J.*, 2020, **26**, 14776–14790.
8. S. C. Karunakaran, B. J. Cafferty, A. Weigert-Muñoz, G. B. Schuster and N. V. Hud, *Angew. Chem., Int. Ed.*, 2019, **58**, 1453–1457.
9. O. Trapp, *Front. Chem.*, 2020, **8**, 1173.
10. J. M. Ribó, C. Blanco, J. Crusats, Z. El-Hachemi, D. Hochberg and A. Moyano, *Chem. – Eur. J.*, 2014, **20**, 17250–17271.
11. J. M. Ribo, J. Crusats, Z. El-Hachemi, A. Moyano and D. Hochberg, *Chem. Sci.*, 2017, **8**, 763–769.
12. J. M. Ribó and D. Hochberg, *Symmetry*, 2019, **11**, 814.
13. J. M. Ribó and D. Hochberg, *Phys. Chem. Chem. Phys.*, 2020, **22**, 14013–14025.
14. D. Hochberg, A. S. Torralba and F. Morán, *Phys. Chem. Chem. Phys.*, 2020, **22**, 27214–27223.

15. A. H. Alberts and H. Wynberg, *J. Am. Chem. Soc.*, 1989, **111**, 7265–7266.
16. K. Soai and T. Kawasaki, *Top. Curr. Chem.*, 2008, **284**, 1–33.
17. S. B. Tsogoeva, *Chem. Commun.*, 2010, **46**, 7662–7669.
18. A. J. Bissette and S. P. Fletcher, *Angew. Chem., Int. Ed.*, 2013, **52**, 12800–12826.
19. D. G. Blackmond, *Chem. Rev.*, 2020, **120**, 4831–4847.
20. T. Buhse, J.-M. Cruz, M. E. Noble-Terán, D. Hochberg, J. M. Ribó, J. Crusats and J.-C. Micheau, *Chem. Rev.*, 2021, **121**, 2147–2229.
21. J.-M. Lehn, *Angew. Chem., Int. Ed.*, 2013, **52**, 2836–2850.
22. J.-M. Lehn, *Angew. Chem., Int. Ed.*, 2015, **54**, 3276–3289.
23. K. Mikami and S. Matsukawa, *Nature*, 1997, **385**, 613–615.
24. K. Mikami, T. Korenaga, M. Terada, T. Ohkuma, T. Pham and R. Noyori, *Angew. Chem., Int. Ed.*, 1999, **38**, 495–497.
25. K. Ding, A. Ishii and K. Mikami, *Angew. Chem., Int. Ed.*, 1999, **38**, 497–501.
26. F. Maier and O. Trapp, *Angew. Chem., Int. Ed.*, 2014, **53**, 8756–8760.
27. G. Storch, F. Maier, P. Wessig and O. Trapp, *Eur. J. Org. Chem.*, 2016, 5123–5126.
28. G. Storch, M. Siebert, F. Rominger and O. Trapp, *Chem. Commun.*, 2015, **51**, 15665–15668.
29. G. Storch and O. Trapp, *Angew. Chem., Int. Ed.*, 2015, **54**, 3580–3586.
30. G. Storch, L. Deberle, J.-M. Menke, F. Rominger and O. Trapp, *Chirality*, 2016, **28**, 744–748.
31. G. Storch, S. Pallmann, F. Rominger and O. Trapp, *Beilstein J. Org. Chem.*, 2016, **12**, 1453–1458.
32. M. Siebert, G. Storch, F. Rominger and O. Trapp, *Synthesis*, 2017, **49**, 3485–3494.
33. G. Storch and O. Trapp, *Nat. Chem.*, 2017, **9**, 179–187.
34. G. Storch and O. Trapp, *Chirality*, 2018, **30**, 1150–1160.
35. J. F. Scholtes and O. Trapp, *Organometallics*, 2019, **38**, 3955–3960.
36. J. F. Scholtes and O. Trapp, *Chirality*, 2019, **31**, 1028–1042.
37. J. F. Scholtes and O. Trapp, *Chem. – Eur. J.*, 2019, **25**, 11707–11714.
38. J. F. Scholtes and O. Trapp, *Angew. Chem., Int. Ed.*, 2019, **58**, 6306–6310.
39. J. F. Scholtes and O. Trapp, *Synlett*, 2021, **32**, 971–980.
40. C. Moberg, *Acc. Chem. Res.*, 2016, **49**, 2736–2745.
41. K. Mikami and M. Yamanaka, *Chem. Rev.*, 2003, **103**, 3369–3400.
42. I. Weissbuch, L. Addadi, Z. Berkovitch-Yellin, E. Gati, M. Lahav and L. Leiserowitz, *Nature*, 1984, **310**, 161–164.
43. D. K. Kondepudi, R. J. Kaufman and N. Singh, *Science*, 1990, **250**, 975–976.
44. B. L. Feringa and R. A. van Delden, *Angew. Chem., Int. Ed.*, 1999, **38**, 3418–3438.
45. H. Zepik, E. Shavit, M. Tang, T. R. Jensen, K. Kjaer, G. Bolbach, L. Leiserowitz, I. Weissbuch and M. Lahav, *Science*, 2002, **295**, 1266.
46. R. R. E. Steendam, M. C. T. Brouwer, E. M. E. Huijs, M. W. Kulka, H. Meekes, W. J. P. V. Enckevort, J. Raap, F. P. J. T. Rutjes and E. Vlieg, *Chem. – Eur. J.*, 2014, **20**, 13527–13530.

47. S. Olsson, P. M. Björemark, T. Kokoli, J. Sundberg, A. Lennartson, C. J. Mckenzie and M. Håkansson, *Chem. – Eur. J.*, 2015, **21**, 5211–5219.
48. D. Guillaneux, S.-H. Zhao, O. Samuel, D. Rainford and H. B. Kagan, *J. Am. Chem. Soc.*, 1994, **116**, 9430–9439.
49. C. Girard and H. B. Kagan, *Angew. Chem., Int. Ed.*, 1998, **37**, 2922–2959.
50. M. Klussmann, H. Iwamura, S. P. Mathew, D. H. Wells, U. Pandya, A. Armstrong and D. G. Blackmond, *Nature*, 2006, **441**, 621–623.
51. T. Satyanarayana, S. Abraham and H. B. Kagan, *Angew. Chem., Int. Ed.*, 2009, **48**, 456–494.
52. C. Puchot, O. Samuel, E. Duiiach, S. Zhao, C. Agami and H. B. Kagan, *J. Am. Chem. Soc.*, 1986, **108**, 2353–2357.
53. M. Kitamura, S. Okada, S. Suga and R. Noyori, *J. Am. Chem. Soc.*, 1989, **111**, 4028–4036.
54. R. Noyori and M. Kitamura, *Angew. Chem., Int. Ed.*, 1991, **30**, 49–69.
55. K. Soai and S. Niwa, *Chem. Rev.*, 1992, **92**, 833–856.
56. F. C. Frank, *Biochim. Biophys. Acta*, 1953, **11**, 459–463.
57. K. Soai, T. Shibata, H. Morioka and K. Choji, *Nature*, 1995, **378**, 767–768.
58. K. Soai and T. Shibata, *J. Synth. Org. Chem., Jpn.*, 1997, **55**, 994–1005.
59. T. Shibata, S. Yonekubo and K. Soai, *Angew. Chem., Int. Ed.*, 1999, **38**, 659–661.
60. K. Soai, T. Shibata and I. Sato, *Acc. Chem. Res.*, 2000, **33**, 382–390.
61. K. Soai and T. Kawasaki, *Chirality*, 2006, **18**, 469–478.
62. K. Soai and T. Kawasaki, *Top. Curr. Chem.*, 2008, **284**, 1–33.
63. T. Gehring, M. Busch, M. Schlageter and D. Weingand, *Chirality*, 2010, **22**, E173–E182.
64. O. Trapp, S. Lamour, F. Maier, A. F. Siegle, K. Zawatzky and B. F. Straub, *Chem. – Eur. J.*, 2020, **26**, 15871–15880.
65. K. Soai, S. Niwa and H. Hori, *J. Chem. Soc., Chem. Commun.*, 1990, 982–983.
66. T. Shibata, K. Choji, T. Hayase, Y. Aizu and K. Soai, *Chem. Commun.*, 1996, 1235–1236.
67. K. Soai and T. Sato, *Chirality*, 2002, **14**, 548–554.
68. C. Romagnoli, B. Sieng and M. Amedjkouh, *Eur. J. Org. Chem.*, 2015, **2015**, 4087–4092.
69. D. A. Singleton and L. K. Vo, *J. Am. Chem. Soc.*, 2002, **124**, 10010–10011.
70. D. A. Singleton and L. K. Vo, *Org. Lett.*, 2003, **5**, 4337–4339.
71. I. Sato, H. Urabe, S. Ishiguro, T. Shibata and K. Soai, *Angew. Chem., Int. Ed.*, 2003, **42**, 315–317.
72. I. Sato, D. Omiya, T. Saito and K. Soai, *J. Am. Chem. Soc.*, 2000, **122**, 11739–11740.
73. T. Kawasaki, M. Shimizu, D. Nishiyama, M. Ito, H. Ozawa and K. Soai, *Chem. Commun.*, 2009, 4396–4398.
74. T. Kawasaki, H. Ozawa, M. Ito and K. Soai, *Chem. Lett.*, 2011, **40**, 320–321.
75. T. Kawasaki, Y. Matsumura, T. Tsutsumi, K. Suzuki, M. Ito and K. Soai, *Science*, 2009, **324**, 492–495.

76. A. Matsumoto, H. Ozaki, S. Harada, K. Tada, T. Ayugase, H. Ozawa, T. Kawasaki and K. Soai, *Angew. Chem., Int. Ed.*, 2016, **55**, 15246–15249.
77. T. Kawasaki, Y. Okano, E. Suzuki, S. Takano, S. Oji and K. Soai, *Angew. Chem., Int. Ed.*, 2011, **50**, 8131–8133.
78. A. Matsumoto, S. Oji, S. Takano, K. Tada, T. Kawasaki and K. Soai, *Org. Biomol. Chem.*, 2013, **11**, 2928–2931.
79. N. A. Hawbaker and D. G. Blackmond, *ACS Cent. Sci.*, 2018, **4**, 776–780.
80. T. Kawasaki, H. Tanaka, T. Tsutsumi, T. Kasahara, I. Sato and K. Soai, *J. Am. Chem. Soc.*, 2006, **128**, 6032–6033.
81. I. Sato, R. Sugie, Y. Matsueda, Y. Furumura and K. Soai, *Angew. Chem., Int. Ed.*, 2004, **43**, 4490–4492.
82. T. Kawasaki, M. Sato, S. Ishiguro, T. Saito, Y. Morishita, I. Sato, H. Nishino, Y. Inoue and K. Soai, *J. Am. Chem. Soc.*, 2005, **127**, 3274–3275.
83. K. Soai, S. Osanai, K. Kadowaki, S. Yonekubo, T. Shibata and I. Sato, *J. Am. Chem. Soc.*, 1999, **121**, 11235–11236.
84. I. Sato, K. Kadowaki and K. Soai, *Angew. Chem., Int. Ed.*, 2000, **39**, 1510–1512.
85. T. Kawasaki, K. Jo, H. Igarashi, I. Sato, M. Nagano, H. Koshima and K. Soai, *Angew. Chem., Int. Ed.*, 2005, **44**, 2774–2777.
86. T. Kawasaki, K. Suzuki, M. Shimizu, K. Ishikawa and K. Soai, *Chirality*, 2006, **18**, 479–482.
87. T. Kawasaki, K. Suzuki, Y. Hakoda and K. Soai, *Angew. Chem., Int. Ed.*, 2008, **47**, 496–499.
88. T. Kawasaki, S. Kamimura, A. Amihara, K. Suzuki and K. Soai, *Angew. Chem., Int. Ed.*, 2011, **50**, 6796–6798.
89. H. Shindo, Y. Shirota, K. Niki, T. Kawasaki, K. Suzuki, Y. Araki, A. Matsumoto and K. Soai, *Angew. Chem., Int. Ed.*, 2013, **52**, 9135–9138.
90. H. Mineki, Y. Kaimori, T. Kawasaki, A. Matsumoto and K. Soai, *Tetrahedron: Asymmetry*, 2013, **24**, 1365–1367.
91. T. Kawasaki, M. Uchida, Y. Kaimori, T. Sasagawa, A. Matsumoto and K. Soai, *Chem. Lett.*, 2013, **42**, 711–713.
92. A. Matsumoto, T. Ide, Y. Kaimori, S. Fujiwara and K. Soai, *Chem. Lett.*, 2015, **44**, 688–690.
93. A. Matsumoto, S. Takeda, S. Harada and K. Soai, *Tetrahedron: Asymmetry*, 2016, **27**, 943–946.
94. F. Lutz, T. Kawasaki and K. Soai, *Tetrahedron: Asymmetry*, 2006, **17**, 486–490.
95. T. Kawasaki, C. Hohberger, Y. Araki, K. Hatase, K. Beckerle, J. Okuda and K. Soai, *Chem. Commun.*, 2009, 5621–5623.
96. G. A. Rance, S. A. Miners, T. W. Chamberlain and A. N. Khlobystov, *Chem. Mater.*, 2013, **557**, 10–14.
97. T. Kawasaki, M. Nakaoda, Y. Takahashi, Y. Kanto, N. Kuruhara, K. Hosoi, I. Sato, A. Matsumoto and K. Soai, *Angew. Chem., Int. Ed.*, 2014, **53**, 11199–11202.

98. A. Matusmoto, S. Fujiwara, Y. Hiyoshi, K. Zawatzky, A. A. Makarov, C. J. Welch and K. Soai, *Org. Biomol. Chem.*, 2017, **15**, 555–558.
99. A. Matsumoto, K. Yonemitsu, H. Ozaki, J. Misek, I. Stary, I. G. Stara and K. Soai, *Org. Biomol. Chem.*, 2017, **15**, 1321–1324.
100. T. Kawasaki, Y. Kaimori, S. Shimada, N. Hara, S. Sato, K. Suzuki, T. Asahi, A. Matsumoto and K. Soai, *Chem. Commun.*, 2021, **57**, 5999–6002.
101. K. Soai, I. Sato, T. Shibata, S. Komiya, M. Hayashi, Y. Matsueda, H. Imamura, T. Hayase, H. Morioka, H. Tabira, J. Yamamoto and Y. Kowata, *Tetrahedron: Asymmetry*, 2003, **14**, 185–188.
102. J. M. Brown, I. Gridnev and J. Klankermayer, *Top. Curr. Chem.*, 2008, **284**, 35–65.
103. K. Micskei, G. Póta, L. Caglioti and G. Pályi, *J. Phys. Chem. A*, 2006, **110**, 5982–5984.
104. D. G. Blackmond and O. K. Matar, *J. Phys. Chem. B*, 2008, **112**, 5098–5104.
105. G. Lente, *Tetrahedron: Asymmetry*, 2011, **22**, 1595–1599.
106. J.-C. Micheau, C. Coudret, J.-M. Cruz and T. Buhse, *Phys. Chem. Chem. Phys.*, 2012, **14**, 13239–13248.
107. B. Barabás, C. Zucchi, M. Maioli, K. Micskei and G. Pályi, *J. Mol. Model.*, 2015, **21**, 33.
108. I. D. Gridnev and A. K. Vorobiev, *ACS Catal.*, 2012, **2**, 2137–2149.
109. I. D. Gridnev and A. K. Vorobiev, *Bull. Chem. Soc. Jpn.*, 2015, **88**, 333–340.
110. J. R. Islas, D. Lavabre, J.-M. Grevy, R. H. Lamoneda, H. R. Cabrera, J.-C. Micheau and T. Buhse, *Proc. Natl. Acad. Sci. U. S. A.*, 2005, **102**, 13743–13748.
111. J.-C. Micheau, J.-M. Cruz, C. Coudret and T. Buhse, *ChemPhysChem.*, 2010, **11**, 3417–3419.
112. F. G. Buono and D. G. Blackmond, *J. Am. Chem. Soc.*, 2003, **125**, 8978–8979.
113. I. D. Gridnev, J. M. Serafimov, H. Quiney and J. M. Brown, *Org. Biomol. Chem.*, 2003, **1**, 3811–3819.
114. D. G. Blackmond, C. R. McMillan, S. Ramdeehul, A. Schorm and J. M. Brown, *J. Am. Chem. Soc.*, 2001, **123**, 10103–10104.
115. D. G. Blackmond, *Tetrahedron: Asymmetry*, 2006, **17**, 584–589.
116. J. Klankermayer, I. D. Gridnev and J. M. Brown, *Chem. Commun.*, 2007, 3151–3153.
117. A. Matsumoto, T. Abe, A. Hara, T. Tobita, T. Sasagawa, T. Kawasaki and K. Soai, *Angew. Chem., Int. Ed.*, 2015, **54**, 15218–15221.
118. I. D. Gridnev, J. M. Serafimov and J. M. Brown, *Angew. Chem., Int. Ed.*, 2004, **43**, 4884–4887.
119. M. Busch, M. Schlageter, D. Weingand and T. Gehring, *Chem. – Eur. J.*, 2009, **15**, 8251–8258.
120. L. Schiaffino and G. Ercolani, *Angew. Chem., Int. Ed.*, 2008, **47**, 6832–6835.

121. L. Schiaffino and G. Ercolani, *ChemPhysChem.*, 2009, **10**, 2508–2515.
122. L. Schiaffino and G. Ercolani, *Chem. – Eur. J.*, 2010, **16**, 3147–3156.
123. G. Ercolani and L. Schiaffino, *J. Org. Chem.*, 2011, **76**, 2619–2626.
124. T. Gehring, M. Quaranta, B. Odell, D. G. Blackmond and J. M. Brown, *Angew. Chem., Int. Ed.*, 2012, **51**, 9539–9542.
125. S. V. Athavale, A. Simon, K. N. Houk and S. E. Denmark, *Nat. Chem.*, 2020, **12**, 412–423.
126. S. V. Athavale, A. Simon, K. N. Houk and S. E. Denmark, *J. Am. Chem. Soc.*, 2020, **142**, 18387–18406.
127. M. Quaranta, T. Gehring, B. Odell, J. M. Brown and D. G. Blackmond, *J. Am. Chem. Soc.*, 2010, **132**, 15104–15107.
128. O. Trapp, *Angew. Chem., Int. Ed.*, 2007, **46**, 5609–5613.
129. A. F. Siegle and O. Trapp, *Anal. Chem.*, 2014, **86**, 10828–10833.
130. A. F. Siegle and O. Trapp, *Anal. Chem.*, 2015, **87**, 11932–11934.
131. M. Wunsch, R. Lehnig, C. Janke and O. Trapp, *Anal. Chem.*, 2018, **90**, 9256–9263.
132. C. J. Welch, X. Gong, W. Schafer, E. C. Pratt, T. Brkovic, Z. Pirzada, J. F. Cuff and B. Kosjek, *Tetrahedron: Asymmetry*, 2010, **21**, 1674–1681.
133. T. Ikai and Y. Okamoto, *Chem. Rev.*, 2009, **109**, 6077–6101.
134. K. J. Laidler, *Chemical Kinetics*, Harper & Row, New York, 3rd edn, 1987.
135. O. Trapp, G. Schoetz and V. Schurig, *Chirality*, 2001, **13**, 403–414.
136. I. D'Acquarica, F. Gasparrini, M. Pierini, C. Villani and G. Zappia, *J. Sep. Sci.*, 2006, **29**, 1508–1516.
137. C. Wolf, *Dynamic Stereochemistry of Chiral Compounds - Principles and Applications*, RSC Publishing, Cambridge, 2008.
138. O. Trapp, *Top. Curr. Chem.*, 2013, **341**, 231–270.
139. O. Trapp and V. Schurig, *J. Am. Chem. Soc.*, 2000, **122**, 1424–1430.
140. O. Trapp, *Anal. Chem.*, 2006, **78**, 189–198.
141. O. Trapp, *Electrophoresis*, 2006, **27**, 534–541.
142. O. Trapp, *Electrophoresis*, 2006, **27**, 2999–3006.
143. F. Maier and O. Trapp, *Angew. Chem., Int. Ed.*, 2012, **51**, 2985–2988.
144. E. Wingstrand, A. Laurell, L. Fransson, K. Hult and C. Moberg, *Chem. – Eur. J.*, 2009, **15**, 12107–12113.
145. L. Fransson, A. Laurell, K. Widyan, E. Wingstrand, K. Hult and C. Moberg, *ChemCatChem*, 2010, **2**, 683–693.
146. A. Laurell and C. Moberg, *Eur. J. Org. Chem.*, 2011, 3980–3984.
147. Y.-Q. Wen, R. Hertzberg, I. Gonzalez and C. Moberg, *Chem. – Eur. J.*, 2014, **20**, 3806–3812.
148. H. Fanlo-Virgós, A.-N. R. Alba, S. Hamieh, M. Colomb-Delsuc and S. Otto, *Angew. Chem., Int. Ed.*, 2014, **53**, 11346–11350.
149. C. Kremer and A. Lützen, *Chem. – Eur. J.*, 2013, **19**, 6162–6196.
150. R. J. Herold, S. L. Aggarwal and V. Neff, *Can. J. Chem.*, 1963, **41**, 1368–1380.

CHAPTER 12

Structure Analysis of Asymmetric Autocatalysis by X-ray Crystallography and Circular Dichroism Spectroscopy

ARIMASA MATSUMOTO,*[a] TSUNEOMI KAWASAKI[b] AND KENSO SOAI[b,c]

[a] Department of Chemistry, Biology, and Environmental Science, Nara Women's University, Kita-Uoya Nishi-machi, Nara 630-8506, Japan; [b] Department of Applied Chemistry, Tokyo University of Science, Kagurazaka, Shinjuku-ku, Tokyo 162-8601, Japan; [c] Research Organization for Nano & Life Innovation, Waseda University, Wasedatsurumaki-cho, Shinjuku-ku, Tokyo 162-0041, Japan
*Email: a-matsumoto@cc.nara-wu.ac.jp

12.1 Mechanism of Asymmetric Autocatalysis

There are many theories as to what brought about molecular homochirality.[1–7] However, irrespective of the origin of homochirality, the initial bias is very small and a process of propagation and amplification of the bias is necessary to explain the homochiral world around us. Frank showed that asymmetric amplification occurs in a very simple model of ''mutual antagonism'', in which the enantiomers replicate themselves while interfering with the production of the other form.[8] However, in spite of this

Catalysis Series No. 43
Asymmetric Autocatalysis: The Soai Reaction
Edited by Kenso Soai, Tsuneomi Kawasaki and Arimasa Matsumoto

Published by the Royal Society of Chemistry, www.rsc.org

apparently simple kinetic model, it is difficult to find a reaction that actually exhibits this amplification behavior.

The discovery of asymmetric autocatalysis in a real reaction by Soai *et al.* in 1990 provided a breakthrough;[9–14] indeed, the asymmetric autocatalysis with pyrimidyl alkanols[15–20] represents a milestone in this field.[21–24] In the asymmetric addition of diisopropylzinc to aldehyde **2**, catalyzed by pyrimidylalkanol **1**, even a slight enantiomeric bias in **1** results in significant chiral amplification (Figure 12.1). It is possible to obtain products with high ee even from isotopic chirality,[25–31] crystal[32–49] or surface chirality,[50,51] circular polarization,[52,53] and other chirality biases that are originally almost undetectable; in fact, it is possible to realize absolute asymmetric synthesis without the need for anything chiral.[54–56] Even now, no other simple chemical reaction is known to induce such a remarkable asymmetric amplification. For this reason, the study of this mechanism has been the focus of much scientific attention.

Although it is not possible to introduce all of them in this chapter, various attempts have been made to unravel the details of this reaction through approaches such as kinetic analysis,[57–65] reaction tracking by HPLC,[66–68] reaction condition screening,[69] analysis by NMR[70–73] or MS,[74,75] modeling by DFT calculations,[76–84] and theoretical kinetics modeling.[85–92] First, if we look at asymmetric reactions in general, not only autocatalysis, the non-linear phenomenon of obtaining a product with a higher ee than the catalyst used

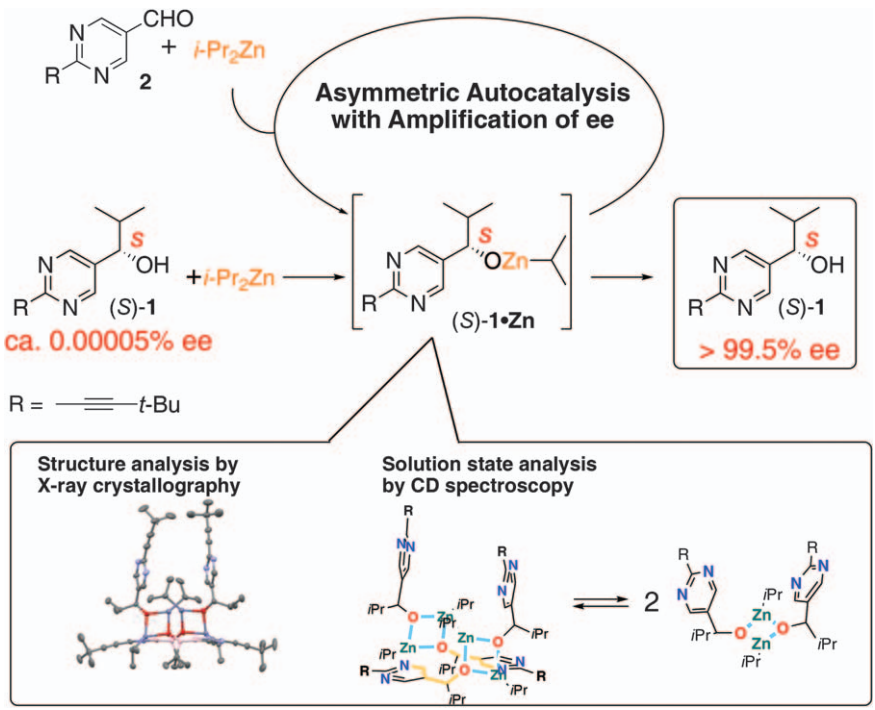

Figure 12.1 Asymmetric autocatalysis of 5-pyrimidyl alkanol and the structure analysis by X-ray crystallography and circular dichroism (CD) spectroscopy.

was discovered by Kagan *et al.* in the asymmetric epoxidation reaction.[93] Noyori *et al.* also reported non-linear amplification of ee in the asymmetric addition of alkylzinc reagents.[94] In the epoxidation, the active species of the catalyst is a dimer, whereas in Noyori's asymmetric addition of alkylzinc, the catalyst is considered to form an inactive dimer. Unlike monomers, homochiral and heterochiral dimers and higher oligomers are no longer enantiomers, but diastereomers. These diastereomers have different reactivity and stability and result in the non-linear relationship between the initial catalyst ee and actual active catalyst. However, various studies have shown that the significant asymmetric amplification of this asymmetric autocatalytic reaction cannot be achieved by simply assuming that an inactive dimer is formed. A pioneering kinetic analysis using reaction calorimetry reported by Blackmond *et al.* showed that there was little difference in the stability of the heterodimer and the homochiral dimer; this suggests that it is more reasonable to consider the dimer as the active species than the possibility of a model in which the active species is the monomer.[57] Soon after, NMR studies by Brown *et al.*[70] and DFT calculations reported by Gridnev *et al.*[76] confirmed that there was no difference in the stability of this dimer. Although several patterns of dimeric structures are possible, a 12-membered macrocycle structure with a nitrogen atom was considered due to the specificity of the pyridine and pyrimidine substrate for asymmetric autocatalysis (Figure 12.2).

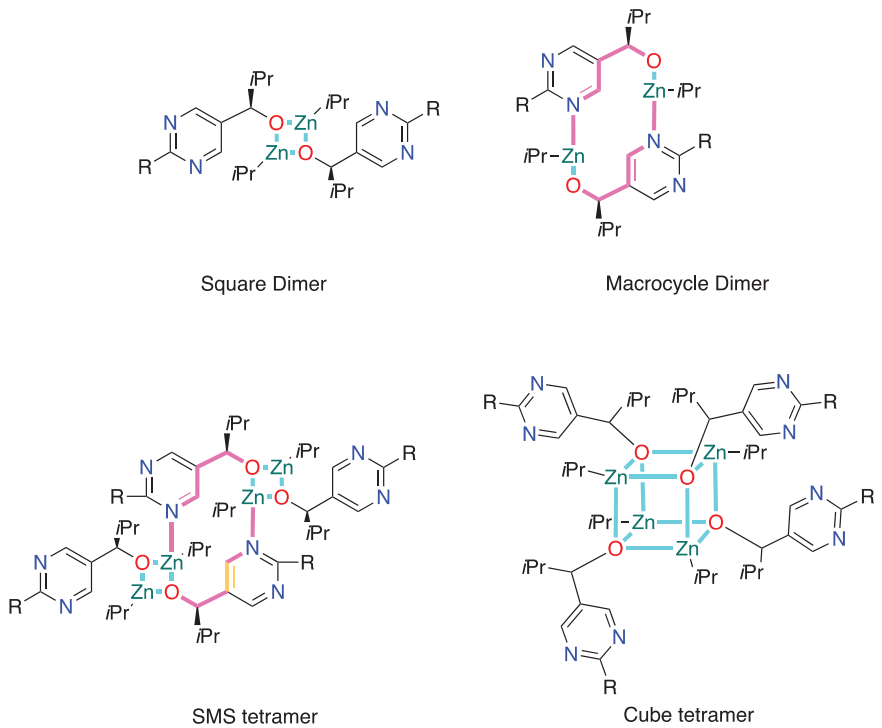

Figure 12.2 Example of possible dimer, tetramer, and oligomer structures of alkoxide **1**·**Zn**.

However, DFT and NMR analyses indicate that the Zn–O–Zn–O structure, which is observed in typical zinc alkoxides,[95] is more stable than the macrocycle structure. The detailed kinetic study by Blackmond *et al.* revealed that the reaction is almost second order on aldehyde **2**, first order in alkanol **1**, and zeroth order on *i*-Pr_2Zn.[59] This kinetic feature was also confirmed by a recent reaction monitoring study using HPLC and MS reported by Trapp *et al.*[74] By using these kinetic parameters Schiaffino and Ercolani proposed a catalytic cycle model based on DFT calculations in which the dimer reacts with two aldehydes to give a tetramer as a resting state.[80] Shortly after that, Gridnev described various possible tetramers or higher oligomer structures and concluded that the Square-Macrocycle-Square type of tetramer is the most stable tetramer of the range examined.[78] Furthermore, DOSY molecular weight analysis also indicated the existence of tetramers, although it is difficult to make a definitive judgment for such relatively small molecules.[71] Some of the remarkable recent results include the finding that NMR analysis indicated the presence of an acetal intermediate in the reaction solution.[73] Although some argue that the acetal is not a direct precursor of the product,[79] the formation of the acetal was confirmed in a high-resolution MS study by Trapp and co-workers, and a reaction model using direct monitoring with high-throughput HPLC has been proposed in which the acetal is the active species.[74]

As described above, the mechanism of this reaction is gradually being elucidated by the contributions of various research groups. All results indicate the importance of the aggregation of zinc alkoxide. In addition to asymmetric amplification, various interesting phenomena have been observed in asymmetric autocatalysis, such as the unusual temperature dependence of the reaction rate,[72] and the change in reaction selectivity depending on the mixture of pyridine and pyrimidine substrates.[96–100] These observations also indicate that the association of zinc alkoxides plays an important role in understanding this reaction. In this chapter, we introduce the crystal structure of zinc alkoxide obtained by single-crystal X-ray diffraction analysis[101,102] and describe the equilibrium state of zinc alkoxide in solution based on CD spectroscopy (Figure 12.2).[103]

12.2 Single Crystal X-ray Analysis of Zinc Alkoxide

Single-crystal X-ray diffraction is the most powerful method for obtaining information on the three-dimensional structure of molecules when crystals are available. Although it is difficult to observe unstable structures such as the transition state of a reaction by crystal diffraction, the structures of intermediates and precursors, which are relatively stable, can provide crucial clues to the reaction mechanism. Alkylzinc reagent is unstable to moisture and oxygen in the air and easily ignites, so care must be taken when handling it. Nevertheless, zinc alkoxide is relatively stable compared with alkylzinc, and once the crystals have grown to a certain size, it is possible to perform measurements for more than one day under the nitrogen flow cryogenic apparatus of the X-ray diffractometer. In this section, we introduce

the crystal structures of the asymmetric autocatalytic pyrimidyl alkanols obtained under various conditions.

12.2.1 Crystal Structures of Enantiopure and Racemic Tetramers

The first crystal with a tetrameric structure was obtained as yellow rod crystals from enantiopure (*S*)-pyrimidyl alkanol **1** dissolved in excess (8.4 equiv.) distilled neat *i*-Pr_2Zn, either without or with a small amount of toluene, under a nitrogen atmosphere (Figure 12.3). Single-crystal X-ray diffraction analysis revealed that this tetramer had a Square-Macrocycle-Square (SMS) tetramer structure. This structure was composed of two Zn_2O_2 square dimers. Each of the Zn atoms in each square dimer co-ordinated with a pyrimidine nitrogen to form a 12-membered macrocycle. The other two atoms, neither of which was involved in the formation of the macrocyclic ring, were found in an unsaturated three-co-ordinated state. This co-ordination-unsaturated zinc could serve as a reaction point with aldehydes by co-ordination of carbonyl oxygen.

Another important feature of this tetramer structure is that excess diisopropylzinc reagent is co-ordinated to the nitrogen atom of the pyrimidine that is not involved in the formation of the macrocyclic ring. Co-ordination of nitrogen atoms to alkylzinc is known to improve the nucleophilicity of alkylzinc reagents.[104,105] This co-ordination of nitrogen atom to diisopropylzinc

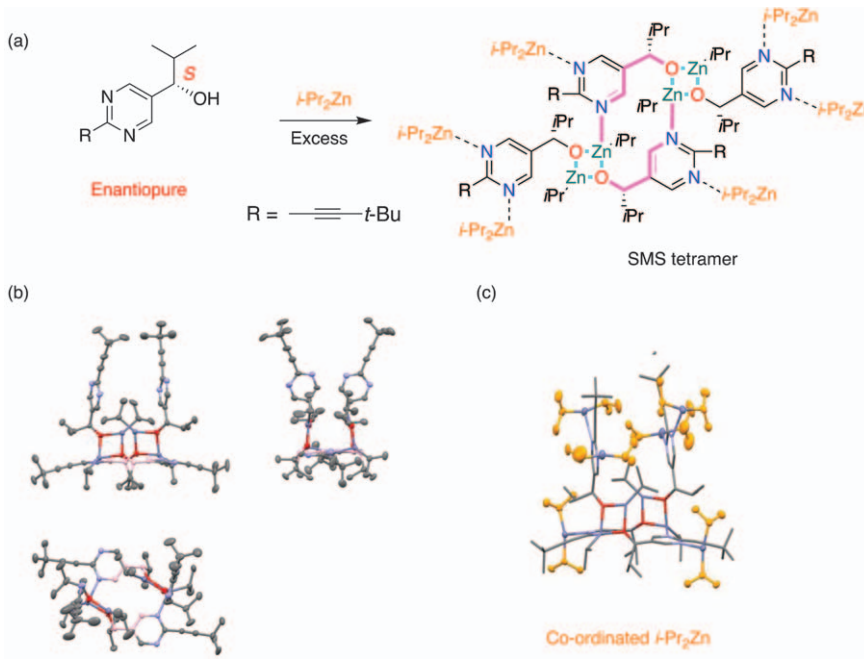

Figure 12.3 Tetramer structure of enantiopure alkoxide **1·Zn**.

slightly extends and bends the Zn–C bond (C–Zn bond, *ca.* 1.99–2.01 Å, C–Zn–C bond, *ca.* 156–164°), although it is small compared to that of the TMED complex.[106] Since asymmetric amplification was observed with pyridine derivatives, it was found that the second nitrogen atom is not necessarily required for asymmetric autocatalysis.[9–14,96–100] However, the advantage of pyrimidine over pyridine in reactivity and amplification efficiency might explain this co-ordination of extra diisopropylzinc. As shown later, oligomeric crystals were obtained in the absence of excess zinc reagent, suggesting that the co-ordination of excess zinc reagent prevents the catalytically active species from aggregating and becoming inactive.

In the case of the racemic alkanol, we also obtained a similar Square-Macrocycle-Square tetramer (Figure 12.4). However, the conformation of the racemic tetramer is completely different from that of the enantiopure tetramer. The enantiopure tetramer has *P*2 symmetry and a square dimer on the same side of the macrocyclic plane. As a result, the two pyrimidine rings occupy the same side of the structure. In the racemic crystal, the crystallographic inversion center is in the center of the tetramer. Thus, the square dimer structure occupies opposite sides. Given the reduced steric hindrance of this centrosymmetric structure, the racemic tetramer is more stable than the enantiopure tetramer by 4.8 kcal mol^{-1} according to DFT calculations. Furthermore, this conformation is quite similar to the

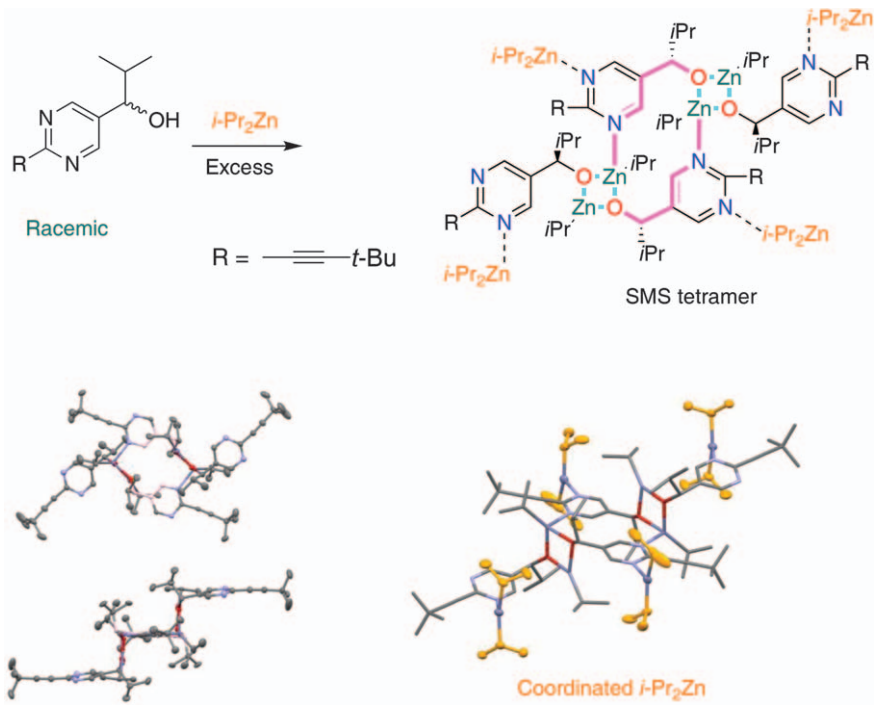

Figure 12.4 Tetramer structure of racemic alkoxide **1**·**Zn**.

structure of the oligomer described in the next section. From this, it can be assumed that the racemic tetramer is more easily oligomerized than the enantiopure form.

Note that no cube-type tetramer was obtained in our several attempts at crystallization. This result supports the hypothesis that the steric hindrance imparted by the isopropyl group prevents the formation of the cube-type tetramer.[99,100]

12.2.2 Structure of Oligomers

In the crystallization of the tetramer, we used an excess of diisopropylzinc and obtained an isopropylzinc-co-ordinated tetramer. It is assumed that the excess zinc co-ordinates to the nitrogen atom of the pyrimidine, preventing further aggregation. In fact, it was found that different crystals appeared when the number of zinc reagent equivalents was reduced (Figure 12.5). In the case of almost equimolar amounts of diisopropylzinc, a 1D-oligomeric structure was obtained for both enantiopure and racemic alkoxide. In this structure, square dimers also bridged by the macrocyclic structure through N–Zn coordination.

Unlike the tetramer structure, both enantiopure and racemic oligomer structures are almost identical if we ignore the orientation of the isopropyl group due to the chirality. In fact, the racemic oligomer crystals show that a disordered structure on the stereocenter of the alkanol, indicating that both enantiomers may crystallize in a partially random arrangement.

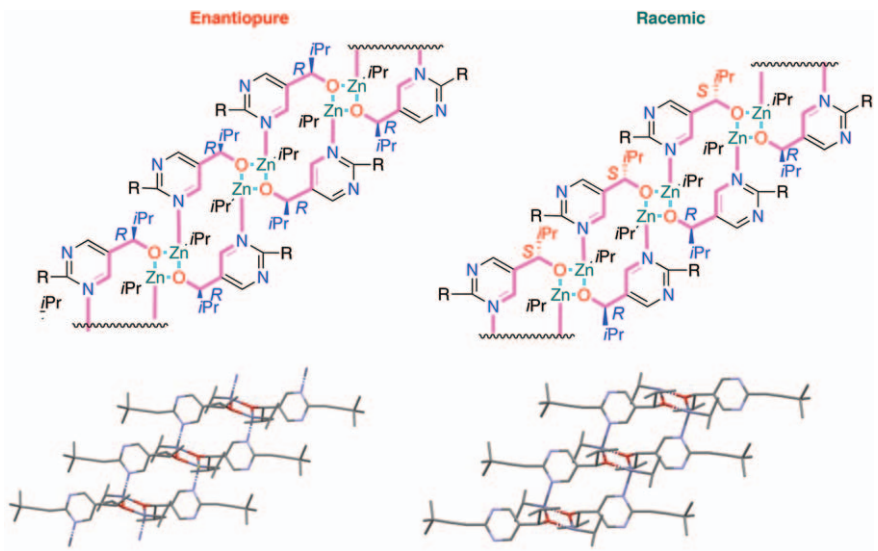

Figure 12.5 Oligomer structure of enantiopure and racemic alkoxide **1**·**Zn**.

Under typical reaction conditions, the zinc reagent is added in excess to the catalyst, and it is unlikely that these oligomers are present in the reaction solution. However, these results clearly show that higher aggregation structures can exist. The formation of reaction-inactive precipitates as oligomers may contribute to asymmetric amplification.

12.2.3 Crystal Structure with Coordinative Solvent

The asymmetric autocatalysis reaction is typically performed in an aromatic solvent such as toluene. Although non-coordinative solvents such as hexane or diethyl ether can also be used as the reaction solvent, the presence of co-ordinative polar solvents such as THF completely suppresses the reaction conversion. A crystal structure of the THF co-ordinated tetramer with enantiopure **1·Zn** was also obtained (Figure 12.6). In this structure, unsaturated zinc is no longer present due to THF co-ordination, and the conformation is changed significantly. Unlike in toluene solution, a sharp NMR spectrum was obtained in the THF solution and it was concluded that the zinc alkoxide is present as a dimer. We could not obtain a good quality crystal of enantiopure dimer crystal with THF, but an enantiopure dimer

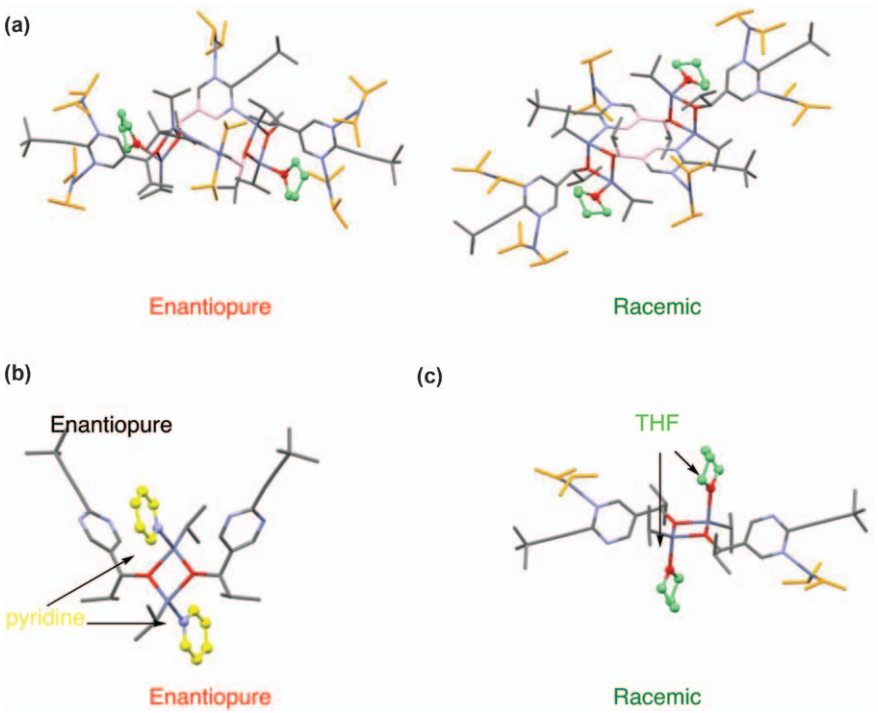

Figure 12.6 Crystal structure of **1·Zn** in co-ordinated solvent. (a) Enantiopure and racemic tetramer with THF; (b) enantiopure dimer with pyridine; (c) racemic dimer with THF.

crystal was isolated with more coordinative pyridine. In the racemic case, a dimer crystal was obtained from THF solution. These observations clearly show why the THF acts as an inhibitor for the reaction and supports the hypothesis that the tetramer is a precursor for the active species.

12.2.4 Crystal Structure with Diethylzinc

Another unique experimental feature of this asymmetric autocatalysis is that efficient asymmetric amplification is observed only with diisopropylzinc reagent as a nucleophile. Diethylzinc has low reactivity and almost no amplification of enantiomeric excess was observed. DFT calculations suggested that the steric hindrance of isopropyl contributes to the stability of the SMS-type tetramer.[78,79] In fact, even when diethylzinc was used in excess, no tetramer was obtained, and oligomeric crystals were obtained (Figure 12.7). In a recent NMR study by Denmark *et al.*, it was hypothesized that the isopropyl group has the effect of preventing the formation of inactive cube-type tetramers.[99,100] We have not yet succeeded in obtaining the crystal structure of the cube-shaped tetramer, because a large amount of fine precipitates formed immediately after mixing in the study using diethylzinc, and it was difficult to obtain crystals of sufficient size for crystal analysis. However, this also supports the hypothesis that the isopropyl group inhibits the formation of inert precipitates.

12.3 CD Spectrum Analysis of Pre-equilibrium of a Zinc Alkoxide

Although X-ray crystallography can provide direct observation of 3D molecular structure, structures that are stable in a crystal do not necessarily

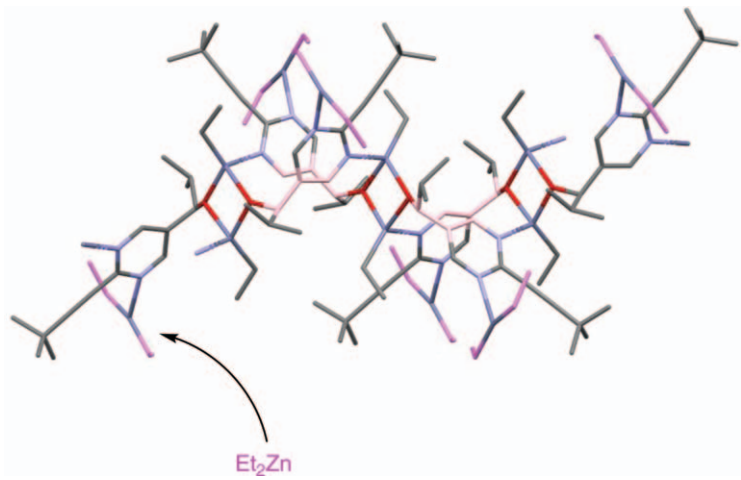

Figure 12.7 Crystal structure of **1** and diethylzinc.

exist in dilute solution. To gain insight into the structure of alkoxides in solution, enantiopure alkoxide solutions were analyzed by CD spectroscopy. CD spectroscopy is a powerful tool for absolute structure determination, but the technique is also useful for conformation analysis: for example, in the analysis of the secondary structure of proteins, because the shapes of the spectra are highly sensitive to conformational changes compared with the normal absorbance spectrum.

In the CD spectrum of a solution of **1**·**Zn**, it was found that the spectra changed reversibly upon changes in temperature (Figure 12.8). Because an isosbestic point is observed in the CD spectrum, this solution is mainly composed of two components. DFT simulations indicate that the spectrum obtained at −20 °C is similar to that of the tetramer obtained from the crystal structure. The spectrum at room temperature resembled that of the structure of the square dimer. This change was more pronounced at higher concentrations, and the reproducibility of the change was less in the absence of an excess of zinc reagent. These results suggest that the dimer exists in equilibrium with the tetramer in solution, supporting the conclusions suggested by NMR analysis and DFT calculations that the dimer is stable in solution and that the multimer forms at low temperatures.

Furthermore, in THF, the shape of the spectrum was invariant with temperature, and DFT simulations showed that the shape of the spectrum was similar to that of the THF-co-ordinated dimer. This result also suggests that tetramer formation is suppressed by THF co-ordination.

12.4 Summary

In this chapter, the aggregation states of various alkoxides were shown by single-crystal X-ray diffraction. The tetramer structure containing a macrocycle was identified in the crystal, and analysis of the circular dichroism spectra supports the conclusion that the tetramer actually exists in equilibrium with the dimer in solution. In addition, oligomer formation was observed without an excess of diisopropylzinc. Co-ordination of excess diisopropyl zinc may play an important role in inhibiting inactive oligomer formation. Furthermore, the structure of the alkoxide also changes significantly due to changes in the co-ordination of the solvent and the alkyl group. It is clear that there is a complex self-organized structural equilibrium behind the seemingly simple addition reaction. It was found that the high asymmetric amplification of asymmetric autocatalysis is due to the asymmetric recognition associated with the efficient self-assembly of the alkoxide. This provides some guidance for the elucidation of the asymmetric amplification mechanism and will help in the search for new asymmetric autocatalytic reactions.

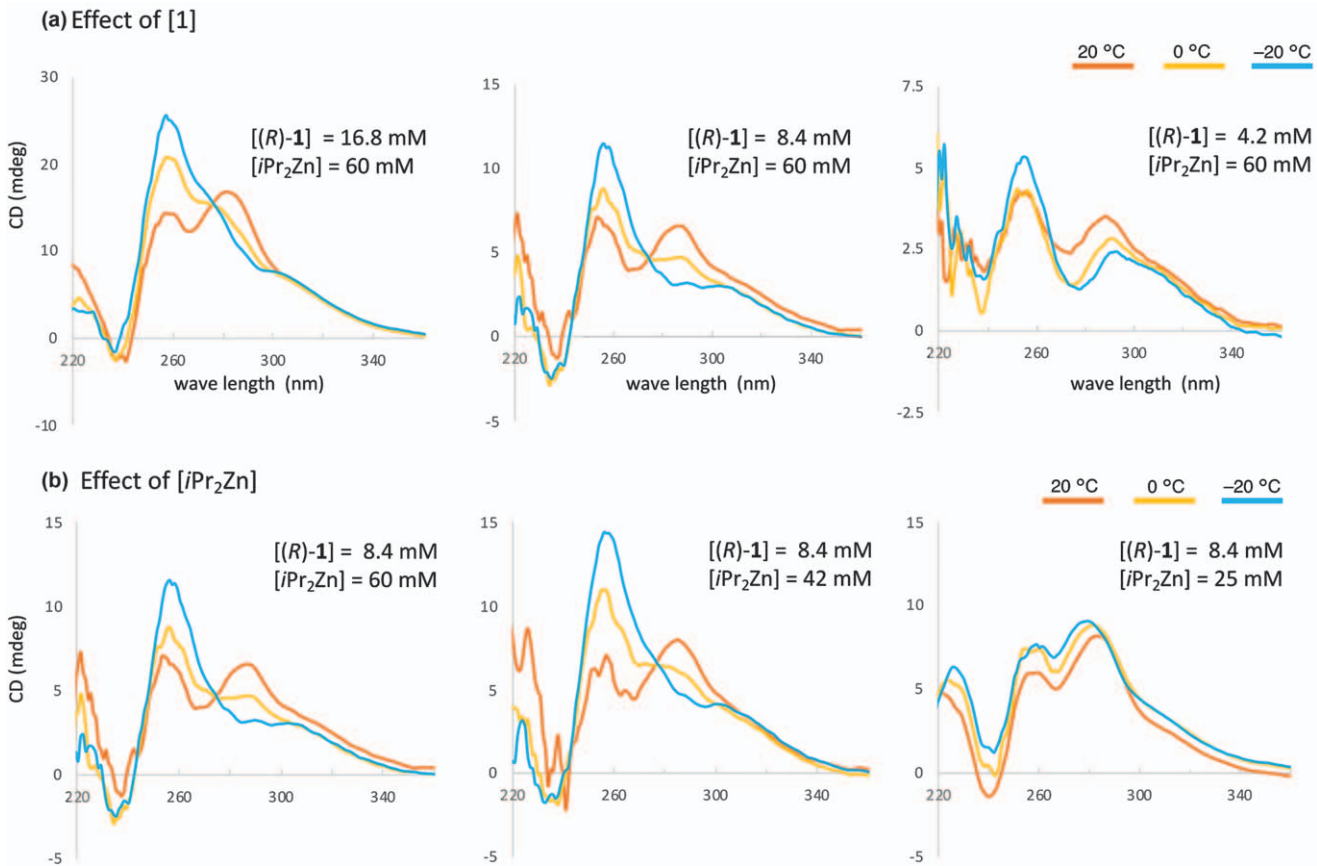

Figure 12.8 CD spectrum of **1**·**Zn** in various concentrations and temperatures.

Acknowledgements

This work was financially supported by JSPS KAKENHI (15H03781, 18H04518, 19K05482, 19K22190, and 20H04674).

References

1. B. L. Feringa and R. A. Van Delden, *Angew. Chem., Int. Ed.*, 1999, **38**, 3418–3438.
2. K. Mislow, *Collect. Czech. Chem. Commun.*, 2003, **68**, 849–864.
3. I. Weissbuch and M. Lahav, *Chem. Rev.*, 2011, **111**, 3236–3267.
4. C. Viedma, *Phys. Rev. Lett.*, 2005, **94**, 065504.
5. D. K. Kondepudi and K. Asakura, *Acc. Chem. Res.*, 2001, **34**, 946–954.
6. S. Pizzarello and A. L. Weber, *Sci.*, 2004, **303**, 1151.
7. R. Breslow and Z.-L. Cheng, *Proc. Natl. Acad. Sci. U. S. A.*, 2010, **107**, 5723–5725.
8. F. C. Frank, *Biochim. Biophys. Acta*, 1953, **11**, 459–463.
9. K. Soai, S. Niwa and H. Hori, *J. Chem. Soc., Chem. Commun.*, 1990, 982–983.
10. T. Shibata, H. Morioka, S. Tanji, T. Hayase, Y. Kodaka and K. Soai, *Tetrahedron Lett.*, 1996, **37**, 8783–8786.
11. S. Tanji, Y. Kodaka, A. Ohno, T. Shibata, I. Sato and K. Soai, *Tetrahedron: Asymmetry*, 2000, **11**, 4249–4253.
12. T. Shibata, K. Choji, H. Morioka, T. Hayase and K. Soai, *Chem. Commun.*, 1996, 751–752.
13. T. Shibata, K. Choji, T. Hayase, Y. Aizu and K. Soai, *Chem. Commun.*, 1996, 1235–1236.
14. I. Sato, T. Nakao, R. Sugie, T. Kawasaki and K. Soai, *Synthesis*, 2004, 1419–1428.
15. K. Soai, T. Shibata, H. Morioka and K. Choji, *Nature*, 1995, **378**, 767–768.
16. T. Shibata, S. Yonekubo and K. Soai, *Angew. Chem., Int. Ed.*, 1999, **38**, 659–661.
17. I. Sato, H. Urabe, S. Ishiguro, T. Shibata and K. Soai, *Angew. Chem., Int. Ed.*, 2003, **42**, 315–317.
18. I. Sato, T. Yanagi and K. Soai, *Chirality*, 2002, **14**, 166–168.
19. F. Lutz, T. Kawasaki and K. Soai, *Tetrahedron: Asymmetry*, 2006, **17**, 486–490.
20. M. Busch, M. Schlageter, D. Weingand and T. Gehring, *Chem. – Eur. J.*, 2009, **15**, 8251–8258.
21. M. Avalos, R. Babiano, P. Cintas, J. L. Jiménez and J. C. Palacios, *Chem. Commun.*, 2000, 887–892.
22. A. J. Bissette and S. P. Fletcher, *Angew. Chem., Int. Ed.*, 2013, **52**, 12800–12826.
23. K. Soai, T. Kawasaki and A. Matsumoto, *Tetrahedron*, 2018, **74**, 1973–1990.
24. K. Soai, *Proc. Jpn. Acad., Ser. B*, 2019, **95**, 89–109.

25. I. Sato, D. Omiya, T. Saito and K. Soai, *J. Am. Chem. Soc.*, 2000, **122**, 11739–11740.
26. T. Kawasaki, M. Shimizu, D. Nishiyama, M. Ito, H. Ozawa and K. Soai, *Chem. Commun.*, 2009, 4396–4398.
27. T. Kawasaki, Y. Matsumura, T. Tsutsumi, K. Suzuki, M. Ito and K. Soai, *Science*, 2009, **324**, 492–495.
28. T. Kawasaki, Y. Okano, E. Suzuki, S. Takano, S. Oji and K. Soai, *Angew. Chem., Int. Ed.*, 2011, **50**, 8131–8133.
29. T. Kawasaki, H. Ozawa, M. Ito and K. Soai, *Chem. Lett.*, 2011, **40**, 320–321.
30. A. Matsumoto, S. Oji, S. Takano, K. Tada, T. Kawasaki and K. Soai, *Org. Biomol. Chem.*, 2013, **11**, 2928–2931.
31. A. Matsumoto, H. Ozaki, S. Harada, K. Tada, T. Ayugase, H. Ozawa, T. Kawasaki and K. Soai, *Angew. Chem., Int. Ed.*, 2016, **55**, 15246–15249.
32. K. Soai, S. Osanai, K. Kadowaki, S. Yonekubo, T. Shibata and I. Sato, *J. Am. Chem. Soc.*, 1999, **121**, 11235–11236.
33. I. Sato, K. Kadowaki and K. Soai, *Angew. Chem., Int. Ed.*, 2000, **39**, 1510–1512.
34. I. Sato, K. Kadowaki, Y. Ohgo and K. Soai, *J. Mol. Catal. A: Chem.*, 2004, **216**, 209–214.
35. H. Shindo, Y. Shirota, K. Niki, T. Kawasaki, K. Suzuki, Y. Araki, A. Matsumoto and K. Soai, *Angew. Chem., Int. Ed.*, 2013, **52**, 9135–9138.
36. A. Matsumoto, H. Ozawa, A. Inumaru and K. Soai, *New J. Chem.*, 2015, **39**, 6742–6745.
37. T. Kawasaki, K. Jo, H. Igarashi, I. Sato, M. Nagano, H. Koshima and K. Soai, *Angew. Chem., Int. Ed.*, 2005, **44**, 2774–2777.
38. T. Kawasaki, K. Suzuki, K. Hatase, M. Otsuka, H. Koshima and K. Soai, *Chem. Commun.*, 2006, **2**, 1869–1871.
39. T. Kawasaki, Y. Harada, K. Suzuki, T. Tobita, N. Florini, G. Pályi and K. Soai, *Org. Lett.*, 2008, **10**, 4085–4088.
40. T. Kawasaki, K. Suzuki, Y. Hakoda and K. Soai, *Angew. Chem., Int. Ed.*, 2008, **47**, 496–499.
41. T. Kawasaki, Y. Hakoda, H. Mineki, K. Suzuki and K. Soai, *J. Am. Chem. Soc.*, 2010, **132**, 2874–2875.
42. T. Kawasaki, M. Nakaoda, N. Kaito, T. Sasagawa and K. Soai, *Origins Life Evol. Biospheres*, 2010, **40**, 65–78.
43. T. Kawasaki, T. Sasagawa, K. Shiozawa, M. Uchida, K. Suzuki and K. Soai, *Org. Lett.*, 2011, **13**, 2361–2363.
44. D. J. Carter, A. L. Rohl, A. Shtukenberg, S. Bian, C. Hu, L. Baylon, B. Kahr, H. Mineki, K. Abe, T. Kawasaki and K. Soai, *Cryst. Growth Des.*, 2012, **12**, 2138–2145.
45. H. Mineki, T. Hanasaki, A. Matsumoto, T. Kawasaki and K. Soai, *Chem. Commun.*, 2012, **48**, 10538–10540.
46. H. Mineki, Y. Kaimori, T. Kawasaki, A. Matsumoto and K. Soai, *Tetrahedron: Asymmetry*, 2013, **24**, 1365–1367.

47. T. Kawasaki, M. Uchida, Y. Kaimori, T. Sasagawa, A. Matsumoto and K. Soai, *Chem. Lett.*, 2013, **42**, 711–713.
48. A. Matsumoto, T. Ide, Y. Kaimori, S. Fujiwara and K. Soai, *Chem. Lett.*, 2015, **44**, 688–690.
49. A. Matsumoto, S. Takeda, S. Harada and K. Soai, *Tetrahedron: Asymmetry*, 2016, **27**, 943–946.
50. T. Kawasaki, S. Kamimura, A. Amihara, K. Suzuki and K. Soai, *Angew. Chem., Int. Ed.*, 2011, **50**, 6796–6798.
51. A. Matsumoto, Y. Kaimori, M. Uchida, H. Omori, T. Kawasaki and K. Soai, *Angew. Chem., Int. Ed.*, 2017, **56**, 545–548.
52. T. Shibata, J. Yamamoto, N. Matsumoto, S. Yonekubo, S. Osanai and K. Soai, *J. Am. Chem. Soc.*, 1998, **120**, 12157–12158.
53. T. Kawasaki, M. Sato, S. Ishiguro, T. Saito, Y. Morishita, I. Sato, H. Nishino, Y. Inoue and K. Soai, *J. Am. Chem. Soc.*, 2005, **127**, 3274–3275.
54. K. Soai, I. Sato, T. Shibata, S. Komiya, M. Hayashi, Y. Matsueda, H. Imamura, T. Hayase, H. Morioka, H. Tabira, J. Yamamoto and Y. Kowata, *Tetrahedron: Asymmetry*, 2003, **14**, 185–188.
55. Y. Kaimori, Y. Hiyoshi, T. Kawasaki, A. Matsumoto and K. Soai, *Chem. Commun.*, 2019, **55**, 5223–5226.
56. D. A. Singleton and L. K. Vo, *Org. Lett.*, 2003, **5**, 4337–4339.
57. D. G. Blackmond, C. R. McMillan, S. Ramdeehul, A. Schorm and J. M. Brown, *J. Am. Chem. Soc.*, 2001, **123**, 10103–10104.
58. D. G. Blackmond, *Adv. Synth. Catal.*, 2002, **344**, 156.
59. F. G. Buono and D. G. Blackmond, *J. Am. Chem. Soc.*, 2003, **125**, 8978–8979.
60. F. G. Buono, H. Iwamura and D. G. Blackmond, *Angew. Chem., Int. Ed.*, 2004, **43**, 2099–2103.
61. D. G. Blackmond, *Proc. Natl. Acad. Sci. U. S. A.*, 2004, **101**, 5732–5736.
62. D. G. Blackmond, *Tetrahedron: Asymmetry*, 2006, **17**, 584–589.
63. N. A. Hawbaker and D. G. Blackmond, *ACS Cent. Sci.*, 2018, **4**, 776–780.
64. N. A. Hawbaker and D. G. Blackmond, *Nat. Chem.*, 2019, **11**, 957–962.
65. D. G. Blackmond, *Chem. Rev.*, 2020, **120**, 4831–4847.
66. I. Sato, D. Omiya, K. Tsukiyama, Y. Ogi and K. Soai, *Tetrahedron: Asymmetry*, 2001, **12**, 1965–1969.
67. I. Sato, D. Omiya, H. Igarashi, K. Kato, Y. Ogi, K. Tsukiyama and K. Soai, *Tetrahedron: Asymmetry*, 2003, **14**, 975–979.
68. F. Lutz, T. Igarashi, T. Kinoshita, M. Asahina, K. Tsukiyama, T. Kawasaki and K. Soai, *J. Am. Chem. Soc.*, 2008, **130**, 2956–2958.
69. T. Gehring, M. Busch, M. Schlageter and D. Weingand, *Chirality*, 2010, **22**(Suppl. 1), E173–E182.
70. I. D. Gridnev, J. M. Serafimov, H. Quiney and J. M. Brown, *Org. Biomol. Chem.*, 2003, **1**, 3811–3819.
71. I. D. Gridnev, J. M. Serafimov and J. M. Brown, *Angew. Chem., Int. Ed.*, 2004, **43**, 4884–4887.
72. M. Quaranta, T. Gehring, B. Odell, J. M. Brown and D. G. Blackmond, *J. Am. Chem. Soc.*, 2010, **132**, 15104–15107.

73. T. Gehring, M. Quaranta, B. Odell, D. G. Blackmond and J. M. Brown, *Angew. Chem., Int. Ed.*, 2012, **51**, 9539–9542.
74. O. Trapp, S. Lamour, F. Maier, A. F. Siegle, K. Zawatzky and B. F. Straub, *Chem. – Eur. J.*, 2020, 15871–15880.
75. O. Trapp, *Front. Chem.*, 2020, **8**, 1–9.
76. I. D. Gridnev and J. M. Brown, *Proc. Natl. Acad. Sci. U. S. A.*, 2004, **101**, 5727–5731.
77. J. J. Klankermayer, I. D. Gridnev and J. M. Brown, *Chem. Commun.*, 2007, 3151–3153.
78. I. D. Gridnev and A. K. Vorobiev, *ACS Catal.*, 2012, **2**, 2137–2149.
79. I. D. Gridnev and A. K. Vorobiev, *Bull. Chem. Soc. Jpn.*, 2015, **88**, 333–340.
80. L. Schiaffino and G. Ercolani, *Angew. Chem., Int. Ed.*, 2008, **47**, 6832–6835.
81. L. Schiaffino and G. Ercolani, *ChemPhysChem*, 2009, **10**, 2508–2515.
82. L. Schiaffino and G. Ercolani, *Chem. – Eur. J.*, 2010, **16**, 3147–3156.
83. G. Ercolani and L. Schiaffino, *J. Org. Chem.*, 2011, **76**, 2619–2626.
84. G. Ercolani, *Tetrahedron: Asymmetry*, 2014, **25**, 405–410.
85. G. Lente, *J. Phys. Chem. A*, 2005, **109**, 11058–11063.
86. É. Dóka and G. Lente, *J. Am. Chem. Soc.*, 2011, **133**, 17878–17881.
87. K. Micskei, G. Póta, L. Caglioti and G. Palyi, *J. Phys. Chem. A*, 2006, **110**, 5982–5984.
88. B. Barabas, L. Caglioti, C. Zucchi, M. Maioli, E. Gal, K. Micskei, G. Pályi, E. Gál, K. Micskei and G. Pályi, *J. Phys. Chem. B*, 2007, **111**, 11506–11510.
89. K. Micskei, G. Rábai, E. Gál, L. Caglioti and G. Pályi, *J. Phys. Chem. B*, 2008, **112**, 9196–9200.
90. M. Maioli, K. Micskei, L. Caglioti, C. Zucchi and G. Pályi, *J. Math. Chem.*, 2008, **43**, 1505–1515.
91. B. Barabás, C. Zucchi, M. Maioli, K. Micskei and G. Pályi, *J. Mol. Model.*, 2015, **21**, 33.
92. J. Crusats, D. Hochberg, A. Moyano and J. M. Ribó, *ChemPhysChem*, 2009, **10**, 2123–2131.
93. T. Satyanarayana, S. Abraham and H. B. Kagan, *Angew. Chem., Int. Ed.*, 2009, **48**, 456–494.
94. M. Kitamura, S. Suga, M. Niwa and R. Noyori, *J. Am. Chem. Soc.*, 1995, **117**, 4832–4842.
95. Ł. Mąkolski, V. Szejko, K. Zelga, A. Tulewicz, P. Bernatowicz, I. Justyniak and J. Lewiński, *Chem. – Eur. J.*, 2021, **27**, 5666–5674.
96. C. Romagnoli, B. Sieng and M. Amedjkouh, *Eur. J. Org. Chem.*, 2015, 4087–4092.
97. M. Funes-Maldonado, B. Sieng and M. Amedjkouh, *Eur. J. Org. Chem.*, 2015, 4081–4086.
98. M. Funes-Maldonado, B. Sieng and M. Amedjkouh, *Org. Lett.*, 2016, **18**, 2536–2539.

99. S. V. Athavale, A. Simon, K. N. Houk and S. E. Denmark, *Nat. Chem.*, 2020, **12**, 412–423.
100. S. V. Athavale, A. Simon, K. N. Houk and S. E. Denmark, *J. Am. Chem. Soc.*, 2020, **142**, 18387–18406.
101. A. Matsumoto, T. Abe, A. Hara, T. Tobita, T. Sasagawa, T. Kawasaki and K. Soai, *Angew. Chem., Int. Ed.*, 2015, **54**, 15218–15221.
102. A. Matsumoto, S. Fujiwara, T. Abe, A. Hara, T. Tobita, T. Sasagawa, T. Kawasaki and K. Soai, *Bull. Chem. Soc. Jpn.*, 2016, **89**, 1170–1177.
103. A. Matsumoto, A. Tanaka, Y. Kaimori, N. Hara, Y. Mikata and K. Soai, *Chem. Commun.*, 2021, **57**, 11209–11212.
104. K. Soai, M. Watanabe and M. Koyano, *Bull. Chem. Soc. Jpn.*, 1989, **62**, 2124–2125.
105. K. Soai and S. Niwa, *Chem. Rev.*, 1992, **92**, 833–856.
106. A. Lennartson, A. Hedström and M. Håkansson, *Acta Crystallogr., Sect. E: Struct. Rep. Online*, 2006, **63**, m123–m125.

CHAPTER 13

Symmetry Breaking in a Heterogenous Phase: Intriguing Intermediates and Side-products During Asymmetric Amplification

MOHAMED AMEDJKOUH* AND GIUSEPPE ROTUNNO

Department of Chemistry, University of Oslo, P.O. Box 1033 Blindern, 0315 Oslo, Norway
*Email: mamou@kjemi.uio.no

13.1 Introduction

13.1.1 Background

The origin of homochirality remains an intriguing scientific question.[1–7] *Absolute asymmetric synthesis* is defined as asymmetric synthesis in the absence of chiral factors.[8–11] It has also been considered a possible explanation for homochirality since it does not require any chiral source. According to statistical theories, the number of enantiomers in a racemic mixture is rarely the same, and these are always subject to small fluctuations: for n molecules, there will be a standard deviation from 50 : 50 of $(n^{1/2})/2$. However, the ee of the product is always below the detection level.[12]

Thus, reactants obtained as single enantiomer crystals can be used in absolute asymmetric synthesis and promote enantioenrichment (ee) without the intervention of chiral catalysts.[13–15] Single phase homochirality without

Catalysis Series No. 43
Asymmetric Autocatalysis: The Soai Reaction
Edited by Kenso Soai, Tsuneomi Kawasaki and Arimasa Matsumoto

Published by the Royal Society of Chemistry, www.rsc.org

counter enantiomer nucleation may also be accessed through crystallization, although no chemical transformation occurs throughout the processes.[16,17] Also, circularly polarized light (CPL) induces crystal growth of a specific enantiomer by action of chiral side products.[18,19] By Viedma ripening of organometallic complexes, six-coordinated Δ- and Λ-$[Co(bpy)_3]^{2+}$ cations and tetrahedral Δ- and Λ-$[Ag(PS)_2]^+$ cations (PS = (2-(methylthio)ethyl)-diphenylphosphine) were successfully obtained in enantiopure forms. The decisive stage showing spontaneous molecular symmetry breaking (SMSB) is the formation of the racemic conglomerate from the racemic mixture of enantiomers.[20,21] Enantioenrichment is also possible by selective crystallization or sublimation.[22,23]

In the field of catalysis, Soai *et al.* showed that the addition of diisopropylzinc to pyridine-3-carbaldehyde **1** could behave autocatalytically (see Scheme 13.1).[24] (*S*)-Pyridyl alcohol **2** with 86% ee was used as a 20% chiral autocatalyst for the enantioselective alkylation of **1**. The product was obtained in 67% yield and 35% ee. Despite the erosion of ee, the predominant configuration of the product was the same as that of the catalyst.

Among other molecular scaffolds, 5-pyrimidine aldehydes were able to give higher enantioselective autocatalysis compared to the other substrates (see Scheme 13.2).[25–30]

The substituent at the 2-position seemed to play an important role in the efficiency of the asymmetric autocatalysis and to prevent the erosion of the final ee. In particular, (*S*)-**4c** was found to be a perfect autocatalyst.[30]

To date, the Soai reaction offers the only example of such an absolute asymmetric catalytic reaction in the absence of chiral polarization.[31–33] Frank envisioned an asymmetric autocatalytic model,[34] where one enantiomer catalyzes its own production at the expense of its opposite enantiomer, giving rise to high asymmetric amplification from extremely low enantiopurity.[35]

Thus, even classical statistical fluctuation in the enantiomeric ratio can lead to spontaneous asymmetric synthesis,[36–38] by virtue of a non-linear relationship (NLE) of a catalyst–product pair, in the form of a homochiral dimer

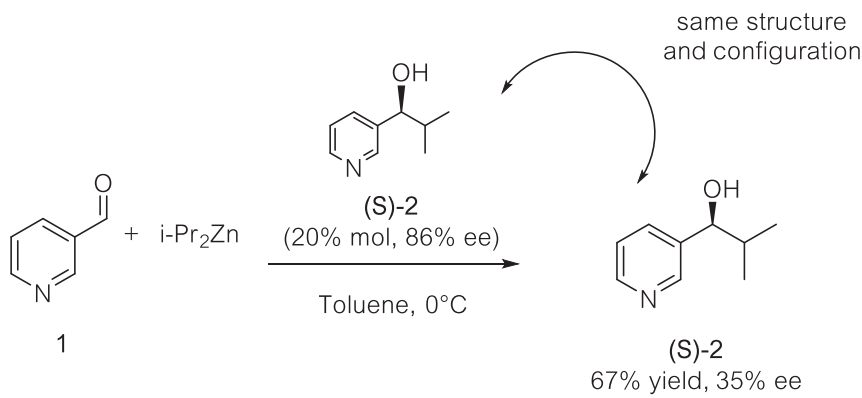

Scheme 13.1 Asymmetric autocatalytic isopropylation of 3-pyridine aldehyde.

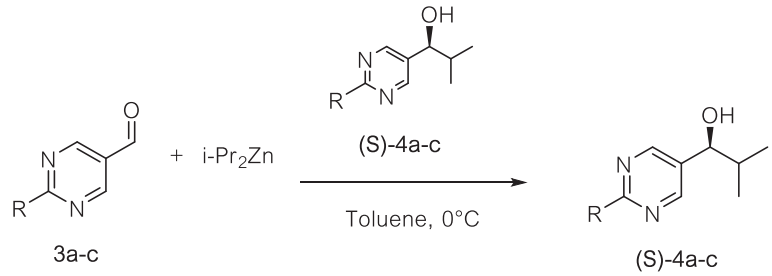

R	Initial *ee*	Final *ee*
a: H	93%	90%
b: Me	>99,5	98,2%
c: t-Bu-C≡C	>99,5	>99,5

Scheme 13.2 Asymmetric autocatalytic isopropylation of 5-pyrimidine aldehydes.

species.[34,39–49] In the Soai reaction those small fluctuations in racemic mixtures can be amplified by the asymmetric autocatalysis, showing mirror-symmetry breaking features. Indeed, Singleton and Soai have demonstrated that reactions of **3b** and **3c** were able to yield enantioenriched alkanols **4b** and **4c** without the requirement of any chiral substance in liquid phase reactions. The products were formed with an approximately stochastic distribution of the two enantiomers.[50,51] Recent developments introduced pyridinyl alkanols **6** as a new autocatalytic family and their amplification in parallel with pyrimidinyl alkanol **3**.[52–54] Further investigations by Denmark *et al.* report on the function of the pyridyl- and pyrimidyl-moiety in the NMR studies revealing a tetrameric structure, also described as a cube escape model.[55]

In this chapter, we focus on alternative mechanistic features to improve our understanding of the autocatalytic amplification behind the Soai reaction. This was made possible by extending the focus to heterogenous conditions of the reaction. This approach involved probing existing hypothesis by physical confinement of reactive species in metal organic framework materials. Also, it draws attention to new chiral products exhibiting autocatalytic features found exclusively while operating under heterogenous conditions. The discussion here demonstrates that their formation is associated with episodes of hydride transfer involving a hemiacetal intermediate and may be key players in the amplification process.

13.1.2 Symmetry Breaking and Spontaneous Absolute Asymmetric Synthesis

In prior work Soai *et al.* revealed that autocatalysis was also possible under heterogenous conditions. Achiral crystals (achiral space group $P\bar{1}$) rising

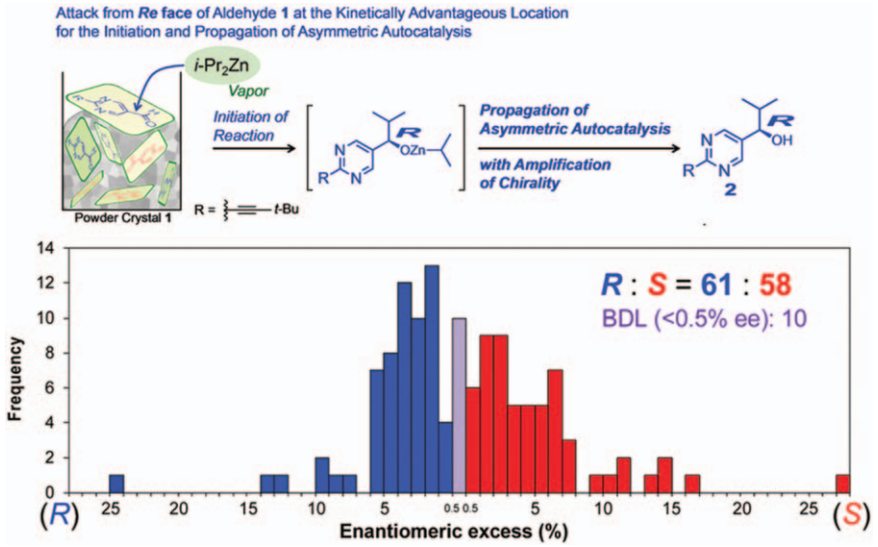

Scheme 13.3 Kinetic heterogenous absolute synthesis in the Soai reaction. Reproduced from ref. 58 with permission from the Royal Society of Chemistry.

from achiral pyrimidine-5-carbaldehyde **3c**, with enantiotopic (001) and (00$\bar{1}$) faces, underwent enantioselective addition of iPr_2Zn vapor. The absolute configuration of the alcohol product correlated with the orientation of the prochiral aldehyde in the achiral crystal lattice.[56,57] Thus, the two-dimensional chirality at the crystal surface dictates the absolute configuration of chiral secondary alcohol **4c**. Then, the newly generated product **4c** was reacted in solution to enhance further ee to greater than 99.5%. Similar reactivity was extended with absolute asymmetric synthesis under kinetic control of vapor–solid phase of reaction of *i*-Pr_2Zn with aldehyde **1** (see Scheme 13.3).[58] The authors analyzed the frequency ratio of distribution of enantiomers and found that reactions provided alkanol 61 times with (*R*) configuration and 58 times as (*S*). Statistical theories revealed that reaction under heterogenous conditions statistical distribution was in line with spontaneous absolute synthesis.[1] In a concomitant report additional products relevant for the mechanism of autocatalysis were identified during a similar process of symmetry breaking.[59]

13.2 Symmetry Breaking with Soai Autocatalysis in MOFs

The reports from the Soai group prompted further studies in order to examine the potential of autocatalysis under heterogenous conditions. Thus, it became relevant to probe confinement effects on the formation of the autocatalytic species and the extent of amplification when possible. Metal–organic

Frameworks (MOFs) were identified for such heterogenous asymmetric catalysis to function as a crystalline sponge for guest inclusion and promote asymmetric reactions in a pocket-like confined space.[60] MOFs are porous crystalline materials, consisting of a 2D or 3D network, with metal containing nodes known as secondary building units (SBUs) linked by multidentate organic ligands (linkers) by strong chemical bonds.[61]

13.2.1 DFT Analysis of Host–Guest Interactions

Soai aldehyde **3c** was preferred as a substrate for the inclusion process, and as stated it was found to be the best performing substrate in solution for the asymmetric autocatalysis with (+)-NLE, and it allows high ee even under absolute conditions. UiO-67 was chosen as a preliminary host material. To evaluate the feasibility of the inclusion process, periodic DFT calculations have been performed to predict the preferred location of guest **3c** inside the unit cell of the host MOF (see Figure 13.1).[60]

Upon physisorption in the octahedral cage of the framework, optimized structures revealed interaction of **3c** with the Zr-cluster, which is characterized by a H-bond between the hydrogen of the hydrated cornerstone of the MOF cluster and the oxygen of the carbonyl group. The location appeared convenient in UiO-67, mainly because **3c** is of comparable size with the

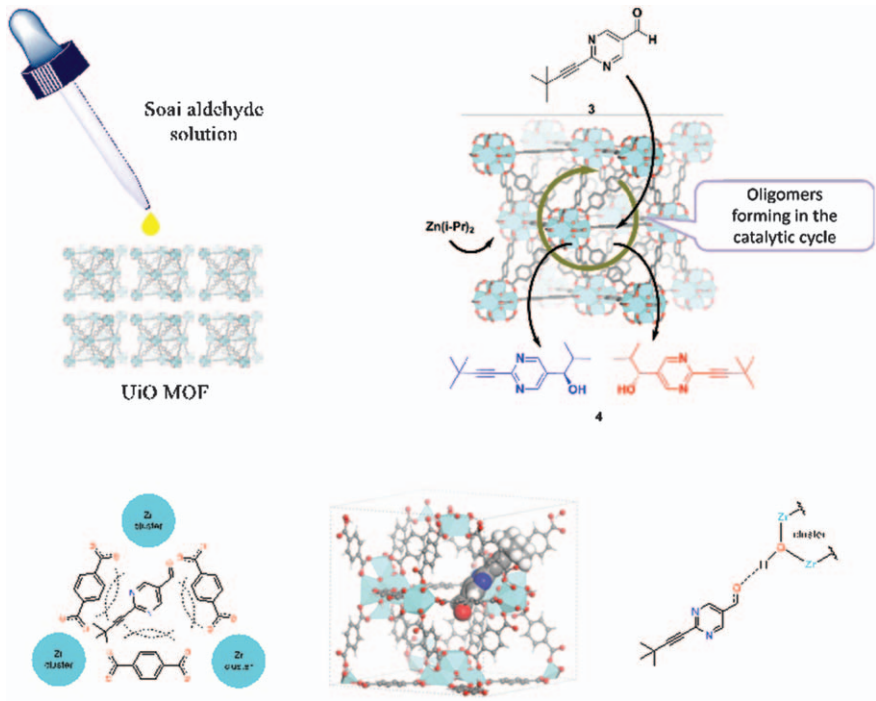

Figure 13.1 Inclusion strategy and DFT model of **3** in cavities of UiO-MOF.

biphenyl dicarboxylate linker of the MOF. However, a similar analysis shows a difference in the accommodation of aldehyde **3c** in UiO-66 with smaller cavities, because of a significantly shorter terephthalic acid linkers (see Figure 13.1). As the DFT calculations showed, high repulsions make energetically disfavored the presence of aldehyde **3c** in the same position as in UiO-67. The optimized structure shows that interactions between **3c** and the framework consisted mainly of week van der Waals interactions with the organic linkers and binding to the clusters.

13.2.2 The Inclusion: Analysis

The inclusion of Soai aldehyde **3c** was performed by soaking the MOF powder in a solution of aldehyde followed by gradual concentration of the substrate in a host–guest interaction. The overall process induces confinement of aldehyde within the framework both at the surface and in the pores of the crystalline material. This requires removing excess aldehyde on the surface by successive washings with solvent. Subsequent PXRD (Powder X-Ray Diffraction) analysis of the host UiO-67 with guest aldehyde confirmed that crystallinity of the solid material was preserved.

In addition, ATR-IR analysis (Infrared Spectroscopy by Attenuated Total Reflectance) revealed a series of signals diagnostic of aldehyde **3c** in the framework (see Figure 13.2 red line, and Figure 13.3 blue line). The aldehyde carbonyl signal is found by stretching at 1700 cm^{-1}, while the peak *ca.* 2200 cm^{-1} is attributed to the stretching of aromatic C–N. The C–H stretching of the terbutyl/isopropyl groups is observed below 3000 cm^{-1}. Furthermore, as predicted by DFT calculations, aldehyde interactions with the O–H stretching of the clusters are indicated by perturbations at 3700 cm^{-1} after inclusion with respect to pristine material.

Comparing the spectra of the two materials after inclusion (Figure 13.4, red and blue lines), a slight shift of the carbonyl stretching around 1700 cm^{-1} to lower wavenumbers is observed in the UiO-67 compared to the UiO-66. This is once again in line with the hypothesis of an interaction for the carbonyl of the aldehyde with the clusters in UiO-67 not present in UiO-66.

13.2.3 Symmetry Breaking and Amplification

In the absence of a chiral inductor, alkylation of aldehyde **3c** in UiO MOFs provide enantiomeric ratios of alcohol **4c** with random distribution: a characteristic feature of absolute asymmetric synthesis. The general features of the reactivity inside the crystalline material are reproduced for different MOF structures and various batches of *i*-Pr_2Zn. Pristine solid Soai aldehyde showed constantly full conversion with very high enantioselectivity in the range of 78–94% ee (see Table 13.1). For the reactions inside MOFs, an interesting difference is that the enantioselectivity was lower even though good conversion was retained. The difference in ee was observed with varying *i*-Pr_2Zn sources in the same MOF series, contrasting with the

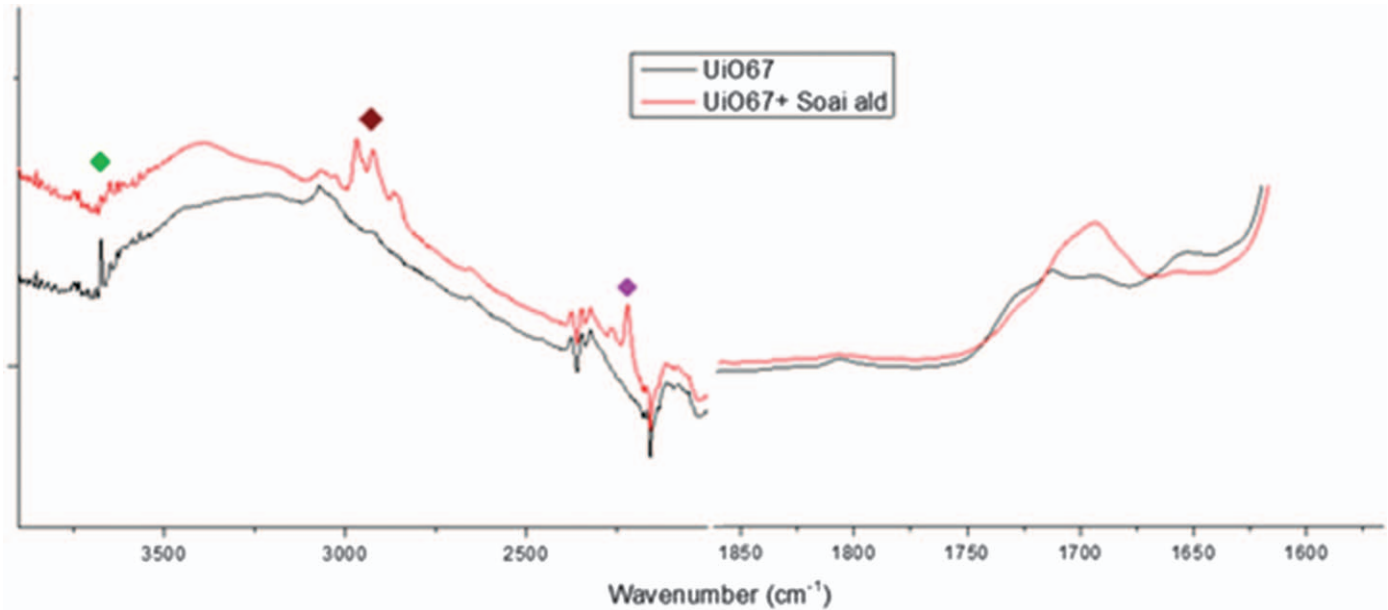

Figure 13.2 IR analysis of UiO-67 (bare) and UiO-67 after inclusion of aldehyde **3c**. On the left, stretching of the hydroxyl groups (in green), stretching of the terbutyl/isopropyl groups (in red), stretching of the C–N of the ring (in purple). On the right, stretching of the carbonyl group. Reproduced from ref. 60 with permission from John Wiley & Sons, Copyright © 2021 The Authors. Chemistry – An Asian Journal published by Wiley-VCH GmbH.

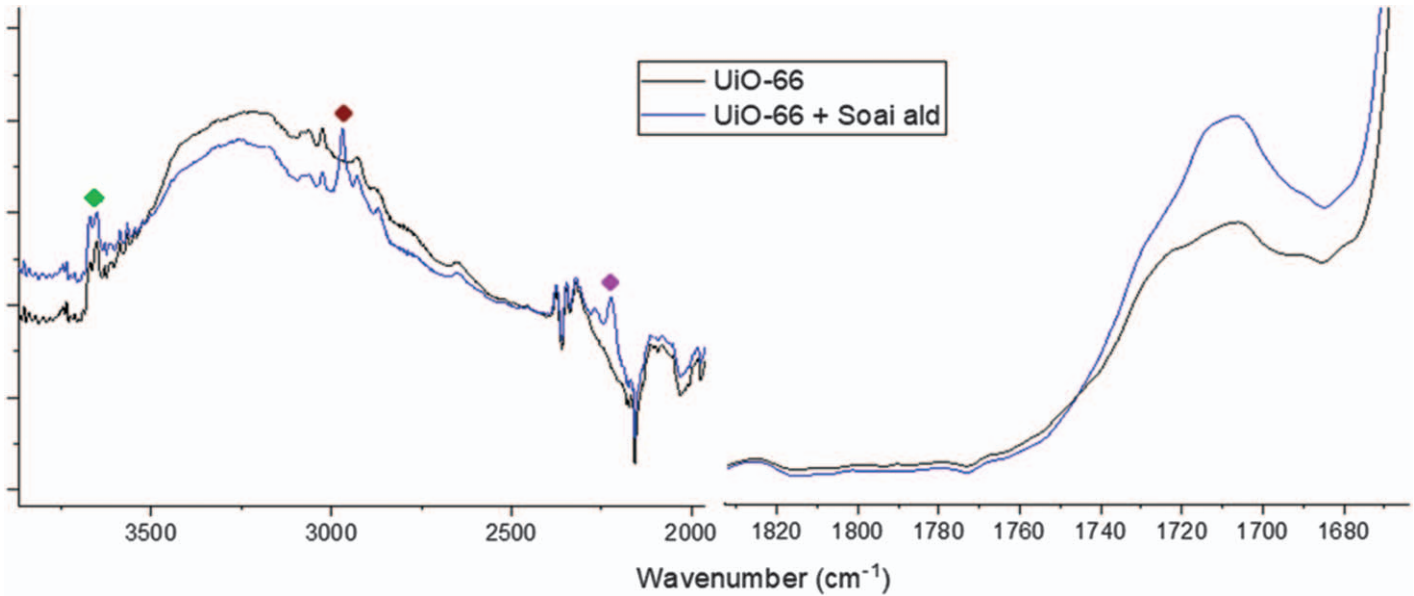

Figure 13.3 IR analysis of UiO-66 and UiO-66 after inclusion of aldehyde **3c**. On the left, stretching of the hydroxyl groups (in green), stretching of the terbutyl/isopropyl groups (in red), stretching of the C–N of the ring (in purple). On the right, stretching of the carbonyl group. Reproduced from ref. 60 with permission from John Wiley & Sons, Copyright © 2021 The Authors. Chemistry – An Asian Journal published by Wiley-VCH GmbH.

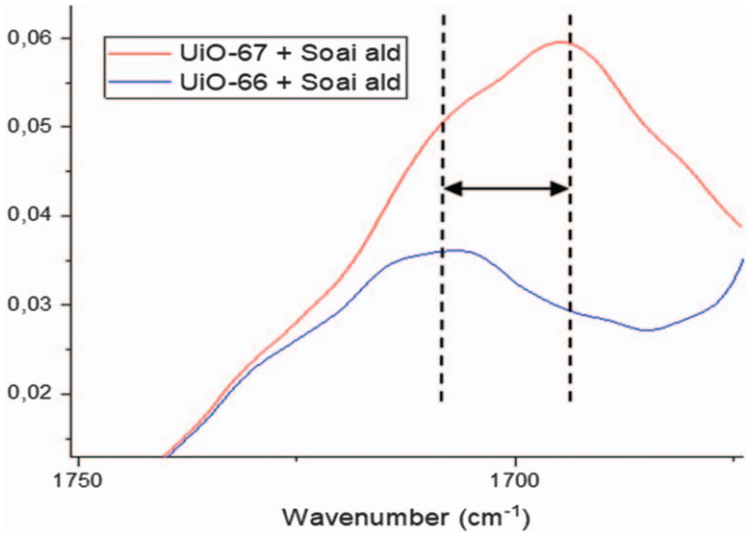

Figure 13.4 Carbonyl stretching in UiO-67 and UiO-66.

Table 13.1 Screening of different UiO MOFs to the vapor phase reaction.[a]

MOF	Zn batch 1 absolute config. **4c** ee/conv. (%)	Zn batch 2 absolute config. **4c** ee/conv. (%)	Zn batch 3 absolute config. **4c** ee/conv. (%)	Zn batch 4 absolute config. **4c** ee/conv. (%)	Zn batch 5 absolute config. **4c** ee/conv. (%)
Soai Aldehyde	**R** **93/99**	**R** **78/99**	**R** **92/99**	**R** **88/99**	**R** **94/99**
UiO-67 (A)	**R** **23/93**	*S* 14/92	**R** **30/93**	**R** **17/92**	**R** **9/91**
UiO-67 (B)	**R** **27/55**	**R** **7/51**	*S* 33/57	*S* 35/35	**R** **45/47**
UiO-67 (C)	*S* 8/83	*S* 31/62	*S* 40/62	*S* 14/65	*S* 23/89
UiO-67 binap	**R** **7/71**	**R** **21/80**	ND	*S* 43/71	**R** **28/82**
UiO-66	**R** **32/55**	**R** **38/20**	**R** **35/51**	*S* 19/15	*S* 16/43
UiO-67 bpy 10%	**R** **18/81**	**R** **11/85**	*S* 26/86	**R** **22/87**	**R** **48/89**

[a]Predominant enantiomers: (*R*) in bold – (*S*) in italic.

behavior of pristine Soai aldehyde. Similarly, the same *i*-Pr_2Zn solution provided alkanol **4** with varying ee in different MOFs. The possible influence of guest accumulation in the host MOF was alleviated by control experiments. On increasing the concentration of aldehyde in UiO-67 from 2.5% to 11.5% enantioselectivity dropped from 28 to 22% ee with comparable conversion at 70%. Similar behavior is observed for the set of experiments with

increasing **3**-UiO-67 loadings with ranges of 43–46% ee and 88–95% conversion. Thus, changes are very significant within the same MOF.

The low amplification level of ee in MOFs compared to the pristine Soai aldehyde is mainly attributed to confinement effects of the framework of the MOF. The pristine aldehyde **3c** can react with no boundaries despite the solid state of the substrate because a continuum in the lattice allows for propagation of the reactive species. In contrast, constraints in the MOF lead to limited diffusion of the oligomeric species involved in the autocatalytic cycles. Thus, autocatalysis is probably confined to several reaction compartments, and the final observed ee consists of a sum of the total autocatalytic cycles occurring in multiple local sites of the MOF. Besides, the rising ee may be reflecting the local chirality in the UiO-MOF series.

The predominance of (*R*)-**4c** in the case of pristine aldehyde could lead to apparent non-stochastic distribution of the enantiomers. This possibility requires pro-*R* crystallization of the Soai aldehyde **3c**. Although this observation is noteworthy, it is in contradiction with the recent work of Soai *et al.* showing a clear frequency of 61 : 58 distribution of *R* : *S* enantiomers.[58] However, a striking difference is the high level of enantiopurity reached in all reactions of pristine aldehyde **3c** under the conditions employed by Amedjkouh *et al.* (*vide infra*). Interestingly, this predominance of one enantiomer is no longer manifested for reactions in MOFs with a frequency of 17 : 13 ratio of *R* : *S* enantiomers, in agreement with Soai's report.[58] Even if (*R*)-**4c** may seem to prevail, this may just be attributed to the small number of experiments performed in the study.

Different setups were used for confined autocatalysis: either individual samples or triplicates for the reaction of *i*-Pr_2Zn vapor on solid aldehyde. Analysis of kinetic plots indicates a trend for reaction conversion. At an early stage, the graphs show a faster transformation after 20 hours in UiO-67 than in the pristine material. In contrast a significantly lower conversion is seen in UiO-66, even when compared to other MOFs (see Figure 13.5). In general, these results suggest comparable reactivities in MOFs of similar structures with a large cavity size derived from the UiO-67. Also, the highest conversion fraction is produced at the early rates, just within the first 5 hours of reaction time. Then, in all cases autocatalysis proceeds at a slower pace. Likewise, symmetry breaking seems to be a sudden event and selectivity is a purely kinetic phenomenon with a significant rise of ee. Amplification tends to peak after 5 hours of reaction in an almost parallel pattern as for fraction conversion.

Capture and diffusion of *i*-Pr_2Zn vapor within the cavities of the solid framework hold as rationale for the observed reactivity. The diffusion depends on the size of the MOF and may influence the organozinc availability to react with aldehyde. Meanwhile, boundary conditions for the supply of aldehyde also have a significant influence on the reactivity. Here again the concentration of aldehyde in the solid is contingent of the size of the MOF host. Upon reaction with *i*-Pr_2Zn molecules of Zn–alkanol are produced and form oligomers with different sizes. Higher oligomers are formed in UiO-67

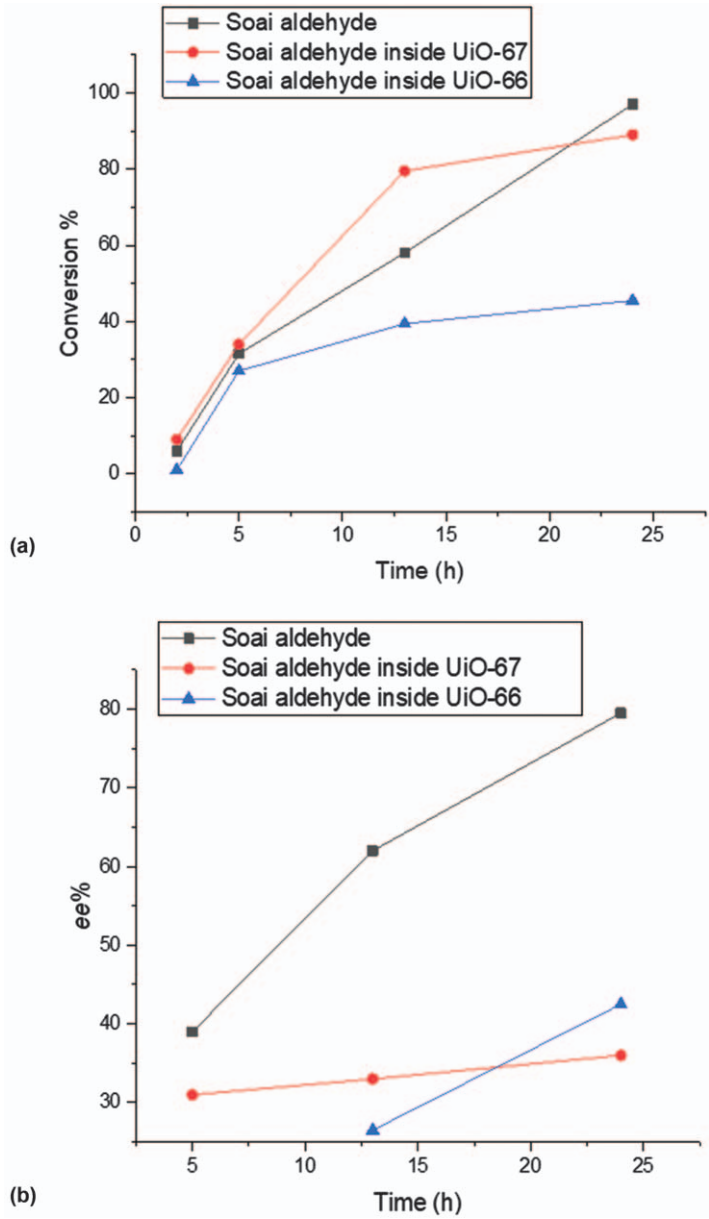

Figure 13.5 (a) Conversion in the three materials. (b) ee% in the three materials. The data point of the ee of the reaction onside UiO-66 after 5 h is missing because of low peak intensity. Reproduced from ref. 60 with permission from John Wiley & Sons, Copyright © 2021 The Authors. Chemistry – An Asian Journal published by Wiley-VCH GmbH.

and lead to higher amplification. On the other hand, short oligomers are also autocatalytically active with high conversion rates, but low enantioselectivity. They are favored in small cavities of the UiO-66, but can also form by dissociation of larger components while migrating between cavities in UiO-66.

13.3 Focus on the Vapor Phase Reaction on Pristine Solid Substrates

13.3.1 Soai Aldehyde

Autocatalysis under heterogenous conditions brought new interesting observations. Indeed, in the well-established amplification under homogenous conditions, only alkanols of type **4** were observed (see Scheme 13.4). Reactions of *i*-P_2Zn vapor on solid aldehydes **3c** and **5c** exhibited a variety of new products in the absolute synthesis.[62] Although these may be considered as side products, their rise during this chemical process tends to suggest a more intricate role in the symmetry breaking and ensuing asymmetric amplification. The most significant observation relates to the formation of chiral esters **9** and **13**. In addition, independent experiments also show amplification of the handedness of the esters subsequent to symmetry breaking. Thus, this observation suggests that formation of esters **9** and **13** exhibits an autocatalytic character. The rationale behind the event of these

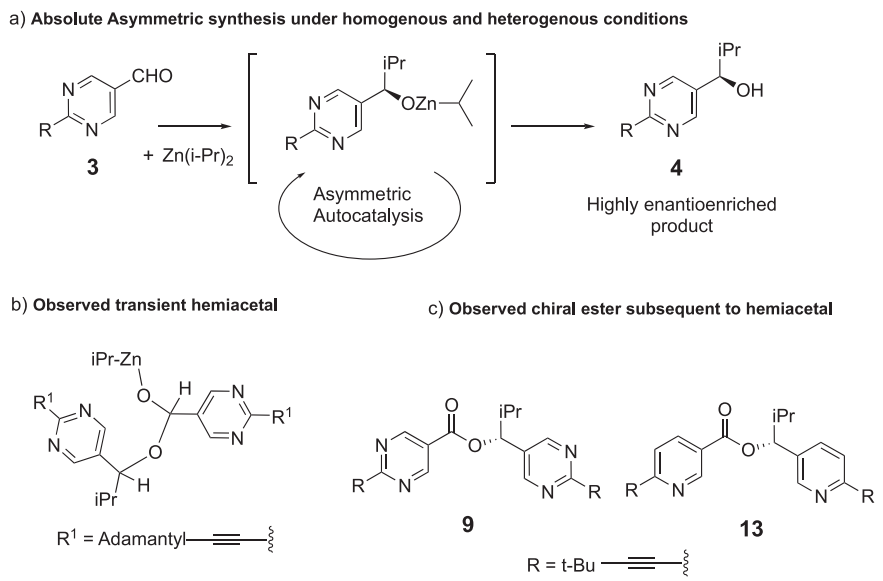

Scheme 13.4 (a) Absolute asymmetric synthesis initiated by symmetry breaking. (b) Observed transient hemiacetal by Brown *et al.* (c) Isolated chiral ester derived from hemiacetal intermediate in recent work.

chiral esters relates to a previously discussed rise of a "*transient hemiacetal*" during the Soai autocatalysis.[63,64]

The results shown above raise the question whether the vapor phase Soai reactions analyzed so far are following the same mechanism and had the same properties as the liquid phase reactions. Generally, under heterogeneous conditions, the conversion slowly increased over time but the ee values were found to be very high immediately following symmetry breaking in the first samples after 30 minutes. Additional experiments focused on the early stages of the reaction. The results summarized in Table 13.2 show slow progress of the reaction and confirmed that ee values were maintained constantly very high throughout all samples over 45 minutes.

Evaluation of the possible effect of $Zn(iPr)_2$ concentration on the high ee values measured for alcohol **4c** revealed some new aspects of the reaction. Under heterogenous conditions, initial experiments were conducted with 2 equivalents of iPr_2Zn vapor on solid Soai aldehyde **3c** at room temperature. This concentration of organozinc corresponds to that used for optimal conditions in solution. Analysis of crude NMR spectra allowed identification of related compounds (side products) consisting of ketone **8** and chiral ester resulting from alkylation of aldehyde, in line with our previous observations (see Scheme 13.5). In addition, the reaction also provided achiral esters **9** rising from reduction alkanol **7**. Side products were not always observed and in several cases with higher concentration in i-Pr_2Zn delivered exclusively alkanol **3c** as the sole product (see Figure 13.6). The results show a steady decay of aldehyde **3c** along with forming alkanol **4c** and reduction alkanol **7** already in the early stages of the reaction. In all runs, chiral ester **9** was

Table 13.2 Conversion and ee% for **4c** in the early stages of the reaction.

Time (min)	ee% **4c**	Conversion **4c** (%)
5	89	2.6
10	89	2.2
15	82.5	3.8
30	81	3.3
45	90.5	5

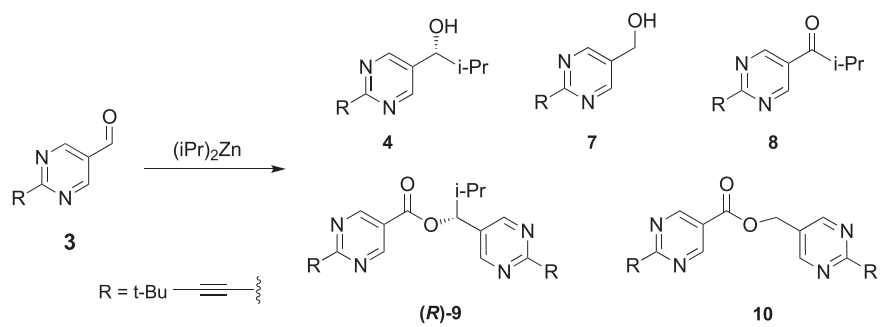

Scheme 13.5 Spontaneous absolute catalysis in the pyrimidine series.

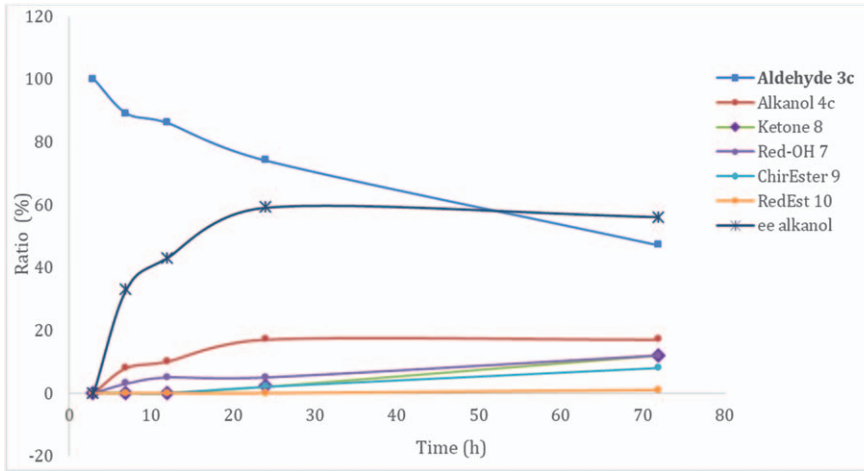

Figure 13.6 Product distribution *vs.* time for the reaction with a 1 : 0.5 ratio of **3c** : *i*-Pr_2Zn.

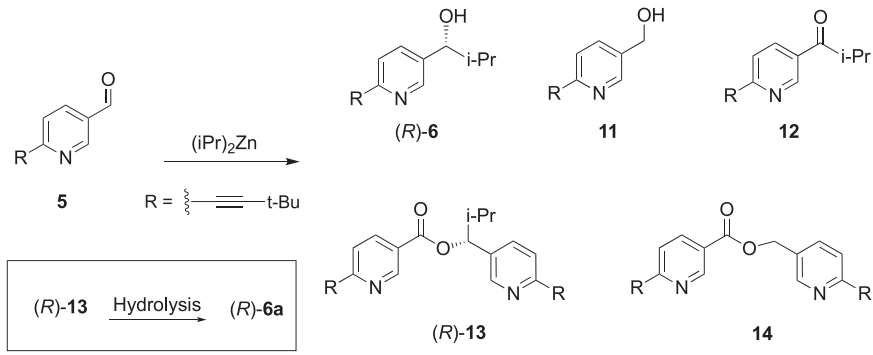

Scheme 13.6 Spontaneous absolute catalysis in the pyridine series.

formed with the same absolute configuration of **4c**, and for example, the ee values were found comparable for both (*R*)-**9** and (*R*)-**4c**.

13.3.2 Analyses of the Reaction Crude in the Pyridine Series

Single crystal analysis showed that aldehyde **5a** crystallized in the achiral $Pca2_1$ space group. This establishes that **5a**, when used in powder form as the starting material, does not provide chiral polarization behind the symmetry breaking. The products formed in the reaction at rt and the respective yields are reported in Scheme 13.6. In previous studies in solution, primary alcohol **11** was the only reported side-product formed in homogenous phase.[54] Interestingly, under a heterogenous phase, reactions of *i*-Pr_2Zn vapor with solid aldehyde produced ketone **12** and two esters, a chiral compound **13**, and another achiral **14**, in the mixture. While compounds

7–10 in the pyrimidine series, with the exception of ketone **8**, were found in low amount and only in particular conditions, the pyridine side products (see Scheme 13.5) were found in comparable amounts to the main product **6a** and in almost all runs. It seemed clear that **6a** and **13**, as well as **11** and **14**, were related to the reaction mechanism. Hydrolysis of chiral ester **13** delivered alkanol **6a** with predominant absolute configuration identical to the main product **6a**. It should be noted that both **6a** and **13** were formed invariably with the same absolute configuration.

Analysis of ee progression for the two chiral compounds over time (see Figure 13.7) revealed higher ee values for (*R*)-**6a** than for (*R*)-**13** at early rates of reaction. However, over time, while the ee of (*R*)-**13** remained consistently high, the ee of (*R*)-**6a**, after reaching a maximum, steadily decreased towards the end of the reaction. Experiments carried out as independent sets of triplicates confirmed the later observation in almost all entries. Alkanol (*R*)-**6a** remained constantly at lower ee than (*R*)-**13**. Also, here, both **6a** and **13** were obtained with a random distribution of enantiomers.

13.3.3 Kinetic Analyses on the Vapor Phase Reaction at Different Temperatures

Initially, the reaction was analyzed at rt as summarized in Figure 13.8. No product was observed after 30 minutes of reaction, while in the following samples the amount of **5a** decreased slowly with concomitant increase of other reaction products with similar trends except for compound **14**.

A general consequence of low temperature is reflected in the decreasing vapor tension of *i*-Pr_2Zn resulting in slower alkylation, as shown by the high amount of recovered aldehyde **5a**. Also, these conditions did not allow easy analysis at early stages due to difficult detection of products. The formation of the other side products is also slower. In contrast, in the reaction at −15 °C most of the side-products are suppressed. In this case, after 24 hours, **6a** was the only product found in the reaction crude. Other side products were detected on the samples after 72 hours of reaction. In general, all reactions at lower temperature provided symmetry breaking and amplification with a final ee slightly higher than the average at rt (see Figure 13.9). At rt the ee for **6a** is lower than **13**.

13.3.4 Analyses with Varying Concentration of $Zn(i\text{-}Pr)_2$

At higher concentration and down to an equimolar *i*-P_2Zn ratio, the graph shows high conversion of aldehyde **5a** (see Figure 13.9). Reduction alcohol **11** prevails in all reactions, while the corresponding ester **14** was kept to a minimum. Meanwhile, with excess *i*-P_2Zn ketone **12** is formed to a much larger extent, which might suggest a second alkylation by reaction with ester **13** or **14**. This observation is important for the interpretation of hemiacetal's contribution in the mechanism of amplification. Remarkably, chiral ester **13**

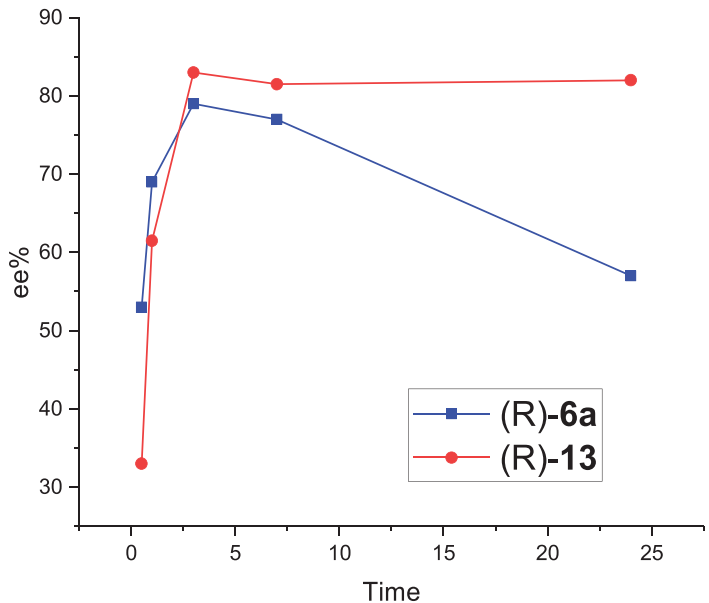

Figure 13.7 Parallel amplification of ee for alkanol **6a** and ester **13.**

Entry	ee% (R)-6a	ee% (R)-13
1	48	72
2	53	65
3	62	83
4	55	54
5	47	25
6	63	79
7	67	81
8	50	57
9	49	66

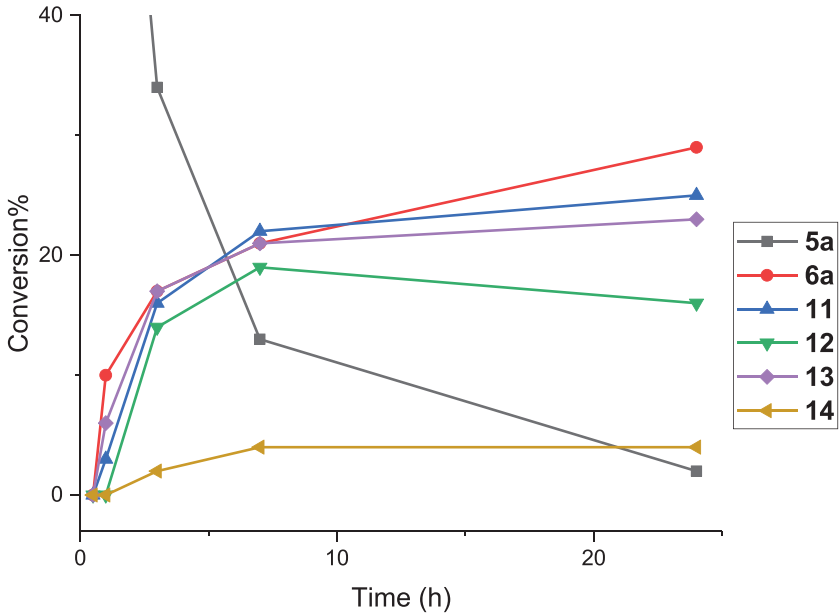

Figure 13.8 Graphical representation of the progress of the reaction (cut over 40% conversion).

is always formed in the range of 16–20% molar ratio and this remains at the expense of alkanol **6a**. Expectedly, with half equivalent *i*-P_2Zn, a low yield of alcohol **6a** was achieved and remains the minor product of the reaction. This can easily be attributed to the subsequent formation of chiral ester **13**, in which a significant portion of chiral alkanol is converted. Here, again the trend in enantiopurity prevails. The ee values for the reaction end products show a significantly higher amplification for ester **13** over that of alkanol **6a** (see Table 13.3). Even in the case with low concentration in *i*-P_2Zn amplification of both **6a** and **13** remained high although with a smaller difference in ee between the two products.

13.3.5 Proposed Mechanism for the Vapor Phase Reaction

On the basis of information gained from the experiments above, it is possible to delineate a mechanism for this transformation upon vapor–solid interaction of *i*-Pr_2Zn and aldehyde **5a** (see Scheme 13.7). We identify at least four different processes taking place at the same time:

- SMSB in the interaction of $Zn(iPr)_2$ and **5a** and amplification of ee% of **6a**
- Formation of **11** and **12** through a Meerwein–Ponndorf–Verley mechanism

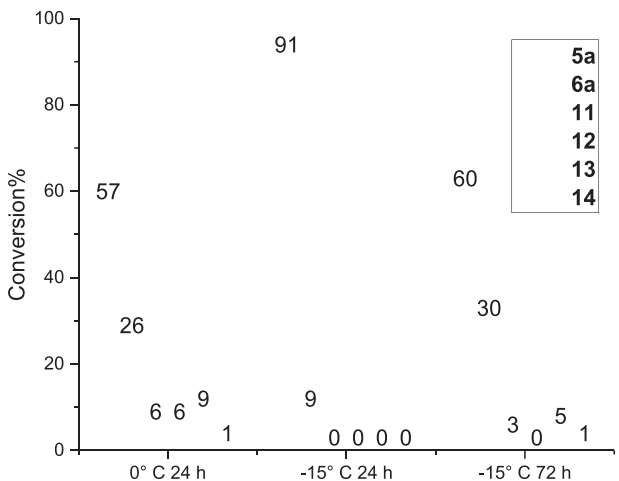

Product	0° C 24 h	-15° C 24 h	-15° C 72 h
6a	91% ee	60% ee	83% ee
13	86% ee	/	81% ee

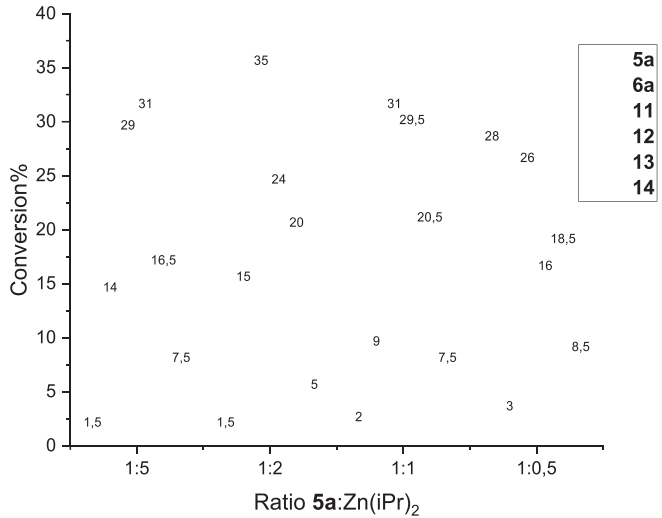

Product	1:5	1:2	1:1	1:0,5
6a	34%	22%	20%	53%
13	56%	70%	59%	63%

Figure 13.9 Conversion of **5a** at different temperatures (left); and at rt with different concentrations of $Zn(iPr)_2$ (right).

Table 13.3 Ee values of **6a** and **13** at different concentrations of *i*-P_2Zn.

	Aldehyde : *i*-P_2Zn ratio (%)			
Compound	1 : 5	1 : 2	1 : 1	1 : 0.5
6a	34	22	20	53
13	56	70	59	63

- Formation of **13** and **14** through a Claisen–Tishchenko disproportionation
- Amplification of ee of **13** by reversible hemiacetal formation in step 1.

Experiments at low temperature indicate that the first step of the reaction mechanism is the interaction between $Zn(iPr)_2$ and aldehyde **5a** to form alkoxide **6a***. Symmetry breaking occurs during attack by organozinc vapors on enantioface of **5a** as a random event. This induces the initial ee imbalance of **6a*** under kinetic control and followed by a subsequent amplification by asymmetric autocatalytic.

The Meerwein–Ponndorf – Verley (MPV) rearrangement involves a reversible hydride transfer from a secondary alcohol to a carbonyl substrate activated through coordination to a Lewis acidic metal center (see Scheme 13.8). This step can be considered as a parasitic side reaction of chiral alkanol **6a**, which may account for the depletion of ee in some occasions.

An alternative reaction of alkoxide **6a*** consists in the Claisen–Tishchenko (CT) reaction with **5a**.[65–68] Thus, a disproportionation occurs on an aldehyde in the presence of an alkoxide to produce the corresponding ester (Scheme 13.8). Unlike the commonly known ester synthesis by reaction of carboxylic acids with alcohols, no side product is formed. The accepted mechanism for the reaction is the Ogata–Kawasaki model, on which the reaction pathways described in Scheme 13.7 are based.[69] Zinc catalysts, are known to catalyze this reaction, and chiral hemiacetals have been observed in intramolecular condensation of Zn–alkoxides subsequent to a first alkylation of dialdehyde with Et_2Zn.[70,71] Further oxidation of the hemiacetal intermediate leads to the corresponding chiral ester.[71] Also both intra- and inter-molecular Claisen–Tishchenko are catalyzed by metallic zinc, although achiral.[72]

The existence of Zn–hemiacetal has been described as a transient intermediate in previous NMR studies, suggesting its association in a transition state in the Soai reaction.[63] In these studies by Brown *et al.*, although at low concentration, the formation of acetal intermediate was correlated to a high concentration of aldehyde. The extent of formation of this acetal increased further at a lower temperature of 0 °C and below. The implied structure involved three pyridines, consisting of two alkoxides and one aldehyde, and resulted into two DFT model structures Act-A and Act-B (see Figure 13.10). This species forms in the early stage of the amplification and lasts until complete consumption of aldehyde. Consistent with this description, aldehyde **5a** is always in large excess upon reaction with organozinc vapor. Then,

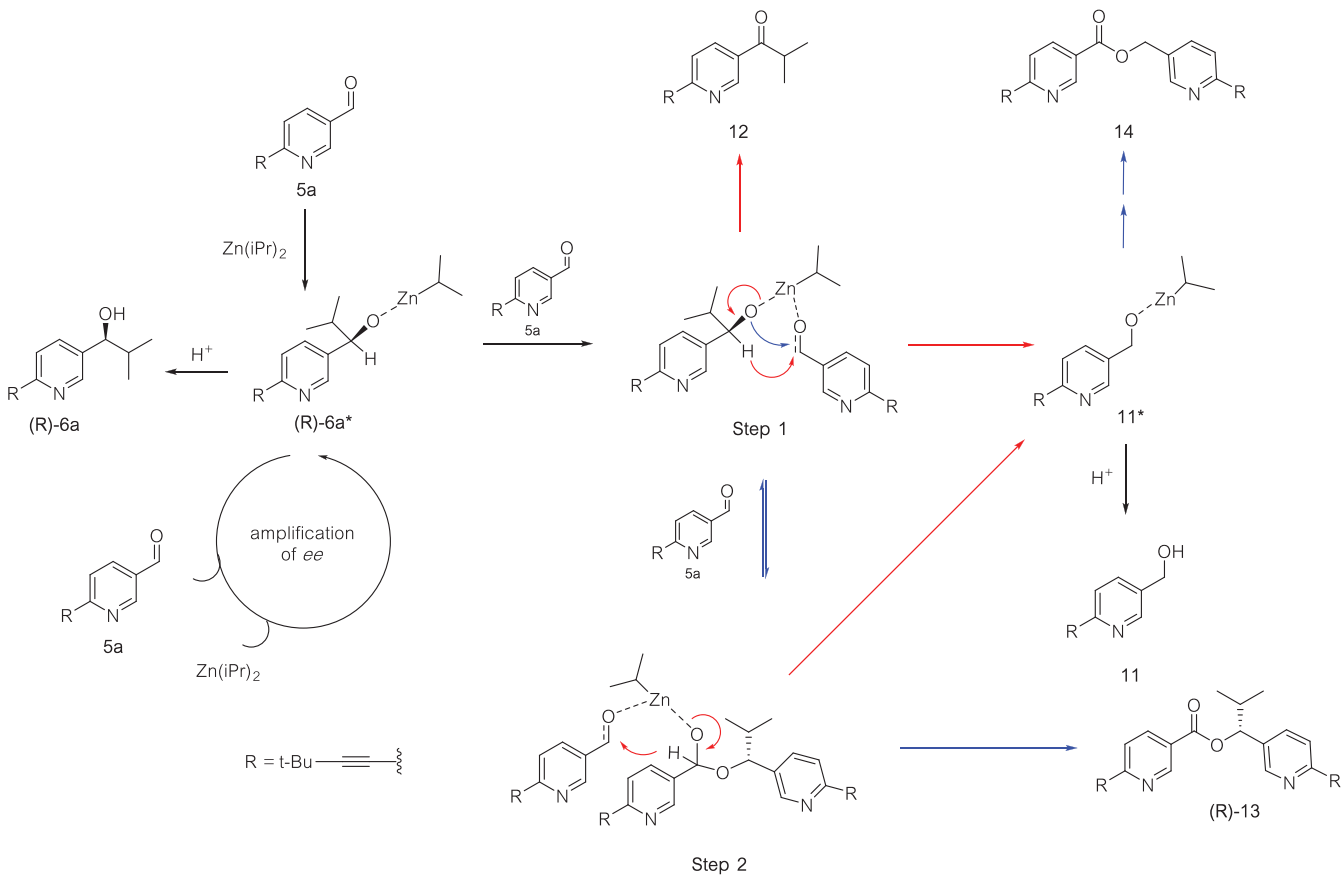

Scheme 13.7 Mechanism of the formation involved in the vapor phase reaction.

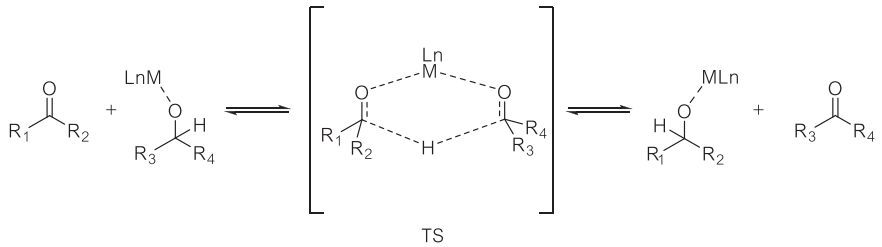

Scheme 13.8 Mechanism of the Meerwein–Ponndorf–Verley reduction.

it can enter the coordination sphere of Zn–alkoxide (Step 1). This approach requires consideration of two pathways envisioned after the coordination step (see Scheme 13.7). The red arrows in Step 1 illustrate the MPV pathway, with the hydride transfer from **6a*** to **5a** and formation of **11*** and **12**. Alternatively, a second possibility represented by blue arrows, involves a nucleophilic attack of Zn–alkoxide **6a*** on the carbonyl of **5a**. This pathway will result in Step 2, forming the hemiacetal intermediate. Through the coordination of another molecule of **5a** and a second MPV rearrangement, yielding ester **13** and alkoxide **11***.

The CT disproportionation can also take place starting from alkoxide **11***. The identical two-step pathways lead to ester **14**. Some confirmations to this mechanism can be found in the reaction conversions shown previously. For example, in the proposed reaction mechanism, ketone **12** can be formed by the MPV rearrangement in Step I, while alcohol **11** can be formed by both MPV rearrangements in Steps I and II. As discussed above, ketone **12** may rise by alkylation of ester **11** or **13**.

The formation of ester **13** starts from alkoxide **6a***, whose ee is continuously increasing through autocatalytic asymmetric amplification. Over time (*R*)-**13** is obtained with a constantly higher ee that is related to the improving ee of (*R*)-**6a**. This explains how, following the first part of the graph representing the ee of (*R*)-**6a** and (*R*)-**13** in Figure 13.7, showing the same trend. It is observed from Figure 13.7 that the final ee of (*R*)-**13** remained constantly higher than the final ee of (*R*)-**6a**.

A report by Gridnev on DFT computations proposed a model mechanism for the formation of the acetal from the same intermediate as the reaction product.[73] With a similar rearrangement occurring between Step I and II in Scheme 13.7, in the presence of excess of aldehyde, ''*unstable*'' adduct P_5Ac is obtained, which dissociates immediately into homodimer P_2 – which has been considered the most stable species in the reaction pool – and P_3Ac consisting of a hemiacetal coordinating aggregate. The later further dissociates to form another P_2 along with a Zn–hemicetal Pac. Eventually, product P and aldehyde A are recovered by break down of the acetal (see Scheme 13.9). To sum up, the acetal intermediate is supposed to form in an off-loop of the catalytic cycle and it yields the reaction product after decay.

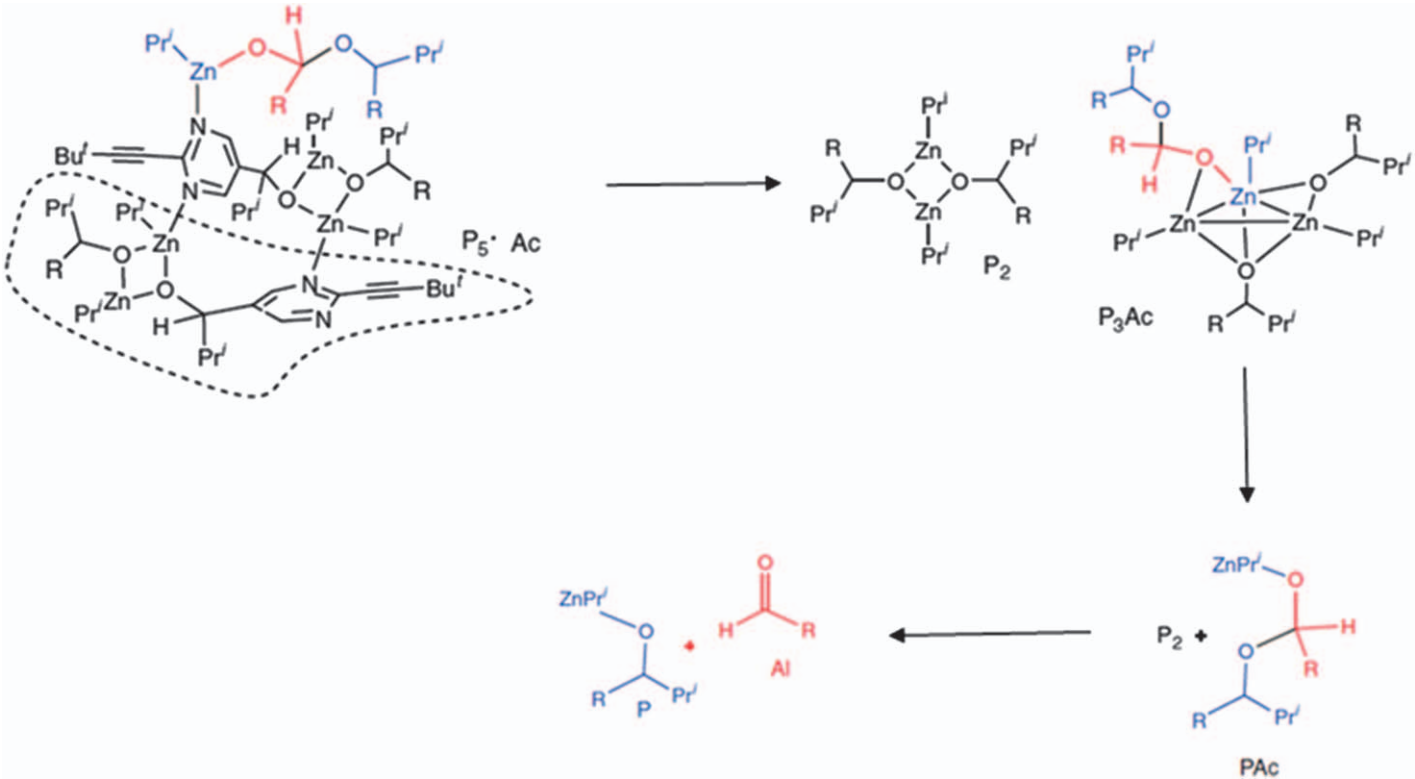

Scheme 13.9 Degradation of transient hemiacetal aggregate.

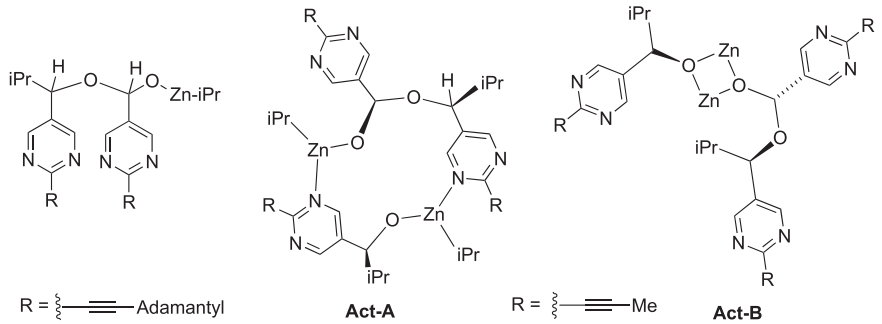

Figure 13.10 Acetal structures as reported by Brown *et al.* Reproduced from ref. 42 with permission from John Wiley & Sons, Copyright © 2012 Wiley-VCH Verlag GmbH & Co. KGaA, Weinheim.

In contrast, a more recent work by Trapp *et al.* concluded to a more catalytically active hemiacetal species. A combined kinetic analyses and mass spectrometric measurements suggested formation of a transient Zn–hemiacetal complex. This is further corroborated with help of doping experiments, by transferring aliquots of a ''live Soai autocatalysis'' to a nascent autocatalytic reaction, resulting in acceleration of the latter with higher amplification. These mixing experiments are in agreement with previous work on parallel autocatalysis using **4a** as a trigger for accelerated amplification of alkanol **6a**.[54,74]

In the case of the vapor phase reaction, the intermediate is still part of an off-loop cycle but it is neither transient nor unstable. The formation of a chiral ester with increasing ee demonstrates that the hemiacetal plays a key role in enantio-discrimination, which can be envisioned as a ''*sorting component*''. A possible explanation for this behavior may call for considering a reversible process in the formation of diastereomeric hemiacetal intermediates. The subsequent hydride transfer could ensure enantioselectively, with the preferential formation of (*R*)-**13**, while the opposite diastereoisomer could preferably revert back to Step I. In this way the amplification of (*R*)-**13** would happen at the expenses of (*R*)-**6a**. Taking in consideration again the results in Table 13.2, the formation of **6a** reached 21% in the first 7 hours, and increased by only 8% in the subsequent 17 hours. Figure 13.7 shows that the depletion of ee for (*R*)-**6a** begins after the first 4–5 hours of reaction. The amplification of ee% of (*R*)-**6a** is not affected by the formation of (*R*)-**13** in the first hours of reaction because new (*R*)-**6a** is continually generated from **5a** with high ee. While the reaction slows down following decay of **5a**, the enantioselective formation of (*R*)-**13** keeps pace.

The experiments in Figure 13.9 provide additional information on the relationship between the different and simultaneous pathways in the reaction. It can be observed that no $Zn(iPr)_2$ takes part in the MPV and CT mechanisms after the formation of alkoxide **6a***. This is confirmed by the fact that all the side products form in almost the same proportions. In the

reaction performed in the deficiency of $Zn(iPr)_2$, the lack of Zn reagent negatively affects the autocatalytic cycle, which is not efficient enough to completely convert **5a**. The extent of the formation of **6a** is naturally limited by a low organozinc concentration, and most of it is converted into the other side products. This explains the low amount of **6a** found in the 1 : 0.5 experiment compared to the other entries.

13.4 Miscellaneous

Certainly, the initial amount of **6a** forming in the beginning could enter the autocatalytic cycle and react with excess aldehyde to form hemiacetal and thus chiral ester **13** at an even earlier stage of the reaction. This would plausibly decrease or eventually suppress the formation of side products. Experiments including 0.1 equiv. of (*R*)-**6a** with 15% ee revealed the formation of side products in comparable proportions, following the same trend as the reaction under absolute catalysis. With no substantial difference from the previous reactions, (*R*)-**6a** and (*R*)-**13** were obtained in 39% and in 81% ee, respectively. In the same manner, reactions with opposite hand (*S*)-**6a** in the reaction mixture provided both (*S*)-**6a** and (*S*)-**13**. This means that the reaction under heterogenous conditions is sensitive to the handedness of a chiral trigger initially present in the powder mixture consisting of **6a** and **5a**. This allows control of the preferential formation of one or the other enantiomer with a judicious source of chirality.

It seemed interesting to perform the vapor phase reaction on **5a** confined within the UiO-67 to probe whether the framework of the MOF would have played a role in the formation of the side products. After the reaction, all side products except for **14** were found in the reaction crude, with a higher percentage of unreacted **5a** compared to the reaction performed on the pristine material. (*R*)-**6a** was obtained in 3% ee and (*R*)-**13** in 23.5% ee. As for the reactions performed on aldehyde **3c** in the MOFs, it seems that the framework of the MOF is not helping the autocatalytic reaction of the substrate, obtaining only moderate ees.

13.5 Conclusion and Future Prospects

Absolute asymmetric synthesis produces chiral alkanols by the action of organozinc vapor on a solid aldehyde substrate. These heterogenous conditions promote symmetry breaking with a more significant chiral induction if compared to corresponding reactions in solution. The recent observation of an X-ray structure of an oligomer inspired encapsulation of the reaction components within a metalorganic framework to function as nanoreactors with well-defined size. The differences observed under host–guest interactions imply that the active species is subject to confinement effects, which is suggested by the moderate ee values observed although amplification keeps pace. An explanation for this aspect is that autocatalytically active oligomers are subject to size discrimination by the nature of the hosting

MOF. Here, models are required to accommodate such oligomers and their distribution, as a reactive homodimer and unreactive heterodimer, in the cavities of the MOFs.

A fundamental observation in these studies is the entry of a chiral ester – with high enantioenrichment – derived from the chiral alkanol. Perhaps more remarkable is the parallel amplification of this ester with even higher ee values than the actual alkanol. A crucial function here is the hemiacetal intermediate, a dissociative species, built under kinetic control. In this case, amplification may arise from a reversible and nonlinear dissociation of the homo- and hetero-chiral hemiacetal. Indeed, the hemiacetal forms as two diastereomers with a kinetically preferred intermediate for a hydride transfer converting into chiral ester (step II: thermodynamic sink), while the other diastereomer reverts back to the starting Zn–alkoxide and aldehyde.[75,76] It is obvious that the formation of chiral ester, a thermodynamic product, is favored by the high concentration of aldehyde under heterogeneous conditions. Studies are in progress with isotopically-labeled substrates to evaluate the implications of the hydride (H/D) transfer in Step II of Scheme 13.5. Finally, another aspect of the heterogenous autocatalysis remaining to be clarified is whether amplification of chiral ester (through hemiacetal) operates at the expense of the chiral alkanol.

Acknowledgements

This work was financially supported by the Research Council of Norway (TOPFORSK program 250795), the University of Oslo, and COST Action ''Emergence and Evolution of Complex Chemical Systems'' (CM 1304).

References

1. K. Mislow, *Collect. Czech. Chem. Commun.*, 2003, **68**, 849–864.
2. M. Bolli, R. Micura and A. Eschenmoser, *Chem. Biol.*, 1997, **4**, 309–320.
3. B. L. Feringa and R. A. van Delden, *Angew. Chem., Int. Ed.*, 1999, **38**, 3419–3438.
4. S. Pizzarello and A. L. Weber, *Science*, 2004, **303**, 1151.
5. I. Weissbuch and M. Lahav, *Chem. Rev.*, 2011, **111**, 3236–3267.
6. J. S. Siegel, *Chirality*, 1998, **10**, 24–27.
7. J. M. Ribo, C. Blanco, J. Crusats, Z. El-Hachemi, D. Hochberg and A. Moyano, *Chem. – Eur. J.*, 2014, **20**, 17250–17271.
8. M. Sakamoto, *Chem. – Eur. J.*, 1997, **3**, 684–689.
9. K. Mislow, *Collect. Czech. Chem. Commun.*, 2003, **68**, 849.
10. B. L. Feringa and R. A. van Delden, *Angew. Chem., Int. Ed.*, 1999, **38**, 3418–3438.
11. T. Buhse, J.-M. Cruz, M. E. Noble-Terán, D. Hochberg, J. M. Ribó, J. Crusats and J.-C. Micheau, *Chem. Rev.*, 2021, **121**, 2147–2229.
12. C. H. L. Caglioti, O. Holczknecht, L. Zékány, C. Zucchi, K. Micskei and G. Pályi, *Viva Origino*, 2006, **34**, 62–80.

13. T. T. Mai, M. Branca, D. Gori, R. Guillot, C. Kouklovsky and V. Alezra, *Angew. Chem., Int. Ed.*, 2012, **51**, 4981–4984.
14. S. Olsson, A. Lennartson and M. Hakansson, *Chem. – Eur. J.*, 2013, **19**, 12415–12423.
15. A. Lennartson, S. Olsson, J. Sundberg and M. Hakansson, *Angew. Chem., Int. Ed.*, 2009, **48**, 3137–3140.
16. D. K. Kondepudi, R. J. Kaufman and N. Singh, *Sci.*, 1990, **250**, 975–976.
17. C. Viedma, *Phys. Rev. Lett.*, 2005, **94**, 065504.
18. W. L. Noorduin, T. Izumi, A. Millemaggi, M. Leeman, H. Meekes, W. J. P. Van Enckevort, R. M. Kellogg, B. Kaptein, E. Vlieg and D. G. Blackmond, *J. Am. Chem. Soc.*, 2008, **130**, 1158–1159.
19. W. L. Noorduin, A. A. C. Bode, M. van der Meijden, H. Meekes, A. F. van Etteger, W. J. P. van Enckevort, P. C. M. Christianen, B. Kaptein, R. M. Kellogg, T. Rasing and E. Vlieg, *Nat. Chem.*, 2009, **1**, 729–732.
20. P. M. Bjoremark, J. Jonsson and M. H. Hakansson, *Chem. – Eur. J.*, 2015, **21**, 10630–10633.
21. P. M. Bjoremark, S. Olsson, T. Kokoli and M. Hakansson, *Chem. – Eur. J.*, 2015, **21**, 8750–8753.
22. Y. Hayashi, M. Matsuzawa, J. Yamaguchi, S. Yonehara, Y. Matsumoto, M. Shoji, D. Hashizume and H. Koshino, *Angew. Chem., Int. Ed.*, 2006, **45**, 4593–4597.
23. V. A. Soloshonok, H. Ueki, M. Yasumoto, S. Mekala, J. S. Hirschi and D. A. Singleton, *J. Am. Chem. Soc.*, 2007, **129**, 12112–12113.
24. K. Soai, S. Niwa and H. Hori, *J. Chem. Soc., Chem. Commun.*, 1990, 982–983.
25. T. H. K. Soai, C. Shimada and K. Isobe, *Tetrahedron: Asymmetry*, 1994, **5**, 789–792.
26. K. Soai, T. Hayase and K. Takai, *Tetrahedron: Asymmetry*, 1995, **6**, 637–638.
27. T. Shibata, K. Choji, H. Morioka, T. Hayase and K. Soai, *Chem. Commun.*, 1996, 751–752.
28. T. Shibata, H. Morioka, S. Tanji, T. Hayase, Y. Kodaka and K. Soai, *Tetrahedron Lett.*, 1996, **37**, 8783–8786.
29. T. Shibata, H. Morioka, T. Hayase, K. Choji and K. Soai, *J. Am. Chem. Soc.*, 1996, **118**, 471–472.
30. T. Shibata, S. Yonekubo and K. Soai, *Angew. Chem., Int. Ed.*, 1999, **38**, 659–661.
31. K. Soai, T. Shibata, H. Morioka and K. Choji, *Nature*, 1995, **378**, 767–768.
32. T. Shibata, S. Yonekubo and K. Soai, *Angew. Chem., Int. Ed.*, 1999, **38**, 659–661.
33. I. Sato, H. Urabe, S. Ishiguro, T. Shibata and K. Soai, *Angew. Chem., Int. Ed.*, 2003, **42**, 315–317.
34. A. J. Bissette and S. P. Fletcher, *Angew. Chem., Int. Ed.*, 2013, **52**, 12800–12826.
35. F. C. Frank, *Biochem. Biophys. Acta*, 1953, **11**, 459–463.
36. K. Soai, I. Sato, T. Shibata, S. Komiya, M. Hayashi, Y. Matsueda, H. Imamura, T. Hayase, H. Morioka, H. Tabira, J. Yamamoto and Y. Kowata, *Tetrahedron: Asymmetry*, 2003, **14**, 185–188.

37. D. A. Singleton and L. K. Vo, *Org. Lett.*, 2003, **5**, 4337–4339.
38. T. Kawasaki, K. Suzuki, M. Shimizu, K. Ishikawa and K. Soai, *Chirality*, 2006, **18**, 479–482.
39. D. G. Blackmond, *Proc. Natl. Acad. Sci. U. S. A.*, 2004, **101**, 5732–5736.
40. J. M. Brown, I. Gridnev and J. Klankermayer, *Top. Curr. Chem.*, 2008, **284**, 35–65.
41. I. D. Gridnev and A. K. Vorobiev, *ACS Catal.*, 2012, **2**, 2137–2149.
42. T. Gehring, M. Quaranta, B. Odell, D. G. Blackmond and J. M. Brown, *Angew. Chem., Int. Ed.*, 2012, **51**, 9539–9542.
43. E. Doka and G. Lente, *J. Am. Chem. Soc.*, 2011, **133**, 17878–17881.
44. O. Fulop and B. Barabas, *J. Math. Chem.*, 2016, **54**, 10–17.
45. B. Barabas, R. Kurdi, C. Zucchi and G. Palyi, *Chirality*, 2018, **30**, 913–922.
46. B. Barabas, J. Toth and G. Palyi, *J. Math. Chem.*, 2010, **48**, 457–489.
47. D. G. Blackmond, *Tetrahedron: Asymmetry*, 2006, **17**, 584–589.
48. J.-C. Micheau, C. Coudret, J.-M. Cruz and T. Buhse, *Phys. Chem. Chem. Phys.*, 2012, **14**, 13239–13248.
49. T. Satyanarayana, S. Abraham and H. B. Kagan, *Angew. Chem., Int. Ed.*, 2009, **48**, 456–494.
50. D. A. Singleton and L. K. Vo, *Org. Lett.*, 2003, **5**, 4337–4339.
51. K. Soai, I. Sato, T. Shibata, S. Komiya, M. Hayashi, Y. Matsueda, H. Imamura, T. Hayase, H. Morioka, H. Tabira, J. Yamamoto and Y. Kowata, *Tetrahedron: Asymmetry*, 2003, **14**, 185–188.
52. M. Funes-Maldonado, B. Sieng and M. Amedjkouh, *Eur. J. Org. Chem.*, 2015, 4081–4086.
53. M. Funes-Maldonado, B. Sieng and M. Amedjkouh, *Org. Lett.*, 2016, **18**, 2536–2539.
54. C. Romagnoli, B. Sieng and M. Amedjkouh, *Eur. J. Org. Chem.*, 2015, 4087–4092.
55. S. V. Athavale, A. Simon, K. N. Houk and S. E. Denmark, *Nat. Chem.*, 2020, **12**, 412–423.
56. T. Kawasaki, S. Kamimura, A. Amihara, K. Suzuki and K. Soai, *Angew. Chem., Int. Ed.*, 2011, **50**, 6796–6798.
57. K. Penzien and G. M. J. Schmidt, *Angew. Chem., Int. Ed. Engl.*, 1969, **8**, 608–609.
58. Y. Kaimori, Y. Hiyoshi, T. Kawasaki, A. Matsumoto and K. Soai, *Chem. Commun.*, 2019, **55**, 5223–5226.
59. G. Rotunno, D. Petersen and M. Amedjkouh, *ChemSystemsChem*, 2020, **2**, e1900060.
60. G. Rotunno, G. Kaur, A. Lazzarini, C. Buono and M. Amedjkouh, *Chem. – Asian J.*, 2021, **16**, 2361–2369.
61. R. Batten Stuart, R. Champness Neil, X.-M. Chen, J. Garcia-Martinez, S. Kitagawa, L. Öhrström, M. O'Keeffe, M. Paik Suh and J. Reedijk, *Pure Appl. Chem.*, 2013, **85**, 1715–1724.
62. M. Amedjkouh and G. Rotunno, 2021, DOI: 10.33774/chemrxiv-2021-ls95s.
63. T. Gehring, M. Quaranta, B. Odell, D. G. Blackmond and J. M. Brown, *Angew. Chem., Int. Ed.*, 2012, **51**, 9539–9542.

64. O. Trapp, S. Lamour, F. Maier, A. F. Siegle, K. Zawatzky and B. F. Straub, *Chem. – Eur. J.*, 2020, **26**, 15871–15880.
65. L. Claisen, *Ber. Dtsch. Chem. Ges.*, 1887, **20**, 646–650.
66. V. E. Tishchenko, *J. Russ. Phys. Chem. Soc.*, 1906, **38**, 355–418.
67. V. E. Tishchenko, *J. Russ. Phys. Chem. Soc.*, 1906, **38**, 482–540.
68. A. O. K. A. M. P. Koskinen, *Org. React.*, 2015, **86**, 105–410.
69. Y. Ogata, A. Kawasaki and I. Kishi, *Tetrahedron*, 1967, **23**, 825–830.
70. K. Soai, Y. Inoue, T. Takahashi and T. Shibata, *Tetrahedron*, 1996, **52**, 13355–13362.
71. M. Watanabe, N. Hashimoto, S. Araki and Y. Butsugan, *J. Org. Chem.*, 1992, **57**, 742–744.
72. M. Miyagawa and T. Akiyama, *Chem. Lett.*, 2018, **47**, 78–81.
73. I. D. Gridnev and A. K. Vorobiev, *Bull. Chem. Soc. Jpn.*, 2015, **88**, 333–340.
74. C. Romagnoli, B. Sieng and M. Amedjkouh, *Chirality*, 2020, **32**, 1143–1151.
75. D. Drahoňovský and J.-M. Lehn, *J. Org. Chem.*, 2009, **74**, 8428–8432.
76. L. You, J. S. Berman and E. V. Anslyn, *Nat. Chem.*, 2011, **3**, 943–948.

CHAPTER 14

Unusual Aspects of Asymmetric Induction and Amplification Observed in the Soai Reaction

TSUNEOMI KAWASAKI,*[a] ARIMASA MATSUMOTO[b] AND KENSO SOAI[a,c]

[a] Department of Applied Chemistry, Tokyo University of Science, Kagurazaka, Shinjuku-ku, Tokyo 162-8601, Japan; [b] Department of Chemistry, Biology, and Environmental Science, Nara Women's University, Kita-Uoya Nishi-machi, Nara 630-8506, Japan; [c] Research Organization for Nano & Life Innovation, Waseda University, Wasedatsurumaki-cho, Shinjuku-ku, Tokyo 162-0041, Japan
*Email: tkawa@rs.tus.ac.jp

14.1 Introduction

Living organisms use only one of the two enantiomers of chiral compounds, such as seen in L-amino acids and the D-sugars. This is a common phenomenon among all terrestrial life; thus, the origin and amplification of overwhelming enantioenrichment have been a long-term mystery and of broad interest in many scientific fields because they may give rise to the origin of life.

Among the credible theories,[1–15] asymmetric autocatalysis with amplification of enantiomeric excess (ee)[16–19] has been considered to play a key role in the chemical evolution of chiral organic compounds.[20–22] Asymmetric autocatalysis is a reaction in which the chiral product acts as a chiral catalyst

Catalysis Series No. 43
Asymmetric Autocatalysis: The Soai Reaction
Edited by Kenso Soai, Tsuneomi Kawasaki and Arimasa Matsumoto

Published by the Royal Society of Chemistry, www.rsc.org

for its own production. In the chemical evolution of enantioenriched chiral organic compounds, after the suggested chiral factor triggers the enantioimbalance of initially forming a chiral product, the autocatalytic mechanism might start to proceed and automultiply the chiral compounds with improved enantioenrichment. Because asymmetric autocatalysis provides a suitable amplification and multiplication method of chiral compounds, the study on the asymmetric autocatalysis of 5-pyrimidyl alkanol in the addition of diisopropylzinc (*i*-Pr_2Zn) to pyrimidine-5-carbaldehyde; that is, the Soai reaction can provide many discoveries toward the origin of biological homochirality.[23–43]

During the research on asymmetric autocatalysis, we encountered some unusual observations, in which, for example, a unique chiral source can give both enantiomeric products that depend on the reaction conditions including achiral or chiral additives and reaction temperatures. These observations suggest the possibility that the origin of chirality that triggers the autocatalytic production of L-product such as amino acids might induce the formation of oppositely configured D-product under the different reaction conditions during the prebiotic generation of chiral biological compounds (see Figure 14.1). Thus, only the original trigger does not necessarily determine the absolute handedness of the current homochirality.

From the practical synthetic perspective, the present observations are closely related to the stereodivergent reactions,[44,45] which would be one of the useful methods to address both enantiomeric products from the unique chiral source, because it is often difficult to address both enantiomeric source compounds.

Moreover, when examining the asymmetric autocatalysis of bis-pyrimidine compounds, a very rapid improvement of stereoselectivity was observed with a remarkable decrease of *meso*-compounds in the reaction products.[46] The unusual ultra-remote intramolecular 1,39-asymmetric induction, based on the principle of the direct orientation of catalytic and reactive moieties, is discussed in this chapter.

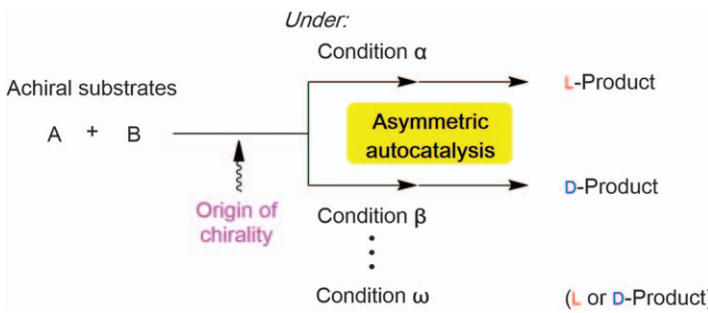

Figure 14.1 The origin of chirality triggers the asymmetric autocatalytic formation of both enantiomers of L- and D-products depending on the reaction conditions.

14.2 Asymmetric Autocatalysis Induced by a Mixture of Two Co-operative Chiral and Achiral Compounds

Asymmetric catalysis is one of the most important research areas in the field of synthetic organic chemistry because it is a powerful method to address large amounts of enantioenriched chiral compounds.[47] The use of achiral additives in asymmetric catalysis is one of the promising optimizations to achieve higher reactivity and enantioselectivity.[48–52] In these reactions, achiral additives often show no catalytic activity by themselves, and their functional groups differ from that of chiral catalysts or ligands.

During the research on asymmetric autocatalysis initiated with chiral β-amino alcohols, we found that 5-pyrimidyl alkanol **2** with an opposite configuration could be induced by utilizing a mixture of chiral and achiral β-amino alcohols as a chiral initiator compared with the reaction initiated with chiral β-amino alcohol alone (see Figure 14.2). Therefore, the enantioselectivity was reversed by the addition of achiral β-amino alcohols, which have the same functional groups as that of the chiral one; thus, the achiral additive can work co-operatively with chiral β-amino alcohol in asymmetric autocatalysis.[53,54]

In addition, chiral diol such as butane-2,3-diol can act as a chiral trigger for asymmetric autocatalysis to afford highly enantioenriched 5-pyrimidyl alkanol **2** with the corresponding absolute configurations to that of chiral diols.[55] We observed that asymmetric autocatalysis, *i.e.*, asymmetric

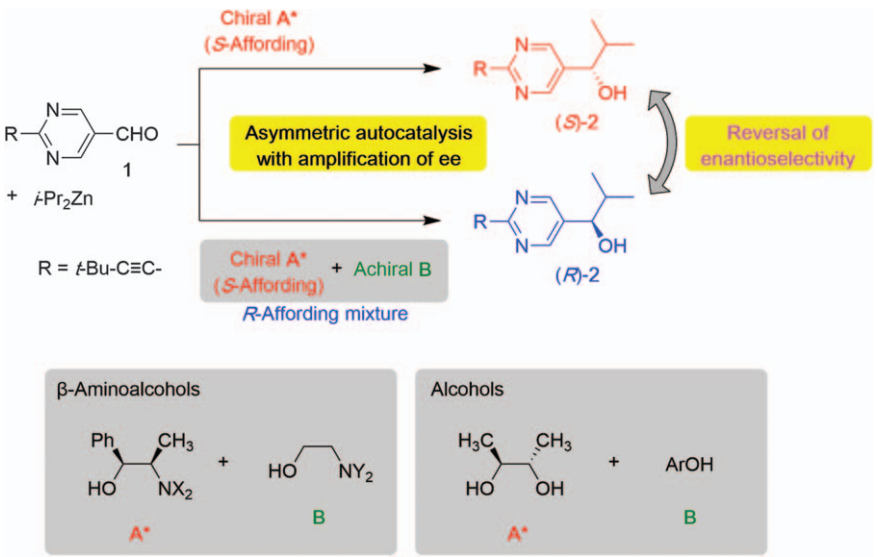

Figure 14.2 Reversal in the sense of enantioselectivity by the chiral and achiral co-operative compounds in asymmetric autocatalysis.

addition of *i*-Pr_2Zn to pyrimidine-5-carbaldehyde **1**, proceeds with reversed enantioselectivity by the addition of achiral alcohols such as phenol (see Figure 14.2). Thus, after the amplification of ee by asymmetric autocatalysis, enantiomeric (*S*)- and (*R*)-5-pyrimidyl alkanols **2** could be synthesized in a highly enantioselective manner by using the unique chiral diols as a chiral trigger.

Moreover, some asymmetric reactions have been demonstrated in which the chiral compounds acted as chiral cocatalysts to improve the reactions.[56–58] However, there have been no reports on the change of enantioselectivity by using a mixture of two chiral catalysts with the same functionalities. We demonstrate the reversal of enantioselectivity in the addition of *i*-Pr_2Zn to **1** by using a mixture of two chiral β-amino alcohol catalysts.[59] Chiral product **2** could be formed by using a mixture of two chiral β-amino alcohols with opposite enantioselectivity to that of individual β-amino alcohols.

14.2.1 Small Amounts of Achiral β-Amino Alcohols Reverse the Sense of Enantioselectivity in Chiral β-Amino Alcohol-initiated Asymmetric Autocatalysis

The addition of dialkylzincs to aldehydes, catalyzed by chiral amino alcohols to form chiral secondary alcohols, is one of the most powerful and well-studied enantioselective catalyses and is a highly enantioselective carbon–carbon bond-forming reaction.[60–62] Various chiral β-amino alcohols have been developed as highly efficient chiral ligands for the addition reactions.

Among the available chiral ligands, *N,N*-dialkylnorephedrines can enantioselectively catalyze the addition of dialkylzincs to various aromatic and aliphatic aldehydes.[63,64] *N,N*-Dialkylnorephedrines with (1*R*,2*S*)-configuration catalyze the formation of (*R*)-alcohols from aromatic aldehydes, whereas (*S*)-alcohols can be obtained using (1*S*,2*R*)-configured *N,N*-dialkylnorephedrines as the chiral catalyst.

When examining β-amino alcohol-initiated asymmetric autocatalysis, we found that (1*S*,2*R*)-*N,N*-dimethylnorephedrine (DMNE) affords (*S*)-5-pyrimidyl alkanol **2** in the asymmetric *i*-Pr_2Zn addition to pyrimidine-5-carbaldehyde **1** in high enantioselectivity (see Figure 14.3).[53] However, oppositely configured (*R*)-**2** can also be obtained by using a mixture of (1*S*,2*R*)-DMNE and achiral *N,N*-dibutylaminoethanol (DBAE). Therefore, both enantiomers could be formed with >98% ee from the same chiral source, that is, (1*S*,2*R*)-DMNE.

In greater detail, the addition of *i*-Pr_2Zn to pyrimidine-5-carbaldehyde **1** was carried out using a mixture of (1*S*,2*R*)-DMNE and DBAE in various proportions in toluene. The total concentration of DMNE and DBAE was constant at 20 mol%. The change of ee and configuration of alkanol **2** were monitored with respect to the composition of the catalytic mixture. As noted, (1*S*,2*R*)-DMNE alone afforded (*S*)-**2**. When the reaction was carried out in the

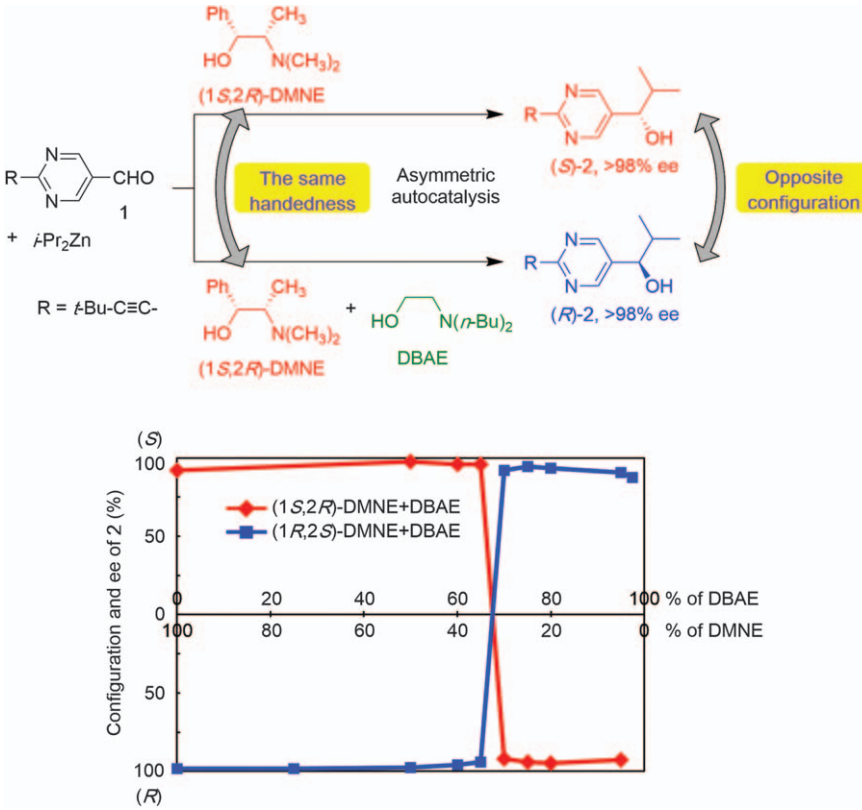

Figure 14.3 Reversal of the sense of enantioselectivity in asymmetric autocatalysis by using a mixture of chiral DMNE and achiral DBAE.

presence of achiral DBAE and (1*S*,2*R*)-DMNE at the ratio of 65 : 35, (*S*)-**2** was obtained as expectedly. In sharp contrast, when the ratio was slightly changed to 70 : 30 (DBAE : DMNE), reversal of the enantioselectivity occurred; thus, (*R*)-**2** was formed in high ee after the amplification of enantiopurity by asymmetric autocatalysis. Of course, symmetrical results could be obtained when a mixture of chiral (1*R*,2*S*)-DMNE and DBAE was used.

When the reaction was performed in hexane, a smaller amount of achiral DBAE could reverse the enantioselectivity of chiral DMNE. Thus, a mixture of DBAE (5 mol%) and (1*S*,2*R*)-DMNE (15 mol%) initiated the production of (*R*)-alkanol **2** (98% ee) with the opposite configuration to that of the reaction using (1*S*,2*R*)-DMNE alone.

Note that the reversal of enantioselectivity could be observed in various chiral and achiral β-amino alcohols (see Figure 14.4); thus, it seems quite general for the class of compounds.

Further kinetic and enantioselectivity studies[65] revealed that the reversal of the sense of enantioselectivity is because of the preferential formation of a catalytically active chiral hetero-aggregate derived from zinc alkoxides of

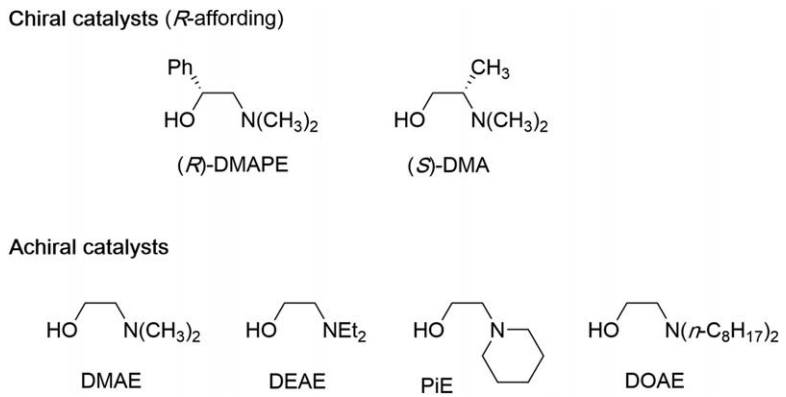

Figure 14.4 The chemical structures of chiral and achiral β-amino alcohols that show the reversal of enantioselectivity in asymmetric autocatalysis.

chiral and achiral β-amino alcohols. These studies might also provide some new insights on the reaction mechanism of catalytic enantioselective addition of dialkylzincs to aldehydes and may have implications for the origin of non-linear effects in these reactions.[58,66,67]

14.2.2 Achiral Alcohols Reverse the Sense of Enantioselectivity in Asymmetric Autocatalysis Initiated with Chiral Diols

Chiral diols are important scaffolds as chiral catalysts and ligands for enantioselective catalyses such as tartrate, α,α,α′,α′-tetraaryl-2,2-disubstituted 1,3-dioxolane-4,5-dimethanol (TADDOL) and 1,1′-bi-2-naphthol (BINOL) derivatives.[68–70] We have investigated asymmetric autocatalysis initiated with chiral diols.[55,71] As a result, a reversal of enantioselectivity was observed in the co-operative induction by a mixture of chiral diol and achiral monoalcohols as a chiral trigger for asymmetric autocatalysis of 5-pyrimidyl alkanol **2** in the alkylation of pyrimidine-5-carbaldehyde **1** (see Figure 14.5).

(2*R*,3*R*)-Butane-2,3-diol alone induced the production of (*S*)-pyrimidyl alkanol **2** with high ee, while (*R*)-alkanol **2** was enantioselectively synthesized by asymmetric autocatalysis when the reaction was initiated with a mixture of (2*R*,3*R*)-butane-2,3-diol (4 mol%) and phenol (32 mol%). Thus, phenol reversed the direction of the chiral induction of butane-2,3-diol in the asymmetric addition of *i*-Pr_2Zn to aldehyde **1**.

When using (2*S*,3*S*)-butane-2,3-diol in the presence and absence of phenol, the reversal of enantioselectivity also showed symmetrical results. When the molar ratio of butane-2,3-diol and phenol was 25 : 75, the reversal did not occur. However, in sharp contrast, when slightly changing the ratio of the alcohols to 20 : 80, the enantioselectivity reversed; thus, there is a critical point at which the enantioselectivity changes between the ratios 25 : 75 and 20 : 80 (butane-2,3-diol : phenol).

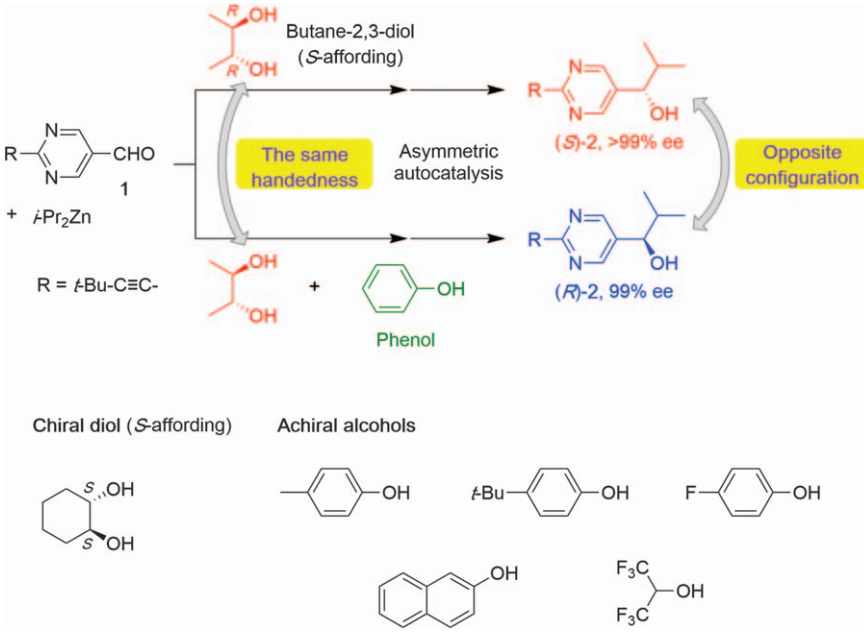

Figure 14.5 Reversed sense of enantioselectivity in the asymmetric autocatalysis initiated with a mixture of chiral diol and achiral phenols and acidic alcohols.

The reversal of enantioselectivity was also observed in the co-operative usage of cyclohexane-1,2-diol and phenol as a chiral initiator of asymmetric autocatalysis. In addition to phenol, *para*-substituted acidic alcohols, 2-naphthol, and fluorinated 2-propanol reversed the direction of the asymmetric induction of butane-2,3-diol.

Therefore, by choosing the presence or absence of achiral alcohols, chiral 1,2-diol-induced asymmetric autocatalysis could synthesize both enantiomeric (*S*)- and (*R*)-pyrimidyl alkanol **2** with high ee because of the amplification of enantiopurity.

14.2.3 Reversal of the Sense of Enantioselectivity in Asymmetric Autocatalysis by the Co-operative Operation of Two Chiral β-Amino Alcohols

There are some examples where chiral compounds acted as chiral cocatalysts in catalytic asymmetric syntheses to enhance the catalytic activity[56] and enantioselectivity.[57,58] However, to our knowledge, there are no reports on the change of the direction of asymmetric induction when the mixture of two chiral catalysts was submitted to the reaction as a chiral initiator. The reversal of enantioface selectivity in the asymmetric addition of *i*-Pr_2Zn to pyrimidine-5-carbaldehyde **1** was observed by mixing two chiral β-amino

alcohols.[59] The opposite enantiomeric product **2** was formed by using a mixture of two chiral β-amino alcohols that possess individual enantioselectivity, that is, a mixture of two *R*-affording chiral β-amino alcohols acting co-operatively gave (*S*)-pyrimidyl alkanol **2** with high ee in conjunction with asymmetric autocatalysis (see Figure 14.6).

The asymmetric addition of *i*-Pr_2Zn to aldehyde **1** using (1*R*,2*S*)-*N*,*N*-dimethylnorephedrine (DMNE) alone afforded, after the amplification of ee,

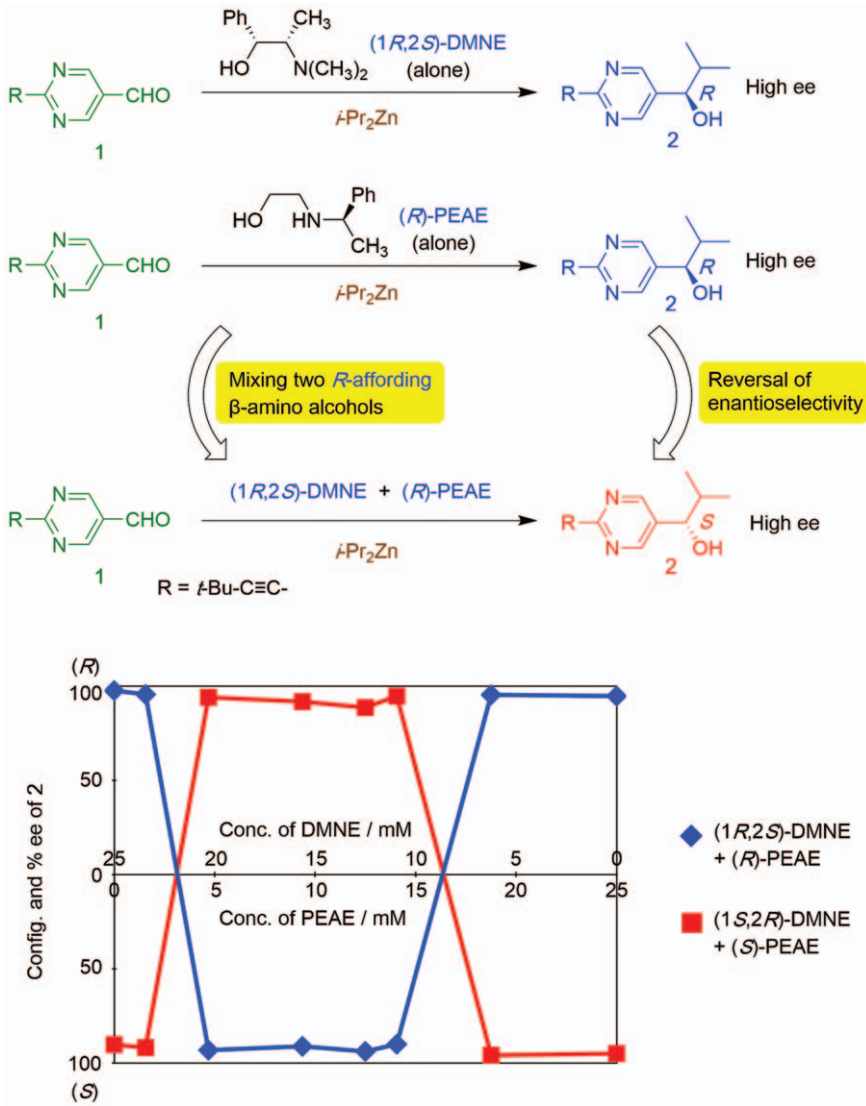

Figure 14.6 A mixture of two *R*-affording catalysts, (1*R*,2*S*)-DMNE and (*R*)-PEAE, acts as the reversed *S*-affording catalyst in asymmetric autocatalysis.

(*R*)-5-pyrimidyl alkanol **2** with high ee, and (*R*)-2-[(1-phenylethyl)amino]ethanol (PEAE) alone also catalyzed the production of (*R*)-**2** with high ee (see Figure 14.6). However, by mixing these β-amino alcohols and utilizing them as a chiral initiator for asymmetric autocatalysis, (*S*)-**2** with reversed configuration was synthesized in a highly enantioselective manner.

In greater detail, the molar ratio of catalytic species was changed subsequently, keeping the sum of molar concentrations constant at 25 mmol L^{-1}, and the critical ratio to change the enantioselectivity was examined. When 23 mmol L^{-1} of (1*R*,2*S*)-DMNE and 2 mmol L^{-1} of (*R*)-PEAE were cooperatively employed as a mixed catalyst, the predicted enantioselectivity was obtained to form (*R*)-**2**. However, by changing the ratio of (1*R*,2*S*)-DMNE (20 mM) and (*R*)-PEAE (5 mM), the reaction was directed to the opposite configured (*S*)-**2** with 94% ee. Among these compositions, the key catalytic species might have changed to reverse the enantioselectivity. Furthermore, when the concentration of PEAE increased to 19 mmol L^{-1} (6 mmol L^{-1} for (1*R*,2*S*)-DMNE), the enantioselectivity reverted to form (*R*)-alkanol **2** with high ee. When the reactions were performed using an enantiomeric pair, *i.e.*, (1*S*,2*R*)-DMNE in combination with (*S*)-PEAE, the symmetrical results could be obtained (see Figure 14.6).

Moreover, to compare the asymmetric power of chiral β-amino alcohols with only a slight difference in chemical structures, we carried out asymmetric autocatalysis by using a mixture of two competing chiral catalysts bearing opposite enantioselectivity. This would be able to determine which chiral catalyst has stronger asymmetric power by the absolute configuration of the resulting 5-pyrimidyl alkanol **2**.[72] Asymmetric power might be influenced by the relative enantioselectivity and reactivity between the two catalysts at the initial stage of asymmetric autocatalysis. If this research is conducted under a conventional asymmetric reaction, it may be difficult to compare the catalysts with similar efficiency because the ee value of the product is supposed to be quite small. Asymmetric autocatalysis enables amplification of such as slight difference to afford highly enantioenriched alkanol **2** with the absolute configuration corresponding to the asymmetric catalyst with a slightly higher catalytic activity than the others.

First, the induction efficiency of *N,N*-dipropylnorephedrine (DPNE) and *N,N*-dibutylnorephedrine (DBNE) as chiral catalysts in the addition of *i*-Pr_2Zn to pyrimidine-5-carbaldehyde **1** was compared (see Figure 14.7). When the reaction was performed using 10 mol% of (1*S*,2*R*)-DPNE (*S*-affording) and 10 mol% of (1*R*,2*S*)-DBNE (*R*-affording) as a mixed catalyst, (*R*)-**2** with 95% ee was given after the amplification of ee. Therefore, DBNE is more powerful under the present reaction than DPNE.

Next, compared with DPNE and *N,N*-diethylnorephedrine (DENE), asymmetric autocatalysis was conducted in the presence of 10 mol% of (1*S*,2*R*)-DPNE (*S*-affording) and 10 mol% of (1*R*,2*S*)-DENE (*R*-affording) under a competitive catalyst mixture to give (*S*)-**2** with 93% ee. Therefore, DPNE possesses a higher catalytic efficiency than DENE. Thus, by utilizing the

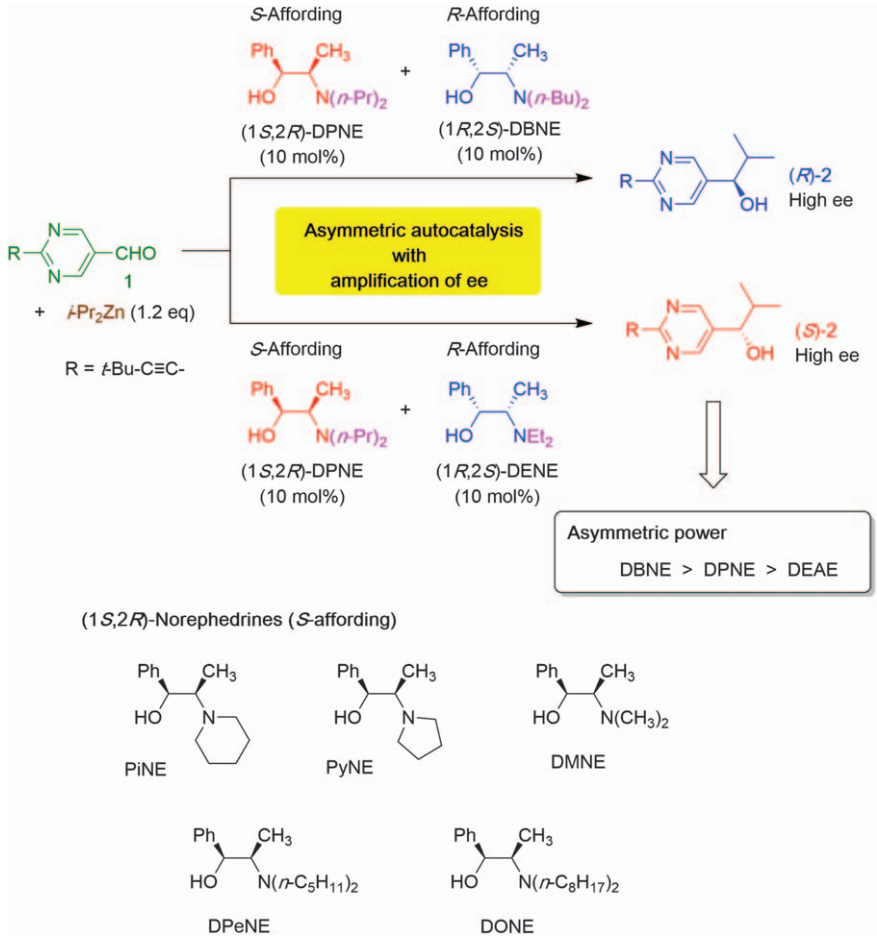

Figure 14.7 Comparison of the asymmetric power of *N,N*-dialkylnorephedrines by competitive asymmetric autocatalysis.

present technique, the asymmetric powers of other dialkylnorephedrines were systematically evaluated.

Note that this method can quantitatively evaluate the asymmetric power of chiral ligands. When asymmetric autocatalysis was carried out using a mixture of an equimolar amount of (1*R*,2*S*)-DMNE (10 mol%) and (1*S*,2*R*)-DBNE (10 mol%), (*S*)-**2** was synthesized in 96% ee; thus, DBNE is more powerful than DMNE. However, by increasing the proportion of DMNE to 74 : 26, the enantioselectivity reversed to afford (*R*)-**2**, while the catalyst mixture in the ratio of 73 : 27 gave (*S*)-product **2**. The critical ratio in which enantioselectivity reversal occurred seems to be the ratio 73.5 : 26.5 (=2.8); thus, it may be conceivable that the asymmetric power of DBNE is 2.8-fold larger than that of DMNE.

Slightly biased enantioselectivity of the catalysis using a mixture of two competing chiral β-amino alcohols can be easily detectable as the absolute configuration of highly enantioenriched **2** because of the significant amplification of ee by asymmetric autocatalysis.

14.3 Anomalous Effect of the Reaction Temperature in Asymmetric Autocatalysis

Asymmetric autocatalysis with the addition of *i*-Pr_2Zn to pyrimidine-5-carbaldehyde **1** proceeds with significant amplification of ee, *i.e.*, a large positive non-linear effect.[15] The mechanism of asymmetric amplification in the Soai reaction should provide deep insight into the origin and amplification of biological homochirality. Thus, many approaches to studying the mechanism of asymmetric autocatalysis have been reported from several research groups,[23–39] including ours.[41–43] Because the reaction shows a large non-linear effect, the aggregation structure of catalytic species should be the key. The aggregation structure or its formation cycle might be influenced by, for example, the reaction temperature, concentration, ee of the species, or the reaction solvent. In this section, unusual reaction outcomes as a result of reaction temperature are discussed.

14.3.1 Unusual Temperature Dependence on the Reaction Rate in the Asymmetric Autocatalysis

Blackmond, Brown and co-workers reported[73] the temperature dependence in asymmetric autocatalysis by kinetic study using calorimetry with substrates **3** and **4** bearing the adamantly ethynyl group at the 2-position of the pyrimidine ring, which was independently developed by Gering *et al.* (see Figure 14.8).[74] The addition of *i*-Pr_2Zn to aldehyde **3** was carried out in the presence of alkanol **4** with low ee, and the reaction calorimetric profiles were examined based on the reaction temperatures.

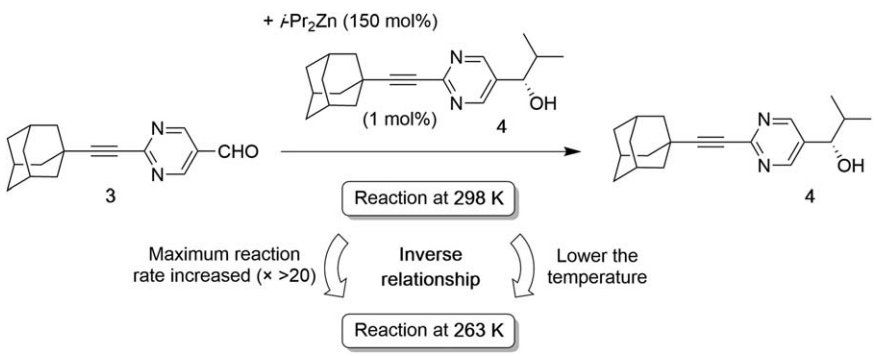

Figure 14.8 Higher maximum reaction rate of asymmetric autocatalysis at a lower temperature (263 K) than room temperature (298 K).

As a result, increase of the maximum reaction rate was observed as the temperature decreased. The reaction at 263 K showed the maximum rate, that is, more than 20 times higher than that observed at room temperature (298 K). In addition, the incubation period until the autocatalytic reaction start was also shorter at 263 K than that observed at room temperature, *i.e.*, the *i*-Pr_2Zn addition reaction proceeded readily at a lower temperature (263 K) compared with the reaction at room temperature. Therefore, an inverse relationship was observed between the reaction rate and reaction temperature. Further kinetic and NMR studies for the isopropylzinc alkoxide of **4** suggest the formation of a homochiral tetramer.

14.3.2 Temperature-dependent Inversion of Enantioselectivity in Asymmetric Catalysis

When addressing both enantiomers of chiral products in an enantioselective reaction, it is usually required to use both enantiomeric substrates, catalysts or ligands. Thus, the method to obtain either an enantiomer of the product only by changing the reaction conditions is an emerging challenge. Although various enantioselectivity reversal affected by changing the solvent, additives, and metals have been reported,[75–77] enantioselectivity reversal under simple temperature control is rare.

In the presence of (*S*)-1-phenethyl alcohol, the addition reaction of *i*-Pr_2Zn to pyrimidine-5-carbaldehyde **1** affords (*S*)-pyrimidyl alkanol **2** in high ee at 0 °C (see Figure 14.9).[78] However, when the same reaction is carried out at −44 °C, the same chiral source, (*S*)-1-phenethyl alcohol, shows the opposite enantioselectivity to give (*R*)-alkanol **2**. The results are reproducible.

Therefore, the temperature-dependent reversal of enantioselectivity was observed in the addition reaction of *i*-Pr_2Zn to pyrimidine-5-carbaldehyde **1** triggered by 1-phenethyl alcohol. The temperature-dependent reversal of enantioselectivity was also observed in the asymmetric autocatalysis triggered by other aromatic alcohols and amines with the relevant structure of 1-phenethyl alcohol (see Figure 14.9).

14.4 Reversal of the Sense of Enantioselectivity in Aza[6]helicene-induced Asymmetric Autocatalysis Depending on the Position of the Nitrogen Atom

Helicenes, polycyclic aromatic compounds, comprise the representative structural motifs of chiral molecules because of their unique helical structures. When examining helicene-induced highly enantioselective asymmetric autocatalysis, we reported that [5]helicene, [6]helicene,[79] and tetrathia[7]helicenes[80] are capable of acting as highly efficient chiral initiators to give highly enantioenriched 5-pyrimidyl alkanol **2** with the

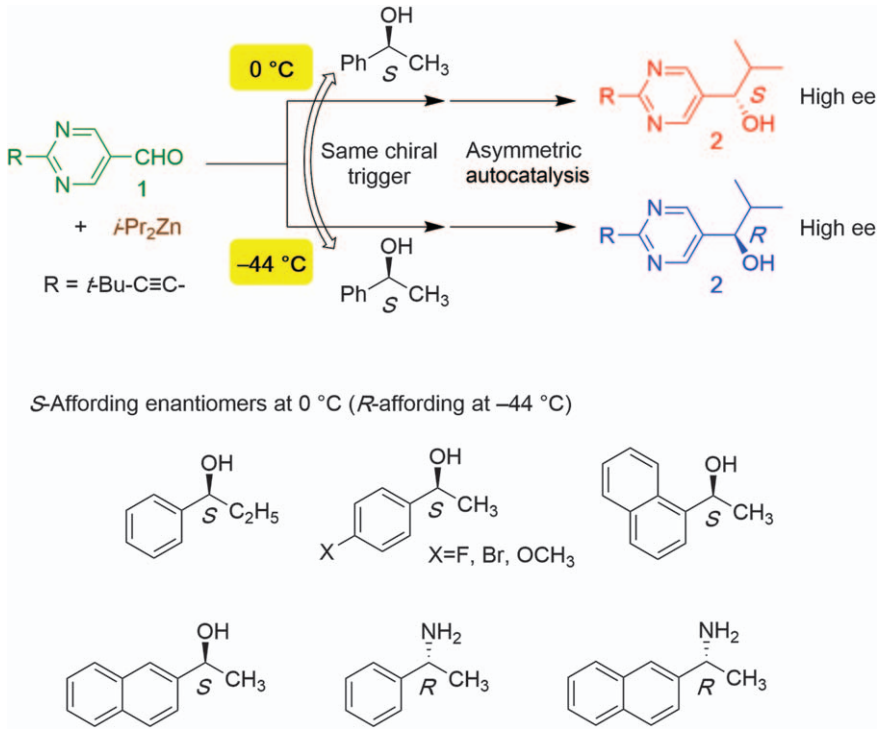

Figure 14.9 Reversal in enantioselectivity by controlling the reaction temperature in asymmetric autocatalysis.

corresponding absolute configurations to that of helicenes (see Figure 14.10). Although we proposed different induction modes between helicenes and thiahelicenes, (*P*)-(+)-(hetero)helicenes induced the production of (*S*)-**2**, while (*M*)-(−)-enantiomers promoted the formation of (*R*)-**2** without exception, regardless of the absence or presence of heteroatoms and the length of polycycles.

To our knowledge, the use of azahelicenes[81] in enantioselective catalysis has been rare. We demonstrated the highly enantioselective synthesis induced by azahelicenes in combination with asymmetric autocatalysis.[82] In addition, an unusual reversal of enantioselectivity was observed depending on the position of nitrogen atoms in the chemical structures of azahelicenes.

When asymmetric addition of *i*-Pr_2Zn to pyrimidine-5-carbaldehyde **1** was carried out in the presence of (*P*)-(+)-1-aza[6]helicene with >99% ee as the chiral initiator, (*S*)-pyrimidyl alkanol **2** with 99% ee was synthesized in 89% yield (see Figure 14.10). In contrast, (*M*)-(−)-1-aza[6]helicene with 99% ee gave the opposite configured (*R*)-**2** with 97% ee. The stereochemical relationship between azahelicene and alkanol **2** is reproducibly constant. Compared with previous reports using [5]helicene, [6]helicene, and

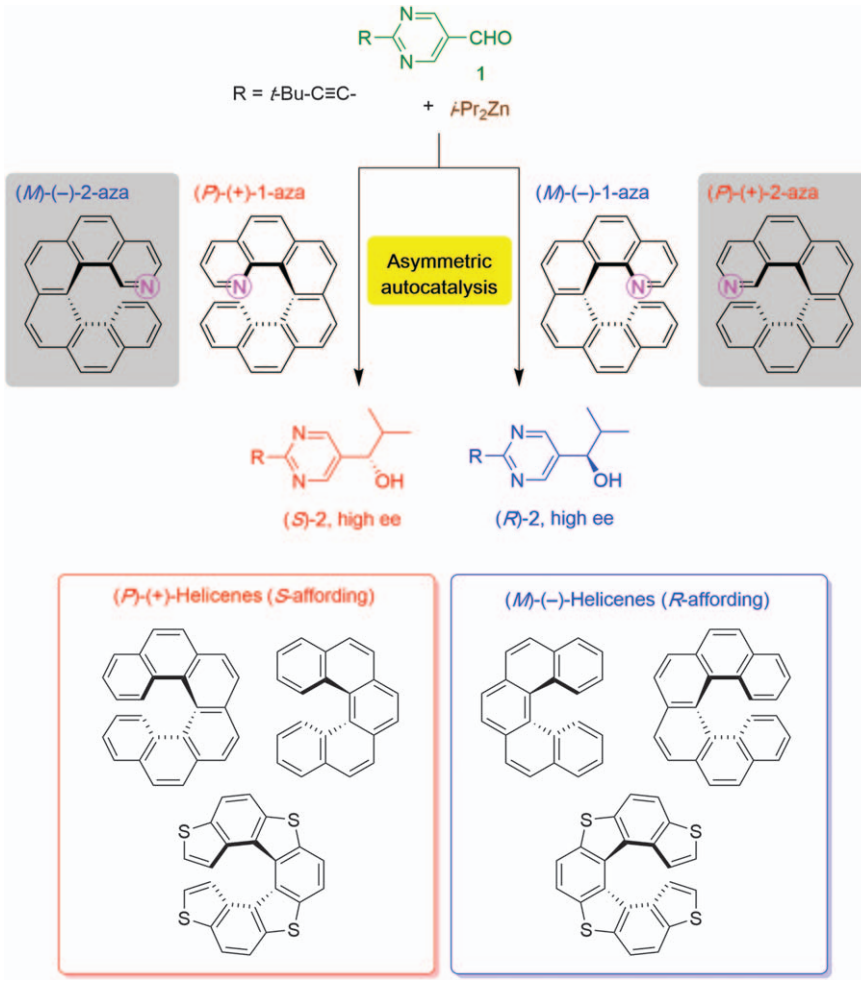

Figure 14.10 Asymmetric autocatalysis induced by helicenes and heterohelicenes and the reversal of enantioselectivity by the positions of the nitrogen atoms of 1- and 2-aza[6]helicenes.

tetrathia[7]helicene, the stereochemical relationship is the same, *i.e.*, (*P*)-(+)- and (*M*)-(−)-helicenes induce the production of (*S*)- and (*R*)-**2**, respectively.

Unexpected reaction outcomes were obtained, *i.e.*, reversal of enantioselectivity occurred when 2-aza[6]helicene was subjected as the chiral initiator of asymmetric autocatalysis. In the presence of (*P*)-(+)-2-aza[6]helicene, (*R*)-alkanol **2** with 93% ee was formed instead of the expected (*S*)-**2** by the *i*-Pr_2Zn addition to aldehyde **1**.[82] The enantiomer (*M*)-(−)-2-aza[6]helicene gave (*S*)-**2** with 97% ee. These reversed stereochemical outcomes compared with 1-aza[6]helicene were reproducible.

Chiral induction by 2-aza[6]helicene might have occurred in a different manner from other helicenes because of the existence of accessible less

hindered and easily coordinating nitrogen atoms at the 2-position. Thus, coordination between its nitrogen and other reactive species including zinc atoms influences the chiral induction at the initial stage of asymmetric autocatalysis.

14.5 Point-to-Point Ultra-remote Asymmetric Control of Bis(pyrimidine) Moieties Connected with Flexible Linker

Developing an efficient asymmetric autocatalyst with multiple reaction points is one of the emerging challenges in the field of stereochemistry and synthetic chemistry. Based on the origin of biological homochirality, the implication of this reaction might include the self-replication and self-improvement of chiral artificial large molecules with multiple reaction sites. In our research, the molecules with multi-asymmetric carbon centers were designed based on 5-pyrimidyl alkanol **2**, which acts as a highly efficient asymmetric autocatalyst in asymmetric *i*-Pr_2Zn addition to the corresponding aldehyde.[83] During the research using bis(pyrimidyl alkanols) with long alkyl spacers, we have found ultra-remote intramolecular 1,39-asymmetric induction under the principle of the direct orientation of catalytic and reactive moieties.[46]

First, asymmetric autocatalysis with amplification of ee was developed using (*S,S*)-bis(pyrimidyl alkanol) **6** (see Figure 14.11). When bis(pyrimidine-5-carbaldehyde) **5**, tethered with a 1,12-disilyldodecane chain, was submitted to *i*-Pr_2Zn addition in the presence of the corresponding (*S,S*)-**6** with the diastereomeric ratio of DL : *meso* = 62 : 38 and 7% ee as an initial autocatalyst, chirally improved product (*S,S*)-diol **6** could be synthesized with DL : *meso* = 73 : 27 and 56% ee as a mixture of initial asymmetric autocatalyst **6**. The obtained mixture **6** was subsequently subjected as the asymmetric autocatalyst of the next round of reaction; then, after four rounds of consecutive reactions, the ratios of enantiomers and diastereomers were both significantly enhanced to achieve >99.5% ee and DL : *meso* = 96 : 4. During four rounds of asymmetric autocatalysis, (*S,S*)-**6** automultiplied *ca.* 2000 times, while *meso*- and (*R,R*)-**6** multiplied *ca.* 76 and 6 times, respectively (see Figure 14.11).

The remarkable improvement in the ratio of DL : *meso*, *i.e.*, decrease of *meso*-**6**, cannot be solely explained by the mechanism of asymmetric autocatalysis. In asymmetric catalysis using a bifunctional substrate, the formation of the *meso* isomer would often contribute to a higher enantioselectivity than that of a monofunctional substrate.[84] Thus, the intramolecular long-range asymmetric induction,[85–89] which realizes high stereoselectivity, might be supposed as a key mechanism in this reaction (see Figure 14.12). We hypothesize that (*S*)-alkoxide formed in the initial reaction with *i*-Pr_2Zn induces the formation of the same *S*-configuration when an intramolecular aldehyde reacts with *i*-Pr_2Zn. Therefore, the point-to-point

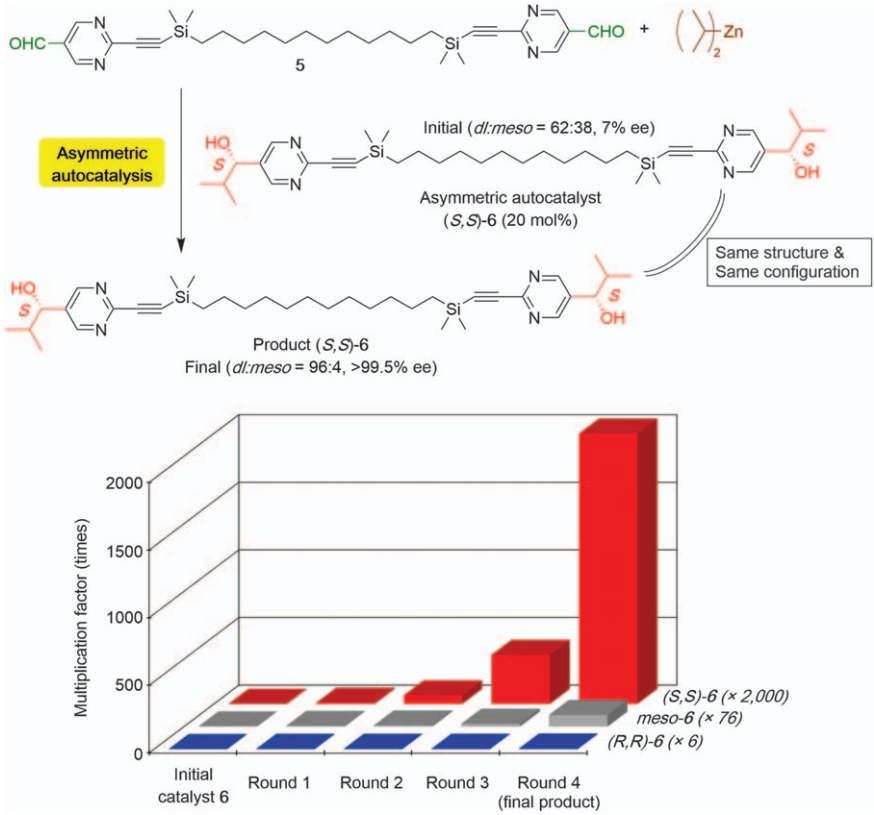

Figure 14.11 Asymmetric autocatalysis of bis(5-pyrimidyl alkanol) **6** with amplification of de and ee.

supramolecular orientation of catalytic and reactive moieties at each terminal of a conformationally flexible simple methylene chain should occur (see Figure 14.12).

To evaluate the intramolecular asymmetric induction, (*S*)-hydroxyaldehyde **7** with various ee was submitted to an isopropylation reaction (see Figure 14.13). When (*S*)-**7** with 88% ee was treated with *i*-Pr_2Zn, (*S*,*S*)-diol **8** with >99.5% ee and DL : *meso* = 91 : 9 was obtained; when (*S*)-**7** with a moderate 48% ee was used as a substrate, (*S*,*S*)-diol **8** with 82% ee was formed in the ratio of DL : *meso* = 77 : 23. Moreover, the racemic **7** was converted to racemic diol **8** in the ratio of DL : *meso* = 70 : 30.

These highly stereoselective results support the assertion that the *i*-Pr_2Zn addition occurs under far remote intramolecular 1,39-stereocontrol. However, there is the possibility that intermolecular asymmetric induction occurred because the substrate has the pyrimidine moiety possessing asymmetric autocatalytic activity.

Thus, we next performed the addition of *i*-Pr_2Zn to (*S*)-**7** in the presence of (*R*)-alkanol **9** as a competitor, which induces *R*-chirality to the newly formed

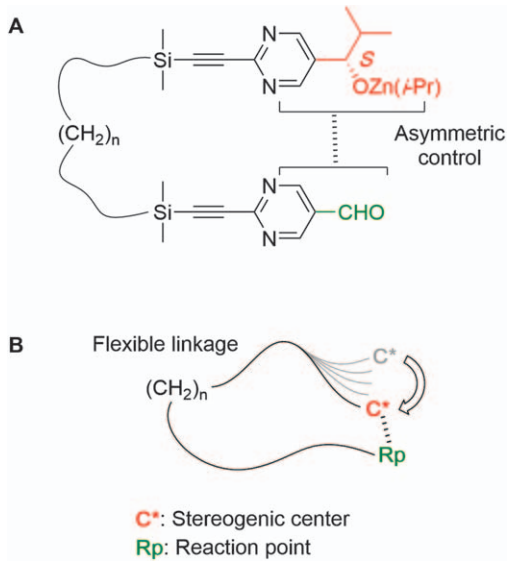

Figure 14.12 Ultra-remote intramolecular asymmetric control with flexible linkers.

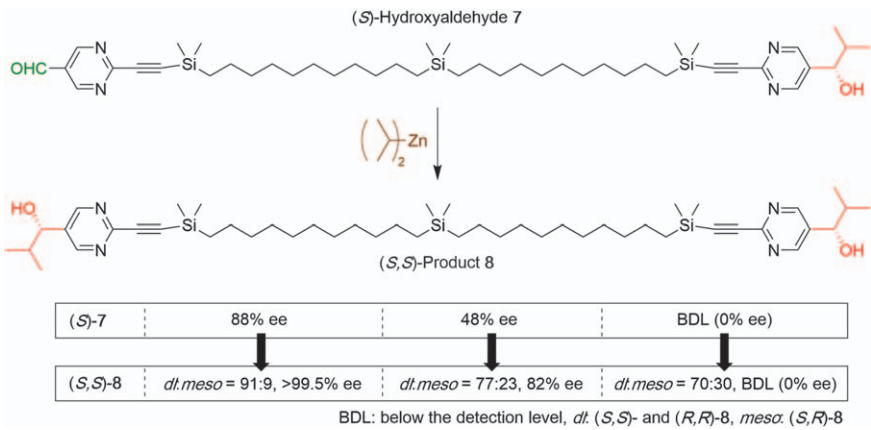

Figure 14.13 Far remote intramolecular 1,39-stereocontrol in asymmetric autocatalysis.

alkanol intermolecularly (see Figure 14.14). When (*S*)-hydroxyaldehyde **7** was treated with *i*-Pr_2Zn in the presence of an excess amount (103 mol%) of (*R*)-hydroxyacetal **9** as a reaction competitor to induce opposite chiral direction, (*S*,*S*)-**8** with >99.5% ee and dr = 93 : 7 was newly formed in 76% yield. The formation of (*S*,*S*)-**8** from (*S*)-**7** in the *R*-excess form can only be explained by intramolecular asymmetric induction, which preferably occurred over the intermolecular alkoxide.

Therefore, we have provided evidence of unprecedented ultra-remote point-to-point asymmetric control (1,39-asymmetric induction) in the

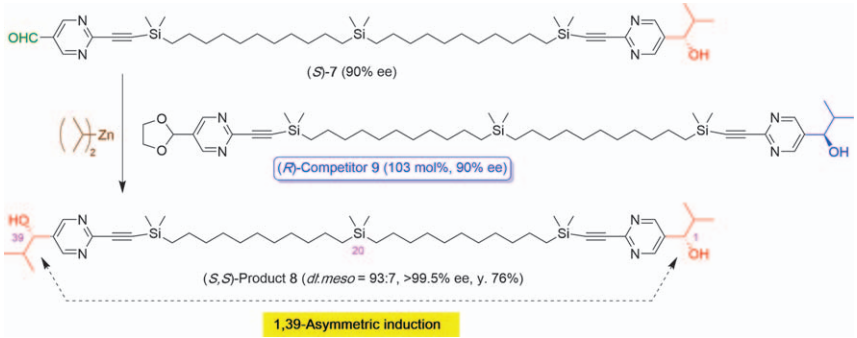

Figure 14.14 Direct evidence of point-to-point intramolecular 1,39-asymmetric induction in asymmetric autocatalysis; the addition of *i*-Pr_2Zn to (*S*)-hydroxyaldehyde in the presence of a (*R*)-configured competitor.

asymmetric autocatalysis of bis(pyrimidyl alkanol), in which two active pyrimidine moieties are tethered with a conformationally flexible long alkyl chain.

14.6 Conclusions

We have summarized the unusual aspect of the Soai reaction, *i.e.*, asymmetric autocatalysis with amplification of ee. When the reaction was carried out using a mixture of two chiral/achiral and chiral/chiral compounds such as β-amino alcohols, the co-operative action of the two β-amino alcohols in the dialkylzinc addition could be sensitively detected as the enantioface selectivity of the product of asymmetric autocatalysis. Achiral β-amino alcohols can reverse the enantioselectivity of chiral β-amino alcohols; thus, both enantiomers of the product could be synthesized from the unique chiral sources. In the reaction using two competing chiral β-amino alcohols, asymmetric autocatalysis can enhance the slight difference in the asymmetric power of the two compounds. The reaction temperature can control not only the reaction rate but also enantioface selectivity and thus can change the aggregation structure of reactive sources. Even though the same chiral source with the same handedness was used as a chiral trigger for asymmetric autocatalysis, highly enantioenriched (*S*)- and (*R*)-products could be obtained depending on the reaction temperature. In addition, 1-aza[6]helicene and 2-aza[6]helicene with the same helical senses showed opposite enantioselectivity in the *i*-Pr_2Zn addition to pyrimidine-5-carbaldehyde depending on the position of the nitrogen atom. In examining the asymmetric autocatalysis of bis(5-pyrimidyl alkanol), unprecedented ultra-remote intramolecular 1,39-asymmetric induction was demonstrated.

Acknowledgements

This work was financially supported by KAKENHI 19K05482, 19K22190 and 20H04674 from JSPS.

References

1. A. Guijarro and M. Yus, *The Origin of Chirality in the Molecules of Life*, The Royal Society of Chemistry, Cambridge, 1st edn, 2009.
2. K.-H. Ernst, *Phys. Status Solidi*, 2012, **249**, 2057.
3. B. L. Feringa and R. A. van Delden, *Angew. Chem., Int. Ed.*, 1999, **38**, 3418.
4. J. M. Ribó, J. Crusats, F. Sagués, J. Claret and R. Rubires, *Science*, 2001, **292**, 2063.
5. I. Weissbuch and M. Lahav, *Chem. Rev.*, 2011, **111**, 3236.
6. T. Kawasaki, Y. Matsumura, T. Tsutsumi, K. Suzuki, M. Ito and K. Soai, *Science*, 2009, **324**, 492.
7. Y. Inoue, *Chem. Rev.*, 1992, **92**, 741.
8. K. Mislow, *Collect. Czech. Chem. Commun.*, 2003, **68**, 849.
9. M. Bolli, R. Micura and A. Eschenmoser, *Chem. Biol.*, 1997, **4**, 309.
10. R. Naaman, Y. Paltiel and D. H. Waldeck, *Nat. Rev. Chem.*, 2019, **3**, 250.
11. C. Viedma, *Phys. Rev. Lett.*, 2005, **94**, 065504.
12. G. Rikken and E. Raupach, *Nature*, 1997, **390**, 493.
13. J. Han, O. Kitagawa, A. Wzorek, K. D. Klia and V. A. Soloshonok, *Chem. Sci.*, 2018, **9**, 1718.
14. G. Storch and O. Trapp, *Nat. Chem.*, 2017, **9**, 179.
15. T. Satyanarayana, S. Abraham and H. B. Kagan, *Angew. Chem., Int., Ed.*, 2009, **48**, 456.
16. K. Soai, T. Shibata, H. Morioka and K. Choji, *Nature*, 1995, **378**, 767.
17. K. Soai, T. Kawasaki and A. Matsumoto, *Acc. Chem. Res.*, 2014, **47**, 3643.
18. K. Soai, A. Matsumoto and T. Kawasaki, *Isr. J. Chem.*, 2021, **61**, 507.
19. K. Soai, T. Kawasaki and A. Matsumoto, *Symmetry*, 2019, **11**, 694.
20. F. C. Frank, *Biochim. Biophys. Acta*, 1953, **11**, 459.
21. J. Crusats, D. Hochberg, A. Moyano and J. M. Ribó, *ChemPhysChem*, 2009, **10**, 2123.
22. D. G. Blackmond, *Chem. Rev.*, 2020, **120**, 4831.
23. D. G. Blackmond, C. R. McMillan, S. Ramdeehul, A. Schorm and J. M. Brown, *J. Am. Chem. Soc.*, 2001, **123**, 10103.
24. T. Gehring, M. Quaranta, B. Odell, D. G. Blackmond and J. M. Brown, *Angew. Chem., Int. Ed.*, 2012, **51**, 9539.
25. G. Ercolani and L. Schiaffino, *J. Org. Chem.*, 2011, **76**, 2619.
26. I. D. Gridnev and A. K. Vorobiev, *ACS Catal.*, 2012, **2**, 2137.
27. I. D. Gridnev and A. K. Vorobiev, *Bull. Chem. Soc. Jpn.*, 2015, **88**, 333.
28. J. R. Islas, D. Lavabre, J.-M. Grevy, R. H. Lamoneda, H. R. Cabrera, J.-C. Micheau and T. Buhse, *Proc. Natl. Acad. Sci. U. S. A.*, 2005, **102**, 13743.
29. J.-C. Micheau, J. M. Cruz, C. Coudret and T. Buhse, *ChemPhysChem*, 2010, **11**, 3417.
30. J.-C. Micheau, C. Coudret, J. M. Cruz and T. Buhse, *Phys. Chem. Chem. Phys.*, 2012, **14**, 13239.
31. M. E. Noble-Teran, J.-M. Cruz, J.-C. Micheau and T. W. Buhse, *ChemCatChem*, 2018, **10**, 642.

32. K. Micskei, G. Rábai, E. Gál, L. Caglioti and G. Pályi, *J. Phys. Chem. B*, 2008, **112**, 9196.
33. M. Maioli, K. Micskei, L. Caglioti, C. Zucchi and G. Pályi, *J. Math. Chem.*, 2008, **43**, 1505.
34. B. Barabás, L. Caglioti, K. Micskei and G. Pályi, *Bull. Chem. Soc. Jpn.*, 2009, **82**, 1372.
35. É. Dóka and G. Lente, *J. Am. Chem. Soc.*, 2011, **133**, 17878.
36. G. Lente, *J. Phys. Chem. A*, 2005, **109**, 11058.
37. Y. Saito and H. Hyuga, *Top. Curr. Chem.*, 2008, **284**, 97.
38. S. Athavale, A. Simon, K. N. Houk and S. E. Denmark, *Nat. Chem.*, 2020, **12**, 412.
39. S. V. Athavale, A. Simon, K. N. Houk and S. E. Denmark, *J. Am. Chem. Soc.*, 2020, **142**, 18387.
40. O. Trapp, S. Lamour, F. Maier, A. F. Siegle, K. Zawatzky and B. F. Straub, *Chem. – Eur. J.*, 2020, **26**, 15871.
41. I. Sato, D. Omiya, H. Igarashi, K. Kato, Y. Ogi, K. Tsukiyama and K. Soai, *Tetrahedron: Asymmetry*, 2003, **14**, 975.
42. A. Matsumoto, T. Abe, A. Hara, T. Tobita, T. Sasagawa, T. Kawasaki and K. Soai, *Angew. Chem., Int. Ed.*, 2015, **54**, 15218.
43. A. Matsumoto, S. Fujiwara, T. Abe, A. Hara, T. Tobita, T. Sasagawa, T. Kawasaki and K. Soai, *Bull. Chem. Soc. Jpn.*, 2016, **89**, 1170.
44. I. P. Beletskaya, C. Naǰera and M. Yus, *Chem. Rev.*, 2018, **118**, 5080.
45. W. Cao, X. Feng and X. Liu, *Org. Biomol. Chem.*, 2019, **17**, 6538.
46. T. Kawasaki, Y. Ishikawa, Y. Minato, T. Otsuka, S. Yonekubo, I. Sato, T. Shibata, A. Matsumoto and K. Soai, *Chem. – Eur. J.*, 2017, **23**, 282.
47. I. Ojima, *Catalytic Asymmetric Synthesis*, John Wiley & Sons, Inc., Hoboken, New Jersey, 3rd edn, 2010.
48. K. Soai, T. Hayasaka and S. Ugajin, *Chem. Commun.*, 1989, 516.
49. E. M. Vogl, H. Groöger and M. Shibasaki, *Angew. Chem., Int. Ed.*, 1999, **38**, 1570.
50. L. C. Wieland, H. Deng, M. L. Snapper and A. H. Hoveyda, *J. Am. Chem. Soc.*, 2005, **127**, 15453.
51. A. M. Costa, C. Jimeno, J. Gavenonis, P. J. Carroll and P. J. Walsh, *J. Am. Chem. Soc.*, 2002, **124**, 6929.
52. M. Reetz and G. Mehler, *Tetrahedron Lett.*, 2003, **44**, 4593.
53. F. Lutz, T. Igarashi, T. Kawasaki and K. Soai, *J. Am. Chem. Soc.*, 2005, **127**, 12206.
54. D. Lavabre, J.-C. Micheau, J. R. Islas and T. Buhse, *J. Phys. Chem. A*, 2007, **111**, 281.
55. T. Shibata, H. Tarumi, T. Kawasaki and K. Soai, *Tetrahedron: Asymmetry*, 2012, **23**, 1023.
56. Y. N. Belokon, M. North, V. I. Maleev, N. V. Voskoboev, M. A. Moskalenko, A. S. Peregudov, A. V. Dmitriev, N. S. Ikonnikov and H. B. Kagan, *Angew. Chem., Int. Ed.*, 2004, **43**, 4085.
57. M. T. Reetz, T. Sell, A. Meiswinkel and G. Mehler, *Angew. Chem., Int. Ed.*, 2003, **42**, 790.

58. M. Kitamura, S. Suga, M. Niwa and R. Noyori, *J. Am. Chem. Soc.*, 1995, **117**, 4832.
59. T. Kawasaki, Y. Wakushima, M. Asahina, K. Shiozawa, T. Kinoshita, F. Lutz and K. Soai, *Chem. Commun.*, 2011, **47**, 5277.
60. K. Soai and S. Niwa, *Chem. Rev.*, 1992, **92**, 833.
61. R. Noyori and M. Kitamura, *Angew. Chem., Int. Ed.*, 1991, **30**, 49.
62. L. Pu and H.-B. Yu, *Chem. Rev.*, 2001, **101**, 757.
63. K. Soai, S. Yokoyama, K. Ebihara and T. Hayasaka, *Chem. Commun.*, 1987, 1690.
64. K. Soai, S. Yokoyama and T. Hayasaka, *J. Org. Chem.*, 1991, **56**, 4264.
65. F. Lutz, T. Igarashi, T. Kinoshita, M. Asahina, K. Tsukiyama, T. Kawasaki and K. Soai, *J. Am. Chem. Soc.*, 2008, **130**, 2956.
66. M. Kitamura, S. Okada, S. Suga and R. Noyori, *J. Am. Chem. Soc.*, 1989, **111**, 4028.
67. Y. Geiger, T. Achard, A. M.-François and S. B.-Laponnaz, *Nat. Cat.*, 2020, **3**, 422.
68. T. Katsuki and K. B. Sharpless, *J. Am. Chem. Soc.*, 1980, **102**, 5974.
69. D. Seebach, A. K. Beck and A. Heckel, *Angew. Chem., Int. Ed.*, 2001, **40**, 92.
70. Y. Chen, S. Yekta and A. K. Yudin, *Chem. Rev.*, 2003, **103**, 3155.
71. T. Kawasaki, Y. Okano, E. Suzuki, S. Takano, S. Oji and K. Soai, *Angew. Chem., Int. Ed.*, 2011, **50**, 8131.
72. F. Lutz, I. Sato and K. Soai, *Org. Lett.*, 2004, **6**, 1613.
73. M. Quaranta, T. Gehring, B. Odell, J. M. Brown and D. G. Blackmond, *J. Am. Chem. Soc.*, 2010, **132**, 15104.
74. M. Busch, M. Schlageter, D. Weingand and T. Gehring, *Chem. – Eur. J.*, 2009, **15**, 8251.
75. B. H. Buschmann, H. Scharf, N. Hoffmann and P. Esser, *Angew. Chem., Int. Ed.*, 1991, **30**, 477.
76. J. Escorihuela, M. I. Burguete and S. V. Luis, *Chem. Soc. Rev.*, 2013, **42**, 5595.
77. Y. Nagata, T. Nishikawa, M. Suginome, S. Sato, M. Sugiyama, L. Porcar, A. Martel, R. Inoue and N. Sato, *J. Am. Chem. Soc.*, 2018, **140**, 2722.
78. A. Matsumoto, S. Fujiwara, Y. Hiyoshi, K. Zawatzky, A. Makarov, C. J. Welch and K. Soai, *Org. Biomol. Chem.*, 2017, **15**, 555.
79. I. Sato, R. Yamashima, K. Kadowaki, J. Yamamoto, T. Shibata and K. Soai, *Angew. Chem., Int. Ed.*, 2001, **40**, 1096.
80. T. Kawasaki, K. Suzuki, E. Licandro, A. Bossi, S. Maiorana and K. Soai, *Tetrahedron: Asymmetry*, 2006, **17**, 2050.
81. J. Míšek, F. Teplý, I. G. Stará, M. Tichý, D. Šaman, I. Císařová, P. Vojtíšek and I. Starý, *Angew. Chem., Int. Ed.*, 2008, **47**, 3188.
82. A. Matsumoto, K. Yonemitsu, H. Ozaki, J. Míšek, I. Starý, I. G. Stará and K. Soai, *Org. Biomol. Chem.*, 2017, **15**, 1321.
83. T. Kawasaki, M. Nakaoda, Y. Takahashi, Y. Kanto, N. Kuruhara, K. Hosoi, I. Sato, A. Matsumoto and K. Soai, *Angew. Chem., Int. Ed.*, 2014, **53**, 11199.

84. K. Soai, H. Hori and M. Kawahara, *J. Chem. Soc., Chem. Commun.*, 1992, 106.
85. K. Mikami, M. Shimizu, H.-C. Zhang and B. E. Maryanoff, *Tetrahedron*, 2001, **57**, 2917.
86. K. Budt, J. Vatele and Y. Kishi, *J. Am. Chem. Soc.*, 1986, **108**, 6080.
87. P. Linnane, N. Magnus and P. Magnus, *Nature*, 1997, **385**, 799.
88. J. Clayden, A. Lund, L. Vallverdu and M. Helliwell, *Nature*, 2004, **431**, 966.
89. L. Byrne, J. Solà, T. Boddaert, T. Marcelli, R. W. Adams, G. A. Morris and J. Clayden, *Angew. Chem., Int. Ed.*, 2014, **53**, 151.

Subject Index